Mechanistic Investigations and Development of Ni-Catalyzed Cross-Electrophile Coupling Reactions

Thesis by

Raymond F. Turro

In Partial Fulfillment of the Requirements

for the Degree of

Doctor of Philosophy

CALIFORNIA INSTITUTE OF TECHNOLOGY

Pasadena, California

2023

(Defended May 22, 2023)

Raymond Turro

ORCID: 0000-0001-9774-4556

To my parents for unwavering support,
Bridget for inspiration,
and Larissa for compassion and strength.
I couldn't have made it without you.

ACKNOWLEDGEMENTS

I am extremely grateful for all the opportunities and support that I have been given that has led to where I am today. It has been such a privilege to join the ranks of the brilliant minds of the scientists and engineers here at Caltech. I have gained so much from interacting with my peers and mentors here and it truly is a "special place" as many before me have said. I would not have made it to this point without all of the love and support I received during my time before Caltech and while I was here

I have to begin by thanking my advisor, Professor Sarah Reisman, for giving me the opportunity to research in her lab for my Ph.D. studies. My time under Sarah's guidance over these years has forged who I am as a scientist. I could not have asked for a more supportive, motivating, rigorous, and exciting environment to do my graduate studies. I'm not sure there would be another place where I could be aligning light sources for spectroelectrochemical detection of a key reaction intermediate with an exotic electronic structure one day, then scaling up material to scout out new routes in our synthesis the next. Sarah has shown compassion and kindness when it matters and has pushed me to achieve the best of my abilities. I am grateful to have worked for someone who puts so much into what she loves and is such a force for good in our field.

I would also like to thank the rest of my committee: Prof. Max Robb, Prof. Brian Stoltz and Prof. Theo Agapie, for their insight over the years and constructive feedback on my progress. As stressful as our meetings have been, they are such an opportunity for intellectual growth. You are all perfect role models for the scientist that I should be and have always been so respectful and facilitative during my journey. I would like to thank Max for being a great committee chair who has made each step of this degree feel

productive and treats me with a refreshing combination of kindness and professionalism. Theo has been a great committee member yet I think I will remember him more for his excellent teaching skills as I don't think I would have passed Ch112 with another professor or set of TAs. I would also like to specifically thank my committee member, and "academic grandfather", Brian for being a great second advisor to us in the Reisman lab and a friend outside of the lab. You are another great example of a compassionate researcher who is truly an expert in their field and always can offer a fresh perspective.

I have had the pleasure of working with many talented scientists over the years on the 3rd floor of Schlinger. I need to start by acknowledging my amazing mentor, Dr. Julie L. H. Wahlman, for welcoming me into the lab and introducing me to graduate-level research. Although we only overlapped in the lab briefly, I learned so much about how to be a successful graduate student in terms of time management, data acquisition, and good scientific practices. I am truly lucky to have worked with Julie and I am relieved to know that you are training the next generation of scientists at Cal State Long Beach. I would also like to acknowledge all of the previous work done by Julie and the rest of Team Nickel Dr. Kelsey Poremba, Dr. Caitlin Lacker, Dr. Alex Shimozono, and Dr. Travis DeLano who dedicated time with me to ensure their knowledge and skills survived in the lab after they left.

I would also like to acknowledge my other senior student mentor in the group, and close friend, Dr. Nicholas Fastuca. Over the years in Pasadena, I had so many positive experiences with him in and out of the lab. He eventually recruited me onto his new synthesis project and taught me about the practical aspects of total synthesis research. When we weren't making natural products in the lab, we were making them in my

apartment as we learned how to brew beer together. Many of these experiences kept me grounded and gave me much needed perspective during my time in graduate school. It also helps that Nick was a part of a wonderful class with Dr. Catilin Lacker and Dr. Skyler Mendoza who were also great friends (and cat sitters) to me. The three of you really lead by example by gave so much of yourselves to the lab and the people in it over the years. The lab has never really been the same without you all.

Another star Reisman class that made a huge impression on me was the year ahead of me consisting: Dr. Mike Maser, Dr. Alex Shimozono, Dr. Travis DeLano, and Dr. Karli Holman. All of these people were model senior lab members when I joined and made us all feel welcomed and wanted. Alex not only played a big role in recruiting me to the Reisman lab but also went above and beyond in supporting me early on. I look forward to our continued friendships into the future, especially with my future neighbors, Karli and Travis, in Boston.

I was fortunate enough to have many great project partners and collaborators over the years. These people were essential intellectual collaborators and spent the time to teach me so much about different aspects of organic, physical, or analytical chemistry. In particular, my partner in Ni, Jaron Tong has been an invaluable asset to my degree and a great friend. I truly would have been lost if it weren't for Jaron's intelligence and patience as a collaborator and was thrilled when he joined our lab. I also was lucky enough to work on a project with Dr. Marco Brandstätter whose creativity, attention to detail, and laboratory skills was such an inspiration. I also worked on projects with Emily Chen and Nathan Friede in our lab and collaborated with Dr. Brendon McNicholas, Dr. Daniel Bim, and Professor Ryan Hadt. While not an official project partner I have to also thank Dr.

David Hill for his mentorship, friendship, and help with analytical techniques I never thought I would be doing. I learned so much from these people and developed so many skills I never thought I would pick up in graduate school which I am truly grateful.

I was joined by two very talented post-docs on the total synthesis project Dr. Sven Richter and Dr. Philip Böhm. Both of them came to the lab with excellent experimental skills in method development which they were both quickly able to translate to progress on our synthesis. It's always a pleasure to sit down with them as a team and brainstorm new ideas. I was also joined by a very impressive and ambitious Caltech undergraduate student, Tessa Pierce, who joined our group as an FSRI student before her freshman year. Despite having no college-level chemistry background she tackled a summer of organic chemistry research and signed up to continue to work on total synthesis throughout her Freshman year into that summer. It was a pleasure working with a beginning scientist like Tessa and I can't wait to see what she does after Caltech.

I have really felt like I was a part of a community these last 5 years (COVID aside) working on the 3rd floor of Schlinger. Working so close to the Stoltz lab has allowed me to make some important connections with them over the years in particular: Zack Sercel, Alexia Kim, Tyler Casselman, Ali Stanko, Dr. Eric Welin, Dr. Nick Hafeman, Dr. Eric Alexy, Dr. Chris Reimann (go Yankees!), and especially Alex Cusumano. Whether it was in the classroom or playing ping-pong I gained a lot from overlapping with these amazing scientists. I could say the same to the friends I've made beyond the 3rd floor including: Dr. Brooke Versaw, Anna Overholts, May Zeng, Chloe Williams, and Sepand Nistanki.

I didn't have to leave the lab to forge great friendships over the years with Reisman lab members. I am incredibly grateful to have had such tight-knit class of students to join

the group with me. Dr. Yujia Tao, Dr. Sara Dibrell, and Jeff Kerkovius are all incredibly hard-working and intelligent scientists who have never stopped making me feel humble. I have to credit a lot of my education over the last few years by just working in proximity to such ambitious and intelligent people. I can't wait to see what we all do from here.

It is very safe to say that I would not be a scientist if it were not for my undergraduate institution, Juniata College, and the stellar Chemistry & Biochemistry Department. I got to learn amongst an amazing class of students including: James McGettigan, Kevin Schofield, Sam Gary, Andrew Guide, Margret Vos, and Larissa Bubb who all made college as fun as it was educational. In particular James McGettigan was truly a great friend who toughed out so many difficult classes and assignments with me. I was a part of the last class at Juniata to take part in the "organic first" experiment where all (STEM) students take organic chemistry as the introductory chemistry course. It was here that a science class actually clicked for me and I realized that this "boogeyman" of a subject was perfect for someone like me. This spark of passion was truly nurtured in the chemistry department by the best teachers I have ever had. The amount of work that professors like Dr. William Ames, Dr. Richard Hark, Dr. Dan Dries, Dr. Ursula Williams, Dr. Sharon Yohn, Dr. Peter Baran, Dr. Alec Brown, and Dr. John Unger put into teaching students and introducing them to research felt truly unique.

I could probably write a page to each of those people but I have explicitly thank my advisor Dr. John Unger. John is a great teacher who always kept are attention like when he brought the president of Juniata into class to drink enough scotch that blowing on some Jones reagent would cause it to change color. He is also a great research advisor who was always encouraging and willing to get in the lab to show you a new technique or decode a

mysterious piece of data. All of the encouragement he gave me to go to conferences, take up leadership roles in the department, get summer internships, etc... played a huge role in my development as a chemist to get me where I am today.

When I was not doing research at Juniata, was in Dallas working with an incredible set of researchers that taught me a lot about the field and what graduate school was like. In particular I really enjoyed working with and learning from Dr. Aaron Nash, Dr. Chris Sleet, Dr. Vaishnavi Nair, Dr. Mohammed Sharique, Dr. Bin Xu, and Dr. Madhu Manna. Others in the group, like Dr. Liela Bayeh-Romero and Dr. Jackson Gartman, went above and beyond with mentoring me in not only how to be successful in the lab but also taught me important lessons that prepared me for graduate school. Of course I need to thank Dr. Uttam Tambar who I can probably credit for most of the opportunities I have been afforded on my path to a career in research. It was during that first summer in Uttam's group that I knew I wanted to get a Ph.D. in organic chemistry. Even though I was in undergrad he spent so much time talking to me about chemistry and introducing me to advanced topics as well as showing me how to do basic lab techniques like column chromatography and pTLC. Even now as I look back, I think I am still riding the enthusiasm he instilled in me to the end of this degree.

None of my research would have been possible without the amazing support staff and facilities we have access to at Caltech. Most importantly, I have to thank Dr. Scott Virgil who never hesitates to help you solve a problem, develop an assay, or purify the impossible. Beyond all he does for us in the lab I will miss his and Silva's wonderful Christmas parties as they really made me feel like I was at a home away from home. I would also like to thank the instrumentation staff: Dr. David VanderVelde, Dr. Mona

Shahgholi, Dr. Paul Oyala, Dr. Nathan Dalleska, and Dr. Jay Winkler.

I have to thank those who are closest to me for helping me get to Caltech as much as they helped me get through it. My younger sister Bridget is such an inspiration to me and a joy in my life. Despite all of the adversity she faces, she always perseveres and laughs while doing it. She truly keeps me grounded and I am happy we have become so close even though I have been living across the country. Her and I have always found relentless support from our parents, whose love fuels us to keep moving. They have been great role models teaching me to be compassionate towards others and do the right thing. Throughout my life they have also been there to listen and provide support even if I didn't want it at the time or know what was best for me. I hope I have reflected the values they instilled in me while I was at Caltech and continue to do so with my own family.

I have to thank the Bubbs/Hackenbergs as well who have welcomed me into their family with open arms. I fondly look back at all the visits or vacations we took with Mike and Tammy over the years. Whether it is playing board games, fishing, horse-riding, or a raucous Hackenberg family gathering, you all really feel like family. You were also able to make Pasadena feel more like home by visiting during Thanksgiving and other important life events. I admire all your hard-work and ambition and will carry that with me as I start my new life.

Most importantly, I have to thank the most impactful person in my life, Larissa. Without of the support, love, and companionship over the last eight years this book would end right here. I could not have asked for a better partner to take on this monumental task while you achieve so much on your own. She took a big chance on me to move across the country and stick out the madness of graduate school and now we leave as a married couple

with a bright future. I am proud to be your partner and will never forget all you have done for me. I cannot wait to start our new life together in Cambridge and begin a new chapter of our story.

ABSTRACT

Transition metal-catalyzed cross-coupling reactions have proven to be a powerful technology for the modular construction of carbon-carbon and carbon-heteroatom bonds over the last half century. More recently, reductive cross-coupling catalyzed by nickel has emerged as a complementary synthetic approach that couples electrophilic fragments and is rendered catalytic by the inclusion of a terminal reductant. These reactions are advantageous because the use electrophiles as coupling partners which display greater stability, functional group tolerance, and commercial availability over the corresponding nucleophilic coupling partners. Additionally, Ni catalysts are less prone to β-hydride elimination compared to later transition metals which enables $C(sp^3)$–$C(sp^n)$ couplings. The challenge with using coupling partners of the same polarity is developing a catalyst that can activate each electrophile in a mechanistically distinct way in order to get high levels off cross-selectivity, over statistical mixtures of cross- and homocoupled products.

Herein, we describe a mechanistic investigation on Ni-catalyzed cross-electrophile couplings developed in our lab; specifically, the asymmetric reductive alkenylation of *N*-hydroxyphthalimide (NHP) esters and benzylic chlorides. Investigations of the redox properties of the Ni-bis(oxazoline) catalyst, the reaction kinetics, and mode of electrophile activation show divergent mechanisms for these two related transformations. Notably, the mechanism of $C(sp^3)$ activation changes from a Ni-mediated process when benzyl chlorides and Mn^0 are used to a reductant-mediated process that is gated by a Lewis acid when NHP esters and tetrakis(dimethylamino)ethylene is used. Kinetic experiments show that changing the identity of the Lewis acid can be used to tune the rate of NHP ester reduction. Spectroscopic studies support a Ni^{II}–alkenyl oxidative addition complex as the

catalyst resting state. DFT calculations suggest an enantiodetermining radical capture step and elucidate the origin of enantioinduction for this Ni-BOX catalyst.

Efforts to expand the scope of coupling partners in XEC reactions to include novel classes of electrophiles, such as *N*-alkyl imines, are also described. The preparation of heterobenzylic amines by a Ni-catalyzed reductive cross-coupling between heteroaryl imines and $C(sp^3)$ electrophiles is reported. This umpolung-type alkylation proceeds under mild conditions, avoids the pre-generation of organometallic reagents, and exhibits good functional group tolerance. Mechanistic studies are consistent with the imine substrate acting as a redox-active ligand upon coordination to a low-valent Ni center. The resulting bis(2-imino)heterocycle·Ni complexes can engage in alkylation reactions with a variety of $C(sp^3)$ electrophiles, giving heterobenzylic amine products in good yields.

PUBLISHED CONTENT AND CONTRIBUTIONS

Portions of the work described herein were disclosed in the following publications:

1. Turro, R. F.; Brandstätter, M.; Reisman, S. E. Nickel-Catalyzed Reductive Alkylation of Heteroaryl Imines**. *Angew. Chem. Int. Ed.* **2022**, *61*, e202207597, Copyright © 2022 Wiley-VCH GmbH. This article is available online at: https://onlinelibrary.wiley.com/doi/full/10.1002/anie.202207597

R. F. T. contributed to the design of the reaction, conducted experiments, and participated in preparation of the supporting data and writing of the manuscript.

2. Turro, R. F.; Wahlman, J. L. H.; Tong, Z. J.; Chen, X.; Yang, M.; Chem. E. P.; Hong, X.; Hadt, R. H.; Houk, K. N., Yang, Y. F.; Reisman, S. E. Mechanistic Investigation of Ni-Catalyzed Reductive Cross-Coupling of Alkenyl and Benzyl Electrophiles. *J. Am. Chem. Soc.* **2023**, *Accepted Manuscript*. DOI pending, Copyright © 2023 American Chemical Society.

R. F. T. contributed to design of mechanistic experiments, conducted experiments, and participated in preparation of the supporting data and writing of the manuscript.

TABLE OF CONTENTS

LIST OF ABBREVIATIONS

–	minus
%	percent
°	degrees
+	plus
<	less than
=	equals
>	greater than
∝	proportional to
~	approximately
λ	lambda (wavelength)
α	alpha
A	ampere
Å	angstrom(s)
$[\alpha]_D$	angle of optical rotation of plane-polarized light
Ac	acetyl
acac	acetylacetonate
AcOH	acetic acid
Anal.	combustion elemental analysis
anti	opposite or same side
approx	approximately
aq	aqueous
Ar	aryl group
Ar^F	perfluorinated aryl group
atm	atmosphere(s)
AU	arbitrary units
avg	average
β	beta
BHT	2,6-di-*tert*-butyl-4-methylphenol ("butylated hydroxytoluene")
BiOX	bi(oxazoline)
BiM	bi(imidazoline)
Bn	benzyl
Boc	*tert*-butoxycarbonyl
BOX	bis(oxazoline)

bp	boiling point
bpy	2,2'-bipyridine
br	broad
BS	broken symmetry calculations
Bu	butyl
Bz	benzoyl
/C	supported on activated carbon charcoal
°C	degrees Celcius
^{13}C	carbon-13 isotope
c	concentration of sample for measurement of optical rotation
calc'd	calculated
CAM	cerium ammonium molybdate
Cbz	benzyloxycarbonyl
cis	on the same side
cm	centimeters
cm^{-1}	wavenumber(s)
CoPc	cobalt(II) phthalocyanine
COSY	homonuclear correlation spectroscopy
Cp	cyclopentyldienyl
CV	cyclic voltammetry
δ	chemical shift in ppm
D	deuterium
d	deutero or dextrorotatory
d	doublet
Δ	heat or difference
DCM	dichloromethane
DEAD	diethyl azodicarboxylate
DFT	Density Functional Theory
ΔG	change in Gibb's free energy
DHA	dihydroanthracene
DHPs	dihydropyridines
DIBAL	diisobutylaluminum hydride
diglyme	diethylene glycol dimethyl ether
DIPEA	*N*,*N*-diisopropylethylamine
DMA	*N*,*N*-dimethylacetamide
DMAP	4-(dimethylamino)pyridine
dme	1,2-dimethoxyethane

DMEDA	*N,N'*-dimethylethylenediamine
DMF	*N*,*N*-dimethylformamide
DMP	Dess-Martin periodinane
DMPU	1,3-dimethyl-3,4,5,6-tetrahydro-2(1H)-pyrimidinone
DMS	dimethylsulfide
DMSO	dimethylsulfoxide
dppf	1,1'-bis(diphenylphosphino)ferrocene
dpph	1,6-bis-(diphenylphosphino)hexane
dr	diastereomeric ratio
dtbbpy	4,4'-di-*tert*-butyl-2,2'-bipyridine
E	*trans* (entgegen) olefin geometry or potential
e.g.	for example (Latin: *exempli gratia*)
E^+	electrophile
EA	elemental analysis
EDC	1-ethyl-3-(3-dimethylaminopropyl)carbodiimide
ee	enantiomeric excess
EI	electron impact
E_{pa}	anodic peak potential
E_{pc}	cathodic peak potential
$E_{pc/2}$	cathodic half peak potential
$E_{1/2}$	reduction potential
EPR	electron paramagnetic resonance
equiv	equivalent(s)
er	enantiomeric ratio
ESI	electrospray ionization
Et	ethyl
et al.	and others (Latin: *et alii*)
Et_2O	diethyl ether
Et_3N	triethylamine
etc	and the rest (Latin: *et cetera*)
EtOAc	ethyl acetate
EtOH	ethanol
^{19}F	fluorine-19 isotope
FAB	fast atom bombardment
Fc	ferrocene
Fc^+	ferrocenium cation

FD	Field Desorption
FID	flame ionization detector
FTIR	fourier transform infrared spectroscopy
G	gauss
g	gram(s)
g-value	dimensionless magnetic moment value
g/mL	grams per milliliter
GC	gas chromatography or glassy carbon
GHz	gigahertz
^{1}H	proton
h	hour(s)
HAT	hydrogen atom transfer
HC	homocoupling
Het	hetero
HMBC	heteronuclear multiple-bond correlation spectroscopy
HMDS	hexamethyldisilazide
HOMO	highest occupied molecular orbital
HPLC	high performance liquid chromatography
HRMS	high resolution mass spectrometry
HSQC	heteronuclear single quantum coherence spectroscopy
hυ	irradiation with light
Hz	hertz
i	current
i-Bu	*iso*-butyl
i-Pr	isopropyl
i-Pr_2NH	diisopropyl amine
i-PrAc	isopropyl acetate
i-PrOH	isopropanol
i.e.	that is (Latin: *id est*)
in situ	in the reaction mixture
IPA	isopropanol
IR	infrared
J	coupling constant in Hz
K	Kelvin
k	rate constant
k_0	initial rate constant
k_c	equilibrium constant

kcal	kilocalorie(s)
kg	kilogram(s)
k_{obs}	observed reaction rate
KO*t*Bu	potassium tert-butoxide
L	liter
l	levorotatory
LC-MS	liquid chromatography–mass spectrometry
LDA	lithium diisopropylamide
LED	light emitting diode
ln	natural logarithm
log	logarithm
LRMS	low resolution mass spectrometry
LUMO	lowest unoccupied molecular orbital
M	metal or Molar
m	multiplet or meter(s)
[M]	parent mass
m	*meta*
M^{-1}	inverse molarity
m.p.	melting point
m/z	mass-to-charge ratio
*m*CPBA	*meta*-chloroperbenzoic acid
Me	methyl
MeCN	acetonitrile
MeI	methyl iodide
MeOH	methanol
mg	milligram(s)
mg/mL	milligrams per milliliter
MHz	megahertz
MIDA	methyliminodiacetic acid
min	minute(s)
µ	micro
µL	microliter(s)
mL	milliliter(s)
mL/min	milliliters per minute
mM	millimolar
mm	millimeter(s)
µm	micrometer(s)

mm Hg	millimeters mercury
mmol	millimole(s)
mol	mole(s)
mol %	mole percent
Ms	methanesulfonyl (mesyl)
MS	molecular sieves
MsCl	methanesulfonyl chloride
MSD	mass selective detector
^{14}N	nitrogen-14 isotope
n	number
ν	scan rate
n-Bu	*norm-butyl*
n-BuLi	*norm*-butyl lithium
n-Hex	*norm*-hexyl
n-Pr	*norm*-propyl
NaOTf	sodium triflate
NBS	*N*-bromosuccinimide
Nf	perfluorobutanesulfonyl
NHP	*N*-hydroxyphthalimide
NIR	near infrared
nm	nanometer(s)
NMP	*N*-methyl pyrrolidinone
NMR	nuclear magnetic resonance
Nuc^-	nucleophile
o	*ortho*
^{31}P	phosphorus-31 isotope
p	*para*
p-TsOH	*para*-toluenesulfonic acid
Pc	phthalocyanine
PDT	product
pH	hydrogen ion concentration in aqueous solution
Ph	phenyl
phen	1,10-phenanthroline
PhH	benzene
PhMe	toluene
PHOX	phosphinooxaozoline
Phth	phthalimide

Pin	pinacol
pm	picometer(s)
PMP	*para*-methoxyphenyl
ppm	parts per million
Pr	propyl
psi	pounds per square inch
Py	pyridine
PyBOX	pyridine bis(oxazoline)
pyr	pyridine
q	quartet
quant.	quantitative
R	generic (alkyl) group
R	rectus (right)
R^2	coefficient of determination
RCC	reductive cross-coupling
ref	reference
RVC	reticulated vitreous carbon foam
R_F	pefluorinated alkyl
R_f	retention factor
RF	response factor
RPKA	reaction progress kinetic analysis
rpm	revolutions per minute
rr	regioisomeric ratio
RS	Randles-Sevcik
rt	room temperature
σ	Hammett coefficient
s	singlet or seconds
S	sinister
sat.	saturated
SCE	saturated calomel electrode
SFC	supercritical fluid chromatography
STD	standard
syn	same side
T	temperature
t	triplet or time
t-Bu	*tert*-butyl
t-BuLi	tert-butyl lithium

taut.	tautomerize
TBA	tetra-n-butylammonium
TBABr	tetra-*n*-butylammonium bromide
TBACl	tetra-*n*-butylammonium chloride
TBAF	tetra-*n*-butylammonium fluoride
TBAI	tetra-*n*-butylammonium iodide
TBAX	tetra-*n*-butylammonium salt
TBDPS	*tert*-butyldiphenylsilyl
TBDPSCl	tert-butyldiphenylsilyl chloride
TBS	*tert*-butyldimethylsilyl
TBSCl	*tert*-butyldimethylsilyl chloride
TDAE	tetrakis(dimethylamino)ethylene
TD-DFT	time-dependent density functional theory
TEA	triethylamine
temp	temperature
TEMPO	2,2,6,6-tetramethylpiperidine 1-oxyl
TEOA	triethanolamine
TES	triethylsilyl
Tf	trifluoromethanesulfonyl
Tf_2O	trifluoromethanesulfonic anhydride
TFA	trifluoroacetic acid
THF	tetrahydrofuran
TIPS	triisopropylsilyl
TLC	thin layer chromatography
TMEDA	*N,N,N′,N′*-tetramethylethylenediamine
TMHD	2,2,6,6-tetramethyl-3,5-heptanedione
TMS	trimethylsilyl
TMSBr	trimethylsilyl bromide
TMSCl	trimethylsilyl chloride
TMSOTf	trimethylsilyl trifluoromethanesulfonate
TOF	time-of-flight
Tol	tolyl
terpy	2,2';6',2"-terpyridine
t_R	retention time
trans	on the opposite side
TS	transition state
Ts	*para*-toluenesulfonyl (tosyl)

TTF	tetrathiafulvalene
UV	ultraviolet
V	volt(s)
vide infra	see below
vide supra	see above
V_{max}	maximum rate
vs.	versus
VTNA	Variable Time Normalization Analysis
W	watt(s)
w/	with
wt%	weight percent
X	anionic ligand or halide or chiral auxillary
XAT	x-atom abstraction
XC	cross-coupled
XEC	cross-electrophile coupling
X_{major}	fraction of mixture as major enantiomer
X_{minor}	fraction of mixture as minor enantiomer
Z	*cis* (zusammen) olefin geometry

Chapter 1

Mechanistically-Guided Strategies for Developing Selective Ni-Catalyzed Cross-Electrophile Couplings

1.1 INTRODUCTION

Transition metal-catalyzed cross-coupling reactions have proven to be one of the most powerful developments in synthetic chemistry over the last few decades. This technology has enabled the efficient and selective formation of carbon–carbon and carbon–heteroatom bonds with applications ranging from bioactive pharmaceuticals and agrochemicals, to materials science, as well as electronics.[1] More recently, cross-electrophile coupling (XEC) reactions have emerged as a complementary method to couple electrophilic fragments. These electrophilic fragments, usually organic halides, make up a class of compounds that are abundant from commercial sources or can be readily synthesized; making them an attractive alternative to organometallic nucleophiles used in traditional, redox-neutral, cross-coupling reactions which are less stable and less tolerant of functional

groups. In the context of cross-coupling, electrophiles are substrates that undergo C-X activation through a reductive mechanism such as oxidative addition or single-electron reduction. As a consequence of using two electrophiles, a stoichiometric reductant is needed in order to render the process catalytic.[2]

Figure 1.1. *Comparison of Ni and Pd as catalysts in cross-coupling reactions.*

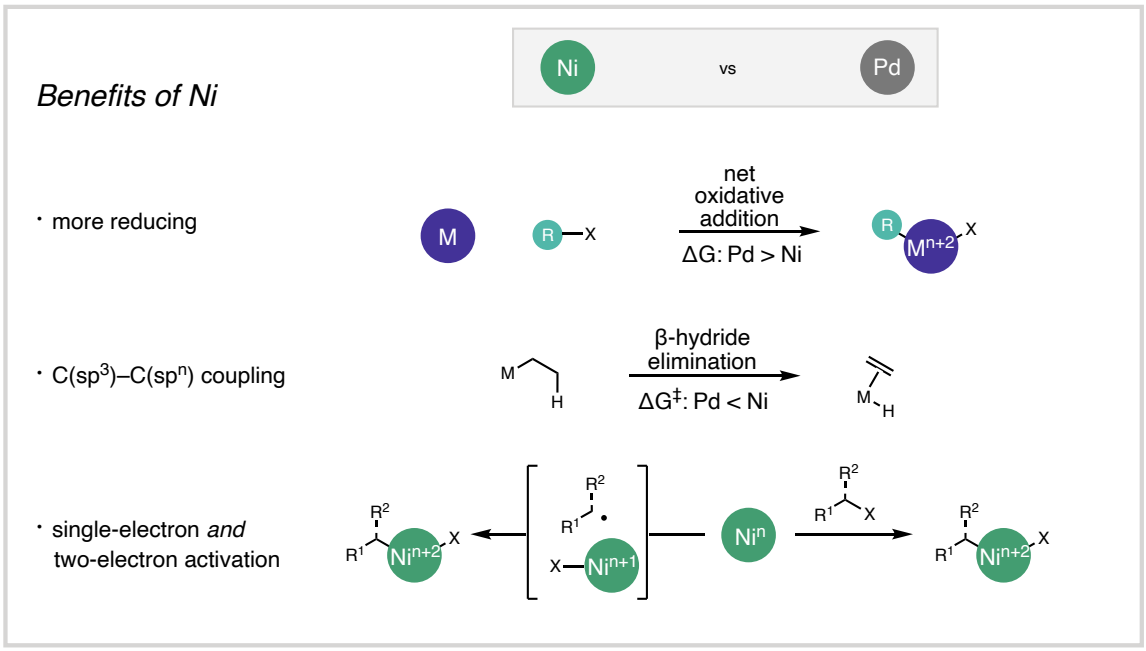

Nickel has proven to be an effective transition-metal catalyst for XEC reactions. This is due to the favorable properties of the metal in terms of reactivity, cost, and sustainability relative to 2nd or 3rd row transition metals popular in traditional cross-couplings. Ni has accessible odd-electron oxidation states ($Ni^{0/I/II/III/IV}$) meaning it can engage in either one or two-electron elementary steps with a substrate. Compared to Pd ($Pd^{0/II}$, E^0 = 0.95 V vs. SHE), there is a greater driving force for oxidation of Ni ($Ni^{0/II}$, E^0 = –0.26 V vs. SHE) making substrate reduction reactions, like oxidative addition, facile. Additionally, intermediate Ni-alkyl complexes are less prone to β-hydride elimination making Ni

amenable to C(sp^3)–C(sp^n) couplings.[3] The intrinsic reactivity of Ni makes it attractive for XEC reactions as it can activate substrates through a variety of mechanisms; however, its promiscuity can make the design of a general and selective catalyst challenging (Figure 1.1).[4]

Figure 1.2. *General scheme for Ni-catalyzed XEC reactions.*

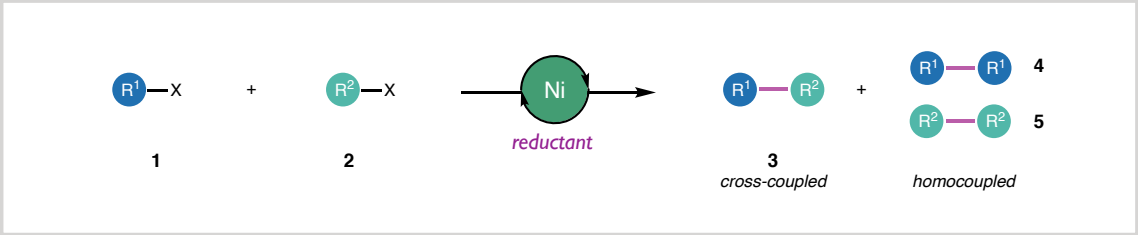

The challenge that arises from using two electrophilic coupling partners (**1** and **2**) is achieving high levels of cross-selectivity over statistical mixtures of cross- (**3**) and homocoupled (**4-5**) products. A cross-selective reaction is achieved by using a catalyst system that activates each electrophile through a distinct mechanism, such that the activation of **1** then **2** can outcompete sequential activation of two equivalents of **1** or **2** (Figure 1.2).[5] This poses a challenge when designing or optimizing XEC reactions due to the ambiguity in how modifying reaction parameters influences the relative rates of electrophile activation (e.g., how electronic perturbations on a ligand may impact the reduction of one coupling partner over the other). Over the last decade of research on XEC reactions, several mechanistically-guided strategies have emerged to achieve remarkable selectivity, enabling exceptionally mild methods for modular construction of strategic bonds.

1.2 Background and Scope

1.2.1 Evolution of Selective Ni-Catalyzed XEC

Scheme 1.1. *Early examples of reductive couplings using Ni.*

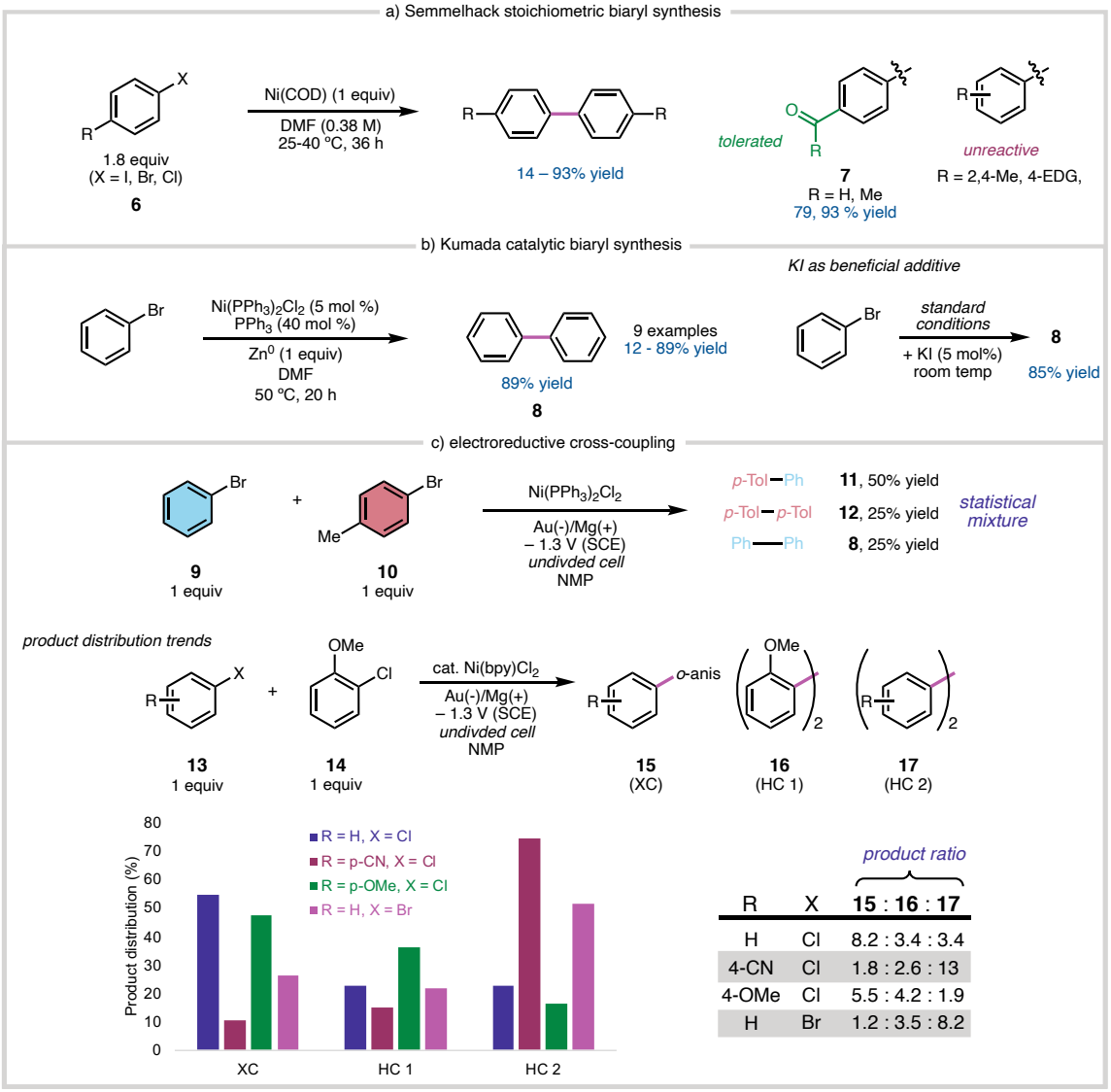

Early investigations of Ni in reductive coupling reactions were performed by Semmelhack and coworkers through the 1970-1980s. These examples utilized stoichiometric Ni^0 complexes and were limited to homocoupling of reactive aryl halides **6**

but demonstrated functional group tolerance (**7**) not seen with traditional couplings that employ organometallic coupling partners (Scheme 1.1a).[6,7,8] Following these early reports, Kumada and coworkers in the late 1970s demonstrated that aryl bromide homocoupling could be made catalytic in Ni when Zn^0 is used as a stoichiometric reductant. Kumada also observes a significant rate acceleration upon the inclusion of KI as an additive enabling the reaction to proceed at room temperature to give **8** in 85% yield (Scheme 1.1b).[9] It was not until 1986 that Périchon and coworkers observed the first cross-coupled products in an electroreductive coupling using aryl bromides (**9** and **10**) with similar reactivity, albeit as a statistical mixture of cross- (**11**) and homocoupled (**8** and **12**) products.[10] Subsequent reports showed the distribution of products (**15-17**) could be perturbed as a function of varying steric and electronic properties of an aryl halide coupling partner **13** when the other coupling partner was an *ortho*-substituted aryl halide **14** (Scheme 1.1c).[11]

Scheme 1.2. *Early example of Ni-catalyzed XEC and proposed mechanism.*

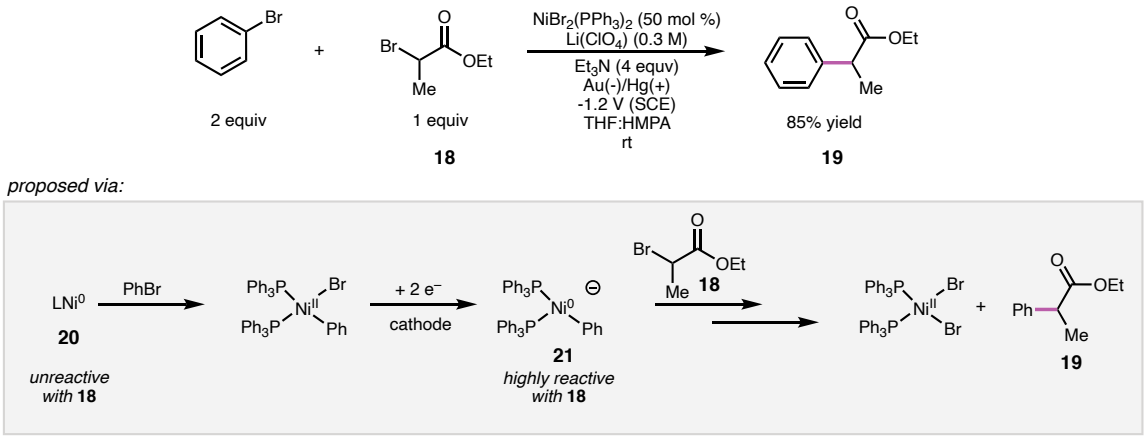

Shortly after their initial report, Périchon and coworkers attained greater cross-selectivity in an electroreductive coupling with electrophiles of different hybridization, in this case, α-bromoesters **18** and aryl halides produced high yields of α-arylated products

19.[12] Subsequent electroanalytical experiments suggest that the origin of selectivity in this case is due to a change in the relative rates of electrophile activation at different oxidation states of Ni where a Ni^0 complex **20** preferentially reacts with aryl halides and the subsequent nickelate complex **21** would react with **18** (Scheme 1.2).[13] These studies in the 1980s and 1990s laid the foundation for how the field would come to think about XEC reactions going forward. Although redox-neutral cross-couplings dominated the literature in the 1990s and 2000s, reductive couplings would undergo a renaissance in the early 2010s that continues to this day.

1.2.2 Proposed Mechanisms of Substrate Activation by Ni in XEC

Mechanistic studies on the oxidative addition of reduced Ni complexes into C–X bonds constitute an ongoing area of research that predates Ni-catalyzed XEC. It is evident that there are numerous pathways that could be operative for a given combination of substrates, ligand environment, and reductant.[3] The evidence and origin of these mechanistic nuances are beyond the scope of this review and unnecessary as a guiding principle in reaction optimization. Instead, we will focus on a practical overview of general mechanisms that have been proposed for $C(sp^2)$ and $C(sp^3)$ electrophile activation in XEC reactions.

The mechanisms of $C(sp^2)$–X oxidative addition with Ni have been proposed to proceed through both one- and two-electron mechanisms. These reactions have been studied extensively for aryl **22** electrophiles but are underexplored for the corresponding alkenyl **23** or acyl **24** electrophiles. In the context of catalytic couplings as well as stoichiometric reactions, oxidative addition with aryl halides have been proposed from both Ni^0 and Ni^I.[14,16,43,15] Proposed C–X activation mechanisms can be summarized as either a

concerted oxidative addition[16,17,43], polar S_NAr,[18] or a stepwise $S_{RN}1$[19] mechanism (Figure 1.3a).

Figure 1.3. *Mechanisms of oxidative addition into C(sp²)–X bonds.*

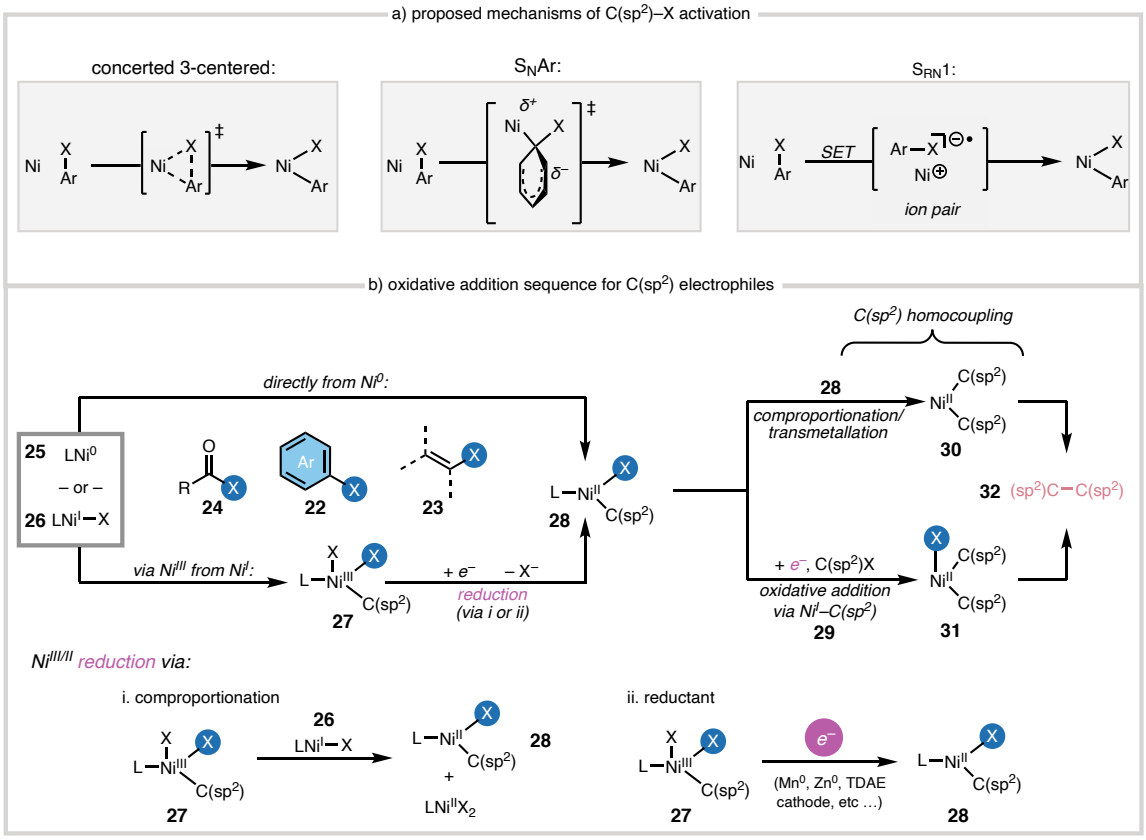

Reactions involving oxidative addition from a Ni^I complex (**26**) yield a high-valent $Ni^{III}Ar$ (**27**) via a radical or two-electron mechanism (Figure 1.3a). This electron-poor intermediate **27** will undergo subsequent reduction reactions by either comproportionation with another equivalent of **26** or by single electron transfer (SET) from the terminal reductant to give Ni^{II} (**28**).[20,101] Alternatively, oxidative addition from Ni^0 **25** would directly furnish complex **28**. Deleterious $C(sp^2)$–$C(sp^2)$ homocoupling reactions have been proposed to occur from disproportionation of **28** to **30** followed by reductive elimination.[21]

Subsequent reduction of oxidative addition complex **28** to a Ni^{I}–Ar **29** has been proposed in Ni-catalyzed XEC reactions, and is a key step in sequential activation mechanisms (*vide infra*).[3,22] Alternatively, **29** can undergo a second oxidative addition of C(sp^2)–X and furnish Ni^{III} species **31** which can undergo reductive elimination to give biaryl product **32** (Figure 1.3b).

Figure 1.4. *Mechanisms of oxidative addition into C(sp^3)–X bonds.*

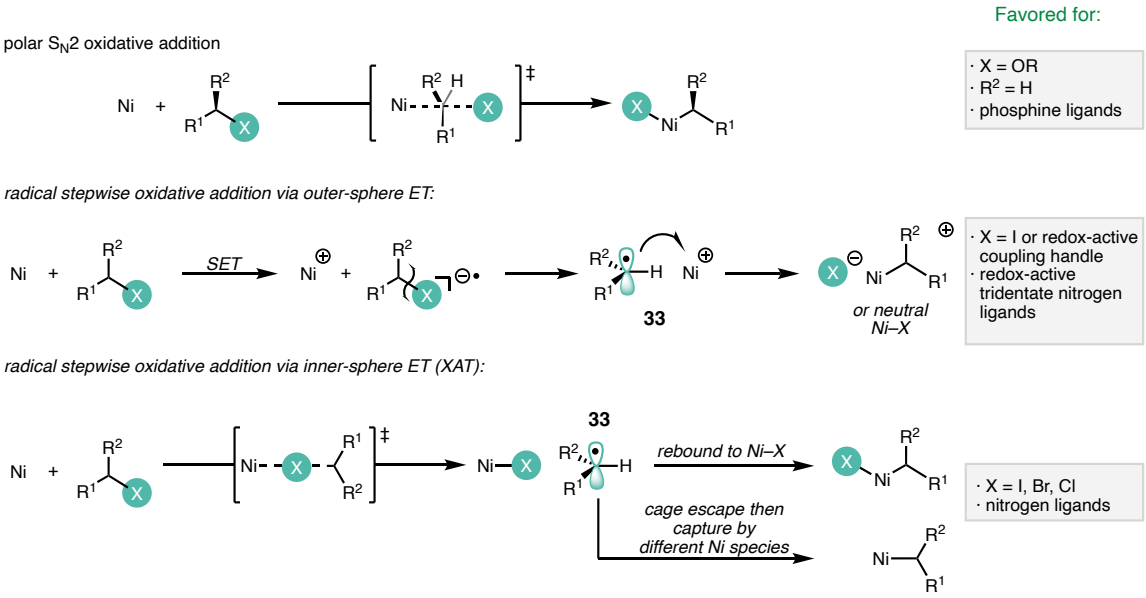

The oxidative addition of Ni into C(sp^3) electrophiles can proceed through several mechanisms depending on the substitution on C, identity of the coupling handle, and ligand environment of the Ni catalyst. This includes two-electron reactions that proceed through an S_N2 mechanism to displace the leaving group to forge a Ni–C bond.[23] This polar mechanism is favored for oxygen-based electrophiles, primary electrophiles, or Ni–phosphine/NHC catalysts.[24] Radical mechanisms have been proposed for various alkyl halide and redox-active coupling handles that proceed through an inner-sphere X-atom transfer (XAT)[25,26,27,28] or by an outer-sphere $S_{RN}1$ process.[29,30,31,32] These proceed through

an alkyl radical intermediate **33** that either rapidly recombines or will escape the solvent cage to be intercepted by another Ni complex (Figure 1.4). In this review, cases will also be discussed where the Ni–C(sp^3) bond is formed by capture of a free radical that was generated through a non-Ni mediated process,[69,33,34,118,83] or by transmetalation of an *in situ* generated organometallic species.[35]

1.2.3 Mechanistic Models of Ni-Catalyzed XEC Reactions

From studies on Ni-catalyzed XEC reactions, several mechanistic frameworks have emerged that can be used to rationalize reactivity during reaction development. Here, we will define two general categories that encompass proposed mechanisms of Ni-catalyzed XEC: 1) sequential activation[36] and 2) parallel activation.[37] Practically, these models are not always distinguishable without extensive mechanistic studies as the difference can come down to accessibility of certain oxidation states for the Ni catalyst, or whether the reduction of a given catalytic intermediate is kinetically feasible.[38] These models can be useful for honing in on challenging processes in a XEC that are responsible for their poor performance such that hypothesis-driven modifications to the reaction conditions can be made in subsequent optimization experiments.

In a $Ni^{I/III}$ sequential activation mechanism, a reduced Ni catalyst (**26**) is proposed to activate the more reactive electrophile **1** via oxidative addition to give **34**. This high-valent intermediate **34** is then reduced to Ni^{I} (**36**) by the terminal reductant which can react with the other electrophile **2** via oxidative addition. The resulting Ni^{III} (**37**) can then undergo reductive elimination to regenerate **26** and furnish product **3** (Figure 1.5a). For this to be cross-selective, the oxidative addition of **1** by **26** must outcompete pathways leading to

homocoupling that can arise from **26** reacting with **2** or **36** reacting with **1**. The preference for **26** reacting with **1** over **2** has been attributed to matching of the steric and electronic properties of reduced Ni intermediates **26** and **36** modulating their respective reactivities towards oxidative addition of either **1** or **2** (Figure 1.5b).[3,27,39]

Figure 1.5. *Sequential activation mechanism.*

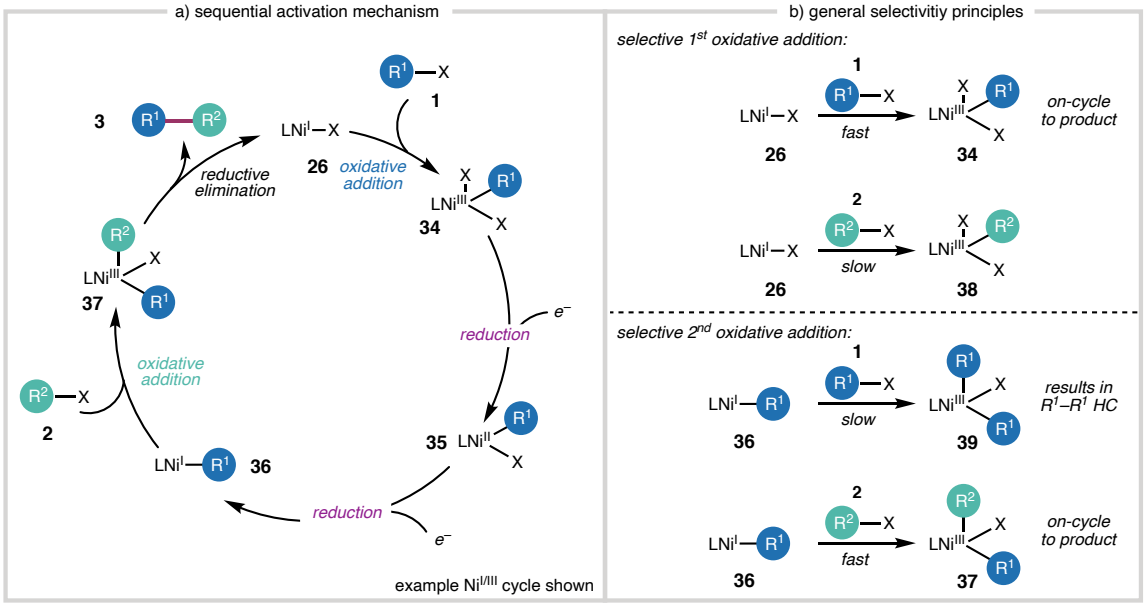

In a $Ni^{I/III}$ parallel activation mechanism, a reduced Ni catalyst (**26**) will react with electrophile **1** to give **34** which is followed by reduction to Ni^{II} **35**. This intermediate **35** then intercepts the activated form of the other electrophile **40** (Y = radical or metal), to forge the second Ni–C bond and give **37**. This Ni^{III} **37** can then undergo reductive elimination to give **26** and cross-coupled product **3**. In versions of this mechanism where **26** acts as chain carrying radical, **26** then goes on to activate electrophile **2** followed by reduction of **41** to turn over the catalyst. This can also be thought of as two parallel catalytic cycles where one Ni catalyst **26** activates one electrophile and another catalyst (possibly

26) can activate the other electrophile. In either case, the origin of cross-selectivity can be explained by comparable rates of converting electrophiles **1** and **2** to their corresponding activated intermediates **35** and **40** in combination with slow homocoupling of the activated intermediate **35** derived from the more reactive electrophile (Figure 1.6). This framework is analogous to the persistent radical effect[40] and the terminology has been extended to cross-coupling as the persistent metal effect (PME).[41]

Figure 1.6. *Parallel activation mechanism.*

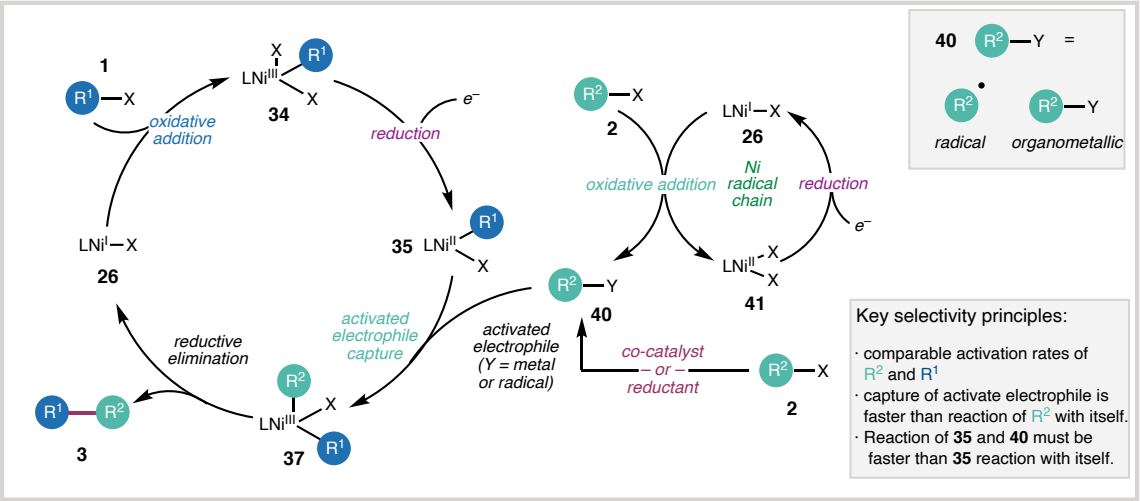

These models can be used to interpret the reaction outcomes in a Ni-catalyzed XEC optimization. No different from any other optimization, the conversion of the starting materials and their distribution among potential products is the experimental output for every input set of conditions. Specifically, the electrophile conversion as a ratio of desired cross-coupled to undesired homocoupled or decomposed products can be informative of the relative rates electrophile activation. For example, if a set of conditions results in significant conversion of one electrophile **A** to homocoupled **A–A** with poor conversion of the other electrophile **B** then this may indicate that **A** activation needs to be slowed or **B**

activation needs to be accelerated (Figure 1.7a).

Figure 1.7. *Ni-catalyzed XEC principles of cross-selectivity relevant to optimization.*

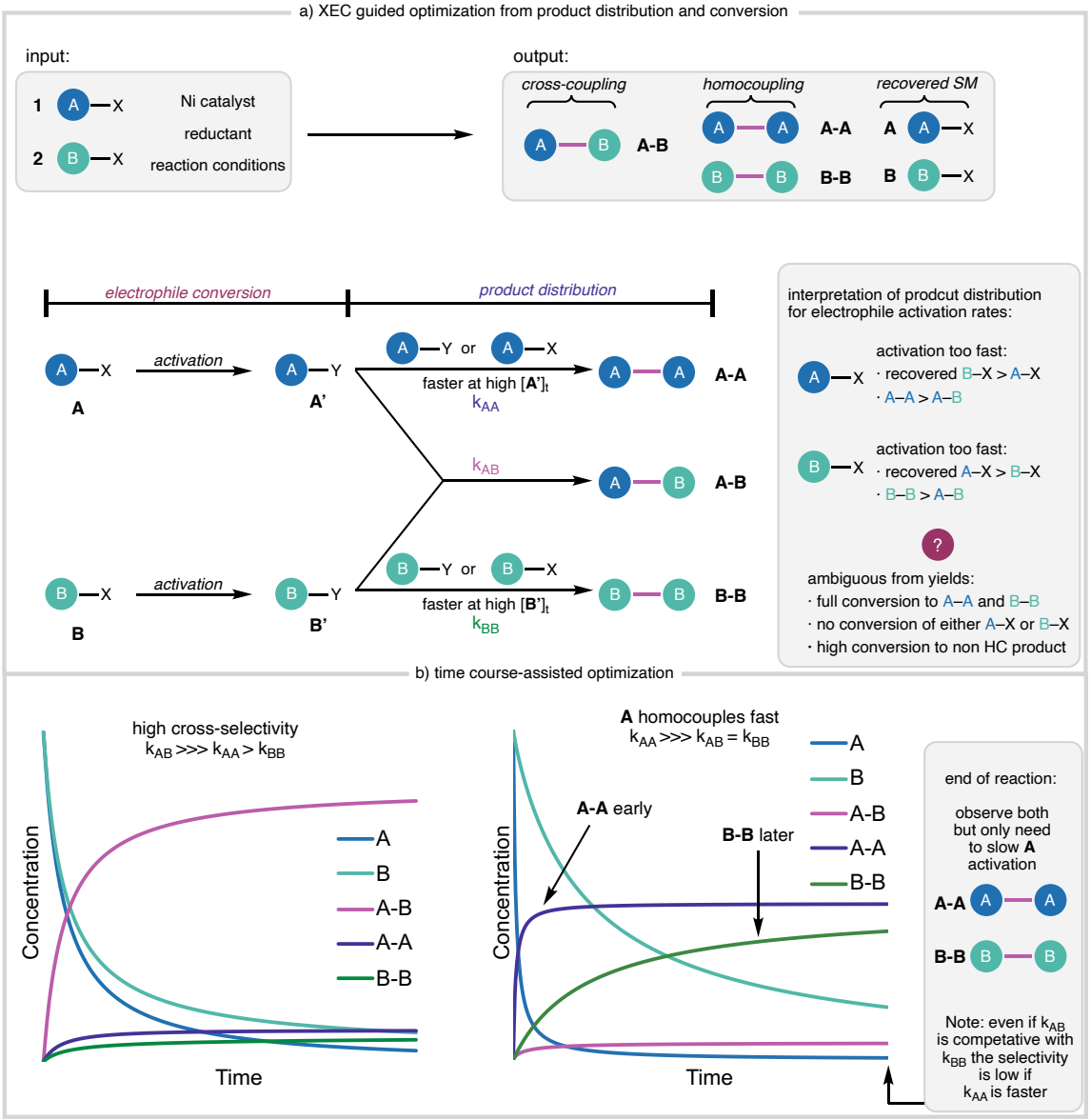

The output obtained from typical optimization by screening (i.e., the yield/ee/dr at the end of the reaction) may not be sufficiently representative of relative rates and obtaining temporal conversion data may be necessary. For example, if it is found that both electrophiles (**A** and **B**) convert to their corresponding homocoupled products (**A–A** and

B–B, respectively) at the end of the reaction then it is not clear which one is activated faster as one could be completely consumed before the other starts converting. This can be investigated by monitoring the electrophile conversion over time to gauge the relative activation rates. Reaction monitoring like this is certainly more resource intensive and may not be feasible for every set of conditions tested, but can be informative for calibrating optimization efforts and generating mechanistic hypotheses (Figure 1.7b).

1.2.4 General Strategies for Cross-Selective XEC Reactions

In this review we will attempt to formalize general classes of strategies that researchers have employed to achieve selectivity in Ni-catalyzed XEC reactions. Specifically, these methods utilize a mechanistic hypothesis regarding the rate of electrophile activation in order to increase yields of cross-coupled products. This notably does not include the well-established, and still frequently employed, strategy of using a large excess of one coupling partner to get high yields of cross-coupled product. This strategy is undoubtedly effective but typically results in concomitant formation of undesired homocoupled products, limiting the efficiency of these transformations. For this reason, *examples that use greater than 2-fold excess of one coupling partner are not considered successful examples of cross-selective XECs* in this review.

Given the explosion in XEC literature that has evolved after Weix initially formalized XEC optimization strategies in 2014,[5] the community's understanding of how these reactions work has grown with the field. The principles that dictate how a given combination of substrates may perform in an XEC still hold true but recent advances have given synthetic chemists more options to modulate substrate reactivity in order to improve

cross-selectivity. These strategies will be classified as: 1) electrophilic coupling-handle modifications, 2) Ni-catalyst or co-catalyst design, 3) reductant or external driving force control (Figure 1.8). Each of these methods uses a mechanistically-driven hypothesis to accelerate the rate of activation of one electrophile over the other. These strategies are attractive in that they are readily accessible within a traditional reaction optimization campaign and do not require expensive mechanistic studies or extensive ligand design.

Figure 1.8. *Summary of strategies for cross-selective XEC reactions.*

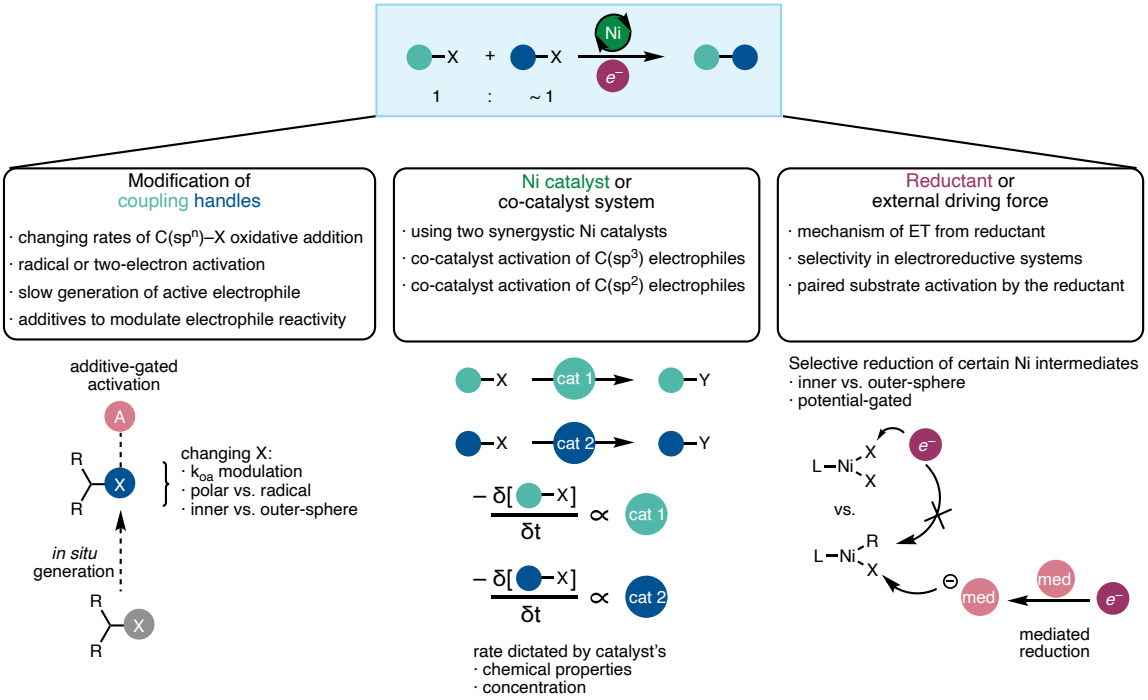

1.3 Tuning the Electrophilic Coupling Handle

The rate of electrophile (R–X) activation is dictated by the identity of the electrophile (X) as much as it is dictated by the inherent stereoelectronic properties of the substrate (R). As previously mentioned, the coupling handle can also influence particular mechanisms of oxidative addition by the Ni-catalyst from a concerted, two-electron process to a step-wise,

radical sequence (Figure 1.4). For a given combination of fragments in a cross-coupling, the reactivity of the electrophiles is directly modulated through the choice of coupling handles. Tuning the reactivity of the coupling handle is a complementary strategy to the later-discussed (Section 1.4) catalyst-based strategies, but obviates resource-intensive screening of catalysts which can be difficult to rationally design *a priori*. In these cases, selectivity is achieved through careful consideration of coupling partners that are synthetically accessible or can be generated *in situ* at a controlled rate.

1.3.1 Coupling Handle Modifications for Changing C(sp^2)–X Activation Rates

While there continues to be major advances in our understanding the mechanism of Ni-catalyzed XEC reactions, extensive studies on the relative rates of oxidative addition as a function of coupling handles across ligand-catalyst frameworks is limited. Kinetic studies using a bidentate phosphine Ni^0 catalyst (**L1**Ni(COD)) with various aryl electrophiles **42** have observed, in the case of aryl halides, that weaker Ar–X bonds undergo faster oxidative addition (I > Br > Cl >> F) via a concerted mechanism. Interestingly, sulfonates or esters were all slower than Ar-Cl following the trend Cl > OTs > CO_2R > OTf >> OMe (Figure 1.9a).[42] Studies on acyl **43** and alkenyl halides **44** have observed much faster reactivity over aryl substrates, although the quantitative rate was not determined for a more precise comparison (Figure 1.9b).[43]

Figure 1.9. *Highlighted mechanistic studies on aryl halide oxidative addition.*

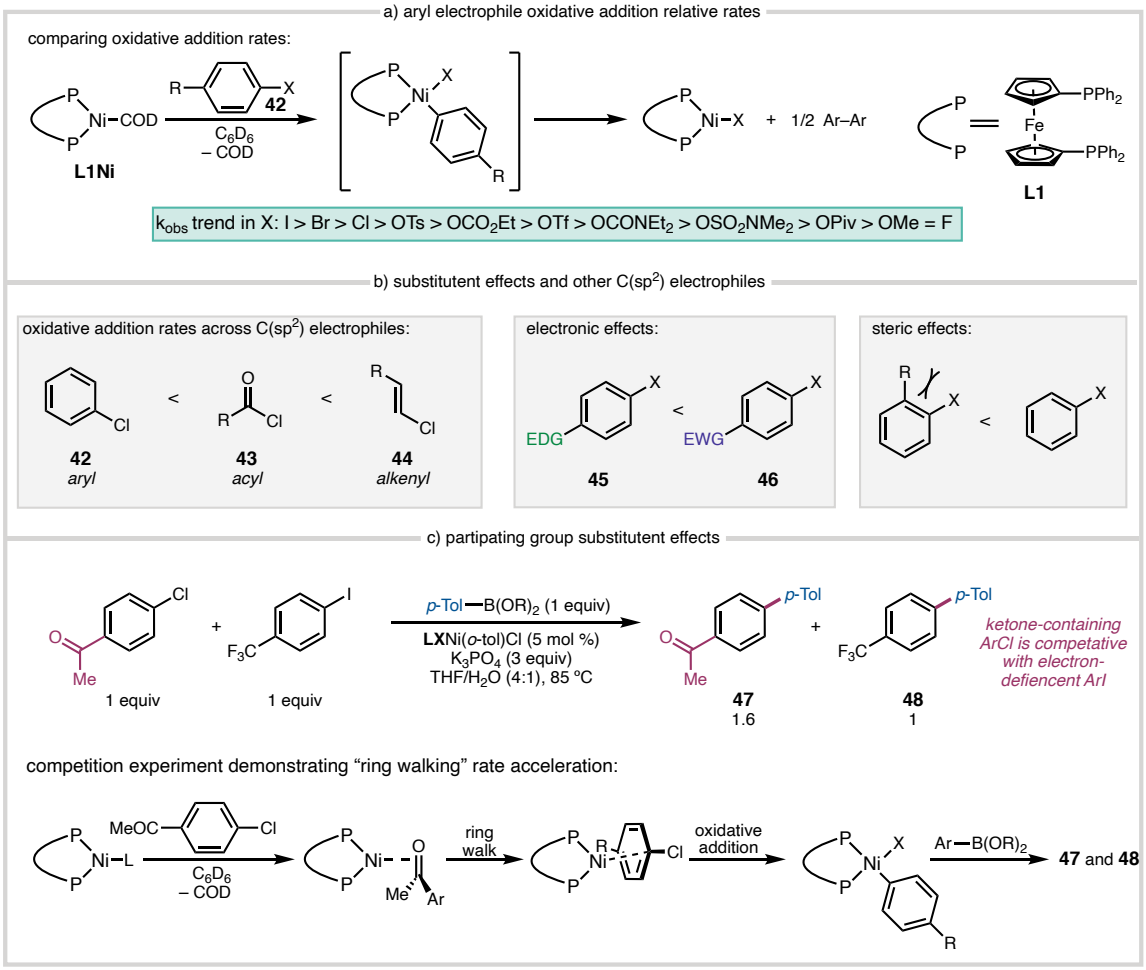

In addition to the coupling handle, it is important to consider stereoelectronic effects of the substrate itself. For example, electron-deficient aryl electrophiles **46** will undergo faster oxidative addition than the corresponding electron-rich substrates **45**.[15,16,42] Sterics also play an important role where a more hindered C–X bond will undergo slower oxidative addition,[42] however the resulting oxidative addition complexes display greater kinetic stability towards homocoupling (Figure 1.9b).[**Error! Bookmark not defined.**,27] There are also significant substituent effects that can impact the reactivity that are well understood to the

point where the regioselectivity of polyhalogenated (hetero)arenes oxidative addition can be reliably predicted.[44,45] Additionally, substituents that can assist in the binding or association of the Ni catalyst with the C(sp^2) electrophile can also effect a profound rate increase (Figure 1.9c).[43]

Scheme 1.3. *Selective C(sp^2)-C(sp^2) cross-couplings.*

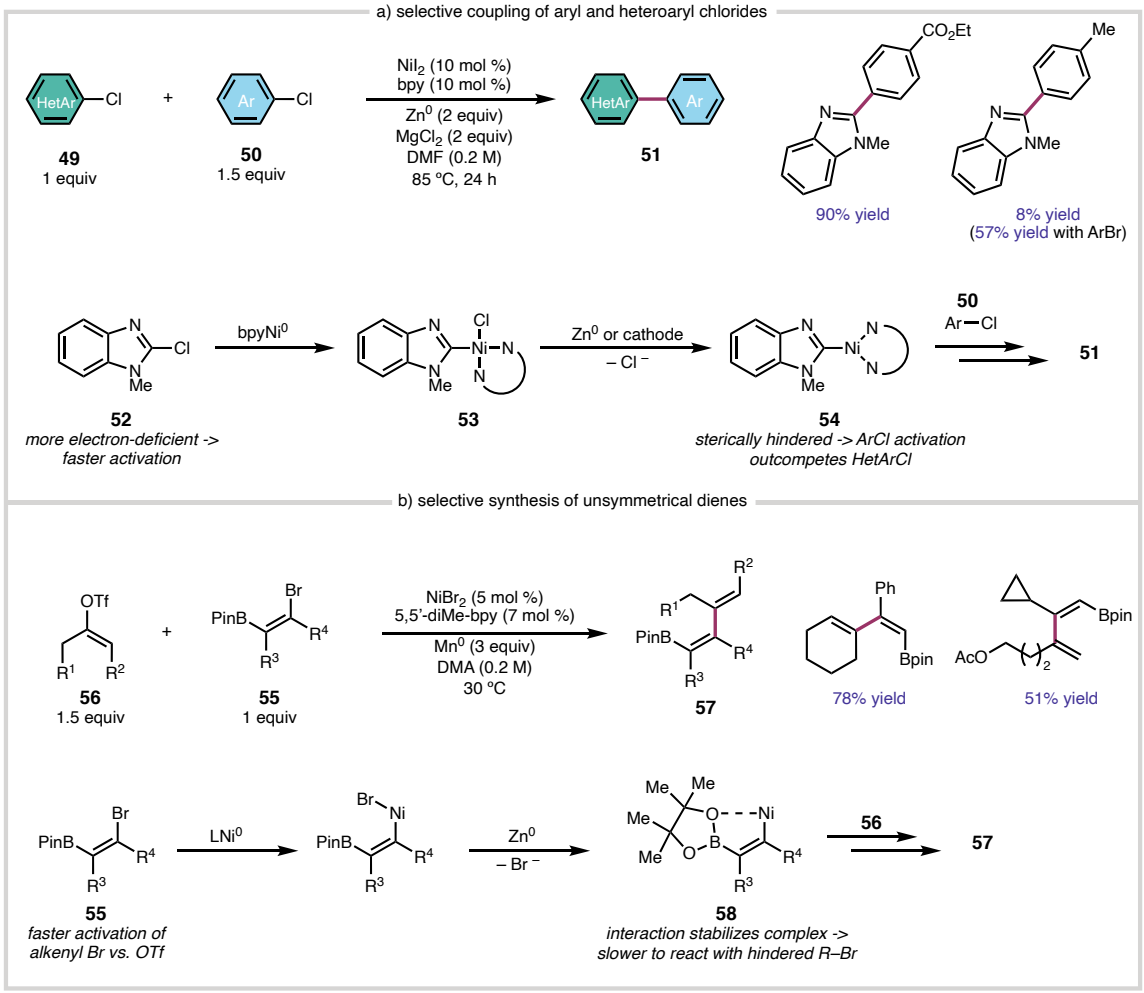

Out of these guiding principles, selective XEC reactions of aryl halides have been developed with remarkable cross-selectivity. In a report from Lautens and coworkers, the XEC of aryl chlorides **50** and heteroaryl chlorides **49** was achieved with a 1.5:1

stoichiometry. This sequential activation mechanism leverages the fast oxidative addition into 2-chlorobenzimidazoles **52** as well as the slow homocoupling of the oxidative addition complex **54** due to the electron-deficient nature of the C bound to Ni and the steric environment. For less reactive aryl chlorides they demonstrate that the cross-selectivity can be recovered by moving to the more reactive Br coupling handle.[46] This has also been leveraged in an electroreductive biaryl synthesis from heteroaryl chlorides and aryl bromides. Notably, the high cross-selectivity here is also attributed to the faster reduction of the electron-deficient Ni^{II} complex **53** to give Ni^{I}–heteroaryl **54**. This complex is hindered and reactive enough to activate the electron-rich aryl bromide, outcompeting deleterious homocoupling processes (Scheme 1.3a).[47]

The corresponding strategy can be used for the cross-coupling of alkenyl (pseudo)halides to make unsymmetrical dienes. Important considerations with alkenyl electrophiles are that 1) oxidative addition is faster,[43] and 2) Ni insertion to C(sp^2)-X bonds is more readily reversible for alkenyl halides compared to that of aryl halides.**Error! Bookmark not defined.** This means in systems with multiple halides, scrambling of the alkenyl halide can occur, thus accumulating the thermodynamic C–X species.[48] In an example from Shu and coworkers, the more reactive bromide coupling handle was used on the more sterically hindered boron-substituted alkenyl electrophile **55** and the triflate handles were used on the more reactive alkenyl electrophile **56** to achieve impressive cross-selectivity. Evidence supports the interaction of the Bpin group with the adjacent Ni-center **58** which occupies a coordination site to stabilize the intermediate towards homocoupling (Scheme 1.3b).[49]

1.3.2 Coupling Handle Modifications for Changing C(sp^3)–X Activation Rates

Analogous principles from C(sp^2)–X modifications can be applied to tune the reactivity of C(sp^3) electrophiles. However, there are additional considerations with C(sp^3) substrates because activation via an organic radical intermediate can occur depending on the substrate, coupling handle, and the catalyst. For C(sp^3) halides, the rate of activation generally follows trends according to C–X bond strength (I > Br > Cl).[50] In the cases where oxygen electrophiles are employed or when ligands that favor 2-electron pathways are used, the relative reactivity is dependent on the stability of the displaced coupling handle, similar to leaving group stability trends in organic S_N2-type reactions.[51]

There are many examples where modifications of the C(sp^3) electrophile's coupling handle improves cross-selectivity when the activation rate of the other substrate is vastly different than what the system was optimized for. A informative case study of this in practice from Baran and coworkers is the Ni-catalyzed XEC of *in situ* generated anhydrides **60** (from the corresponding carboxylic acid **59**) with NHP esters **61** to make ketone products **62**. This reaction is uniquely modular given both electrophiles are derived from carboxylic acids meaning either coupling fragment can be employed as the C(sp^2) electrophile (**59**) or the C(sp^3) electrophile (**61**) if it is pre-functionalized as the NHP ester to access the same product. The authors report a reactivity guide for how different alkyl electrophiles perform as either the "acyl electrophile" **60** or the "radical electrophile" **63** across different substrate classes which reflects the combinations that are activated at similar rates (Figure 1.10a).[52]

Figure 1.10. *Examples of changing C(sp^3) coupling handle for different C(sp^2) electrophiles.*

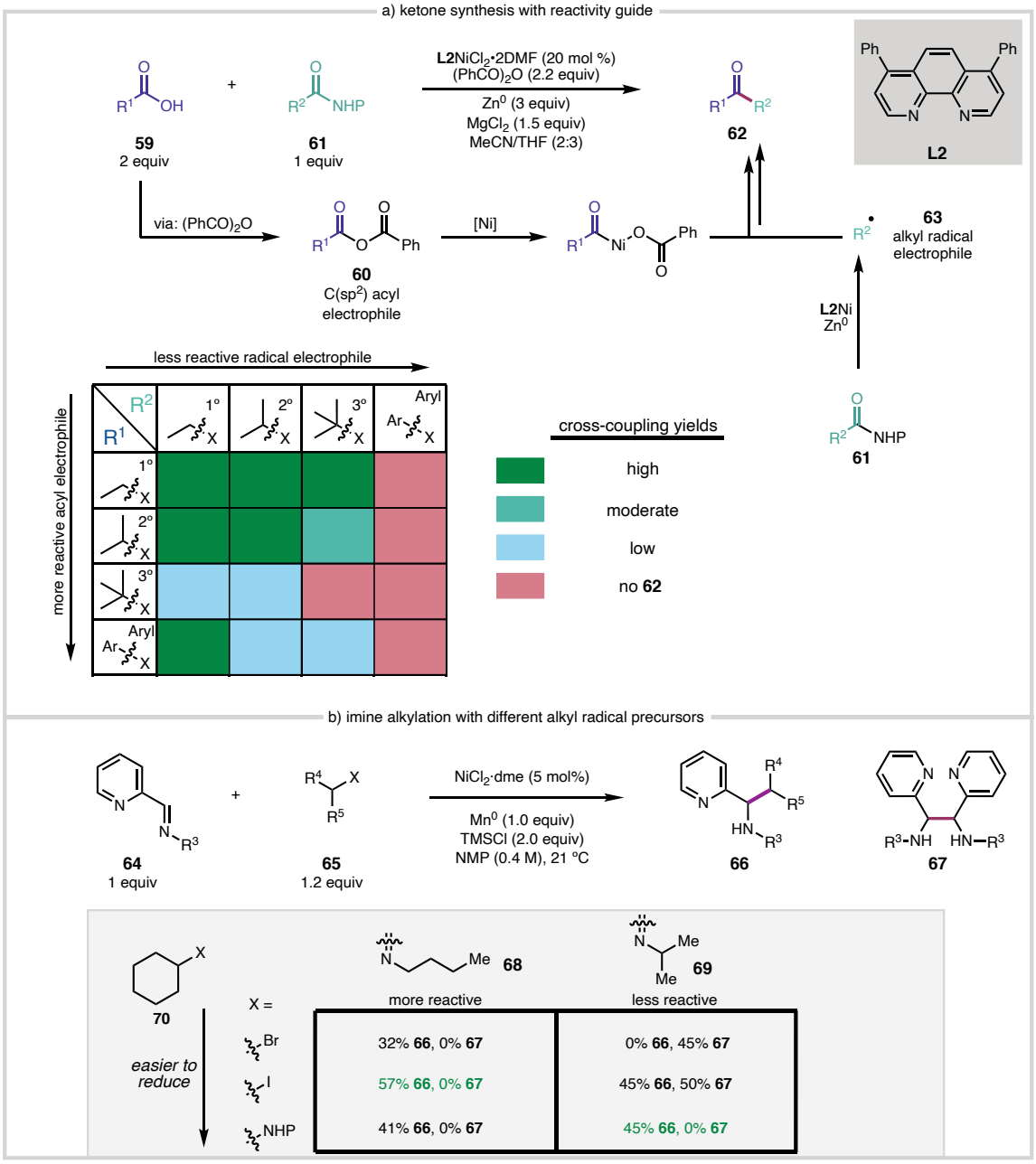

Another case study can be seen in the XEC of redox-active imines **64** and alkyl electrophiles **65** to give benzyl amine products **66** from Reisman and coworkers. In this

reductive alkylation reaction, more hindered *N*-alkyl imine **69** produced significant quantities of homocoupled diamine **67** with 2º alkyl electrophiles (**70**), while the less hindered *N*-alkyl imine **68** exclusively produced the desired cross-coupled product **66**. It was found that by using alkyl radical precursors that were easier to reduce than alkyl bromides or iodides (E^{red} = –2.06 V vs. SCE for **70** X = I),[53] like NHP esters (E^{red} = –1.4 V vs. SCE),[54] cross-coupling could then outcompete deleterious homocoupling for the more challenging sterically-hindered imines (Figure 1.10b).[55]

Scheme 1.4. *Controlled in situ generation of alkyl halide electrophile.*

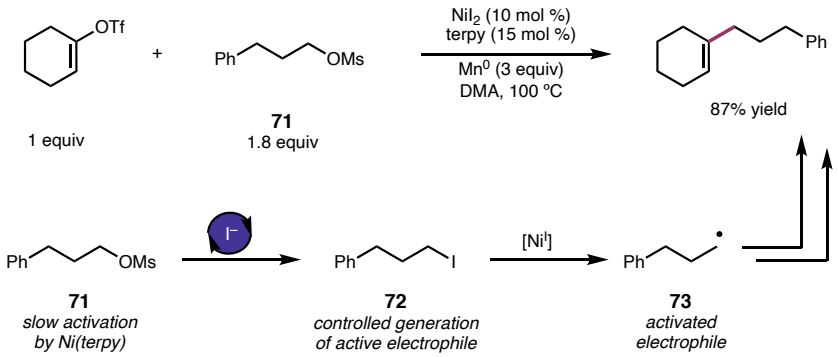

deviation from standard	*yield*
$NiCl_2$	< 5%
$NiBr_2$	15%
$NiBr_2$ + NaI	63%
72 instead of **71**	35%
slow addition **72**	63%

Another approach is to keep the concentration of the active electrophile low by generating it *in situ* from a less reactive precursor. While this strategy is not limited to *reductive* Ni-catalysis,[56,57] it has been used both intentionally to improve selectivity or uncovered as an operative mechanism afterwards. Alkyl tosylates[58] or mesylates **71** have been used as precursor electrophiles to generate alkyl halides from the addition of a catalytic halide salt or from the halide counter ions on the Ni precatalyst. Here, the tridentate Ni catalyst is slow at alkyl mesylate **71** activation via a polar mechanism but can rapidly react with 1º alkyl iodides **72** via a radical mechanism to give a radical intermediate **73**. This allows for control of the concentration of the active electrophile by changing the

halide additive concentration enabling higher yields of cross-coupled products compared to using the alkyl iodide (**72**) as a coupling partner directly (Scheme 1.4).[59] This has also been used to convert relatively unreactive halide precursors to more reactive halide electrophiles. Weix and coworkers utilized this halide exchange in the cross-coupling of challenging aryl chlorides with alkyl chlorides employing catalytic iodide to generate low concentrations of alkyl iodide *in situ* from the alkyl chloride.[60]

Figure 1.11. *Regioselective activation of strained heterocycles with additives.*

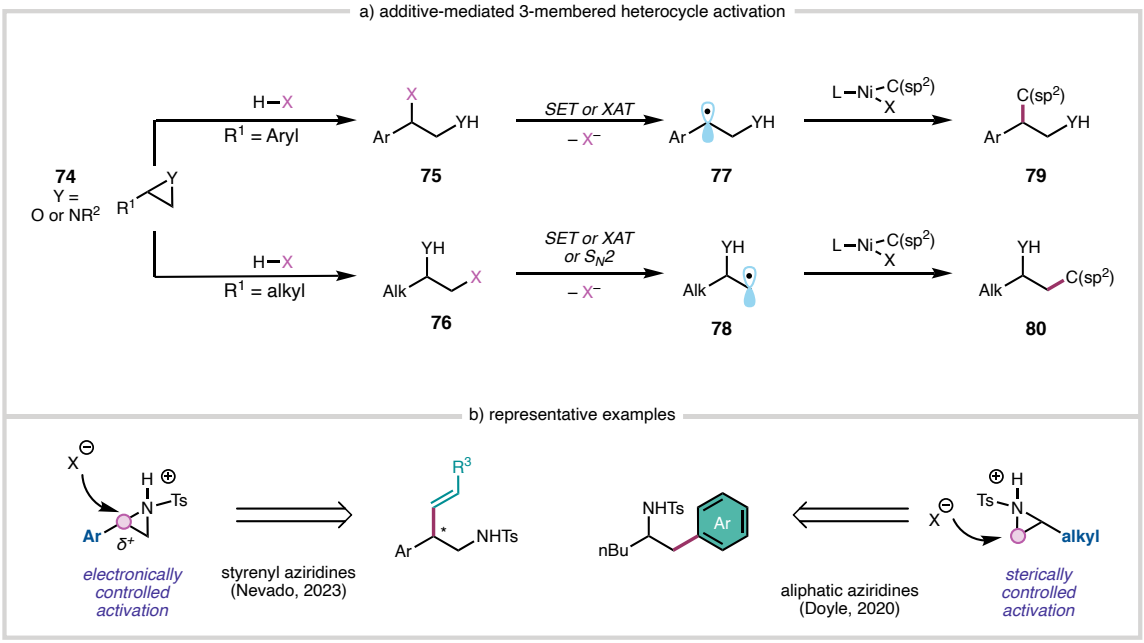

Strained heterocycles, like azirines and epoxides **74**, have been used extensively as C(sp^3) electrophiles. These substrates can be directly activated by the Ni-catalysts via oxidative addition,[616263] or they can undergo C–O/N bond activation through other mechanisms for a controlled release of the activated species. Redox-active co-catalyst systems will be addressed later (see section 1.4.2), but halide additives have also been used to generate reactive bromo/iodohydrin intermediates (**75** or **76**) that proceed through

radical intermediates (**77** or **78**) like other alkyl halides (Figure 1.11a).

The Doyle group has leveraged this to achieve selective coupling to give arylated products at either the more substituted position, if benzylic, or less substituted position if aliphatic.[64] This has also been used by Nevado and coworkers in an electroreductive alkenylation of aziridines. In this transformation, anodically-generated acid mediates the formation of β-amino halide from the aziridine (**75**, Y = NTs) as the active electrophile.[65] The regioselectivity here in these cases is dictated by the substitution of the heterocycle towards nucleophilic substitution where resonance stabilizing groups can direct addition to the more substituted position otherwise the more sterically accessible position is preferred. These examples exhibit great regioselectivity along with improved cross-selectivity over using the less stable β-halo amines of halohydrins directly (Figure 1.11b).

Coupling handle-based rate-tuning has also been achieved by derivatizing or modifying a parent coupling handle. The Baran lab has popularized the use of redox-active radical precursors, like NHP esters or Barton esters, in Ni-catalyzed XEC reactions. They have used both the parent NHP ester as well as more reactive derivatives for a myriad of Ni-catalyzed reactions, albiet in fairly unselective processes requiring >3 equivs of one component in some cases.[66] Recently, the Weix group has used these derivatives **81** to rationally optimize a selective cross-couplings with aryl iodides **82**. For less reactive aryl iodides they observed improved yields when more electron-rich (harder-to-reduce) NHP ester derivatives were employed. They could also extend the scope to include aryl bromides when electron-rich NHP ester derivatives are used (Figure 1.12a).[67]

Figure 1.12. *Methods of controlling rate of NHP ester activation.*

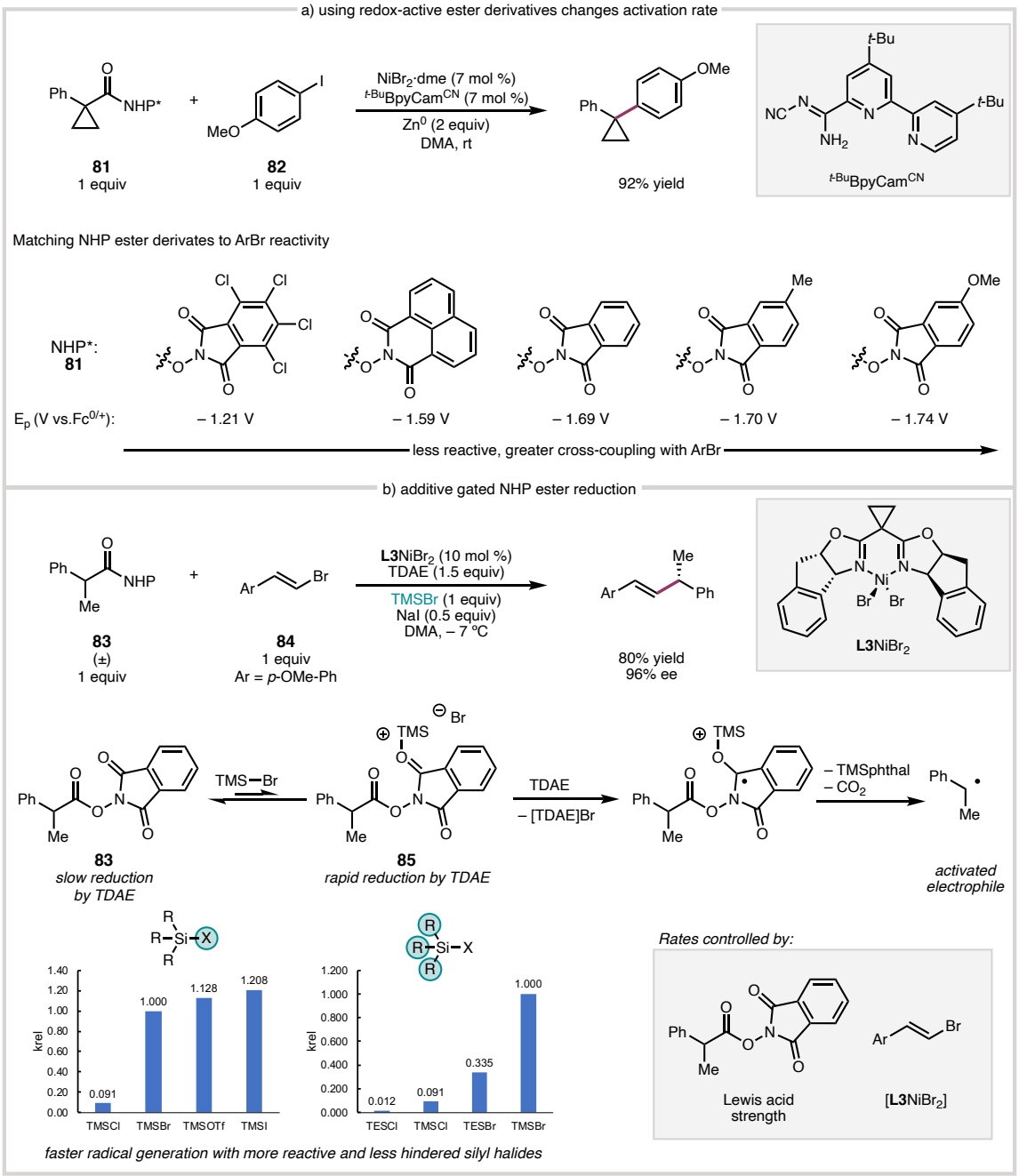

A conceptually related strategy from Reisman and coworkers uses Lewis acid additives to gate the reduction of NHP esters. In this specific system, it was determined that the NHP ester electrophile **X** was not activated by the Ni catalyst **X** but instead by the terminal

reductant, *N,N'*-tetrakis(dimethylamino)ethane (TDAE), in the reported asymmetric XEC of alkenyl bromides **84** with NHP esters **83**.[68] It was found that the TMSBr additive facilitates NHP ester activation by acting as a Lewis acid to give a species **85** that is easier to reduce such that SET from TDAE is kinetically competent. The rate of reduction can then be modulated by changing the Lewis acid where less hindered acids and better leaving groups led to faster radical generation (Figure 1.12b). This could then be used to lower the catalyst loading to 1 mol % of the chiral catalyst to achieve highly cross-selective coupling when a less reactive Lewis acid was used.[69] Similar Lewis acid effects with NHP esters have been observed in other XECs that employ metal powder reductants.[70]

Scheme 1.5. *Additive-gated activation of aldehyde electrophiles*

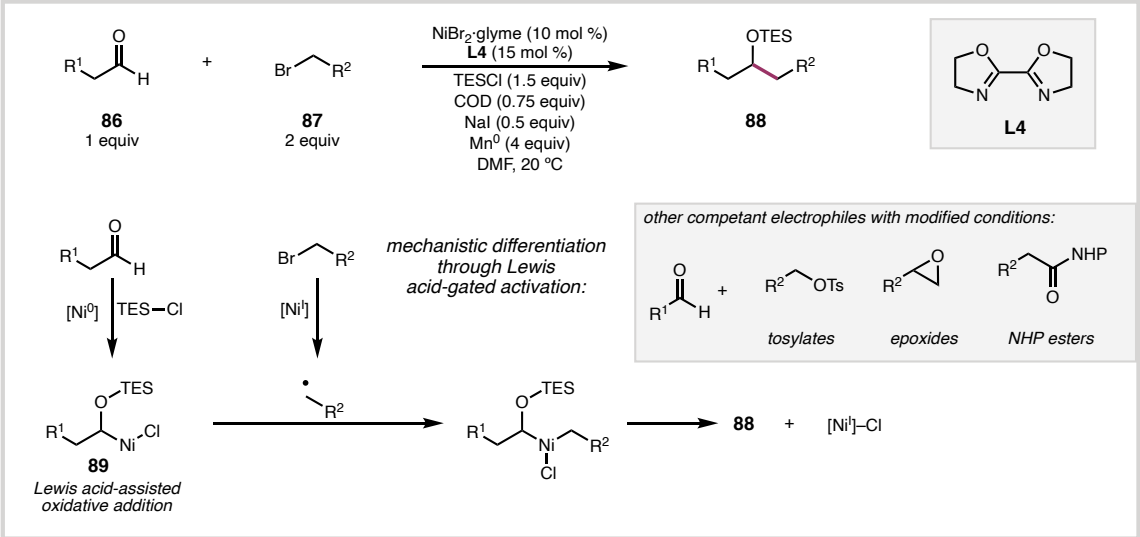

Lewis acids have also been used to activate aldehyde electrophiles for Ni-catalyzed XEC. The Montgomery group has published several XEC couplings of aliphatic aldehydes **86** and alkyl electrophiles **87** to synthesize 2º silyl ether products **88**. These reactions are proposed to proceed through α-oxy-Ni species **89** mediated by the halosilane additive.

Accessing these products from a direct alkyl-alkyl coupling would be quite challenging due to the matched hybridization of the electrophiles,[71] but by activating the aldehyde *in situ* to generate the alkyl–Ni intermediate **89** through an orthogonal mechanism to other pathways to access an alkyl–Ni.[72] Silyl halides have also been used to trigger the generation of oxonium ions from the corresponding dialkyl acetals in Ni-catalyzed XEC to access similar products.[73] In related mechanistic studies, it was found the efficiency of this reaction is sensitive to the sterics of the halosilane, suggesting that the rate of acetal activation could also be tuned by the Lewis acid additive (Scheme 1.5).[74]

1.4 Modulating Electrophile Activation Rates with Ni Catalysts and Co-Catalyst

A conceptually distinct strategy from the aforementioned substrate control-based approaches is to achieve selective reactions through catalyst-control. While there are many examples of Ni catalysts that alone can activate each electrophile in a mechanistically distinct way, this reactivity is challenging to predict as changes to the catalyst can impact the rate of activation for both electrophiles. Instead of relying on one Ni catalyst to activate both substrates, it can be enabling to employ a co-catalyst system where a Ni catalyst activates one electrophile and a different catalyst activates the other. The added complexity of optimizing two catalyst systems is offset by the ability to tune the activation rate of each electrophile independently. This is achieved by changing the chemical properties of the catalysts or their relative concentration to modulate the rate of one electrophile conversion to match the other.

1.4.1 Dual Ni Catalyst Systems

The use of two Ni-catalysts in XEC reactions has proven to be a powerful technique for achieving high levels of cross-selectivity. This is typically done by using two ligands whose sum is approximately equal to the amount of nickel precatalyst that is added. In this case one ligand forms a catalyst that is optimal for the activation of one substrate and is slow to react with the other electrophile and vice versa. The substrate activation rates are then tuned by changing the relative ligand ratio and thus the concentration of each active catalyst in solution. Considerations about the speciation, equilibrium binding to Ni, and reduction potentials of each catalyst must be taken into account when designing these systems.

Scheme 1.6. *Dual Ni-catalysis with bidentate phosphine and nitrogen catalysts.*

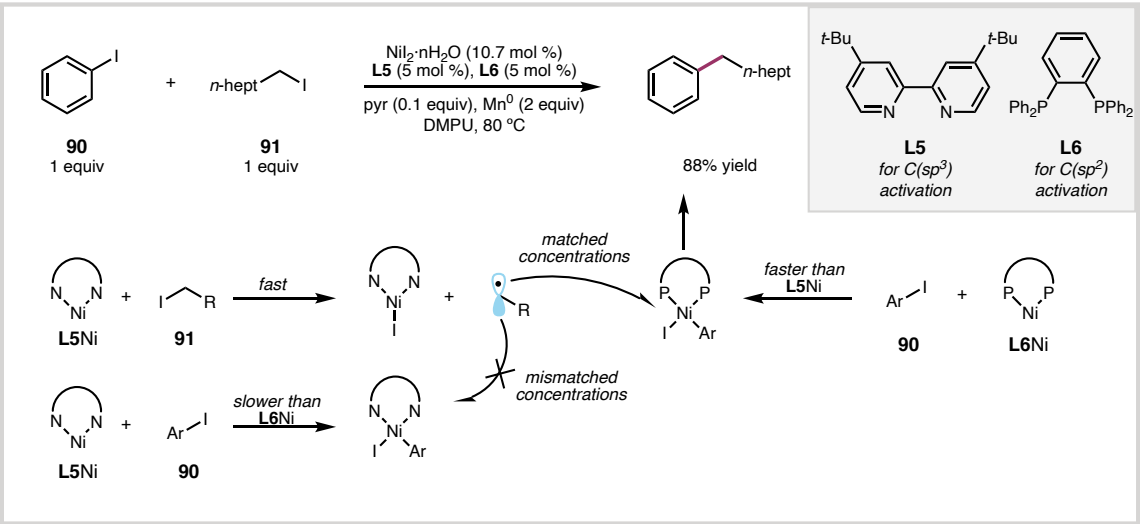

This strategy was used by Weix and coworkers in 2010 for the coupling of alkyl iodides **91** and aryl iodides **90**. In this report, a combination of a bidentate phosphine ligand **L6** and a bidentate pyridine ligand **L5** in a 1:1 ratio with ~2 equiv of Ni^{II} precatalyst. Here,

good selectivity is only seen when both ligands are employed and if one is omitted, significant quantities of homocoupled product is observed. The observed homocoupling trends suggests that the bidentate phosphine-ligated **L6**Ni catalyst is well-suited to activate the aryl electrophile **90** via a 2-electron oxidative addition,[43] while the **L5**Ni complex preferentially reacts with the alkyl halide electrophile **91** via a radical mechanism. For particularly activated aryl iodides, it was found the phosphine ligand can be omitted, as oxidative addition with the **L5**Ni ligand is fast enough to match activation of **91** (Scheme 1.6).[75,76]

This strategy was used by Kishi and coworkers in a method for the coupling of alkyl iodides **92** with thiopyridine esters **93** to make ketone products **94**. Here, they observe that the activation of the acyl electrophile **93** was fast with bidentate Ni complex **L8**Ni and alkyl halide **92** activation was slow. Conversely, a tridentate Ni^{I} complex **L7**Ni[29] was found to rapidly react with the alkyl halide **92** and was relatively inert towards thioester **93** activation. By using these independently prepared catalysts in a 1:1 ratio efficient cross-coupling was achieved with 1:1 electrophile equivalency and catalyst loadings as low as 1 mol % (Scheme 1.7a). Once optimized, this was applied in a convergent fragment coupling towards the synthesis of Halichondrin B, using significantly more complex substrates **96** and **97**. By modifying the conditions for these substrates to a 4:1 ratio of **L8**Ni: **L7**Ni the complex ketone product **98** was obtained in 80% yield on 100 mg scale (Scheme 1.7b).[77]

Scheme 1.7. *Dual Ni-catalyzed XEC with application to complex molecule synthesis.*

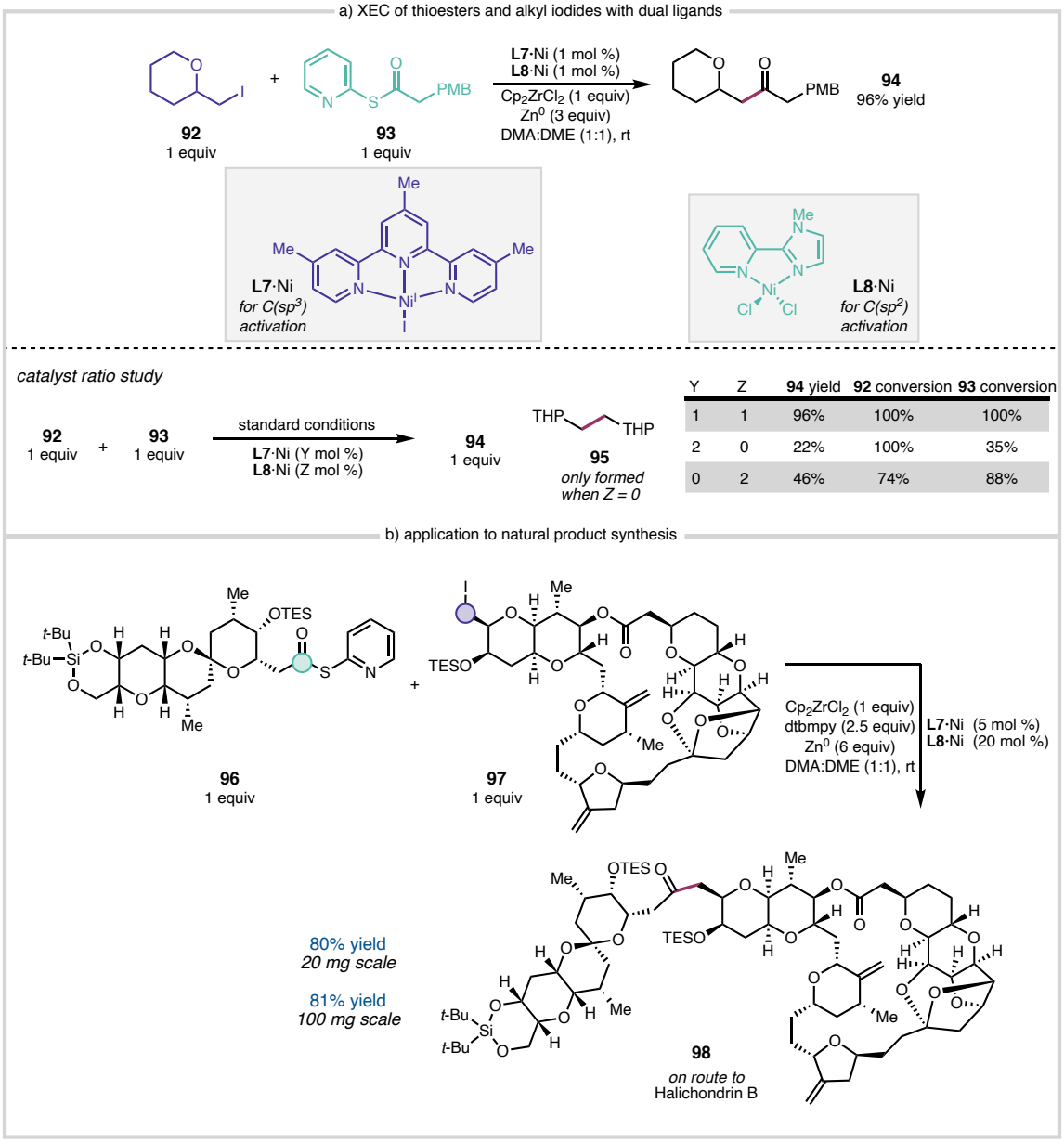

Dual Ni catalysts has also found use in selective electroreductive XEC reactions. This was first done in a collaborative study from between the Weix group and the Pfizer process team in a reductive coupling of 1° alkyl bromides **99** and aryl bromides **100**. This reaction utilized a divided cell under constant current electrolysis (CCE) as a means to drive the

reaction in their dual catalytic system. Selective coupling was achieved by using a combination of tridentate **L9** and bidentate **L5** ligands with varied stoichiometric ratios of **L9**:**L5** based on the substrate combination. The reaction could also be extended to more reactive 2° alkyl bromides **101** by increasing the relative amount of **L5** (Scheme 1.8a).[78] A follow-up study from the Weix group achieved the same transformation in an undivided cell and highlights how the selectivity changes as a function of **L9**:**L5** for several substrates. This provides a roadmap for how to extend this methodology to new substrates that are not included in the scope by performing a small screen varying 0 – 100% **L9**:**L5** to identify the ideal ligand ratio (Scheme 1.8b).[79]

Another example of dual Ni catalysts in electrochemical XEC comes from Sevov and coworkers. This mechanistically-guided study identified the optimal combination of ligands to be bidentate P,N ligand **L11** and tridentate **L10**$NiBr_2$, for the coupling of aryl (pseudo)halides (**102**, X = Cl, Br, OTf) with 3° alkyl bromides (**103**). The design principle here is based on the observations that **L10**NiX_2 is readily reduced at the cathode (–1.4 V vs. $Fc^{0/+}$, 0.1 M KPF_6 in DMF) to give a **L10**Ni^I complex (**104**) that can readily react with **103** to give radical **105**. This is in contrast to **L11**NiX_2 which is difficult to reduce (no cathodic wave in solvent window), but the (**L11**)$_2Ni^0$ complex rapidly reacts with **102** and slowly reacts with **103**. Spectroelectrochemical experiments reveal that ligand exchange is possible following reduction of **L10**NiX_2 resulting in the formation of (**L11**)$_2Ni^0$ when **L11** is present in solution. Additionally, they show that following oxidation addition of (**L11**)$_2Ni^0$ to **102**, the resulting complex (**106**) can undergo another ligand exchange with **L10** to give **107** which is competent at capturing the hindered radical **105** to give product

108 (Figure 1.13). This leverages the dual ligand strategy to not only influence the relative concentration active catalyst in solution, but also the accessible oxidation states of Ni where Ni^0 and Ni^I have can have different rates and mechanisms of oxidative addition.[80]

Scheme.1.8. *Dual Ni-catalyzed electroreductive coupling.*

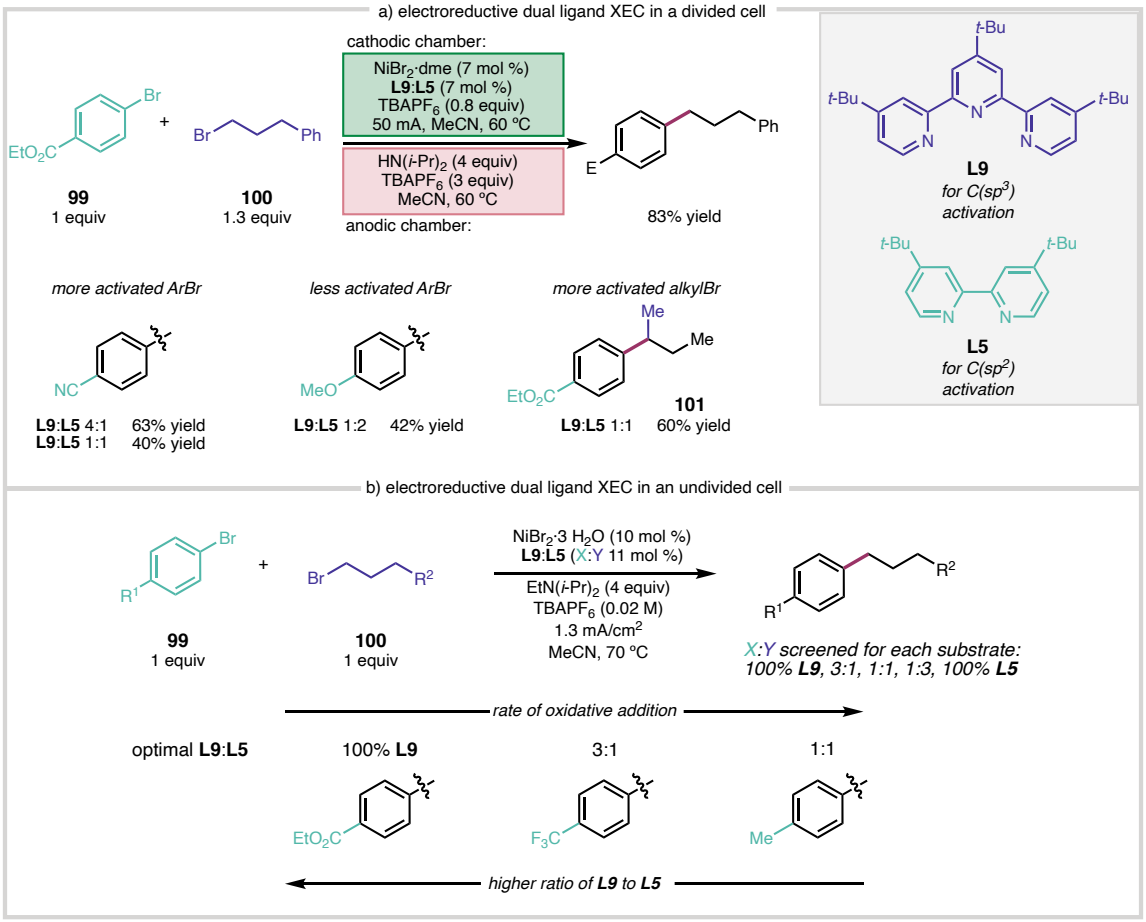

Figure 1.13. *Dynamic ligand exchange for dual catalytic sequential activation.*

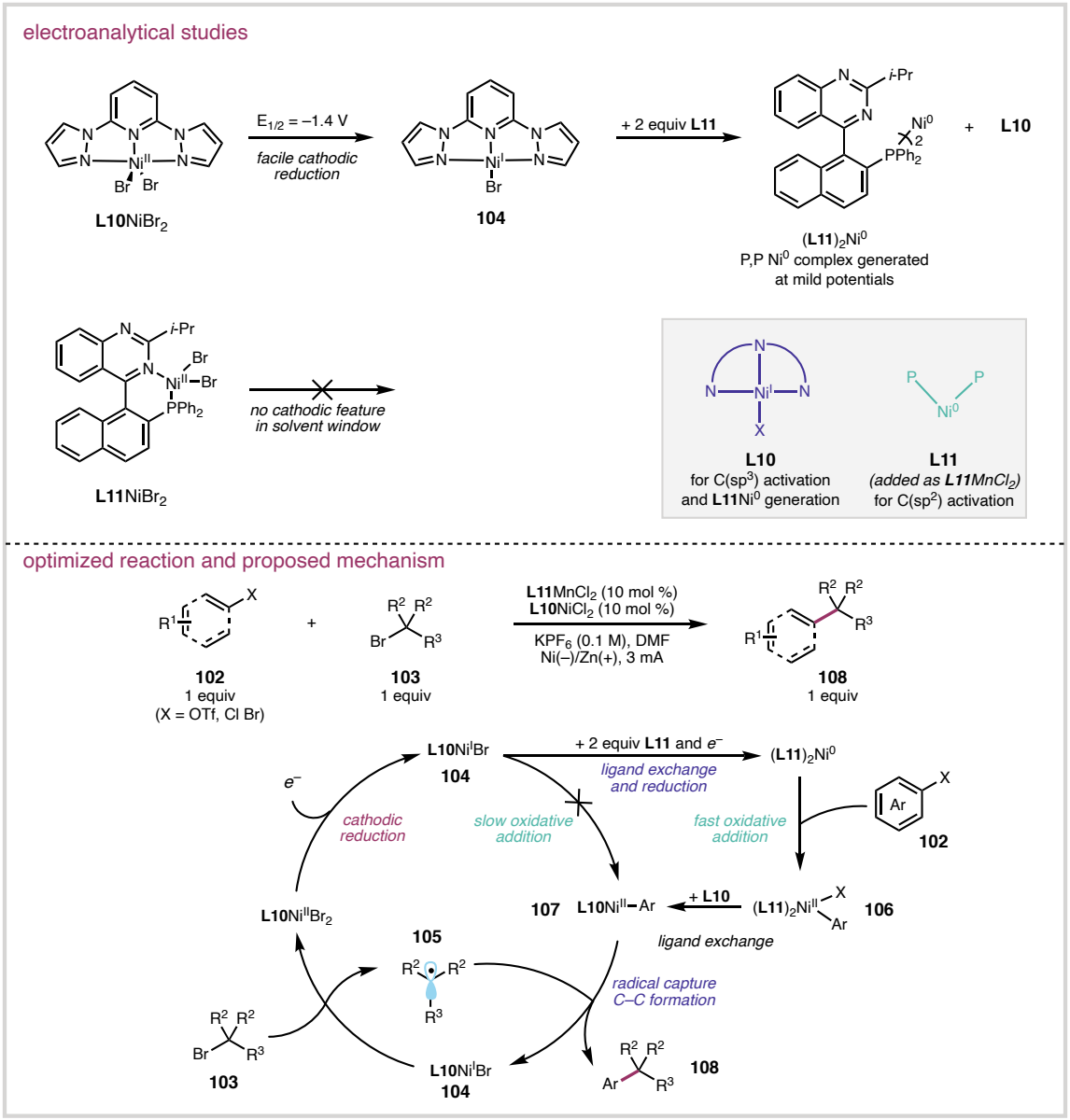

1.4.2 Transition Metal Co-Catalysts for C(sp³)–X Activation

Beyond dual Ni catalysis, other transition metals capable of oxidative addition to activate substrates have also been used as co-catalysts for Ni-catalyzed XEC. Perhaps the most popular is the use of cobalt catalysts to activate C(sp^3)–X electrophiles through

orthogonal mechanisms invoked for Ni. Specifically, nucleophilic square planar Co^{I} complexes **109** will rapidly react with alkyl electrophiles **110** to give an alkyl–Co^{III} **111** via an S_N2 reaction. Reduction or photolysis of **111** triggers Co–C homolysis thus releasing an alkyl radical that can be captured by a Ni catalyst (Figure 1.14).[81] This is complementary to Ni catalysis because it proceeds though an overall distinct mechanism to generate alkyl radicals and, unlike Ni, they are slow to react with C(sp^2)–X electrophiles.[25,26,27,28] This allows for more precise control of alkyl radical generation by making changes to the ligand on Co as well as the Co catalyst loading.

Figure 1.14. *Mechanism of alkyl radical generation with square-planar Co^{I} catalysts.*

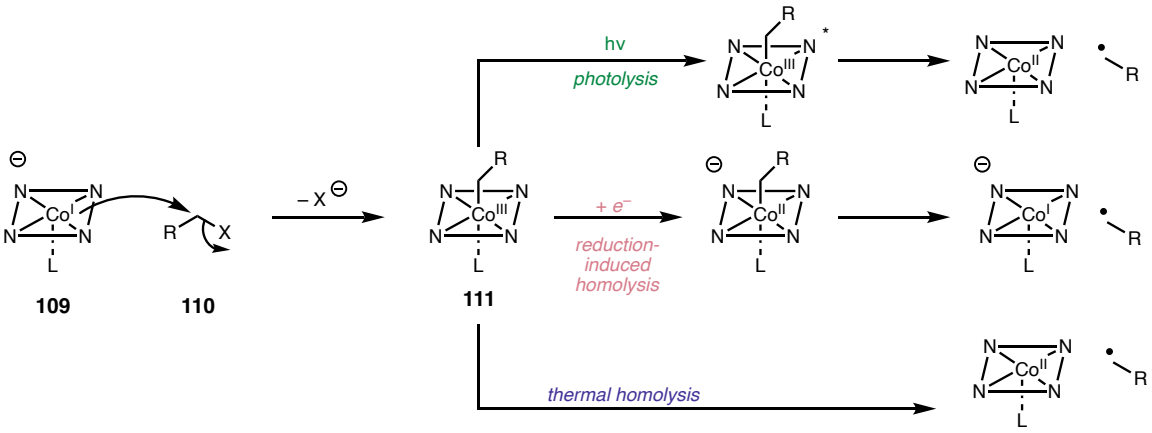

This strategy was first used in Ni-catalyzed XEC by Weix coworkers for the coupling of benzyl electrophiles **112** (X = OMs **112**, $O_2P(OEt)_2$ **113**) with aryl halides **114** (X = Br or I). Activation of 1° benzyl halides with reduced **L5**Ni (**117**) is much faster than activation of the aryl halide **114** coupling partner to such a degree that selective cross-coupling is challenging and would require extensive ligand optimization. The reaction of reduced Ni complex **117** with the corresponding benzyl mesylate **112** is much slower and provides some cross-coupled product **115** with reactive coupling partners, like aryl iodides.

They observed greater control over the rate of benzyl radical (**118**) formation when CoPc was used as the mesylate **112** activator in a 7:1 ratio of **L5**Ni:CoPc to successfully suppress formation of **116** and favor product **115**. For less reactive benzyl electrophiles like **113**, the concentration of CoPc had to be increased to compensate for the slower benzyl electrophile activation where ~1:1 Co:Ni was found to be optimal (Scheme 1.9).[82]

Scheme 1.9. *Dual Ni/Co arylation of benzyl electrophiles.*

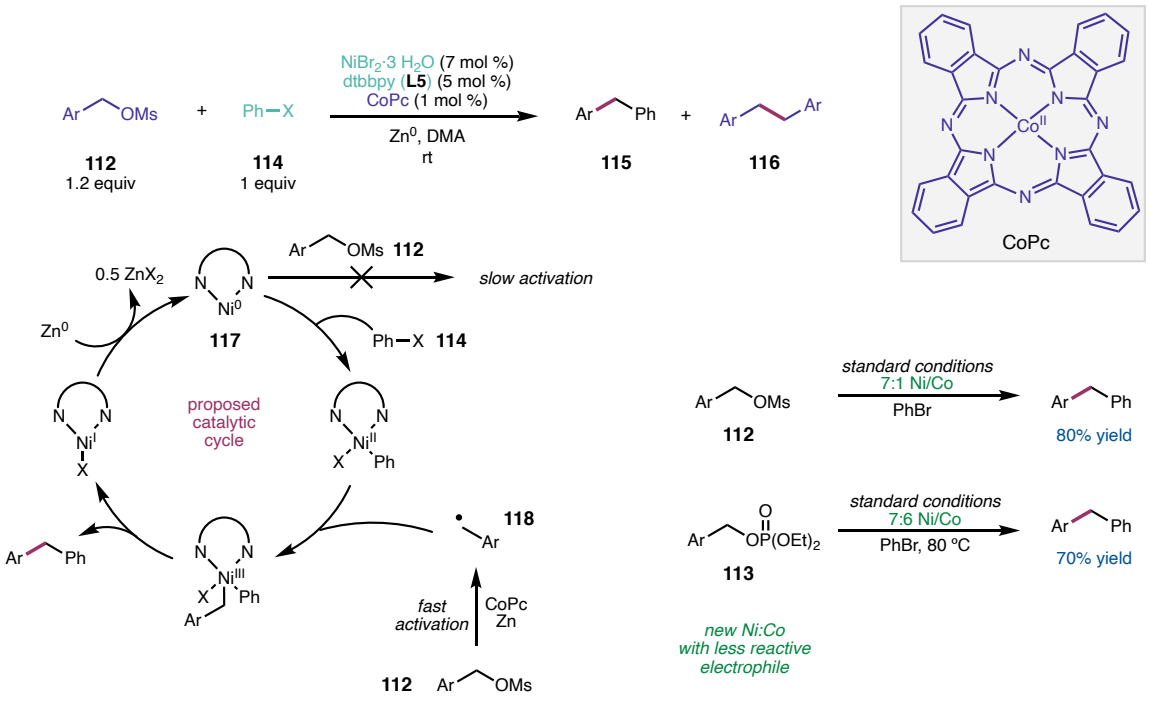

In a related system reported by Hazari and coworkers, CoPc was used to facilitate the coupling of various alkyl electrophiles **119** with aryl and alkenyl halides **120** employing a TDAE as a reductant. Here, they show how adjusting the ratio of Ni:Co can enable cross-coupling of fragments to accommodate diverse coupling handles, electronics, and steric properties (Scheme 1.10a). They also show how this could be used for a 3-component alkylation of dihalogenated aryl substrates **121** containing an iodo and bromo coupling

handle. In this system, alkylation first occurs at the C_{Ar}–I position with the more activated alkyl electrophile **122** then at the C_{Ar}–Br position with a less activated alkyl halide substrate **123**. This can be achieved in one pot with fine tuning of the catalyst concentrations or by supplementing the reaction after the first cross-coupling is complete with additional catalyst to change the ratio so that it is optimal for the second coupling (Scheme 1.10b).[83]

Scheme 1.10. *Varying catalyst ratios for different substrates in Ni/Co catalyzed XEC.*

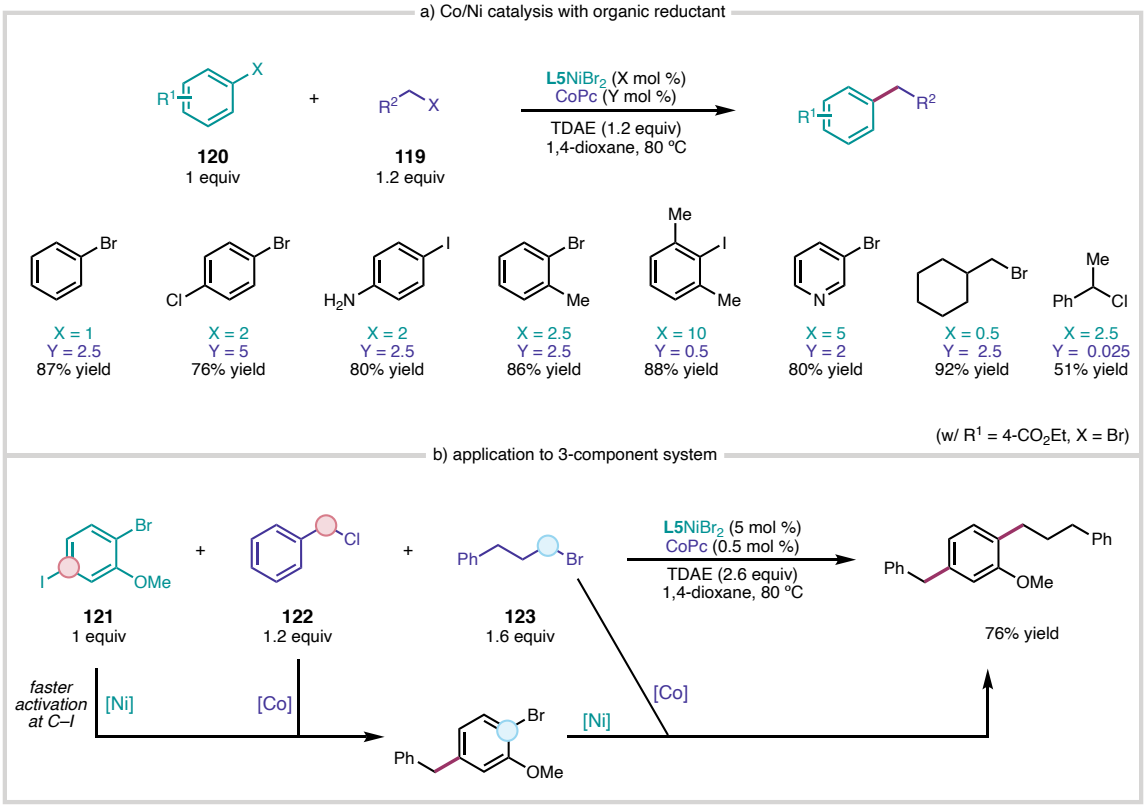

The ligand environment on the Co catalyst can also be used to modulate the reactivity in order to achieve high levels of selectivity. In the coupling of aryl iodides with epoxides **124** developed by Gryko, Giedyk, and coworkers, the regioselective epoxide opening was achieved with cyanocobalamin (Vitamin B_{12}), a square planar Co complex, as a cocatalyst. Notably, the opposite regioselectivity is observed in this system for styrenyl epoxides

compared to other epoxide couplings (Figure 1.11) that proceed through the more stable benzyl radical intermediate **77**. Arylation occurs at the less sterically hindered carbon as it is more accessible for the large Co catalyst toward activation via S_N2 oxidative addition. The alkyl radical **125** is then generated by photolysis of the Co^{III}–alkyl which can outcompete the thermal pathway that requires reduction to Co^{II} by the heterogenous Zn reductant. Judicious choice of Co catalyst and Co–R homolysis mechanism allows for precise control of the concentration of the desired activated epoxide intermediate **125** to achieve high levels of regioselective cross-coupling product **126** (Scheme 1.11).[84]

Scheme 1.11. *Ti and Co co-catalyzed epoxide openings.*

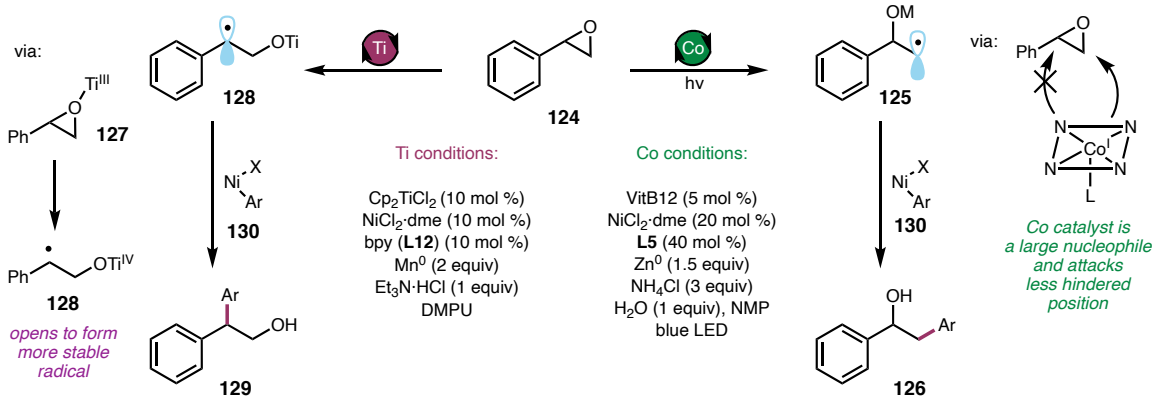

Ti catalysts, or more specifically titanocenes, have been used as co-catalysts with Ni in XEC with epoxide electrophiles. In contrast to the aforementioned iodide[64a] or Co[84] co-catalyst systems, epoxide **126** activation occurs by coordination of a Ti^{III} species **127** to the oxygen resulting in C–O homolysis to give an alkyl radical **128**. The regioselectivity of epoxide opening is dictated by the stability of the resulting radical species. Weix and coworkers have demonstrated that XEC with aryl halides can be achieved with Cp_2TiCl_2 to access regioisomer **129** (Scheme 1.11).[85] In a subsequent report they demonstrate that

by using a chiral titanocene catalyst, meso-epoxides could be symmetrized to give the chiral Ti-alkoxide radical intermediate. This intermediate can then engage with a Ni-aryl oxidative addition complex **130** to give the chiral ring-opened products in good yields, diastereoselectivity, and enantioselectivity.[86]

1.4.3 Transition Metal Co-Catalysts for C(sp²)–X Activation

Pd has been used as a co-catalyst to achieve highly cross-selective Ni-catalyzed XEC reactions. As previously discussed, the reactivity of Pd is quite different than Ni despite both being group 10 metals. This includes differences with Pd including: trends in relative rates of oxidative addition, affinity for 2-electron elementary steps, and stability of key organometallic intermediates. For example, oxidative addition into aryl triflates is faster than aryl bromides for Pd^0,[87] although this can be overturned with ligand design,[88] this is inherently different than Ni, where aryl bromide oxidative addition is intrinsically faster.[43] The ligand transfer in these systems is distinct to the aforementioned first row co-catalyst systems and instead of proceeding through a radical intermediates, C–C bond formation is proposed to occur through the transmetalation of a fragment on one catalyst to the other.[41]

In the seminal example from Weix and coworkers, a selective aryl-aryl cross-coupling of aryl bromides **132** and aryl triflates **131** is achieved with a dual **L12**Ni and **L13**Pd system. This system takes advantage of the fact **L12**Ni oxidative addition of Ar–X follows k_{oa} Br > OTf and **L13**Pd oxidative addition of Ar–X follows k_{oa} Br < OTf. This results in the generation of a **L12**Ni^{II}Ar complex **137** that can transmetalate the Ar^1 fragment to **L13**Pd^{II}Ar intermediate **138** which can then undergo reductive elimination from Pd^{II} **139** to form the cross-coupled product **133**. They demonstrate that both catalysts are necessary

for cross-coupling and that changing the ratio of Pd:Ni from the optimized conditions lowers the selectivity resulting in homocoupled **134** and **135**.[89] This was later extended to aryl chlorides (activated by Ni) with the addition of LiCl as a key additive which is hypothesized to accelerate the rate of oxidative addition by **L12**Ni such that it is competitive with **L13**Pd activation of the aryl triflate.[90] Subsequent reports found heteroaryl substrates could be cross-coupled when a less-activated tridentate ligand was used on Ni (Scheme 1.12a).[91]

A follow-up study achieved a similar cross-coupling to prepare dienes from alkenyl bromides and alkenyl triflates. Mechanistic studies revealed that the Zn^{2+} salts from the Zn^0 reductant were non-innocent in the reaction where stoichiometric alkenyl-Zn species were detected in the reaction mixture.[92,93] The beneficial role of Zn salts was further explored and enabled the challenging coupling of aryl triflates **131** with aryl tosylates **136** by a Ni/Pd catalyst system. Mechanistic studies reveal that the concentration of Ar–M (where M = Ni, Zn, or Pd) never exceeds the combined catalyst loading (Pd + Ni) when both Pd and Ni are present but will accumulate in the absence of Pd. This suggests the steady state concentration of **140** is very low and transmetalation from Ni to Zn to Pd is faster than the direct Ni to Pd transmetalation outcompeting homocoupling pathways. A low concentration of **137** or **138** is desirable as the accumulation of either activated electrophile will result in unproductive homocoupling. Given this net aryl transfer from Ni to Pd is the selectivity-determining step, the acceleration afforded by Zn^{2+} results in higher levels of selectivity (Scheme 1.12b).[94]

Scheme 1.12. *Dual Ni/Pd-catalyzed biaryl formation.*

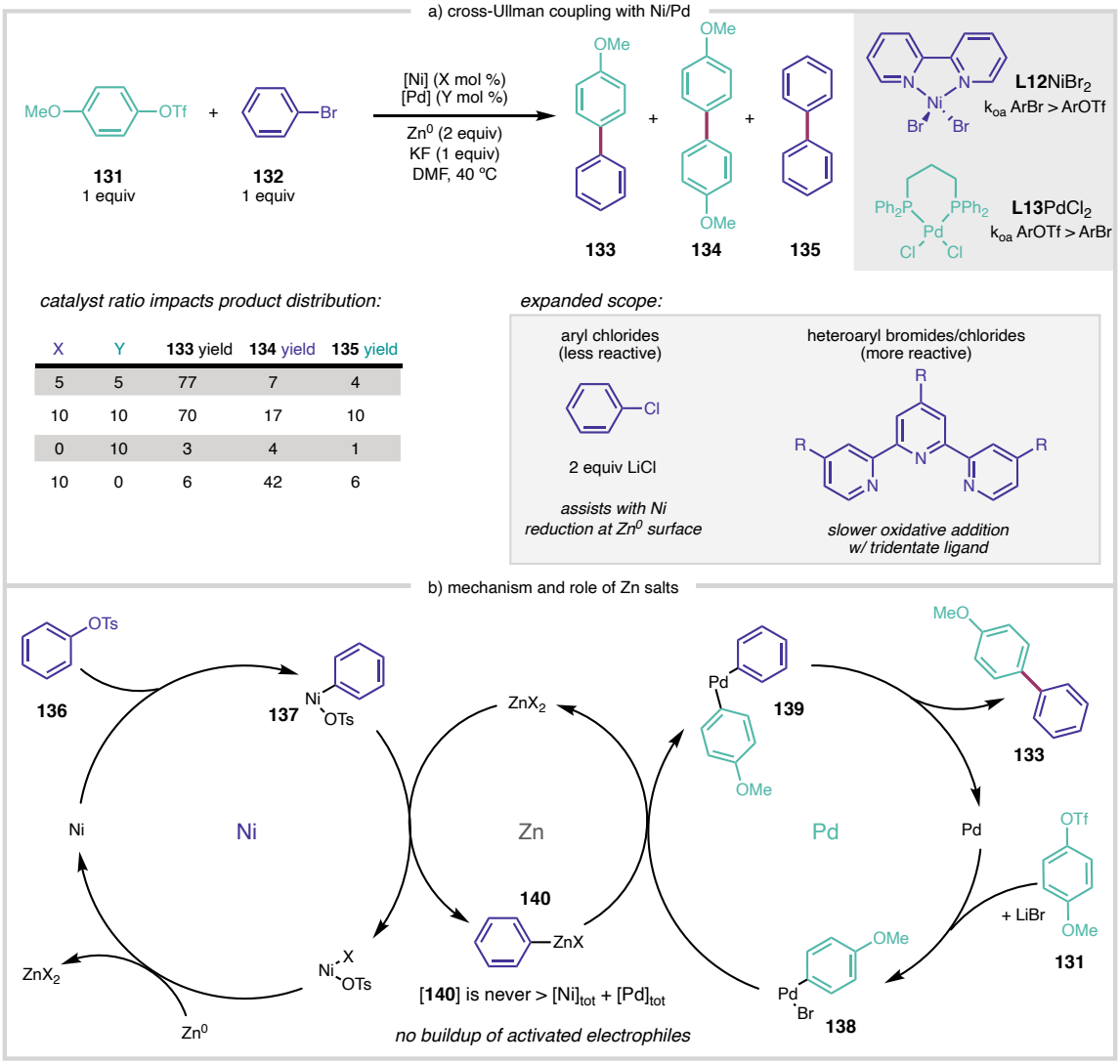

1.5 Modulating Electrophile Activation with Reductants

Figure 1.15. *Mechanisms of reduction and important redox potentials.*[95]

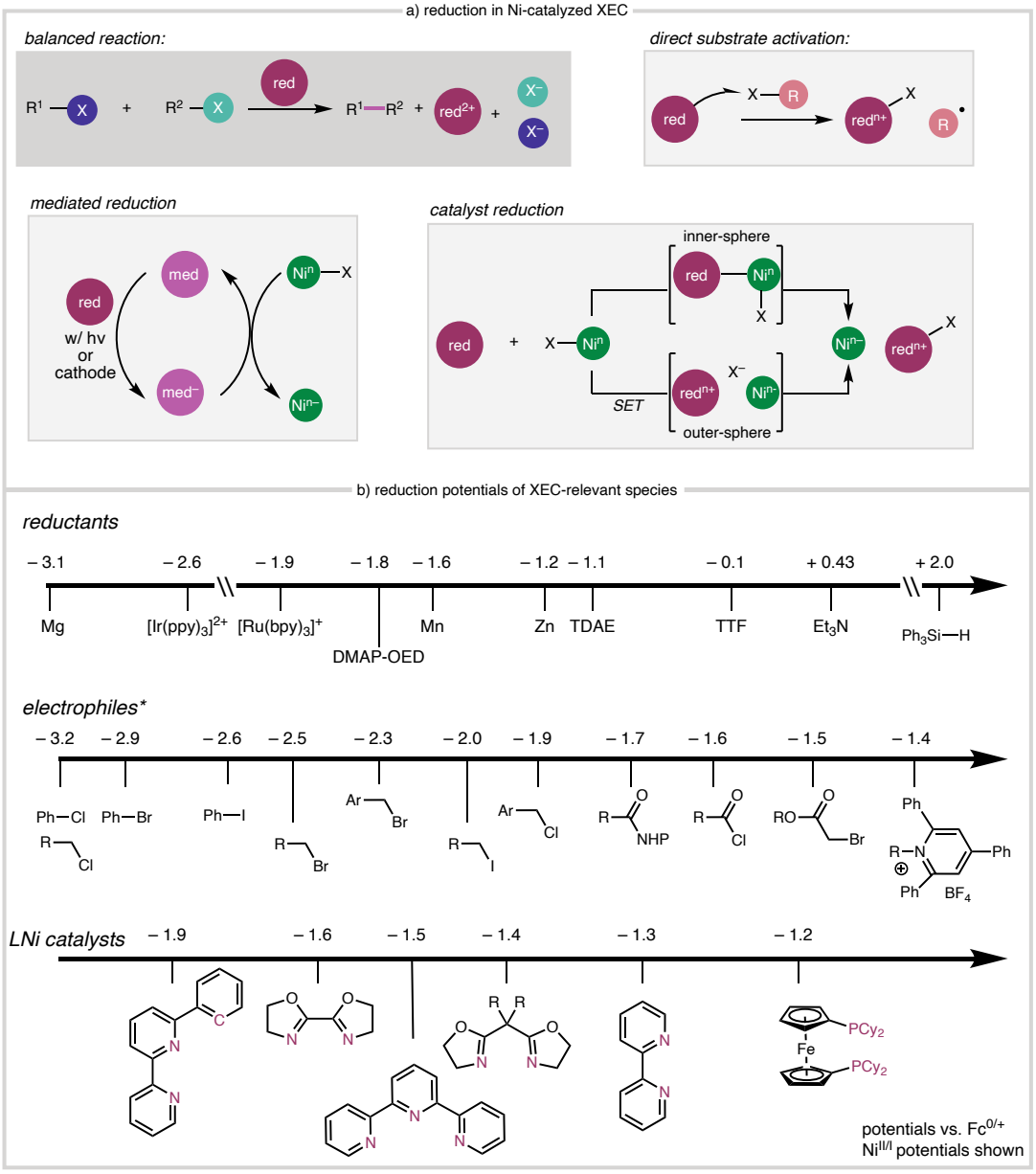

A crucial component to any XEC is the reductant that renders this net reductive reaction catalytic in Ni. The source of electrons and the means by which they are delivered to a substrate or catalyst has a profound impact on the outcome of these transformations. The

use of mediators, or electron-transfer catalysts, can be used as an additional control element in the net reduction of a catalytic intermediate or substrate. An external driving force, like photon absorption or a potential gradient, can also be used to drive XEC from otherwise prohibitively weak reductants (Figure 1.15a).[96] Over the last decade, reductants with diverse properties and reduction potentials have proven competent for driving XEC reactions (Figure 1.15b).[2,97,98]

1.5.1 Leveraging Reduction Mechanisms for Selectivity

More important than the thermodynamic aspects of the reductant in the context of catalysis are the kinetics of electron transfer (ET) from the reductant to other species in solution. While the redox potentials of the reductant and reaction components do impact the rate of electron transfer, the solubility and reduction mechanism play an outsized role. Heterogenous reductants (e.g., Mn^0, Zn^0, Mg^0, Sm^0) are most commonly employed in Ni-catalyzed XEC. These species have well-defined reduction potentials, are generally inexpensive,[99] and can be handled under air. Their insolubility means reduction is plagued by capricious mass-transfer effects rendering scale up[100] and mechanistic studies challenging. This is reflected in kinetics studies on Ni-catalyzed XEC, which uniformly show significant reaction rate dependence on stir rate and suggest rate-limiting reduction of the Ni-catalyst.[69,76,101]

Homogenous reductants, like TDAE, B_2Pin_2, dimethoxymethylsiloxane (DEMS), MeLi, etc... are generally more expensive and air sensitive but do not suffer from mass transport limited reduction and can proceed through inner- and outer-sphere mechanisms (Figure 1.15a). This can have significant effects on the mechanism of the reaction as

reduction of the catalyst may no longer be turnover-limiting or other electron-transfer reactions may become kinetically competitive. For example, Reisman and coworkers observed divergent kinetics across two related asymmetric reductive alkenylation reactions (ARA). By using a soluble reductant TDAE, they found the reaction is under saturation kinetics with regards to the Ni catalyst while the Mn^0-mediated reaction is first order in catalyst (**L3**NiX_2) reflecting the turnover-limiting catalyst reduction (Scheme 1.13a).[69]

Scheme.1.13. *Mechanistic changes with soluble reductant and their tunability.*

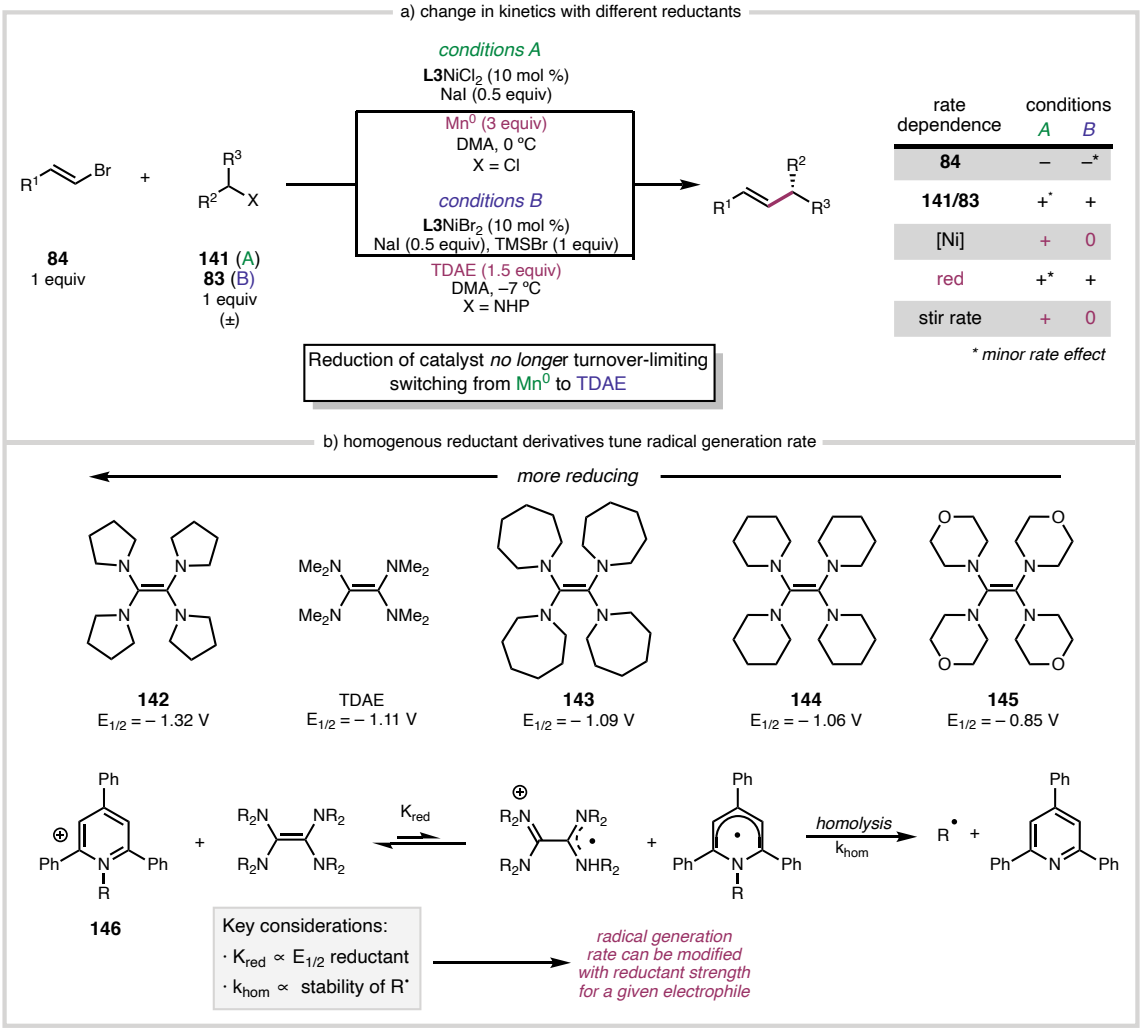

For homogenous reductants, the sterics and electronics influence the chemical properties, including reduction potential. In an example from Hazari and coworkers, various dialkyltetraaminoethylenes (**142**-**145**) were synthesized and compared to TDAE in an XEC coupling of Katritzky salts **146** with aryl iodides. These TDAE derivatives span ~500 mV in reducing strength and some of the less reactive agents can be handled under air. The reduction of Katritzky salts by any of these designer reductants is reversible and the subsequent C–N homolysis to generate the alkyl radical intermediate is rate-limiting, meaning the rate of alkyl radical generation is dependent on the reduction potential of the reductant. They further demonstrate highly selective XEC reactions achieved by changing the strength of the reductant to modulate the rate of radical generation to match the activation of aryl iodides (Scheme 1.13b).[102]

Figure 1.16. *Mechanism of reduction with diborane and thermodynamics.*

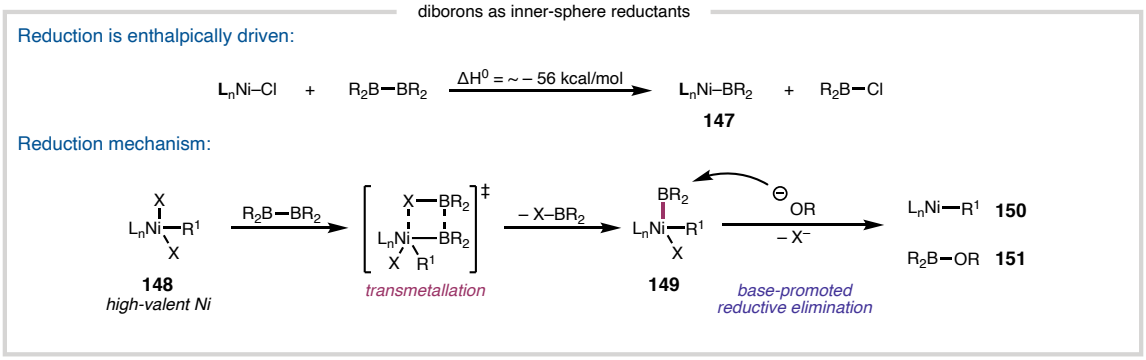

ET from a reductant to a substrate or catalyst can occur via a covalently-bound intermediate (i.e., inner-sphere). For homogenous reductants, both mechanisms can be operative depending on the identity of the reductant and the substrates.[97] The mechanisms of inner-sphere reduction makes the ET highly selective for components that can form a favorable covalent adduct with the reductant. Several examples can be found from Gong

and coworkers of selective reactions using diboranes as inner-sphere terminal reductants, like B_2pin_2. Reduction with diboranes is proposed to proceed through a Ni–BR_2 **147** intermediate. This can form either from transmetalation of **148** and R_2B–BR_2 driven by the formation of a strong B–X bond over the weak B–B bond to give **149**. From these Ni–B intermediates, either direct or base-promoted reductive elimination of X–Bpin **151** yields the reduced Ni complex **150** (Figure 1.16).[103]

Figure 1.17. *Diborane-mediated alkyl-alkyl couplings.*

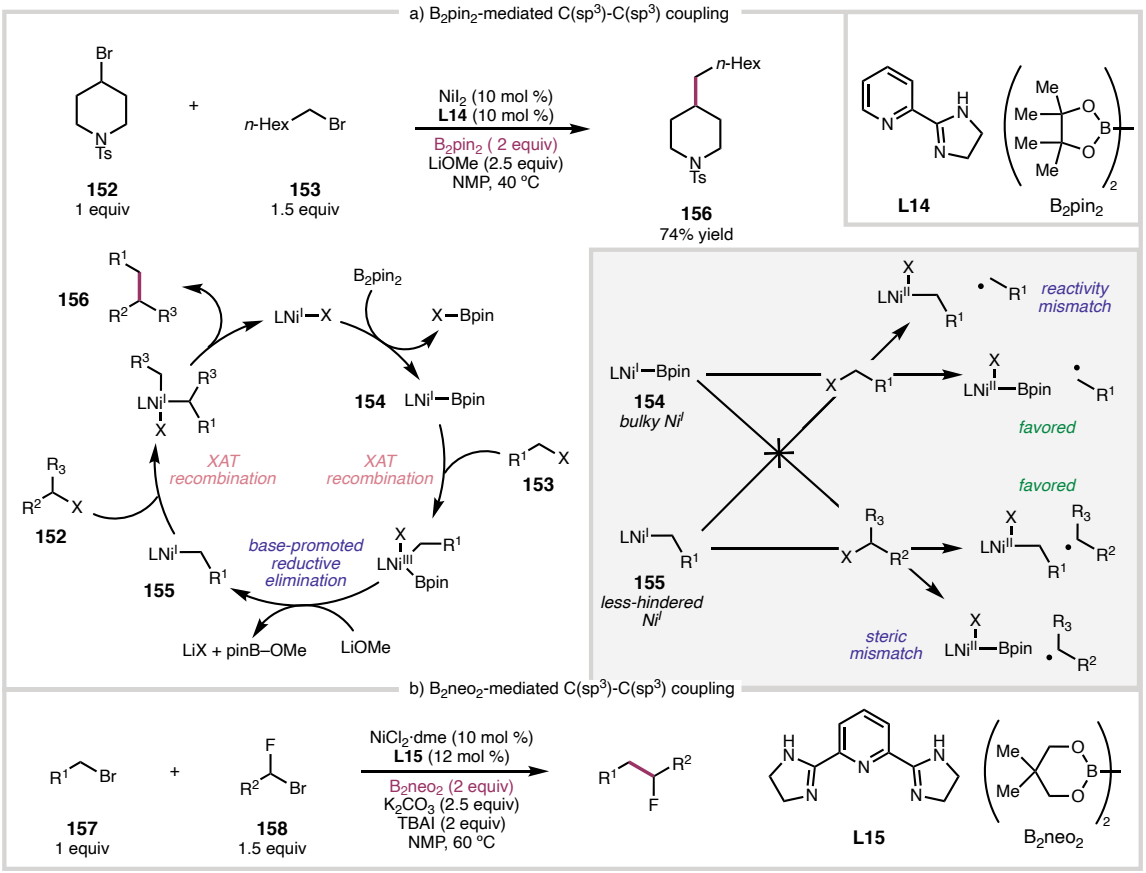

In the Gong group's $C(sp^3)$–$C(sp^3)$ coupling of 2° **152** and 1° **153** alkyl halides, the diborane reductant is credited for selective cross-coupling of these chemically similar electrophiles via a sequential activation mechanism. Upon reduction with B_2Pin_2, a Ni^I–

Bpin **154** is formed which will react with the 1º electrophile **153** faster than the 2º electrophile **152** due to the steric bulk of the Bpin group. This ultimately gives alky-Ni **155** after LiOMe-promoted XBpin reductive elimination. This less hindered Ni^{I}-alkyl complex **155** can then undergo oxidative addition with the more activated 2º substrate **152** which give product **156** following reductive elimination. Overall the cross-selectivity is attributed to the steric environment of the covalently-bound reductant in **154** as well as the mechanism of catalyst reduction via X–BPin-producing reductive elimination which is practically selective for Ni^{III}–X intermediates. It is notable that the yield of cross-coupled product decreases when either Mn^0 or Zn^0 reductants are employed, supporting the important mechanistic role of B_2Pin_2 (Figure 1.17a).[104] This same strategy was used by Wang and coworkers to cross-couple 1º alkyl halides **157** with α-fluoro 1º bromides **158**, a combination that is less sterically differentiated than the previous example. Adjusting the sterics of the diborane reducing agent led to impressive levels of cross-selectivity where $B_2(neo)_2$ was found to be optimal (Figure 1.17b).[105]

1.5.2 Selectivity in Electroreductive Systems

Electrolysis is well-suited for Ni-catalyzed XEC reactions as it enables direct manipulation of the rate electrons are delivered to the reaction (current, *i*) as well as their reducing power (potential, *E*). These are fundamentally heterogenous reactions as the reduction of intermediates, mediators, or substrates occurs at the surface of the cathode with oxidation of the reductant at the anode or oxidation of the anode itself.[106] These considerations offer several methods to favorably tune the delivery of electrons into the catalytic cycle by changing the cell current, the electrode materials, or by adding an

electroactive mediator with desirable electrochemical properties.

The use of Ni complexes as mediators in Ni-catalyzed XEC has been shown to ameliorate the challenges associated with heterogenous cathodic reduction. Sevov and coworkers have used coordinatively-saturated Ni complexes Ni–**S1** in combination with a Ni XEC catalyst **L16**Ni to couple aryl bromides **159** and alkyl bromides **160** in good yields. The mediators, like Ni–**S1**, are not reactive towards alkyl or aryl bromides, but have favorable ET kinetics given the minimal reorganization upon reduction and demonstrate remarkable stability in both oxidation states (Figure 1.17a).[107]

The authors reason that the mediator can not only deliver electrons to the Ni complex catalyzing the XEC in the bulk solution, but also prevent deleterious reactions caused by cathodic reduction of the substrates. This is because the catalyst turnover frequency (TOF) operative at the beginning of the reaction, when there are ample quantities of substrates, is higher than later stages of the reaction, after most substrates are consumed. This is accompanied by an increase in cell potential as the reaction progresses due to the lower driving force for product formation. The electrochemical stability of the mediator prevents this "overcharging" of the cell as it can undergo anodic oxidation if there is not enough **L16**Ni catalyst to reduce ($i > k_{cat}$), satisfying the reaction current while avoiding deleterious overreduction. While this reduces the faradaic efficiency of the reaction due to the unproductive reduction then reoxidation of the mediator Ni–**S1** (i.e., short circuiting), it can also maintain a more mild cell potential, resulting in a more selective reaction (Figure 1.17b).[108]

Figure 1.17. *Electrochemical mediators for overcharge protection.*

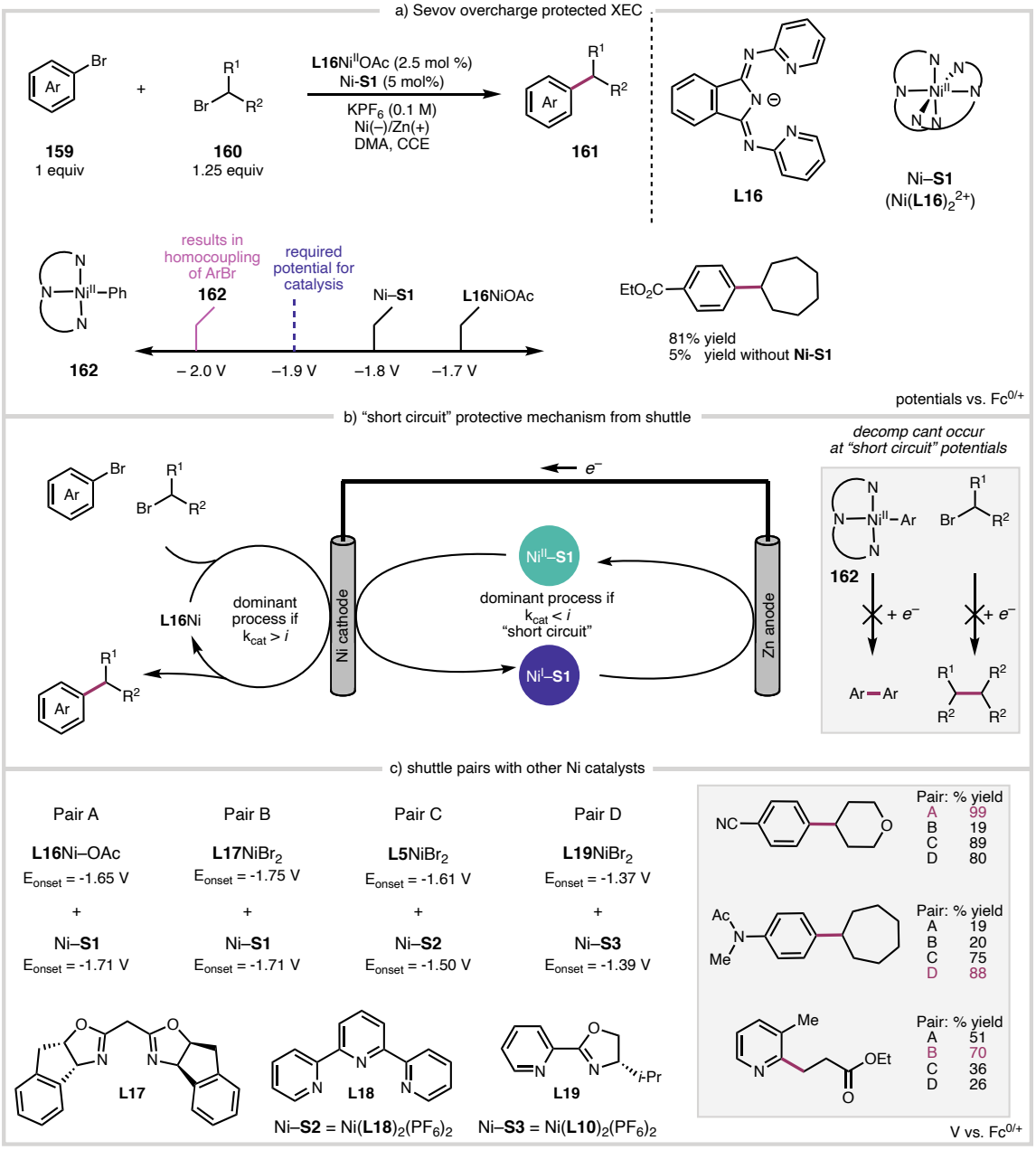

Subsequent studies demonstrated that this can be generalized to other catalysts and mediators (Ni–**S1**-Ni–**S3**) where the combinations of catalysts (**L16**, **L17**, **L5**, and **L19**) and mediators (**S1**, **S2**, and **S3**) with similar cathodic onset potentials results in higher

yields. The Sevov group demonstrate how this can be used to optimize the reaction for particular substrate combinations where catalyst/mediators can be screened as pairs (4 reactions for 4 mediators and 4 catalysts) as opposed to a more laborious combinatorial screening approach (12 reactions for 4 catalysts and 3 mediators) (Figure 1.17c).[109] A similar effect could presumably be achieved by running the reaction under constant potential electrolysis where the cell potential is set to the reduction potential of the Ni catalyst and anodic to the reduction potential substrates. This may be less general, as the overpotential (kinetic barrier) may change for a given set of substrates and issues with conversion are known for constant potential reactions.[110]

Figure 1.18. *Functionalized electrodes to favor productive catalyst reduction.*

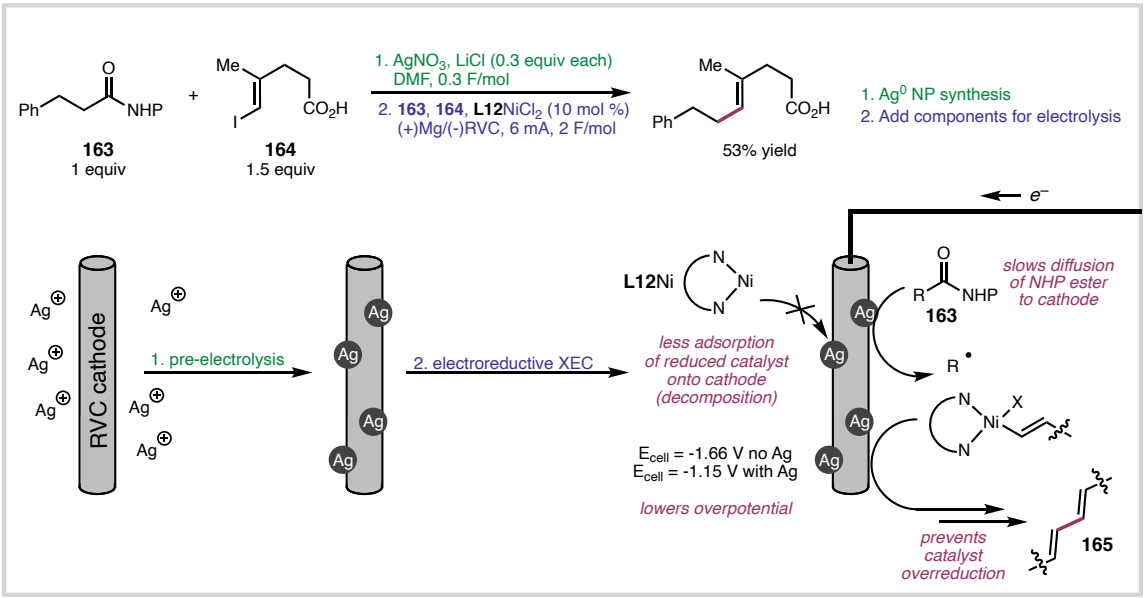

Manipulating the rates of electron transfer to specific reaction components can also be achieved by modifying the cathode itself as demonstrated in a Ni-catalyzed coupling of NHP esters **163** and alkenyl iodides **164** from Baran and coworkers. Initial optimization efforts were hampered by catalyst decomposition, overreduction of the activated alkenyl

electrophile **165**, and unproductive reduction of the NHP ester **163** at the RVC cathode. After extensive optimization, selectivity was improved when the cathode was functionalized by electrodeposition of Ag nanoparticles onto the surface. Monitoring the potential of the reaction with a reference electrode revealed a more mild cell potential during the electrolysis with the functionalized electrode, thus mitigating the undesired reduction processes. Electroanalytical studies revealed that deleterious deposition of the Ni catalyst **L12**Ni was decreased with the Ag/RVC electrode and diffusion of the NHP ester **163** to the electrode surfaced was slowed thus slowing unproductive cathodic reduction. Taken together, the passivation of the electrode surface with Ag nanoparticles tuned the electron transfer kinetics, mass-transport, and cell potential to a regime where the major reaction occurring at the cathode was productive turnover of the catalyst (Figure 1.18).[111]

Another benefit to electrochemical reactions is that the potential gradient generated by the power source (potentiostat or battery) expands the pool of reductants that can be used. This enables the use of mild reductants that would not be able to reduce catalytically relevant Ni complexes directly (Figure 1.15), to act as an electron source by anodic oxidation. Pairing the electroreductive reaction with oxidation of a soluble species is beneficial from a sustainability and scalability perspective,[106] while also allowing for more functional group tolerant reductants to be employed in these reactions (e.g., Et_3N $Ep_{/2}$ = ~ 0.41 V vs. $Fc^{0/+}$ [112] while most Ni catalysts are $E_{1/2}$ < –1.0 V vs. $Fc^{0/+}$).[113] There are several examples of reductants like alkyl amines, phosphines, and silanes being used as reductants for Ni-catalyzed XEC in both undivided[79,114,115,116] and divided cells[78] for cases where the oxidized reductant could interfere with productive catalysis.

1.5.3 Coupled Reductant Oxidation with Substrate Activation

The emergence of photoredox in XEC coupling reactions has enabled selective Ni-catalyzed XEC reactions and has expanded the classes of competent electrophiles. Like electrochemistry, tapping into an external driving force enables the generation of highly reactive intermediates under otherwise mild conditions, except in this case through photon absorption. This energy can be used to mediate the reduction of a Ni catalyst, co-catalyst, reagent, or electrophile from exceptionally mild reductants like triethanolamine,[117] silanes,[118,119] as well as dihydropyridines.[120]

In the seminal photoredox Ni-catalyzed XEC report from MacMillan and coworkers, a silane reductant, $(TMS)_3SiH$, was used in combination with Ir photoredox catalyst as a mediator to couple aryl **166** and alkyl bromides **167**. In this system, the excited state photoredox catalyst can oxidize bromide ions to generate a bromine radical which can undergo exothermic HAT with $(TMS)_3SiH$ yielding HBr and silyl radical **169**. This can then activate the alkyl bromide **167** substrate via XAT to give alkyl radical **170** that can be intercepted by **171** generated from the reduced photocatalyst. They demonstrate that the rate of **167** activation can be tuned by changing the properties of the silane where the bulky and more electron rich $(TMS)_3SiH$ was found to be optimal (Scheme 1.14a).[118]

In a follow-up study, they were able to achieve selective alkyl-alkyl coupling of alkyl bromides **172** and in situ generated alkyl bromide from alkyl tosylates **173**. Key to achieving high levels of selectivity was the reoptimization of the reductant to $(TMS)_3SiOH$ in addition to slow generation of the less hindered electrophile (Scheme 1.14b).[119] Mechanistic studies on this system conducted by the Lloyd-Jones group using photo-LED

NMR reaction monitoring rigorously characterized the kinetic driving forces towards cross-coupled and homocoupled products. Despite the complexity of the system, they determined that the identity of the silane as well as the alkyl bromide are the most important drivers of cross-selectivity.[121] Some of the decomposition pathways they identified, like photoinduced Ni–Ar (**171**) homolysis, are important considerations for these photoredox reactions as these complexes are known to be light-sensitive.[122]

Scheme 1.14. *Silane reductant-mediated substrate activation.*

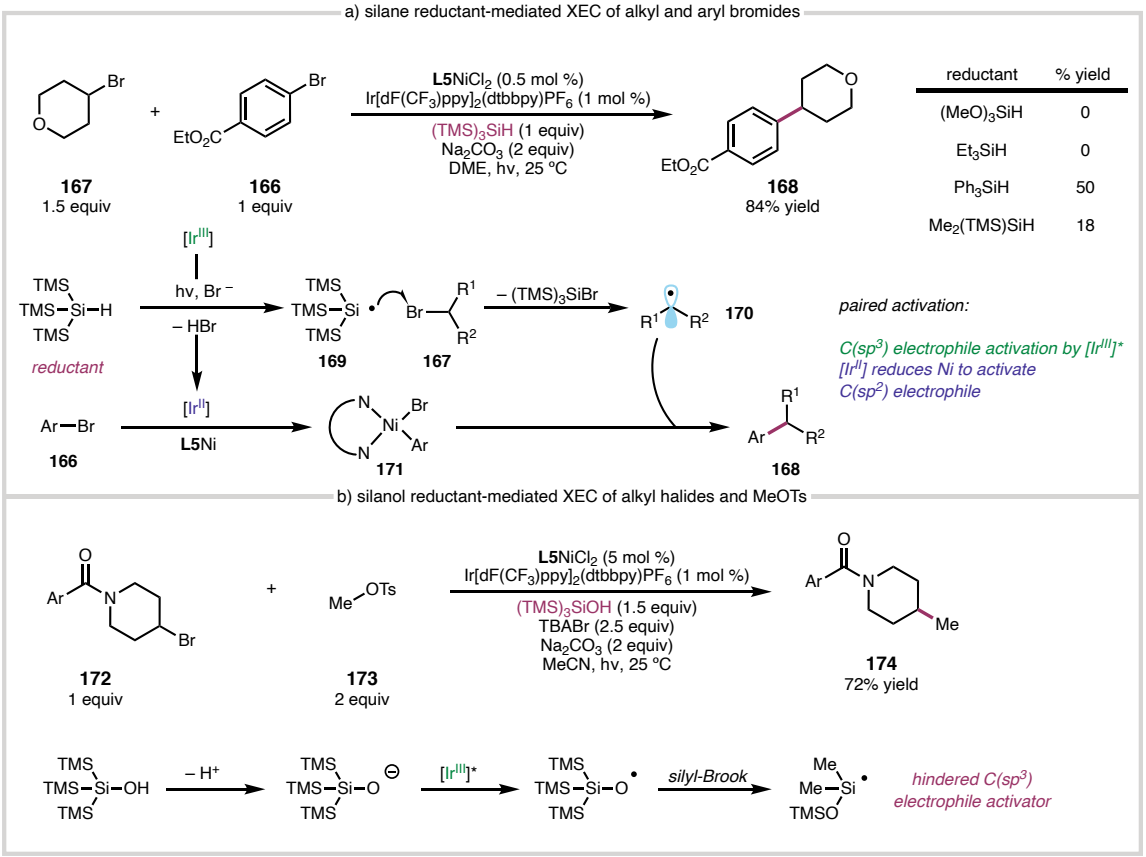

The oxidation of a mild reductant in paired electrolysis has been used for selective electrophile activation in electroreductive couplings. In a report from Mei and coworkers, the asymmetric XEC of α-chloroesters **175** and aryl or alkenyl bromides **176** is driven by

the oxidation of a silane reductant. Mechanistic studies revealed that the activation of the α-chloroester **175** is not mediated by **L20**Ni, but instead by the oxidized silane. This proceeded through a similar pathway as aforementioned photoredox system (Scheme 1.14a) where the bromine-mediated anodic oxidation of the silane affords silyl radical **169** which can undergo a chloride atom abstraction to give the activated radical derived from **175**. Given the anodically-trigger C(sp^3) electrophile activation is paired to the cathodically-triggered C(sp^2) activation ensures the rate of electrophile activation occurs at similar rates throughout catalysis. Additionally, mediating electrophile's activation with distinct species allows for the independent modulation of each electrophiles activation by modification of either the silane or Ni catalyst (Scheme 1.15).**Error! Bookmark not defined.**

Scheme 1.15. *Paired electrolysis with silane reductant.*

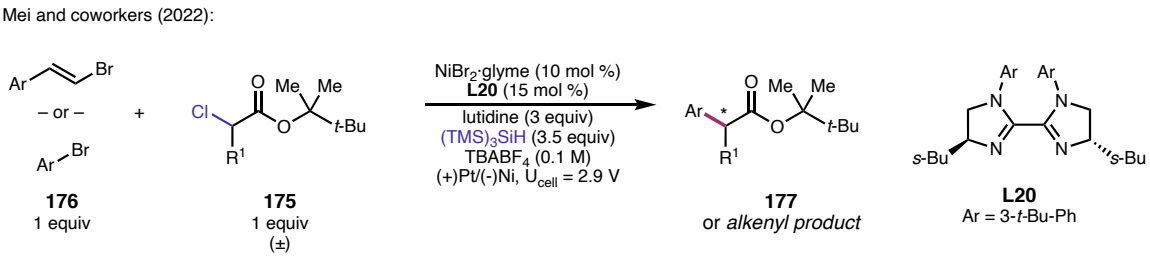

Utilizing the oxidized reductant to activate electrophiles has been leveraged in to make alcohols competent electrophilic coupling handles in electroreductive systems. In an example from Li and coworkers, the electroreductive coupling of aryl bromides **178** and alcohols **179** is driven by the oxidation of a PPh_3 reductant. The anodically generated Br_2 reacts with PPh_3 in solution to generate phosphonium ion **181**, which undergoes an *in situ* Appel-type reaction with the alcohol **179** to give the corresponding alkyl bromide **182**. The alkyl bromide **182** is then the active electrophile in the Ni-catalyzed XEC to give cross-

coupled product **180**. This method is impressive in that it can directly utilize alcohols as coupling handles; however, it is apparent this mode of C(sp^3) electrophile activation is challenging to control as these conditions are not cross-selective, requiring 3 equivalents of **178** for generality (Scheme 1.16).[123]

Scheme 1.16. *Paired electrolysis with phosphine reductant for alcohol activation.*

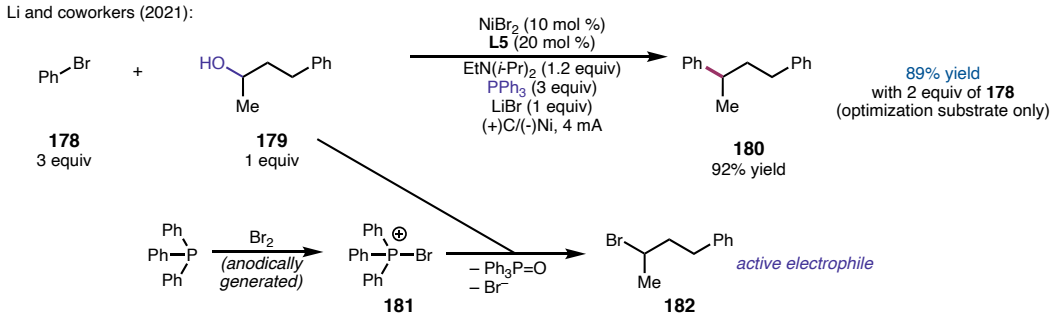

In a remarkably more selective arylation **183** of alcohols **184** from MacMillan and coworkers, the terminal reductant is also used for substrate activation. In this metallaphotoredox XEC, a *N*-heterocyclic carbene (NHC) reductant (**NHC-1**) is used which can undergo a formal O–H insertion with **184** to give **186** which can be oxidized by the photocatalyst to give radical **187**. This triggers a fragmentation process releasing the NHC-derived carbamate **188** and an alkyl radical **189** which can engage with the Ni catalyst and give product **185** (Scheme 1.17). In analogy to the NHP ester derivative strategy for selective reactions (Figure 1.12a),[67] the rate of alkyl radical generation is perturbed by adjusting the reducing strength of the NHC reductant as changing the NHC is shown to impact yields of cross-coupled product.[124]

Scheme 1.17. *Photoredox XEC with NHC reductant for alcohol activation.*

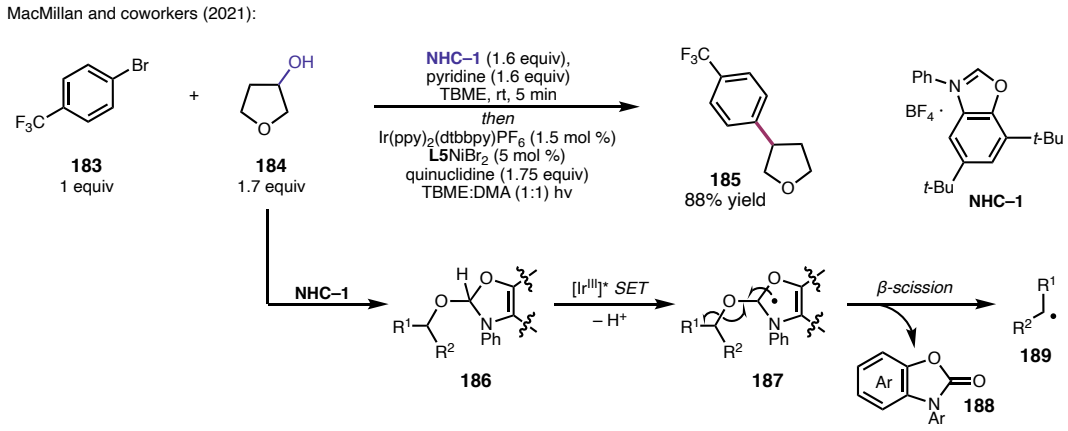

1.6 CONCLUDING REMARKS

Herein, we present mechanistic principles to guide cross-selective Ni-catalyzed XEC reaction optimization with examples of practical strategies that have been previously employed. These strategies aim to match the rate of electrophile activation by fine-tuning of the reaction conditions. We categorized the strategies based on the aspects of the reaction they modulated to attain cross-selectivity in the coupling of two fragments: 1) coupling handles, 2) catalyst/co-catalyst system, 3) reductant or mediated reduction. These are much more efficient than methods that obtain high yields of cross-coupled products, at the expense of sacrificing one electrophile by using a large excess.

While it is easy to rationalize why certain aspects of optimized reaction conditions lead to highly selective reactions *post-hoc,* the challenge remains on how to rationally optimize XEC reactions by determining what factors modulate one electrophile's relative activation/decomposition rate. Additionally, our ability to predict these factors *in lieu* of resource-intensive, empirically-derived models is lacking, in part due to the complexity of

these reactions, but can largely be attributed to a lack of *general* understanding of how these transformations work. As a result, identification of optimal reaction conditions by generating large data sets through brute-force screening is usually more rapid, especially as technology makes high-throughput experimentation (HTE) more accessible.[125] HTE is a powerful way to arrive at relatively general conditions representing a local maxima in chemical space; however, mechanistic understanding opens up an alternative form of generality which provides a road map for traversing into new chemical space.[126]

Valuable mechanistic work has historically been outpaced by reaction development making it challenging to formulate *predictive* mechanistic hypothesis during an optimization campaign. Recent advances in technology and computer science as well as the cumulative mechanistic knowledge in Ni-catalyzed XEC has facilitate the formulation of these mechanistic models. Modern mechanistic experiments have enabled a more rapid way to perform kinetic analysis of a reaction such as RPKA/VTNA-treated time course studies,[127] or electroanalytical techniques.[17] These simplify the process of obtaining qualitative or quantitative data on how different catalysts interact with reaction components and can be used to derive reactivity trends.[128] It would be enabling if pre-screening reaction conditions for each electrophile could be done in short order to determine parameters that can tune relative rates of activation and indicate which parameters to modulate next in an optimization screening campaign.

Thesis techniques are also being used in conjunction with computational and data science tools to create general models for reaction development. In practice, a machine-learning algorithm is trained on mechanistic data or early screening results so it can learn

about the transformation in order to predict reaction conditions for a given substrate combination. [129] Due to the fact that these models are usually trained on large, representative data sets, this can be used in tandem with HTE to generate training data. In practice the mechanistic data is used in parameterization of the reaction components and the model can then relate this to performance in a reaction with large HTE data sets. Ideally, this could then be simplified by pre-screening with virtual ligand/catalyst libraries, obviating the need to do expensive HTE screens.[130]

1.7 NOTES AND REFERENCES

(1) (a) Buskes, M. J.; Blanco, M.-J. Impact of Cross-Coupling Reactions in Drug Discovery and Development. *Molecules* **2020**, *25*, 3493. (b) Xu, S.; Kim, E. H.; Wei, A.; Negishi, E. Pd- and Ni-Catalyzed Cross-Coupling Reactions in the Synthesis of Organic Electronic Materials. *Sci. Tech. Adv. Mater.* **2014**, *15*, 044201. (c) Devendar, P.; Qu, R.-Y.; Kang, W.-M.; He, B.; Yang, G.-F. Palladium-Catalyzed Cross-Coupling Reactions: A Powerful Tool for the Synthesis of Agrochemicals. *J. Agric. Food Chem.* **2018**, *66*, 8914–8934. (d) Ruiz-Castillo, P.; Buchwald, S. L. Applications of Palladium-Catalyzed C–N Cross-Coupling Reactions. *Chem. Rev.* **2016**, *116*, 12564–12649.

(2) Goldfogel, M. J.; Huang, L.; Weix, D. J. Cross-Electrophile Coupling. In *Nickel Catalysis in Organic Synthesis*; John Wiley & Sons, Ltd, 2020; pp 183–222.

(3) Diccianni, J. B.; Diao, T. Mechanisms of Nickel-Catalyzed Cross-Coupling Reactions. *TRECHEM* **2019**, *1*, 830–844.

(4) Ananikov, V. P. Nickel: The "Spirited Horse" of Transition Metal Catalysis. *ACS Catal.* **2015**, *5*, 1964–1971.

(5) Everson, D. A.; Weix, D. J. Cross-Electrophile Coupling: Principles of Reactivity and Selectivity. *J. Org. Chem.* **2014**, *79*, 4793–4798.

(6) Semmelhack, M. F.; Helquist, P. M.; Jones, L. D. Synthesis with Zerovalent Nickel. Coupling of Aryl Halides with Bis(1,5-Cyclooctadiene)Nickel(0). *J. Am. Chem. Soc.* **1971**, *93* (22), 5908–5910.

(7) Semmelhack, M. F.; Ryono, L. S. Nickel-Promoted Synthesis of Cyclic Biphenyls. Total Synthesis of Alnusone Dimethyl Ether. *J. Am. Chem. Soc.* **1975**, *97*, 3873–3875.

(8) Semmelhack, M. F.; Helquist, P.; Jones, L. D.; Keller, L.; Mendelson, L.; Ryono, L. S.; Gorzynski Smith, J.; Stauffer, R. D. Reaction of Aryl and Vinyl Halides with Zerovalent Nickel - Preparative Aspects and the Synthesis of Alnusone. *J. Am. Chem. Soc.* **1981**, *103*, 6460–6471.

(9) Zembayashi, M.; Tamao, K.; Yoshida, J.; Kumada, M. Nickel-Phosphine Complex-Catalyzed Homo Coupling of Aryl Halides in the Presence of Zinc Powder. *Tetrahedron Letters* **1977**, *18*, 4089–4091.

(10) Rollin, Y.; Troupel, M.; Tuck, D. G.; Perichon, J. The Coupling of Organic Groups by the Electrochemical Reduction of Organic Halides: Catalysis by 2,2′-Bipyridinenickel Complexes. *Journal of Organometallic Chemistry* **1986**, *303*, 131–137.

(11) Meyer, G.; Rollin, Y.; Perichon, J. A Zerovalent Nickel-2,2′-Bipyridine Complex: An Efficient Catalyst for Electrochemical Homocoupling of Ortho-Substituted Halides and Their Heterocoupling with Meta- and Para-Substituted Halides. *Journal of Organometallic Chemistry* **1987**, *333*, 263–267.

(12) Folest, J. C.; Périchon, J.; Fauvarque, J. F.; Jutand, A. Synthèse électrochimique d'esters arylacétique et arylpropionique via des complexes du nickel. *Journal of Organometallic Chemistry* **1988**, *342*, 259–261.

(13) Marzouk, H.; Rollin, Y.; Folest, J. C.; Nédélec, J. Y.; Périchon, J. Electrochemical Synthesis of Ketones from Acid Chlorides and Alkyl and Aryl Halides Catalysed by Nickel Complexes. *Journal of Organometallic Chemistry* **1989**, *369*, C47–C50.

(14) Bajo, S.; Laidlaw, G.; Kennedy, A. R.; Sproules, S.; Nelson, D. J. Oxidative Addition of Aryl Electrophiles to a Prototypical Nickel(0) Complex: Mechanism and Structure/Reactivity Relationships. *Organometallics* **2017**, *36*, 1662–1672.

(15) Till, N. A.; Oh, S.; MacMillan, D. W. C.; Bird, M. J. The Application of Pulse Radiolysis to the Study of Ni(I) Intermediates in Ni-Catalyzed Cross-Coupling Reactions. *J. Am. Chem. Soc.* **2021**, *143*, 9332–9337.

(16) Ting, S. I.; Williams, W. L.; Doyle, A. G. Oxidative Addition of Aryl Halides to a Ni(I)-Bipyridine Complex. *J. Am. Chem. Soc.* **2022**, *144*, 5575–5582.

(17) Tang, T.; Hazra, A.; Min, D. S.; Williams, W. L.; Jones, E.; Doyle, A. G.; Sigman, M. S. Interrogating the Mechanistic Features of Ni(I)-Mediated Aryl Iodide Oxidative Addition Using Electroanalytical and Statistical Modeling Techniques. *J. Am. Chem. Soc.* **2023**. *ASAP.*

(18) (a) Fahey, D. R. The Reaction of Aryl and Vinyl Halides with Nickel(0) Complexes. *J. Am. Chem. Soc.* **1970**, *92*, 402–404. (b) Fahey, D. R.; Mahan, J. E. Oxidative Additions of Aryl, Vinyl, and Acyl Halides to Triethylphosphinenickel(0) Complexes. *J. Am. Chem. Soc.* **1977**, *99*, 2501–2508.

(19) Tsou, T. T.; Kochi, J. K. Mechanism of Oxidative Addition. Reaction of Nickel(0) Complexes with Aromatic Halides. *J. Am. Chem. Soc.* **1979**, *101*, 6319–6332.

(20) Kawamata, Y.; Vantourout, J. C.; Hickey, D. P.; Bai, P.; Chen, L.; Hou, Q.; Qiao, W.; Barman, K.; Edwards, M. A.; Garrido-Castro, A. F.; deGruyter, J. N.; Nakamura, H.; Knouse, K.; Qin, C.; Clay, K. J.; Bao, D.; Li, C.; Starr, J. T.; Garcia-Irizarry, C.; Sach, N.; White, H. S.; Neurock, M.; Minteer, S. D.; Baran, P. S. Electrochemically Driven, Ni-Catalyzed Aryl Amination: Scope, Mechanism, and Applications. *J. Am. Chem. Soc.* **2019**, *141*, 6392–6402.

(21) Yamamoto, T.; Wakabayashi, S.; Osakada, K. Mechanism of C-C Coupling Reactions of Aromatic Halides, Promoted by Ni(COD)2 in the Presence of 2,2′-Bipyridine and PPh3, to Give Biaryls. *Journal of Organometallic Chemistry* **1992**, *428*, 223–237.

(22) Biswas, S.; Weix, D. J. Mechanism and Selectivity in Nickel-Catalyzed Cross-Electrophile Coupling of Aryl Halides with Alkyl Halides. *J. Am. Chem. Soc.* **2013**, *135*, 16192–16197.

(23) (a) Tollefson, E. J.; Hanna, L. E.; Jarvo, E. R. Stereospecific Nickel-Catalyzed Cross-Coupling Reactions of Benzylic Ethers and Esters. *Acc. Chem. Res.* **2015**, *48* (8), 2344–2353. (b) Zhou, Q.; Cobb, K. M.; Tan, T.; Watson, M. P. Stereospecific Cross Couplings To Set Benzylic, All-Carbon Quaternary Stereocenters in High Enantiopurity. *J. Am. Chem. Soc.* **2016**, *138* (37), 12057–12060.

(24) Thane, T. A.; Jarvo, E. R. Ligand-Based Control of Nickel Catalysts: Switching Chemoselectivity from One-Electron to Two-Electron Pathways in Competing Reactions of 4-Halotetrahydropyrans. *Org. Lett.* **2022**, *24*, 5003–5008.

(25) Diccianni, J. B.; Katigbak, J.; Hu, C.; Diao, T. Mechanistic Characterization of (Xantphos)Ni(I)-Mediated Alkyl Bromide Activation: Oxidative Addition, Electron Transfer, or Halogen-Atom Abstraction. *J. Am. Chem. Soc.* **2019**, *141*, 1788–1796.

(26) Schley, N. D.; Fu, G. C. Nickel-Catalyzed Negishi Arylations of Propargylic Bromides: A Mechanistic Investigation. *J. Am. Chem. Soc.* **2014**, *136*, 16588–16593.

(27) Lin, Q.; Fu, Y.; Liu, P.; Diao, T. Monovalent Nickel-Mediated Radical Formation: A Concerted Halogen-Atom Dissociation Pathway Determined by Electroanalytical Studies. *J. Am. Chem. Soc.* **2021**, *143*, 14196–14206.

(28) Kehoe, R.; Mahadevan, M.; Manzoor, A.; McMurray, G.; Wienefeld, P.; Baird, M. C.; Budzelaar, P. H. M. Reactions of the Ni(0) Compound Ni(PPh3)4 with Unactivated Alkyl Halides: Oxidative Addition Reactions Involving Radical Processes and Nickel(I) Intermediates. *Organometallics* **2018**, *37*, 2450–2467.

(29) Anderson, T. J.; Jones, G. D.; Vicic, D. A. Evidence for a NiI Active Species in the Catalytic Cross-Coupling of Alkyl Electrophiles. *J. Am. Chem. Soc.* **2004**, *126*, 8100–8101.

(30) Ni, S.; Li, C.-X.; Mao, Y.; Han, J.; Wang, Y.; Yan, H.; Pan, Y. Ni-Catalyzed Deaminative Cross-Electrophile Coupling of Katritzky Salts with Halides via C─N Bond Activation. *Science Advances* **2019**, *5*, eaaw9516.

(31) Jones, G. D.; Martin, J. L.; McFarland, C.; Allen, O. R.; Hall, R. E.; Haley, A. D.; Brandon, R. J.; Konovalova, T.; Desrochers, P. J.; Pulay, P.; Vicic, D. A. Ligand Redox Effects in the Synthesis, Electronic Structure, and Reactivity of an Alkyl−Alkyl Cross-Coupling Catalyst. *J. Am. Chem. Soc.* **2006**, *128*, 13175–13183.

(32) Wuttig, A.; Derrick, J. S.; Loipersberger, M.; Snider, A.; Head-Gordon, M.; Chang, C. J.; Toste, F. D. Controlled Single-Electron Transfer via Metal–Ligand Cooperativity Drives Divergent Nickel-Electrocatalyzed Radical Pathways. *J. Am. Chem. Soc.* **2021**, *143*, 6990–7001.

(33) Jouffroy, M.; Primer, D. N.; Molander, G. A. Base-Free Photoredox/Nickel Dual-Catalytic Cross-Coupling of Ammonium Alkylsilicates. *J. Am. Chem. Soc.* **2016**, *138*, 475–478.

(34) Nakajima, K.; Nojima, S.; Nishibayashi, Y. Nickel- and Photoredox-Catalyzed Cross-Coupling Reactions of Aryl Halides with 4-Alkyl-1,4-Dihydropyridines as Formal Nucleophilic Alkylation Reagents. *Angew. Chem. Int. Ed.* **2016**, *55*, 14106–14110.

(35) Xu, G.-L.; Liu, C.-Y.; Pang, X.; Liu, X.-Y.; Shu, X.-Z. Nickel-Catalyzed Cross-Electrophile Vinyl–Vinyl Coupling: An Approach to Structurally Versatile Dienylboronates. *CCS Chemistry* **2021**, *4*, 864–871.

(36) Also known as sequential reduction or sequential oxidative addition.

(37) Also known as “radical chain” mechanism in cases with a single Nickel catalyst. This mechanistic category has been expanded here to include dual catalytic systems

as well as systems where substrate activation occurs from the reductant or other reaction components.

(38) We note that the differences in the sequential reduction mechanism in ref. 101 and the radical chain mechanism starting from Ni^0 proposed in ref. 21 (Weix) is the sequence of reduction events. Namely, the two electron reduction to Ni0 that allows for the radical chain mechanism to occur without intermediate reduction reactions or reduction to Ni^I where an intermediate reduction is needed and proposed to occur with the reduction of $Ni^{II}ArX$ instead of NiX_2.

(39) Wagner, C. L.; Herrera, G.; Lin, Q.; Hu, C. T.; Diao, T. Redox Activity of Pyridine-Oxazoline Ligands in the Stabilization of Low-Valent Organonickel Radical Complexes. *J. Am. Chem. Soc.* **2021**, *143*, 5295–5300.

(40) Leifert, D.; Studer, A. The Persistent Radical Effect in Organic Synthesis. *Angew. Chem. Int. Ed.* **2020**, *59*, 74–108.

(41) Ackerman-Biegasiewicz, L. K. G.; Kariofillis, S. K.; Weix, D. J. Multimetallic-Catalyzed C–C Bond-Forming Reactions: From Serendipity to Strategy. *J. Am. Chem. Soc.* **2023**, *145*, 6596–6614.

(42) Bajo, S.; Laidlaw, G.; Kennedy, A. R.; Sproules, S.; Nelson, D. J. Oxidative Addition of Aryl Electrophiles to a Prototypical Nickel(0) Complex: Mechanism and Structure/Reactivity Relationships. *Organometallics* **2017**, *36*, 1662–1672.

(43) Greaves, M. E.; Humphrey, E. L. B. J.; Nelson, D. J. Reactions of Nickel(0) with Organochlorides, Organobromides, and Organoiodides: Mechanisms and Structure/Reactivity Relationships. *Catal. Sci. Technol.* **2021**, *11* (9), 2980–2996.

(44) (a) Legault, C. Y.; Garcia, Y.; Merlic, C. A.; Houk, K. N. Origin of Regioselectivity in Palladium-Catalyzed Cross-Coupling Reactions of Polyhalogenated Heterocycles. *J. Am. Chem. Soc.* **2007**, *129* (42), 12664–12665. (b) Garcia, Y.; Schoenebeck, F.; Legault, C. Y.; Merlic, C. A.; Houk, K. N. Theoretical Bond Dissociation Energies of Halo-Heterocycles: Trends and Relationships to Regioselectivity in Palladium-Catalyzed Cross-Coupling Reactions. *J. Am. Chem. Soc.* **2009**, *131* (18), 6632–6639.

(45) For Handy's rules see: Handy, S. T.; Zhang, Y. A Simple Guide for Predicting Regioselectivity in the Coupling of Polyhaloheteroaromatics. *Chem. Commun.* **2006**, No. 3, 299–301.

(46) Mirabi, B.; Marchese, A. D.; Lautens, M. Nickel-Catalyzed Reductive Cross-Coupling of Heteroaryl Chlorides and Aryl Chlorides. *ACS Catal.* **2021**, *11*, 12785–12793.

(47) Sengmany, S.; Vitu-Thiebaud, A.; Le Gall, E.; Condon, S.; Léonel, E.; Thobie-Gautier, C.; Pipelier, M.; Lebreton, J.; Dubreuil, D. An Electrochemical Nickel-Catalyzed Arylation of 3-Amino-6-Chloropyridazines. *J. Org. Chem.* **2013**, *78*, 370–379

(48) (a) Hofstra, J. L.; Poremba, K. E.; Shimozono, A. M.; Reisman, S. E. Nickel-Catalyzed Conversion of Enol Triflates into Alkenyl Halides. *Angew. Chem. Int. Ed.* **2019**, *58* (42), 14901–14905. (b) Suzuki, N.; Hofstra, J. L.; Poremba, K. E.; Reisman, S. E. Nickel-Catalyzed Enantioselective Cross-Coupling of N-Hydroxyphthalimide Esters with Vinyl Bromides. *Org. Lett.* **2017**, *19*, 2150–2153.

(49) Xu, G.-L.; Liu, C.-Y.; Pang, X.; Liu, X.-Y.; Shu, X.-Z. Nickel-Catalyzed Cross-Electrophile Vinyl–Vinyl Coupling: An Approach to Structurally Versatile Dienylboronates. *CCS Chemistry* **2021**, *4*, 864–871.

(50) (a) Gosden, C.; Healy, K. P.; Pletcher, D. Reaction of Electrogenerated Square-Planar Nickel(I) Complexes with Alkyl Halides. *J. Chem. Soc., Dalton Trans.* **1978**, No. 8, 972–976. (b) Greaves, M. E.; Ronson, T. O.; Lloyd-Jones, G. C.; Maseras, F.; Sproules, S.; Nelson, D. J. Unexpected Nickel Complex Speciation Unlocks Alternative Pathways for the Reactions of Alkyl Halides with Dppf-Nickel(0). *ACS Catal.* **2020**, *10* (18), 10717–10725.

(51) Thane, T. A.; Jarvo, E. R. Ligand-Based Control of Nickel Catalysts: Switching Chemoselectivity from One-Electron to Two-Electron Pathways in Competing Reactions of 4-Halotetrahydropyrans. *Org. Lett.* **2022**, *24* (28), 5003–5008.

(52) Ni, S.; Padial, N. M.; Kingston, C.; Vantourout, J. C.; Schmitt, D. C.; Edwards, J. T.; Kruszyk, M. M.; Merchant, R. R.; Mykhailiuk, P. K.; Sanchez, B. B.; Yang, S.; Perry, M. A.; Gallego, G. M.; Mousseau, J. J.; Collins, M. R.; Cherney, R. J.; Lebed, P. S.; Chen, J. S.; Qin, T.; Baran, P. S. A Radical Approach to Anionic Chemistry:

Synthesis of Ketones, Alcohols, and Amines. *J. Am. Chem. Soc.* **2019**, *141*, 6726–6739.

(53) Gerroll, B. H. R.; Bird, S. P.; Martin, E. T.; Mubarak, M. S.; Peters, D. G. Cyclohexyl Bromide and Iodide: Direct Reduction at Vitreous Carbon Cathodes Together with Nickel(I) Salen- and Cobalt(I) Salen-Catalyzed Reductions in Dimethylformamide. *ChemElectroChem* **2018**, *5*, 902–910.

(54) Okada, Keiji.; Okamoto, Kazushige.; Oda, Masaji. A New and Practical Method of Decarboxylation: Photosensitized Decarboxylation of N-Acyloxyphthalimides via Electron-Transfer Mechanism. *J. Am. Chem. Soc.* **1988**, *110*, 8736–8738.

(55) Turro, R. F.; Brandstätter, M.; Reisman, S. E. Nickel-Catalyzed Reductive Alkylation of Heteroaryl Imines. *Angew. Chem. Int. Ed.* **2022**, *61*, e202207597.

(56) Do, H.-Q.; Chandrashekar, E. R. R.; Fu, G. C. Nickel/Bis(Oxazoline)-Catalyzed Asymmetric Negishi Arylations of Racemic Secondary Benzylic Electrophiles to Generate Enantioenriched 1,1-Diarylalkanes. *J. Am. Chem. Soc.* **2013**, *135*, 16288–16291.

(57) Hewitt, K. A.; Herbert, C. A.; Jarvo, E. R. Synthesis of Vicinal Carbocycles by Intramolecular Nickel-Catalyzed Conjunctive Cross-Electrophile Coupling Reaction. *Org. Lett.* **2022**, *24*, 6093–6098.

(58) Liang, Z.; Xue, W.; Lin, K.; Gong, H. Nickel-Catalyzed Reductive Methylation of Alkyl Halides and Acid Chlorides with Methyl p-Tosylate. *Org. Lett.* **2014**, *16*, 5620–5623.

(59) Duan, J.; Du, Y.-F.; Pang, X.; Shu, X.-Z. Ni-Catalyzed Cross-Electrophile Coupling between Vinyl/Aryl and Alkyl Sulfonates: Synthesis of Cycloalkenes and Modification of Peptides. *Chem. Sci.* **2019**, *10*, 8706–8712.

(60) Kim, S.; Goldfogel, M. J.; Gilbert, M. M.; Weix, D. J. Nickel-Catalyzed Cross-Electrophile Coupling of Aryl Chlorides with Primary Alkyl Chlorides. *J. Am. Chem. Soc.* **2020**, *142*, 9902–9907.

(61) Dongbang, S.; Doyle, A. G. Ni/Photoredox-Catalyzed C(Sp3)–C(Sp3) Coupling between Aziridines and Acetals as Alcohol-Derived Alkyl Radical Precursors. *J. Am. Chem. Soc.* **2022**, *144* (43), 20067–20077.

(62) (a) Lin, B. L.; Clough, C. R.; Hillhouse, G. L. Interactions of Aziridines with Nickel Complexes: Oxidative-Addition and Reductive-Elimination Reactions That Break and Make C−N Bonds. *J. Am. Chem. Soc.* **2002**, *124*, 2890–2891.

(63) Desnoyer, A. N.; Geng, J.; Drover, M. W.; Patrick, B. O.; Love, J. A. Catalytic Functionalization of Styrenyl Epoxides via 2-Nickela(II)Oxetanes. *Chem. Eur. J* **2017**, *23*, 11509–11512.

(64) (a) Lau, S. H.; Borden, M. A.; Steiman, T. J.; Wang, L. S.; Parasram, M.; Doyle, A. G. Ni/Photoredox-Catalyzed Enantioselective Cross-Electrophile Coupling of Styrene Oxides with Aryl Iodides. *J. Am. Chem. Soc.* **2021**, *143* (38), 15873–15881. (b) Dongbang, S.; Doyle, A. G. Ni/Photoredox-Catalyzed C(Sp3)–C(Sp3) Coupling between Aziridines and Acetals as Alcohol-Derived Alkyl Radical Precursors. *J. Am. Chem. Soc.* **2022**, *144* (43), 20067–20077. (c) Steiman, T. J.;

Liu, J.; Mengiste, A.; Doyle, A. G. Synthesis of β-Phenethylamines via Ni/Photoredox Cross-Electrophile Coupling of Aliphatic Aziridines and Aryl Iodides. *J. Am. Chem. Soc.* **2020**, *142* (16), 7598–7605. (d) Woods, B. P.; Orlandi, M.; Huang, C.-Y.; Sigman, M. S.; Doyle, A. G. Nickel-Catalyzed Enantioselective Reductive Cross-Coupling of Styrenyl Aziridines. *J. Am. Chem. Soc.* **2017**, *139* (16), 5688–5691.

(65) Hu, X.; Cheng-Sánchez, I.; Cuesta-Galisteo, S.; Nevado, C. Nickel-Catalyzed Enantioselective Electrochemical Reductive Cross-Coupling of Aryl Aziridines with Alkenyl Bromides. *J. Am. Chem. Soc.* **2023**, *145*, 11, 6270-6279.

(66) Zhang, B.; Gao, Y.; Hioki, Y.; Oderinde, M. S.; Qiao, J. X.; Rodriguez, K. X.; Zhang, H.-J.; Kawamata, Y.; Baran, P. S. Ni-Electrocatalytic Csp3–Csp3 Doubly Decarboxylative Coupling. *Nature* **2022**, *606* (7913), 313–318.

(67) Salgueiro, D. C.; Chi, B. K.; Guzei, I. A.; García-Reynaga, P.; Weix, D. J. Control of Redox-Active Ester Reactivity Enables a General Cross-Electrophile Approach to Access Arylated Strained Rings. *Angew. Chem. Int. Ed.* **2022**, *61*, e202205673.

(68) Suzuki, N.; Hofstra, J. L.; Poremba, K. E.; Reisman, S. E. Nickel-Catalyzed Enantioselective Cross-Coupling of N-Hydroxyphthalimide Esters with Vinyl Bromides. *Org. Lett.* **2017**, *19* (8), 2150–2153.

(69) Turro, R. F.; Wahlman, J. L. H.; Tong, Z. J.; Chen, X.; Yang, M.; Chem. E. P.; Hong, X.; Hadt, R. H.; Houk, K. N., Yang, Y. F.; Reisman, S. E. Mechanistic

Investigation of Ni-Catalyzed Reductive Cross-Coupling of Alkenyl and Benzyl Electrophiles. *J. Am. Chem. Soc.* **2023**, *Accepted.*

(70) (a) Gabbey, A. L.; Michel, N. W. M.; Hughes, J. M. E.; Campeau, L.-C.; Rousseaux, S. A. L. Synthesis of α-Aryl Secondary Amides via Nickel-Catalyzed Reductive Coupling of Redox-Active Esters. *Org. Lett.* **2022**, *24*, 3173–3178. (b) Michel, N.; Edjoc, R.; Fagbola, E.; Hughes, J.; Campeau, L.-C.; Rousseaux, S. Nickel-Catalyzed Reductive Arylation of Redox Active Esters for the Synthesis of α-Aryl Nitriles – Role of a Chlorosilane Additive. ChemRxiv April 21, 2021.

(71) Cruz, C. L.; Montgomery, J. Nickel-Catalyzed Reductive Coupling of Unactivated Alkyl Bromides and Aliphatic Aldehydes. *Chem. Sci.* **2021**, *12*, 11995–12000. (b) Xiao, J.; Li, Z.; Montgomery, J. Nickel-Catalyzed Decarboxylative Coupling of Redox-Active Esters with Aliphatic Aldehydes. *J. Am. Chem. Soc.* **2021**, *143*, 21234–21240. (c) Shimkin, K. W.; Montgomery, J. Synthesis of Tetrasubstituted Alkenes by Tandem Metallacycle Formation/Cross-Electrophile Coupling. *J. Am. Chem. Soc.* **2018**, *140* (23), 7074–7078.

(72) Ogoshi, S.; Kamada, H.; Kurosawa, H. Reaction of (H2-Arylaldehyde)Nickel(0) Complexes with Me3SiX (X=OTf, Cl). Application to Catalytic Reductive Homocoupling Reaction of Arylaldehyde. *Tetrahedron* **2006**, *62*, 7583–7588.

(73) Arendt, K. M.; Doyle, A. G. Dialkyl Ether Formation by Nickel-Catalyzed Cross-Coupling of Acetals and Aryl Iodides. *Angew. Chem. Int. Ed.* **2015**, *54*, 9876–9880.

(74) Hatano, B.; Nagahashi, K.; Habaue, S. Reductive Coupling of Aromatic Dialkyl Acetals Using the Combination of Zinc and Chlorotrimethylsilane in the Presence of Potassium Carbonate. *Chem. Lett.* **2007**, *36*, 1418–1419.

(75) Everson, D. A.; Shrestha, R.; Weix, D. J. Nickel-Catalyzed Reductive Cross-Coupling of Aryl Halides with Alkyl Halides. *J. Am. Chem. Soc.* **2010**, *132*, 920–921.

(76) Everson, D. A.; Jones, B. A.; Weix, D. J. Replacing Conventional Carbon Nucleophiles with Electrophiles: Nickel-Catalyzed Reductive Alkylation of Aryl Bromides and Chlorides. *J. Am. Chem. Soc.* **2012**, *134*, 6146–6159.

(77) Umehara, A.; Kishi, Y. Further Studies on Ni/Zr-Mediated One-Pot Ketone Synthesis: Use of a Mixture of NiI- and NiII-Catalysts Greatly Improves the Molar Ratio of Coupling Partners. *Chem. Lett.* **2019**, *48*, 947–950.

(78) Perkins, R. J.; Hughes, A. J.; Weix, D. J.; Hansen, E. C. Metal-Reductant-Free Electrochemical Nickel-Catalyzed Couplings of Aryl and Alkyl Bromides in Acetonitrile. *Org. Process Res. Dev.* **2019**, *23*, 1746–1751.

(79) Franke, M. C.; Longley, V. R.; Rafiee, M.; Stahl, S. S.; Hansen, E. C.; Weix, D. J. Zinc-Free, Scalable Reductive Cross-Electrophile Coupling Driven by Electrochemistry in an Undivided Cell. *ACS Catal.* **2022**, *12*, 12617–12626.

(80) Hamby, T. B.; LaLama, M. J.; Sevov, C. S. Controlling Ni Redox States by Dynamic Ligand Exchange for Electroreductive Csp3–Csp2 Coupling. *Science* **2022**, *376*, 410–416.

(81) Demarteau, J.; Debuigne, A.; Detrembleur, C. Organocobalt Complexes as Sources of Carbon-Centered Radicals for Organic and Polymer Chemistries. *Chem. Rev.* **2019**, *119*, 6906–6955.

(82) Ackerman, L. K. G.; Anka-Lufford, L. L.; Naodovic, M.; Weix, D. J. Cobalt Co-Catalysis for Cross-Electrophile Coupling: Diarylmethanes from Benzyl Mesylates and Aryl Halides. *Chem. Sci.* **2015**, *6*, 1115–1119.

(83) Charboneau, D. J.; Barth, E. L.; Hazari, N.; Uehling, M. R.; Zultanski, S. L. A Widely Applicable Dual Catalytic System for Cross-Electrophile Coupling Enabled by Mechanistic Studies. *ACS Catal.* **2020**, *10*, 12642–12656.

(84) Potrząsaj, A.; Musiejuk, M.; Chaładaj, W.; Giedyk, M.; Gryko, D. Cobalt Catalyst Determines Regioselectivity in Ring Opening of Epoxides with Aryl Halides. *J. Am. Chem. Soc.* **2021**, *143*, 9368–9376.

(85) Zhao, Y.; Weix, D. J. Nickel-Catalyzed Regiodivergent Opening of Epoxides with Aryl Halides: Co-Catalysis Controls Regioselectivity. *J. Am. Chem. Soc.* **2014**, *136*, 48–51.

(86) Zhao, Y.; Weix, D. J. Enantioselective Cross-Coupling of Meso-Epoxides with Aryl Halides. *J. Am. Chem. Soc.* **2015**, *137*, 3237–3240.

(87) Jutand, A.; Mosleh, A. Rate and Mechanism of Oxidative Addition of Aryl Triflates to Zerovalent Palladium Complexes. Evidence for the Formation of Cationic (σ-Aryl)Palladium Complexes. *Organometallics* **1995**, *14* (4), 1810–1817.

(88) Kamikawa, T.; Hayashi, T. Control of Reactive Site in Palladium-Catalyzed Grignard Cross-Coupling of Arenes Containing Both Bromide and Triflate. *Tetrahedron Letters* **1997**, *38* (40), 7087–7090.

(89) Ackerman, L. K. G.; Lovell, M. M.; Weix, D. J. Multimetallic Catalysed Cross-Coupling of Aryl Bromides with Aryl Triflates. *Nature* **2015**, *524* (7566), 454–457.

(90) Huang, L.; Ackerman, L. K. G.; Kang, K.; Parsons, A. M.; Weix, D. J. LiCl-Accelerated Multimetallic Cross-Coupling of Aryl Chlorides with Aryl Triflates. *J. Am. Chem. Soc.* **2019**, *141* (28), 10978–10983.

(91) Kang, K.; Loud, N. L.; DiBenedetto, T. A.; Weix, D. J. A General, Multimetallic Cross-Ullmann Biheteroaryl Synthesis from Heteroaryl Halides and Heteroaryl Triflates. *J. Am. Chem. Soc.* **2021**, *143*, 21484–21491.

(92) Olivares, A. M.; Weix, D. J. Multimetallic Ni- and Pd-Catalyzed Cross-Electrophile Coupling To Form Highly Substituted 1,3-Dienes. *J. Am. Chem. Soc.* **2018**, *140*, 2446–2449.

(93) Yanagi, T.; Somerville, R. J.; Nogi, K.; Martin, R.; Yorimitsu, H. Ni-Catalyzed Carboxylation of C(Sp2)–S Bonds with CO2: Evidence for the Multifaceted Role of Zn. *ACS Catal.* **2020**, *10*, 2117–2123.

(94) Kang, K.; Huang, L.; Weix, D. J. Sulfonate Versus Sulfonate: Nickel and Palladium Multimetallic Cross-Electrophile Coupling of Aryl Triflates with Aryl Tosylates. *J. Am. Chem. Soc.* **2020**, *142* (24), 10634–10640.

(95) Caution should be exercised comparing potentials as not all species are reversible or soluble. This should serve as rough comparison across XEC reaction components. Potentials were obtained from: (a) ref. 113, (b) ref. 112 (c) ref. 96 (d) ref. 97.

(96) Tay, N. E. S.; Lehnherr, D.; Rovis, T. Photons or Electrons? A Critical Comparison of Electrochemistry and Photoredox Catalysis for Organic Synthesis. *Chem. Rev.* **2022**, *122*, 2487–2649.

(97) Charboneau, D. J.; Hazari, N.; Huang, H.; Uehling, M. R.; Zultanski, S. L. Homogeneous Organic Electron Donors in Nickel-Catalyzed Reductive Transformations. *J. Org. Chem.* **2022**, *87*, 7589–7609.

(98) Richmond, E.; Moran, J. Recent Advances in Nickel Catalysis Enabled by Stoichiometric Metallic Reducing Agents. *Synthesis* **2018**, *50*, 499–513.

(99) As of 4/12/23 a Reaxys search yields current prices for these metals but representative prices from Oakwood Chemical are shown – Zn^0: \$65/kg, Mn^0: \$212/kg. This translates to \$4.2/mol for Zn^0 and \$11.64/mol for Mn^0. By comparison TDAE can be purchased from Sigma Aldrich for \$1,430 for 50g which is \$28.6/g or \$5,720/mol.

(100) Nimmagadda, S. K.; Korapati, S.; Dasgupta, D.; Malik, N. A.; Vinodini, A.; Gangu, A. S.; Kalidindi, S.; Maity, P.; Bondigela, S. S.; Venu, A.; Gallagher, W. P.; Aytar, S.; González-Bobes, F.; Vaidyanathan, R. Development and Execution of an Ni(II)-

Catalyzed Reductive Cross-Coupling of Substituted 2-Chloropyridine and Ethyl 3-Chloropropanoate. *Org. Process Res. Dev.* **2020**, *24*, 1141–1148.

(101) Lin, Q.; Diao, T. Mechanism of Ni-Catalyzed Reductive 1,2-Dicarbofunctionalization of Alkenes. *J. Am. Chem. Soc.* **2019**, *141*, 17937–17948.

(102) Charboneau, D. J.; Huang, H.; Barth, E. L.; Germe, C. C.; Hazari, N.; Mercado, B. Q.; Uehling, M. R.; Zultanski, S. L. Tunable and Practical Homogeneous Organic Reductants for Cross-Electrophile Coupling. *J. Am. Chem. Soc.* **2021**, *143*, 21024–21036.

(103) Zhang, G.; Xie, Y.; Wang, Z.; Liu, Y.; Huang, H. Diboron as a Reductant for Nickel-Catalyzed Reductive Coupling: Rational Design and Mechanistic Studies. *Chem. Commun.* **2015**, *51*, 1850–1853.

(104) Xu, H.; Zhao, C.; Qian, Q.; Deng, W.; Gong, H. Nickel-Catalyzed Cross-Coupling of Unactivated Alkyl Halides Using Bis(Pinacolato)Diboron as Reductant. *Chem. Sci.* **2013**, *4*, 4022–4029.

(105) Sheng, J.; Ni, H.-Q.; Ni, S.-X.; He, Y.; Cui, R.; Liao, G.-X.; Bian, K.-J.; Wu, B.-B.; Wang, X.-S. Diversity-Oriented Synthesis of Aliphatic Fluorides via Reductive C(Sp3)−C(Sp3) Cross-Coupling Fluoroalkylation. *Angew. Chem. Int. Ed.* **2021**, *60*, 15020–15027.

(106) Claraz, A.; Masson, G. Recent Advances in C(Sp3)–C(Sp3) and C(Sp3)–C(Sp2) Bond Formation through Cathodic Reactions: Reductive and Convergent Paired Electrolyses. *ACS Org. Inorg. Au* **2022**, *2*, 126–147.

(107) (a) Hogue, R. W.; Toghill, K. E. Metal Coordination Complexes in Nonaqueous Redox Flow Batteries. *Curr. Opin. Electrochem*. **2019**, 18, 37−45. (b) . (46) Sevov, C. S. S. C. S.; Fisher, S. L. S. L.; Thompson, L. T. L. T.; Sanford, M. S. M. S. Mechanism-Based Development of a Low Potential, Soluble, and Cyclable Multielectron Anolyte for Nonaqueous Redox Flow Batteries. *J. Am. Chem. Soc*. **2016**, 138, 15378− 15384.

(108) Truesdell, B. L.; Hamby, T. B.; Sevov, C. S. General C(Sp2)–C(Sp3) Cross-Electrophile Coupling Reactions Enabled by Overcharge Protection of Homogeneous Electrocatalysts. *J. Am. Chem. Soc.* **2020**, *142*, 5884–5893.

(109) Zackasee, J. L. S.; Al Zubaydi, S.; Truesdell, B. L.; Sevov, C. S. Synergistic Catalyst–Mediator Pairings for Electroreductive Cross-Electrophile Coupling Reactions. *ACS Catal.* **2022**, *12*, 1161–1166.

(110) Nutting, J. E.; Gerken, J. B.; Stamoulis, A. G.; Bruns, D. L.; Stahl, S. S. "How Should I Think about Voltage? What Is Overpotential?": Establishing an Organic Chemistry Intuition for Electrochemistry. *J. Org. Chem.* **2021**, *86*, 15875–15885.

(111) Palkowitz, M. D.; Laudadio, G.; Kolb, S.; Choi, J.; Oderinde, M. S.; Ewing, T. E.-H.; Bolduc, P. N.; Chen, T.; Zhang, H.; Cheng, P. T. W.; Zhang, B.; Mandler, M. D.; Blasczak, V. D.; Richter, J. M.; Collins, M. R.; Schioldager, R. L.; Bravo, M.; Dhar, T. G. M.; Vokits, B.; Zhu, Y.; Echeverria, P.-G.; Poss, M. A.; Shaw, S. A.; Clementson, S.; Petersen, N. N.; Mykhailiuk, P. K.; Baran, P. S. Overcoming

Limitations in Decarboxylative Arylation via Ag–Ni Electrocatalysis. *J. Am. Chem. Soc.* **2022**, *144*, 17709–17720.

(112) Roth, H. G.; Romero, N. A.; Nicewicz, D. A. Experimental and Calculated Electrochemical Potentials of Common Organic Molecules for Applications to Single-Electron Redox Chemistry. *Synlett* **2016**, *27*, 714–723.

(113) Lin, Q.; Dawson, G.; Diao, T. Experimental Electrochemical Potentials of Nickel Complexes. *Synlett* **2021**, *32*, 1606–1620.

(114) Hu, X.; Cheng-Sánchez, I.; Cuesta-Galisteo, S.; Nevado, C. Nickel-Catalyzed Enantioselective Electrochemical Reductive Cross-Coupling of Aryl Aziridines with Alkenyl Bromides. *J. Am. Chem. Soc.* **2023**, *145*, 6270–6279.

(115) Li, Z.; Sun, W.; Wang, X.; Li, L.; Zhang, Y.; Li, C. Electrochemically Enabled, Nickel-Catalyzed Dehydroxylative Cross-Coupling of Alcohols with Aryl Halides. *J. Am. Chem. Soc.* **2021**, *143*, 3536–3543.

(116) Liu, D.; Liu, Z.-R.; Wang, Z.-H.; Ma, C.; Herbert, S.; Schirok, H.; Mei, T.-S. Paired Electrolysis-Enabled Nickel-Catalyzed Enantioselective Reductive Cross-Coupling between α-Chloroesters and Aryl Bromides. *Nat Commun* **2022**, *13*, 7318.

(117) Paul, A.; Smith, M. D.; Vannucci, A. K. Photoredox-Assisted Reductive Cross-Coupling: Mechanistic Insight into Catalytic Aryl–Alkyl Cross-Couplings. *J. Org. Chem.* **2017**, *82*, 1996–2003.

(118) Zhang, P.; Le, C. "Chip"; MacMillan, D. W. C. Silyl Radical Activation of Alkyl Halides in Metallaphotoredox Catalysis: A Unique Pathway for Cross-Electrophile Coupling. *J. Am. Chem. Soc.* **2016**, *138*, 8084–8087.

(119) Smith, R. T.; Zhang, X.; Rincón, J. A.; Agejas, J.; Mateos, C.; Barberis, M.; García-Cerrada, S.; de Frutos, O.; MacMillan, D. W. C. Metallaphotoredox-Catalyzed Cross-Electrophile Csp3–Csp3 Coupling of Aliphatic Bromides. *J. Am. Chem. Soc.* **2018**, *140*, 17433–17438.

(120) Guan, H.; Zhang, Q.; Walsh, P. J.; Mao, J. Nickel/Photoredox-Catalyzed Asymmetric Reductive Cross-Coupling of Racemic α-Chloro Esters with Aryl Iodides. *Angew. Chem. Int. Ed.* **2020**, *59*, 5172–5177.

(121) Ben-Tal, Y.; Lloyd-Jones, G. C. Kinetics of a Ni/Ir-Photocatalyzed Coupling of ArBr with RBr: Intermediacy of ArNiII(L)Br and Rate/Selectivity Factors. *J. Am. Chem. Soc.* **2022**, *144*, 15372–15382.

(122) Cagan, D. A.; Stroscio, G. D.; Cusumano, A. Q.; Hadt, R. G. Multireference Description of Nickel–Aryl Homolytic Bond Dissociation Processes in Photoredox Catalysis. *J. Phys. Chem. A* **2020**, *124*, 9915–9922.

(123) Li, Z.; Sun, W.; Wang, X.; Li, L.; Zhang, Y.; Li, C. Electrochemically Enabled, Nickel-Catalyzed Dehydroxylative Cross-Coupling of Alcohols with Aryl Halides. *J. Am. Chem. Soc.* **2021**, *143* (9), 3536–3543.

(124) Dong, Z.; MacMillan, D. W. C. Metallaphotoredox-Enabled Deoxygenative Arylation of Alcohols. *Nature* **2021**, *598* (7881), 451–456.

(125) Reetz, M. T. New Methods for the High-Throughput Screening of Enantioselective Catalysts and Biocatalysts. *Angew. Chem. Int. Ed.* **2002**, *41*, 1335–1338.

(126) (a) Wagen, C. C.; McMinn, S. E.; Kwan, E. E.; Jacobsen, E. N. Screening for Generality in Asymmetric Catalysis. *Nature* **2022**, *610*, 680–686. (b)Kim, H.; Gerosa, G.; Aronow, J.; Kasaplar, P.; Ouyang, J.; Lingnau, J. B.; Guerry, P.; Farès, C.; List, B. A Multi-Substrate Screening Approach for the Identification of a Broadly Applicable Diels–Alder Catalyst. *Nat. Commun.* **2019**, *10*, 770.

(127) (a) Nielsen, C. D.-T.; Burés, J. Visual Kinetic Analysis. *Chem. Sci.* **2019**, *10*, 348–353. (b) Blackmond, D. G. Reaction Progress Kinetic Analysis: A Powerful Methodology for Mechanistic Studies of Complex Catalytic Reactions. *Angew. Chem. Int. Ed.* **2005**, *44*, 4302–4320.

(128) Taylor, C. J.; Pomberger, A.; Felton, K. C.; Grainger, R.; Barecka, M.; Chamberlain, T. W.; Bourne, R. A.; Johnson, C. N.; Lapkin, A. A. A Brief Introduction to Chemical Reaction Optimization. *Chem. Rev.* **2023**, *123*, 3089–3126.

(129) Kariofillis, S. K.; Jiang, S.; Żurański, A. M.; Gandhi, S. S.; Martinez Alvarado, J. I.; Doyle, A. G. Using Data Science To Guide Aryl Bromide Substrate Scope Analysis in a Ni/Photoredox-Catalyzed Cross-Coupling with Acetals as Alcohol-Derived Radical Sources. *J. Am. Chem. Soc.* **2022**, *144*, 1045–1055.

(130) (a) Matsuoka, W.; Harabuchi, Y.; Maeda, S. Virtual Ligand Strategy in Transition Metal Catalysis Toward Highly Efficient Elucidation of Reaction Mechanisms and

Computational Catalyst Design. *ACS Catal.* **2023**, *13*, 5697–5711. (b) Short, M. A. S.; Tovee, C. A.; Willans, C. E.; Nguyen, B. N. High-Throughput Computational Workflow for Ligand Discovery in Catalysis with the CSD. *Catal. Sci. Technol.* **2023**, *13*, 2407–2420. (c) Rosales, A. R.; Wahlers, J.; Limé, E.; Meadows, R. E.; Leslie, K. W.; Savin, R.; Bell, F.; Hansen, E.; Helquist, P.; Munday, R. H.; Wiest, O.; Norrby, P.-O. Rapid Virtual Screening of Enantioselective Catalysts Using CatVS. *Nat Catal* **2019**, *2*, 41–45. (d) Burai Patrascu, M.; Pottel, J.; Pinus, S.; Bezanson, M.; Norrby, P.-O.; Moitessier, N. From Desktop to Benchtop with Automated Computational Workflows for Computer-Aided Design in Asymmetric Catalysis. *Nat Catal* **2020**, *3*, 574–584.

Chapter 2

Mechanistic Investigation of Ni-Catalyzed Reductive Cross-Coupling of Alkenyl and Benzyl Electrophiles[†]

2.1 INTRODUCTION

Mechanistic investigations of the Ni-catalyzed asymmetric reductive alkenylation of *N*-hydroxyphthalimide (NHP) esters and benzylic chlorides are reported. Investigations of the redox properties of the Ni-bis(oxazoline) catalyst, the reaction kinetics, and mode of electrophile activation show divergent mechanisms for these two related transformations. Notably, the mechanism of C(sp^3) activation changes from a Ni-mediated process when benzyl chlorides and Mn^0 are used to a reductant-mediated process that is gated by a Lewis acid when NHP esters and tetrakis(dimethylamino)ethylene is used. Kinetic experiments show that changing the identity of the Lewis acid can be used to tune the rate of NHP ester reduction.

[†] Portions of this chapter have been reproduced from a published manuscript.[1] Fellowship support was provided by the NIH (R35GM118191-01). J. L. H. Wahlman was supported by the NSF (DGE-1144469). R.G.H. acknowledges support from the NIH (National Institute of General Medical Sciences, R35-GM142595). Y.-F. Y. is grateful to the National Natural Science Foundation of China (21978272), the Fundamental Research Funds for the Provincial Universities of Zhejiang (RF-C2022006).

Spectroscopic studies support a Ni^{II}–alkenyl oxidative addition complex as the catalyst resting state. DFT calculations suggest an enantiodetermining radical capture step and elucidate the origin of enantioinduction for this Ni-BOX catalyst.

2.2 Background and Scope

Ni-catalyzed reductive cross-couplings (RCCs) of organic electrophiles have emerged as useful reactions for $C(sp^2)$–$C(sp^3)$ bond formation.[2] These reactions provide direct access to cross-coupled products from readily available organic electrophiles, such as halides, precluding the need to pre-generate an organometallic coupling partner. The use of a metal powder (Mn^0, Zn^0) or an organic electron donor such as tetrakis(dimethylamino)ethylene (TDAE)[3] provides reducing equivalents to render the system catalytic in Ni. Ni-catalyzed RCC reactions can also be driven electrochemically using either sacrificial anodes or paired electrolysis systems.[4] A key challenge in the development of these reactions is achieving selectivity for the cross-coupled product over possible homo-coupling products; this requires a catalyst that oxidatively adds each electrophile in sequence, or a catalyst system with mechanistically distinct modes of activating each coupling partner. Despite this challenge, several different Ni catalysis systems have been developed that afford high selectivity for cross-coupled products.[2,5,6]

Our lab has developed several Ni-catalyzed asymmetric reductive alkenylation (ARA) reactions (Figure 2.1), which leverage the intermediacy of $C(sp^3)$ radicals to enable stereoconvergent, enantioselective bond formation.[7,8,9] In 2014, we reported an ARA between benzylic chlorides **201** and alkenyl bromides **200** using cyclopropyl-containing IndaBOX ligand (**L3**) and Mn^0 as the terminal reductant (Figure 2.1a).[7] We subsequently developed a related ARA that uses the same ligand (**L3**), but employs redox-active *N*-hydroxyphthalimide (NHP) esters **202** as the $C(sp^3)$ coupling partner.[8] In this case, TDAE was used as the reductant, and trimethylsilyl bromide (TMSBr) was identified as a key additive (Figure 2.1b). In addition

to chiral ligand **L3** being optimal for both reactions, the use of DMA as solvent and NaI as an additive was shared between the two transformations. Given their similarities, we identified this pair of transformations as well suited for investigating how the mechanism of Ni-catalyzed RCCs might change depending on the C(sp^3) coupling partner.

Figure 2.1. *Ni-catalyzed ARA investigated in this study.*

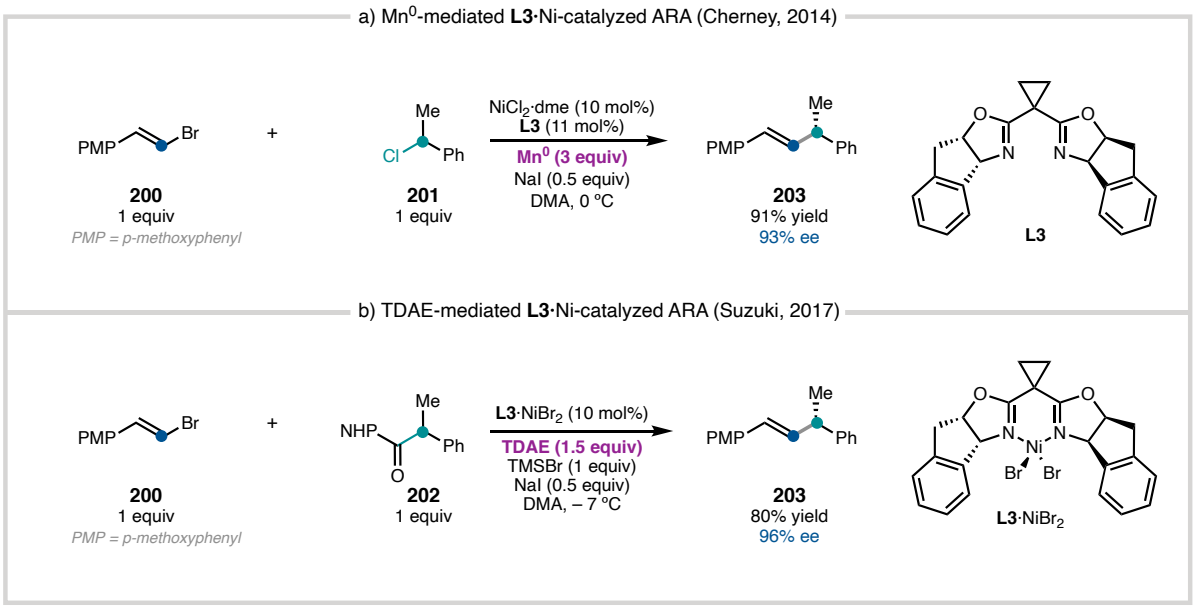

Since many RCCs use heterogenous terminal reductants, the mechanisms of these reactions have been difficult to elucidate. Nonetheless, insightful studies of reductive arylation have been disclosed by the groups of Weix[10], Diao[11]; these systems have primarily focused on reactions in which catalytically relevant Ni^{II}(aryl)X complexes can be isolated and characterized. Diao has also recently investigated bi(oxazoline)[11a,b] and pyridine-oxazoline[11c] ligands in reductive arylation; however, mechanistic studies of reductive alkenylation and of Ni-catalysts supported by chiral bis(oxazolines) such as **L3** are lacking.[12] Here, we report our mechanistic investigations of two **L3**·Ni-catalyzed ARA reactions. In this study we sought to: (1) determine the kinetic driving forces and resting state for the homogenous reaction of alkenyl bromide **200** with NHP ester **202**; (2) investigate the redox properties of the **L3**·$Ni^{II}X_2$ precatalysts and determine whether **L3**·Ni^0 is accessible using common reductants; (3) interrogate the

mechanism of electrophile activation for both **201** and **202**; (4) use computational methods to understand the enantioselectivity determining step. These studies have revealed that chloride **201** and NHP ester **202** are activated through distinct mechanisms and provide insights that can guide the optimization of reaction conditions for Ni-catalyzed RCC reactions.

2.3 INVESTIGATION OF HOMOGENOUS ARA REACTION

2.3.1 Redox properties of L3NiX$_2$ Precatalyst

Figure 2.2. *Cyclic Voltammetry of* ***L3***·*NiX$_2$ complexes.*

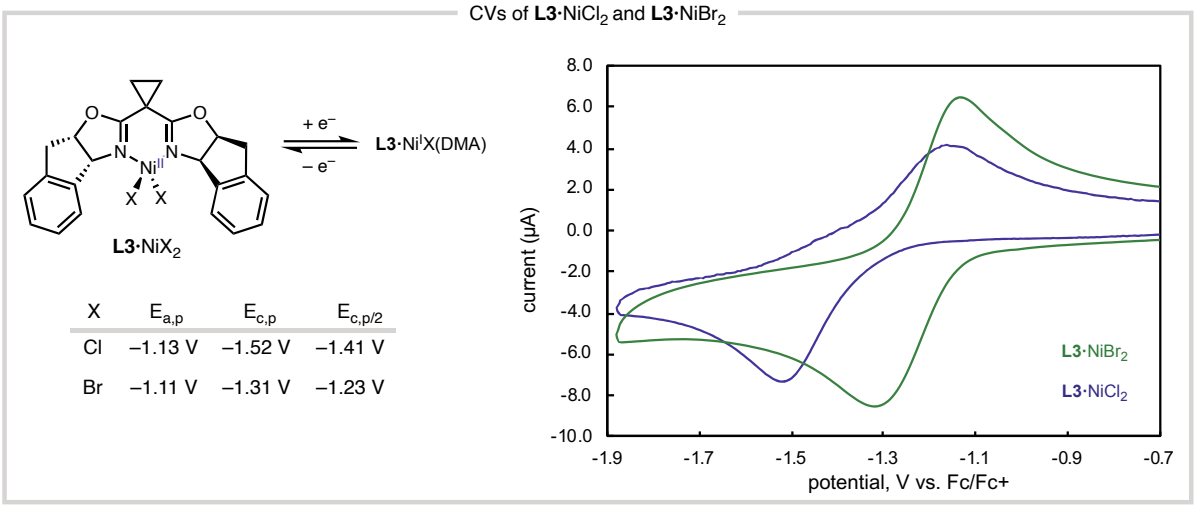

We first used cyclic voltammetry (CV) to determine the reduction potentials of **L3**·Ni^{II}Br$_2$ and **L3**·Ni^{II}Cl$_2$; these complexes (isolable as crystalline solids) catalyze the reductive alkenylations of both benzylic chlorides **201** and NHP esters **202** in comparable yields and slightly improved ee relative to *in situ* catalyst generation.[7,8] Electrochemically, **L3**·Ni^{II}Cl$_2$ and **L3**·Ni^{II}Br$_2$ exhibit irreversible reduction waves at $E_{p/2}$ = –1.47 V and –1.23 V vs. Fc$^{0/+}$, respectively (Figure 2.2). These reduction events have a large peak separation with the corresponding oxidation events, suggesting that a chemical change, such as halide loss, occurs rapidly upon one electron reduction. More detailed electrochemical studies of these pre-catalysts, performed by Hadt and coworkers,[13] support a single-electron reduction event to give

a **L3**·Ni^{I}X·DMA species (**204**). Notably, these studies suggest that reduction to **L3**·Ni^{0} does not proceed within the solvent window of DMA.

To verify the ability of TDAE to reduce **L3**·Ni^{II}Br$_2$ to **L3**·Ni^{I}Br (**204**), a solution of **L3**·Ni^{II}Br$_2$ in DMA was treated with TDAE ($E_{1/2}$ = –1.1 V vs. $Fc^{0/+}$); the resulting solution was frozen and analyzed by electron paramagnetic resonance (EPR) spectroscopy. A strong signal at g = 2.02 is assigned to the organic TDAE$^{+\bullet}$ radical **205**,[14] and the weaker signal (g_1 = 2.07, g_2 = 2.08, g_3 = 2.330) is assigned to a reduced **L3**·Ni^{I}Br species **204** (Figure 2.3, also see section 2.9.8.1). The same **L3**·Ni^{I}Br signal is observed when **L3**·Ni^{II}Br$_2$ is reduced with Ni(cod)$_2$. When Zn^{0} is used as the reductant, more pronounced changes are observed, which could potentially arise from the interaction between a **L3**·Ni^{I} species with the Zn^{II} formed upon oxidation (Figure 2.3).[15] We note that electrochemical and spectroscopic studies by Hadt and coworkers suggest that DMA can bind to both **L3**·Ni^{I} and **L3**·Ni^{II} redox states.[13] Given the strong variation of EPR signals and speciation of **L3**·Ni^{I} species observed herein, no formal assignments of the EPR signals are provided. Nevertheless, these data support the presence of **L3**·Ni^{I}X species forming from reduction under cross-coupling reaction conditions, and the nature of these species is clearly dependent on the reaction conditions.

Figure 2.3. *EPR analysis of reduced* ***L3***·NiX_2 *species.*

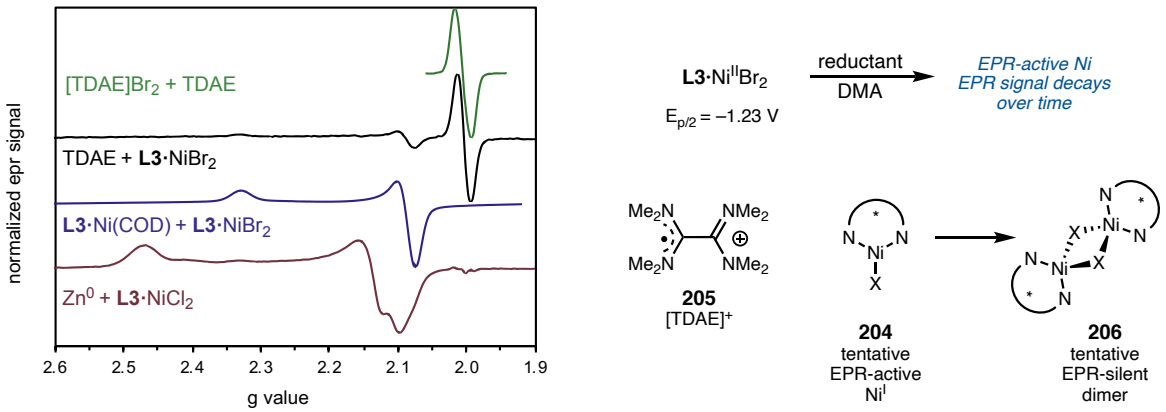

A time course of the Zn^{0} reduction of **L3**·NiCl$_2$ revealed that the observed EPR signals decrease over time (Figure 2.76-2.77, section 2.9.8.3) in concert with a change in the

corresponding UV-vis-NIR spectra (Figure 2.79-2.80, section 2.9.8.3), and the terminal EPR-silent mixture was catalytically inactive. Attempts to isolate **L3**·$Ni^{I}X$ complexes were unsuccessful; this might be due to the formation of **L3**·Ni^{I} oligomers like **206** in the absence of electrophiles **200**-**202**, or due to the difference in stability between DMA-bound and un-bound species (Figure 2.3).[10a,16,17]

2.3.2 Reactivity of Reduced Precatalyst with Substrates

To test whether the putative **L3**·$Ni^{I}Cl$ species formed upon reduction of **L3**·$Ni^{II}Cl_2$ can react with alkenyl bromide **200**, a series of CV studies were performed in the presence of **200** (Figure 2.4). A concentration-dependent increase in current was observed as [**200**] increased, which was accompanied by a loss of re-oxidation current. Taken together, these studies are consistent with reaction between **L3**·$Ni^{I}X$ and alkenyl bromide **200**.

Figure 2.4. *Investigating the reactivity of reduced* ***L3***·$NiCl_2$ *with substrates by CV.*

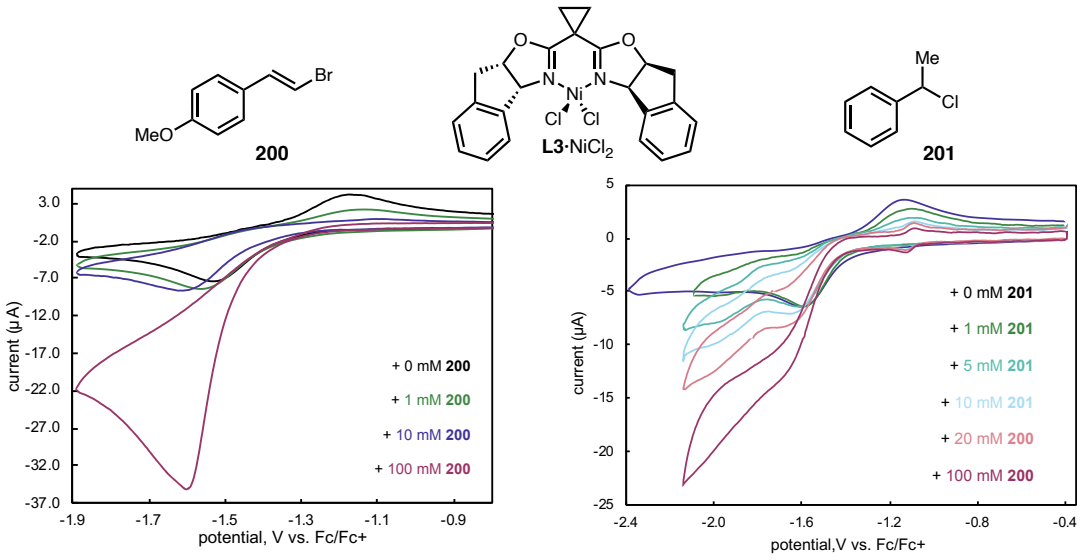

CV studies were also performed to investigate the reaction of in situ generated **L3**·$Ni^{I}Cl$ with **201**. CVs were acquired for **L3**·$Ni^{II}Cl_2$ (1.0 mM) in the presence of varying concentrations of **201** (1 – 100 mM), which also showed a concentration-dependent current with cathodic shifting of the onset potential and loss of the anodic return wave (Figure 2.4). This current

likely results from the reaction of the reduced **L3**·Ni complex reacting with **201**, presumably corresponding to the catalytic homocoupling to give **207**. In the presence of 100 mM **200** and **201**, regardless of the order of addition, a catalytic current consistent with the reaction with **200** is observed (Figure 2.5). The observation of a catalytic current resembling the reaction of **L3**·$NiCl_2$ and **200** when both electrophiles are present suggests that the reduced catalyst reacts more rapidly with **200**.

Figure 2.5. *Comparison of catalytic currents with substrates.*

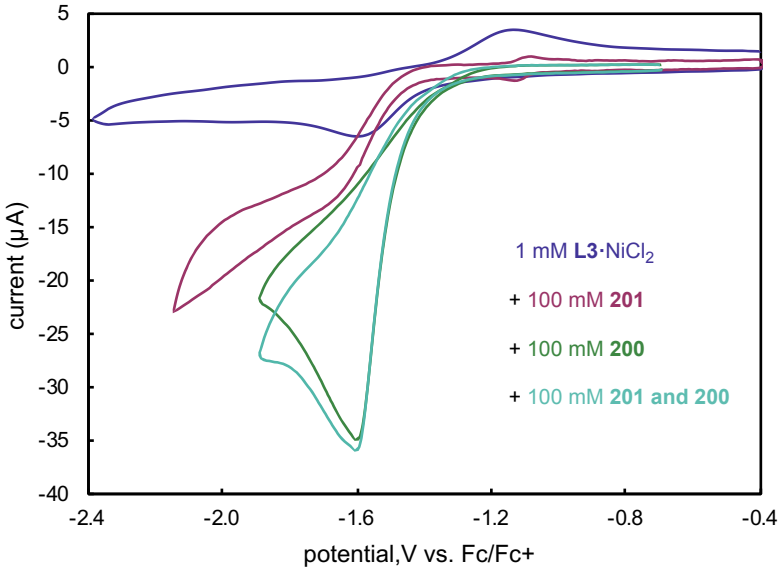

To interrogate the role of Ni in the activation of benzylic chloride **201**, a DMA solution of **201** was treated with Mn^0 (3.0 equiv) and NaI (0.5 equiv) and the formation of homodimer **207** was monitored (see section 2.9.5). No conversion of **201** or formation of **207** was observed at 0 or 23 °C, even with extended reaction times. In contrast, when **201** was subjected to identical conditions but **L3**·$Ni^{II}Cl_2$ (10 mol %; standard reaction conditions minus **200**) was added, **201** was cleanly converted to homodimer **207** over 60 min (Figure 2.55, section 2.9.5). These findings suggest that **L3**·$Ni^{I}X$ can activate **201**. This is consistent with the Mn-mediated Ni-catalyzed homodimerization reactions of **200** and **201**, in which the conversion of **200** is faster than the conversion of **201** under otherwise identical conditions (Figure 2.6). Taken together

with the CV studies, these data qualitatively suggests that the reductively generated **L3**·Ni^{I}Cl reacts faster with **200** and is consistent with previous RCC studies investigating the relative rates of Ni(I) complexes with aryl and alkyl electrophiles.[10b,11a,19]

Figure 2.6. *Stoichiometric homocoupling for comparing rates of electrophile activation.*

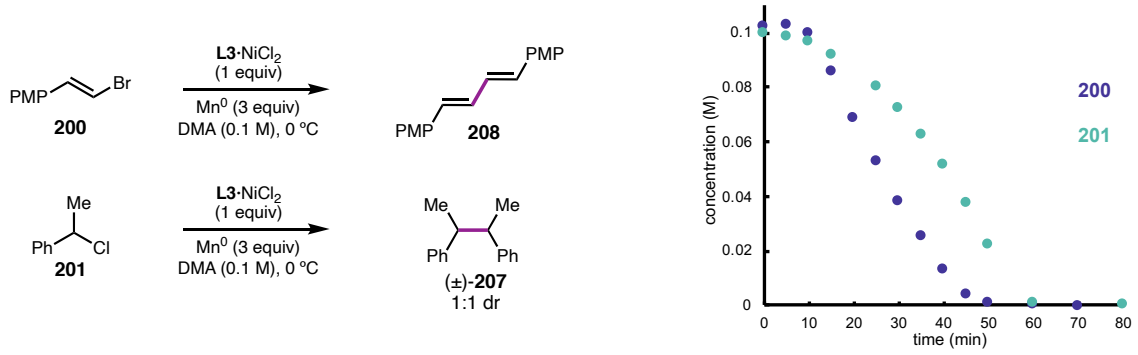

The mechanism shown in Section 2.6.3 is consistent with our observation that **L3**·Ni^{I}X (**204**) can react with both **200** and **201**, but that **200** reacts with **204** more rapidly. While we have demonstrated that **L3**·Ni^{I}Cl can perform the halogen atom transfer from benzylic chloride **201**, we cannot rule out the possibility that **212** is reduced and that the corresponding **L3**·Ni^{I}(alkenyl) species – which is calculated to be a stronger reductant[13] – mediates the XAT. We note that recent studies by Diao and coworkers have suggested that reduction of similar (biox)Ni^{II}(aryl)X complexes are unlikely to be reduced by Mn^{0}.[11b]

2.3.3 Kinetics of TDAE-Mediated ARA

Since the TDAE-driven **L3**·Ni-catalyzed ARA[8] is homogeneous and does not suffer from an induction period, we initiated our kinetic studies by determining the kinetic orders in **200**, **202**, and **L3**·NiBr$_2$ under standard reaction conditions (Figure 2.7a). For this, we employed Variable Time Normalization Analysis[18] (VTNA) to analyze the results of different excess experiments (Figure 2.7b–d). These experiments revealed a 1st order rate dependence on the concentration of NHP ester **202** (Figure 2.7c) and an inverse fractional order rate dependence on the concentration of **201** (Figure 2.7b). The inverse order in C(sp^2) electrophile observed in

this reaction (and the Mn^0-mediated reaction, *vide infra*) has also been observed previously for a related (bpy)Ni-catalyzed RCC of aryl and alkyl halides.[10a] Interestingly, there is an apparent 0^{th} order rate dependence on **L3**·$NiBr_2$ at loadings similar to the optimized conditions (5 and 10 mol %, Figure 2.7d); however, a positive rate dependence develops at low catalyst loadings (<1 mol %). The observation that the catalyst loading does not influence the rate of product **203** formation has not been previously reported for Ni-catalyzed RCC reactions.[10,11]

Figure 2.7. *Kinetic orders in substrates and catalyst.*

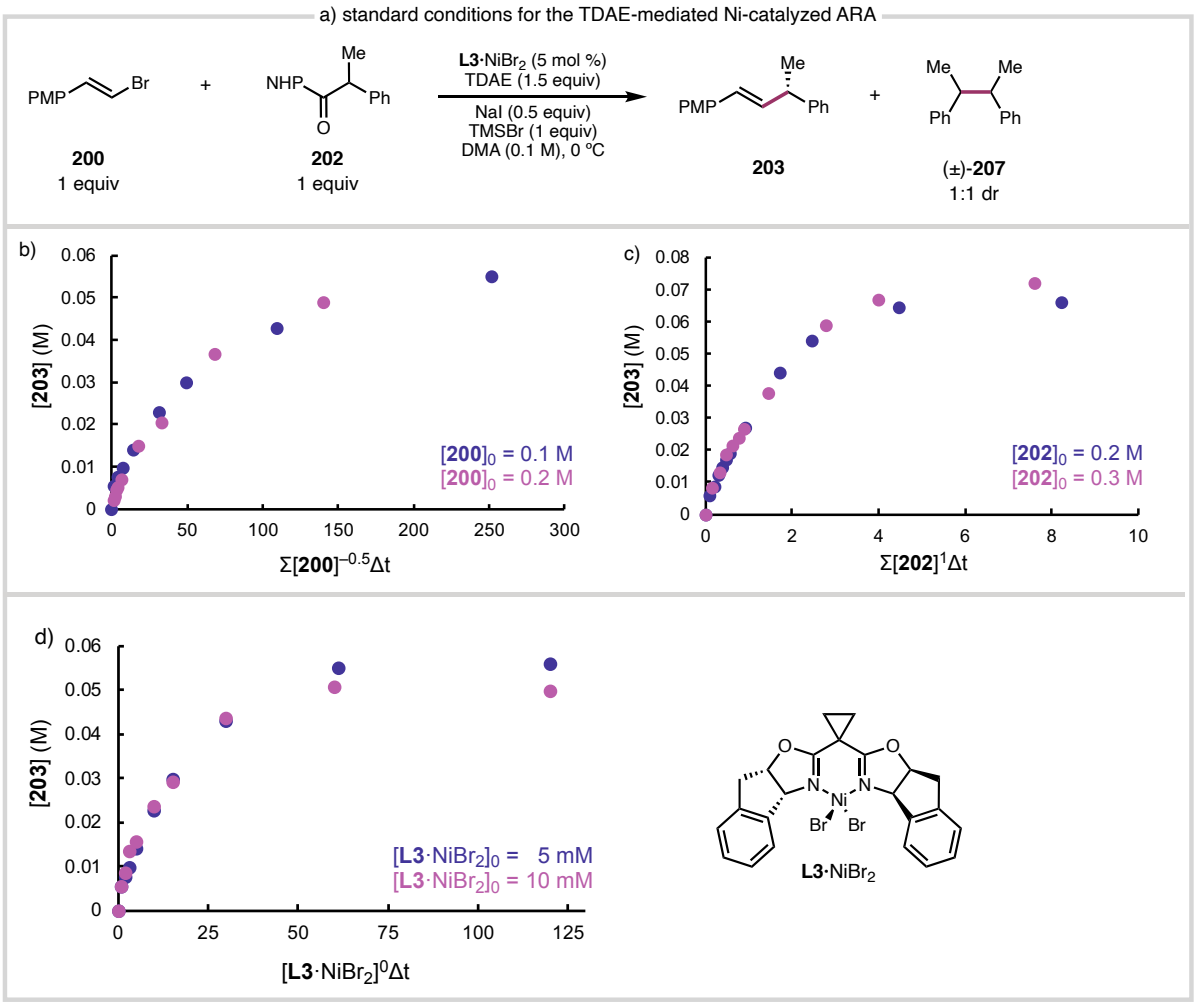

Figure 2.8. *Rate dependence on TDAE reductant and TMSBr additive.*

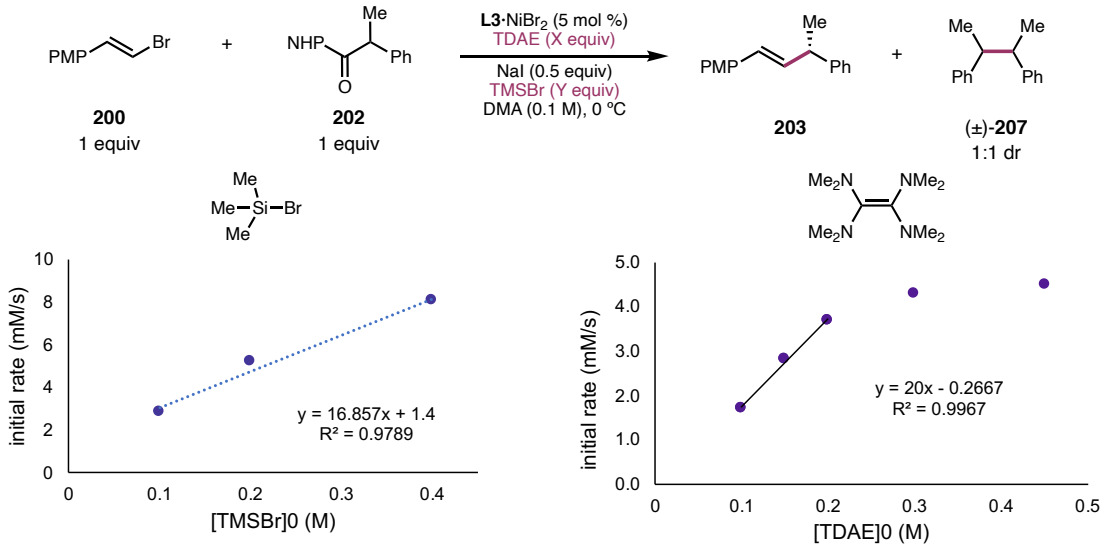

The reaction rate as a function of [TDAE] and [TMSBr] was also studied by method of initial rates due to the inability to quantify the concentration of the respective species as we did in the VTNA experiments. In the absence of either component no product **203** is produced but **200** is converted to homocoupled **208** in the absence of TMSBr with no conversion of **202**. These experiments show that by varying the initial concentration of TMSBr from 1 to 4 equivalents, shows a positive rate dependence with little change to the product distribution (Figure 2.8). Similarly, the TDAE reductant also has a positive rate dependence from 1-2 equiv and then becomes saturated, or pseudo 0^{th}-order, at >2 equiv (Figure 2.8).

Figure 2.9. *Electrophile conversion and byproduct formation as a function of catalyst loading.*

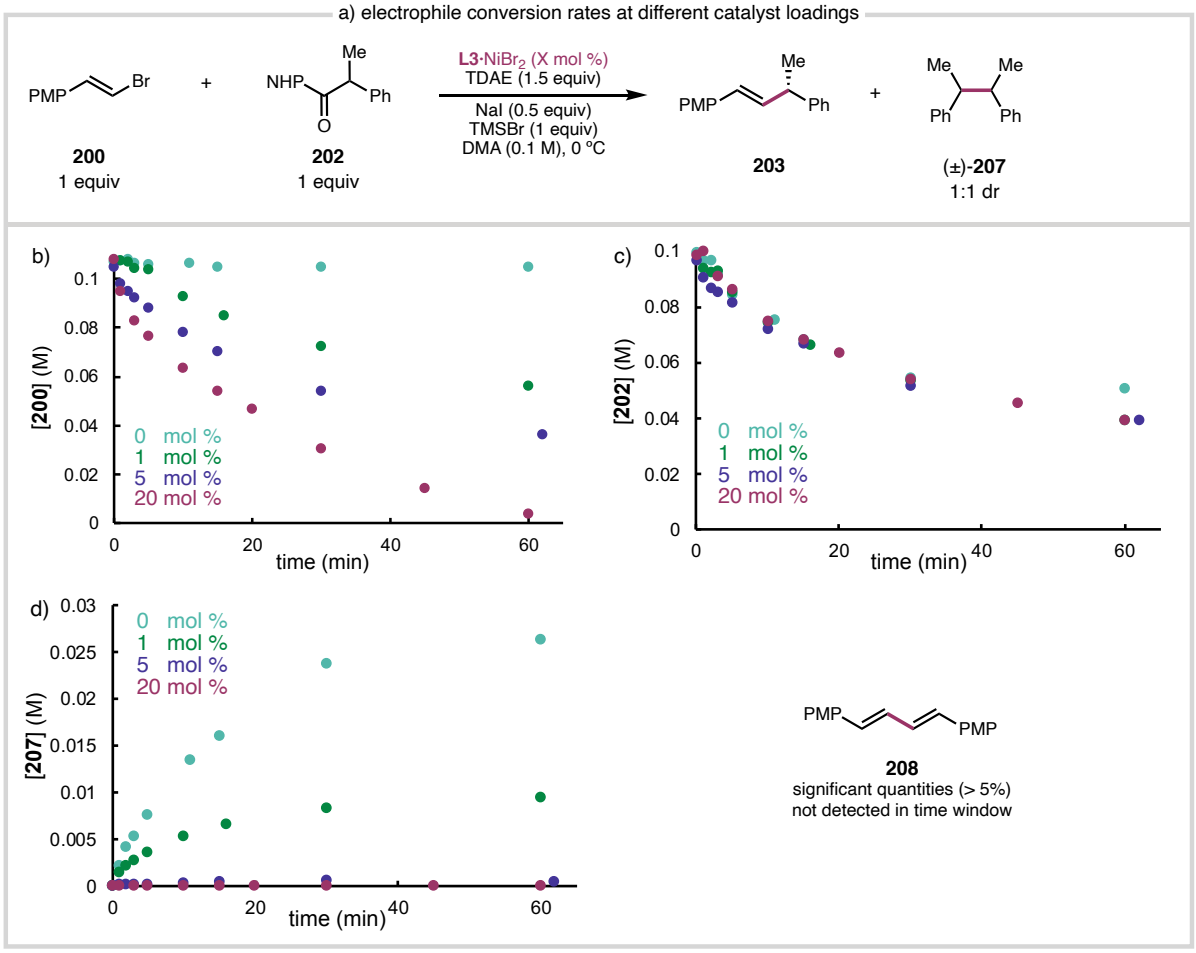

To further investigate this unusual rate dependence on catalyst **L3**·$NiBr_2$, the concentration of **200**, **202**, and homodimer **207** were monitored over time, at different concentrations of Ni (Figure 2.9b-d). The conversion of alkenyl bromide **200** shows a clear rate dependence on the concentration of Ni (Figure 2.9b). In contrast, the rate of conversion of NHP ester **202** is independent of [Ni]: even in experiments where **L3**·$Ni^{II}Br_2$ is omitted, **202** is consumed at the same rate as when using 20 mol % Ni (Figure 2.9d). Correspondingly, as the concentration of Ni decreases, the yield of cross-coupled product **203** decreases and the yield of homocoupled product **207** (formed as a 1:1 diastereomeric mixture) increases (Figure 2.9d). These data are consistent with generation of a cage-escaped benzylic radical from **202** by a non-Ni-catalyzed process. This represents a distinct mode of NHP ester activation for the **L3**·Ni-catalyzed RCC

in comparison to the (bpy)Ni-mediated coupling of NHP esters reported by Weix[19] and Baran,[20] in which a (bpy)Ni^{I}–Ar is proposed to reduce the NHP ester by single electron transfer (SET).

2.4 DETERMINING THE CATALYST RESTING STATE

2.4.1 Using EPR to Detect a Paramagnetic Catalyst Resting State

Figure 2.10. *Reaction monitoring by EPR to detect paramagnetic Ni resting state.*

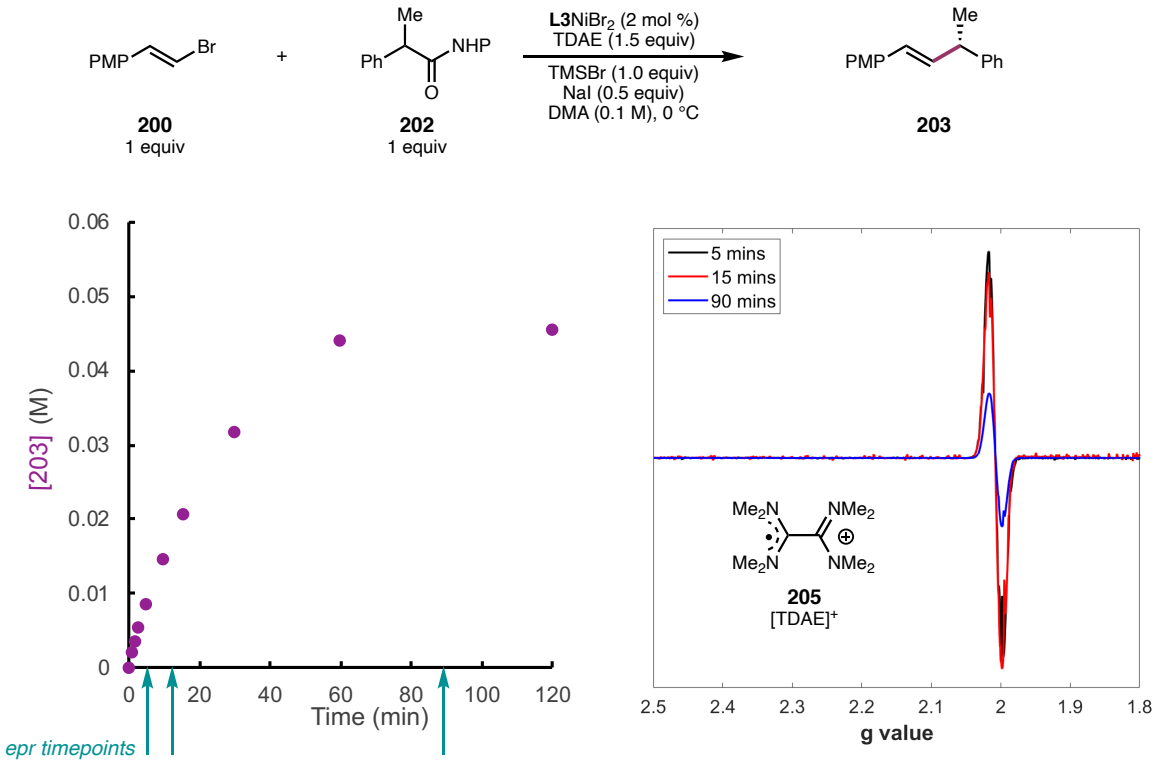

At this stage, we sought to determine the resting state of the Ni catalyst under the reaction conditions. If a Ni^{I} or Ni^{III} intermediate were the resting state, then it could be observable by EPR. The Ni-catalyzed reaction of **200** and **202** was performed using 2 mol % **L3**·$NiBr_2$ under otherwise standard conditions and aliquots were removed, filtered, and frozen in an EPR tube. No signal corresponding to a metal-based radical was observed by EPR; instead, a signal consistent with an organic radical was observed, which decreased in intensity over time (Figure 2.10). This species was assigned as **205** by comparison to an independently prepared sample

(Figure 2.71, section 2.9.8) and previously reported spectra.[14] Although this does not rule out a Ni^{I} or Ni^{III} resting state, we sought to investigate other possibilities.

2.4.2 NMR Reaction Monitoring For Diamagnetic Resting State

Figure 2.11. *Electrophile conversion and byproduct formation as a function of catalyst.*

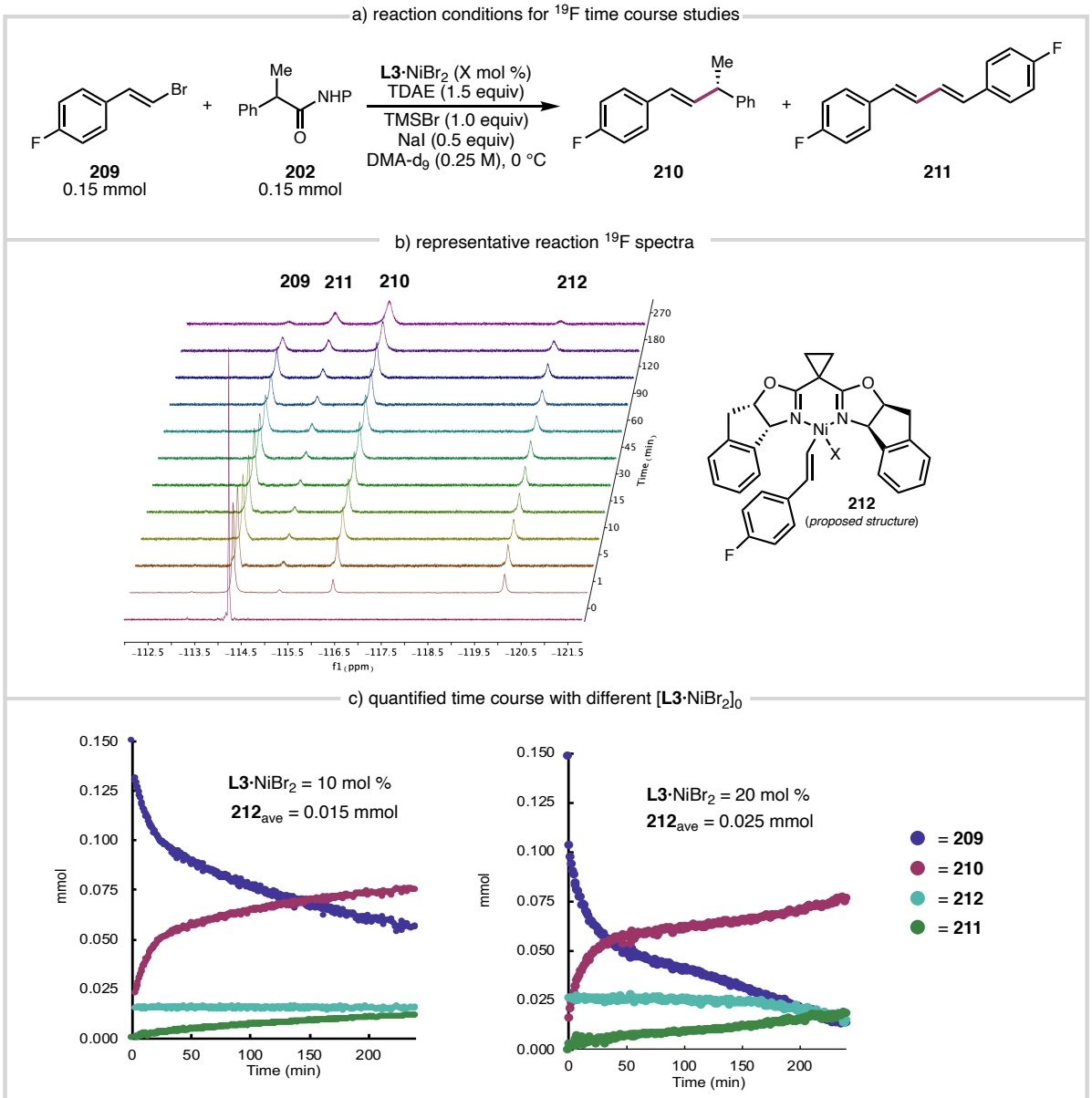

Given the rapid reaction of **L3**·Ni^{I}Cl with alkenyl bromide **200** (Figure 2.5), and prior RCC mechanistic studies,[10b,11a] we hypothesized that the catalyst resting state likely resides after oxidative addition of the C(sp^2)-electrophile. To monitor the reaction by *in situ* ^{19}F NMR, ^{19}F-labeled alkenyl bromide **209** was used and all alkenyl bromide-derived species were tracked

over the course of the reaction (Figure 2.11a). Upon the addition of TDAE (0.23 mmol, 1.5 equiv) to a solution of **209** (0.15 mmol), **202** (0.15 mmol), **L3**·$NiBr_2$ (0.015 mmol, 10 mol %), TMSBr (0.15 mmol), and NaI (0.075 mmol) in DMA-d_9, the signal corresponding to **209** decreases and several signals emerge that were assigned to product **210** (δ =–116.5 ppm), homocoupled diene **211** (δ =–115 ppm), and a new, broad signal at δ =–120 ppm (Figure 2.11b). This species persisted throughout the reaction, maintaining steady concentration corresponding to 15 μmol, or 10 mol %, which is the concentration of **L3**·$NiBr_2$ used in the reaction. When this experiment was repeated with 20 mol% **L3**·$NiBr_2$, the concentration of this species corresponded to 17 mol% (25 μmol) for the first 2.5 hours of catalysis and then decreased as the reaction approached the last few turnovers, eventually disappearing at the end of the reaction (Figure 2.11c). Although attempts to isolate this species or prepare it independently have been unsuccessful due to its instability, we assign this intermediate as a diamagnetic Ni^{II} oxidative addition complex **212**.[21]

2.4.3 Mechanistic Summary of TDAE-Mediated Reaction

Taken together, a mechanism for the TDAE mediated Ni-catalyzed RCC is proposed in Figure 6. Upon reduction of the Ni precatalyst, the resulting **L3**·$Ni^{I}Br$ (**204**) rapidly reacts with alkenyl bromide to give Ni^{III} species **213** which can be reduced to furnish resting state species **212**. Given Hadt and coworker's studies,[13] it is possible that DMA is coordinated to **204** during oxidative addition. While the reductant in this oxidative addition-reduction sequence is not known, we propose that the oxidative addition step is fast and reversible since we can observe the formation of alkenyl iodide and chloride products (when a Cl^- source is present).[8,22] The Ni^{II} complex **212** can then intercept NHP ester-derived radical **214** to give Ni^{III} complex **215** which can undergo reductive elimination to give product **203**. NHP ester **202** is activated by TMSBr followed by reduction with TDAE in the turnover-limiting step (*vide infra*). This reduced species undergoes N–O homolysis and subsequent decarboxylation to give **214** (Figure

2.12).

Figure 2.12. *Mechanism of TDAE-mediated ARA.*

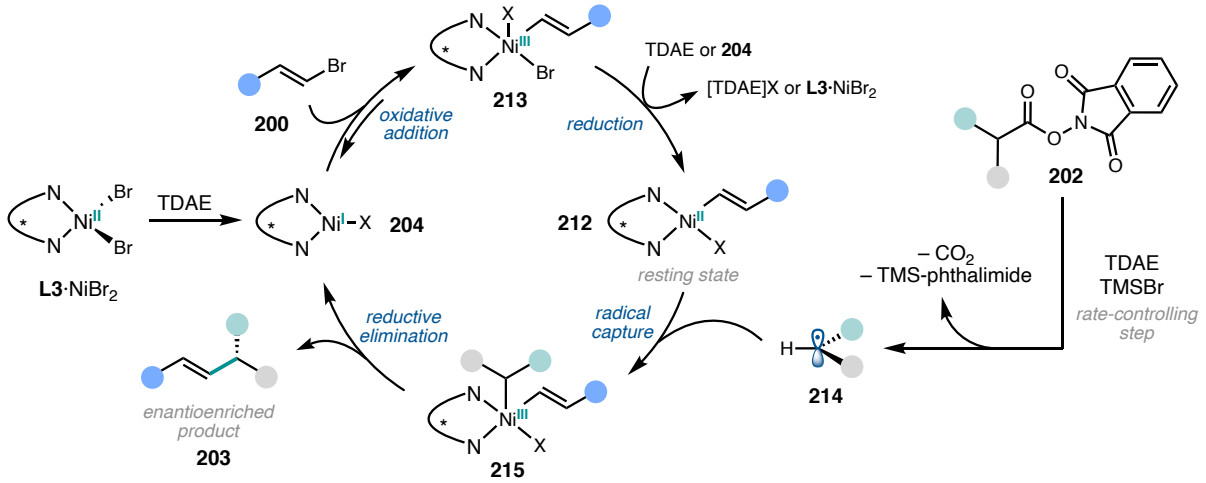

2.5 MECHANISM OF NHP ESTER ACTIVATION

2.5.1 NHP Ester Reduction

Given that the kinetic studies revealed that the NHP ester **202** is not reduced by Ni, we hypothesized that it is instead reduced by TDAE. To test this hypothesis, NHP ester **202** was treated with TDAE in DMA and the formation of homodimer **207** was monitored as an indirect measurement of benzylic radical (**214**) generation. In the absence of additional additives, the mixture of **202** and TDAE results in minimal conversion to homodimer **207**, even at ambient temperature (Figure 2.13a, purple). This can be rationalized by the difference in reduction potential of NHP ester **202** ($E_{p/2} = -1.62$ V vs. $Fc^{0/+}$), which is 0.5 V more cathodic than TDAE ($E_{1/2} = -1.11$ V vs. $Fc^{0/+}$); the irreversible loss of CO_2 following SET does not appear to be sufficient to drive the thermodynamically unfavorable process. Similarly, the mixture of **202**, TDAE, and NaI also fail to produce homodimer **207** (Figure 2.13a, green).

In contrast, when TDAE is added to a mixture of **202** and TMSBr (1.0 equiv), **202** is converted to **207** at a rate that is comparable to the rate of **202** conversion in the catalytic

reaction (Figure 2.13a, teal). We note that TMSBr is essential to form **203** in high yields under standard reaction conditions (19% yield **203** when TMSBr is excluded). The rate is increased further (k_{rel} = 1.5) when both TMSBr and NaI are present, presumably through the *in situ* generation of TMSI (Figure 2.13a, maroon). We propose that the silyl halide additive functions as a Lewis acid to lower the reduction potential[23] of the NHP ester through formation of **216** which can be reduced by TDAE to furnish radical **214** (Figure 2.13b).

Figure 2.13. *Additive effects on NHP ester reduction by TDAE.*

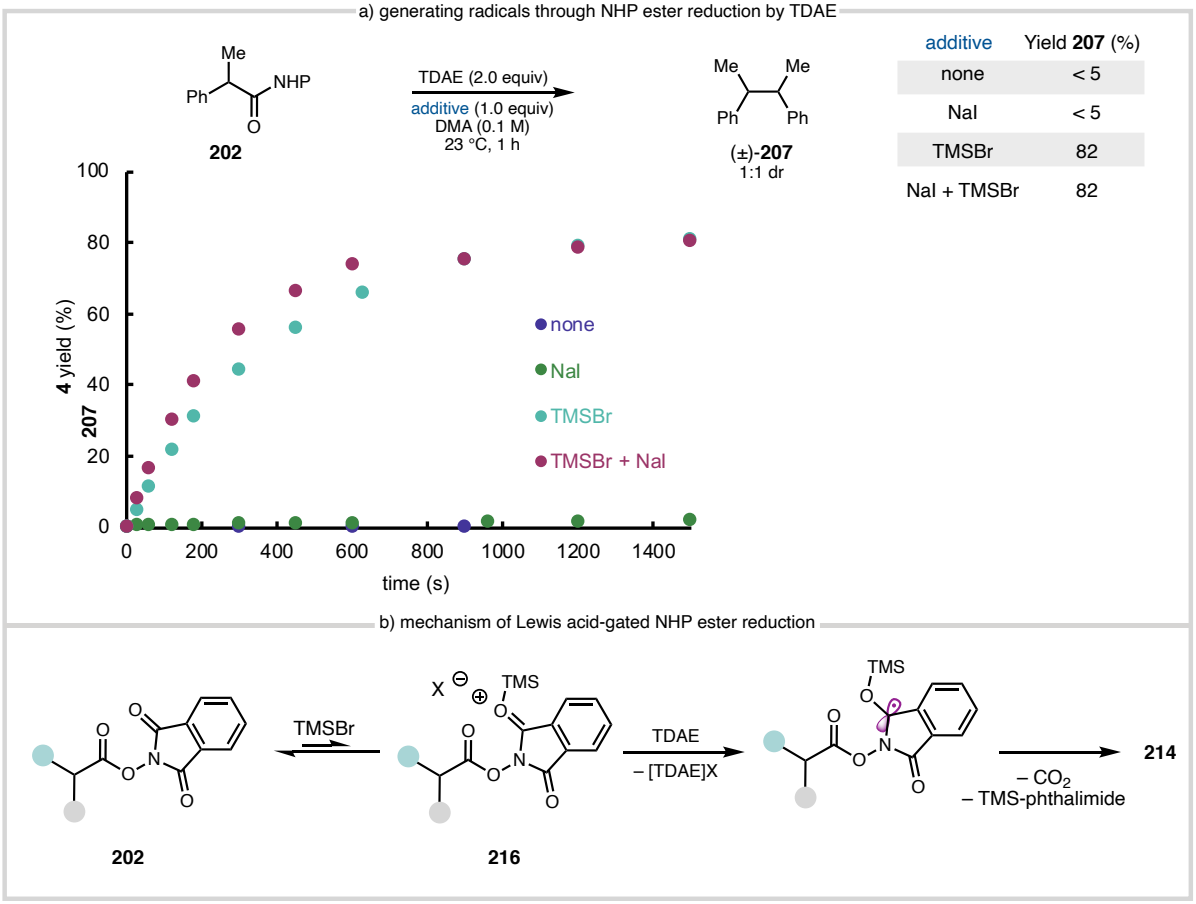

2.5.2 Additive Effects on Rate of NHP Ester Reduction by TDAE

The observation that a Lewis acid gates NHP ester reduction inspired us to question whether the rate of radical generation could be tuned by using TDAE in combination with different Lewis acids, similar to Weix's work tuning rate of radical generation by using derivatized NHP esters.[24,25] To test this, we measured the rate of radical generation (as

d[**207**]/dt) in the presence of a variety of Lewis acids (Figure 2.14a). The more sterically hindered triethylsilyl bromide (TESBr) results in a 3-fold decrease in the rate (k_{rel} = 0.34) of radical generation. Further investigation of different silyl halides revealed an intuitive trend in sterics (TBS<TES<TMS), with larger groups slowing down radical generation, as well as the leaving group identity (Cl<Br<OTf<I)[26], with the better leaving group accelerating radical generation (Figure 2.14b). As observed with TMSBr (Figure 2.13a, purple), addition of NaI as a co-additive to various R_3Si–Cl additives can increase the rate by more than 2-fold. Increasing the concentration of TMSBr increases the rate (k_{rel} = 1.68), presumably by driving the equilibrium to increase the concentration of silylated NHP ester **216**. Additionally, non-silyl Lewis acids can also increase the rate of **202** reduction by TDAE. We have quantified the ability of several common additives[27] to modulate the rate of radical generation, with rates spanning three orders of magnitude (Figure 2.14a).

Figure 2.14. *Kinetics of NHP ester reduction with different Lewis acids.*

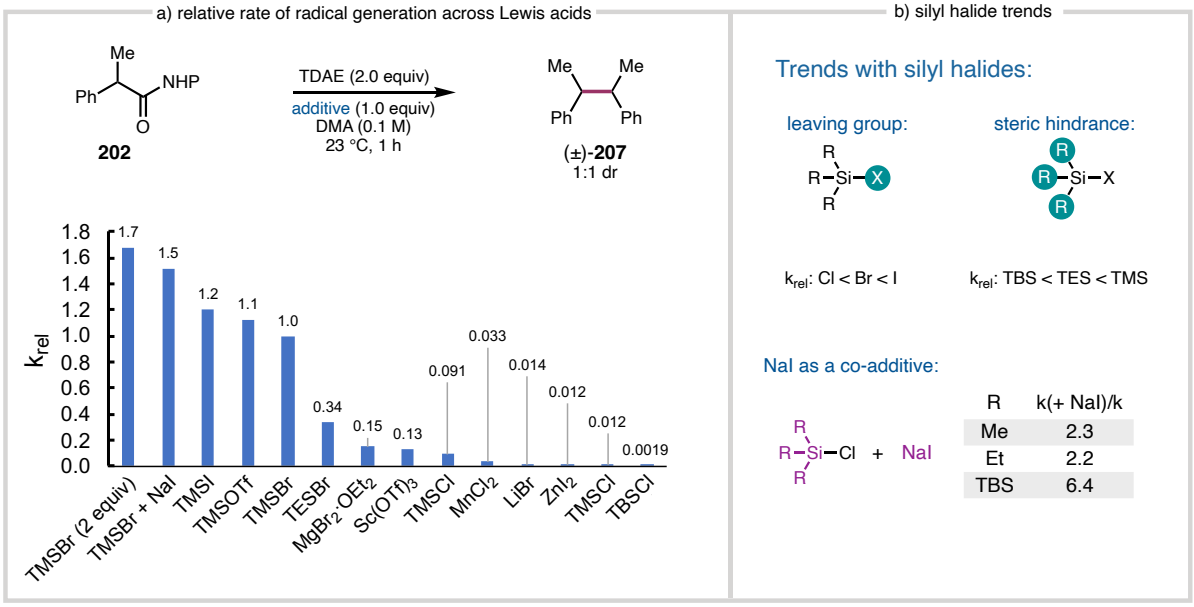

2.5.3 Reevaluating Optimized ARA Conditions

Figure 2.15. *Impact of Lewis acid on optimal catalyst loadings.*

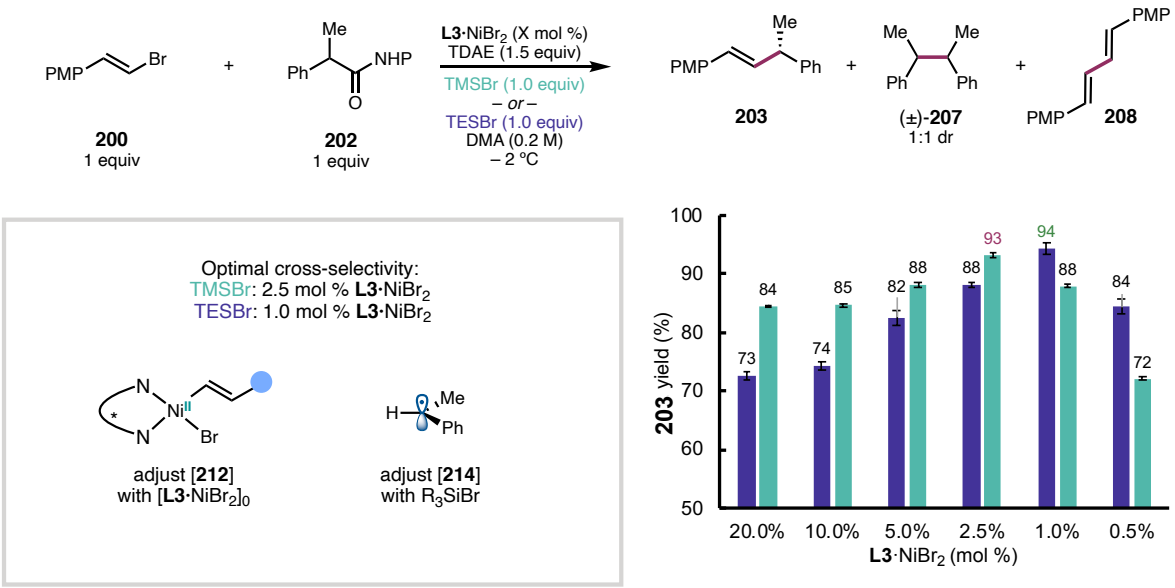

After demonstrating the rate of NHP ester activation can be tuned with different Lewis acid additives, we sought to investigate how the yield of product was effected by the silyl additive. Although the ARA reaction between **200** and **202** was initially reported using TMSBr, we observed that at lower catalyst loadings, increased amounts of benzyl dimer **207** is formed (Figure 2.9d). We hypothesized that slower rate of radical generation could improve the yield of **203** at low catalyst loadings by better matching of the relative concentrations of the resting state species **212** and benzylic radical **214**. Given that TESBr decreases the rate of benzylic radical formation by 3-fold (Figure 2.14a), we performed a series of experiments varying the concentration of **L3**·$NiBr_2$ in the presence of either TMSBr or TESBr (Figure 2.15). First, we note that for this well-performing substrate pair, high yields can be maintained using 1 mol% **L3**·$NiBr_2$. Second, we note that TMSBr performs better relative to TESBr when 20 mol% **L3**·$NiBr_2$ is used (higher concentration of resting state **212**) and performs worse than TESBr at 0.5 mol% **L3**·$NiBr_2$, when rapid release of benzyl radical would outpace radical capture by resting state **212** (Figure 2.15). Using 0.5 mol% **L3**·$NiBr_2$, higher yield of **203** was obtained

with TESBr (84% yield) than with TMSBr (72% yield), which we propose results from slower release of the benzyl radical. Analysis of the product profiles for each bromosilane shows that the ratio of cross-coupled to homocoupled products reaches a maxima at 2.5 mol % Ni for TMSBr (k_{rel} = 1.0) and 1 mol % Ni for TESBr (k_{rel} = 0.34) (Figure 2.82 and 2.83, section 2.9.9), which is consistent with the trends observed in yield. We anticipate these data can serve as a roadmap for optimizing reaction conditions for new substrate combinations.

2.6 INVESTIGATION OF HETEROGENOUS ARA REACTION

2.6.1 Kinetic Studies on ARA with Benzyl Chlorides

Kinetic studies of the heterogenous metal-powder conditions (Figure 2.1a) proved more challenging than the homogenous TDAE-mediated reaction (Figure 2.1b). We observe long induction periods (up to 90 minutes) and reaction times of 6 hours using previously reported conditions.[7] The induction period and reaction times can be shortened to 30 and 100 min, respectively, by pre-activating the Mn^0 with HCl. Use of Zn^0 powder further improved the reaction times (5–10 minute induction period and 45 minute reaction times, Figure 2.36, section 2.9.3.1) and provided product in comparable yield and with only slightly lower enantioselectivity as Mn^0 (Zn: 91% yield, 90% ee; Mn: 96% yield, 96% ee). Both Mn^0 and Zn^0 gave reactions with linear rates of product formation, indicative of mass transport-limited reduction; however, Zn^0 displayed a less significant stir rate dependence that saturated >1000 rpm (Figure 2.35, section 2.9.3.1). Use of 6 equiv Zn^0 slightly increased the reaction rate by a factor of 1.1, similar to observations by Weix[10b] and Diao[11a] in related arylation reactions (Figure 2.37, section 2.9.3.1). These modified reaction conditions (Figure 2.16a) enabled the collection of reproducible kinetic data where the heterogenous reduction events are not as significantly rate limiting, allowing us to probe the rate influences of other reaction components.

Figure 2.16. *Kinetics of Mn-mediated ARA reaction.*

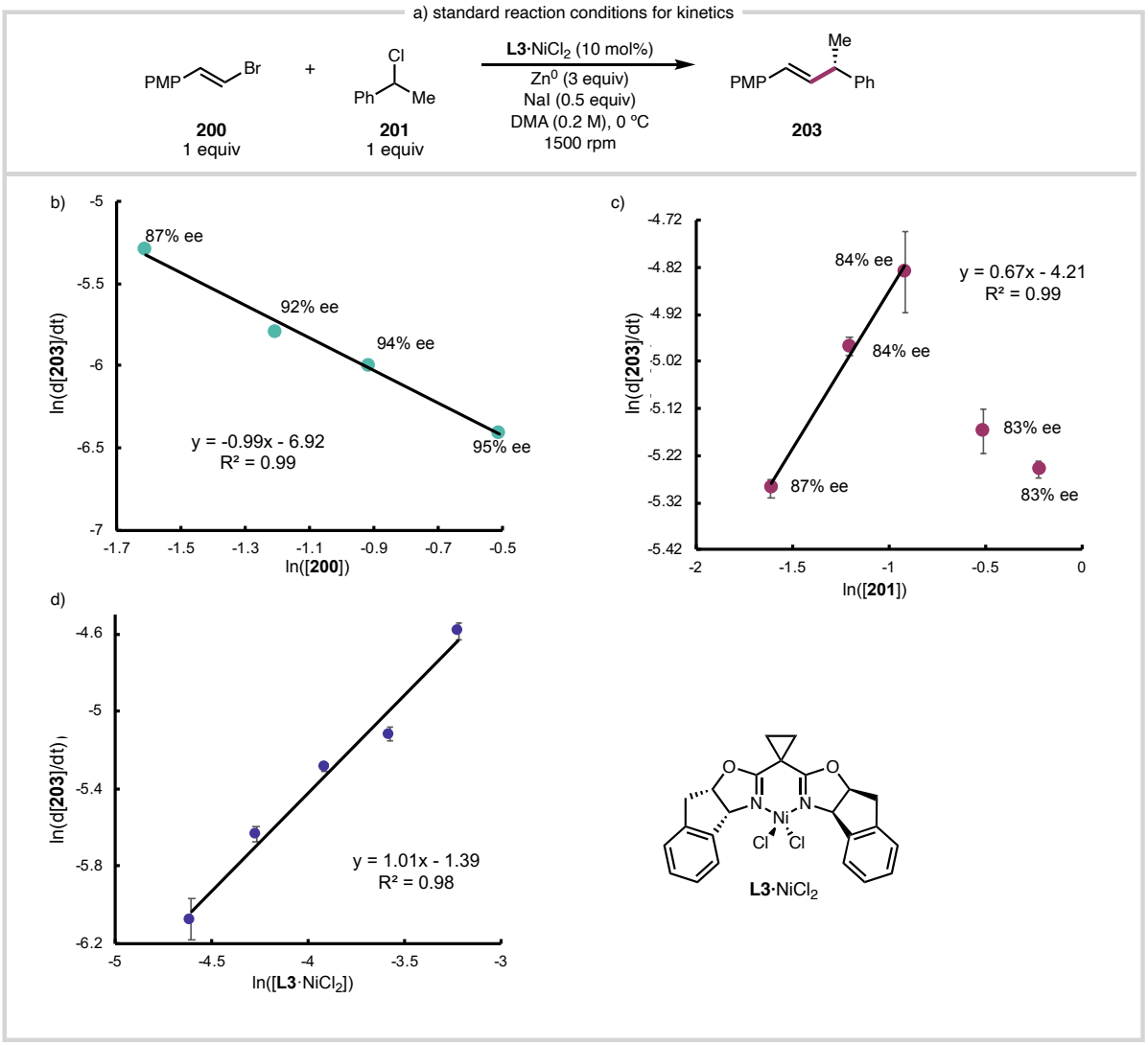

Kinetics experiments reveal a first-order rate dependence on [**L3**·$NiCl_2$], unlike the TDAE system, across catalyst loadings ranging from 5 mol % to 20 mol % (Figure 2.16d). The reaction exhibits a negative first-order rate dependence on $[\mathbf{200}]_0$ (Figure 2.16b), similar the TDAE-mediated system but to a lesser extent (Figure 2.7b). The rate dependence on $[\mathbf{201}]_0$ is more complex: a fractional positive rate dependence was observed at 1.0 and 2.0 equivalents of **201**, but the rate decreases again when >2.0 equiv **201** is employed (Figure 2.16c). Notably, as $[\mathbf{201}]_0$ increases, the ee of **203** decreases. Taken together, these data might indicate that there are competing mechanisms that depend on the concentration of $[\mathbf{201}]_0$. One possibility is that when [**201**]>>[**200**], the reaction of **L3**·$Ni^{I}X$ with **201** begins to compete with the reaction

between **L3**·Ni^{I}X and **201**, therefore reversing the order of oxidative addition of the electrophiles to Ni.

2.6.2 Stoichiometric Experiments

Scheme 2.1. *Stoichiometric Ni^{0} couplings with both C(sp^{3}) electrophiles.*

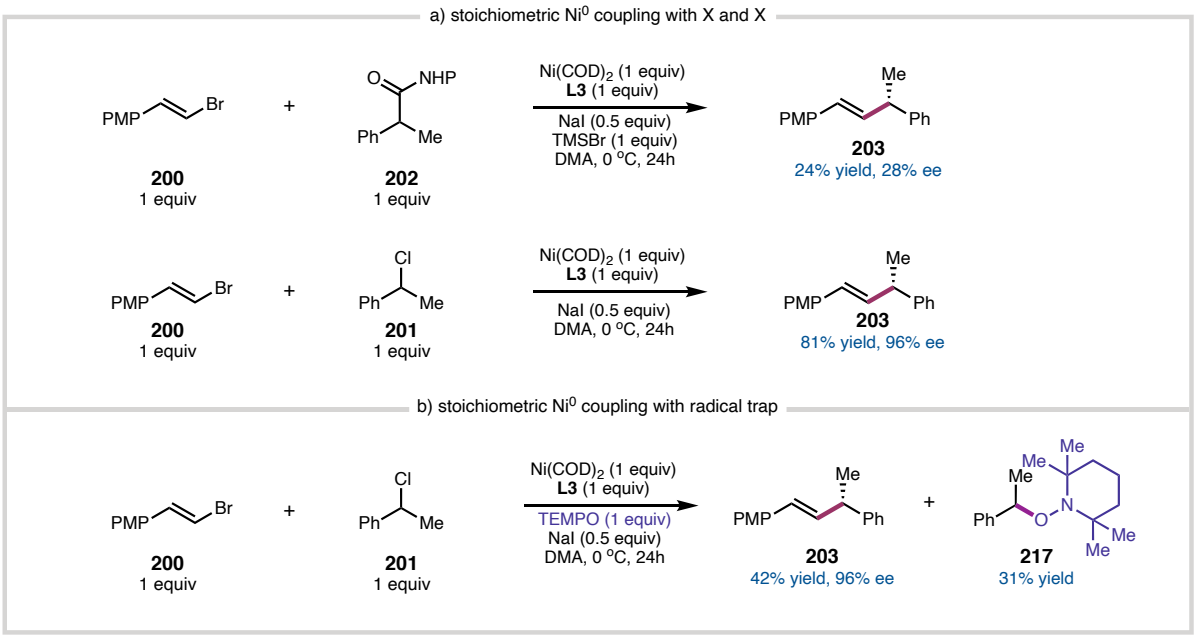

While the inclusion of a stoichiometric reductant is required to render the reaction catalytic, we wanted to investigate if reagents like Zn^{0}, Mn^{0}, or TDAE are required for product formation. A stoichiometric reaction was conducted using equimolar quantities of **L3**, Ni(cod)$_{2}$, alkenyl bromide **200**, and benzyl chloride **201** or NHP ester **202** (Scheme 2.1a) in the *absence* of exogenous reductant. The Ni-mediated reaction with **201** gave product **203** in 78% yield and 96% ee while using NHP ester **202** also formed **203** albiet in 24% yield and 28% ee. Addition of radical trap 2,2,6,6-tetramethyl-1-piperidinyloxy (TEMPO) significantly reduced the yield of **203** (42% yield, 96% ee) due to the formation of the benzyl-tempo adduct **217** (31% yield) (Scheme 2.1b). This shows that the **L3**·Ni^{0} can facilitate the enantioselective RCC reaction with **202**, possibly through a mechanism that is less selective than the optimized reaction conditions.

2.6.3 Mechanistic Summary of Mn-Mediated Reaction

Based on our experimental studies, a proposed mechanism for the Mn-mediated Ni-catalyzed ARA is shown in Figure 2.17. Upon reduction of precatalyst **L3**·$Ni^{II}Cl_2$ the resulting complex **204** reacts with alkenyl bromide **200** in an oxidative addition-reduction step to give **L3**·Ni(II) complex **213**. This could proceed by a bimolecular oxidative addition as proposed by Diao,[11a] or by reduction of the transiently formed Ni(III) species **213** by Mn^0. Ni-catalyzed halide atom abstraction (XAT) from benzylic chloride **201** gives rise to a cage-escaped radical **214** that can be captured by **212** to yield product **203** following reductive elimination.

Figure 2.17. *Mechanism of Mn-mediated ARA*

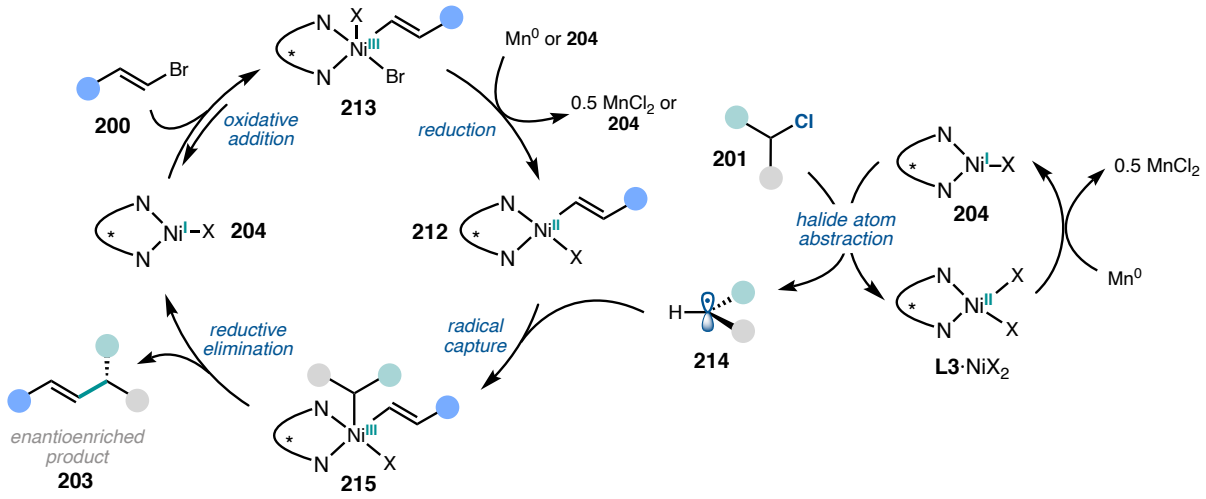

2.7 COMPUTATIONAL INVESTIGATION ON THE ORIGIN OF ENANTIOSELECTIVITY

Figure 2.18. *ee's of products produced from Mn- and TDAE-mediated ARA are similar.*

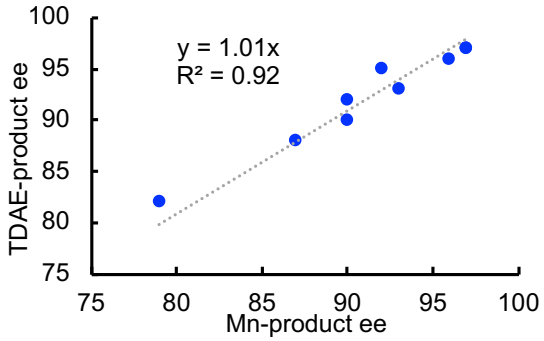

A comparison of the enantioenrichment of the common products isolated from the optimized TDAE conditions (Figure 2.1b) and Mn^0 conditions (Figure 2.1a) shows a good correlation across the two reactions (Figure 2.18).[8] This suggests that despite the differences in mechanism, conditions, and radical precursors, the enantiodetermining step may be the same in both reactions. This inspired our team to investigate the enantiodetermining step of the reaction as well as the origin of enantioinduction in this stereoconvergent transformation.

Figure 2.19. *Sterics of chiral ligand effects diastereoselective radical capture.*

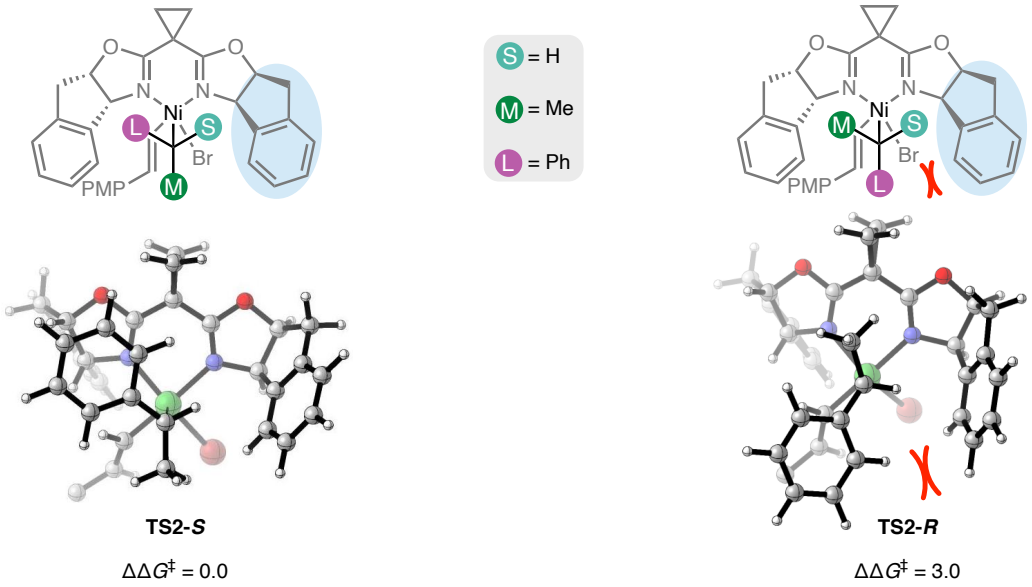

To explore the origins of enantioinduction, the structures and relative Gibbs free energies of the competing transition states for addition of radical **214** to resting state complex **212** were computed (Figure 2.19). The free energy difference between **TS2-*S*** and **TS2-*R*** is computed to be 3.0 kcal/mol, which slightly overestimates the enantioselectivity for the reaction. In both transition states, the smallest substituent of the approaching benzyl radical (**214**), hydrogen, is pointing towards the sterically bulky part of the ligand (highlighted in teal in Figure 2.19). This allows the largest substituent, the phenyl group, to project away from this region of the ligand in the favored transition state **TS2-*S***. In the disfavored transition state **TS2-*R***, the phenyl group is proximal to the bulky region of the ligand. This results in an almost perfectly staggered approach of the benzyl radical with respect to the Ni ligands in **TS2-*S***, while steric repulsion from the ligand forces the benzyl radical to adopt a more eclipsed conformation in **TS2-*R***.[28] Subsequent reductive elimination for **215-*S*** is facile with a computed barrier of 0.9 kcal/mol (Figure 2.20) for the major pathway. These calculations suggest the facial selectivity of the enantiodetermining radical addition is influenced by the steric environment of BOX ligand **L3** (Figure 2.20).

Figure 2.20. *Potential energy surface of radical capture and reductive elimination.*

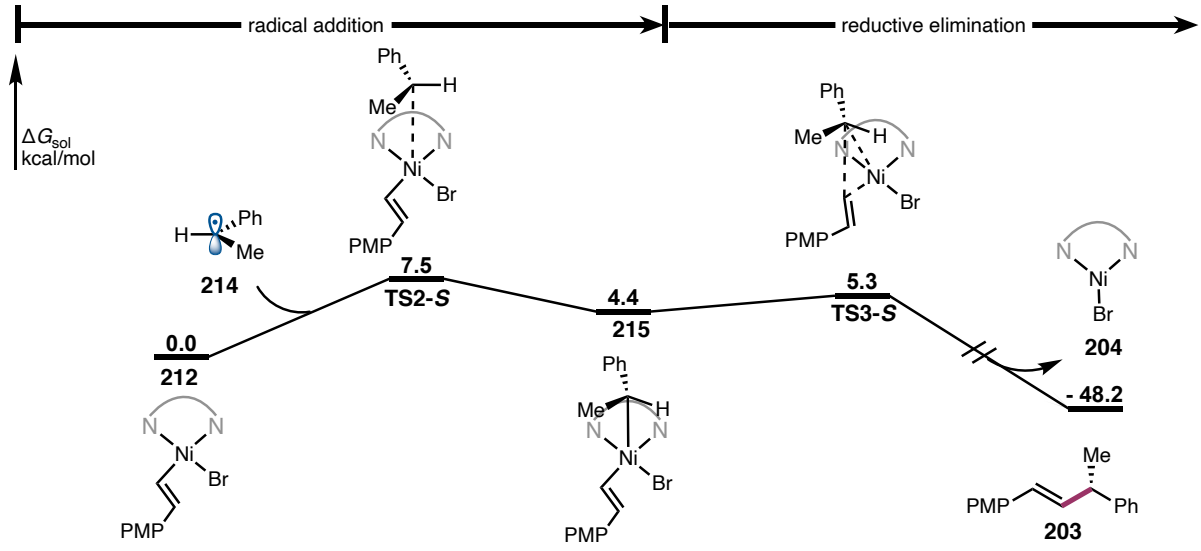

2.8 CONCLUDING REMARKS

In summary, we have investigated two Ni-catalyzed asymmetric RCC reactions to determine how changing the reductant and C(sp^3) electrophile influences the reaction mechanism. These reactions proceed through a $Ni^{I/III}$ cycle with fast activation of the alkenyl bromide electrophile by a Ni^{I} species. Both reactions have a rate-determining activation of the C(sp^3) electrophile to furnish a cage escaped benzyl radical. We have demonstrated that Ni is not required for NHP ester activation; instead, the combination of TDAE and TMSBr results in reductive decarboxylation to give the benzylic radical. The radical can then be intercepted by a Ni^{II}–alkenyl resting state that we were able to detect spectroscopically.

The fact that reduction of NHP esters by TDAE is Lewis acid-mediated, rate controlling, and independent of the alkenyl bromide activation has significant implications for the development of other Csp^3-Csp^n RCCs. This mechanistic regime allows for independent tuning of the rates of electrophile activation where d[Csp^3]/dt can be tuned with additives and d[Csp^2]/dt through catalyst design. It is our hope that these findings aid in the adoption of C(sp^2)–X reductive couplings with NHP ester fragments in more complex settings by providing a framework to guide reaction optimization.

2.9 EXPERIMENTAL SECTION

2.9.1 Materials and Methods

Unless otherwise stated, reactions were performed under a N_2 atmosphere using freshly dried solvents. All reagents were purchased from commercial suppliers (Sigma Aldrich, Combi- Blocks, TCI, Enamine, Strem) and used without further purification unless mentioned otherwise. Tetrahydrofuran (THF), acetonitrile (MeCN), and methylene chloride (CH_2Cl_2) were dried by passing through activated alumina columns. Anhydrous dimethylacetamide (DMA) was purchased from Aldrich and stored in a N_2-filled glovebox. $NiCl_2$·dme was purchased from Strem and stored in the glovebox. Manganese powder (~325 mesh, 99.3%) was purchased from Alfa Aesar. Zinc dust (97.5%) was purchased from Strem. NaI (anhydrous, 99%) was purchased from Strem and stored in a N_2-filed glovebox. Flash column chromatography was performed as described by Still et al. using silica gel (230-400 mesh, Silicycle).[29] Purified compounds were dried on a high vacuum line (0.2 torr) to remove trace solvent. ^1H and ^{13}C NMR spectra were recorded on a Bruker Avance III HD with Prodigy cryoprobe (at 400 MHz and 101 MHz, respectively), a Varian 400 MR (at 400 MHz and 101 MHz, respectively), or a Varian Inova 500 (at 500 MHz and 126 MHz, respectively). ^1H and ^{19}F NMR spectra were also recorded on a Varian Inova 300 (at 300 MHz and 282 MHz, respectively). NMR data is reported relative to internal $CHCl_3$ (^1H, $\delta = 7.26$) and $CDCl_3$ (^{13}C, $\delta = 77.0$) or C_6F_6 (^{19}F -164.9 ppm). HRMS were acquired from the Caltech Center for Catalysis and Chemical Synthesis Facility using electrospray ionization (ESI-TOF). Analytical chiral SFC was performed with a Mettler SFC supercritical CO_2 analytical chromatography system with Chiralcel AD-H, OD-H, AS-H, OB-H, and OJ-H columns (4.6 mm x 25 cm). Analytical achiral GC was performed with an Agilent 6850 GC utilizing an HP-1 capillary column (methyl siloxane, 30.0 m x 320 μm x 0.25 μm, Agilent) column with a splitless injection and a helium

flow of 7.3 mL/min. The temperature program began at 50 °C and was held for 2 min, increased to 250 °C at 25 °C/min and then held at 250 °C for 3 min. X-band perpendicular mode EPR spectra were recorded on a Bruker EMX spectrometer at 77 K using a LN_2 immersion dewar. Parallel mode EPR were recorded at 5K using a LHe cryostat. EPR spectra were simulated with Easyspin (version 5.2.35)[30]. Electronic absorption spectra were obtained using CARY 300 spectrophotometer. Electroanalytical experiments were conducted in the Beckman Resource Laser Resource Center at the California Institute of Technology using a Bio-Logic SP300 potentiostat/galvanostat. Cyclic voltammetry experiments we conducted with a glassy carbon disk working electrode, a platinum wire counter electrode, and a silver wire reference electrode containing a 10 mM $AgNO_3$ solution with 0.1 M $TBAPF_6$ in MeCN.

2.9.2 Synthetic Procedures

2.9.2.1 Substrate and Catalyst Synthesis

Figure 2.21. *Substrates and catalysts used in mechanistic studies*

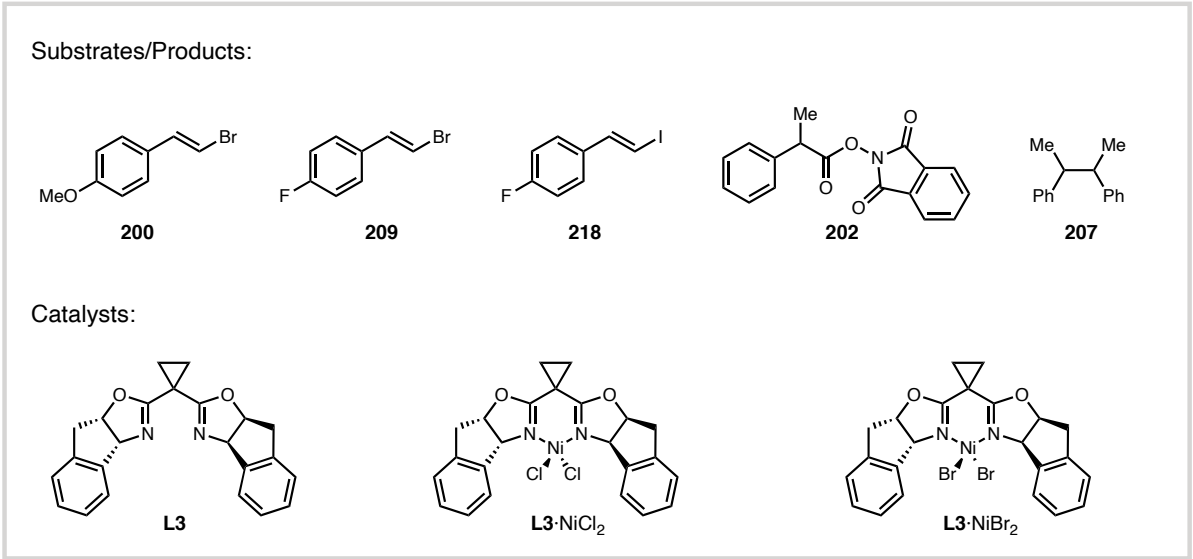

Catalysts:(3a*R*,3a'*R*,8a*S*,8a'*S*)-2,2'-(Cyclopropane-1,1-diyl)bis(3a,8a-dihydro-8*H*-indeno[1,2-*d*]-oxazole) (**L3**) was synthesized according to our previously published procedure [31] Complexation with $NiBr_2$ or $NiCl_2$ were prepared according to previously reported synthesis of

L3·$NiCl_2$[9a] and **L3**·$NiBr_2$.[8] Complexes were recrystallized once by vapor diffusion of pentane in a saturated DCM solution for use in catalytic reactions and 3 times for use in electroanalytical experiments.

Substrates: Coupling partners **200**, **209**, and **202** were synthesized according to the procedure described in the initial disclosure.[7,8]

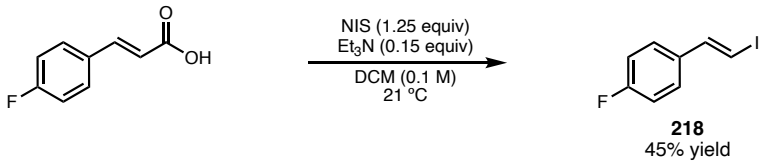

218
45% yield

(*E*)-1-fluoro-4-(2-iodovinyl)benzene (**218**): To a 250 mL oven-dried round bottom flask with a stir bar was added (*E*)-4-fluorocinnamic acid (831.6mg, 5.0 mmol, 1 equiv). The acid was then suspended in 50 mL (0.1 M) DCM then triethylamine (105 μL, 0.75 mmol, 0.15 equiv) was added and the reaction was stirred under N_2. To the stirring solution was then added *N*-iodosuccinimide (1.41 g, 6.25 mmol, 1.25 equiv) in one portion. After 12 minutes, the reaction solution had turned red and then deep black after 20 minutes. After 1h the starting material was consumed by TLC and the reaction mixture was concentrated *in vacuo*. Residue was taken up in 30 mL EtOAc and washed with 25 mL sat. $Na_2S_2O_3$ solution. The aqueous layer was then extracted two more times and combined organics were dried over $MgSO_4$, filtered through celite, rinsed with EtOAc then concentrated in vacuo to give a brown solid. The crude was then purified by filtration through SiO_2 with pentane to give alkenyl iodide **218** (558 mg, 2.3 mmol, 45% yield). *Note:* we observed significant discoloration and decomposition upon prolonged exposure to light so storage at -20 ºC in the darkness under Ar is essential to prevent decomposition. Spectral data is in good agreement with literature reports.[32]

2.9.3 Kinetics and Time Course Experiments

Methods of GC-FID Quantification: For each reaction component and product, authentic samples were isolated to determine response factors for GC-FID analysis. Three standards were made for each analyte to normalize the GC-FID area counts and convert the obtained data into reaction concentration (M) values. The analyte and dodecane standard were each added to a 20 mL vial and massed on a balance. The mixture was dissolved in 10 mL of EtOAc and transferred to a GC vial for analysis. The density of dodecane (0.75 g/mL) was also used to convert the area values to concentration.

2.9.3.1 Heterogeneous Reaction Kinetics

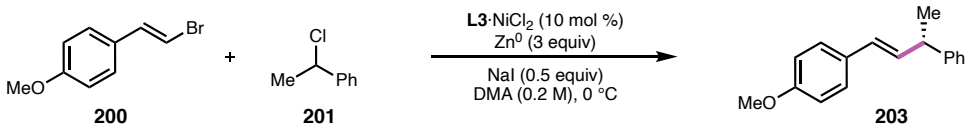

General Procedure 2.1 (Zn^0 powder): A 10 mL round bottom flask with a small magnetic stirring rod was charged with the sodium iodide (22.5 mg, 0.15 mmol, 0.5 equiv) and zinc powder (58.8 mg, 0.9 mmol, 3 equiv). The flask was sealed with a rubber septum, purged with N_2, and cooled to 0 °C by being placed in an ice water bath. The alkenyl bromide **200** (85.2 mg, 0.4 mmol) and **L3**·$NiCl_2$ complex (19.4 mg, 0.04 mmol) were added to a 2 mL volumetric flask, sealed with a rubber septum, and purged with N_2. The benzyl chloride **201** (53 μL, 0.4 mmol) and *n*-dodecane (48 μL) as an internal standard were added via syringe to the volumetric flask. Then anhydrous DMA was added to the volumetric flask until it reached the 2 mL line. A small stir bar was added to the volumetric flask and the solution was stirred until all of the **L3**·$NiCl_2$ complex was dissolved. The solution was taken up into a 2 mL syringe to ensure homogeneity, and then 1.5 mL of the solution was added to the round bottom flask. The reaction was stirred under a positive N_2 flow by using an IKA stir plate set to a stirring speed

of 1500 rpm. At appropriate time points, approximately 50 μL of the solution was removed by syringe (syringe and needle were pre-flushed with N_2), loaded onto a short silica plug (1 cm) in a glass pipette packed with cotton. The crude mixture was flushed through the silica plug with 2 mL of 10% EtOAc/hexane directly into GC vials and analyzed by GC-FID.

All data runs obtained from the GC-FID instrument were appropriately integrated for the product and the dodecane standard. The integrated data points were further processed by normalizing each product area value by its corresponding standard area value. The normalized areas were then converted to concentration by using calculated response factors obtained from preparing known mixtures of the standard and purified reaction product. Each reaction was analyzed and graphed to show the product concentration (M) as a function of reaction time (min). All data points were plotted with black markers (•) as shown below, while only the data points included in the linear fit are shown with red markers (•). The best-fit linear regression line is also shown and the y = mx+b equation is given. Each reaction was run in duplicates as indicated by Trial 1 and Trial 2.

Figure 2.22. *Standard reaction conditions:* [**200**]$_0$ = 0.2 M, [**201**]$_0$ = 0.2 M, [**L3**·$NiCl_2$] = 0.02 M.

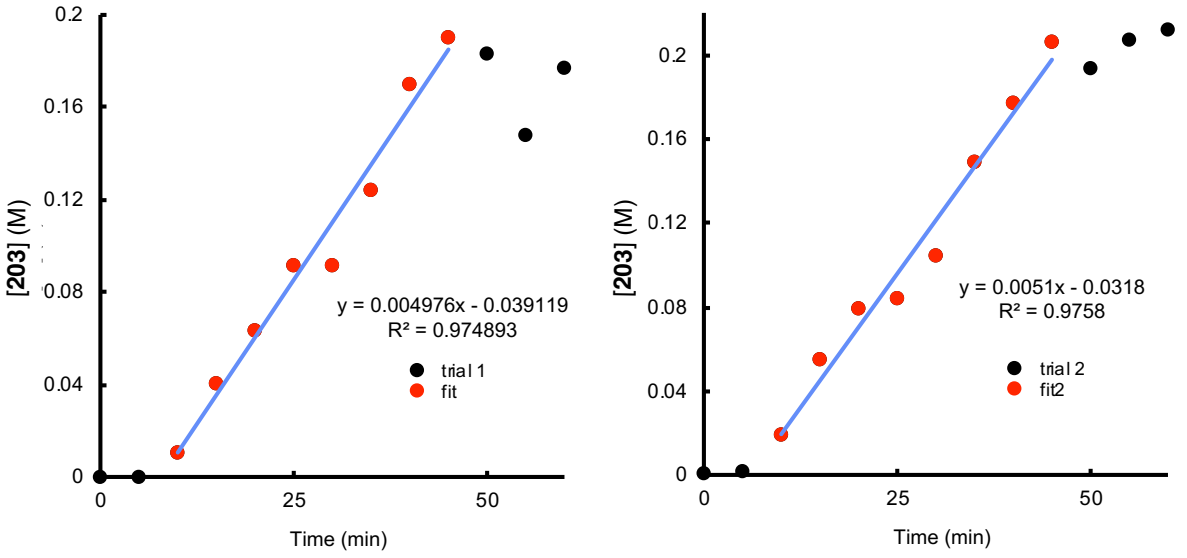

Effect of Changing [L3·$NiCl_2$]

The general procedure 2.1 was followed except varying the amounts of **L3**·$NiCl_2$ were used to give final loadings of 5%, 7%, 14%, and 20%.

Figure 2.23. *Catalyst loading 5 mol %:* [**200**]$_0$ = 0.2 M, [**201**]$_0$ = 0.2 M, [**L3**·$NiCl_2$] = 0.01 M.

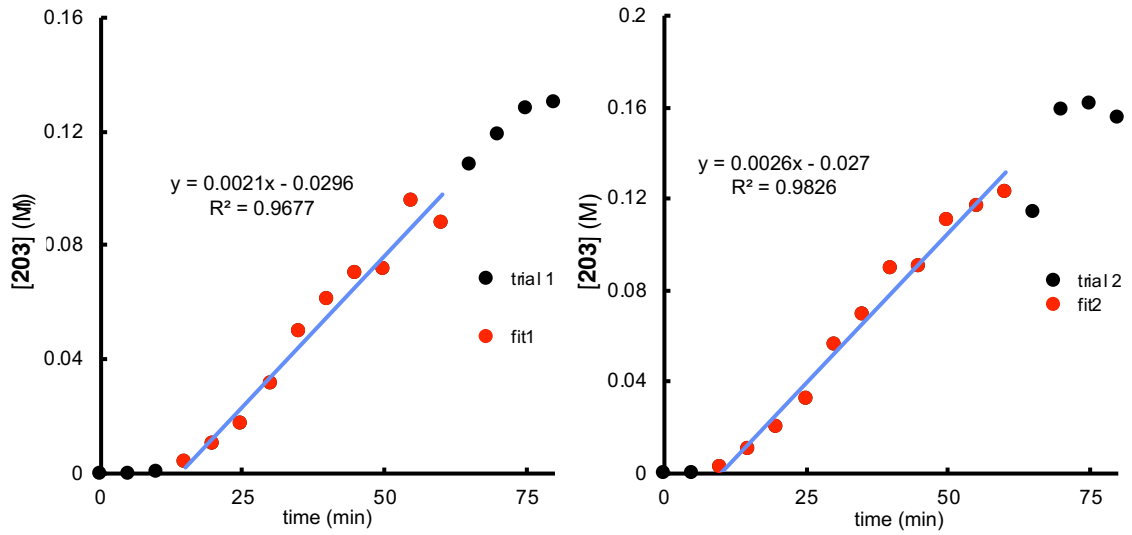

Figure 2.24. *Catalyst loading 7 mol %:* [**200**]$_0$ = 0.2 M, [**201**]$_0$ = 0.2 M, [**L3**·$NiCl_2$] = 0.014 M.

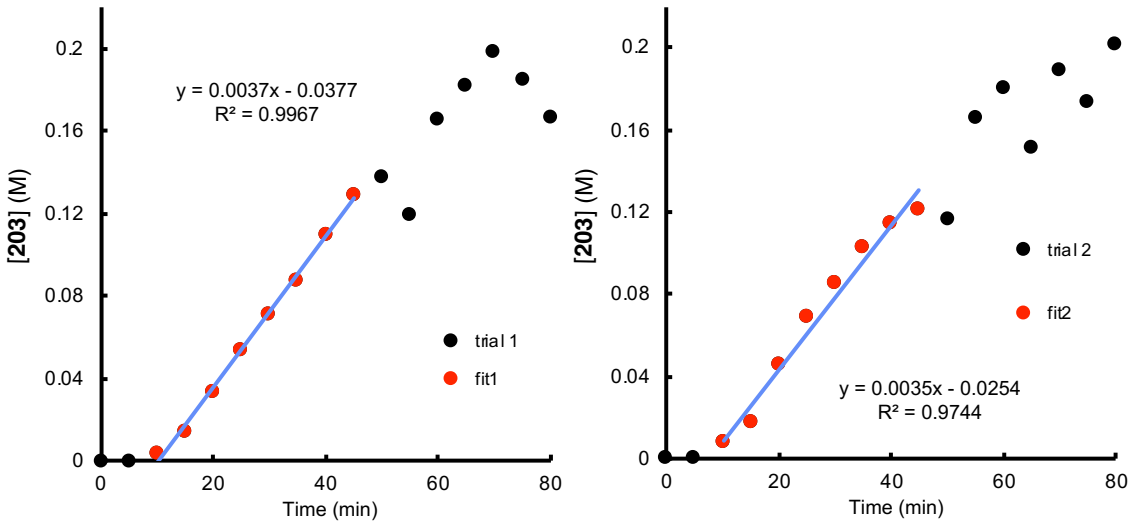

Figure 2.25. *Catalyst loading 14 mol %:* [**200**]$_0$ = 0.2 M, [**201**]$_0$ = 0.2 M, [**L3**·$NiCl_2$] = 0.028 M.

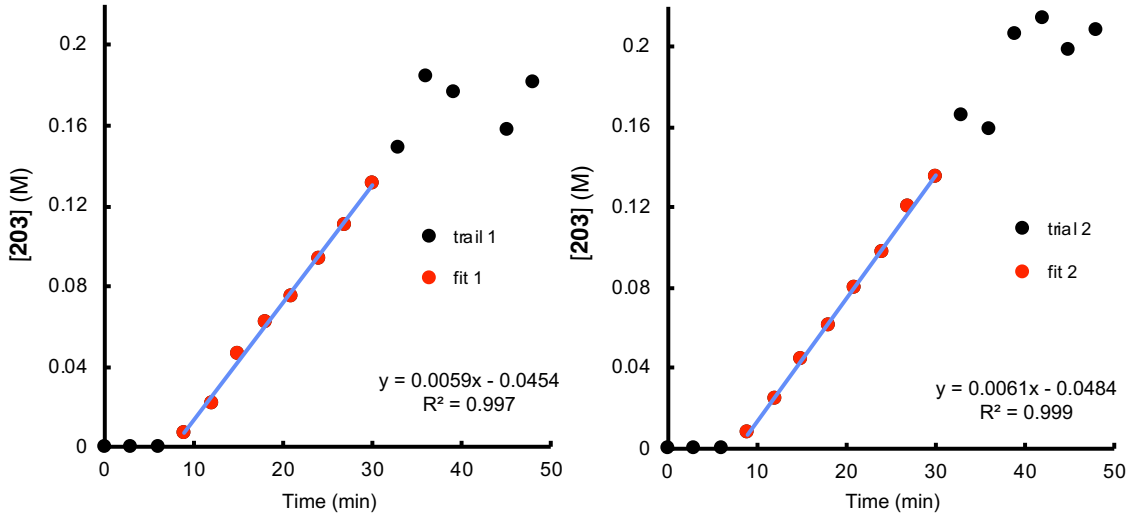

Figure 2.26. *Catalyst loading 20 mol %:* [**200**]$_0$ = 0.2 M, [**201**]$_0$ = 0.2 M, [**L3**·$NiCl_2$] = 0.04 M.

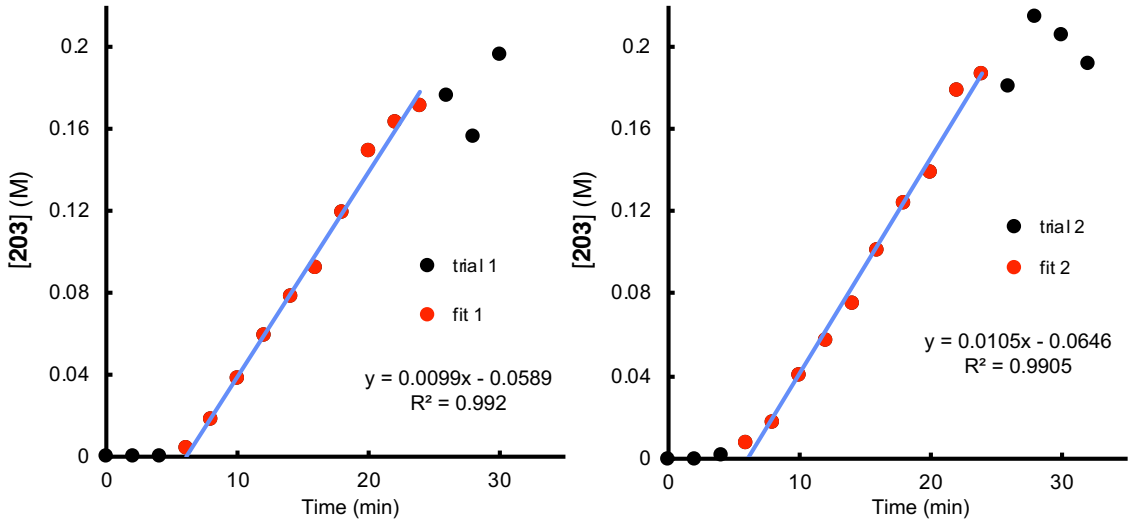

Effect of Changing Alkenyl Bromide (200) Equivalents

The general procedure 2.1 was followed except varying the amounts of [**200**]$_0$ were used to give final amounts of 1.5, 2, 3, and 4 equivalents.

Figure 2.27. *Order in **200** 1.5 equiv:* [**200**]$_0$ = 0.3 M, [**201**]$_0$ = 0.2 M, [**L3**·$NiCl_2$] = 0.02 M.

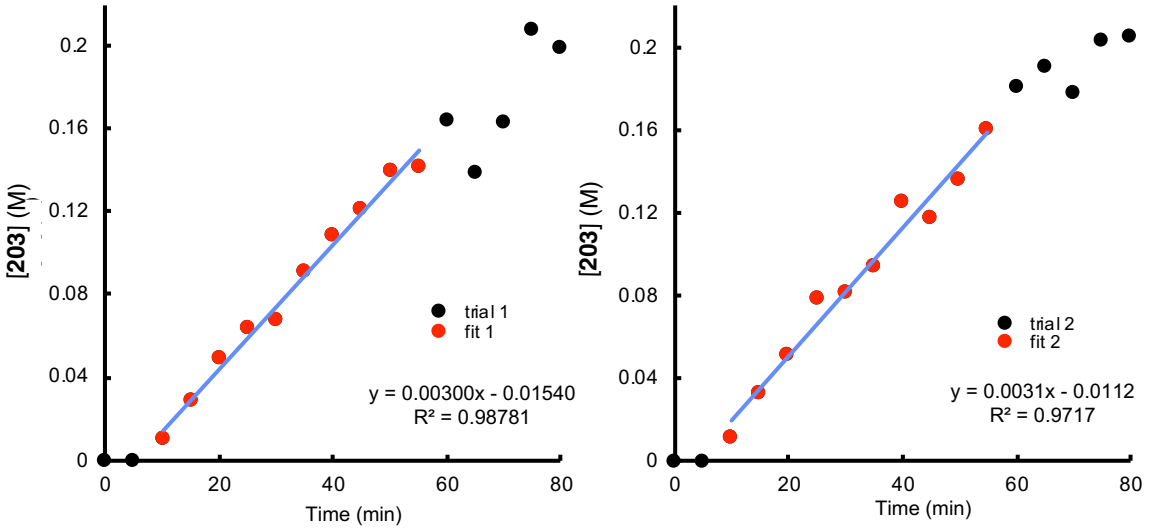

Figure 2.28. *Order in* ***200*** *2.0 equiv:* [**200**]$_0$ = 0.4 M, [**201**]$_0$ = 0.2 M, [**L3**·$NiCl_2$] = 0.02 M.

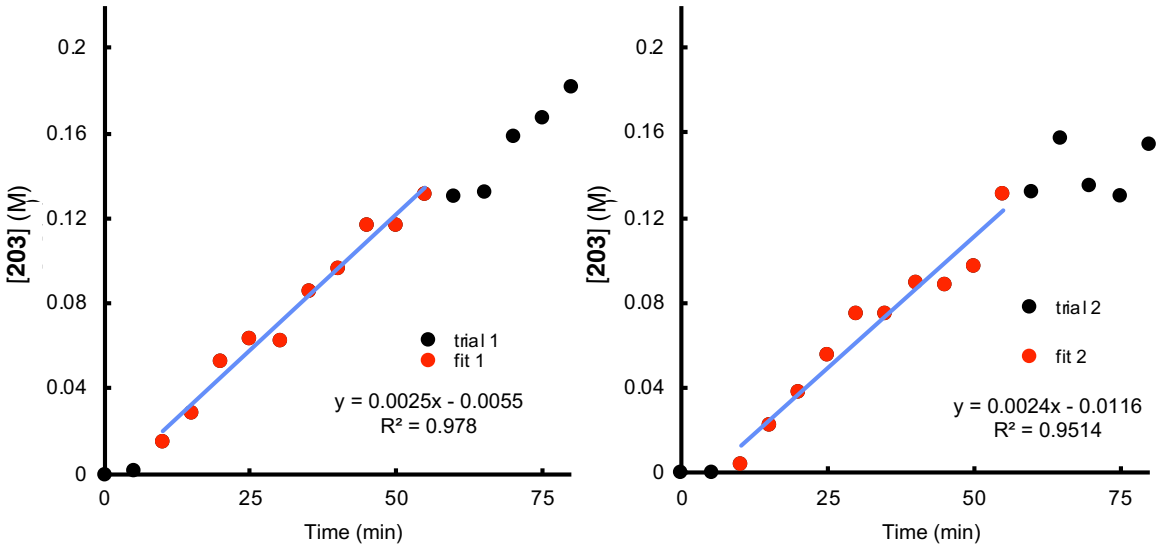

Figure 2.29. *Order in* ***200*** *3.0 equiv:* $[\mathbf{200}]_0 = 0.6$ M, $[\mathbf{201}]_0 = 0.2$ M, $[\mathbf{L3}\cdot NiCl_2] = 0.02$ M.

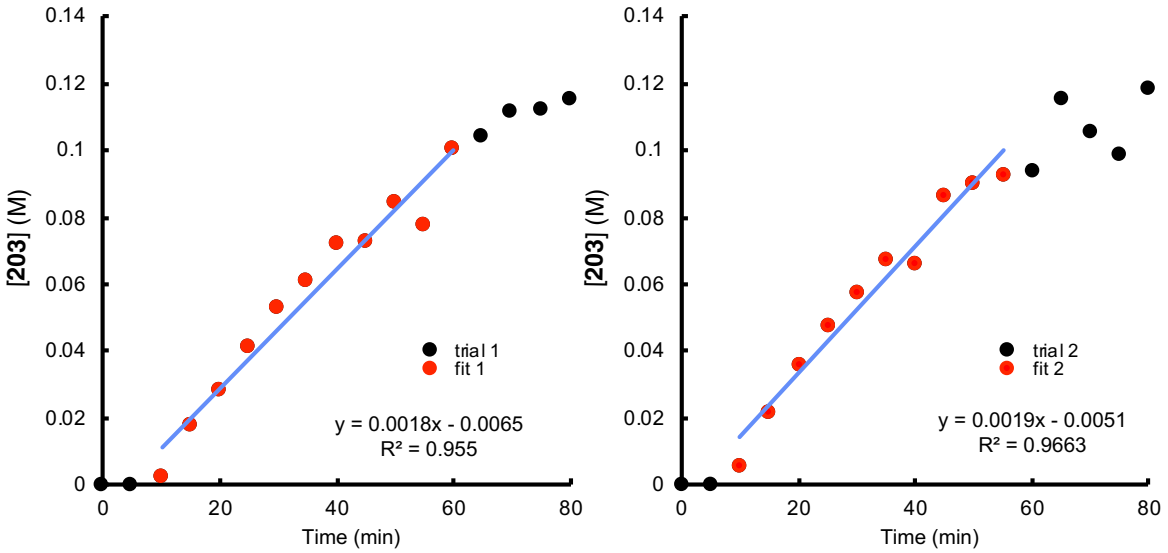

Figure 2.30. *Order in* ***200*** *4.0 equiv:* $[\mathbf{200}]_0 = 0.8$ M, $[\mathbf{201}]_0 = 0.2$ M, $[\mathbf{L3}\cdot NiCl_2] = 0.02$ M.

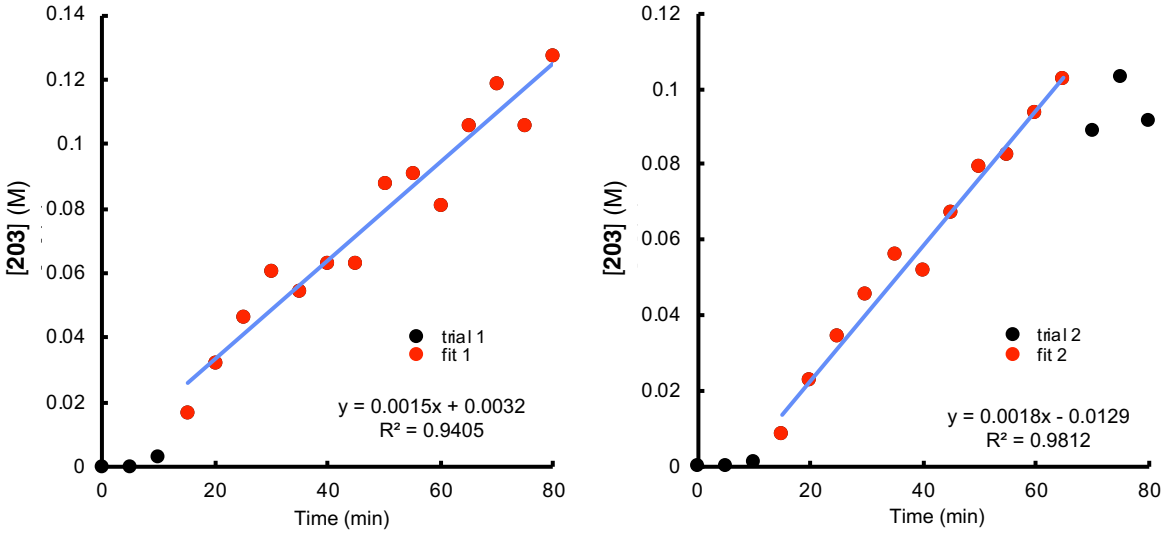

Effect of Changing Benzyl Chloride (201) Equivalents

The general procedure 2.1 was followed except varying the amounts of $[\mathbf{201}]_0$ were used to give final amounts of 1.5, 2, 3, and 4 equivalents.

Figure 2.31. *Order in* ***201*** *1.5 equiv:* [**200**]$_0$ = 0.2 M, [**201**]$_0$ = 0.3 M, [**L3**·$NiCl_2$] = 0.02 M.

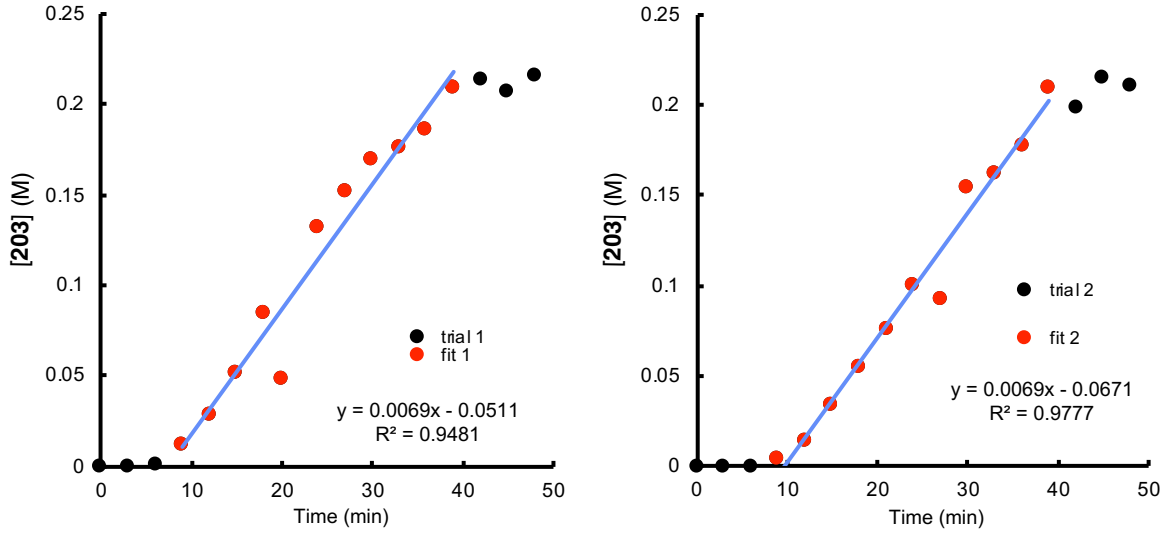

Figure 2.32. *Order in* ***201*** *2.0 equiv:* [**200**]$_0$ = 0.2 M, [**201**]$_0$ = 0.4 M, [**L3**·$NiCl_2$] = 0.02 M.

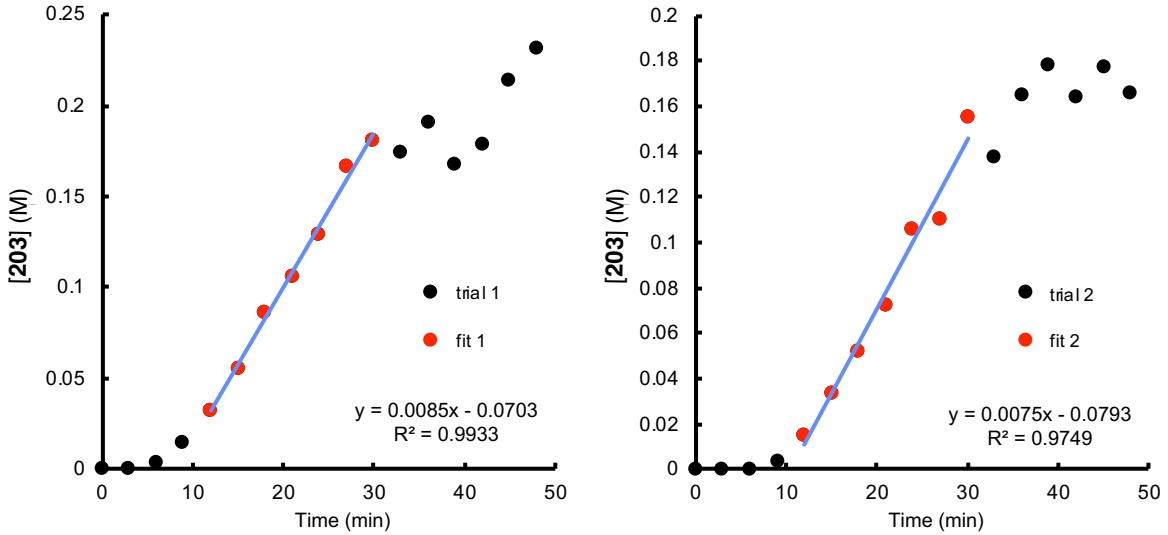

Figure 2.33. *Order in* ***201*** *3.0 equiv:* [**200**]$_0$ = 0.2 M, [**201**]$_0$ = 0.6 M, [**L3**·$NiCl_2$] = 0.02 M.

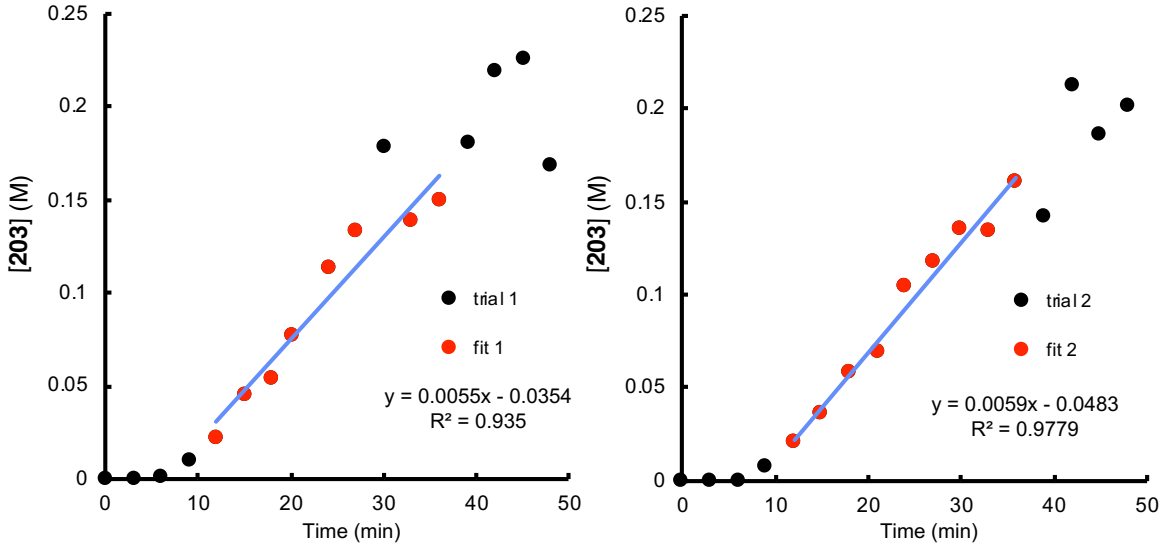

Figure 2.34. *Order in* ***201*** *4.0 equiv:* [**200**]$_0$ = 0.2 M, [**201**]$_0$ = 0.8 M, [**L3**·$NiCl_2$] = 0.02 M.

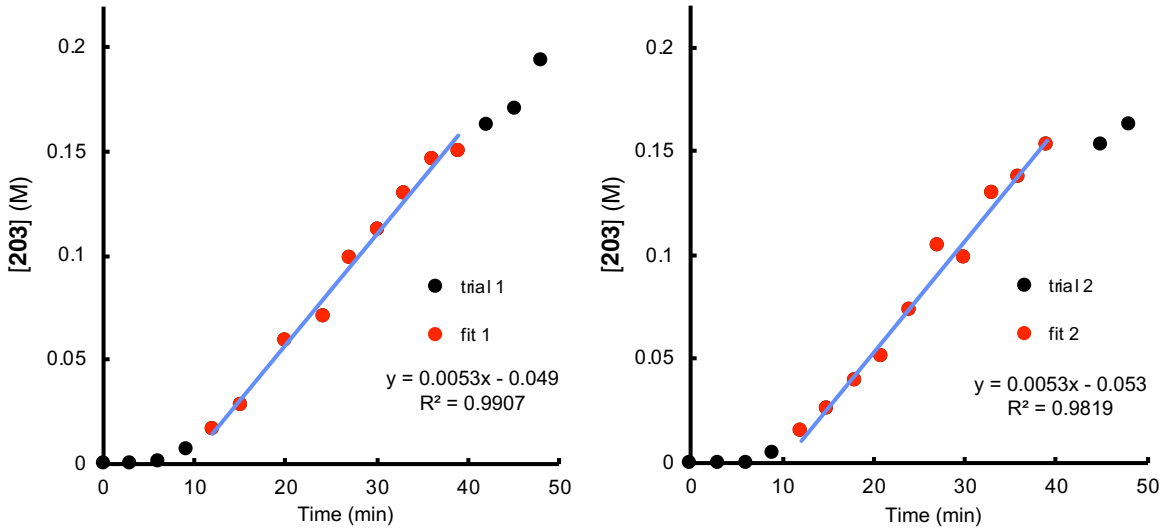

Tabulated Summary of Heterogeneous Kinetics Data:

Table 2.1. *Tabulated rate data for each run varying [**L3**·$NiCl_2$]$_0$.*

[**L3**$NiCl_2$]$_0$ (M)	Trial 1 Rate (M/min)	Trial 2 Rate (M/min)	Average Rate (M/min)	Standard deviation	**203** ee at End of Trial 1	**203** ee at End of Trial 2
0.02	0.0050	0.0051	0.0050	0.0001	93	93
0.01	0.0025	0.0021	0.0023	0.0003	87	88
0.014	0.0035	0.0037	0.0036	0.0001	89	89
0.028	0.0061	0.0059	0.0060	0.0002	86	85
0.04	0.0099	0.011	0.010	0.0004	85	85

Table 2.2. *Tabulated rate data for each run varying [**200**]$_0$.*

[**200**]$_0$ (M)	Trial 1 Rate (M/min)	Trial 2 Rate (M/min)	Average Rate (M/min)	Standard deviation	**203** ee at End of Trial 1	**203** ee at End of Trial 2
0.2	0.0050	0.0051	0.0050	0.0001	93	93
0.3	0.0030	0.0031	0.0030	0.0001	93	91
0.4	0.0025	0.0025	0.0025	0.0001	94	94
0.6	0.0016	0.0017	0.0017	0.00003	95	95
0.8	0.0018	0.0015	0.017	0.0002	95	95

Table 2.3. *Tabulated rate data for each run varying [**201**]$_0$.*

[**201**]$_0$ (M)	Trial 1 Rate (M/min)	Trial 2 Rate (M/min)	Average Rate (M/min)	Standard deviation	**203** ee at End of Trial 1	**203** ee at End of Trial 2
0.2	0.0050	0.0051	0.0050	0.0001	93	93
0.3	0.0069	0.0067	0.0068	0.0001	83	84
0.4	0.0075	0.0085	0.0080	0.0007	84	83
0.6	0.0055	0.0059	0.0057	0.0003	82	83
0.8	0.0052	0.0053	0.0053	0.0001	83	83

Impact of Stir Rate

Figure 2.35. *Rate of product* ***203*** *formation at different stir rates.*

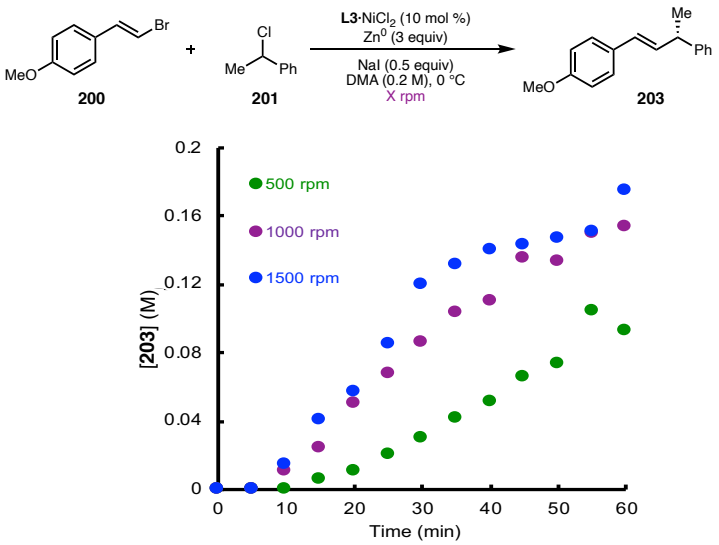

Rate of **203** formation at different stir rates (average of 2 runs shown). There is a significant rate dependence on stirring from 500 rpm to 1000 rpm and a smaller difference between 1000 rpm and 1500 rpm. The stir rate dependence is smaller at high stir rates and kinetic runs measured runs at 1500 rpm are reproducible.

Mn^0 vs. Zn^0 Profile:

Figure 2.36. *Rate of product* ***203*** *formation with Mn^0 and Zn^0 reductants.*

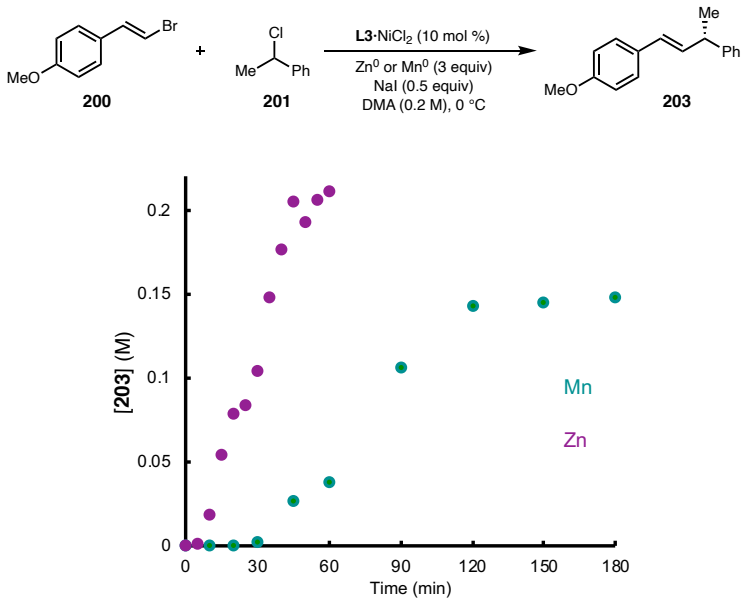

Rate of **203** formation at 1500 rpm shows a longer induction period and overall longer reaction times with Mn^0 reductant compared to Zn^0.

Excess Zn^0 Profile

Figure 2.37. *Rate of product* ***203*** *formation with 3 and 6 equivalents of Zn^0 reductant.*

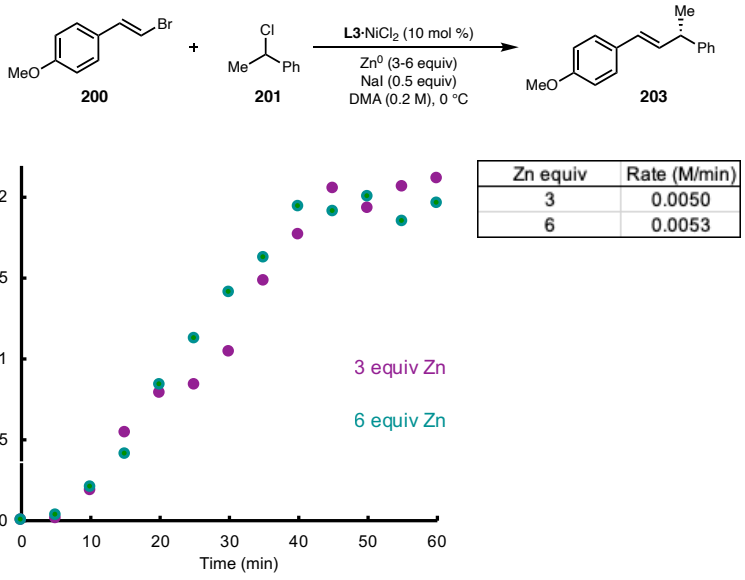

Zn equiv	Rate (M/min)
3	0.0050
6	0.0053

2.9.3.2 Homogenous Reaction Kinetics

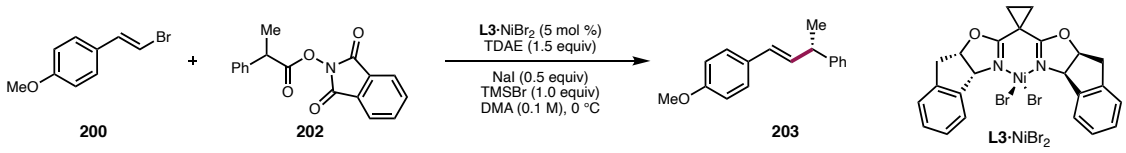

General Procedure 2.2: To a 2mL volumetric flask was added (*E*)-1-(2-bromovinyl)-4-methoxybenzene (**200**, 65.6 mg, 0.308 mmol, 1.0 equiv), 1,3-dioxoisoindolin-2-yl 2-phenylpropanoate (**202**, 90.9 mg, 0.308 mmol, 1.0 equiv) and **L3**·$NiBr_2$ (8.8 mg, 0.0154 mmol, 5 mol%) on the bench. The volumetric flask was then placed under argon and sealed with a septa. In a N_2-filled glovebox was then added sodium iodide (23.1 mg, 0.154 mmol, 0.5 equiv) to the volumetric flask which was then filled to volume with DMA (0.154 M). A stir bar was then added and the solution was stirred for 15 minutes. In a 1mL volumetric flask was added *N,N'*-tetrakis(dimethylamino)ethylene (TDAE, 100µL, 0.43 mmol, 1.5 equiv) and then filled to volume with DMA (0.43 M) in the glovebox and sealed with a rubber septum and tape. Then 1.3mL of the homogeneous solution in the 2 mL volumetric flask was then added to a 10mL oven-dried round bottom flask with a 2 dram stir bar. The flask was then sealed with a rubber septum and electrical tape. To the 10mL round bottom flask was added 15µL of dodecane as the internal standard followed by TMSBr (26.4 µL, 0.2 mmol, 1.0 equiv). The round bottom flask was then quickly removed from the glovebox and placed in an ice bath under N_2 and stirred. A ~50 µL aliquot were removed by an N_2-purged 1mL syringe for a t = 0 timepoint. Once cooled, TMSBr (26.4 µL, 0.2 mmol, 1.0 equiv) was added via syringe and the reaction was stirred for 30 seconds before 0.7 mL of the cooled TDAE solution was added initiating the reaction. ~50 µL aliquots were removed by an N_2-purged 1mL syringe and quenched into a 1-dram vial containing EtOAc and 1M $HCl_{(aq)}$. The vial was then capped and shaken then the organic layer was removed and pushed through a $MgSO_4$ plug into a GC vial for analysis. All

samples were analyzed directly by GC-FID. Each experiment was run in duplicate with representative profiles shown below.

Figure 2.38. *Standard reaction conditions under general procedure 2.2:* [**200**]$_0$ = 0.1 M, [**202**]$_0$ = 0.1 M, [**L3**·NiBr$_2$] = 0.005 M.

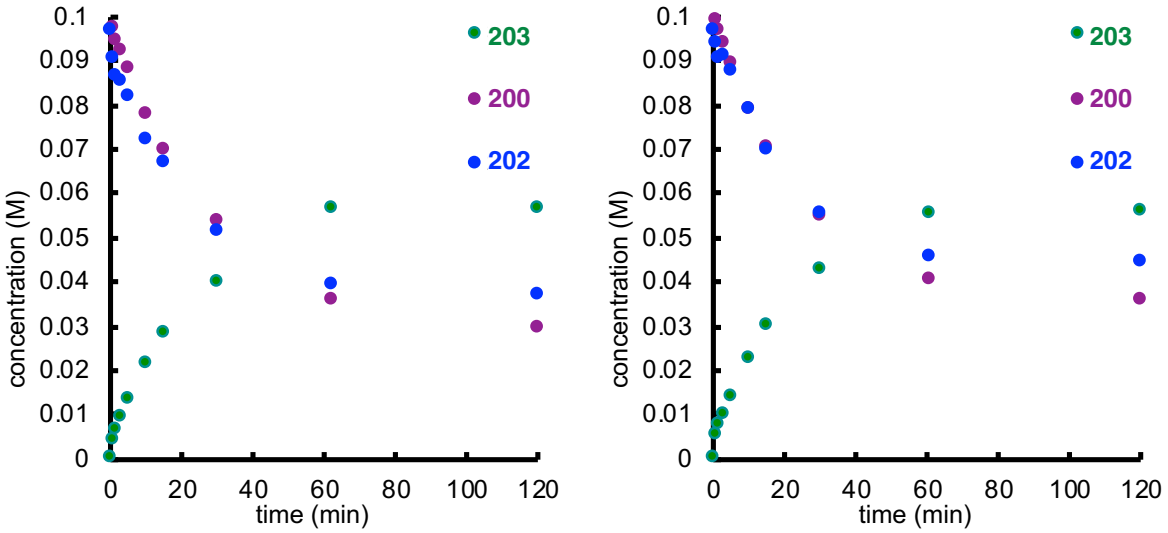

Reaction Profiles for Experiments Varying [L3·NiBr$_2$]$_0$

Figure 2.39. *Order in **L3**·NiBr$_2$ 20 mol %:* [**200**]$_0$ = 0.1 M, [**202**]$_0$ = 0.1 M, [**L3**·NiBr$_2$] = 0.02 M.

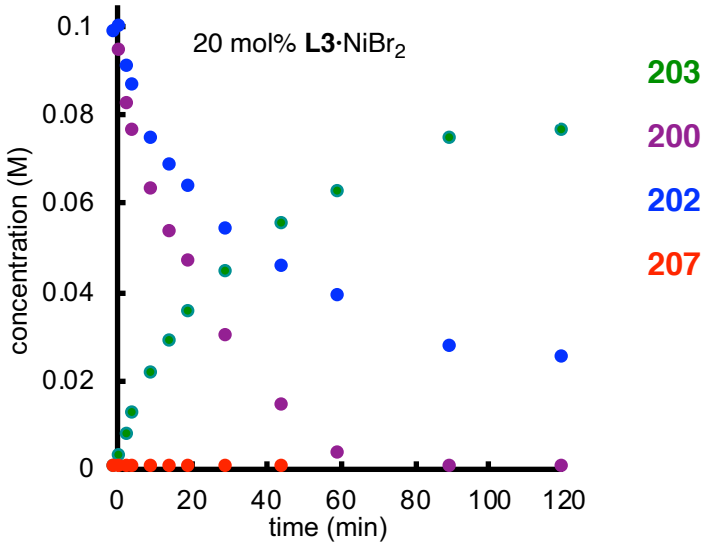

Figure 2.40. *Order in* ***L3***·*NiBr₂ 10 mol %:* [**200**]$_0$ = 0.1 M, [**202**]$_0$ = 0.1 M, [**L3**·NiBr$_2$] = 0.01 M.

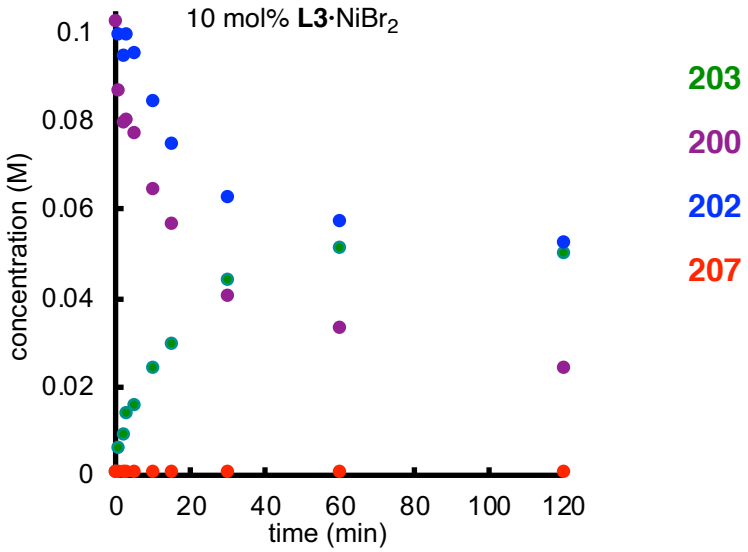

Figure 2.41. *Order in* ***L3***·*NiBr₂ 5 mol %:* [**200**]$_0$ = 0.1 M, [**202**]$_0$ = 0.1 M, [**L3**·NiBr$_2$] = 0.05 M.

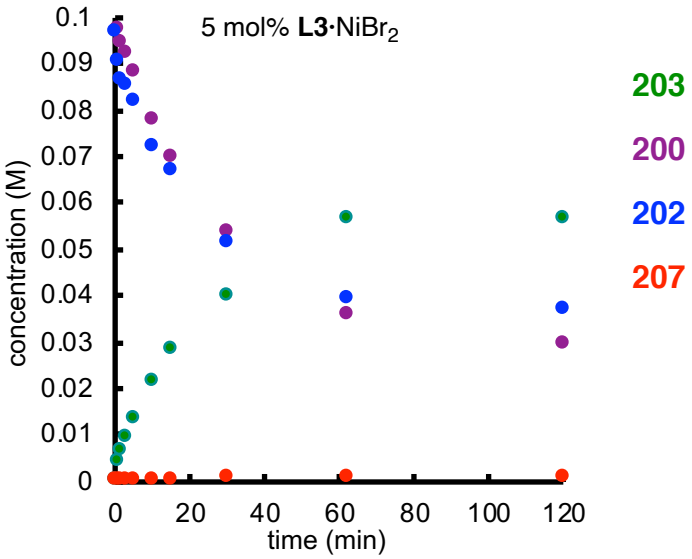

Figure 2.42. *Order in* ***L3***·*NiBr₂ 1 mol %:* [**200**]$_0$ = 0.1 M, [**202**]$_0$ = 0.1 M, [**L3**·NiBr$_2$] = 0.01 M.

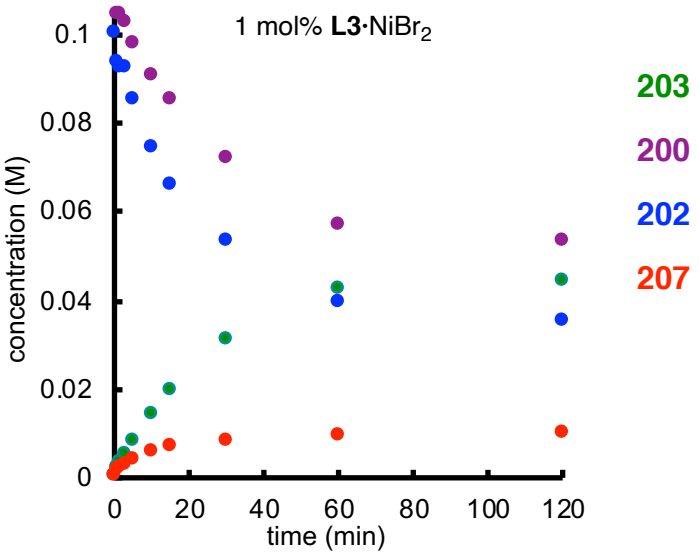

Figure 2.43. *Order in* ***L3***·*NiBr₂ 0 mol %:* [**200**]$_0$ = 0.1 M, [**202**]$_0$ = 0.1 M, [**L3**·NiBr$_2$] = 0 M.

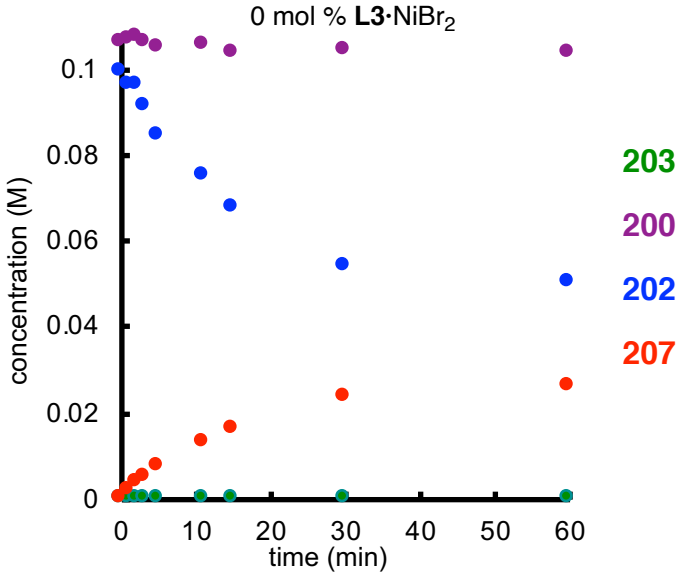

Reaction Profiles for Experiments Varying [200]$_0$

Figure 2.44. *Order **200** 2 equiv:* [**200**]$_0$ = 0.2 M, [**202**]$_0$ = 0.1 M, [**L3**·$NiBr_2$] = 0.05 M.

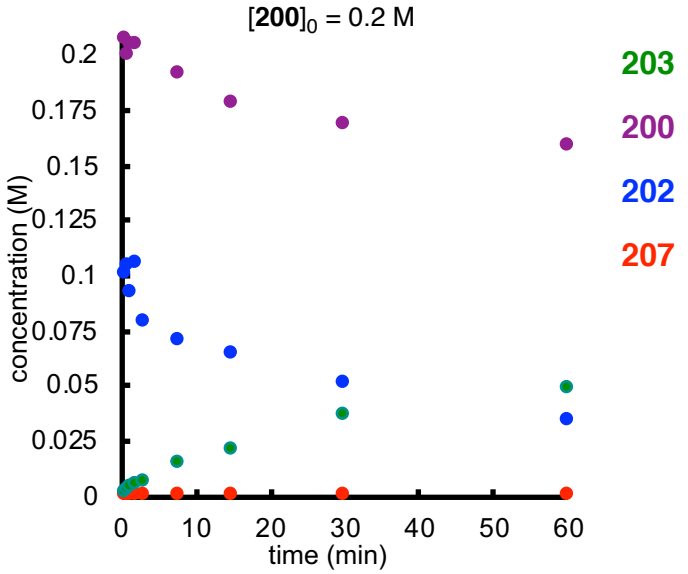

Figure 2.45. *Order **200** 5 equiv:* [**200**]$_0$ = 0.5 M, [**202**]$_0$ = 0.1 M, [**L3**·$NiBr_2$] = 0.05 M.

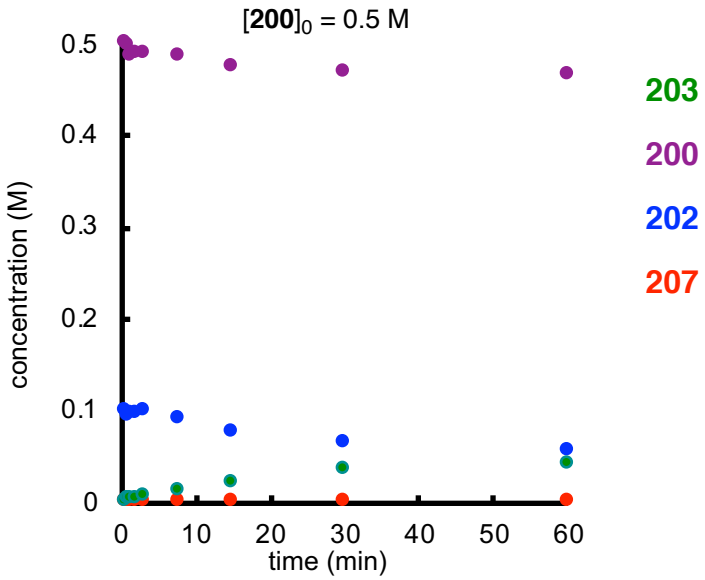

Reaction Profiles for Experiments Varying [202]$_0$

Figure 2.46. *Order* ***202*** *2 equiv:* [**200**]$_0$ = 0.1 M, [**202**]$_0$ = 0.2 M, [**L3**·NiBr$_2$] = 0.05 M.

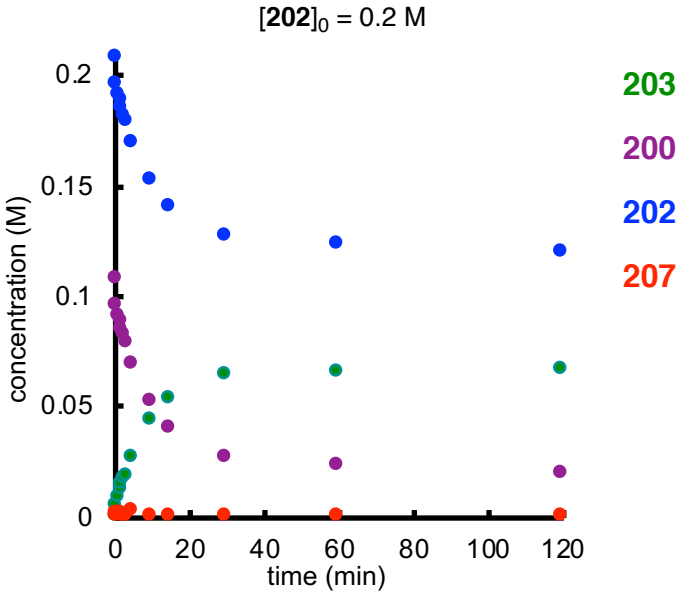

Figure 2.47. *Order* ***202*** *3 equiv:* [**200**]$_0$ = 0.1 M, [**202**]$_0$ = 0.3 M, [**L3**·NiBr$_2$] = 0.05 M.

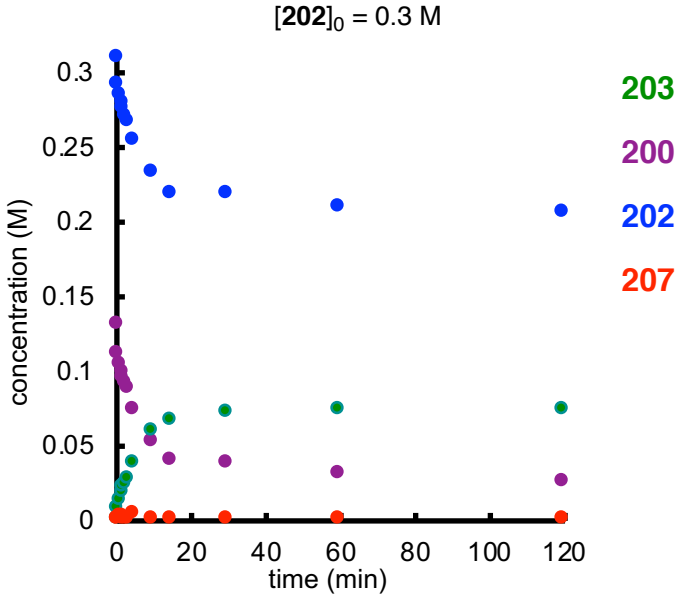

Figure 2.48. *Grid of reactions analyzed by Variable Time Normalization Analysis (VTNA) showing the coefficients that result in the best profile overlay next to coefficients that show poor overlay.*

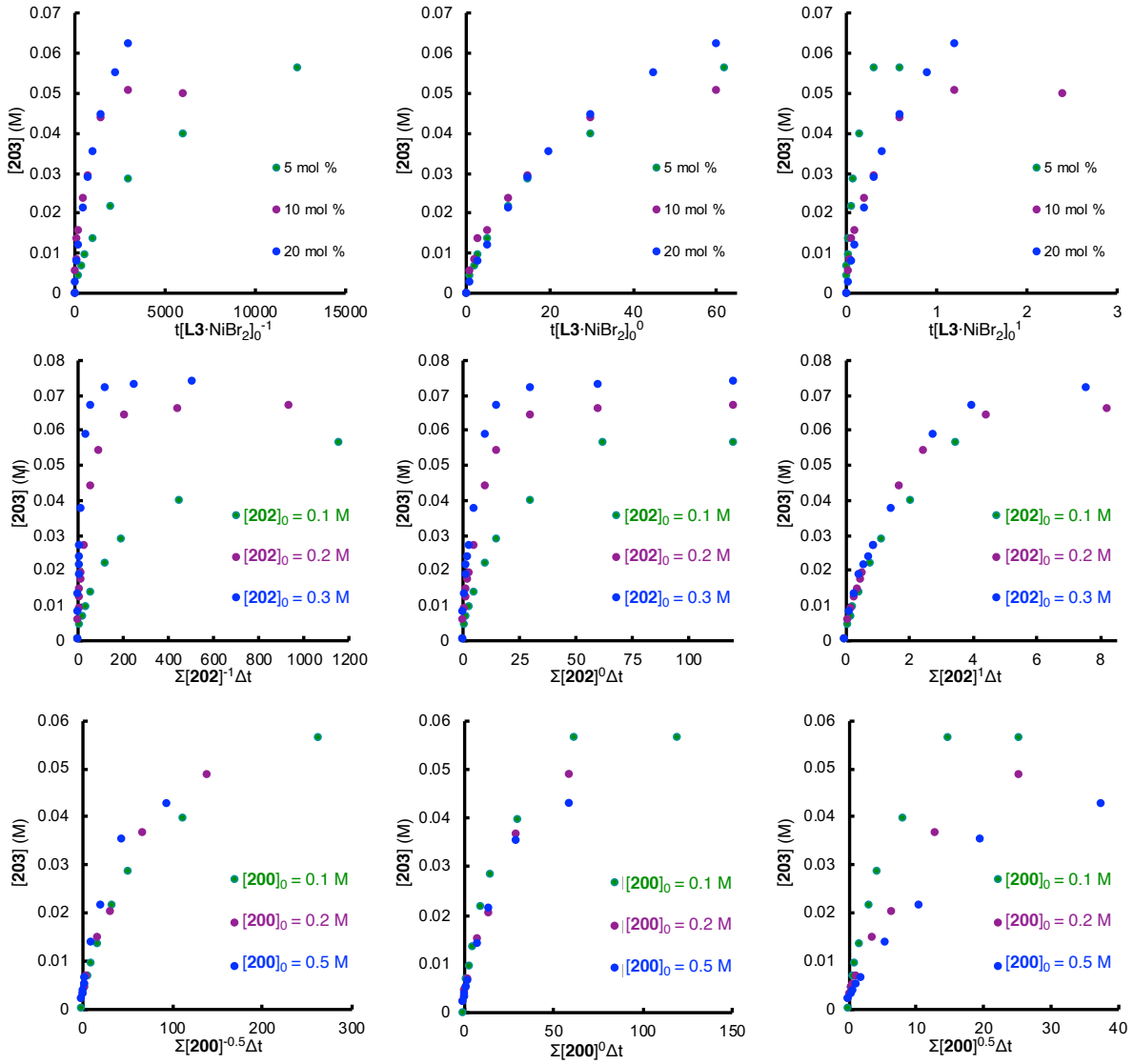

2.9.4 Mechanism of Substrate Activation Experiments

2.9.4.1 Additive Effects on NHP Ester Reduction Rate

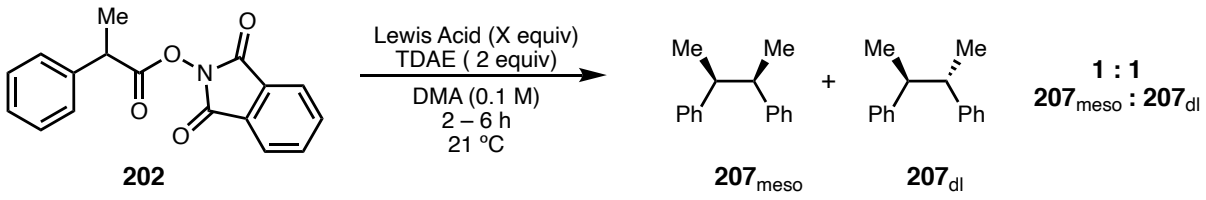

202 **207**$_{meso}$ **207**$_{dl}$

General Procedure 2.3: To an oven-dried 10 mL round bottom flask with a stir bar was added 1,3-dioxoisoindolin-2-yl 2-phenylpropanoate (**202**, 59.1 mg, 0.20 mmol, 1.0 equiv). The flask was then brought into a N_2-filled glovebox where NaI (if applicable), DMA (2.0 mL, 0.1 M) and *n*-dodecane (target: 20 μL, 0.088 mmol, 0.44 eqiuv, actual mass was recorded for each experiment) internal standard was added. The solution was stirred until homogenous and then the respective Lewis acid (0.2 mmol, 1 equiv) was added and the flask was sealed with a septa and electrical tape. The flask was removed from the glovebox and placed under N_2 and stirred. A ~50 μL aliquot of the solution was removed with a N_2-purged syringe then quenched into a 1-dram vial containing EtOAc and 1M $HCl_{(aq)}$ and the organic layer was passed through a $MgSO_4$ plug into a GC vial then further diluted with EtOAc for the appropriate concentration for GC analysis. To the stirring solution was then added *N,N'*-tetrakis(dimethylamino)ethylene (93.1 μL, 0.40 mmol, 2.0 equiv) to start the reaction (t = 0). The reaction was then aliquoted with the same procedure previously described at regular intervals.

Data Analysis: The calculated concentrations of **202**, meso-**207** and dl-**207** were calculated from the analyte:standard integral ratios measured by GC-FID at each timepoint. The measured response for each component was used to calculate the amount of analyte which was then converted to concentration corresponding to 2 mL reaction volume. In all cases, diastereomers of **207** were produced in a 1:1 ratio and summed to determine the total amount of product produced ($[\mathbf{207}]_{meso} + [\mathbf{207}]_{dl} = [\mathbf{207}]_{tot}$, noted as [**207**] throughout the remainder of the text). Due to the fact that the formation of **207** from the diffusion-limited termination of two **202**-derived radicals is much faster than the reactions leading to the generation of the radical species it is reasonable to treat the rate of radical generation as the rate of [**207**] formation.

The relative rate of **202**-derived radical formation was determined from the [**207**] vs. time profiles for each Lewis acid additive. The rates were determined in a similar method as described by Weix and coworkers[33] using equation 2.1 to linearize the data.

$$\frac{1}{(1-f)} = mt \qquad \textbf{(equation 2.1)}$$

where f is the fraction of [**207**]$_t$ over the theoretical yield of [**207**]. The rate was then extracted from the slope determined from least-squares linear regression. To calculate the relative rate (k_{rel}) the absolute rate obtained from experiments employing 1 equivalent of TMSBr was used as a baseline according to equation 2.2 due to its use in the optimized catalytic reaction.

$$k_{rel} = \frac{k_{Lewis\ acid}}{k_{TMSBr}} \qquad \textbf{(equation 2.2)}$$

Representative Concentration Profiles and Rate Determination:

Figure 2.49. *Representative profile from general procedure 2.3 with product* ***207*** *shown as individual diastereomers (left) and combined yield (right).*

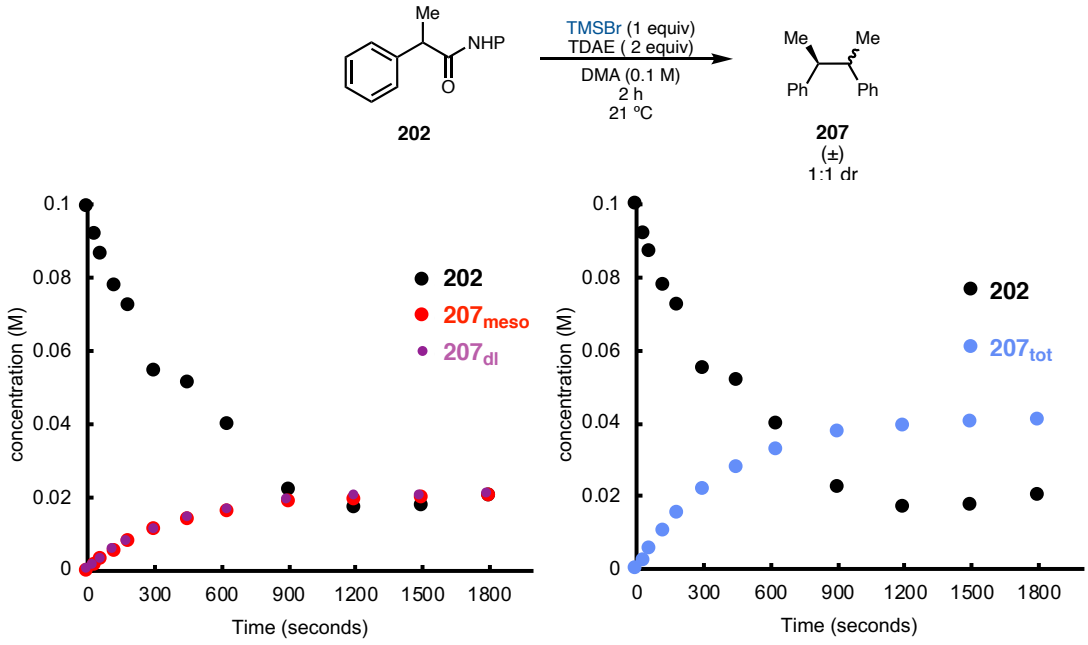

Figure 2.50. *Representative profile from general procedure 2.3 under standard conditions in duplicate to show reproducibility.*

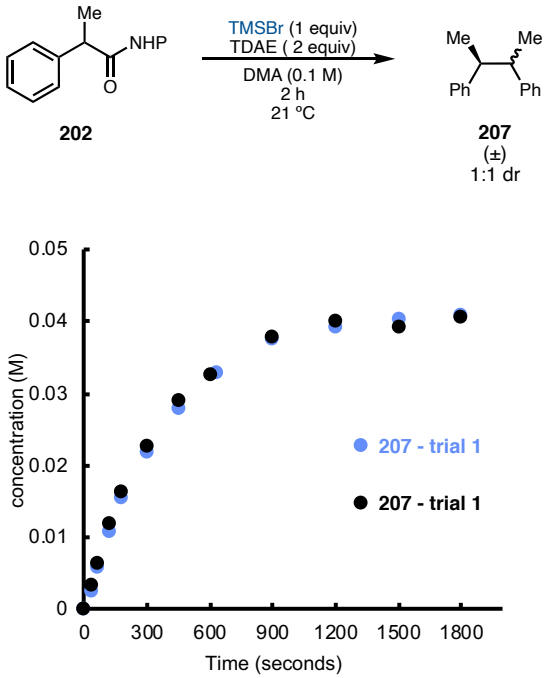

Figure 2.51. *Comparative reaction profiles for different Lewis acids (left) and the corresponding linearized data.*

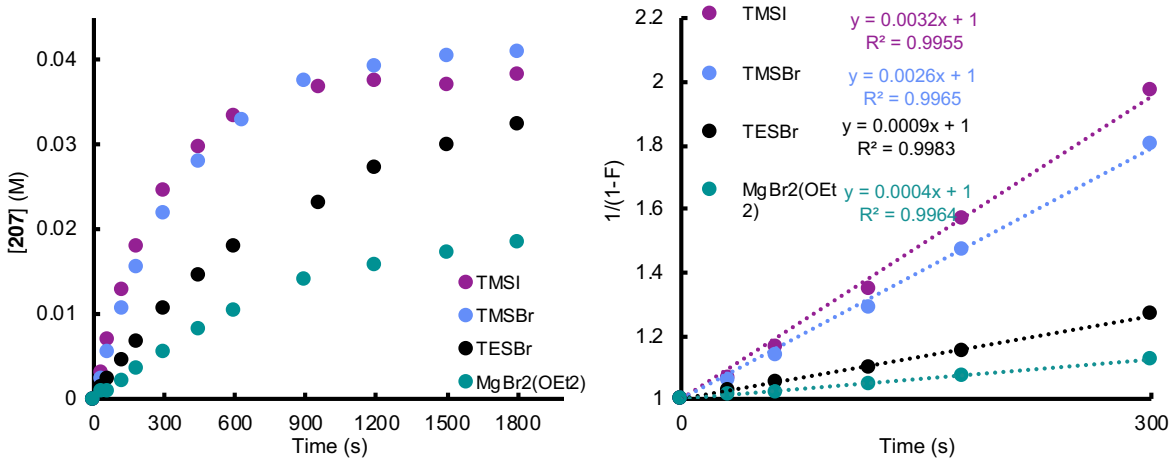

Tabulated Rate Data:

Table 2.4. *Reaction data and linearization by general procedure 2.3. $[TMSBr]_0 = 0.1$ M.*

Lewis Acid	TMSBr	1 equiv
k	0.002625	
krel	1.000	
Time (s)	**[207] (M)**	**1/(1-F)**
0	0.000	1.00
30	0.002	1.05
60	0.006	1.13
120	0.011	1.27
180	0.016	1.45
300	0.022	1.78
450	0.028	2.27
630	0.033	2.91
900	0.038	4.04
1200	0.039	4.70
1500	0.040	5.20
1800	0.041	5.59
2700	0.041	5.62
3600	0.041	5.88
5400	0.039	4.61
7202	0.043	6.88

Table 2.5. *Reaction data and linearization by general procedure 2.3. $[TMSI]_0 = 0.1$ M.*

Lewis Acid	TMSI	1 equiv
k	0.00317	
krel	1.210	
Time (s)	**[207] (M)**	**1/(1-F)**
0	0.000	1.00
30	0.003	1.07
60	0.007	1.17
120	0.013	1.35
180	0.018	1.57
300	0.025	1.97
450	0.030	2.48
600	0.033	3.02
960	0.037	3.83
1200	0.038	4.03
1500	0.037	3.85
1800	0.038	4.25
2700	0.038	4.27
3600	0.038	4.15
5400	0.039	4.42

Table 2.6. *Reaction data and linearization by general procedure 2.3. $[TMSOTf]_0$ = 0.1 M.*

Lewis Acid	TMSOTf	1 equiv
k	0.00296	
krel	1.128	
Time (s)	**[207] (M)**	**1/(1-F)**
0	0.000	1.00
30	0.003	1.07
60	0.007	1.16
120	0.013	1.36
180	0.018	1.55
300	0.023	1.88
450	0.028	2.24
600	0.030	2.52
960	0.033	2.91
1200	0.033	2.97
1500	0.034	3.08
1800	0.034	3.16
2700	0.035	3.24
3600	0.034	3.22
5400	0.034	3.19

Table 2.7. *Reaction data and linearization by general procedure 2.3. $[TESBr]_0$ = 0.1 M.*

Lewis Acid	TESBr	1 equiv
k	0.00088	
krel	0.335	
Time (s)	**[207] (M)**	**1/(1-F)**
0	0.000	1.00
30	0.002	1.03
60	0.002	1.05
120	0.005	1.10
180	0.007	1.15
300	0.011	1.27
450	0.015	1.41
600	0.018	1.56
960	0.023	1.87
1200	0.027	2.21
1500	0.030	2.51
1800	0.032	2.84
2700	0.036	3.53
3600	0.037	3.85
5400	0.038	4.05

Table 2.8. *Reaction data and linearization by general procedure 2.3. $[TMSBr]_0$ = 0.2 M.*

Lewis Acid	TMSBr	2 equiv
k	0.0044	
krel	1.676	
Time (s)	**[207] (M)**	**1/(1-F)**
0	0.000	1.00
30	0.005	1.11
60	0.010	1.24
120	0.016	1.47
180	0.021	1.75
300	0.029	2.38
450	0.035	3.39
600	0.039	4.73
900	0.045	10.23
1200	0.048	32.81
1500	0.051	-70.94

Table 2.9. *Reaction data and linearization by general procedure 2.3. $[TMSCl]_0$ = 0.1 M.*

Lewis Acid	TMSCl	1 equiv
k	0.00024	
krel	0.091	
Time (s)	**[207] (M)**	**1/(1-F)**
0	0.000	1.00
30	0.001	1.02
60	0.001	1.02
120	0.002	1.04
180	0.002	1.05
300	0.004	1.08
450	0.005	1.12
600	0.007	1.15
900	0.010	1.24
1200	0.013	1.34
1500	0.015	1.44
1800	0.017	1.53
2700	0.023	1.84
3600	0.026	2.06
5400	0.031	2.59

Table 2.10. *Reaction data and linearization by general procedure 2.3. $[TESCl]_0$ = 0.1 M.*

Lewis Acid	TESCl	1 equiv
k	0.000031	
krel	0.012	
Time (s)	**[207] (M)**	**1/(1-F)**
0	0.000	1.00
30	0.000	1.00
60	0.000	1.00
120	0.000	1.01
180	0.000	1.01
300	0.000	1.01
450	0.001	1.01
600	0.001	1.02
960	0.001	1.02
1200	0.001	1.03
1500	0.001	1.03
1800	0.002	1.03
2700	0.002	1.05
3600	0.003	1.07
5400	0.005	1.12

Table 2.11. *Reaction data and linearization by general procedure 2.3. $[TBSCl]_0$ = 0.1 M.*

Lewis Acid	TBSCl	1 equiv
k	0.0000049	
krel	0.002	
Time (s)	**[207] (M)**	**1/(1-F)**
0	0.000	1.00
300	0.000	1.00
600	0.000	1.00
900	0.000	1.00
1800	0.000	1.01
2700	0.000	1.01
3600	0.001	1.01
5400	0.001	1.02
7200	0.001	1.03
9000	0.002	1.03
10860	0.002	1.05
12600	0.002	1.05
14400	0.003	1.07
18000	0.004	1.10

Table 2.12. *Reaction data and linearization by general procedure 2.3. $[MnCl_2]_0$ = 0.1 M.*

Lewis Acid	MnCl2	1 equiv
k	0.000094	
krel	0.036	
Time (s)	**[207] (M)**	**1/(1-F)**
0	0.000	1.00
30	0.000	1.01
60	0.001	1.01
120	0.001	1.02
180	0.001	1.02
300	0.002	1.03
450	0.002	1.05
600	0.003	1.07
900	0.004	1.10
1200	0.006	1.13
1500	0.007	1.15
1800	0.007	1.18
2700	0.010	1.26
3600	0.013	1.35
5400	0.016	1.49

Table 2.13. *Reaction data and linearization by general procedure 2.3. $[MgBr_2{\cdot}OEt_2]_0$ = 0.1 M.*

Lewis Acid	MgBr2(OEt2)	1 equiv
k	0.00044	
krel	0.147	
Time (s)	**[207] (M)**	**1/(1-F)**
0	0.000	1.00
30	0.001	1.02
60	0.001	1.02
120	0.002	1.05
180	0.004	1.08
300	0.006	1.13
450	0.008	1.20
600	0.011	1.27
900	0.014	1.39
1200	0.016	1.47
1500	0.017	1.53
1800	0.019	1.59
2700	0.019	1.59
3600	0.019	1.64
6300	0.020	1.67
9000	0.021	1.70

Table 2.14. *Reaction data and linearization by general procedure 2.3. $[Sc(OTf)_3]_0$ = 0.1 M.*

Lewis Acid	Sc(OTf)3	1 equiv
k	0.00038	
krel	0.127	
Time (s)	**[207] (M)**	**1/(1-F)**
0	0.000	1.00
30	0.001	1.02
60	0.002	1.03
120	0.003	1.06
180	0.004	1.08
300	0.006	1.14
450	0.008	1.20
600	0.010	1.25
900	0.013	1.36
1200	0.016	1.47
1500	0.018	1.57
1800	0.021	1.72
2700	0.026	2.07
3600	0.030	2.51
5400	0.036	3.70

Table 2.15. *Reaction data and linearization by general procedure 2.3. $[LiBr]_0$ = 0.1 M.*

Lewis Acid	LiBr	1 equiv
k	0.000043	
krel	0.014	
Time (s)	**[207] (M)**	**1/(1-F)**
0	0.000	1.00
30	0.000	1.01
60	0.000	1.01
120	0.000	1.01
180	0.000	1.01
300	0.001	1.01
450	0.001	1.02
600	0.001	1.02
900	0.002	1.04
1200	0.002	1.05
1500	0.003	1.06
1800	0.003	1.07
2700	0.005	1.12
3600	0.007	1.15
5400	0.010	1.26
7200	0.013	1.35

Table 2.16. *Reaction data and linearization by general procedure 2.3. $[ZnI_2]_0$ = 0.1 M.*

Lewis Acid	ZnI2	1 equiv
k	0.000037	
krel	0.012	
Time (s)	**[207] (M)**	**1/(1-F)**
0	0.000	1.00
30	0.001	1.01
60	0.001	1.02
120	0.001	1.02
180	0.002	1.03
300	0.002	1.04
450	0.002	1.05
600	0.003	1.06
900	0.003	1.07
1200	0.004	1.08
1500	0.004	1.09
1800	0.004	1.10
2700	0.005	1.12
3600	0.006	1.14
5400	0.007	1.17
7200	0.008	1.19

Table 2.17. *Reaction data and linearization by general procedure 2.3. $[TMSBr]_0$ = 0.1 M, $[NaI]_0$ = 0.05 M.*

Lewis Acid	TMSBr, NaI	1 equiv, 0.5 equiv
k	0.0046	
krel	1.533	
Time (s)	**[207] (M)**	**1/(1-F)**
0	0.000	1.00
30	0.004	1.09
60	0.008	1.20
120	0.015	1.43
180	0.020	1.69
300	0.028	2.24
450	0.033	2.96
600	0.037	3.79
900	0.038	4.01
1200	0.039	4.68
1500	0.040	5.11
1800	0.040	4.98
2700	0.041	5.60
3600	0.041	5.76
5400	0.042	6.07

Table 2.18. *Reaction data and linearization by general procedure 2.3. $[TMSCl]_0$ = 0.1 M, $[NaI]_0$ = 0.1 M*

Lewis Acid	TMSCl, NaI	1 equiv, 1 equiv
k	0.000549	
krel	0.209	
Time (s)	**[207] (M)**	**1/(1-F)**
0	0.000	1.00
30	0.001	1.02
60	0.002	1.04
120	0.003	1.07
180	0.004	1.10
300	0.007	1.16
450	0.009	1.23
600	0.012	1.31
960	0.015	1.43
1200	0.018	1.58
1500	0.021	1.72
1800	0.022	1.76
2700	0.026	2.07
3600	0.028	2.28
5400	0.031	2.65
7200	0.034	3.10

Table 2.19. *Reaction data and linearization by general procedure 2.3. $[TESCl]_0$ = 0.1 M, $[NaI]_0$ = 0.1 M.*

Lewis Acid	TESCl, NaI	1 equiv, 1 equiv
k	0.000068	
krel	0.026	
Time (s)	**[207] (M)**	**1/(1-F)**
0	0.000	1.00
30	0.000	1.00
60	0.000	1.01
120	0.001	1.01
180	0.001	1.02
300	0.001	1.02
450	0.002	1.03
600	0.002	1.04
1200	0.003	1.06
1500	0.003	1.06
1800	0.003	1.07
2700	0.004	1.09
3600	0.006	1.13
5400	0.008	1.18
7200	0.010	1.25

Table 2.20. *Reaction data and linearization by general procedure 2.3. $[TBSCl]_0$ = 0.1 M, $[NaI]_0$ = 0.1 M.*

Lewis Acid	TBSCl, NaI	1 equiv, 1 equiv
k	0.000032	
krel	0.012	
Time (s)	**[207] (M)**	**1/(1-F)**
0	0.000	1.00
30	0.000	1.00
60	0.000	1.00
120	0.000	1.01
180	0.000	1.01
300	0.000	1.01
450	0.001	1.01
600	0.001	1.01
900	0.001	1.02
1200	0.001	1.02
1500	0.001	1.02
1800	0.001	1.03
2700	0.002	1.03
3600	0.002	1.04
5400	0.003	1.06
7200	0.003	1.07

2.9.4.2 Comparison of 200 and 201 Activation Rates by L3·NiCl₂

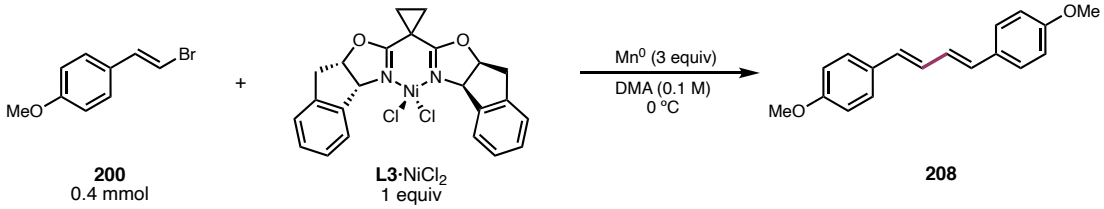

200
0.4 mmol

L3·$NiCl_2$
1 equiv

208

Reaction of L3·$NiCl_2$ with 200: To an oven-dried 10 mL round bottom flask with a stir bar was added (*E*)-1-(2-bromovinyl)-4-methoxybenzene (**200**, 85.2 mg, 0.40 mmol, 1 equiv) and Mn^0 powder (65.9 mg, 1.2 mmol, 3 equiv). In a 2-dram oven-dried vial with a stir bar was added **L3**·$NiCl_2$ (1.1 times the needed amount, 213.4 mg, 0.44 mmol, 1.1 equiv). The flask and vial were then brought into a N_2-filled glovebox where 4.4 mL of DMA was added to the vial and the contents were stirred until homogenous to make a 0.1 M stock solution of **L3**·$NiCl_2$. To the flask was then added *n*-dodecane (target: 40 μL, 0.176 mmol, 0.44 eqiuv, actual mass was recorded for each experiment) internal standard was added followed by 4 mL of the **L3**·$NiCl_2$ stock solution. The flask was then sealed with a septa and electrical tape then removed from the glovebox where it was placed under N_2 and submerged in an ice bath. A ~50 μL aliquot of the solution was removed with a N_2-purged syringe then pushed through a SiO_2 plug and eluted with 10% EtOAc:hexanes into a GC vial then further diluted with EtOAc. Once cooled, the solution was then stirred at 1500 rpm to start the reaction (t = 0). The reaction was then aliquoted with the same procedure previously described at regular intervals.

Figure 2.52. *Profile for the stoichiometric reaction of* ***L3***·$NiCl_2$ *and* ***200****.*

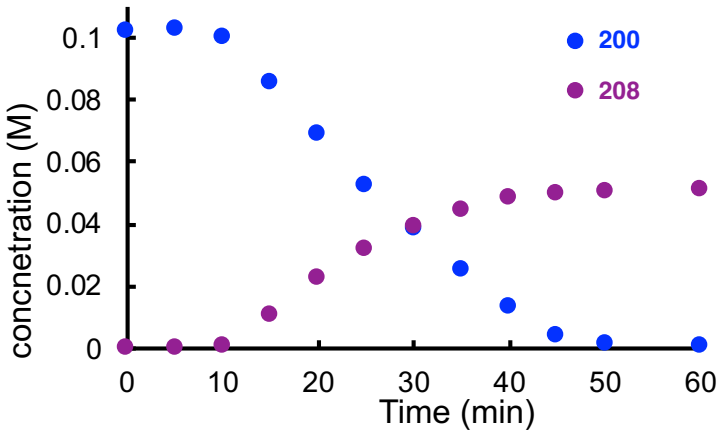

Reaction:	**200** with **L3**·$NiCl_2$	
Time (min)	**200** (M)	**208** (M)
0	0.1025	0.0000
5	0.1030	0.0000
10	0.1003	0.0007
15	0.0859	0.0108
20	0.0689	0.0227
25	0.0528	0.0322
30	0.0388	0.0396
35	0.0255	0.0450
40	0.0134	0.0487
45	0.0043	0.0497
50	0.0014	0.0506
60	0.0007	0.0510

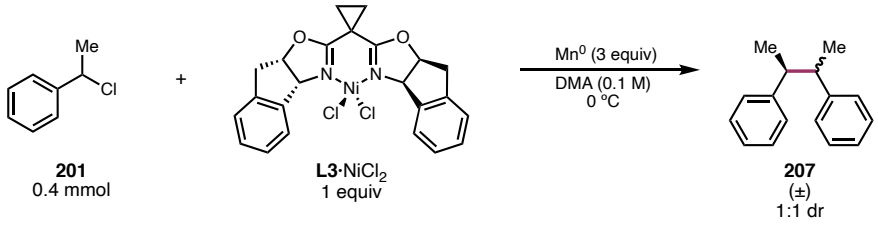

Reaction of L3·$NiCl_2$ with 201: To an oven-dried 10 mL round bottom flask with a stir bar was added Mn^0 powder (65.9 mg, 1.2 mmol, 3 equiv). In a 2-dram oven-dried vial with a stir bar was added **L3**·$NiCl_2$ (1.1 times the needed amount, 213.4 mg, 0.44 mmol, 1.1 equiv). The flask and vial were then brought into a N_2-filled glovebox where 4.4 mL of DMA was added to the vial and the contents were stirred until homogenous to make a 0.1 M stock solution of **L3**·$NiCl_2$. To the flask was added (1-Chloroethyl)benzene (**201,** 53.1 µL, 0.40 mmol, 1 equiv) and *n*-dodecane (target: 40 µL, 0.176 mmol, 0.44 equiv, actual mass was recorded for each experiment) internal standard. The **L3**·$NiCl_2$ (4 mL) stock solution was then added to the flask before it was sealed with a septa and electrical tape

then removed from the glovebox where it was placed under N_2 and submerged in an ice bath. A ~50 µL aliquot of the solution was removed with a N_2-purged syringe then pushed through a SiO_2 plug and eluted with 10% EtOAc:hexanes into a GC vial then further diluted with EtOAc. Once cooled, the solution was then stirred at 1500 rpm to start the reaction (t = 0). The reaction was then aliquoted with the same procedure previously described at regular intervals.

Figure 2.53. *Profile for the stoichiometric reaction of* ***L3***·$NiCl_2$ *and* ***201****.*

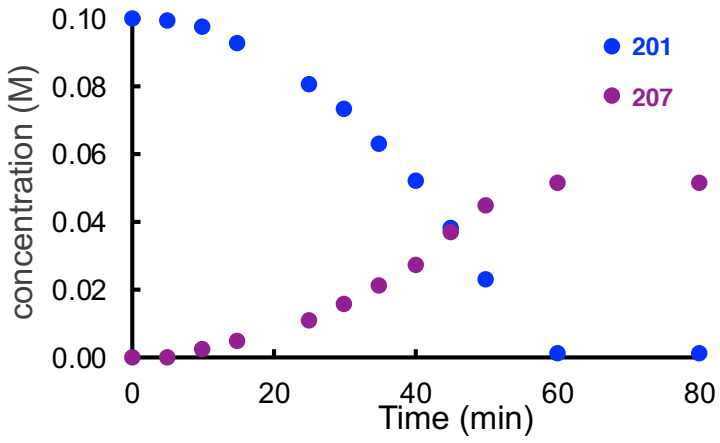

Reaction:	**201** with **L3**·$NiCl_2$	
Time (min)	**201** (M)	**207** (M)
0	0.0998	0.0000
5	0.0987	0.0000
10	0.0971	0.0021
15	0.0921	0.0046
25	0.0804	0.0108
30	0.0728	0.0153
35	0.0628	0.0210
40	0.0516	0.0272
45	0.0381	0.0367
50	0.0228	0.0446
60	0.0013	0.0511
80	0.0008	0.0513

Figure 2.54. *Overlaid reaction profiles of* ***L3***·$NiCl_2$ *with* ***200*** *and* ***201*** *(left) with simulated starting material consumption curves (right).*

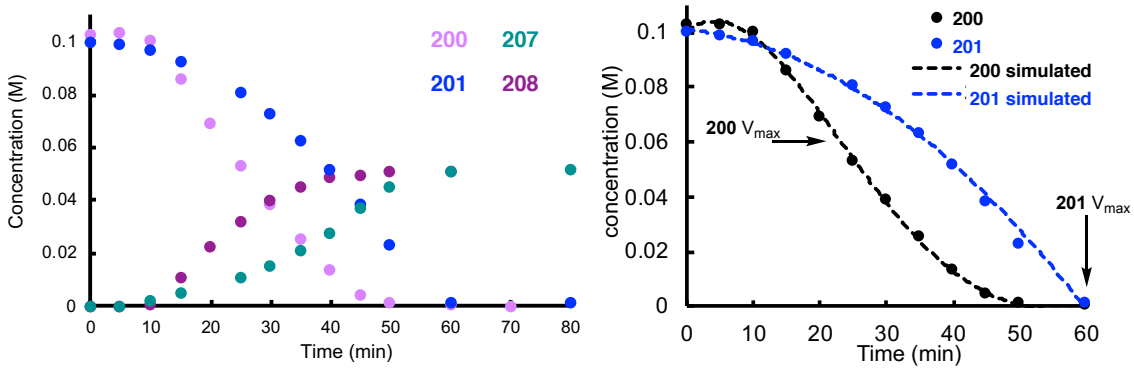

Estimating k_{rel} for 200 and 201 Activation

To estimate the relative rates of **200** and **201** activation the concentration profiles were fitted with an appropriate n^{th}-order polynomial. The simulated profile from these equations (Figure S31, right) were then derived with the power rule to obtain an expression for d[**200**]/dt and d[**201**]/dt. Comparing the rates at 15% conversion gives a **200**:**201** k_{rel} = 4.1 whereas comparison of the maximum rates (V_{max}) gives a **200**:**201** k_{rel} = 1.3. These values are reasonable based on the reaction kinetic data that shows **200** activation is faster yet **201** is competitive at higher concentrations of **201** (Figure 2.16c).

2.9.5 Catalyst-Mediated 201 Activation Control Experiments

Figure 2.55. *Control experiments probing necessary components for* ***201*** *activation.*

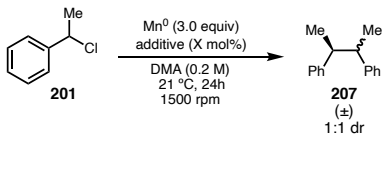

additive	**207** yield %
NA	ND
NaI (50 mol%)	< 5
$MnCl_2$ (10 mol%)	ND
L3·$NiCl_2$ (10 mol%)	82
$NiCl_2$•dme (10 mol%)	63
L3 (10 mol%)	ND

Procedure for Control Experiments: To an oven dried 1 dram vial with a stir bar was added Mn^0 powder (8.2 mg, 0.15 mmol, 3 equiv). The vial was then brought into a N_2-filled glovebox where (1-chloroethyl)benzene (**201**, 6.6 µL, 0.050 mmol, 1 equiv), *n*-dodecane internal standard, and the respective additive (if applicable) was added. DMA (0.25 mL, 0.2 M) was then added to the vial before it was sealed with a teflon-lined cap and removed from the glovebox. The reactions were allowed to stir at ambient temperature for 24h at 1500 rpm. Upon completion the crude reaction mixture was filtered through SiO_2 plug and eluted with 10% EtOAc:hexanes into a GC vial then further diluted with EtOAc,

then analyzed by GC-FID. Reaction were run in duplicate and no other **201**-derived byproducts (other than **207**) were detected.

These control experiments show that Ni is required for **201** activation meaning a reductant-mediated activation pathway, like **202**, is unlikely.

2.9.6 Cyclic Voltammetry Experiments

General Details: Cyclic voltammograms were obtained in a N_2-filled glovebox using a standard three electrode cell consisting of a freshly polished (0.3 μm then 0.05 μm alumina) glassy carbon working electrode, platinum counter electrode, and a silver wire non-aqueous reference electrode containg a 10 mM $AgNO_3$, 0.1 M $TBAPF_6$, MeCN filling solution. Data were collected using a Biologic SP-300 potentiostat and analyzed in EC-Lab. All cyclic voltammograms were measured in DMA with 0.1 M $TBAPF_6$ or 0.1 M $TBAClO_4$ supporting electrolyte and then referenced to freshly sublimed ferrocene (Fc). $TBAPF_6$ was recrystallized from boiling absolute ethanol and stored in a N_2-filled gloveox. The reduction potentials are reported versus the reduction potential of the Fc/Fc^+ peak. Ohmic drop compensation was done with all samples before each scan using positive-feedback iR-compensation at 85% of uncompensated resistance (R_u) measured from potentio electrochemical impedence spectroscopy (PEIS). The first scan is shown in the following section and the main text unless otherwise specified.

2.9.6.1 CVs of L3·NiX₂ Complexes and Individual Reaction Components

Figure 2.56. *CV of* ***L3***·$NiBr_2$ *(1 mM) in 0.1 M* $TBAPF_6$ *DMA,* ***ν = 100 mv/s.***

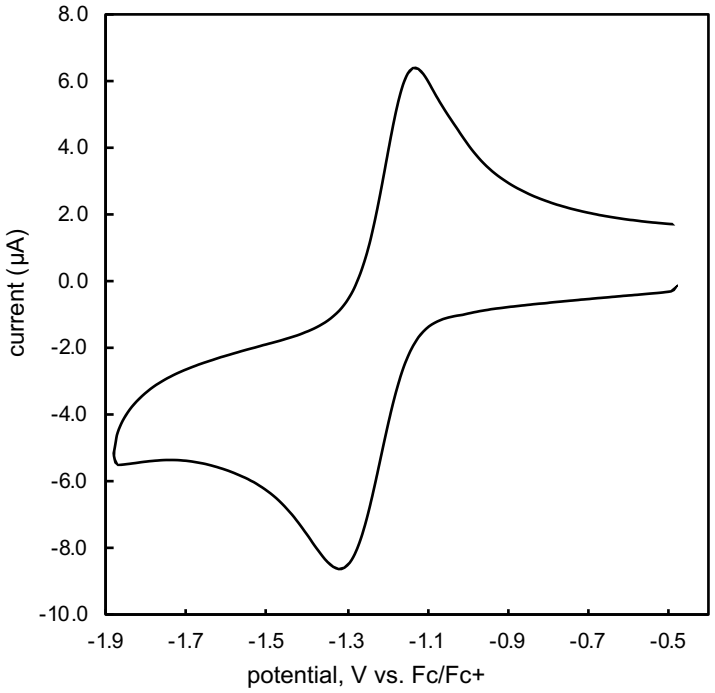

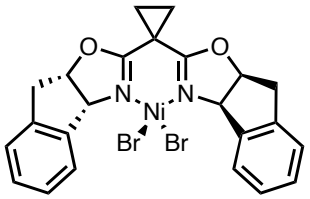

Analyte	**L3**·$NiBr_2$
Epc (Fc/Fc+)	– 1.31 V
Epc/2 (Fc/Fc+)	– 1.23 V
Epa (Fc/Fc+)	– 1.11 V

Figure 2.57. *CV of* ***L3***·$NiCl_2$ *(1 mM) in 0.1 M* $TBAPF_6$ *DMA,* ν *= 100 mv/s.*

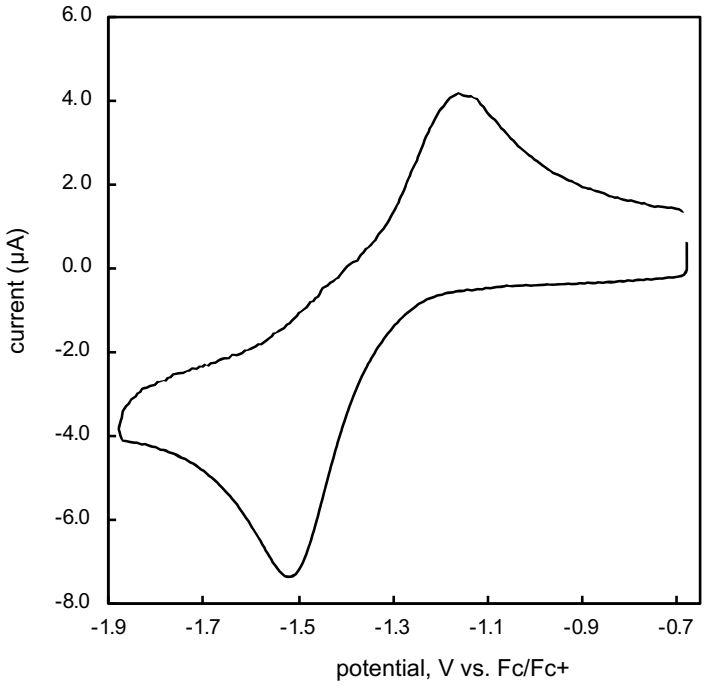

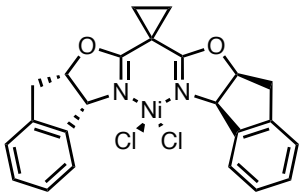

Analyte	**L3**·$NiCl_2$
Epc (Fc/Fc+)	– 1.52 V
Epc/2 (Fc/Fc+)	– 1.41 V
Epa (Fc/Fc+)	– 1.13 V

Figure 2.58. *CV of TDAE (1 mM) in 0.1 M* $TBAPF_6$ *DMA,* ν *= 100 mv/s.*

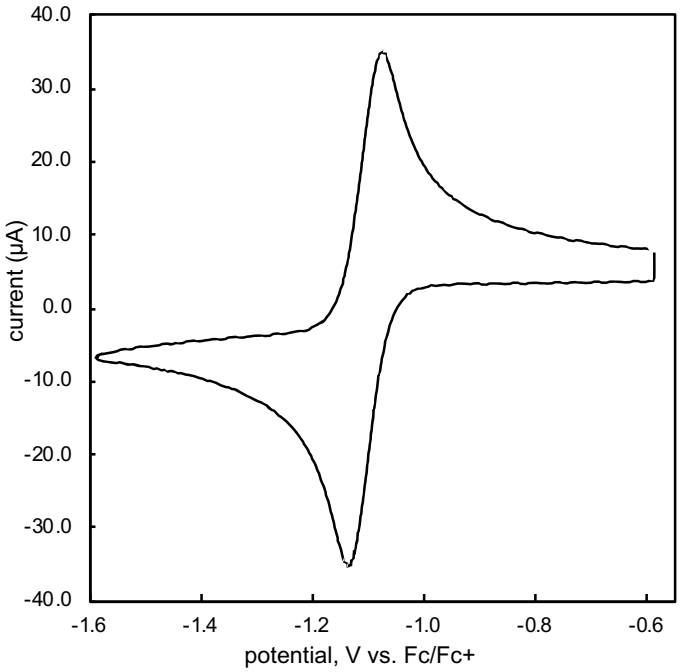

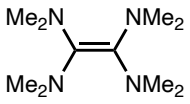

Analyte:	TDAE
E1/2(Fc/Fc+)	-1.11 V

Figure 2.59. *CV of* ***202*** *(1 mM) in 0.1 M $TBAPF_6$ DMA, ν = 100 mv/s.*

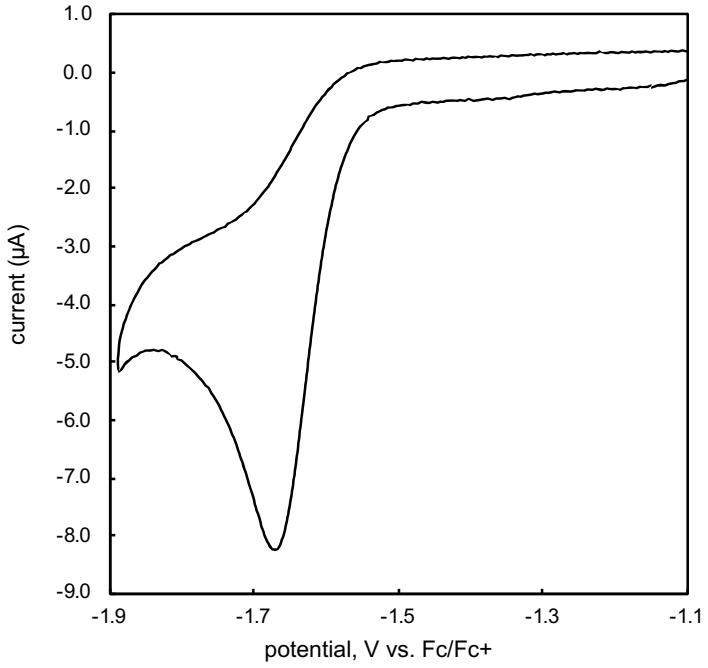

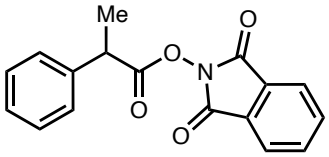

Analyte:	**202**
Ep (Fc/Fc+)	-1.67 V
Ep/2 (Fc/Fc+)	-1.61 V

Figure 2.60. *CV of* ***202*** *(1 mM) alone and* ***202*** *(1 mM) with TMSBr (1 mM) in 0.1 M $TBAClO_4$ DMA, ν = 100 mv/s.*

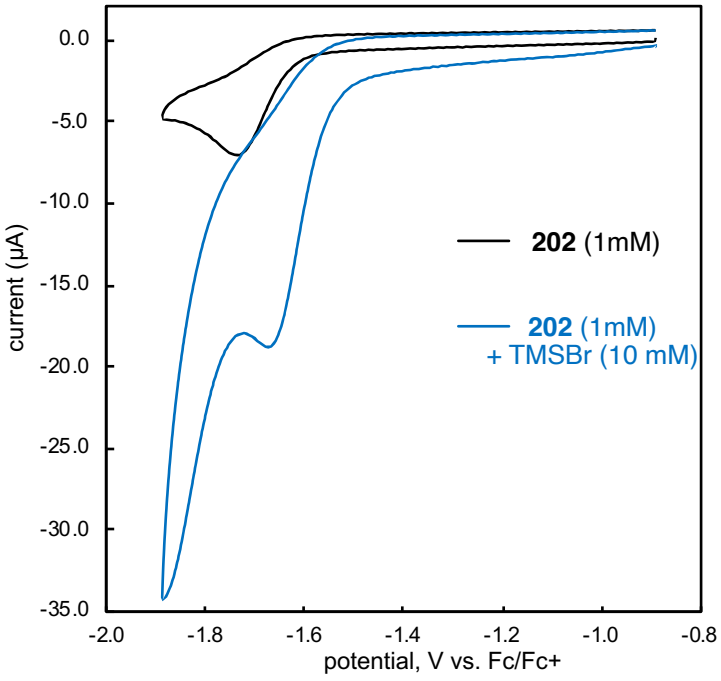

2.9.6.2 Substrate Titration and Catalytic Current Comparison

Procedure for Substrate Titration for Current response of L3·$NiCl_2$: For these experiments CVs were taken of 1 mM **L3**·$NiCl_2$ followed by the addition of an appropriate amount of **200** or **201** was added for subsequent scans. At the end of each titration the substrate that was not previously titrated in was then added in equimolar amounts.

Figure 2.61. *CV of titration of **200** to 1 mM **L3**·$NiCl_2$ (left) and then addition of a large excess to **201** to compare catalytic currents (right). 0.1 M $TBAPF_6$ DMA, ν = 100 mv/s.*

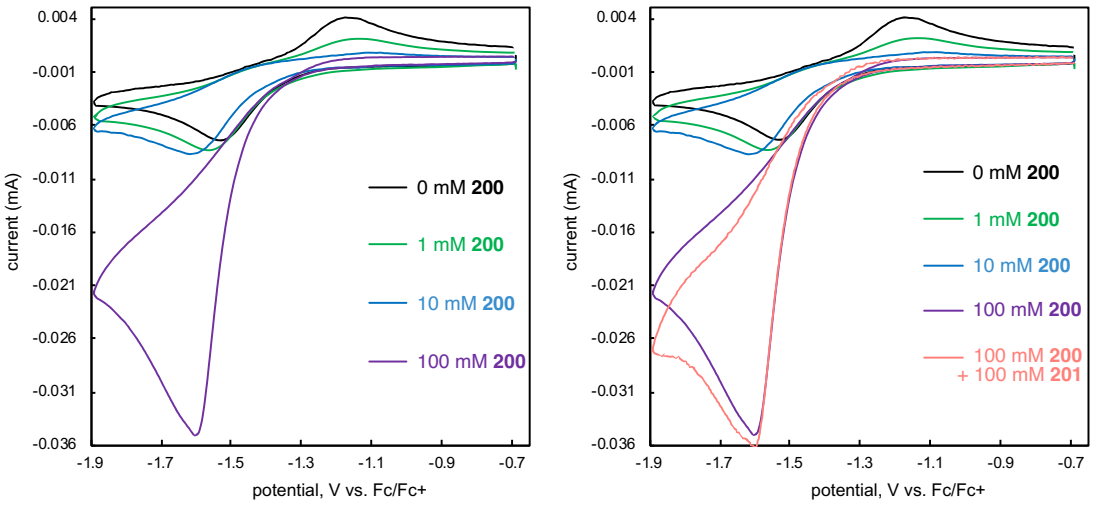

Figure 2.62. *CV of titration of* ***201*** *to 1 mM* ***L3***·$NiCl_2$ *(left) and then addition of a large excess to* ***200*** *to compare catalytic currents (right). 0.1 M $TBAPF_6$ DMA, ν = 100 mv/s.*

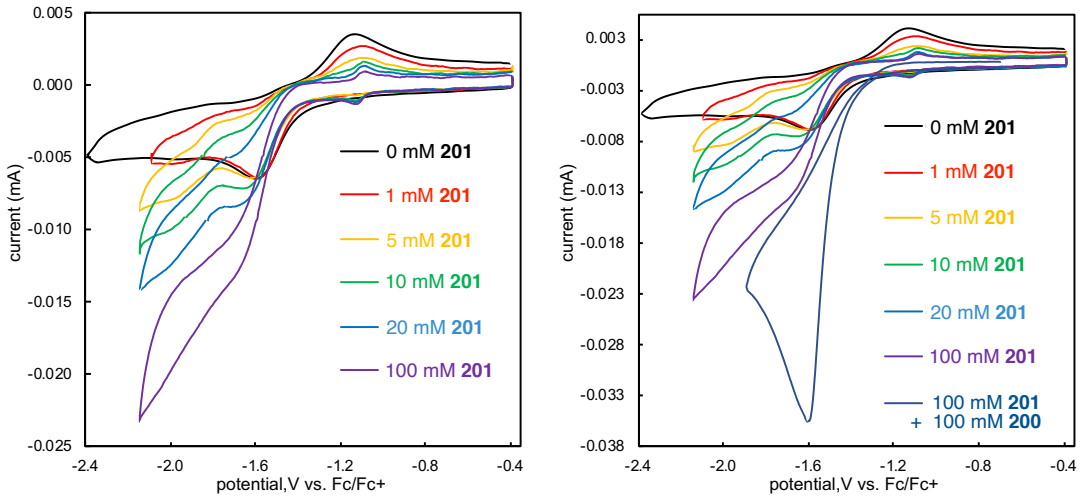

2.9.7 NMR Reaction Monitoring

2.9.7.1 Monitoring ARA of NHP Ester with ^{19}F NMR

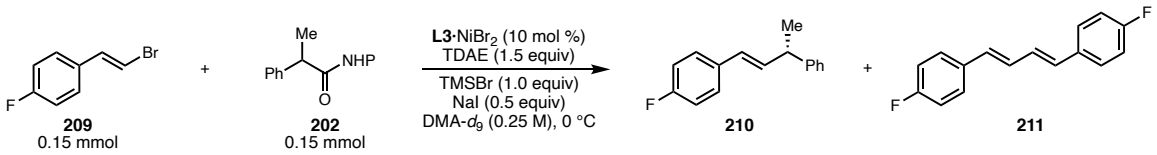

General procedure 2.4 for ^{19}F Reaction Monitoring: In a N_2-filled glovebox (*E*)-1-(2-bromovinyl)-4-fluorobenzene (**209**, 30.2 mg, 0.15 mmol, 1 equiv), 1,3-dioxoisoindolin-2-yl 2-phenylpropanoate (**202,** 44.3 mg, 0.15 mmol, 1 equiv), **L3**·$NiBr_2$ (8.6 mg, 0.015 mmol, 0.1 equiv), NaI (11.2 mg, 0.075 mmol, 0.5 equiv), and hexafluorobenzene internal standard were added to a dry 1 dram vial with a stir bar. The contents were then dissolved in 0.3 mL

of DMA-d^9 then transferred to a dry J-young NMR tube. The vial was rinsed with 0.3 mL of DMA (0.6 mL final volume, 0.25 M final concentration) to ensure quantitative transfer. The NMR tube was then sealed and removed from the glovebox where it was then cooled to 0 ºC in the NMR instrument (air bath cooling to 0 ºC). The sample was locked/shimmed and an initial quantitative ^{19}F NMR measurement was taken in order to determine starting concentration. The tube was then removed from the instrument, submerged in an ice bath, fitted with a septa, and Ar balloon. The tube was opened then TMSBr (19.8 uL, 0.15 mmol, 1 equiv) was added via syringe and the tube was agitated to ensure adequate mixing. After 30 seconds TDAE (52.3 µL, 0.225 mmol, 1.5 equiv) was added to start the reaction and the tube was immediately sealed, placed back in the NMR instrument, and qNMR (single scan, 27s interscan delay) scans (measured 3 minute delay from TDAE addition to completion of first measurement). Measurements were taken every 30 seconds for the first 3 hours of the reaction and then every minute for the next 3 hours (6 hours total). At the end of the reaction the product was isolated to determine ee of **210** as 93% by SFC analysis (OJ-H, 7% IPA:CO_2, t_{major} = 7.07 min, t_{minor}=5.86 min).**Error! Bookmark not defined.**

Modifications to General Procedure for 20 mol % Catalyst Loadings: For this experiment more **L3**·$NiBr_2$ (17.2 mg, 0.030 mmol, 0.2 equiv) added to 1 dram vial. The delay between TDAE addition and the first scan was shortened to one minute instead of three minutes. Scan taken every one minute for the entire experiment and the reaction was monitored for 5 hours total.

Representative Spectra (full window):

Figure 2.63. *^{19}F NMR full window view of reaction mixture before TDAE is added.*

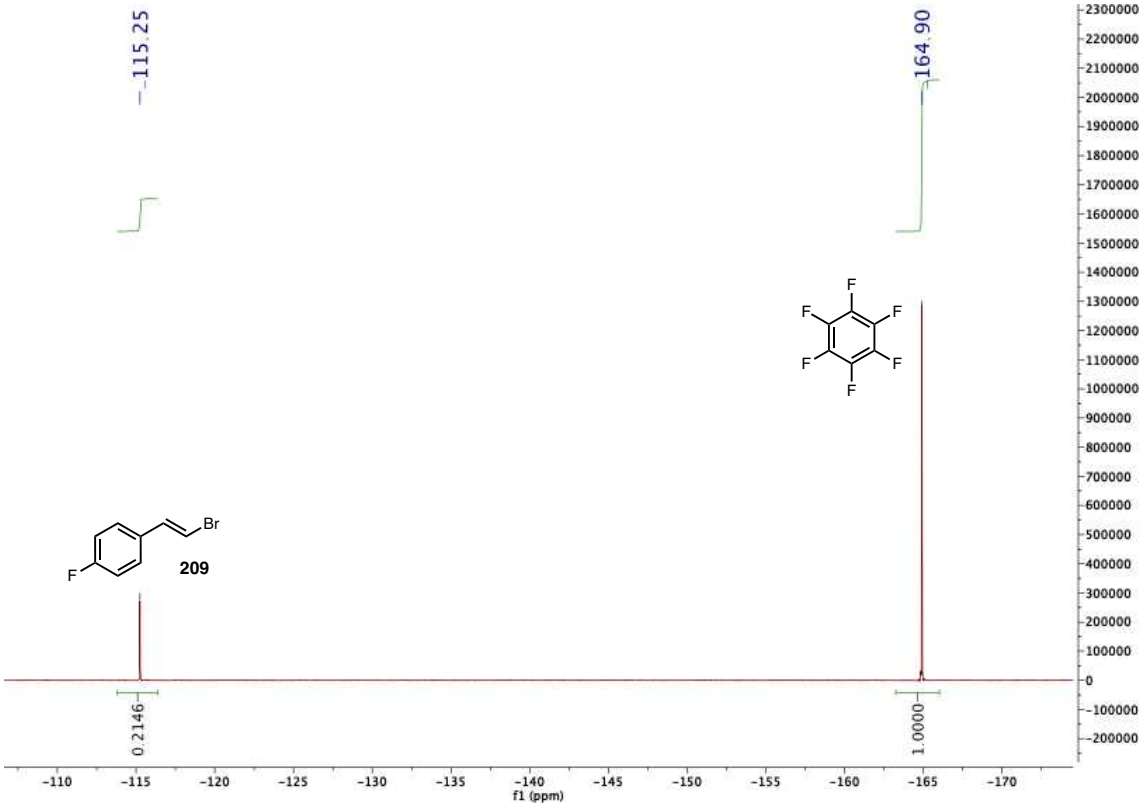

Figure 2.64. *^{19}F NMR full window view of reaction mixture 3 minutes after TDAE is added*

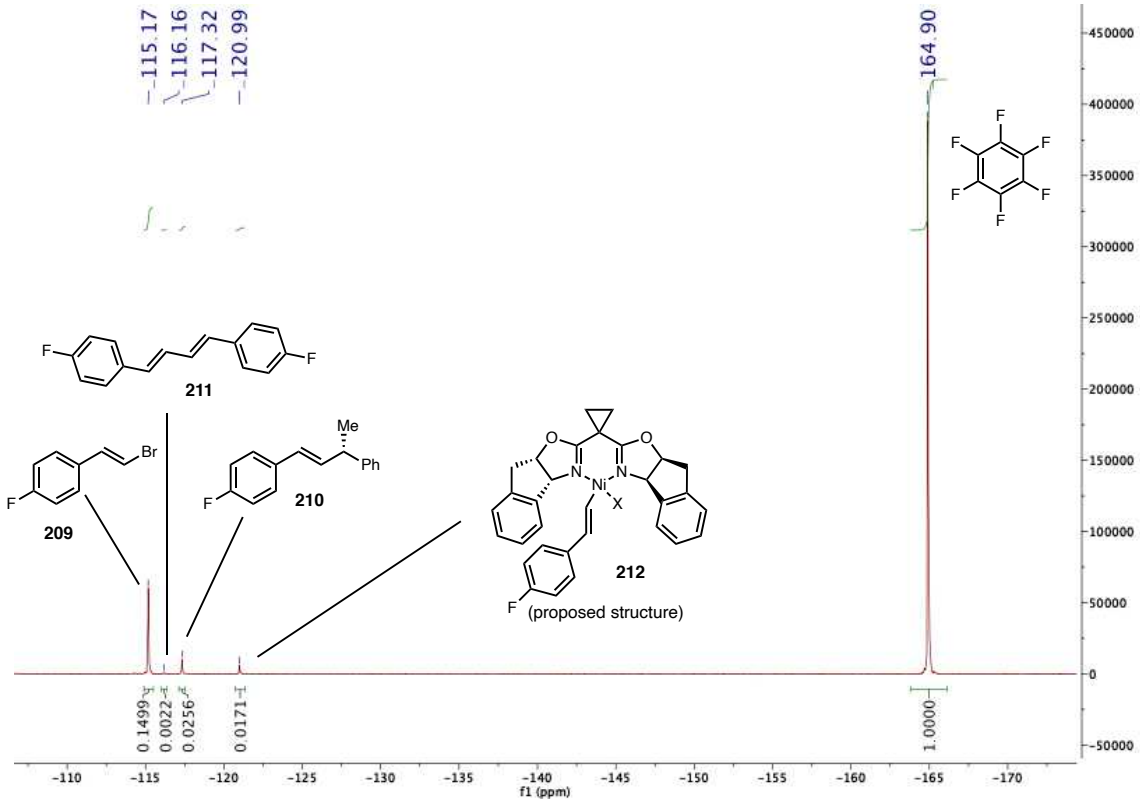

Figure 2.65. *^{19}F NMR full window view of reaction mixture 3 hours after TDAE is added.*

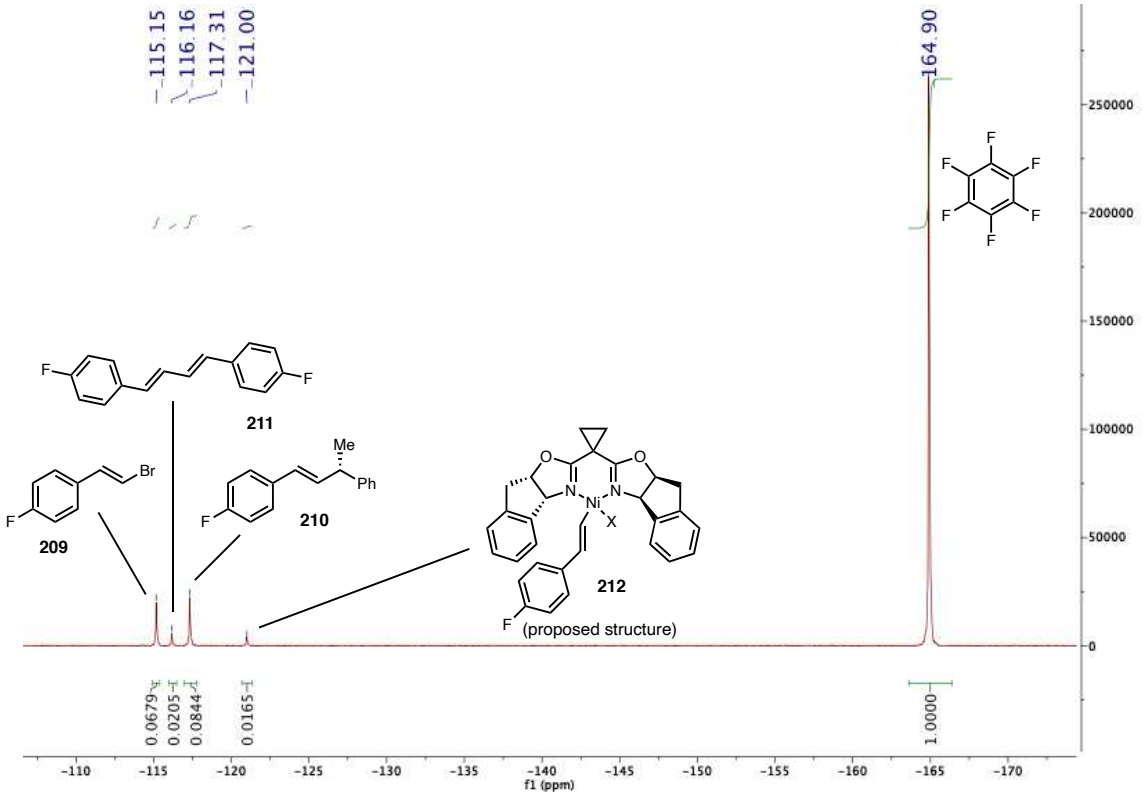

Independently prepared, C_6F_6-referenced (C_6F_6 = -164.9 ppm) NMR characterization in $CDCl_3$ of possible **209**-derived species. This includes species like 4-fluorostyrene and **218** that were not observed in the reaction mixture. It is noteworthy that while the absolute chemical shifts of independently prepared species in $CDCl_3$ are different than those observed in the reaction mixture in DMA-d_9 (Figure 2.63-65), the relative shifts are the same (Table 2.21).

Figure 2.66. *^{19}F NMR chemical shifts for reaction components and potential byproducts. No species corresponds to the observed intermediate assigned as* ***212****. Reported shifts are referenced such that C_6F_6 = -164.9 ppm.*

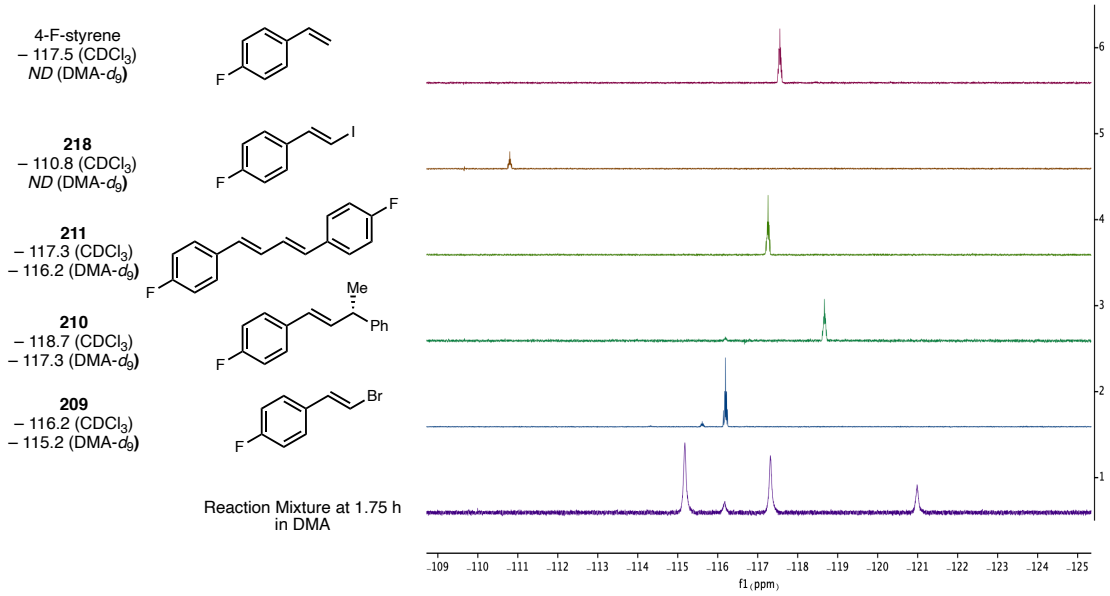

Table 2.21. *Tabulated ^{19}F NMR chemical shifts in $CDCl_3$ and DMA-d_9 as well as relative shifts compared to* ***209*****.**

	4-F-styrene	**218**	**211**	**210**	**209**	Resting State
CDCl3 (ppm)	-117.5	-110.8	-117.3	-118.7	-116.2	ND
DMA-d9 (ppm)	ND	ND	-116.2	-117.3	-115.2	-120.99
Δ to **209** ppm (CDCl3)	-1.3	5.4	-1.1	-2.5	0	–
Δ to **209** ppm (DMA-d9)	–	–	-1	-2.1	0	-5.79

Table 2.22. *Comparison between observed and DFT-predicted ^{19}F chemical shifts***.**

Δ to C_6F_6 (DMA)	**209**	**211**	**212**
Observed	51.00	50.00	45.00
DFT Predicted	47.00	46.00	37.00

Processed Reaction Data:

Figure 2.67. *Quantified amount of each species for ^{19}F NMR time course shown in main text.*

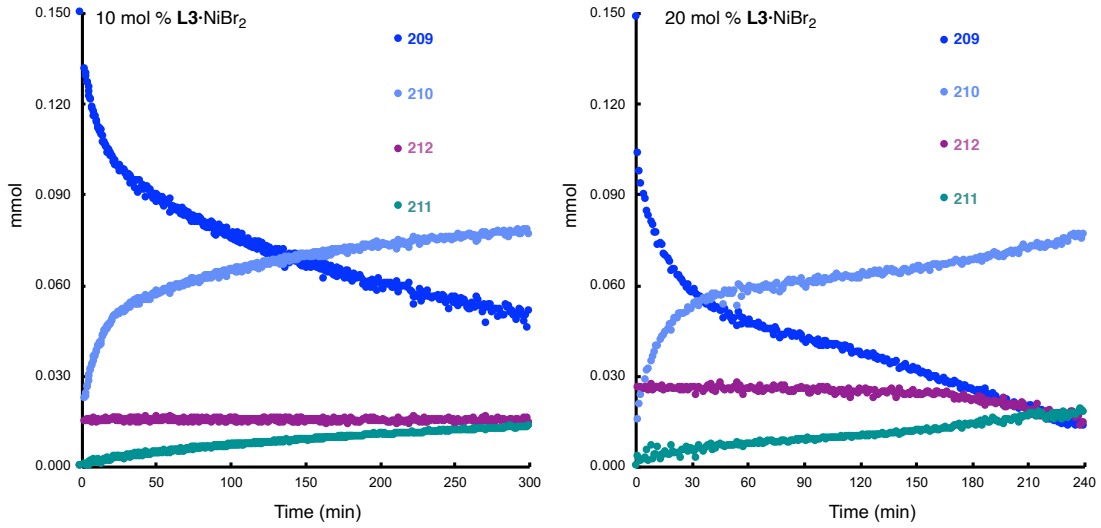

Figure 2.68. *Comparison of the resting state concentration for experiments starting with10 and 20 mol % **L3**·$NiBr_2$ including table showing how average concentration was calculated for each experiment.*

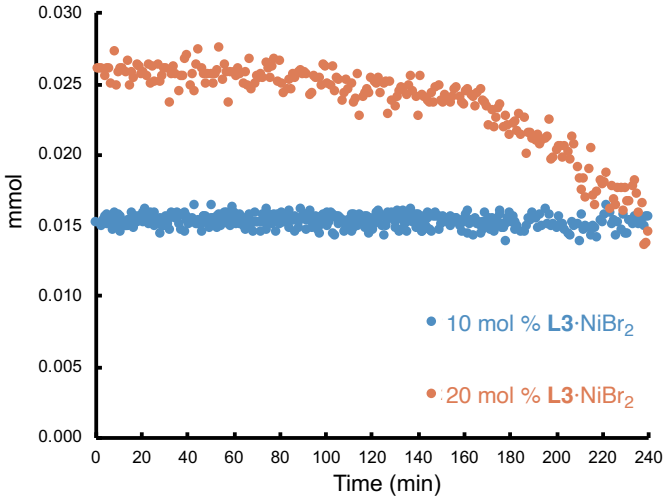

L3·$NiBr_2$ loading	Avg **L3**·$NiBr_2$ (mmol/mol %)	Std Dev (mmol)	Period Used for Avg
10 mol %	0.015 / 10.1	0.0005	3 min – 5 h
20 mol %	0.025 / 16.9	0.0008	1 min – 2 h

2.9.7.2 Room Temperature NMR Experiments

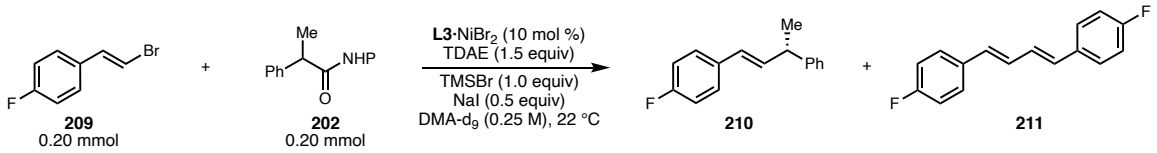

Ambient Temperature NMR Reaction: In a N_2-filled glovebox (*E*)-1-(2-bromovinyl)-4-fluorobenzene (**209**, 40.2 mg, 0.20 mmol, 1 equiv), 1,3-dioxoisoindolin-2-yl 2-phenylpropanoate (**202**, 59.1 mg, 0.2 mmol, 1 equiv), **L3**·$NiBr_2$ (11.5 mg, 0.020 mmol, 0.1 equiv), NaI (15.0 mg, 0.10 mmol, 0.5 equiv), and hexafluorobenzene internal standard were added to a dry 1 dram vial with a stir bar. The contents were then dissolved in 0.4 mL of DMA-d_9 then transferred to a dry J-young NMR tube. The vial was rinsed with 0.4 mL of DMA (0.6 mL final volume, 0.25 M final concentration) to ensure quantitative transfer. The NMR tube was then sealed and removed from the glovebox. The sample was locked/shimmed and an initial quantitative ^{19}F NMR measurement was taken in order to determine starting concentration. The tube was then removed from the instrument, fit with a septa, and Ar balloon. To the tube was then added TMSBr (26.4 μL, 0.20 mmol, 1 equiv) was added via syringe and the tube was agitated to ensure adequate mixing. After 30 seconds TDAE (69.8 μL, 0.30 mmol, 1.5 equiv) was added to start the reaction and the tube was immediately sealed, placed back in the NMR instrument and monitored at 22 ºC.

Figure 2.69. *Concentration of **209**-derived species over the course of the reaction (left). Concentration of resting state species **212** during the time course (right).*

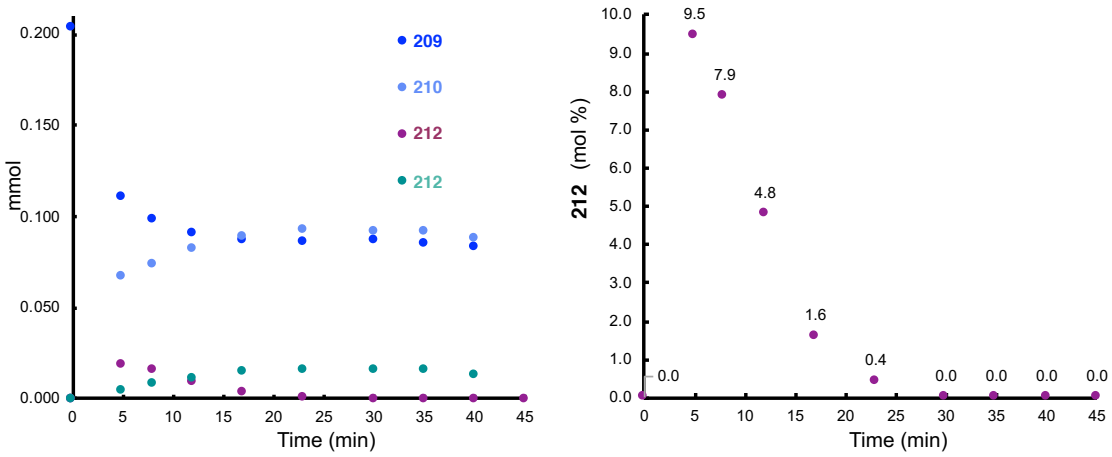

2.9.8 EPR Experiments

2.9.8.1 Generation of Ni(I) from Chemical Reduction of L3·NiX₂

Reduction of L3·NiBr₂ by TDAE: To an oven-dried 20 mL was added **L3**·$NiBr_2$ (5.7 mg, 0.010 mmol, 1 equiv). The vial was brought into a N_2-filled glovebox and the solid was dissolved in 10 mL of anhydrous DMA. To this vial TDAE (2.33 uL, 0.010 mmol, 1 equiv) was added. The reaction was stirred for 2 h, after which an aliquot was removed by a syringe, filtered, and transferred to an oven-dried EPR tube. The tube was sealed, removed from the glovebox, and then frozen in LN_2 for analysis by EPR at 77 K.

Figure 2.70. *Observed and simulated spectra of reduction of* ***L3***·$NiBr_2$ *by TDAE. The EPR spectra were collected at 9.371 GHz with a micropower of 2 mW, a modulation amplitude of 4 G, and a conversion time of 40.96 ms. The spectrum shown here was averaged over 4 scans. Nickel signals were simulated with g = [2.078, 2.089, 2.335] with a linewidth of 4 mT. TDAE$^{\bullet+}$ signals were simulated with g_{iso} = 2.0069 with a linewidth of 3 mT. The two species exist in a 1:0.78 ratio.*

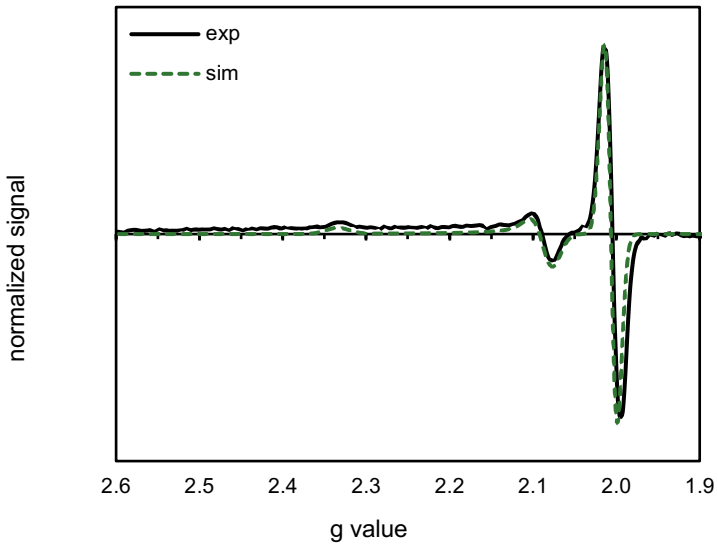

Figure 2.71. *Observed and simulated spectra of [TDAE]Br (left). Overlay of independent [TDAE]Br and* ***L3***·$NiBr_2$ *from Figure 2.70 (right). The EPR spectra were collected at 9.370 GHz with a micropower of 2 mW, a modulation amplitude of 4 G, and a conversion time of 40.96 ms. The spectrum shown here was averaged over 4 scans. The isotropic signal was simulated with* g_{iso} *= 2.006 with a linewidth of 3.8 mT prepared by mixing TDAE and isolated*

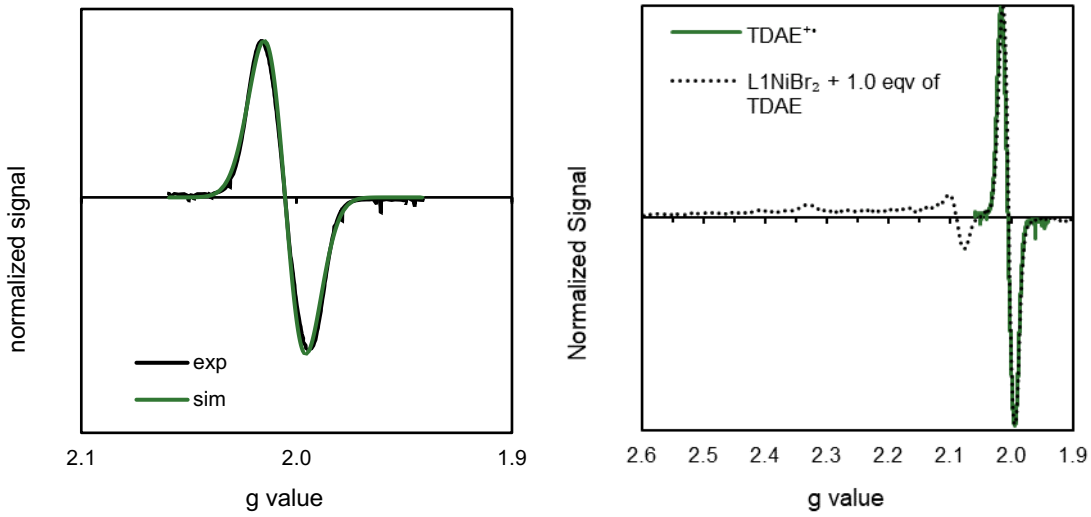

Reduction of L3·$NiBr_2$ by L3·Ni(cod): In a N_2-filled glovebox $Ni(cod)_2$ (8.3 mg, 0.030 mmol, 1 equiv) and **L3** (10.7 mg, 0.030 mmol, 1 equiv) were added to an oven-dried 20 mL scintillation and dissolved in 7.5 mL of anhydrous DMA. The reaction was stirred for 1.5 h for and then **L3**·$NiBr_2$ (17.2 mg, 0.030 mmol, 1 equiv) was added. After 1 min of stirring, a 300 uL aliquot was removed by a syringe and transferred to an oven-dried EPR tube. The tube was sealed, removed from the glovebox, and then frozen in LN_2 for analysis by EPR at 77 K.

Figure 2.72. *Observed and simulated spectra of reduction of* ***L3***·$NiBr_2$ *by* ***L3***·*Ni(cod). The EPR spectra were collected at 9.392 GHz with a micropower of 2.0 mW, a modulation amplitude of 4 G, and a conversion time of 4 ms. The spectrum shown here was averaged over 9 scans. Nickel signals were simulated with g = [2.075, 2.085, 2.328] with a linewidth of 4 mT.*

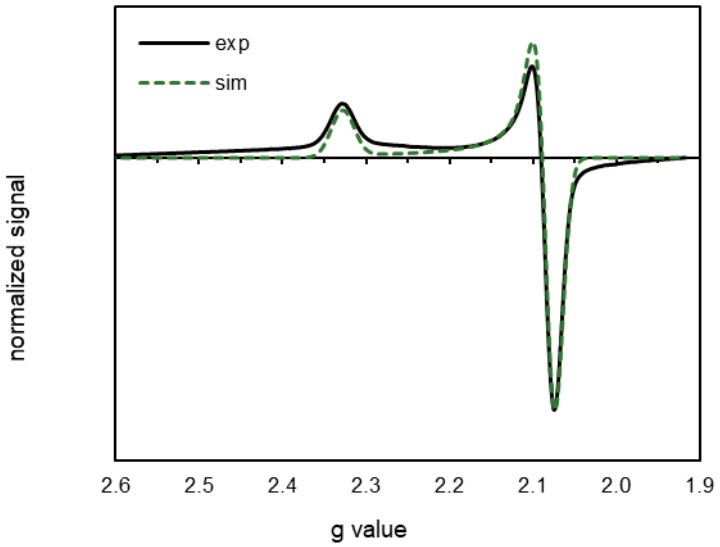

Reduction of L3·$NiCl_2$ by Zn: For preparation procedure see section 2.9.8.3.

Figure 2.73. *Observed and simulated spectra of reduction of **L3**·$NiCl_2$ by Zn at 2.75 h. The EPR spectra were collected at 9.368 GHz with a micropower 2.0 mW, a modulation amplitude of 4 G, and a conversion time of 40.96 ms. The spectrum shown here was averaged over 9 scans. The nickel signals were simulated with g = [2.095, 2.141, 2.471] with a nitrogen superhyperfine tensor A = [30, 40, 40] MHz and a linewidth of 4 mT.*

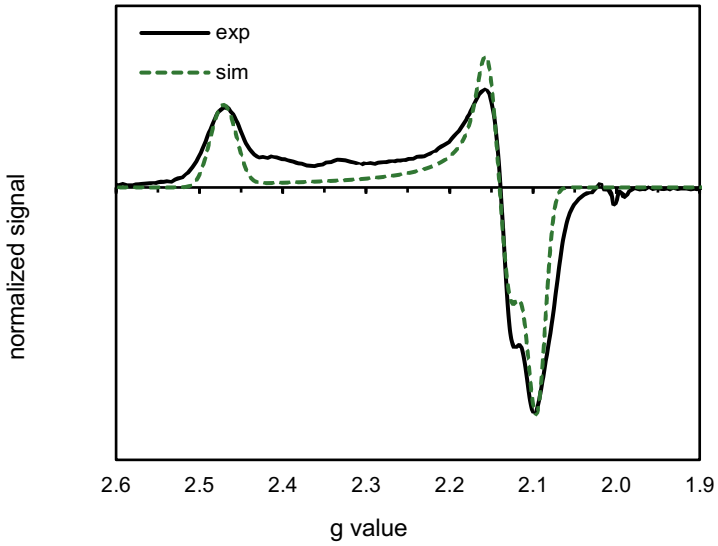

2.9.8.2 Reaction of L3·Ni(COD) with 200

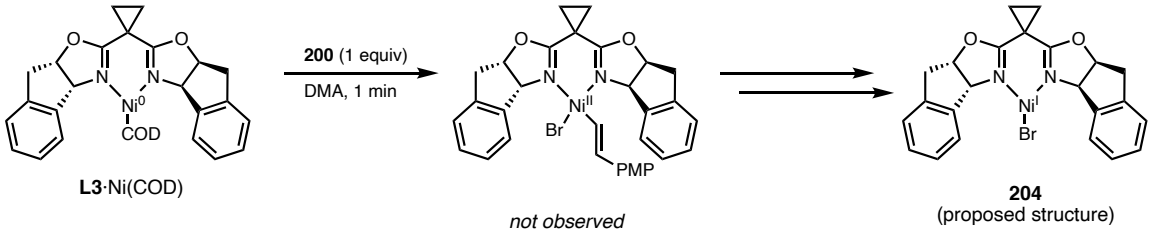

Oxidative addition of 200 by L3·Ni(cod): In a N_2-filled glovebox $Ni(cod)_2$ (2.8 mg, 0.010 mmol, 1 equiv) and **L3** (3.7 mg, 0.010 mmol, 1 equiv) were added to an oven-dried 2-dram vial. The mixture was dissolved in DMA and stirred for 24 h at 30 °C, after which **200** (2.1

mg, 0.100 mmol, 1 equiv) was added . In a separate vial, 21.4 mg of **200** was dissolved in 100 uL of anhydrous DMA; 10 uL (0.010 mol, 1 equiv) or 5 uL (0.005 mol, 0.5 equiv) of this 1M stock solution was added **L3**·Ni(cod). The reaction was stirred for 1 min after which an aliquot was removed and transferred to an oven-dried EPR tube. The tube was sealed, removed from the glovebox, and then frozen in LN_2 for analysis by EPR at 77 K.

Figure 2.74. *Truncated observed and simulated spectra of the stoichiometric mixture of* ***L3***·*Ni(cod) (1.0 equivalent) and* ***200*** *(1.0 equivalent). The EPR spectrum was collected at 9.511 GHz with a micropower of 6.4 mW, a modulation amplitude of 4 G, and a conversion time of 40.96 ms. No additional signals were observed for g values between 2.60 and 6.80 that would suggest S ≠ ½ species were present. The nickel signals were simulated with g = [2.078, 2.085, 2.330] with a linewidth of 4 mT.*

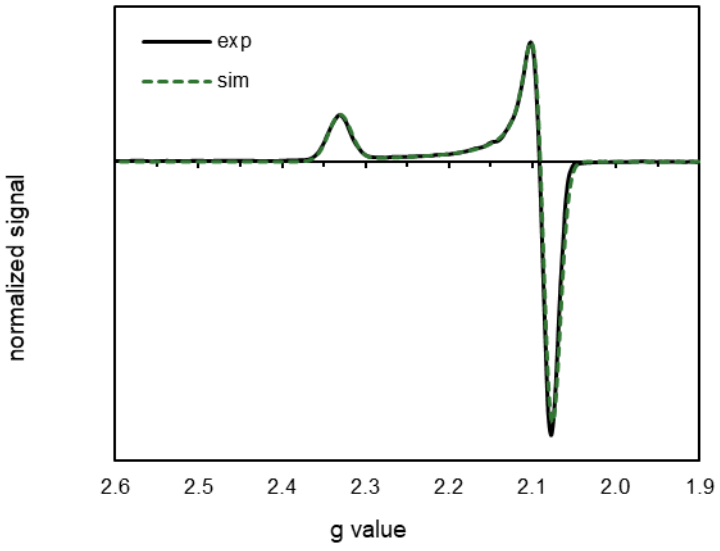

Figure 2.75. *Same as Figure 2.74 but with* ***L3***·*Ni(cod) (2.0 equivalent) and* ***200*** *(1.0 equivalent).*

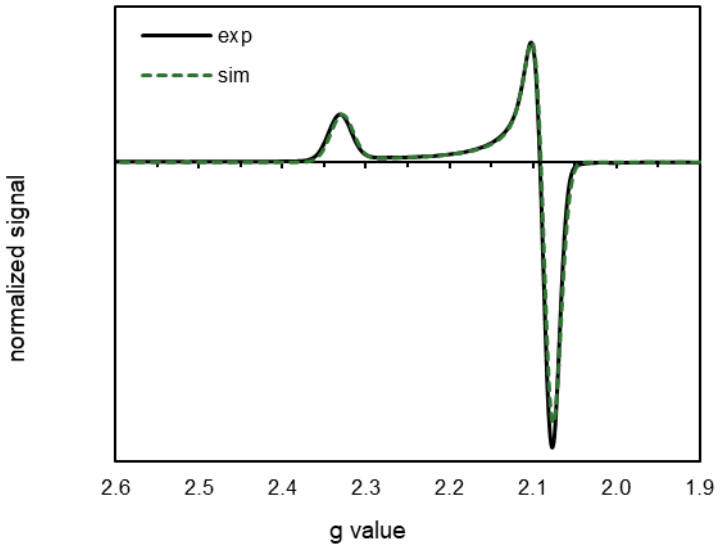

2.9.8.3 Time Course Reduction of L3·NiCl₂ with Zn⁰

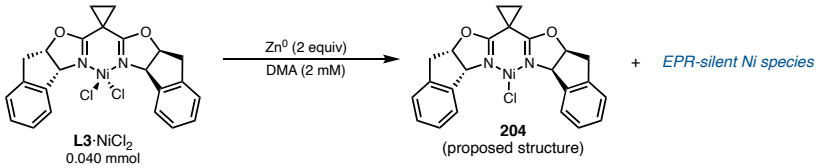

Reduction Reaction and Sample Preparation Procedure: To an oven-dried 50 mL round bottom flask was added Zn^0 powder (5.2 mg, 0.080 mmol, 2 equiv) and **L3**·$NiCl_2$ (19.4 mg, 0.040 mmol, 1 equiv). The flask was then brought into a N_2-filled glovebox where DMA (20 mL, 2 mM) was added. Before the reaction was stirred, a 2 mL aliquot was removed by a syringe fit with a 0.45 μm filter and added to a 10 mm pathlength optical cell and an oven-dried EPR tube. The tube was then removed from the glovebox and frozen in LN_2 for analysis by perpendicular mode EPR at 77 K and parallel mode EPR at 5 K. The optical cell was sealed and removed from the glovebox for analysis by optical

spectroscopy. The reaction mixture was then stirred at 1000 rpm to start the reaction and aliquots (same procedure as before) were removed at regular intervals: 0.5 h, 1 h, 1.5 h, 2.75 h, 5 h, 8 h, and 30 h.

Figure 2.76. *Observed perpendicular mode EPR spectra during the first 2.75 h of reaction. The EPR spectra were taken at 9.368 GHz (0 h), 9.364 GHz (0.5 h), 9.375 GHz (1 h), 9.368 GHz (1.5 h), and 9.368 GHz (2.75 h). Spectrum at each timepoint was averaged over 9 scans. The spectra were collected at microwave power of 2.0 mW with a modulation amplitude of 4 G and conversion time of 40.96 ms.*

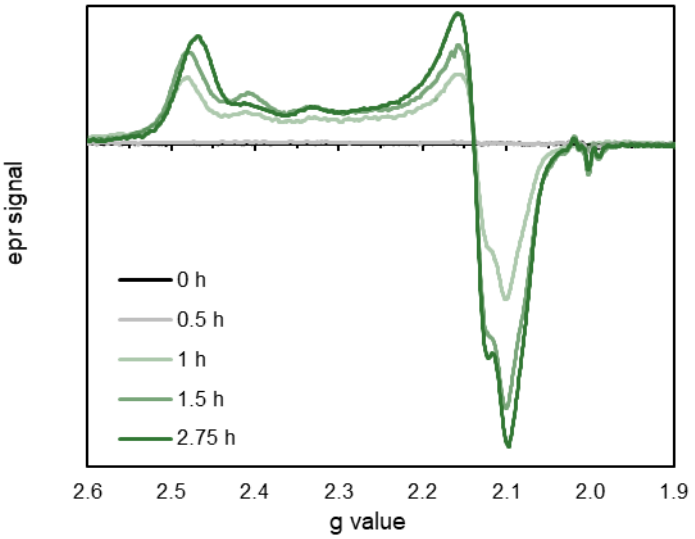

Figure 2.77. *Same reaction as Figure 2.76 showing later timepoints.*

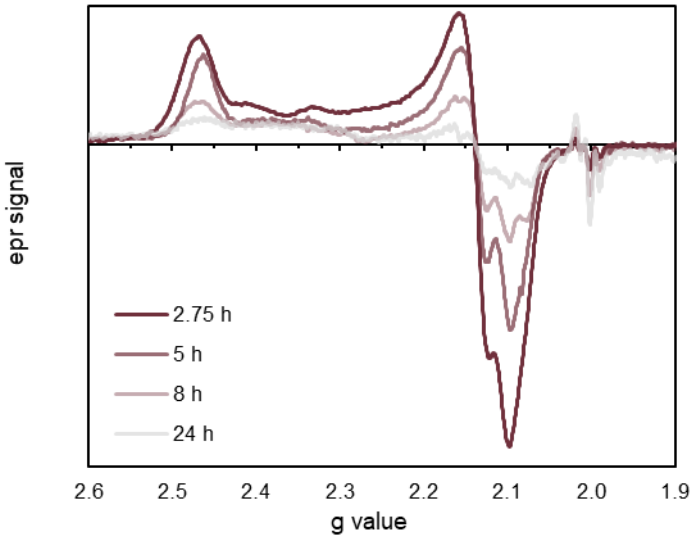

Figure 2.78. *Concentration of EPR active species quantified with an external calibration curve.*[34]

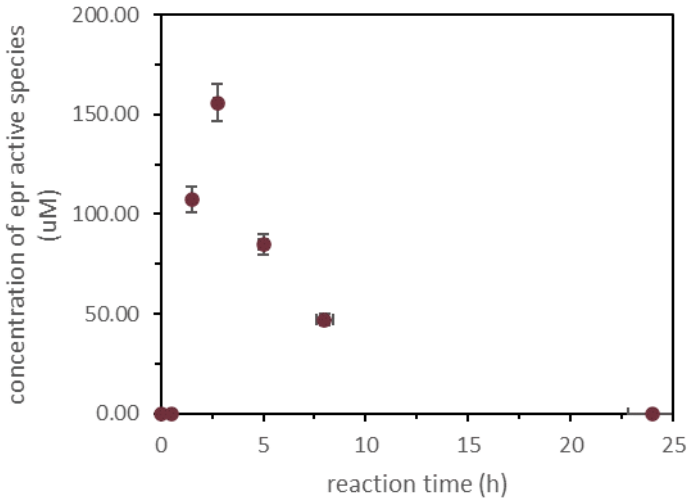

Figure 2.79. *Corresponding optical spectra during the first 2.75h of the reaction.*

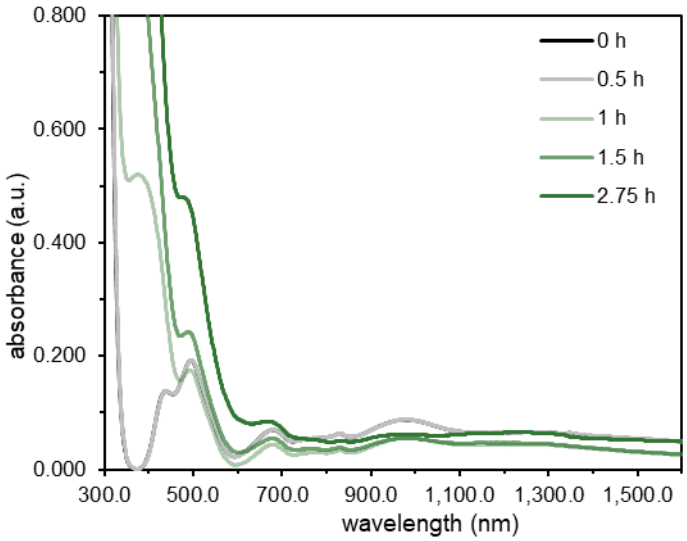

Figure 2.80. *Corresponding optical spectra after first 2.75h of the reaction.*

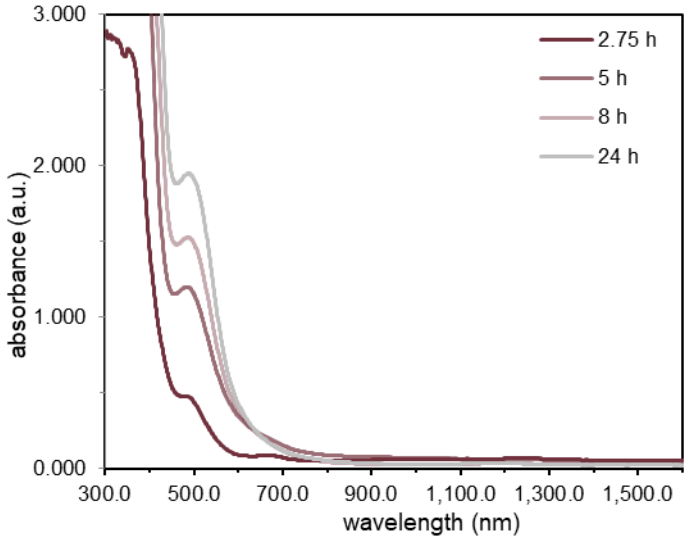

2.9.8.4 Reaction Monitoring with EPR

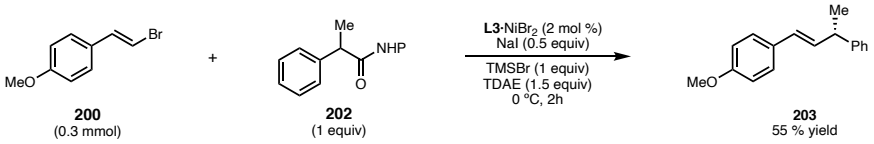

Cross-Coupling Reaction and Sample Preparation Procedure: In a dry 20 mL scintillation vial with a stir bar was added (*E*)-1-(2-bromovinyl)-4-methoxybenzene (**200**, 63.9 mg, 0.30 mmol, 1 equiv) 1,3-dioxoisoindolin-2-yl 2-phenylpropanoate (**202**, 88.6 mg, 0.30 mmol, 1 equiv), **L3**·$NiBr_2$ (3.5 mg, 6.0 μmol, 0.02 equiv), and NaI (22.5 mg, 0.15 mmol, 0.5 equiv). The vial was then placed under Ar, sealed and brought into a N_2-filled glovebox. The contents of the vial were dissolved in DMA (3.0 mL, 0.1 M) and cooled to 0 ºC in a cold well. Once cooled, TMSBr (39.6 μL, 0.30 mmol, 1 equiv) was added and the reaction was stirred for 5 min before TDAE (105 μL, 0.45 mmol, 1.5 equiv) was added to start the reaction. After 5 minutes, a ~0.4 mL aliquot was removed by syringe fitted with a 0.45 μm filter and transferred to an oven-dried EPR tube. The tube was then rapidly removed from the glove box and frozen in LN_2 for EPR analysis. The same procedure was done at 15 min and 90 min. After the final aliquot was removed, the reaction was quenched with 0.5 mL 1M HCl, further diluted with 3 mL H_2O then extracted three times with 5 mL of Et_2O. The combined organics were then washed with 3 mL 1M LiCl, dried over $MgSO_4$, then filtered and concentrated. The crude mixture was then diluted with 10 mL EtOAc and analyzed by GC-FID to confirm the presence of product **203** (55% yield). The EPR spectra were taken at 9.360 GHz (5 mins), 9.360 GHz (15 mins), and 9.362GHz (90 mins). Spectrum at each timepoint was averaged over 4 scans. The spectra were collected at a modulation amplitude of 4 G and conversion time of 40.96 ms. The spectra were taken at

0.5 mW (shown here), 2.0 mW, and 8.0 mW, which showed EPR no oversaturation occurred for a microwave power below 2.0 mW.

Figure 2.81. *EPR spectra taken over the course of the reaction.*

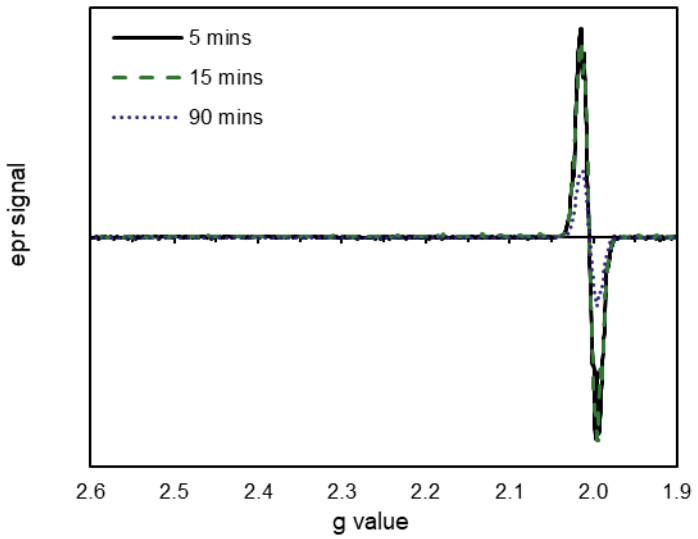

2.9.9 Catalyst Loading Study (Figure 2.15)

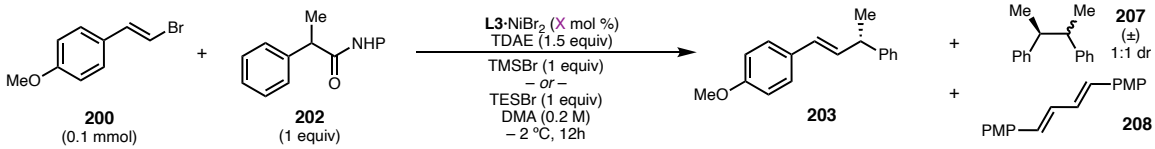

Changing Lewis Acid at Different Catalyst Loadings Cross-Coupling Procedure: In a N_2-filled glovebox to an oven-dried 20 mL scintillation vial was added **200**, **202**, *n*-dodecane internal standard and dry DMA to make a 0.4 M stock solution of substrates. In an oven-dried 1-dram vial with a stir bar was added **L3**·$NiBr_2$ complex followed by dry DMA to make a 0.08 M catalyst stock solution. Stock solutions of substrates and catalyst were added to oven-dried 1 dram vials with a stir bar then diluted with dry DMA (final reaction concentration 0.2 M). This was done such that there was 6 different catalyst loadings: 20, 10, 5, 2.5, 1.0, 0.5 mol% and done in triplicate for each loading (total 18

reactions for each Lewis acid). Each reaction was then cooled to –2 ºC and stirred at 200 rpm. *Note: Julabo LH45 chiller was set to 0 ºC however we measured a reaction temperature of –2 ºC for these experiments.* Once cooled, either TMSBr (13.2 μL, 0.10 mmol, 1 equiv) or TESBr (17.2 μL, 0.10 mmol, 1 equiv) was added to each reaction and they were allowed to stir for 10 minutes before TDAE (35 μL, 0.15 mmol, 1.5 equiv) was added to start the reaction. Each reaction was allowed to stir for 12 hours at –2 ºC. Upon completion the reactions were diluted with EtOAc and quenched with 1M HCl. An aliquot of the organic layer was extracted and filtered through MgSO4 then further diluted for GC analysis. For one sample reaction of each Lewis acid/catalyst loading combination the remaining crude was purified by preparative-TLC for chiral SFC analysis to determine ee.

Data analysis: Reaction yields and conversions were determined by GC-FID analysis against *n*-dodecane internal standard. In Figure 2.15 the average of three runs is displayed with the error bars representing the standard deviation of the three runs. Yields of homocoupled products **207** and **208** are not based on their theoretical yields (0.05 mmol) but instead of the reaction product's theoretical yield (0.10 mmol) to allow for facile comparison of relative mass balance across reactions.

Table 2.23. *Raw data from catalyst loading screen with TMSBr.*

run #	Ni mol %	**203** yield (%)	**207** yield (%)	**208** yield (%)
1	20	84	3	0
2	20	84	3	0
3	20	85	3	0
1	10	85	4	0
2	10	84	5	0
3	10	85	4	0
1	5.0	87	4	0
2	5.0	88	4	0
3	5.0	88	4	0
1	2.5	93	3	0
2	2.5	93	3	0
3	2.5	94	3	0
1	1.0	87	5	1
2	1.0	88	5	0
3	1.0	89	5	0
1	0.5	72	14	0
2	0.5	72	14	0
3	0.5	71	14	0

Table 2.24. *Raw data from catalyst loading screen with TESBr.*

run #	Ni mol %	**203** yield (%)	**207** yield (%)	**208** yield (%)
1	20	73	8	13
2	20	74	8	15
3	20	71	8	13
1	10	75	8	12
2	10	75	9	13
3	10	73	9	10
1	5.0	80	7	9
2	5.0	83	7	1
3	5.0	85	7	11
1	2.5	87	5	8
2	2.5	88	5	11
3	2.5	89	5	9
1	1.0	92	3	11
2	1.0	95	3	9
3	1.0	96	3	8
1	0.5	82	9	8
2	0.5	87	3	9
3	0.5	84	9	8

Table 2.25. *Average yield data and error analysis for all runs.*

	Ni mol %	**203** avg yield ± STDEV	**207** avg yield ± STDEV	**208** avg yield ± STDEV	**203** ee (%)
TMSBr	20	84 ± 0.4	3 ± 0	0 ± 0	96
	10	85 ± 0.6	4 ± 0.2	1 ± 0	95
	5	88 ± 0.6	4 ± 0	2 ± 0	93
	2.5	93 ± 0.8	3 ± 0	3 ± 0	88
	1	88 ± 0.8	5 ± 0	4 ± 0	82
	0.5	72 ± 0.6	14 ± 0.2	5 ± 0	76
TESBr	20	73 ± 1.2	8 ± 0	14 ± 1.2	95
	10	74 ± 1.4	9 ± 0.2	12 ± 1.2	94
	5	82 ± 2.4	7 ± 0	7 ± 5.4	93
	2.5	88 ± 0.8	5 ± 0	9 ± 1.2	90
	1	94 ± 2.0	3 ± 0	9 ± 1.4	85
	0.5	84 ± 2.6	7 ± 3.6	58± 0.6	78

Figure 2.82. *TMSBr reaction data in graphical form similar to Figure 2.15.*

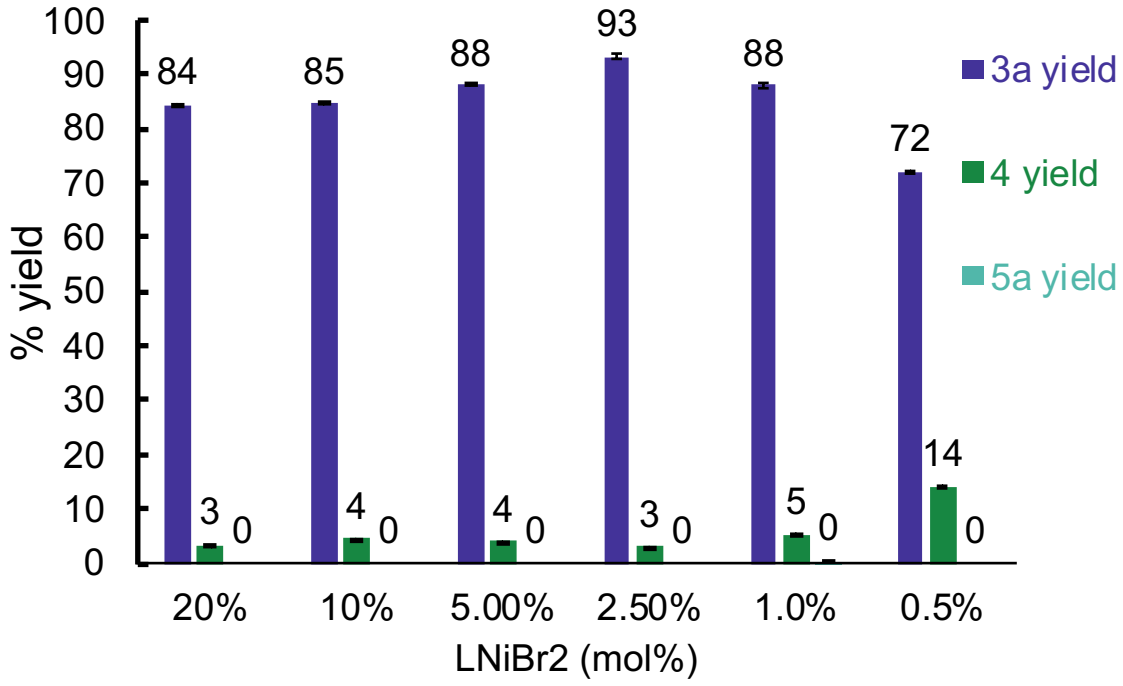

Figure 2.83. *TESBr reaction data in graphical form similar to Figure 2.15.*

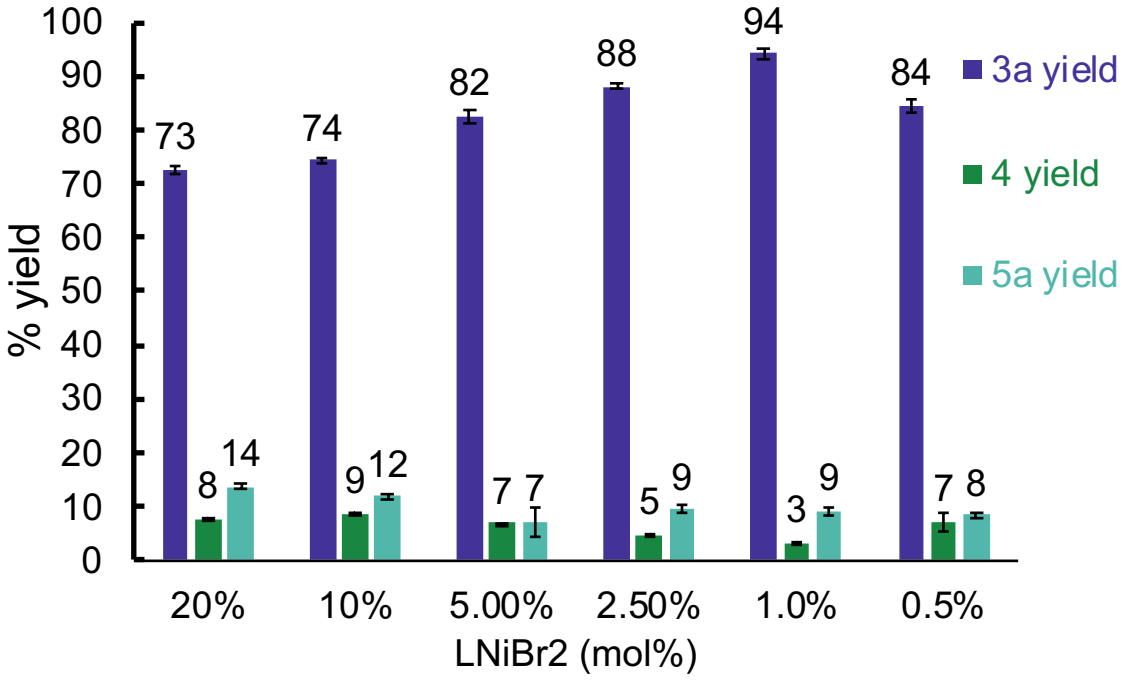

2.9.10 Computational Data

Unless otherwise noted, all calculations were carried out with the Gaussian 16 package.[35] Geometry optimization and energy calculations were performed with B3LYP-D3.[36] The LANL2DZ basis set[37] with ECP was used for Ni, and the 6-31G(d) basis set[38] was used for other atoms. Frequency analysis was conducted at the same level of theory to verify that the stationary points are minima or saddle points. To ensure that the correct unrestricted wave functions were obtained, a stability test was carried out with the Gaussian keyword *stable = opt*. Single point energies were calculated at the M06[39]/6-311+G(d,p)-SDD[40] level using SMD solvation model[41] (solvent = DMA). Computed structures were visualized using CYLview.[42]

^{19}F Chemical shifts were carried out with ORCA 4.2.1 package.[43] Geometry optimizations and frequency calculations were performed with BP86. Chemical shifts calculation were performed with TPSSh and accelerated with RIJCOSX approximation using SMD solvation model (solvent = DMA). All atoms were described with def2-TZVPP basis set.

2.9.10.1 DFT-Computed Gibbs Free Energy Barriers for Radical Addition and Reductive Elimination

Figure 2.84. *DFT-computed Gibbs free energy barriers for radical addition transition states. Energies in kcal/mol, only the α-carbon of aryl group (p-OMe-Ph) is shown for simplicity.*

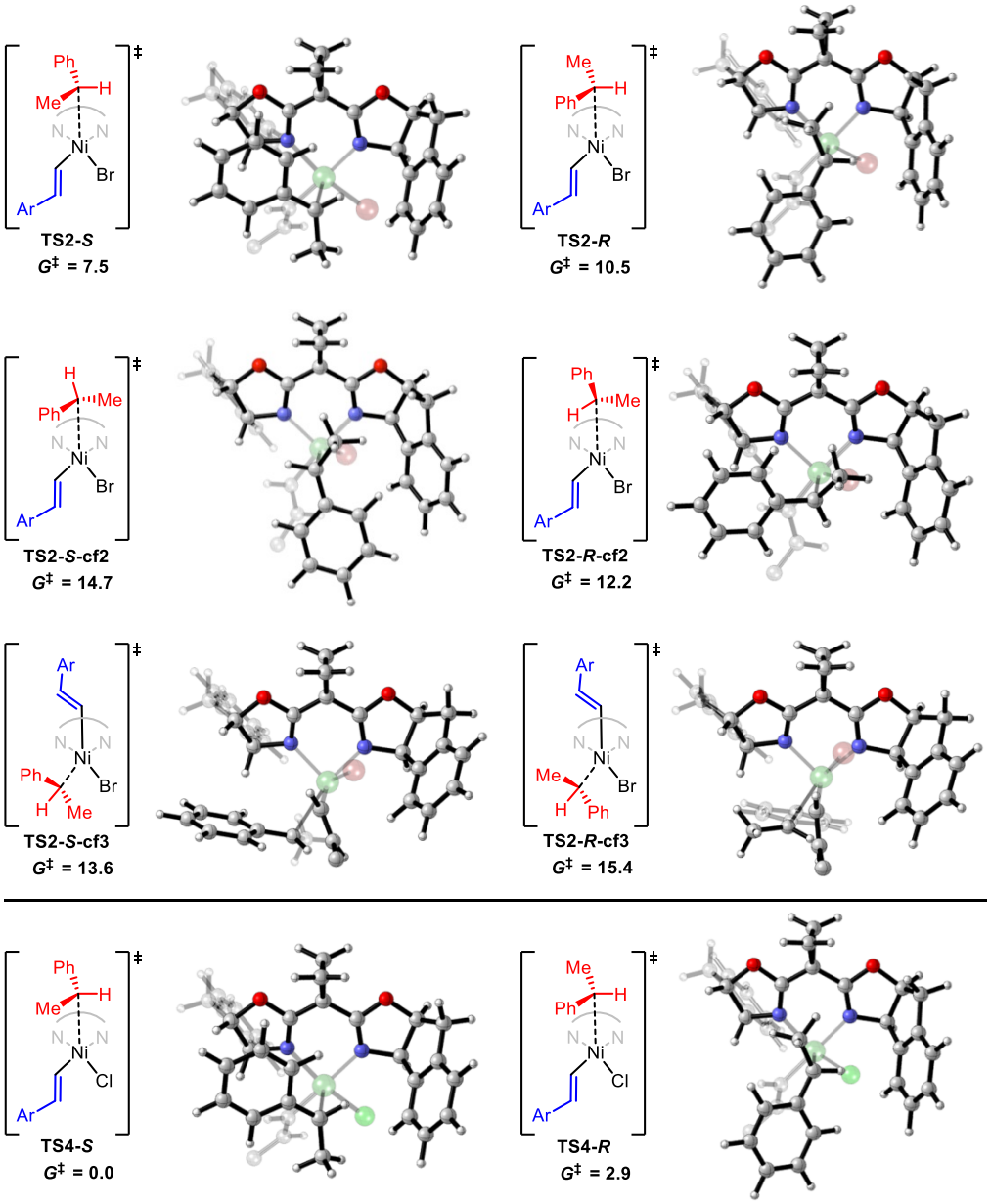

Figure 2.85. *DFT-computed Gibbs free energy barriers for reductive elimination transition states. Energies in kcal/mol, only the α-carbon of aryl group (p-OMe-Ph) is shown for simplicity.*

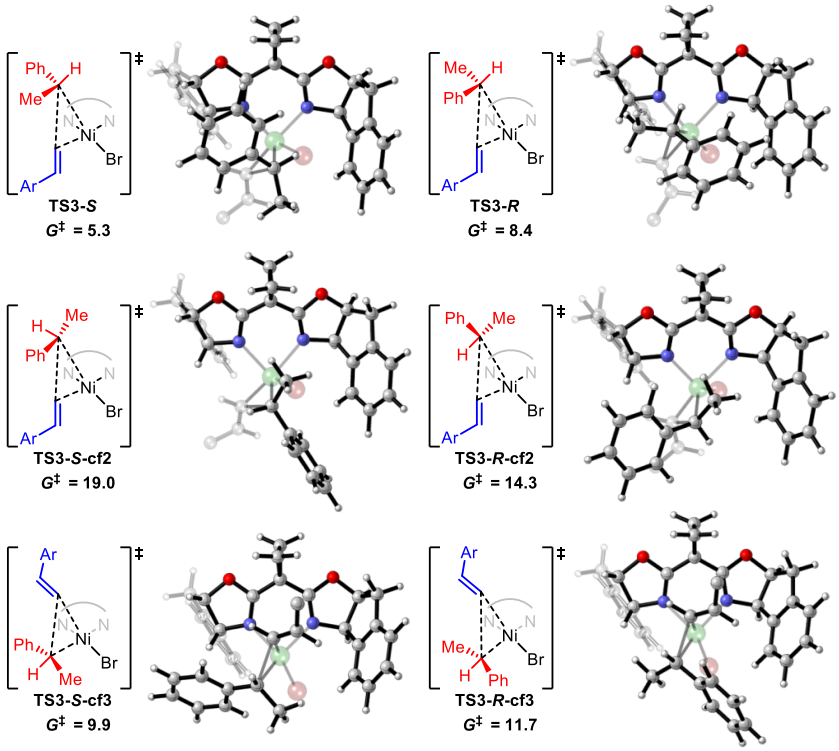

2.9.10.2 Table of Energies

Table 2.26. *Zero-point correction (ZPE), thermal correction to enthalpy (TCH), thermal correction to Gibbs free energy (TCG), energies (E), enthalpies (H), and Gibbs free energies (G) (in Hartree) of the structures calculated at the M06/6-311+G(d,p)-SDD-SMD(DMA)//B3LYP-D3/6-31G*-LANL2DZ level of theory.*

structures	*ZPE*	*TCH*	*TCG*	*E*	*H*	*G*	Imaginary Frequency
200	0.157103	0.168714	0.118363	-2994.814718	-2994.813774	-2994.864125	—
214	0.143410	0.151702	0.111157	-310.086145	-310.085200	-310.125745	—
203	0.305310	0.322803	0.258415	-733.546167	-733.545222	-733.609611	—
204(Br)	0.387446	0.412098	0.330548	-3888.876796	-3888.875852	-3888.957402	—
213	0.545058	0.582077	0.471467	-6883.698127	-6883.697183	-6883.807793	—
212	0.544906	0.579268	0.475840	-4312.265954	-4312.265010	-4312.368438	—
215	0.693066	0.735906	0.613379	-4622.384353	-4622.383409	-4622.505936	—
L3·NiBr$_2$	0.389305	0.415738	0.330948	-6460.314111	-6460.313167	-6460.397957	—
L3·NiCl$_2$	0.390313	0.416097	0.334385	-2237.879255	-2237.878311	-2237.960023	—
TS1	0.544407	0.580802	0.470800	-6883.686941	-6883.685997	-6883.795998	77.97*i*
TS2-*S*	0.691161	0.733509	0.612775	-4622.377688	-4622.376744	-4622.497478	86.29*i*
TS2-*S*-cf2	0.690994	0.733306	0.613450	-4622.366077	-4622.365133	-4622.484988	99.49*i*
TS2-*S*-cf3	0.689948	0.732831	0.609722	-4622.368744	-4622.367800	-4622.490909	43.26*i*
TS2-*R*	0.690489	0.733056	0.610999	-4622.369068	-4622.368124	-4622.490181	93.39*i*
TS2-*R*-cf2	0.691202	0.733535	0.613484	-4622.373867	-4622.372923	-4622.492974	122.69*i*
TS2-*R*-cf3	0.690101	0.732833	0.611372	-4622.363507	-4622.362563	-4622.484024	29.39*i*
TS3-*S*	0.692081	0.734347	0.612426	-4622.378747	-4622.377802	-4622.499724	228.06*i*
TS3-*S*-cf2	0.693128	0.735204	0.613722	-4622.360576	-4622.359631	-4622.481113	188.10*i*
TS3-*S*-cf3	0.692833	0.734938	0.616204	-4622.384026	-4622.383082	-4622.501816	163.77*i*
TS3-*R*	0.692106	0.734445	0.612125	-4622.370255	-4622.369311	-4622.491631	250.12*i*
TS3-*R*-cf2	0.693082	0.735002	0.614428	-4622.367556	-4622.366612	-4622.487187	213.19*i*
TS3-*R*-cf3	0.692876	0.734861	0.616167	-4622.379267	-4622.378323	-4622.497017	195.93*i*
TS4-*S*	0.691521	0.733615	0.613914	-2511.159973	-2511.159029	-2511.278730	91.24*i*
TS4-*R*	0.690833	0.733155	0.611956	-2511.150744	-2511.149799	-2511.270998	102.88*i*

2.9.10.3 Cartesian Coordinates for Calculated Species

200

Br	3.88090800	-0.05446600	-0.00003200
C	2.04318100	0.44922200	0.00055600
C	1.05264300	-0.45014700	-0.00077900
H	1.91071500	1.52387800	0.00210800
H	1.32134700	-1.50469200	-0.00207000
C	-0.38593400	-0.16251700	-0.00053200
C	-1.29087000	-1.23408600	-0.00023400
C	-0.92482900	1.14221900	-0.00060600
C	-2.67281500	-1.03722800	0.00012800
H	-0.90780400	-2.25189200	-0.00022900
C	-2.29264800	1.35456200	-0.00024800
H	-0.26441000	2.00430200	-0.00106700
C	-3.18250600	0.26592200	0.00014900
H	-3.33165300	-1.89772700	0.00037100
H	-2.70717900	2.35770000	-0.00033600
O	-4.50597500	0.58767300	0.00046800
C	-5.45497000	-0.46821100	0.00085400
H	-6.43595400	0.01042300	0.00109800
H	-5.35854200	-1.09783700	-0.89418800
H	-5.35801300	-1.09766100	0.89596200

214

C	1.83322100	-0.65199900	0.00004500
H	2.08025400	-1.71111700	0.00002500
C	0.46218600	-0.30019600	0.00000800
C	-0.54340000	-1.31146300	-0.00004900
C	0.02037200	1.05542000	0.00002500
C	-1.89146700	-0.98836800	-0.00008600
H	-0.23452900	-2.35444100	-0.00006300
C	-1.33233400	1.36765200	-0.00001200
H	0.75473700	1.85543900	0.00006800
C	-2.30004300	0.35380700	-0.00006800
H	-2.63543400	-1.78104500	-0.00012900
H	-1.64206100	2.40984800	0.00000200
H	-3.35692000	0.60491000	-0.00009600
C	2.95955100	0.33474300	0.00010600
H	2.92767900	0.99432600	0.88074100
H	3.92999900	-0.16984900	0.00014200
H	2.92775500	0.99434700	-0.88051600

203

C	-0.89419600	1.51166900	-0.25111200
C	-0.15813300	0.39239600	-0.18067500
H	-0.39834100	2.48271600	-0.27730500
H	-0.67988500	-0.56313700	-0.16658600
C	1.30641100	0.29100500	-0.12049800
C	1.90139600	-0.97895400	-0.09917500
C	2.17066300	1.40603900	-0.07970400
C	3.28615800	-1.15298300	-0.04467500
H	1.26489100	-1.86058800	-0.12772600
C	3.54627000	1.25264500	-0.02497100
H	1.75879600	2.41092300	-0.08770300
C	4.11939100	-0.03019900	-0.00767100
H	3.69536400	-2.15666900	-0.03153000
H	4.20849300	2.11234000	0.00722700
O	5.48282900	-0.06751800	0.04718400
C	6.11699800	-1.33581400	0.06792300
H	7.18939400	-1.13548200	0.11138700
H	5.82198500	-1.92183900	0.94946400
H	5.89322300	-1.91542500	-0.83845200
C	-3.76795400	-1.61797800	1.24498500
C	-3.09639200	-0.40683900	1.08072400
C	-3.12430200	0.27252900	-0.14728000
C	-3.83962100	-0.30001600	-1.20522200
C	-4.51513700	-1.51275800	-1.04629100
C	-4.48253500	-2.17559600	0.18098000
H	-3.73292100	-2.12811700	2.20427700
H	-2.53161600	0.01210800	1.90912000
H	-3.86867400	0.21005400	-2.16565900
H	-5.06563600	-1.93737500	-1.88189200
H	-5.00711600	-3.11878800	0.30870500
C	-2.40640000	1.60109200	-0.32528000
H	-2.65336600	1.97333900	-1.33257200
C	-2.92710700	2.66358000	0.67098300
H	-2.70693900	2.37690400	1.70482300
H	-2.45217700	3.63420100	0.48451900
H	-4.01117200	2.78605500	0.57418800

204(Br)

C	-0.36197700	-3.82183400	0.64792100
C	0.00000000	-2.47192800	-0.00001700
C	0.36197200	-3.82181600	-0.64799500
H	0.18960700	-4.06808200	1.54864200
H	-1.41774200	-4.06938300	0.65315900
H	-0.18961400	-4.06803400	-1.54872400
H	1.41773600	-4.06936800	-0.65324100
C	-1.10716600	-1.70895600	-0.61880500
C	-3.06015700	-1.54459400	-1.76366800
C	-2.53247600	-0.14513900	-1.32829900
H	-3.01912600	-1.73277600	-2.83888600
H	-2.37605000	0.55621300	-2.15238100
C	1.10716800	-1.70897900	0.61879400
C	3.06017000	-1.54465700	1.76364500
C	2.53248400	-0.14518800	1.32833100
H	3.01915100	-1.73287600	2.83885700
H	2.37606300	0.55613500	2.15244000
O	-2.10340100	-2.46199700	-1.14717300
O	2.10340700	-2.46203800	1.14712900
N	-1.22318600	-0.43422100	-0.70416200
N	1.22319200	-0.43424600	0.70418900
C	-4.46409300	-1.72539100	-1.15867200
C	4.46410100	-1.72543000	1.15862800
C	-3.54941100	0.33992800	-0.31837500
C	-3.48867700	1.49828700	0.45643100
C	-4.60775700	-0.56504900	-0.19674200
C	-4.51932700	1.73749600	1.36871600
H	-2.64978600	2.18386500	0.36262900
C	-5.63598400	-0.32103700	0.71362800
C	-5.58356300	0.83571300	1.49640300
H	-4.49123300	2.63128600	1.98564800
H	-6.46422000	-1.01821700	0.81551500
H	-6.37708300	1.03668000	2.21147900
H	-5.22433100	-1.68760200	-1.94973800
H	-4.55216900	-2.70631900	-0.67813200
C	3.54940800	0.33991900	0.31841600
C	3.48866000	1.49830400	-0.45635000
C	4.60775600	-0.56505100	0.19674100
C	4.51930200	1.73755000	-1.36863500
H	2.64976400	2.18387300	-0.36252200
C	5.63597300	-0.32100200	-0.71362900
C	5.58354100	0.83577600	-1.49636200
H	4.49119700	2.63136000	-1.98553800
H	6.46421000	-1.01817500	-0.81554900
H	6.37705400	1.03677100	-2.21143800
H	5.22434700	-1.68767000	1.94968900
H	4.55217300	-2.70633900	0.67805000
Ni	0.00001800	0.98322500	0.00002100
Br	-0.00000700	3.30195300	-0.00002900

213

C	0.20675000	-2.54672700	3.05661000
C	0.03498500	-1.58269300	1.87478600
C	1.19881500	-2.59681300	1.95455000

H	0.49681700	-2.08791500	3.99491300
H	-0.53276200	-3.33647300	3.12341000
H	1.15151600	-3.41383200	1.24289500
H	2.18238300	-2.16494000	2.10339200
C	-1.02381500	-1.88678400	0.88607300
C	-2.39906900	-3.30249000	-0.23413400
C	-2.52780200	-1.84666600	-0.77356500
H	-1.94855800	-4.00772800	-0.93569000
H	-2.27520000	-1.72498300	-1.82946800
C	0.39108200	-0.16529000	2.09780700
C	1.61222800	1.47096700	3.04715000
C	0.61588700	2.06680800	2.01173600
H	1.51882700	1.88684600	4.05026800
H	-0.20560100	2.65989000	2.42130500
O	-1.44839600	-3.16904600	0.87296800
O	1.22156200	0.06828800	3.14127300
N	-1.52886800	-1.09422700	0.01645900
N	0.02388000	0.84961900	1.41041100
C	-3.78662500	-3.74120000	0.27310900
C	3.03277600	1.62805700	2.44868000
C	-3.94785300	-1.44736400	-0.45393200
C	-4.54915500	-0.21142200	-0.68368000
C	-4.63897500	-2.49450200	0.16188100
C	-5.87288400	-0.03575500	-0.27509200
H	-3.98994500	0.59831800	-1.13912700
C	-5.96260800	-2.31747500	0.56360500
C	-6.57318500	-1.07942900	0.34257500
H	-6.35636400	0.92430500	-0.43015400
H	-6.51133900	-3.12545000	1.04167100
H	-7.60262700	-0.92561900	0.65570200
H	-4.17874300	-4.55679000	-0.34780800
H	-3.71251500	-4.12758500	1.29622500
C	1.48661700	2.83756100	1.05038700
C	1.07592300	3.67256600	0.01147900
C	2.83987900	2.57987500	1.28819700
C	2.05449200	4.23853100	-0.81063000
H	0.01718700	3.84637600	-0.15953700
C	3.81485300	3.15802500	0.47559400
C	3.41245700	3.98228900	-0.58069000
H	1.75755200	4.88249400	-1.63333300
H	4.87015500	2.96486800	0.65237600
H	4.16202600	4.43189300	-1.22636000
H	3.75170700	1.99769700	3.18823000
H	3.39722700	0.65175700	2.10364100
Ni	-0.92707600	0.83769700	-0.40361100
C	0.83294900	0.37386400	-1.23372600
C	1.36680000	-0.84896800	-1.26035100
H	1.36873700	1.30987700	-1.36783000
H	0.69918200	-1.70847900	-1.25223700
C	2.79813400	-1.17381100	-1.18318900
C	3.20396200	-2.51663100	-1.18074700
C	3.80213800	-0.19179000	-1.03335800
C	4.54430300	-2.88656200	-1.04412500
H	2.45386300	-3.29677800	-1.29386700
C	5.13421400	-0.54335000	-0.89371900

H	3.53290300	0.85912500	-1.01500600
C	5.52095200	-1.89516200	-0.89761100
H	4.80906100	-3.93766700	-1.05440700
H	5.90493400	0.21273800	-0.77831600
O	6.85661100	-2.12784700	-0.74797000
C	7.30923700	-3.47240100	-0.76347400
H	8.39296400	-3.42633900	-0.64070000
H	6.87577200	-4.05496200	0.06142100
H	7.07274400	-3.96747300	-1.71530300
Br	-1.32480800	0.84804800	-2.78048400
Br	-2.49495900	2.56254800	0.39800900

212

C	-3.45641300	3.36847900	-0.98383400
C	-2.66854600	2.04467700	-1.00132200
C	-3.53683000	2.50615100	-2.18818400
H	-4.30326500	3.38899400	-0.30678800
H	-2.85835700	4.27160800	-1.02792200
H	-2.98697800	2.80395000	-3.07468200
H	-4.43920700	1.92925900	-2.35828100
C	-1.20617000	2.13914900	-1.15655300
C	0.68871900	3.11618700	-1.93015500
C	0.99951800	1.99017500	-0.91734500
H	0.90072700	2.87416100	-2.97495400
H	1.73024400	1.25570500	-1.25560600
C	-3.18988600	0.93986300	-0.17270400
C	-4.85197600	-0.19178200	0.86671700
C	-3.49898100	-0.94150700	0.97129300
H	-5.19273100	0.27843000	1.79271000
H	-3.19176300	-1.21613900	1.98086600
O	-0.76827000	3.23463800	-1.81353300
O	-4.53586500	0.89705500	-0.06265500
N	-0.31176000	1.32645900	-0.71209000
N	-2.51442500	0.02584900	0.42316000
C	1.36886600	4.39452300	-1.42567600
C	-5.87072400	-1.14659200	0.23234900
C	1.44608500	2.74305500	0.32116100
C	1.61854400	2.24676400	1.61277600
C	1.63440600	4.09959200	0.03517500
C	2.00526900	3.13511600	2.61959000
H	1.43627600	1.19938800	1.82532800
C	2.02233400	4.98330700	1.04101700
C	2.20996600	4.49088200	2.33578700
H	2.14197000	2.76883500	3.63322700
H	2.16900100	6.03897300	0.82581300
H	2.50870600	5.16900700	3.13084200
H	2.30132200	4.55945700	-1.98193400
H	0.73428300	5.27176300	-1.59281600
C	-3.68524300	-2.13743600	0.05516500
C	-2.72381500	-3.05549000	-0.36784300
C	-5.00971700	-2.22524900	-0.38778500
C	-3.11084300	-4.06542300	-1.25254200
H	-1.70382800	-2.97994500	-0.00614400
C	-5.39374800	-3.23510900	-1.26914000
C	-4.43411200	-4.15446000	-1.70168700

H	-2.37536800	-4.78897300	-1.59350200
H	-6.42176300	-3.30627100	-1.61647300
H	-4.71837500	-4.94528700	-2.39103200
H	-6.52877500	-1.55687200	1.00996600
H	-6.51006600	-0.61959700	-0.48457700
Ni	-0.50635000	-0.30348800	0.37724300
C	1.21759400	-0.85976400	-0.14389600
C	2.36331000	-1.05674100	0.52538300
H	1.21232300	-0.98116700	-1.23799800
H	2.34159100	-0.97215500	1.61168800
C	3.68756900	-1.38278500	-0.03341400
C	4.77353900	-1.57263100	0.83417500
C	3.94746000	-1.50339200	-1.41538900
C	6.05765200	-1.87079800	0.37084200
H	4.61030500	-1.48841300	1.90633700
C	5.21449300	-1.79923300	-1.89371100
H	3.13807800	-1.36609600	-2.12728500
C	6.28459400	-1.98595000	-1.00402000
H	6.86073800	-2.00966600	1.08598200
H	5.40797700	-1.89336400	-2.95824300
O	7.49343300	-2.27094700	-1.58046000
C	8.60330300	-2.48026700	-0.72594200
H	9.45168400	-2.69609900	-1.37910300
H	8.82825100	-1.58771100	-0.12474400
H	8.44144700	-3.33210200	-0.05028200
Br	-0.50214400	-1.74640000	2.22145000

215

C	4.00627100	3.10774600	-0.42997400
C	3.06837500	1.96969500	0.01765400
C	4.15037600	2.55854000	0.94114300
H	4.74434800	2.84057200	-1.17742200
H	3.53272900	4.07521300	-0.55267000
H	3.77753800	3.14072800	1.77610400
H	4.99176600	1.90680100	1.15087100
C	1.66789000	2.35000700	0.30527900
C	0.10029800	3.75994300	1.13717900
C	-0.53839300	2.50240200	0.49004700
H	0.05338300	3.77848000	2.22825100
H	-1.20425400	1.96133200	1.16359700
C	3.33469200	0.63008000	-0.55254300
C	4.72640800	-0.97971200	-1.29225000
C	3.24752800	-1.40728500	-1.46991500
H	5.31432300	-1.00672400	-2.20991200
H	2.87750000	-1.42542000	-2.49794200
O	1.51331000	3.60688800	0.78885500
O	4.63421900	0.41637200	-0.89497300
N	0.61316200	1.64368100	0.15391800
N	2.51035100	-0.32556400	-0.76796600
C	-0.50604300	4.99286200	0.44903800
C	5.31534500	-1.87242800	-0.16936300
C	-1.22369300	3.03146500	-0.75070500
C	-1.78126300	2.29376400	-1.79426800
C	-1.18063900	4.42894800	-0.78480000
C	-2.32288700	2.98935000	-2.87799700

H	-1.76256400	1.20869900	-1.77613300
C	-1.72540500	5.11922800	-1.86701000
C	-2.29991400	4.38927500	-2.91190900
H	-2.75450300	2.43487100	-3.70645000
H	-1.69716800	6.20573100	-1.90399500
H	-2.72329400	4.91445400	-3.76427200
H	-1.22890000	5.47536900	1.12047600
H	0.26761800	5.73588800	0.22520000
C	3.15611500	-2.74374200	-0.78491700
C	2.09825500	-3.64928000	-0.82643600
C	4.31062500	-2.99953800	-0.03756800
C	2.20649000	-4.82900000	-0.08472000
H	1.21462600	-3.41922800	-1.41603700
C	4.41609000	-4.17745100	0.70042900
C	3.35371800	-5.08767400	0.67502200
H	1.39390400	-5.54997600	-0.09754900
H	5.30844600	-4.39086500	1.28380800
H	3.42405000	-6.00974800	1.24592900
H	6.32338100	-2.22755600	-0.41050500
H	5.39592200	-1.28739000	0.75622300
Ni	0.37394900	-0.51206900	-0.36861400
C	-1.47083400	-0.64491500	0.17951300
C	-2.44002300	-1.34902500	-0.41843200
H	-1.68423300	-0.04707100	1.06676400
H	-2.19063900	-1.92639600	-1.30655100
C	-3.85739000	-1.39096200	-0.01669500
C	-4.80051500	-1.96938400	-0.87891300
C	-4.33540300	-0.87892800	1.20821900
C	-6.15917200	-2.03229000	-0.56069100
H	-4.46386500	-2.37634900	-1.82963300
C	-5.67996000	-0.93147300	1.53997100
H	-3.63715900	-0.43844200	1.91477400
C	-6.60708800	-1.50776900	0.65633300
H	-6.84821200	-2.48742600	-1.26313600
H	-6.04455100	-0.53972200	2.48483200
O	-7.90679000	-1.51079500	1.08103200
C	-8.88488900	-2.08167900	0.22905600
H	-9.83800100	-1.97836200	0.75201000
H	-8.94165000	-1.55506900	-0.73395600
H	-8.68864400	-3.14681900	0.04191400
C	0.71852900	-1.43197500	1.56529900
H	1.73763300	-1.70412200	1.28227200
C	0.71604800	-0.35795100	2.57388800
C	1.88987900	0.39168000	2.80284500
C	-0.42907600	-0.00759300	3.32005700
C	1.91152400	1.46178300	3.69077400
H	2.78975400	0.12634600	2.25428000
C	-0.41228200	1.07143700	4.20518000
H	-1.33795300	-0.58990900	3.21209300
C	0.75268100	1.82009000	4.39028400
H	2.83368000	2.01632500	3.84613200
H	-1.31249000	1.32151200	4.76119600
H	0.76646000	2.65370900	5.08729400
C	-0.11050500	-2.67720100	1.82296800
H	-0.11115300	-3.32244100	0.94142400

H	0.32641700	-3.24542000	2.65885200
H	-1.15237700	-2.45879000	2.06445000
Br	0.05704200	-1.05193200	-2.80568000

L3·NiBr$_2$

C	0.35281100	-4.05239100	-0.65177700
C	-0.00013400	-2.70088800	0.00001300
C	-0.35326200	-4.05231400	0.65186400
H	-0.21169000	-4.29370300	-1.54590800
H	1.40866000	-4.29806600	-0.67366300
H	0.21120400	-4.29366300	1.54600700
H	-1.40914600	-4.29784200	0.67376300
C	1.10618800	-1.93484000	0.60579700
C	3.08896300	-1.75477500	1.69404700
C	2.54537800	-0.35989500	1.28288300
H	3.06155700	-1.95980700	2.76632300
H	2.42435000	0.35224900	2.09963700
C	-1.10635800	-1.93472200	-0.60579600
C	-3.08902800	-1.75444900	-1.69419300
C	-2.54538600	-0.35964000	-1.28287600
H	-3.06148000	-1.95943200	-2.76647500
H	-2.42432000	0.35258100	-2.09955700
O	2.12640500	-2.67546300	1.07689300
O	-2.12663700	-2.67523700	-1.07693100
N	1.20169600	-0.65967400	0.72599800
N	-1.20172900	-0.65954600	-0.72599400
C	4.47793200	-1.92368200	1.05843500
C	-4.47809300	-1.92327800	-1.05878300
C	3.50385000	0.10838900	0.20798400
C	3.40038500	1.24656700	-0.59231000
C	4.56102600	-0.79421500	0.05383800
C	4.37780900	1.46286200	-1.56675500
H	2.57687600	1.94162100	-0.46077800
C	5.53802000	-0.57207400	-0.91589400
C	5.43696900	0.56115600	-1.72801400
H	4.31078200	2.33923800	-2.20491400
H	6.36378200	-1.26826300	-1.04134900
H	6.18861900	0.74382000	-2.49142300
H	5.25424300	-1.83256200	1.82931600
H	4.58347600	-2.92005600	0.61476900
C	-3.50388000	0.10856900	-0.20795400
C	-3.40036300	1.24660500	0.59254000
C	-4.56115600	-0.79395600	-0.05402200
C	-4.37783100	1.46283000	1.56695600
H	-2.57678300	1.94160900	0.46118700
C	-5.53819400	-0.57188300	0.91568200
C	-5.43709000	0.56120200	1.72799600
H	-4.31076100	2.33909600	2.20526300
H	-6.36402900	-1.26801600	1.04096500
H	-6.18877700	0.74381800	2.49138000
H	-5.25429200	-1.83194800	-1.82975200
H	-4.58381600	-2.91970400	-0.61527500
Ni	0.00005300	0.77347900	0.00001300
Br	-0.60168700	2.35892200	-1.66454900

Br	0.60199600	2.35881200	1.66461900

L3·NiCl₂

C	0.36934700	3.67764800	0.64258800
C	0.00000100	2.32595500	0.00000000
C	-0.36934600	3.67764100	-0.64260100
H	-0.17237100	3.91868200	1.55077700
H	1.42551800	3.92296700	0.63776900
H	0.17237100	3.91866800	-1.55079200
H	-1.42551800	3.92295900	-0.63778400
C	1.09063800	1.55889300	-0.63047100
C	3.04198500	1.37425300	-1.77216800
C	2.52420300	-0.01632400	-1.31750100
H	2.97370800	1.56203300	-2.84586200
H	2.39777600	-0.75012700	-2.11317000
C	-1.09063600	1.55889700	0.63047700
C	-3.04198700	1.37426400	1.77216700
C	-2.52420400	-0.01631400	1.31750900
H	-2.97371400	1.56205000	2.84586000
H	-2.39778000	-0.75011300	2.11318300
O	2.09531600	2.29789400	-1.13382400
O	-2.09531400	2.29790200	1.13382200
N	1.18788800	0.28228600	-0.74021100
N	-1.18788900	0.28229100	0.74022000
C	4.44989400	1.56501900	-1.18871300
C	-4.44989300	1.56502700	1.18870500
C	3.51063200	-0.44384900	-0.24985100
C	3.43503000	-1.55628900	0.58899900
C	4.56515000	0.46973700	-0.15032000
C	4.43788000	-1.73471100	1.54536000
H	2.61538800	-2.26205000	0.49551000
C	5.56698100	0.28560300	0.80180900
C	5.49408000	-0.82146100	1.65198300
H	4.39445600	-2.59166900	2.21140600
H	6.39045800	0.99085500	0.88432000
H	6.26565400	-0.97493500	2.40182100
H	5.20011200	1.44661000	-1.98147600
H	4.56967100	2.57594200	-0.78328300
C	-3.51062700	-0.44384400	0.24985700
C	-3.43501700	-1.55628800	-0.58898700
C	-4.56514300	0.46974100	0.15031400
C	-4.43786000	-1.73471500	-1.54535500
H	-2.61537500	-2.26204700	-0.49549000
C	-5.56696800	0.28560300	-0.80182100
C	-5.49406000	-0.82146500	-1.65198900
H	-4.39443100	-2.59167400	-2.21139800

H	-6.39044400	0.99085500	-0.88434100
H	-6.26562700	-0.97494200	-2.40183300
H	-5.20011400	1.44661500	1.98146500
H	-4.56967300	2.57595000	0.78327400
Ni	-0.00000200	-1.14356200	0.00000300
Cl	-0.71978600	-2.66568700	1.48657600
Cl	0.71975700	-2.66569100	-1.48657800

TS1

C	-1.05584700	0.89662900	-3.79898300
C	-0.92083500	1.17557100	-2.29343800
C	-1.06769600	2.30559400	-3.32646300
H	-0.16620700	0.51693600	-4.28908200
H	-1.99528800	0.44884900	-4.10598300
H	-2.00856000	2.84351200	-3.30064600
H	-0.17975200	2.90975700	-3.48015400
C	-2.09530300	0.83643400	-1.46137000
C	-4.29566400	0.90548800	-0.94148600
C	-3.51430500	-0.02258700	0.02688400
H	-4.59199000	1.86533200	-0.51392300
H	-3.63456200	0.22184900	1.08420100
C	0.41473600	1.05373700	-1.67121800
C	2.66920900	0.85510800	-1.71649500
C	2.14510400	1.10600700	-0.28042400
H	2.98683100	-0.17258200	-1.91186600
H	2.49463200	0.37043000	0.44594000
O	-3.28871500	1.20140000	-1.96844900
O	1.46357000	1.08268800	-2.52378900
N	-2.09915500	0.19721600	-0.34813100
N	0.67950300	0.99420600	-0.41813200
C	-5.44190700	0.09126400	-1.55083300
C	3.72885000	1.92119100	-2.01636800
C	-3.99803800	-1.41188500	-0.34834300
C	-3.50273900	-2.64360700	0.07883900
C	-5.05237000	-1.34284600	-1.26646300
C	-4.07447500	-3.81104700	-0.43326900
H	-2.69797700	-2.68765900	0.80437500
C	-5.62274600	-2.50862700	-1.77612800
C	-5.12515800	-3.74506400	-1.35621100
H	-3.70012100	-4.77862100	-0.11001500
H	-6.44092900	-2.45778200	-2.49048300
H	-5.55868000	-4.66163200	-1.74753900
H	-6.38671300	0.35341000	-1.05667800
H	-5.56293400	0.31617000	-2.61610300
C	2.60104300	2.51909500	0.02464300
C	2.22385600	3.33003400	1.09353800
C	3.48199100	2.97826000	-0.96083800
C	2.76054300	4.61793600	1.16938500
H	1.48841300	2.98993300	1.81581200
C	4.01768500	4.26278800	-0.88054000
C	3.65324700	5.07902500	0.19418300
H	2.46940700	5.27051000	1.98761100
H	4.70094500	4.62772300	-1.64372300

H	4.05865700	6.08488700	0.26687600
H	4.73044300	1.48068300	-1.92230800
H	3.63604500	2.29146900	-3.04328800
Ni	-0.62992500	0.39158400	1.09701700
C	0.14520600	-1.46090200	1.05306000
C	1.40732100	-1.61682700	1.50717100
H	-0.31299900	-2.04962100	0.26152600
H	1.68174300	-1.10086300	2.42747200
C	2.49157700	-2.32559200	0.82522800
C	3.74667800	-2.44072900	1.44634600
C	2.36658500	-2.85002800	-0.48193600
C	4.82896100	-3.06044800	0.82009200
H	3.87940700	-2.03847100	2.44795200
C	3.43208400	-3.46857700	-1.11546300
H	1.42078100	-2.76087600	-1.00897100
C	4.67635700	-3.58135200	-0.47045400
H	5.77552200	-3.12906600	1.34371200
H	3.33380500	-3.87313600	-2.11815400
O	5.65806800	-4.20007800	-1.18629800
C	6.93347900	-4.35406700	-0.58259200
H	7.55201700	-4.87442800	-1.31620500
H	7.38965200	-3.38248300	-0.34759100
H	6.87577700	-4.95503500	0.33512900
Br	-1.44118600	-1.23197500	2.80236100
Br	-1.30366700	2.56382000	1.96385100

TS2-*S*

C	3.06533600	3.75139600	-0.25459700
C	2.43773300	2.38254800	0.08018700
C	3.34577300	3.13862400	1.06689800
H	3.84222100	3.73508700	-1.00992800
H	2.36947800	4.58111900	-0.30266600
H	2.84254900	3.53642500	1.94074400
H	4.32116600	2.69577400	1.23789300
C	0.98949600	2.38723100	0.34882200
C	-0.90790000	3.32868100	1.14922800
C	-1.20355200	2.05954800	0.31764600
H	-1.01878000	3.20317500	2.22812000
H	-1.83818800	1.33816600	0.82819300
C	3.01699600	1.19812400	-0.58757000
C	4.71129500	0.16140800	-1.67453800
C	3.49998200	-0.79599300	-1.47785700
H	4.88489600	0.46227000	-2.71024600
H	3.07288700	-1.19479400	-2.39845100
O	0.52167700	3.52713300	0.89863900
O	4.30538100	1.36373500	-0.95864400
N	0.13497500	1.46911400	0.07213000
N	2.46071500	0.06827000	-0.83920100
C	-1.71954400	4.47901300	0.54038100
C	5.94182600	-0.46804400	-1.00032700
C	-1.81501400	2.60062400	-0.95816300
C	-2.06009600	1.91699000	-2.14808600
C	-2.08142200	3.96888000	-0.83883600
C	-2.59813500	2.62800800	-3.22388600
H	-1.82825000	0.86058600	-2.22544100

C	-2.61980300	4.67550500	-1.91329000
C	-2.87849700	3.99502200	-3.10681700
H	-2.79664300	2.11477300	-4.16077900
H	-2.82906800	5.73923700	-1.82895300
H	-3.29487300	4.53427700	-3.95368700
H	-2.61429200	4.66205300	1.15040800
H	-1.14110900	5.40943500	0.53072400
C	4.04047400	-1.88375500	-0.57030500
C	3.37611200	-3.01122400	-0.08701500
C	5.38561300	-1.66010800	-0.25579000
C	4.05976700	-3.88257900	0.76377800
H	2.35079300	-3.19728000	-0.38330500
C	6.06861400	-2.53117300	0.59287900
C	5.39348000	-3.63875900	1.11226200
H	3.54949600	-4.75863800	1.15459900
H	7.11341300	-2.35751100	0.83923700
H	5.91280700	-4.32347200	1.77762700
H	6.67311400	-0.78228400	-1.75590000
H	6.44273400	0.26409600	-0.35662100
Ni	0.44699700	-0.43770500	-0.57422900
C	-1.34020500	-0.88513600	-0.08926900
C	-2.37633600	-1.35969400	-0.79547900
H	-1.50812900	-0.62470400	0.95860100
H	-2.21484800	-1.65504500	-1.83081300
C	-3.75781400	-1.53355200	-0.30880400
C	-4.72552000	-2.08282400	-1.16277400
C	-4.18447600	-1.16739000	0.98628500
C	-6.05207300	-2.27175300	-0.76606700
H	-4.43240400	-2.37656000	-2.16825500
C	-5.49578300	-1.34795200	1.39760200
H	-3.47324100	-0.73300000	1.68389900
C	-6.44479700	-1.90323100	0.52425000
H	-6.75881300	-2.70301700	-1.46618000
H	-5.81838800	-1.06543100	2.39544400
O	-7.71013800	-2.03640100	1.02945800
C	-8.70447200	-2.59637600	0.19038300
H	-9.62325400	-2.61462100	0.78063000
H	-8.86601900	-1.98803700	-0.71091500
H	-8.44975300	-3.62154800	-0.11369100
C	0.96679000	-1.54179300	1.75743500
H	1.98701400	-1.52659300	1.38724500
C	0.62295100	-0.48967300	2.66278100
C	1.54986900	0.56303300	2.90315300
C	-0.62920900	-0.40880200	3.33182800
C	1.24074800	1.62863500	3.73492800
H	2.51855300	0.51957200	2.41134200
C	-0.93846000	0.67044400	4.15425700
H	-1.35556900	-1.20472400	3.20600700
C	-0.01266400	1.70002100	4.36291900
H	1.97704600	2.40938300	3.90913800
H	-1.90633100	0.70466400	4.64852400
H	-0.25278200	2.53250400	5.01856300
C	0.26399300	-2.86369700	1.67067800
H	0.35700400	-3.28125500	0.66461400
H	0.70717600	-3.57850200	2.38380900

H	-0.80484800	-2.79535300	1.88649100
Br	0.56273400	-2.22066500	-2.18652600

TS2-*S*-cf2

C	-5.24604100	0.93263800	-1.09771400
C	-3.78020100	0.46035300	-1.07308800
C	-4.72742500	0.15407600	-2.24963500
H	-5.90476600	0.43784500	-0.39323900
H	-5.38939800	2.00062000	-1.21509500
H	-4.50794100	0.67868100	-3.17351100
H	-5.02398900	-0.88431700	-2.35061300
C	-2.74655500	1.49274900	-1.29434100
C	-1.98700200	3.42406000	-2.20753000
C	-0.96486100	2.81826100	-1.20851700
H	-1.70266200	3.34862100	-3.26044300
H	0.03323200	2.68154400	-1.62838100
C	-3.45812900	-0.65564400	-0.15661300
C	-3.95584800	-2.58543100	0.89349500
C	-2.56383100	-2.06153000	1.33506700
H	-4.65722600	-2.72712100	1.71631600
H	-2.51102600	-1.67969700	2.35673600
O	-3.15146000	2.55628200	-2.02782300
O	-4.48810900	-1.50756000	0.07301600
N	-1.53755500	1.49752100	-0.86628200
N	-2.34852700	-0.89515100	0.43738200
C	-2.29907900	4.85454200	-1.74476600
C	-3.71530200	-3.88040700	0.08024000
C	-0.99473400	3.77315600	-0.03206800
C	-0.40792700	3.60279400	1.22151300
C	-1.76991900	4.89979400	-0.32721500
C	-0.60415400	4.59756500	2.18260700
H	0.15652200	2.70512100	1.45229500
C	-1.95947700	5.89195900	0.63363600
C	-1.36958100	5.73318900	1.89111600
H	-0.16606000	4.47731500	3.16917200
H	-2.56087000	6.77063600	0.41295500
H	-1.51413000	6.49578700	2.65203700
H	-1.78308600	5.57546900	-2.39295200
H	-3.37165200	5.06429800	-1.82287900
C	-1.63701400	-3.22968500	1.11404200
C	-0.32240600	-3.37122400	1.55443700
C	-2.29174100	-4.26218300	0.43149700
C	0.33339800	-4.58010100	1.30880200
H	0.16271500	-2.55238700	2.07634500
C	-1.63083300	-5.46401400	0.17928500
C	-0.31473600	-5.61749800	0.62868500
H	1.35947900	-4.70970400	1.63921900
H	-2.13241000	-6.27485600	-0.34340400
H	0.20868400	-6.55261500	0.44675600
H	-4.44056000	-4.66386700	0.32549000
H	-3.82651700	-3.66274500	-0.99024600
Ni	-0.57037800	0.09954800	0.34237500
C	1.19758600	0.77276100	0.08725800
C	2.29005800	0.49311700	0.81753900
H	1.34097700	1.32648500	-0.84872600

H	2.16264300	-0.06577100	1.74245300
C	3.68876100	0.77871900	0.45664600
C	4.72233100	0.11693400	1.13625400
C	4.06738100	1.64744600	-0.58872200
C	6.06653300	0.27757500	0.79072700
H	4.46646400	-0.55885700	1.94895800
C	5.39590500	1.81982100	-0.94714600
H	3.30220700	2.20003800	-1.12725200
C	6.41049900	1.13107300	-0.26287700
H	6.82529300	-0.26400500	1.34449200
H	5.68159500	2.49075000	-1.75189700
O	7.68691800	1.36894400	-0.69721200
C	8.74819700	0.70512800	-0.03467800
H	9.66530500	1.03134600	-0.53002100
H	8.79619600	0.97591900	1.02958500
H	8.66069100	-0.38751700	-0.11963100
C	0.02816900	-1.10197600	-1.99384200
H	0.16064700	-0.07561300	-2.32286600
C	1.23175600	-1.87556800	-1.83920300
C	2.50292300	-1.25761600	-1.95384800
C	1.20378100	-3.26829100	-1.58674900
C	3.67706700	-1.97925900	-1.79379100
H	2.55788800	-0.19373500	-2.15525100
C	2.38227300	-3.99083100	-1.43611600
H	0.25316500	-3.77895600	-1.48118200
C	3.62487900	-3.35413400	-1.53162100
H	4.63222900	-1.46575800	-1.85857900
H	2.33047900	-5.05709900	-1.23090100
H	4.54247300	-3.92228100	-1.40350700
C	-1.26706300	-1.75529500	-2.38832200
H	-2.06450400	-1.01734700	-2.49361900
H	-1.15810800	-2.26936900	-3.35697800
H	-1.59331200	-2.50707600	-1.66326800
Br	-0.44406200	0.11836600	2.80762700

TS2-*S*-cf3

C	-0.47501300	2.80575700	3.30454100
C	-0.91695400	2.30951000	1.91624500
C	-1.67712900	3.41112500	2.67567000
H	-0.61024400	2.10347700	4.11993700
H	0.44560300	3.37997800	3.32015500
H	-1.59936900	4.40606100	2.25314900
H	-2.65391400	3.12822000	3.05175500
C	-0.06998900	2.72342100	0.77504700
C	0.96474700	4.28006000	-0.49971100
C	1.27756800	2.84038900	-0.99239300
H	0.27193000	4.83662200	-1.13485400
H	1.02455900	2.66503100	-2.04073700
C	-1.60267300	1.00403500	1.83219500
C	-2.85384100	-0.67757300	2.69557100
C	-2.66246100	-0.82548600	1.16991900
H	-2.26255700	-1.36870200	3.30234700
H	-2.30112200	-1.80473600	0.86803200
O	0.26562000	4.03419900	0.76312200
O	-2.31380200	0.66269700	2.93519900

N	0.39620500	1.98574700	-0.16097800
N	-1.65885000	0.20273300	0.83144800
C	2.29793000	4.99243100	-0.23850800
C	-4.36105700	-0.72438000	2.97740900
C	2.74952200	2.66870500	-0.66665800
C	3.51999100	1.51158000	-0.75572400
C	3.30765900	3.86638300	-0.20588000
C	4.85776700	1.55627900	-0.35721700
H	3.07449600	0.58488600	-1.09092100
C	4.64576200	3.91554300	0.18410600
C	5.41685900	2.75155600	0.11079700
H	5.45586500	0.65005600	-0.40177800
H	5.08274300	4.84365900	0.54515300
H	6.45803600	2.77564800	0.42216100
H	2.51020000	5.69618700	-1.05429700
H	2.25490200	5.57750700	0.68685900
C	-4.02804700	-0.48532300	0.60918600
C	-4.36323900	-0.19793700	-0.71238300
C	-4.98323300	-0.43032100	1.62852400
C	-5.69301400	0.11018000	-1.00868400
H	-3.59734900	-0.16207700	-1.48013800
C	-6.31143000	-0.12717600	1.33040600
C	-6.66179100	0.13471300	0.00272400
H	-5.97284900	0.34671600	-2.03153200
H	-7.06062600	-0.08201100	2.11725600
H	-7.69214900	0.37777400	-0.24355300
H	-4.63263300	-1.72489200	3.34003100
H	-4.64241300	-0.00964800	3.75859600
Ni	-0.43574700	0.13162200	-0.87840800
C	1.01519800	-0.96171900	-0.10574800
C	2.04267300	-1.55781600	-0.73849400
H	1.08599800	-0.87082900	0.98616300
H	2.02095000	-1.62319100	-1.83192500
C	3.30171100	-2.06014300	-0.15285600
C	4.40947000	-2.29128700	-0.98127800
C	3.47755000	-2.28007300	1.22896200
C	5.64727600	-2.70041800	-0.47553000
H	4.30862500	-2.13483400	-2.05347700
C	4.69504400	-2.69143000	1.74810300
H	2.63940900	-2.12598700	1.90267900
C	5.79557200	-2.90077600	0.90085500
H	6.47385700	-2.86011500	-1.15876900
H	4.82606800	-2.86218700	2.81248500
O	6.95042700	-3.29973900	1.51595100
C	8.09042500	-3.52921400	0.70660600
H	8.88821400	-3.83347200	1.38742200
H	7.91470300	-4.33011000	-0.02542300
H	8.39880500	-2.61958000	0.17185900
C	-1.03792700	-2.22098700	-2.20683500
H	0.04302000	-2.27980200	-2.19687400
C	-1.71452400	-3.03305200	-1.22790200
C	-3.11634700	-3.24115700	-1.25635500
C	-0.97686400	-3.66936900	-0.19176800
C	-3.74802900	-4.01123400	-0.28423800
H	-3.71289300	-2.77234000	-2.03052200

C	-1.61287700	-4.44456000	0.76839600
H	0.09515400	-3.51032100	-0.14714500
C	-3.00571700	-4.61388200	0.73658000
H	-4.82702800	-4.13561600	-0.31873700
H	-1.02567800	-4.91938500	1.55049200
H	-3.50239100	-5.21473700	1.49369900
C	-1.67313000	-1.85503000	-3.51482600
H	-1.82654100	-2.76770300	-4.11535800
H	-2.64517800	-1.36835500	-3.39782000
H	-1.04290800	-1.16617700	-4.07804600
Br	-1.53281300	1.39671500	-2.66981400

TS2-*R*

C	4.22818600	2.95283600	1.33414200
C	3.18356600	1.83386900	1.16632000
C	4.10022600	1.93023200	2.40160700
H	5.07893700	2.89766400	0.66480300
H	3.82535500	3.94320900	1.51214100
H	3.60416200	2.20321200	3.32702500
H	4.86238600	1.16238400	2.47959900
C	1.77025100	2.21715000	1.34853600
C	0.11011700	3.47711000	2.24200700
C	-0.41614800	2.54064400	1.12569800
H	-0.16215500	3.18544500	3.25996600
H	-1.27687800	1.93439100	1.40867100
C	3.49150800	0.77343100	0.17975100
C	4.93449400	-0.58545600	-0.89311200
C	3.47790700	-0.84540200	-1.37080100
H	5.62177100	-0.30810000	-1.69291400
H	3.25789500	-0.54356700	-2.39652100
O	1.56199400	3.30125300	2.13029500
O	4.81611300	0.57575500	-0.02482100
N	0.73657800	1.65885700	0.83299700
N	2.67228000	0.03861900	-0.47876200
C	-0.28571700	4.91117200	1.86837500
C	5.39312200	-1.83634700	-0.10543400
C	-0.70272700	3.48572200	-0.02532200
C	-0.97249000	3.15932200	-1.35400500
C	-0.60495100	4.81774300	0.39145000
C	-1.16281400	4.20186000	-2.26460100
H	-1.00363000	2.12333900	-1.67264500
C	-0.79959500	5.85488700	-0.51944800
C	-1.08251100	5.53726400	-1.85116500
H	-1.36596300	3.96896300	-3.30606200
H	-0.72454500	6.89263900	-0.20340200
H	-1.23144800	6.33543600	-2.57379900
H	-1.16319500	5.21540600	2.45476500
H	0.51901200	5.61618500	2.10438400
C	3.26929600	-2.32335300	-1.13831600
C	2.20105500	-3.11743300	-1.55822600
C	4.32682600	-2.86790800	-0.40232700
C	2.19214700	-4.46753900	-1.19878300
H	1.39258300	-2.67481000	-2.13125200
C	4.31576900	-4.21613100	-0.04584700
C	3.23669500	-5.01137600	-0.44166400

H	1.36478300	-5.09966900	-1.50898300
H	5.13444400	-4.64494800	0.52696700
H	3.21393500	-6.06268300	-0.16740200
H	6.39207300	-2.16756300	-0.41130400
H	5.45139800	-1.59514100	0.96366900
Ni	0.60934800	0.05817200	-0.42880600
C	-1.26167500	-0.14690900	-0.10097900
C	-2.30371300	-0.26818400	-0.93807100
H	-1.45843900	-0.17467300	0.97684300
H	-2.11876000	-0.22913000	-2.00981100
C	-3.71622900	-0.45603400	-0.56020800
C	-4.71807700	-0.32025600	-1.53241900
C	-4.13104800	-0.79107200	0.74594100
C	-6.07359800	-0.48741600	-1.23479700
H	-4.43151900	-0.07317900	-2.55243700
C	-5.47048800	-0.96335500	1.05828600
H	-3.38703700	-0.94706500	1.51952100
C	-6.45672600	-0.80942500	0.07101600
H	-6.80902200	-0.36785300	-2.02264900
H	-5.78361800	-1.23278900	2.06286500
O	-7.74855400	-1.00341700	0.48551600
C	-8.77977700	-0.87281500	-0.47553600
H	-9.71489600	-1.06644500	0.05488000
H	-8.81114300	0.13889800	-0.90479500
H	-8.67034700	-1.60084200	-1.29210200
C	0.88829200	-1.80576800	1.50093000
C	-0.37012000	-2.44243300	1.75272300
C	-1.08484900	-2.26467100	2.96391900
C	-0.95457200	-3.27636200	0.76343700
C	-2.30006700	-2.90993500	3.18178100
H	-0.67330000	-1.62885600	3.74232200
C	-2.16997700	-3.90583200	0.98144600
H	-0.44032400	-3.39050200	-0.18582300
C	-2.85072300	-3.73342600	2.19559900
H	-2.82491300	-2.76483300	4.12287200
H	-2.60319900	-4.52581600	0.20140200
H	-3.80739800	-4.22071100	2.35989900
C	1.62165000	-1.05690700	2.57420500
H	1.05265700	-0.19133100	2.93714000
H	1.81814500	-1.69938800	3.44725100
H	2.58358700	-0.69295700	2.20896000
H	1.47579600	-2.20432600	0.68354400
Br	0.49764500	-0.21368200	-2.86300700

TS2-*R*-cf2

C	4.61806900	2.25812300	0.60197100
C	3.37474000	1.35362400	0.64547200
C	4.29028600	1.55676400	1.86886400
H	5.44315100	1.88693400	0.00490800
H	4.41891800	3.32128300	0.53226300
H	3.85892600	2.13038000	2.68246400
H	4.88486800	0.69611100	2.15601400
C	2.05899600	2.02838300	0.67508300
C	0.68984600	3.75653800	1.20908500
C	-0.05381500	2.66422000	0.39603400

H	0.38796300	3.81603300	2.25498200
H	-0.93675300	2.28253700	0.91035600
C	3.46816500	0.05391000	-0.05514600
C	4.62186600	-1.72761000	-0.84650200
C	3.10916500	-1.84143100	-1.19080400
H	5.27264500	-1.64899100	-1.71859400
H	2.87001600	-1.80945500	-2.25507300
O	2.07253900	3.27406100	1.20366000
O	4.72152900	-0.45018600	-0.14762200
N	0.93544500	1.57407900	0.26011200
N	2.51551400	-0.62810000	-0.57145400
C	0.56148300	5.08104800	0.43954500
C	4.98595400	-2.91163700	0.07805700
C	-0.34392100	3.32173500	-0.93700200
C	-0.84236800	2.72537500	-2.09574100
C	0.02679100	4.67051900	-0.91626000
C	-0.98611000	3.51596600	-3.23862000
H	-1.07740900	1.66569200	-2.11962800
C	-0.12241500	5.45711100	-2.05785600
C	-0.63468700	4.87114800	-3.21899200
H	-1.36378400	3.06709900	-4.15281600
H	0.16242500	6.50657500	-2.04935000
H	-0.75077500	5.47140600	-4.11769200
H	-0.13327900	5.75106400	0.96307000
H	1.52680100	5.59747700	0.39026200
C	2.65934500	-3.11805700	-0.52467600
C	1.38197600	-3.67852900	-0.54102500
C	3.69683300	-3.69415100	0.21430000
C	1.15048200	-4.82762800	0.21864400
H	0.59602800	-3.21165400	-1.12667500
C	3.46430500	-4.84563000	0.96673800
C	2.18288700	-5.40455900	0.96928600
H	0.16119600	-5.27683500	0.22658200
H	4.26320200	-5.29992700	1.54778900
H	1.98761800	-6.29760200	1.55704300
H	5.78994800	-3.51832300	-0.35582900
H	5.35451400	-2.53511000	1.03985500
Ni	0.50392500	-0.26841200	-0.58224000
C	-1.39415800	-0.17808200	-0.41733900
C	-2.29751800	-1.09707200	-0.79584600
H	-1.74718000	0.68600700	0.14846000
H	-1.95679300	-1.95601700	-1.37243900
C	-3.73975200	-1.09323200	-0.49147600
C	-4.51997900	-2.21156300	-0.82307800
C	-4.40250700	-0.01969300	0.14397200
C	-5.88545300	-2.28244900	-0.53578300
H	-4.04510100	-3.05418800	-1.32098500
C	-5.75652700	-0.07285300	0.43721800
H	-3.84391600	0.87236200	0.40975000
C	-6.51276200	-1.20754500	0.10240300
H	-6.44066600	-3.17132700	-0.81374000
H	-6.26135800	0.75804600	0.92132400
O	-7.83865800	-1.15769700	0.43765300
C	-8.65030600	-2.27053500	0.10684700
H	-9.65660000	-2.02426100	0.45256300

H	-8.67392100	-2.44829600	-0.97761300
H	-8.30953500	-3.18655200	0.61015300
C	0.25062300	-1.10137500	1.94414400
C	-0.48815300	-0.07298100	2.63343100
C	0.15497900	0.94275700	3.38612900
C	-1.90626200	-0.04586000	2.59081300
C	-0.57573500	1.93430300	4.03365400
H	1.23818400	0.95268800	3.45754000
C	-2.63176500	0.95239800	3.23201700
H	-2.43019400	-0.81768600	2.03871900
C	-1.97378100	1.95617300	3.95281200
H	-0.05393100	2.69536700	4.60985100
H	-3.71666000	0.94223600	3.16853300
H	-2.54078600	2.73429100	4.45635000
C	1.64870400	-1.44437500	2.37497900
H	2.33135000	-0.58990400	2.31643900
H	1.65008100	-1.77365600	3.42690400
H	2.06438800	-2.24862800	1.77109900
H	-0.33284800	-1.90584700	1.50794100
Br	0.34383600	-1.00613000	-2.91029500

TS2-*R*-cf3

C	-0.39683000	4.14318800	2.26550300
C	-0.78091500	2.98313200	1.33267000
C	-1.71213200	4.18486200	1.57599000
H	-0.37001900	3.90835100	3.32371900
H	0.39652400	4.78695900	1.90093500
H	-1.84023600	4.85211400	0.73126000
H	-2.60572100	3.97051800	2.15238200
C	-0.06979300	2.91798100	0.03741100
C	0.72092400	3.83054300	-1.87658400
C	1.08255800	2.32239800	-1.77055100
H	-0.05688700	4.05837400	-2.60804300
H	0.72242700	1.72320100	-2.61079100
C	-1.20771800	1.70897200	1.94754900
C	-1.94680000	0.44661200	3.68114700
C	-1.92642300	-0.35010400	2.35224100
H	-1.15470600	0.18505300	4.38782500
H	-1.37581400	-1.29114200	2.40546000
O	0.14560200	4.11264600	-0.55909400
O	-1.66286300	1.80683200	3.22125300
N	0.37392000	1.87387700	-0.55354200
N	-1.25088200	0.54944100	1.40261200
C	2.02633400	4.61495000	-2.07226800
C	-3.36398400	0.34121900	4.26341600
C	2.58838100	2.32243000	-1.59858000
C	3.41813800	1.24057300	-1.30754100
C	3.10887900	3.61463600	-1.72804000
C	4.78584600	1.46994300	-1.13632900
H	3.00192600	0.24690900	-1.18621500
C	4.47508500	3.84216000	-1.56360300
C	5.31033300	2.76208200	-1.26363600
H	5.43779400	0.63758500	-0.88729400
H	4.88494200	4.84470800	-1.66146700
H	6.37564500	2.92789200	-1.12534000

H	2.10817300	4.94971300	-3.11479700
H	2.04003200	5.51354100	-1.44548200
C	-3.39414100	-0.51543300	2.01621600
C	-3.94736900	-0.91427200	0.80213700
C	-4.20042800	-0.12575000	3.09053600
C	-5.33854000	-0.97345200	0.69201500
H	-3.31722900	-1.12128700	-0.05427100
C	-5.58899100	-0.18211800	2.97824000
C	-6.15236600	-0.61952800	1.77481200
H	-5.78214200	-1.28426800	-0.24948500
H	-6.22550800	0.12017500	3.80637800
H	-7.23365100	-0.66534100	1.67431600
H	-3.37125800	-0.38521800	5.08709800
H	-3.69007000	1.30093500	4.67919700
Ni	-0.44571300	-0.10150200	-0.41657600
C	1.21958500	-0.85395800	0.35949800
C	2.03015900	-1.88034100	0.03954700
H	1.61439900	-0.14369500	1.09862100
H	1.68696600	-2.63337300	-0.67641600
C	3.40269300	-2.13623400	0.52196100
C	4.01924000	-3.36837900	0.25904100
C	4.16664800	-1.17382200	1.21587700
C	5.32262200	-3.65500100	0.67278500
H	3.46362600	-4.13049600	-0.28387700
C	5.46302800	-1.43894200	1.63152000
H	3.74111200	-0.19401600	1.40941500
C	6.05386700	-2.68489500	1.36657700
H	5.75084300	-4.62507400	0.44659600
H	6.04914600	-0.69223700	2.15908400
O	7.33613900	-2.84170900	1.81705600
C	7.98386900	-4.07644700	1.56556200
H	8.98147100	-3.98858200	2.00114400
H	7.45569100	-4.91635600	2.03865300
H	8.07588000	-4.27519300	0.48838300
C	-1.13227000	-2.76119200	-0.84380000
C	-2.23205400	-2.94461900	-1.74655400
C	-3.48212800	-3.46899200	-1.32767600
C	-2.08275100	-2.62492000	-3.12075800
C	-4.51933600	-3.65802100	-2.23376100
H	-3.63573900	-3.72489100	-0.28471400
C	-3.11796900	-2.82456000	-4.02248100
H	-1.14425100	-2.19575100	-3.45639800
C	-4.34500100	-3.33862600	-3.58558100
H	-5.46735400	-4.06297300	-1.88849400
H	-2.97806300	-2.56559100	-5.06832300
H	-5.15789000	-3.48742900	-4.29119600
C	-1.13460900	-3.33844800	0.54209000
H	-0.23945100	-3.03099600	1.08454000
H	-2.01838100	-3.03171800	1.11378700
H	-1.15755900	-4.43991500	0.50251600
H	-0.16642400	-2.59456400	-1.30825900
Br	-2.03898400	0.56242800	-2.14637500

TS3-*S*

C	3.69301300	3.47518800	-0.64044600

C	2.87608200	2.25666700	-0.17715000
C	3.92036200	2.94410700	0.72701600
H	4.43656200	3.27539700	-1.40339000
H	3.13306400	4.39676300	-0.75072200
H	3.51486200	3.48957400	1.57189700
H	4.82198000	2.37165600	0.91641400
C	1.45774900	2.49811700	0.16155300
C	-0.19782200	3.78491000	1.02321800
C	-0.73611800	2.42898700	0.49739800
H	-0.19403500	3.87388400	2.11195800
H	-1.26959600	1.86585300	1.26365500
C	3.25586800	0.94044400	-0.73613700
C	4.78422300	-0.52787400	-1.51229000
C	3.35974000	-1.15431800	-1.50721500
H	5.25528700	-0.49973600	-2.49548600
H	2.93117000	-1.36118900	-2.49015000
O	1.20101500	3.75145500	0.60763900
O	4.55551700	0.85508800	-1.12218100
N	0.47562100	1.67761900	0.10248900
N	2.52177600	-0.09744700	-0.88128300
C	-0.96701000	4.90318800	0.29980900
C	5.62889000	-1.28380400	-0.45721800
C	-1.58860300	2.79807900	-0.69582600
C	-2.17483900	1.93858700	-1.62485000
C	-1.69215000	4.18723200	-0.82118900
C	-2.89000200	2.49917900	-2.68584600
H	-2.05641000	0.86300500	-1.53653500
C	-2.40870600	4.74273800	-1.88065000
C	-3.00873900	3.88890200	-2.81085000
H	-3.34940800	1.84773300	-3.42369900
H	-2.49507500	5.82149100	-1.98718600
H	-3.56639400	4.30904500	-3.64383700
H	-1.66980100	5.38357500	0.99325700
H	-0.28108100	5.68259900	-0.05073300
C	3.49787000	-2.39400700	-0.65732800
C	2.55069200	-3.39721400	-0.45393200
C	4.75389000	-2.44848200	-0.04481900
C	2.87091500	-4.45234700	0.40420000
H	1.58905000	-3.33620300	-0.95520500
C	5.07262500	-3.50450000	0.80862100
C	4.11978800	-4.50232000	1.03538700
H	2.14435800	-5.24050700	0.58090700
H	6.04766700	-3.55660900	1.28717600
H	4.35576300	-5.32973300	1.69947500
H	6.58988200	-1.61358800	-0.86897500
H	5.85648300	-0.61339800	0.38120700
Ni	0.42576000	-0.37968900	-0.47077600
C	-1.27355900	-0.77182900	0.38256000
C	-2.17501400	-1.65809200	-0.08327500
H	-1.60953400	0.00650800	1.06209400
H	-1.83287500	-2.44363500	-0.75318900
C	-3.61979700	-1.62129300	0.16580100
C	-4.47489600	-2.40903400	-0.62223700
C	-4.22055200	-0.82454700	1.16598300
C	-5.85975900	-2.40649900	-0.44667700

H	-4.04381200	-3.03327800	-1.40127700
C	-5.59317900	-0.81021300	1.35276100
H	-3.59706800	-0.21535500	1.81475200
C	-6.42851900	-1.60004600	0.54549700
H	-6.47622200	-3.03032000	-1.08396400
H	-6.05153000	-0.20036000	2.12546600
O	-7.76582900	-1.51305500	0.81439500
C	-8.65554000	-2.29021100	0.03105200
H	-9.65749100	-2.07125700	0.40607000
H	-8.60039900	-2.02080800	-1.03297500
H	-8.45639400	-3.36582400	0.13753800
C	0.48889000	-1.39203200	1.45009400
H	1.49064700	-1.55089700	1.04096500
C	0.55803400	-0.36160700	2.52330000
C	1.71927700	0.42047300	2.66771800
C	-0.51852800	-0.09739600	3.39023400
C	1.79408700	1.44464200	3.60801800
H	2.56106300	0.22613600	2.00850700
C	-0.44964600	0.93221800	4.33132400
H	-1.41946500	-0.69993100	3.32367900
C	0.70198600	1.71548200	4.43995900
H	2.70509100	2.03203200	3.69510200
H	-1.29822800	1.11971600	4.98452600
H	0.75581600	2.51402900	5.17517200
C	-0.06050700	-2.76299600	1.82618000
H	-0.15124900	-3.38671100	0.93307800
H	0.63863300	-3.25577600	2.51691300
H	-1.04422100	-2.71641400	2.29845600
Br	0.13717800	-1.58531800	-2.63128400

TS3-*S*-cf2

C	-2.89739700	4.22721900	-1.47020700
C	-2.20981200	2.89088400	-1.17188100
C	-3.01969300	3.13035500	-2.46483400
H	-3.75603200	4.46049800	-0.85300000
H	-2.23774500	5.05614600	-1.69585300
H	-2.44138700	3.18603400	-3.38205900
H	-3.95751800	2.58843100	-2.53598900
C	-0.73637200	2.84988600	-1.30260700
C	1.26192000	3.72151800	-1.92966900
C	1.43185600	2.41222500	-1.11350900
H	1.50400100	3.63716300	-2.99240400
H	2.05028600	1.66450800	-1.61186900
C	-2.83676200	2.01614700	-0.14575000
C	-4.57168800	1.46317700	1.19924400
C	-3.38913200	0.45827300	1.35751200
H	-4.80127100	2.03092800	2.10261800
H	-2.92078600	0.43383100	2.34357500
O	-0.17719200	3.95804500	-1.84554200
O	-4.07600200	2.42357600	0.22572800
N	0.05050300	1.90012700	-0.95414500
N	-2.36549600	0.95718400	0.39599000
C	2.04043500	4.82875800	-1.20017900
C	-5.78754600	0.69136000	0.63905400
C	2.01914000	2.87164800	0.20406900

C	2.20669900	2.11728600	1.36143200
C	2.33076000	4.23430600	0.16189700
C	2.72611000	2.75671400	2.48948100
H	1.92341600	1.07061500	1.39790500
C	2.85435300	4.86746100	1.28843400
C	3.05067500	4.11836800	2.45250100
H	2.86575900	2.18950100	3.40513900
H	3.09963600	5.92660400	1.26624000
H	3.45177000	4.60100900	3.33997900
H	2.96516700	5.05622400	-1.74704500
H	1.45531400	5.75426900	-1.16105100
C	-3.98161700	-0.87068500	0.95341200
C	-3.35917300	-2.11501200	0.98328800
C	-5.29123500	-0.72904600	0.48457600
C	-4.04421300	-3.22299400	0.48016000
H	-2.35711900	-2.19945600	1.38214400
C	-5.98279900	-1.83702400	-0.00469700
C	-5.34510100	-3.08201000	-0.01707800
H	-3.55175200	-4.19064100	0.46314000
H	-7.00225900	-1.73736800	-0.37019100
H	-5.86951800	-3.94989500	-0.40870700
H	-6.63931400	0.74698500	1.32831700
H	-6.11392400	1.14289800	-0.30552100
Ni	-0.39367400	-0.02339300	0.03594900
C	1.23964400	-0.77853200	-0.68959600
C	2.10209600	-1.52012700	0.03201000
H	1.61113000	-0.24898900	-1.56455900
H	1.74414200	-2.03257200	0.91882800
C	3.54944300	-1.59267500	-0.20006500
C	4.39357000	-1.98885700	0.84988500
C	4.15998300	-1.26863600	-1.43088200
C	5.78067200	-2.04325100	0.70550400
H	3.95231400	-2.24984500	1.80882000
C	5.53593200	-1.31693900	-1.59048100
H	3.54105600	-0.99708400	-2.28179300
C	6.36143200	-1.70071300	-0.52114000
H	6.38984200	-2.35068700	1.54787100
H	6.00330900	-1.07590600	-2.54048400
O	7.70231200	-1.71595200	-0.78462600
C	8.58241800	-2.10871800	0.25504200
H	9.58896600	-2.05174700	-0.16453500
H	8.51282300	-1.43605800	1.12131900
H	8.38584400	-3.13819700	0.58559900
C	-0.54069500	-1.50446700	-1.57300400
H	0.16019300	-1.46196700	-2.40846700
C	-0.71253300	-2.95930700	-1.18811500
C	-1.06919800	-3.86676800	-2.20141000
C	-0.53320500	-3.46093000	0.10543300
C	-1.26274000	-5.22031100	-1.92736400
H	-1.19420000	-3.50970000	-3.22146700
C	-0.72308000	-4.81660600	0.38462900
H	-0.26751600	-2.78159600	0.90624500
C	-1.09312100	-5.70319300	-0.62721700
H	-1.54013700	-5.89822700	-2.73088600
H	-0.58048200	-5.17384400	1.40138100

H	-1.23969600	-6.75807800	-0.40981400
C	-1.84614600	-0.86747500	-2.10495600
H	-1.69563000	0.18052300	-2.38450900
H	-2.15452900	-1.40839700	-3.01217300
H	-2.66378200	-0.93059600	-1.38780500
Br	-0.25568000	-0.60870500	2.48313100

TS3-*S*-cf3

C	1.60857000	-2.54903300	1.37114900
C	0.45608400	-1.58616000	1.73603300
C	0.92419800	-2.69686000	2.68052600
H	1.39308400	-3.25793300	0.57879500
H	2.59555800	-2.10101300	1.32391400
H	1.43953300	-2.36367100	3.57377200
H	0.23480600	-3.52211700	2.81399800
C	0.84843900	-0.19497600	2.06413500
C	2.11495300	1.34816100	3.11904800
C	1.11042400	2.02252300	2.12996200
H	1.98589300	1.64637100	4.16034700
H	0.34693000	2.65230700	2.59502400
C	-0.82874700	-1.78209800	1.02153600
C	-2.52079900	-3.06716500	0.23160000
C	-2.74840700	-1.56535900	-0.08143500
H	-2.24566200	-3.67713000	-0.63334700
H	-2.93456300	-1.36100900	-1.13283400
O	1.77557800	-0.06607900	3.04881300
O	-1.34984600	-3.03018200	1.10846800
N	0.43043400	0.87276600	1.50354000
N	-1.48158100	-0.92305900	0.32670500
C	3.54341800	1.60966400	2.58521400
C	-3.75393200	-3.57872100	0.99076500
C	1.98903100	2.78958000	1.16722000
C	1.58452900	3.61896800	0.12119500
C	3.34263300	2.54398700	1.41295700
C	2.56416500	4.18922100	-0.69684300
H	0.52693200	3.79343900	-0.05257900
C	4.31917300	3.12546900	0.60331000
C	3.92182100	3.94288300	-0.45941900
H	2.26699300	4.83181600	-1.52110000
H	5.37480500	2.94305600	0.79101600
H	4.67360100	4.39446300	-1.10119500
H	4.19200100	2.04169700	3.35642100
H	3.99745800	0.66011800	2.27506300
C	-3.91607700	-1.18392000	0.80300000
C	-4.42212200	0.09220300	1.04322400
C	-4.46931500	-2.31331400	1.41466300
C	-5.51027700	0.22010400	1.91019400
H	-3.95305900	0.96497900	0.59953100
C	-5.55747400	-2.18243000	2.27697100
C	-6.07604400	-0.90719200	2.51919900
H	-5.91424300	1.20699600	2.11895100
H	-5.99297200	-3.05529100	2.75774700
H	-6.92140500	-0.78960800	3.19241000
H	-4.37570300	-4.18823500	0.32151500
H	-3.45979700	-4.22051300	1.82873700

Ni	-0.60763200	0.90738200	-0.43140800
C	0.75665700	-0.11212200	-1.37031700
C	2.06214200	0.20656700	-1.29386200
H	0.44153900	-1.13633400	-1.57876300
H	2.34412900	1.23946600	-1.09828800
C	3.16677200	-0.76356400	-1.28685200
C	4.39369300	-0.41232100	-0.70032000
C	3.04760000	-2.07930400	-1.78528500
C	5.44663700	-1.32336400	-0.57772500
H	4.52334400	0.59894300	-0.32468400
C	4.08317200	-2.99422800	-1.67229700
H	2.12750400	-2.38372400	-2.27664000
C	5.29290500	-2.62833500	-1.05910500
H	6.37268100	-1.00322500	-0.11319200
H	3.98869600	-4.00361800	-2.06136000
O	6.24436800	-3.60754400	-0.99311000
C	7.49245400	-3.28591300	-0.40344500
H	8.09480800	-4.19502200	-0.45700900
H	8.00349800	-2.48041900	-0.94922300
H	7.37968800	-2.98848100	0.64878200
C	-0.62444500	0.98065600	-2.69355300
H	0.10413900	0.45654400	-3.30561700
C	-1.95964500	0.36373000	-2.91852400
C	-3.17126100	0.98607900	-2.55725900
C	-2.02547400	-0.90869900	-3.52157900
C	-4.39181900	0.35262100	-2.78310100
H	-3.14412200	1.94508400	-2.05254700
C	-3.24829100	-1.54142700	-3.74780300
H	-1.10168700	-1.40160000	-3.81762000
C	-4.44050900	-0.91355400	-3.37624900
H	-5.31137900	0.84635700	-2.48081600
H	-3.27017400	-2.52141200	-4.21842600
H	-5.39543100	-1.40328900	-3.54651500
C	-0.43061000	2.47816000	-2.88724500
H	-0.54848000	2.72445500	-3.95315500
H	-1.13123600	3.07842300	-2.30603900
H	0.58436600	2.76127400	-2.58680700
Br	-2.00361500	2.85830100	0.30308500

TS3-*R*

C	4.83539800	-0.06231100	1.96008100
C	3.42062200	-0.08523600	1.37450400
C	3.75071000	-0.69697900	2.75256000
H	5.55674300	-0.70154300	1.46516500
H	5.19929100	0.90961500	2.27162000
H	3.34909600	-0.16807600	3.61103100
H	3.70560600	-1.78036200	2.80809000
C	2.67159200	1.19678900	1.36864300
C	2.23540200	3.28681300	2.13504700
C	1.33770700	2.91643100	0.92095300
H	1.71828600	3.32121600	3.09753200
H	0.26757200	3.03479000	1.10777000
C	3.15207300	-1.03188000	0.25989400
C	3.67326500	-2.73899900	-1.11892100
C	2.31015400	-2.10070400	-1.51119800

H	4.42201000	-2.71347200	-1.91123300
H	2.30482700	-1.53486900	-2.44683000
O	3.15787800	2.15196700	2.19867600
O	4.17084000	-1.87158100	-0.05615000
N	1.63145900	1.49130500	0.68058500
N	2.07608300	-1.12379000	-0.42435600
C	2.98431100	4.58125700	1.78256900
C	3.37588700	-4.17382700	-0.61909600
C	1.84463500	3.80671900	-0.19337700
C	1.50398700	3.75275300	-1.54395000
C	2.78391500	4.72375400	0.28857100
C	2.11891200	4.65616100	-2.41459700
H	0.81493100	2.99840700	-1.91409600
C	3.39328100	5.62488200	-0.58380800
C	3.05170600	5.58635800	-1.93876500
H	1.87555300	4.62703900	-3.47293900
H	4.12551400	6.34156400	-0.21963900
H	3.52170100	6.28040000	-2.63076500
H	2.54727000	5.42570300	2.33192400
H	4.03649500	4.51565100	2.08097900
C	1.34258000	-3.25512200	-1.53441900
C	0.02288300	-3.24892800	-1.98335500
C	1.94343600	-4.42089800	-1.04824900
C	-0.69617400	-4.44592200	-1.94327900
H	-0.41584200	-2.32820200	-2.35803600
C	1.22501000	-5.61596300	-1.01695200
C	-0.09861200	-5.61983900	-1.46965400
H	-1.72661100	-4.46586400	-2.28643700
H	1.68529400	-6.53197000	-0.65404200
H	-0.66901900	-6.54487100	-1.45143900
H	4.07610500	-4.90638800	-1.03596200
H	3.48846100	-4.21130600	0.47244300
Ni	0.27450100	0.06457800	-0.23961900
C	-1.44634600	0.67227100	0.38217800
C	-2.60835800	0.09474800	0.02235800
H	-1.42958000	1.69473600	0.76332200
H	-2.58824200	-0.96102300	-0.24730300
C	-3.93541600	0.71335300	-0.02553400
C	-5.06961300	-0.10004700	-0.17888300
C	-4.15126000	2.10372300	0.09109500
C	-6.36336600	0.42506500	-0.19913300
H	-4.93631300	-1.17541800	-0.27374000
C	-5.42839500	2.64037200	0.07433300
H	-3.29954700	2.77241200	0.17871700
C	-6.54911400	1.80561900	-0.06917400
H	-7.20685000	-0.24591100	-0.31677700
H	-5.59156700	3.71060000	0.15804300
O	-7.76190200	2.43807700	-0.07502700
C	-8.92472300	1.64683800	-0.24479900
H	-9.76752000	2.34118300	-0.22947700
H	-8.91469200	1.11099600	-1.20438800
H	-9.04279700	0.91751700	0.56925500
C	-0.36751400	-0.53696300	1.84984500
C	-1.07281300	-1.84490000	1.90449200
C	-2.40893200	-1.96567600	2.32882900

C	-0.38572400	-3.01883400	1.55088900
C	-3.02676300	-3.21361400	2.40229900
H	-2.97272700	-1.07641100	2.58928200
C	-0.99859400	-4.26762900	1.62994000
H	0.63881900	-2.94402700	1.19798100
C	-2.32485600	-4.37093300	2.05573200
H	-4.06043500	-3.28093000	2.73237000
H	-0.44158800	-5.15413900	1.34514300
H	-2.80726100	-5.34311200	2.11546500
C	-0.67607200	0.45426800	2.96469400
H	-1.72929200	0.74528500	2.99840900
H	-0.41951600	0.00946400	3.93688500
H	-0.08188800	1.36572800	2.84493600
H	0.70992300	-0.72205600	1.85322900
Br	0.14901400	0.43718100	-2.69357000

TS3-*R*-cf2

C	4.43857400	2.96426800	0.15677300
C	3.37114100	1.87788600	0.37296000
C	4.39798100	2.25552700	1.46056500
H	5.22419700	2.70916400	-0.54490900
H	4.06877600	3.98177200	0.10838100
H	3.99643800	2.77779200	2.32268300
H	5.15359400	1.50567300	1.66898100
C	1.98151900	2.34334300	0.58561100
C	0.45378300	3.87631500	1.27157900
C	-0.22378000	2.63294600	0.63725400
H	0.32593200	3.96163300	2.35378200
H	-0.95454400	2.16115700	1.29651000
C	3.58335600	0.59080000	-0.33179500
C	4.90160400	-1.01478300	-1.22279300
C	3.39437500	-1.35255500	-1.41956400
H	5.46244200	-0.91419200	-2.15274600
H	3.03499900	-1.34154300	-2.45103100
O	1.87414000	3.61629900	1.04045800
O	4.88385800	0.30712100	-0.60824300
N	0.89232200	1.69276300	0.40055900
N	2.70070200	-0.25342500	-0.70497900
C	-0.01827700	5.11301100	0.48944900
C	5.49587400	-2.07893900	-0.26797100
C	-0.81316000	3.14800400	-0.65805900
C	-1.37774000	2.40497500	-1.69484100
C	-0.67271800	4.53675400	-0.74895000
C	-1.82140800	3.08646500	-2.83073900
H	-1.43314300	1.32191400	-1.64570000
C	-1.12128200	5.21335100	-1.88244100
C	-1.69949400	4.47828800	-2.92166900
H	-2.25124600	2.52367700	-3.65408800
H	-1.01653700	6.29276100	-1.96232200
H	-2.04750000	4.99237300	-3.81383200
H	-0.73192500	5.68726800	1.09499000
H	0.82394300	5.77892400	0.27055200
C	3.21253200	-2.69084300	-0.74625400
C	2.05843500	-3.47431000	-0.71191400
C	4.37162700	-3.07312500	-0.06483000

C	2.07528100	-4.64952800	0.04323500
H	1.17616000	-3.15399200	-1.25877900
C	4.38658100	-4.24965200	0.68465000
C	3.22874000	-5.03134800	0.74024000
H	1.18679300	-5.27371700	0.08705100
H	5.28264600	-4.55637100	1.21888600
H	3.22721700	-5.94806900	1.32415200
H	6.38846400	-2.54904900	-0.69767700
H	5.80813800	-1.60196000	0.66924900
Ni	0.58434700	-0.27805000	-0.35984400
C	-1.22083300	-0.54730800	0.30921300
C	-2.05372500	-1.50483300	-0.15440100
H	-1.64671600	0.34776600	0.75671500
H	-1.61869500	-2.39843100	-0.59889400
C	-3.51224000	-1.41175600	-0.19900200
C	-4.23830400	-2.22655900	-1.08450900
C	-4.25212700	-0.53771200	0.62974800
C	-5.62974800	-2.17208800	-1.16842400
H	-3.69614600	-2.90803100	-1.73567000
C	-5.63479900	-0.47371500	0.55693700
H	-3.73349400	0.07645400	1.35943300
C	-6.33791000	-1.28702800	-0.34605000
H	-6.14411800	-2.81579500	-1.87299900
H	-6.20238600	0.19288700	1.19928500
O	-7.69812500	-1.14604100	-0.33597200
C	-8.45757000	-1.93852400	-1.23225900
H	-9.50191300	-1.66633800	-1.06516100
H	-8.19335400	-1.73375700	-2.27921000
H	-8.32803100	-3.01218000	-1.03546200
C	0.13812400	-1.23442500	1.72532600
C	-0.72379000	-0.65805200	2.80860800
C	-0.39373300	0.55573100	3.43688500
C	-1.90375100	-1.30589700	3.21323800
C	-1.21511800	1.10391600	4.42351000
H	0.51069500	1.08013000	3.14419700
C	-2.72040500	-0.76641200	4.20545000
H	-2.19276300	-2.22792900	2.71704600
C	-2.38343200	0.44612700	4.81395400
H	-0.93838100	2.04574600	4.89181200
H	-3.62812300	-1.28885100	4.49559900
H	-3.02322700	0.87177700	5.58214700
C	1.63385500	-1.14848500	2.08596600
H	2.02259100	-0.12789500	2.08838500
H	1.76349500	-1.55237000	3.10179500
H	2.24334800	-1.74146100	1.40717900
H	-0.11552600	-2.27493700	1.52977100
Br	0.21479500	-0.98657100	-2.75061600

TS3-*R*-cf3

C	0.67802800	-3.36424500	0.30548600
C	-0.45266800	-2.44665000	0.82329600
C	-0.28022500	-3.88784100	1.31137200
H	0.58820200	-3.68251700	-0.72756200
H	1.68177000	-3.08418800	0.60791300
H	0.05309900	-3.99525300	2.33692400

H	-1.03961500	-4.58939500	0.98678000
C	-0.04226100	-1.35572100	1.73933700
C	1.02847400	-0.53305200	3.55100400
C	0.37018200	0.61113300	2.71458000
H	0.64544300	-0.62168900	4.56864700
H	-0.42654900	1.16349300	3.22017500
C	-1.56734800	-2.16201100	-0.11069900
C	-3.14829800	-2.78624800	-1.61148100
C	-3.20170800	-1.26275000	-1.31468400
H	-2.74762600	-3.05158200	-2.59403800
H	-3.16281400	-0.63874800	-2.20995400
O	0.62679300	-1.74807600	2.85318600
O	-2.18194600	-3.25740900	-0.62231500
N	-0.23005400	-0.10467700	1.57204500
N	-2.00061000	-1.01531700	-0.49296500
C	2.56125100	-0.33587200	3.49262000
C	-4.54210900	-3.36556500	-1.32927700
C	1.52733800	1.49408700	2.30757500
C	1.47383200	2.68096500	1.57749900
C	2.74736500	0.95062500	2.71883800
C	2.67362900	3.31445800	1.24351600
H	0.51724300	3.08583500	1.26131200
C	3.94394700	1.59181000	2.39635300
C	3.89923600	2.77237100	1.64797600
H	2.64783800	4.22358900	0.65334000
H	4.89784300	1.17837300	2.71630200
H	4.82517300	3.27460900	1.38012500
H	2.99745000	-0.28182000	4.49739100
H	3.02281100	-1.19288600	2.98656300
C	-4.48964900	-1.09266500	-0.53500600
C	-4.92903100	0.04111500	0.14630000
C	-5.22943300	-2.27971900	-0.52928100
C	-6.14570200	-0.02967500	0.82973400
H	-4.31798400	0.93876500	0.18069300
C	-6.44384600	-2.34548700	0.15267900
C	-6.89878700	-1.21047700	0.82987800
H	-6.50346600	0.83967200	1.37440600
H	-7.02456400	-3.26476500	0.16447400
H	-7.84180800	-1.24860700	1.36910300
H	-5.06245600	-3.56163400	-2.27635500
H	-4.46769200	-4.32198200	-0.80012400
Ni	-0.81363800	0.82244300	-0.30445500
C	0.56866000	0.01088100	-1.38804700
C	1.85613000	0.08275200	-1.00429600
H	0.20906700	-0.82334800	-1.99268100
H	2.18302500	0.94165200	-0.42129000
C	2.84390000	-0.99192900	-1.16986300
C	3.92364500	-1.08142500	-0.27610400
C	2.73617300	-1.99967600	-2.15249200
C	4.83854100	-2.13691400	-0.32308100
H	4.04147700	-0.31102100	0.48120200
C	3.63748900	-3.05185700	-2.21316100
H	1.93536900	-1.94774900	-2.88530300
C	4.69488100	-3.13646300	-1.29241500
H	5.65269400	-2.16403600	0.39265800

H	3.55520500	-3.82221100	-2.97405300
O	5.52063100	-4.21652700	-1.43532100
C	6.61865300	-4.33860800	-0.54741100
H	7.14038100	-5.25313900	-0.83661100
H	7.30710700	-3.48633100	-0.63385600
H	6.28826100	-4.42597000	0.49737500
C	-0.35258600	1.75059200	-2.31844200
H	0.09851600	1.17612400	-3.12570100
Br	-2.20814600	2.51441200	0.88022800
C	0.48380800	2.96056000	-2.06102500
C	1.82004400	2.98102000	-2.50439500
C	-0.02564300	4.11865900	-1.44668100
C	2.61316600	4.11747800	-2.35805400
H	2.23401800	2.09220500	-2.97248300
C	0.76755200	5.25729100	-1.30279500
H	-1.03684900	4.11690200	-1.05824400
C	2.08738500	5.26735700	-1.76273300
H	3.63936600	4.10771400	-2.71676500
H	0.34833100	6.14163400	-0.82967000
H	2.69947800	6.15949600	-1.65627200
C	-1.82012300	1.98835600	-2.69192200
H	-1.85601300	2.60690100	-3.60203600
H	-2.31254600	1.03876300	-2.92192700
H	-2.39475400	2.48641500	-1.90980800

TS4-*S*

C	3.23208300	3.56651500	-0.17821100
C	2.55391200	2.20444100	0.07091700
C	3.51707700	2.84573900	1.08674200
H	3.98959300	3.57442900	-0.95313900
H	2.57258900	4.42613900	-0.14592700
H	3.05250600	3.19710200	2.00103200
H	4.47586200	2.35053700	1.19817400
C	1.11377100	2.24595700	0.38011200
C	-0.71817100	3.20386400	1.30393600
C	-1.09123600	2.00074700	0.40711500
H	-0.79969400	3.01482900	2.37595600
H	-1.72930900	1.27068400	0.90054000
C	3.06518200	1.04870000	-0.69427900
C	4.66968200	0.02202600	-1.91729100
C	3.43259300	-0.90272600	-1.72229800
H	4.80580900	0.38580700	-2.93836800
H	2.95499100	-1.23593900	-2.64382500
O	0.70893600	3.36358700	1.01776000
O	4.34442400	1.18830900	-1.10469400
N	0.21487000	1.38084500	0.07243100
N	2.45476800	-0.04007100	-0.99375300
C	-1.50207400	4.42061900	0.79630200
C	5.90451400	-0.69422700	-1.34678500
C	-1.73461600	2.64154600	-0.80555100
C	-2.06259100	2.04116500	-2.02019700
C	-1.93972200	4.00923100	-0.59366300
C	-2.61770200	2.83633400	-3.02612600
H	-1.88337400	0.98193500	-2.16772200
C	-2.49513500	4.80004800	-1.59856200

C	-2.83416300	4.20392400	-2.81673100
H	-2.88079500	2.38837800	-3.98043500
H	-2.65699100	5.86382100	-1.44165900
H	-3.26490800	4.80923400	-3.61008000
H	-2.36368000	4.60448100	1.45203600
H	-0.88417400	5.32515700	0.81655300
C	3.96863200	-2.05511900	-0.89514600
C	3.27947800	-3.17638300	-0.43267900
C	5.33501800	-1.90043800	-0.63560600
C	3.96494500	-4.11490500	0.34199500
H	2.23407200	-3.30441600	-0.68591600
C	6.01952100	-2.83882000	0.13664600
C	5.32294400	-3.94264200	0.63529800
H	3.43697400	-4.98767000	0.71637200
H	7.08098500	-2.71918800	0.34027800
H	5.84331300	-4.67958600	1.24143400
H	6.57823700	-0.99754700	-2.15839000
H	6.47274900	-0.02046900	-0.69533900
Ni	0.44027400	-0.49214000	-0.69145900
C	-1.35322000	-0.91633000	-0.21843700
C	-2.36855400	-1.37681600	-0.96268000
H	-1.53956800	-0.68850300	0.83398800
H	-2.17617100	-1.63860200	-2.00184000
C	-3.75998400	-1.57751300	-0.51671800
C	-4.70841100	-2.07799800	-1.42084900
C	-4.21420700	-1.28694300	0.78805400
C	-6.04305900	-2.28862400	-1.06413100
H	-4.39343300	-2.31452300	-2.43475900
C	-5.53379000	-1.49004800	1.16024100
H	-3.51774400	-0.89510200	1.52468700
C	-6.46359500	-1.99364800	0.23626400
H	-6.73418700	-2.67951800	-1.80249400
H	-5.87762200	-1.26608900	2.16581500
O	-7.73934400	-2.15483200	0.70589600
C	-8.71530600	-2.66469300	-0.18503700
H	-9.64665700	-2.71538600	0.38321800
H	-8.85725500	-2.00568100	-1.05341100
H	-8.45420500	-3.67118200	-0.54160500
C	0.94402300	-1.73548000	1.55048900
H	1.96024300	-1.73528800	1.16805400
C	0.65416500	-0.73047400	2.52700400
C	1.62530000	0.26729900	2.82041600
C	-0.58353200	-0.64627100	3.22144200
C	1.37209600	1.28469500	3.72823600
H	2.58407700	0.22008600	2.30974400
C	-0.83628000	0.38463000	4.12167600
H	-1.34324300	-1.40238500	3.05368600
C	0.13319500	1.36042500	4.38374000
H	2.14142800	2.02310300	3.94065400
H	-1.79422700	0.42232600	4.63471300
H	-0.06293000	2.15391200	5.09962500
C	0.19776500	-3.02887900	1.40754300
H	0.26571900	-3.39825400	0.38110300
H	0.62499300	-3.79140100	2.07995300
H	-0.86582200	-2.93708900	1.63995500

Cl	0.51419300	-2.14139600	-2.26255300

TS4-*R*

C	4.04933100	3.12538100	1.27529700
C	3.06849300	1.95975600	1.05542800
C	3.97254100	2.05562000	2.30067500
H	4.90526300	3.14363200	0.61092700
H	3.59313500	4.08443400	1.49116600
H	3.45822500	2.26281100	3.23331400
H	4.77414900	1.32648000	2.35327700
C	1.63589200	2.26096300	1.23724400
C	-0.09550500	3.43748400	2.11060000
C	-0.56063800	2.47560500	0.98961000
H	-0.36883700	3.13619200	3.12532900
H	-1.39677900	1.83097400	1.25987200
C	3.43702200	0.95398700	0.03153900
C	4.96489000	-0.18572300	-1.18220900
C	3.51832000	-0.64131300	-1.54156700
H	5.51435200	0.24808700	-2.01883700
H	3.19334400	-0.40563900	-2.55624800
O	1.36428600	3.33015600	2.01956100
O	4.76455400	0.88863400	-0.22054900
N	0.63672900	1.64993500	0.71247500
N	2.66546100	0.16088800	-0.61677700
C	-0.55236100	4.85081400	1.72618900
C	5.69422100	-1.38366300	-0.53319400
C	-0.87090700	3.40320600	-0.16906400
C	-1.09958600	3.06073800	-1.50152400
C	-0.84146300	4.73937600	0.24413500
C	-1.32123900	4.09021200	-2.41995000
H	-1.08471000	2.02173600	-1.81241500
C	-1.06626900	5.76351900	-0.67460900
C	-1.30963800	5.42919700	-2.01002200
H	-1.49680600	3.84593100	-3.46385900
H	-1.04448400	6.80466500	-0.36168600
H	-1.48199800	6.21740000	-2.73830500
H	-1.45324100	5.11441200	2.29648000
H	0.21393300	5.59368500	1.97354600
C	3.51911700	-2.12893400	-1.26498700
C	2.51451300	-3.05627700	-1.54783100
C	4.71719900	-2.53038000	-0.66546600
C	2.71136200	-4.38952800	-1.18068000
H	1.60006200	-2.72638700	-2.02986000
C	4.91290200	-3.86289200	-0.30211300
C	3.89776200	-4.78929900	-0.55413900
H	1.93387800	-5.12120000	-1.38194200
H	5.84309400	-4.17875400	0.16412800
H	4.03604600	-5.82981300	-0.27249400
H	6.64414600	-1.59541000	-1.03818100
H	5.93559900	-1.14898300	0.51092800
Ni	0.59428100	0.04388500	-0.53437800
C	-1.26358700	-0.23003600	-0.19873100
C	-2.29302900	-0.35155700	-1.04972600
H	-1.46475600	-0.28733800	0.87669600
H	-2.09740600	-0.28710800	-2.11858700

C	-3.70465300	-0.57052200	-0.68387800
C	-4.71294500	-0.35053100	-1.63338300
C	-4.10903900	-1.01772500	0.59157700
C	-6.06662800	-0.53847800	-1.33953300
H	-4.43367900	-0.01853300	-2.63107900
C	-5.44685200	-1.21152200	0.89924100
H	-3.35794600	-1.24590300	1.34009600
C	-6.44032300	-0.96925300	-0.06258300
H	-6.80802900	-0.35066600	-2.10823800
H	-5.75278600	-1.56810500	1.87856600
O	-7.72973700	-1.19360800	0.34456300
C	-8.76762800	-0.98349400	-0.59481100
H	-9.69914800	-1.21976100	-0.07542700
H	-8.80115200	0.06026800	-0.93886200
H	-8.66495500	-1.64160300	-1.46953200
C	0.94623400	-1.79843300	1.32873700
C	-0.26221600	-2.54276400	1.53836500
C	-1.00842000	-2.46014100	2.74020600
C	-0.76345600	-3.38671700	0.51319200
C	-2.17499000	-3.20207200	2.91403700
H	-0.65990800	-1.82136000	3.54644700
C	-1.93124400	-4.11295300	0.68728900
H	-0.23051600	-3.42573400	-0.43181400
C	-2.64477200	-4.03174500	1.89213400
H	-2.72503400	-3.12787100	3.84904000
H	-2.30183900	-4.73818800	-0.12044700
H	-3.56383100	-4.59574000	2.02280000
C	1.59031600	-1.01557900	2.43498700
H	0.93761200	-0.21684900	2.81001100
H	1.83337500	-1.66079800	3.29448100
H	2.51915000	-0.55403200	2.09481700
H	1.59073000	-2.14468000	0.53059100
Cl	0.49161100	-0.53365900	-2.76197000

C_6F_6 (ORCA)

C	-2.08035480745116	-0.00000002082751	-1.58571637452826
C	-3.23769074609703	-0.35506623649578	-0.88678634286898
C	-0.92301885233540	0.35506620501065	-0.88678633289870
F	-4.34757496386184	-0.69560642286598	-1.55705193271356
F	0.18686535087026	0.69560647574205	-1.55705190979329
C	-3.23769072197718	-0.35506626792560	0.51107006734975
C	-0.92301888078694	0.35506626628939	0.51107007660397
F	-4.34757492081340	-0.69560645694073	1.18133567640156
F	0.18686527613664	0.69560653123027	1.18133569163507
C	-2.08035478998591	-0.00000002292387	1.21000011999390
F	-2.08035478968096	-0.00000002759632	2.55054875632649
F	-2.08035483801706	-0.00000002269656	-2.92626500750795

209

C	-0.60660232044200	-0.64433995736758	-3.38005900922667
H	-1.60460746635295	-0.65333316008541	-2.93305121239365
C	0.45328983433487	-0.63003599455311	-2.55907618308245
H	1.49371646233862	-0.61917515448373	-2.87727047533960
C	-0.57195750470224	-0.64861128117865	-4.84562063603251
C	0.61998802181281	-0.64566072383544	-5.60004674907194

C	-1.79395229994265	-0.65623905033384	-5.54712355152329
C	0.59517064787864	-0.64949435993566	-6.99133310043017
C	-1.83877360137507	-0.66018199574130	-6.94122267777344
C	-0.63805521806712	-0.65660166165618	-7.64189706791389
H	1.58733125793119	-0.64084111737458	-5.09619226931526
H	-2.72959761049744	-0.65893299398530	-4.98438732683538
H	1.51428622431806	-0.64739411187043	-7.57720370736237
H	-2.78463544871623	-0.66600376119840	-7.48253959334636
F	-0.66382938969596	-0.66046915172425	-8.99889893159037
Br	0.28753780217748	-0.62612448467614	-0.66915781976260

211

C	-4.11532733969400	-1.12491356946914	-6.01429941298077
H	-5.16322602983630	-1.18831310673920	-5.69956900909472
C	-3.16762685914312	-1.13905534301137	-5.03808195186337
H	-2.10787415739093	-1.07707981623321	-5.30788545720844
C	-3.91045792977807	-1.03391764636984	-7.45326825019406
C	-2.63517196350950	-0.94763086729187	-8.05638453755352
C	-5.03578889837609	-1.03059708961062	-8.30621104514578
C	-2.48924585320593	-0.86218979261019	-9.43718523379085
C	-4.90926778262523	-0.94565654158294	-9.69165106403804
C	-3.63208872736911	-0.86244512329972	-10.23619868915133
H	-1.73841991553155	-0.94745158212351	-7.43570092957264
H	-6.03294651870383	-1.09641924344777	-7.86583450438134
H	-1.50595499406426	-0.79571102427353	-9.90305274209395
H	-5.78036122167198	-0.94331164978294	-10.34674289253264
F	-3.49132406175592	-0.77912663157127	-11.58447816915054
C	-2.51469059029440	-1.24576756800706	-2.66099915450661
H	-1.46687926140760	-1.18133021087182	-2.97581356345228
C	-3.46240715910281	-1.23201887654516	-3.63721103848032
H	-4.52215243116646	-1.29415602968902	-3.36740962017595
C	-2.71942537499200	-1.33692986135368	-1.22203428823827
C	-3.99440254918885	-1.42969757739758	-0.61920347627904
C	-1.59432007195093	-1.33379279785311	-0.36880889762441
C	-4.14025890510305	-1.51467685159697	0.76162695209982
C	-1.72077805437147	-1.41813833281390	1.01667612550167
C	-2.99765036725211	-1.50753157476434	1.56095297035080
H	-4.89091017520987	-1.43587163754732	-1.24020875430780
H	-0.59740181833295	-1.26311777973175	-0.80897429389443
H	-5.12328860004276	-1.58630054772655	1.22728282564892
H	-0.84986377820378	-1.41537981423140	1.67200496308725
F	-3.13833900772507	-1.59044516645319	2.90926760902267

212(4-F) low spin (ORCA)

Ni	-0.00448447947817	0.00164020935805	0.00239302745841
Br	1.48051895103094	-1.06498553032033	-1.42227277162176
O	-2.14618384754168	2.70992481822853	2.28296153762120
O	2.37980000208120	1.45487800242610	3.14553552778769
N	-1.22320307906186	1.24516125844987	0.82001397365091
N	1.38187625645077	0.45142569725855	1.37268370607038
C	-2.50473685992759	1.69215636182839	0.20028167496512
H	-3.02703521838075	0.81954243180769	-0.21284803429169
C	-2.31414275829491	2.79291707793566	-0.82891167485076
C	-1.51232164190342	2.78354092305962	-1.97151518676158
H	-0.91049815291267	1.90705015537969	-2.21296422085385

C	-1.48667183784918	3.92329934054902	-2.78164286180547
H	-0.86400414733098	3.93421369639543	-3.67748163198082
C	-2.24859325449193	5.05089471093451	-2.45132495367893
H	-2.21699304159929	5.93275922013676	-3.09340087627570
C	-3.04370247594705	5.05993212985855	-1.30037856197006
H	-3.62841865175398	5.94527500807122	-1.04169202149398
C	-3.07032191595432	3.92462134312011	-0.48855181182245
C	-3.84960356218091	3.69579574776801	0.78758163630582
H	-4.92295813349767	3.54333522451468	0.58491826850845
H	-3.77594304049303	4.52241849465255	1.50957617890282
C	-3.24782198837848	2.40494676146387	1.34996429789153
H	-3.96181548987140	1.77984856842228	1.90421276940742
C	-1.09373624482642	1.93610966048983	1.91190877407963
C	0.08827487863875	2.02707353287255	2.78263295351118
C	0.30730255664132	3.36135515193982	3.52746537385254
H	1.34653079630200	3.67037733750601	3.61840043281037
H	-0.41234425523186	4.14546701019410	3.30285053411278
C	-0.14793530388374	2.18122249430214	4.30349516773825
H	-1.18964241399308	2.13532039477542	4.61554073715783
H	0.56860777104095	1.66629142186091	4.94026945293758
C	1.28394818055181	1.27319317310105	2.36563742651106
C	3.48191174327627	0.72368410573533	2.48920495801151
H	4.12422097702651	1.48580470131008	2.02662190639825
C	4.20274200542984	-0.17332887910662	3.49859326451102
H	5.27190389476995	-0.23974757835717	3.23630663075593
H	4.15016485558222	0.24321584348415	4.51544988063502
C	3.51466753766513	-1.51073413328666	3.34409244178004
C	3.63740994066102	-2.64517637862000	4.14876463050819
H	4.27231145295736	-2.63258666009796	5.03739448769345
C	2.93467878923394	-3.80286202606502	3.79970833654877
H	3.02093633812608	-4.69635418451876	4.42049587820722
C	2.12461490652130	-3.82420395829027	2.65754694487539
H	1.58689261393112	-4.73596305778894	2.39252422867949
C	1.99959201633266	-2.68990406879442	1.84907993232279
H	1.38061955905140	-2.70181397824566	0.95098959516874
C	2.69685644850178	-1.53271201153393	2.20372943294103
C	2.72663367802005	-0.18761704582790	1.49388927054575
H	3.16825451112758	-0.25449746077197	0.49010899285342
C	-1.40149009875006	-0.78861801427904	-0.96238725294244
H	-2.03510631596574	-1.28764677439133	-0.20524543892123
C	-1.75652521743068	-0.86523505167258	-2.25838195017227
H	-1.10501207355006	-0.40857308973478	-3.01166561912331
C	-2.95112365620622	-1.51914280490975	-2.81650139221344
C	-3.85728499891261	-2.28306114369508	-2.04982337266299
C	-3.22151252707195	-1.39017338112351	-4.19468295364675
C	-4.97922286924958	-2.87842821603045	-2.62231397369321
C	-4.33992211595134	-1.97850977092046	-4.78764052083420
C	-5.20574311712741	-2.71388056534712	-3.98709027461802
H	-3.67377801332535	-2.42693252758972	-0.98369370994579
H	-2.53258188490982	-0.81230109787859	-4.81459548781304
H	-5.67387381635059	-3.47346317041941	-2.02849829659437
H	-4.54200225250226	-1.87474016712144	-5.85400827132554
F	-6.30308490686389	-3.29527128245169	-4.55036414280337

2.10 Notes and References

(1) Turro, R. F.; Wahlman, J. L. H.; Tong, Z. J.; Chen, X.; Yang, M.; Chem. E. P.; Hong, X.; Hadt, R. H.; Houk, K. N., Yang, Y. F.; Reisman, S. E. Mechanistic Investigation of Ni-Catalyzed Reductive Cross-Coupling of Alkenyl and Benzyl Electrophiles. *J. Am. Chem. Soc.* **2023**, *Accepted.*

(2) For reviews see: (a) Everson, D. A.; Weix, D. J. Cross-Electrophile Coupling: Principles of Reactivity and Selectivity. *J. Org. Chem.* **2014**, *79*, 4793–4798. (b) Knappke, C. E. I.; Grupe, S.; Gärtner, D.; Corpet, M.; Gosmini, C.; Jacobi von Wangelin, A. Reductive Cross-Coupling Reactions between Two Electrophiles. *Chem. Eur. J.* **2014**, 20, 6828–6842. (c) Weix, D. J. Methods and Mechanisms for Cross-Electrophile Coupling of Csp2 Halides with Alkyl Electrophiles. *Acc. Chem. Res*. **2015**, 48, 1767–1775. (d) Wang, X.; Dai, Y.; Gong, H. Nickel-Catalyzed Reductive Couplings. *Top. Curr. Chem.* (Z) **2016**, 374, 43. (e) Richmond, E.; Moran, J. Recent Advances in Nickel Catalysis Enabled by Stoichiometric Metallic Reducing Agents. *Synthesis* **2018**, 50, 499–513. (f) Goldfogel, M. J.; Huang, L.; Weix, D. J. Cross-Electrophile Coupling. In Nickel Catalysis in Organic Synthesis; John Wiley & Sons, Ltd, **2020**; pp 183–222. (g) Poremba, K. E.; Dibrell, S. E.; Reisman, S. E. Nickel-Catalyzed Enantioselective Reductive Cross-Coupling Reactions. *ACS Catal*. **2020**, 10, 8237–8246.

(3) Charboneau, D. J.; Hazari, N.; Huang, H.; Uehling, M. R.; Zultanski, S. L. Homogeneous Organic Electron Donors in Nickel-Catalyzed Reductive Transformations. *J. Org. Chem*. **2022**, 87, 7589–7609.

(4) Zhou, Z.; Xu, S.; Zhang, J.; Kong, W. Nickel-Catalyzed Enantioselective Electroreductive Cross-Couplings. *Org. Chem. Front*. **2020**, 7, 3262–3265.

(5) Diccianni, J. B.; Diao, T. Mechanisms of Nickel-Catalyzed Cross-Coupling Reactions. *TRECHEM* **2019**, 1, 830–844.

(6) For examples using photoredox (a) Zhang, P.; Le, C. "Chip"; MacMillan, D. W. C. Silyl Radical Activation of Alkyl Halides in Metallaphotoredox Catalysis: A Unique Pathway for Cross-Electrophile Coupling. *J. Am. Chem. Soc*. **2016**, 138, 8084–8087. (b) Duan, Z.; Li, W.; Lei, A. Nickel-Catalyzed Reductive Cross-Coupling of Aryl Bromides with Alkyl Bromides: Et_3N as the Terminal Reductant. *Org. Lett*. **2016**, 18, 4012–4015. (c) Yi, J.; Badir, S. O.; Kammer, L. M.; Ribagorda, M.; Molander, G. A. Deaminative Reductive Arylation Enabled by Nickel/Photoredox Dual Catalysis. *Org. Lett*. **2019**, 21, 3346–3351. For Examples using electrochemistry: (d) Perkins, R. J.; Pedro, D. J.; Hansen, E. C. Electrochemical Nickel Catalysis for sp^2-sp^3 Cross-Electrophile Coupling Reactions of Unactivated Alkyl Halides. *Org. Lett*. **2017**, 19, 3755–3758. (e) Truesdell, B. L.; Hamby, T. B.; Sevov, C. S. General $C(sp^2)$–$C(sp^3)$ Cross-Electrophile Coupling Reactions Enabled by Overcharge Protection of Homogeneous Electrocatalysts. *J. Am. Chem. Soc*. **2020**, 142, 5884–5893. (f)

Kumar, G. S.; Peshkov, A.; Brzozowska, A.; Nikolaienko, P.; Zhu, C.; Rueping, M. Nickel-Catalyzed Chain-Walking Cross-Electrophile Coupling of Alkyl and Aryl Halides and Olefin Hydroarylation Enabled by Electrochemical Reduction. *Angew. Chem. Int. Ed.* **2020**, 59, 6513–6519. For examples using metal powder: (g) Durandetti, M.; Gosmini, C.; Périchon, J. Ni-Catalyzed Activation of α-Chloroesters: A Simple Method for the Synthesis of α-Arylesters and β-Hydroxyesters. *Tetrahedron* **2007**, 63, 1146–1153. (h) Nimmagadda, S. K.; Korapati, S.; Dasgupta, D.; Malik, N. A.; Vinodini, A.; Gangu, A. S.; Kalidindi, S.; Maity, P.; Bondigela, S. S.; Venu, A.; Gallagher, W. P.; Aytar, S.; González-Bobes, F.; Vaidyanathan, R. Development and Execution of an Ni(II)-Catalyzed Reductive Cross-Coupling of Substituted 2-Chloropyridine and Ethyl 3-Chloropropanoate. *Org. Process Res. Dev*. **2020**, *24*, 1141–1148.

(7) Cherney, A. H.; Reisman, S. E. Nickel-Catalyzed Asymmetric Reductive Cross-Coupling Between Vinyl and Benzyl Electrophiles. *J. Am. Chem. Soc*. **2014**, *136*, 14365–14368.

(8) Suzuki, N.; Hofstra, J. L.; Poremba, K. E.; Reisman, S. E. Nickel-Catalyzed Enantioselective Cross-Coupling of N-Hydroxyphthalimide Esters with Vinyl Bromides. *Org. Lett*. **2017**, *19*, 2150–2153.

(9) (a) Hofstra, J. L.; Cherney, A. H.; Ordner, C. M.; Reisman, S. E. Synthesis of Enantioenriched Allylic Silanes via Nickel-Catalyzed Reductive Cross-Coupling. *J. Am. Chem. Soc*. **2018**, *140*, 139–142. (b) DeLano, T. J.; Reisman, S. E.

Enantioselective Electroreductive Coupling of Alkenyl and Benzyl Halides via Nickel Catalysis. *ACS Catal*. **2019**, *9*, 6751–6754.

(10) (a) Everson, D. A.; Jones, B. A.; Weix, D. J. Replacing Conventional Carbon Nucleophiles with Electrophiles: Nickel-Catalyzed Reductive Alkylation of Aryl Bromides and Chlorides. *J. Am. Chem. Soc*. **2012**, *134*, 6146–6159. (b) Biswas, S.; Weix, D. J. Mechanism and Selectivity in Nickel-Catalyzed Cross-Electrophile Coupling of Aryl Halides with Alkyl Halides. *J. Am. Chem. Soc*. **2013**, 135, 16192–16197. (c) Wotal, A. C.; Ribson, R. D.; Weix, D. J. Stoichiometric Reactions of Acylnickel(II) Complexes with Electrophiles and the Catalytic Synthesis of Ketones. *Organometallics* **2014**, *33*, 5874–5881.

(11) (a) Lin, Q.; Diao, T. Mechanism of Ni-Catalyzed Reductive 1,2-Dicarbofunctionalization of Alkenes. *J. Am. Chem. Soc*. **2019**, *141*, 17937–17948. (b) Ju, L.; Lin, Q.; LiBretto, N. J.; Wagner, C. L.; Hu, C. T.; Miller, J. T.; Diao, T. Reactivity of (Bi-Oxazoline)Organonickel Complexes and Revision of a Catalytic Mechanism. *J. Am. Chem. Soc*. **2021**, *143*, 14458–14463. (c) Wagner, C. L.; Herrera, G.; Lin, Q.; Hu, C. T.; Diao, T. Redox Activity of Pyridine-Oxazoline Ligands in the Stabilization of Low-Valent Organonickel Radical Complexes. *J. Am. Chem. Soc*. **2021**, *143*, 5295–5300.

(12) Just before the submission of this manuscript, an investigation of an electrochemically driven Ni-catalyzed enantioselective reductive alkenylation using a **L3**·Ni catalyst was reported. Hu, X.; Cheng-Sánchez, I.; Cuesta-Galisteo,

S.; Nevado, C. Nickel-Catalyzed Enantioselective Electrochemical Reductive Cross-Coupling of Aryl Aziridines with Alkenyl Bromides. *J. Am. Chem. Soc.* **2023**. https://doi.org/10.1021/jacs.2c12869.

(13) McNicholas, B. J.; Tong, Z. J.; Bím, D.; Turro, R. F.; Kazmierczak, N. P.; Chalupský, Reisman, S. E.; Hadt, R. G.* Electronic structures of nickel(II)bis(indanyloxazoline)-dihalide catalysts: Understanding ligand field contributions that promote $C(sp^2)$–$C(sp^3)$ cross-coupling. **2023**, *Submitted.*

(14) Kuwata, Keiji.; Geske, D. H. The Cation Radical of Tetrakis(Dimethylamino)Ethylene. *J. Am. Chem. Soc*. **1964**, 86, 2101–2105.

(15) Diccianni, J. B.; Hu, C. T.; Diao, T. Insertion of CO_2 Mediated by a (Xantphos)Ni^{I}–Alkyl Species. *Angew. Chem. Int. Ed.* **2019**, *58*, 13865–13868.

(16) (a) Sun, R.; Qin, Y.; Ruccolo, S.; Schnedermann, C.; Costentin, C.; Daniel G. Nocera. Elucidation of a Redox-Mediated Reaction Cycle for Nickel-Catalyzed Cross Coupling. *J. Am. Chem. Soc*. **2019**, *141*, 89–93. (b) Mohadjer Beromi, M.; Brudvig, G. W.; Hazari, N.; Lant, H. M. C.; Mercado, B. Q. Synthesis and Reactivity of Paramagnetic Nickel Polypyridyl Complexes Relevant to C(Sp2)–C(Sp3)Coupling Reactions. *Angew. Chem. Int. Ed.* **2019**, *58,* 6094–6098.

(17) (a) Ting, S. I.; Williams, W. L.; Doyle, A. G. Oxidative Addition of Aryl Halides to a Ni(I)-Bipyridine Complex. *J. Am. Chem. Soc*. **2022**, 144, 5575–5582. (b) Till, N. A.; Oh, S.; MacMillan, D. W. C.; Bird, M. J. The Application of Pulse Radiolysis

to the Study of Ni(I) Intermediates in Ni-Catalyzed Cross-Coupling Reactions. *J. Am. Chem. Soc*. **2021**, 143, 9332–9337.

(18) Burés, J. Variable Time Normalization Analysis: General Graphical Elucidation of Reaction Orders from Concentration Profiles. *Angew. Chem. Int. Ed.* **2016**, *55*, 16084–16087.

(19) Huihui, K. M. M.; Caputo, J. A.; Melchor, Z.; Olivares, A. M.; Spiewak, A. M.; Johnson, K. A.; DiBenedetto, T. A.; Kim, S.; Ackerman, L. K. G.; Weix, D. J. Decarboxylative Cross-Electrophile Coupling of N-Hydroxyphthalimide Esters with Aryl Iodides. *J. Am. Chem. Soc*. **2016**, *138*, 5016–5019.

(20) Cornella, J.; Edwards, J. T.; Qin, T.; Kawamura, S.; Wang, J.; Pan, C.-M.; Gianatassio, R.; Schmidt, M.; Eastgate, M. D.; Baran, P. S. Practical Ni-Catalyzed Aryl–Alkyl Cross-Coupling of Secondary Redox-Active Esters. *J. Am. Chem. Soc*. **2016**, *138*, 2174–2177.

(21) Calculated ^{19}F NMR chemical shifts (Table 2.21) are also consistent with complex **212** shift of – 115.2 ppm.

(22) Hofstra, J. L.; Poremba, K. E.; Shimozono, A. M.; Reisman, S. E. Nickel-Catalyzed Conversion of Enol Triflates into Alkenyl Halides. *Angew. Chem. Int. Ed.* **2019**, 58, 14901–14905.

(23) CV measurements of **202** in the presence of TMSBr display a more anodic onset potential for reduction and an increase in current consistent with a more facile reduction (Figure 2.60).

(24) Salgueiro, D. C.; Chi, B. K.; Guzei, I. A.; García-Reynaga, P.; Weix, D. J. Control of Redox-Active Ester Reactivity Enables a General Cross-Electrophile Approach to Access Arylated Strained Rings. *Angew. Chem. Int. Ed.* **2022**, 61, e202205673.

.(25) The Rousseaux lab has also reported the rate-enhancing effect of TMSCl of NHP ester reduction using Zn^0 reductant in a preprint article: Michel, N.; Edjoc, R.; Fagbola, E.; Hughes, J.; Campeau, L.-C.; Rousseaux, S. Nickel-Catalyzed Reductive Arylation of Redox Active Esters for the Synthesis of α-Aryl Nitriles – Role of a Chlorosilane Additive. *ChemRxiv* April 20, 2021 (DOI: 10.26434/chemrxiv.14450007.v2).

(26) We observe a counterion effect with triflate salts where the rate of activation is slower than would be expected compared to iodide salts. We attribute this difference to the remarkable solubility of $TDAE(OTf)_2$ salts in DMA. For all halides, $[TDAE]X_2$ salts precipitate out of the reaction mixture which likely acts as an additional driving force for reduction.

(27) Metal additives chosen in this study have been used in reductive NHP ester reactions previously reported in the literature. Although the role of these additives in these selected examples is not known, they are likely non-innocent in the NHP ester reduction process as demonstrated in this study. For examples with Li+ salts: (a) Huang, L.; Olivares, A. M.; Weix, D. J. Reductive Decarboxylative Alkynylation of N-Hydroxyphthalimide Esters with Bromoalkynes. *Angew. Chem.* **2017**, 129, 12063–12067. (b) Qin, T.; Malins, L. R.; Edwards, J. T.; Merchant, R.

R.; Novak, A. J. E.; Zhong, J. Z.; Mills, R. B.; Yan, M.; Yuan, C.; Eastgate, M. D.; Baran, P. S. Nickel-Catalyzed Barton Decarboxylation and Giese Reactions: A Practical Take on Classic Transforms. *Angew. Chem. Int. Ed.* **2017**, 56, 260–265. Examples with Mg^{2+} salts: (c) Zhang, J.-J.; Yang, J.-C.; Guo, L.-N.; Duan, X.-H. Visible-Light-Mediated Dual Decarboxylative Coupling of Redox-Active Esters with α,β-Unsaturated Carboxylic Acids. *Chem. Eur. J.* **2017**, 23, 10259–10263. (d) Lu, X.; Xiao, B.; Liu, L.; Fu, Y. Formation of C(Sp3)–C(Sp3) Bonds through Nickel-Catalyzed Decarboxylative Olefin Hydroalkylation Reactions. *Chem. Eur. J.* **2016**, 22, 11161–11164.

(28) The benzyl radical addition to intermediate **L3**·Ni^{II}(alkenyl)Cl was also studied. The **TS4-R** is 2.9 kcal/mol lower than the **TS4-S** (Figure 2.84). This indicates that the influence of the halide ligand on the enantioselectivity is minimal.

(29) W. C. Still, M. Kahn, A. Mitra, *J. Org. Chem.* **1978**, *43*, 2923–2925.

(30) Stoll, S.; Schweiger, A. Easyspin, a comprehensive software package for spectral simulation and analysis in EPR. *J. Magn. Reson.* **2006**, *178*, 42–45.

(31) L. Hofstra, J. Synthesis of Chiral Bisoxazoline Ligands: (3aR,3a'R,8aS,8a'S)-2,2'-(Cyclopropane-1,1-Diyl)Bis(3a,8a-Dihydro-8H-Indeno[1,2-d]Oxazole). *Org. Synth.* **2020**, *97*, 172–188.

(32) Bull, J. A.; Mousseau, J. J.; Charette, A. B. Convenient One-Pot Synthesis of (E)-β-Aryl Vinyl Halides from Benzyl Bromides and Dihalomethanes. *Org. Lett.* **2008**, *10*, 5485–5488.

(33) Everson, D. A.; Jones, B. A.; Weix, D. J. Replacing Conventional Carbon Nucleophiles with Electrophiles: Nickel-Catalyzed Reductive Alkylation of Aryl Bromides and Chlorides. *J. Am. Chem. Soc.* **2012**, *134* (14), 6146–6159.

(34) Jette, C.I.; Tong, Z.J.; Hadt, R.G.; Stoltz, B.M. Copper-catalyzed enantoselective allylic alkylation with a butyrolactone-derived silyl ketene acetal. *Angew. Chem. Int. Ed.* **2019**, *59*, 2033–2038.

(35) Frisch, M. J.; Trucks, G. W.; Schlegel, H. B.; Scuseria, G. E.; Robb, M. A.; Cheeseman, J. R.; Scalmani, G.; Barone, V.; Petersson, G. A.; Nakatsuji, H.; Li, X.; Caricato, M.; Marenich, A. V.; Bloino, J.; Janesko, B. G.; Gomperts, R.; Mennucci, B.; Hratchian, H. P.; Ortiz, J. V.; Izmaylov, A. F.; Sonnenberg, J. L.; Williams-Young, D.; Ding, F.; Lipparini, F.; Egidi, F.; Goings, J.; Peng, B.; Petrone, A.; Henderson, T.; Ranasinghe, D.; Zakrzewski, V. G.; Gao, J.; Rega, N.; Zheng, G.; Liang, W.; Hada, M.; Ehara, M.; Toyota, K.; Fukuda, R.; Hasegawa, J.; Ishida, M.; Nakajima, T.; Honda, Y.; Kitao, O.; Nakai, H.; Vreven, T.; Throssell, K.; Montgomery, J. A., Jr.; Peralta, J. E.; Ogliaro, F.; Bearpark, M. J.; Heyd, J. J.; Brothers, E. N.; Kudin, K. N.; Staroverov, V. N.; Keith, T. A.; Kobayashi, R.; Normand, J.; Raghavachari, K.; Rendell, A. P.; Burant, J. C.; Iyengar, S. S.; Tomasi, J.; Cossi, M.; Millam, J. M.; Klene, M.; Adamo, C.; Cammi, R.; Ochterski, J. W.; Martin, R. L.; Morokuma, K.; Farkas, O.; Foresman, J. B.; Fox, D. J. Gaussian 16, Revision C.01; Gaussian, Inc.: Wallingford, CT, 2019.

(36) (a) Grimme, S.; Antony, J.; Ehrlich, S.; Krieg, H. A Consistent and Accurate Ab Initio Parametrization of Density Functional Dispersion Correction (DFT-D) for the 94 Elements H-Pu. *J. Chem. Phys.* **2010**, *132*, 154104. (b) Grimme, S.; Ehrlich, S.; Goerigk, L. Effect of the Damping Function in Dispersion Corrected Density Functional Theory. *J. Comput. Chem.* **2011**, *32*, 1456. (c) Witte, J.; Mardirossian, N.; Neaton, J. B.; Head-Gordon, M. Assessing DFT-D3 Damping Functions Across Widely Used Density Functionals: Can We Do Better? *J. Chem. Theory Comput.* **2017**, *13*, 2043.

(37) (a) Hay, P. J.; Wadt, W. R. Ab Initio Effective Core Potentials for Molecular Calculations. Potentials for K to Au Including the Outermost Core Orbitals. *J. Chem. Phys.* **1985**, *82*, 299. (b) Ehlers, A. W.; Böhme, M.; Dapprich, S.; Gobbi, A.; Höllwarth, A.; Jonas, V.; Köhler, K. F.; Stegmann, R.; Veldkamp, A.; Frenking, G. A Set of f-Polarization Functions for Pseudo-Potential Basis Sets of the Transition Metals Sc-Cu, Y-Ag and La-Au. *Chem. Phys. Lett.* **1993**, *208*, 111. (c) Roy, L. E.; Hay, P. J.; Martin, R. L. Revised Basis Sets for the LANL Effective Core Potentials. *J. Chem. Theory Comput.* **2008**, *4*, 1029.

(38) (a) Ditchfield, R.; Hehre, W. J.; Pople, J. A. Self-Consistent Molecular-Orbital Methods. IX. An Extended Gaussian-Type Basis for Molecular-Orbital Studies of Organic Molecules. *J. Chem. Phys.* **1971**, *54*, 724. (b) Hehre, W. J.; Ditchfield, R.; Pople, J. A. Self-Consistent Molecular Orbital Methods. XII. Further Extensions of Gaussian-Type Basis Sets for Use in Molecular Orbital Studies of Organic

Molecules. *J. Chem. Phys.* **1972**, *56*, 2257. (c) Hariharan, P. C.; Pople, J. A. The Influence of Polarization Functions on Molecular Orbital Hydrogenation Energies. *Theoret. Chim. Acta.* **1973**, *28*, 213.

(39) (a) Zhao, Y.; Truhlar, D. G. The M06 Suite of Density Functionals for Main Group Thermochemistry, Thermochemical Kinetics, Noncovalent Interactions, Excited States, and Transition Elements: Two New Functionals and Systematic Testing of Four M06-class Functionals and 12 other Functionals. *Theor. Chem. Acc*. **2008**, *120*, 215. (b) Zhao, Y.; Truhlar, D. G. Density Functionals with Broad Applicability in Chemistry. *Acc. Chem. Res*. **2008**, *41*, 157.

(40) Dolg, M.; Wedig, U.; Stoll, H.; Preuss, H. Energy-Adjusted Ab Initio Pseudopotentials for the First Row Transition Elements. *J. Chem. Phys.* **1987**, *86*, 866.

(41) Marenich, A. V.; Cramer, C. J.; Truhlar, D. G. Universal Solvation Model Based on Solute Electron Density and on a Continuum Model of the Solvent Defined by the Bulk Dielectric Constant and Atomic Surface Tensions. J. *Phys. Chem. B* **2009**, *113*, 6378.

(42) Legault, C. Y. CYLview, 1.0b; Université de Sherbrooke: Canada, 2009. http://www.cylview.org.

(43) Neese, F.; Wennnmohs, F.; Becker, U.; Riplinger, C.; The ORCA quantum chemistry program package. *J. Chem. Phys.* **2020**, *152*, 224108

Chapter 3

Nickel-Catalyzed Reductive Alkylation of Heteroaryl Imines †

3.1 INTRODUCTION

The preparation of heterobenzylic amines by a Ni-catalyzed reductive cross-coupling between heteroaryl imines and C(sp^3) electrophiles is reported. This umpolung-type alkylation proceeds under mild conditions, avoids the pre-generation of organometallic reagents, and exhibits good functional group tolerance. Mechanistic studies are consistent with the imine substrate acting as a redox-active ligand upon coordination to a low-valent Ni center. The resulting bis(2-imino)heterocycle·Ni complexes can engage in alkylation reactions with a variety of C(sp^3) electrophiles, giving heterobenzylic amine products in good yields.

† Portions of this chapter have been reproduced from a published manuscript.[1] Fellowship support was provided by the NIH (R35GM118191-01). M.B. was supported by a fellowship from the Swiss National Science Foundation.

3.2 Development of a Reductive Alkylation of Heteroaryl Imines

3.2.1 Background and Motivation

Benzylic amines are common substructures in a variety of natural products, agrochemicals, and pharmaceuticals.[2] In particular, heterobenzylic amines serve as important nitrogen-containing scaffolds in medicinal chemistry. Two representative examples are Gilead's Phase II/III HIV capsid inhibitor Lenacapavir[3] and Pfizer's commercial anticancer agent Glasdegib[4] (Figure 3.1). Due to broad interest in this structural motif, a variety of synthetic approaches to prepare benzylic amines have been developed.

Figure 3.1. *Pharmaceutical drugs that contain heterobenzylic amines.*

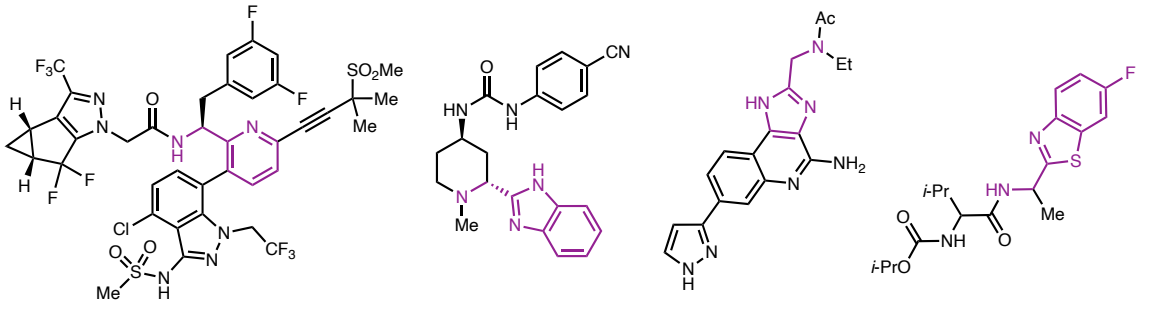

Of these methods, the 1,2-addition of organometallic reagents to imines is one of the most well-established;[5] however, pre-generation of sensitive and reactive organometallic reagents **250** and use of activated imine derivatives is typically required. When simple *N*-alkylimines are employed, stoichiometric Lewis acid additives can be necessary to enhance the reactivity (**251**). Moreover, α-deprotonation of the imine substrate by the basic nucleophiles can be problematic as it isomerizes the imine and quenches the nucleophile (Scheme 3.1).

Scheme 3.1. *Organometallic addition into imine-derivatives.*

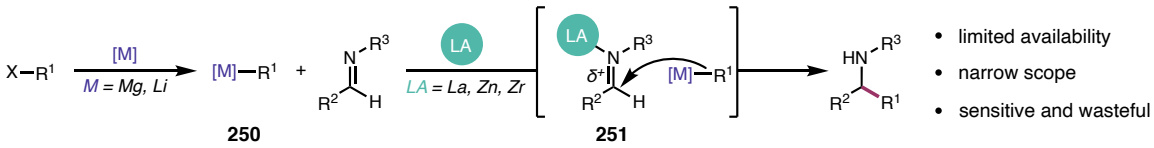

In order to improve access to benzylic amines, chemists have explored complimentary single electron reactions of imines, including the 1,2-addition of organic radicals to imines[6,7,8] and the reductive alkylation of imines via α-amino radicals.[9] These reactions often exhibit improved functional group tolerance by avoiding the use of organometallic reagents; however, they typically require particularly activated substrates. This challenge with radical addition to unactivated C-N π* systems can be attributed to the poor electrophilicity of imines, additionally the resulting *N*-centered radical in the product is typically less stable than the corresponding *C*-centered radical. This problem is resolved when using activated imine derivatives which contain groups that can stabilize the resulting *N*-centered radicals or lower the LUMO to accelerate radical addition. (Figure 3.2a). Due to these stabilizing effects, the vast majority of methods employ imine derivatives such as glyoxime esters **255**,[10] glyoxal sulfoxides **254**,[11] sulfonimines **253**,[12] or hydrazones **252**.[13] Unfortunately, in most cases,[6] harsh conditions are required for radical generation reducing the generality and functional group tolerance of these methods (Figure 3.2b).

Figure 3.2. *Radical addition into activated imines*

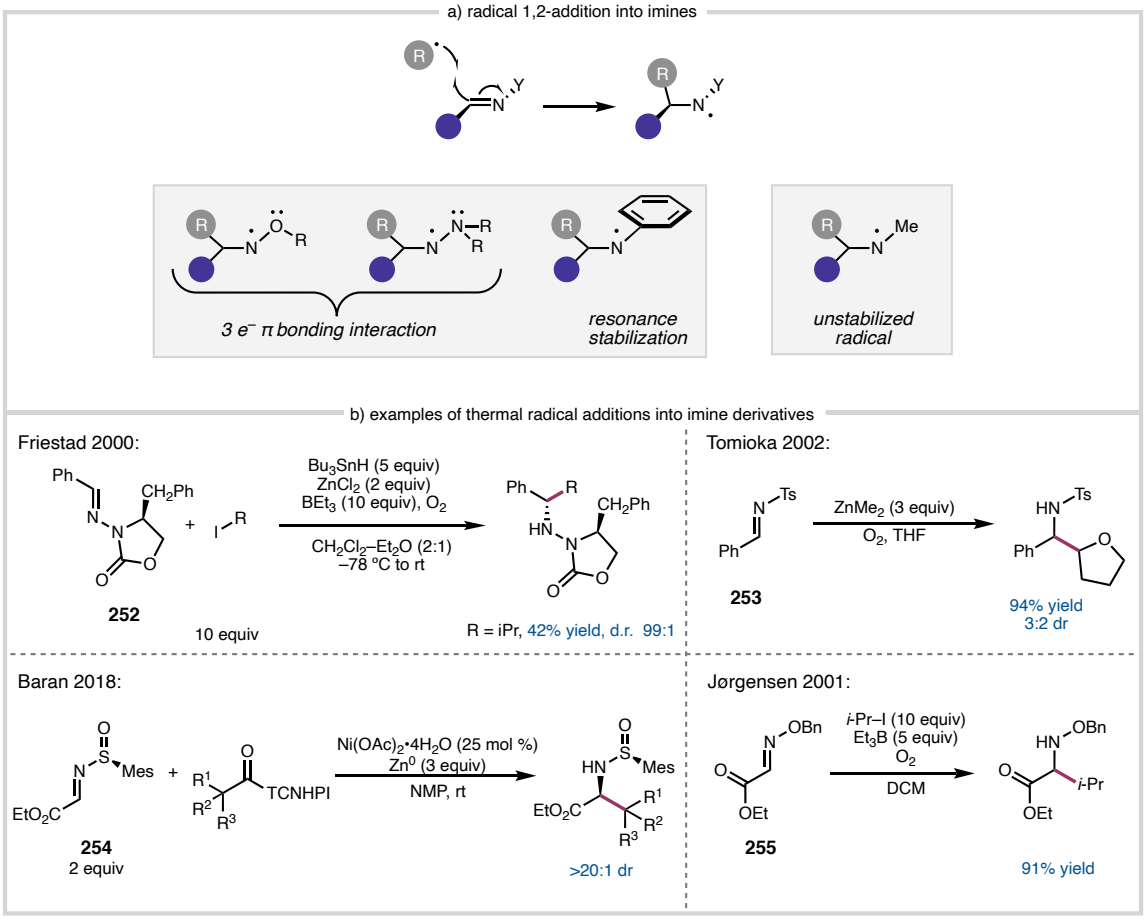

An alternative strategy that circumvents a high-energy *N*-centered radical intermediate, is photoredox-mediated reduction of imines to provide a more stable *N*-centered anion (**256**). The adjacent C-centered radical can then undergo radical-radical coupling reactions with other organic radicals (**257**) in solution. While this strategy has recently gained attention and appears to have broader functional group tolerance, the reducing power required to reduce imines (**261**, – 2.43 V vs. SCE) is not feasible from most photoredox catalysts. This means for photoredox systems, like the aforementioned thermal reactions, stabilizing groups are required to lower the reduction potential like aromatics (**260**, – 1.91 V vs. SCE), sulfonimides (**259**, – 1.45 V vs. SCE), or hydrogen-bond donors **258** (Figure

3.3a).[14] Despite these limitations, there are many methods for photoredox-mediated imine alkylation reactions to give functionalized anilines or sulfonamide products (Figure 3.3b).[15]

Figure 3.3. *Radical reactions with imines the proceed through an α-amino radical.*

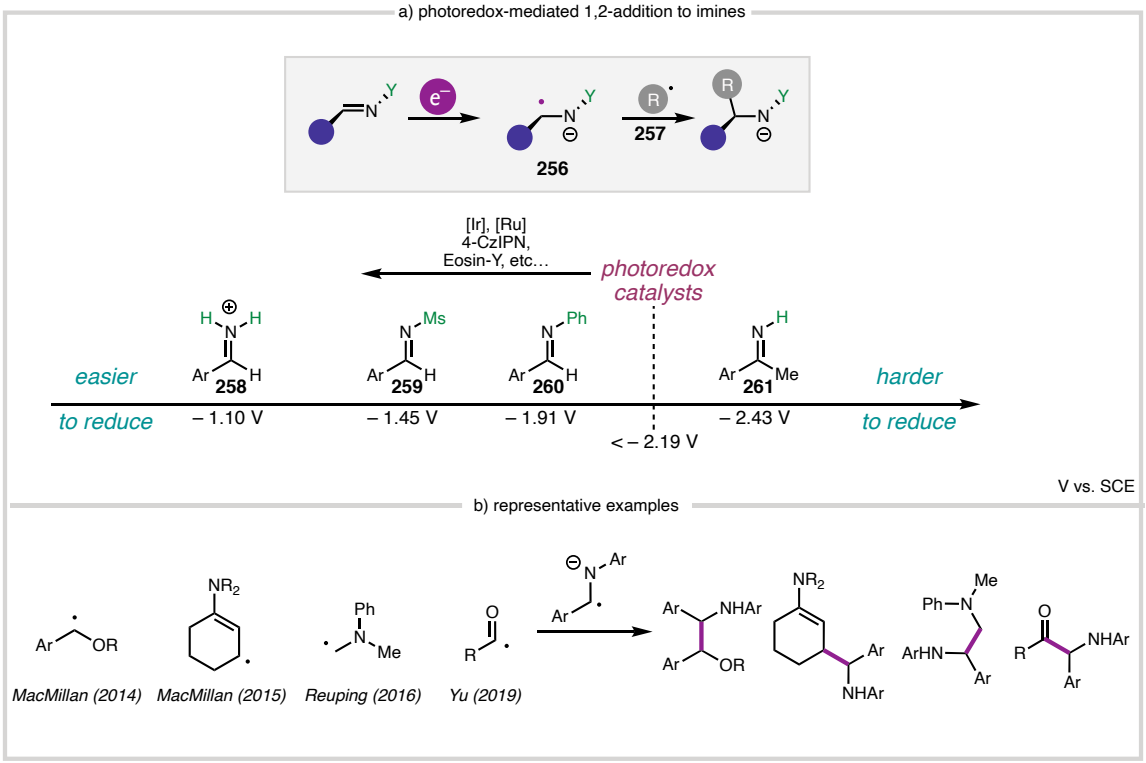

As part of our efforts to broaden the scope of electrophiles for cross-electrophile coupling, we became interested in a mechanistically distinct transition metal-catalyzed reductive alkylation of heterocyclic imines[16,17] that leverages the redox non-innocence of 2-iminoheterocycles **262** as ligands on first-row transition metals. This strategy allows for the mild activation of imines for single-electron alkylation and provides direct access to *N*-alkyl heterobenzylic amines **264** by the equivalent of a C(sp^3)–C(sp^3) coupling reaction (Scheme 3.2). In this report, we describe the development of this method, which provides access to a variety of heterobenzylic *N*-alkylamines **264** in good yields.

Scheme 3.2. *Proposed reductive imine alkylation reaction.*

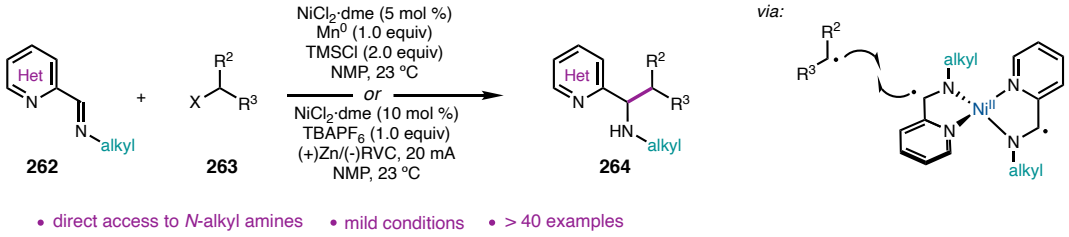

3.2.2 Reaction Design and Redox-Active Iminopyridines

Figure 3.4. *α-aminopyridine as redox-active ligands and catalytic reaction design.*

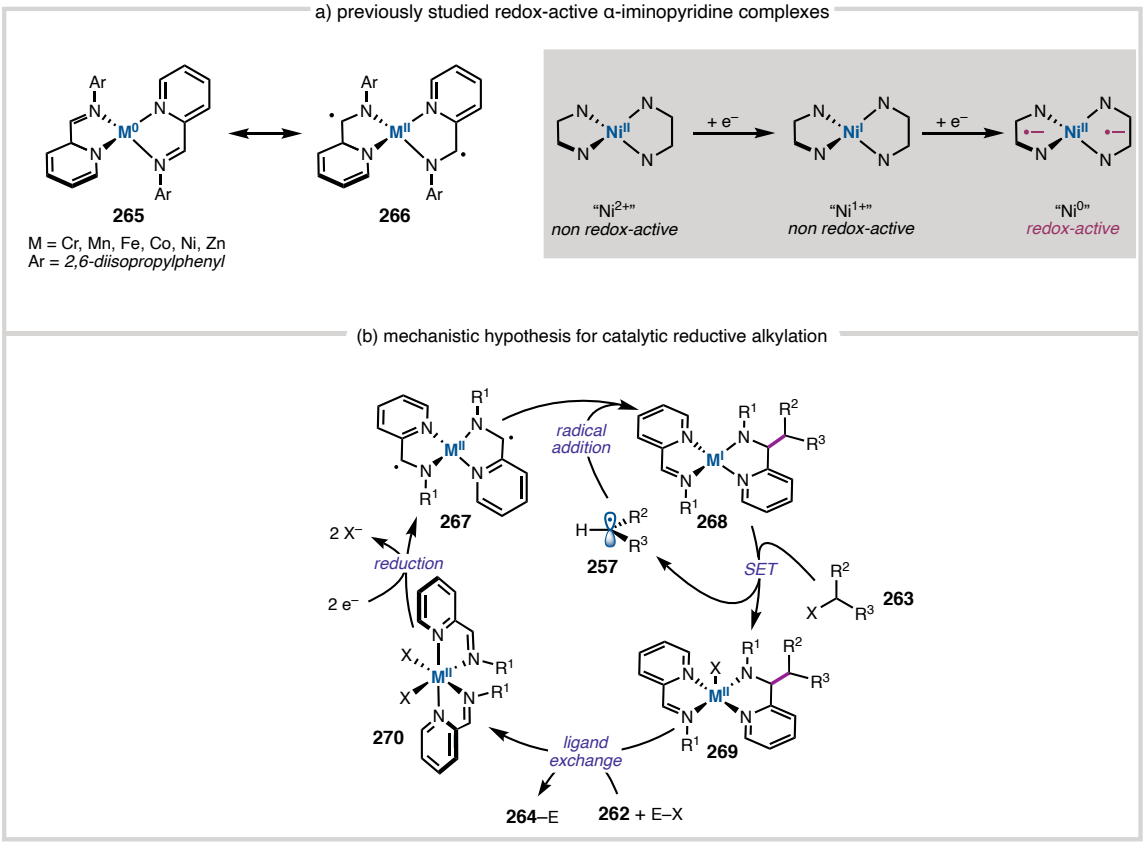

Conjugated nitrogen ligands such as diiminopyridines, α-diimines, and bi- and terpyridines can be electronically non-innocent: their π-systems are able to accept one or two electrons when bound to first-row transition metals.[18] For example, spectroscopic,

electrochemical, and computational investigations conducted by Wieghardt and coworkers demonstrated that low-valent Cr, Mn, Fe, Co, Ni, and Zn bis(2-imino)pyridine complexes (**265**) possess ligand-centered radicals (**266**, Figure 3.4a).[19] Although the alkylation of ligand backbones has been observed previously,[20] this reactivity has not been leveraged for a catalytic cross-coupling.

We hypothesized that these redox-active complexes could be considered persistent α-amino radicals, which might react with alkyl radicals (**257**) to give metal-coordinated imine alkylation products (**267** to **268**). This process could be rendered catalytic if 1) the alkylated product-metal complex **268** could activate a C(sp^3) electrophile to generate an alkyl radical (**268** to **269**), 2) the product could be liberated from complex **269** by exchange with imine **262**, and 3) the bis(2-iminoheterocycle)$M^{II}X_2$ complex **270** could be reduced by a terminal reductant to regenerate the low-valent complex **267**. We envisioned that turnover might be facilitated by a Brönsted acid (H–X) or electrophilic reagent (E–X) able to sequester the anionic nitrogen of **269** (Figure 3.4b).

3.2.3 Optimization of Alkylation Reaction

Table 3.1. *Identifying the optimal transition metal for the imine alkylation reaction.*

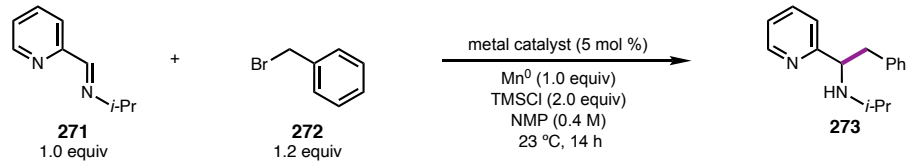

entry	metal catalyst	yield **273** (%)
1	$NiCl_2$·dme	87
2	$CrCl_2$	25
3	$FeBr_2$	50
4	$ZnCl_2$	62
5	$CoCl_2$	80
6	$MnCl_2$	68
7	none	66
8*	none	19

* no TMSCl

Our investigations commenced with the coupling between (*E*)-*N*-isopropyl-1-(pyridin-2-yl)methanimine (**271**) and benzyl bromide (**272**) in the presence of Mn^0 as a stoichiometric reductant, *N*-methylpyrrolidone (NMP) as the solvent, and trimethylsilyl chloride (TMSCl) as an additive. Product **273** was formed in varying yields for a series of metal dihalide salts (entries 1-6, Table 3.1). Of the metals evaluated, $NiCl_2$·dme was found to be optimal providing **273** in 87% yield (entry 1, Table 3.1). Interestingly, when TMSCl is used, the reaction proceeds in the absence of exogenous catalyst (entry 7, Table 3.1). It is likely that the combination of Mn^0 and TMSCl generates $MnCl_2$, which was previously shown by Wieghardt[12] to form a redox-active complex with a similar heteroaryl imine. Use of $MnCl_2$ gives no improvement over just Mn^0 and provides **273** in lower yield than $NiCl_2$·dme (entry 6, Table 3.1).[13,21,22] When TMSCl was omitted from the reaction, **273** was formed in only 19% yield (entry 8, Table 3.1).

Table 3.2. *Optimizing the Ni-catalyzed imine alkylation.*

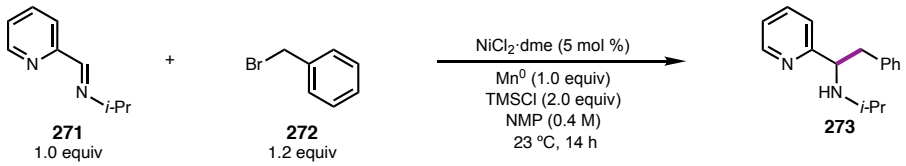

entry	deviation from standard conditions	yield **273** (%)
1	none	87
2	HFIP (5 equiv), no TMSCl	67
3	AcOH (1 equiv), no TMSCl	69
4	Zn^0 (2 equiv), no Mn^0	45
5	TDAE (1.5 equiv), no Mn^0	12
6	1 mol % $NiCl_2$·dme	83
7	0.1 mol % $NiCl_2$·dme	62

Protic additives such as hexafluoroisopropanol (HFIP) (entry 2, Table 3.2) and AcOH (entry 3, Table 3.2) were also beneficial, but inferior to TMSCl.[23] Alternative reductants such as Zn^0 and tetrakis(*N,N*- dimethylamino)ethylene (TDAE) did not perform as well as Mn^0 (entries 4 and 5, Table 3.2). The catalyst loading could be dropped to 1 mol % with only a small decrease in yield (entry 6, Table 3.2); however, lowering the catalyst loading to 0.1 mol % significantly reduced the yield and showed no improvement over the background Mn-mediated reaction ((entry 7, Table 3.2 vs. entry 7, Table 3.1). To investigate the reaction in the absence of Mn^0, a constant current electrolysis protocol was explored for both Ni and Mn salts. The Ni-catalyzed electrolysis provided **273** in good yield (entry 1, Table 3.3) while the Mn-catalyzed reaction provided drastically lower yield of **273** (entry 2, Table 3.3). Although the reaction could be performed with just Mn^0, the addition of $NiCl_2$·dme resulted in higher yields of the imine alkylation product. As a result, the conditions from entry 1 (Table 3.2) were used to evaluate the scope of the reaction using Mn^0 as the terminal reductant.

Table 3.3. *Comparing the Ni and Mn-catalyzed reactions in the absence of Mn^0.*

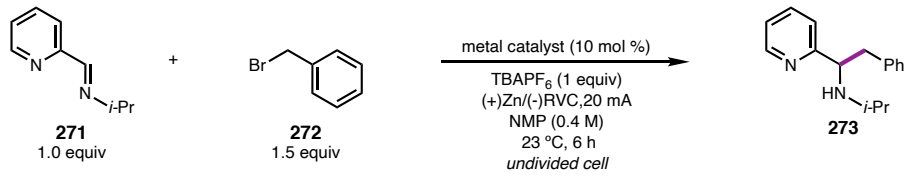

entry	metal catalyst	yield **273** (%)
1	$NiCl_2$·dme	76
2	$MnCl_2$	23

3.2.4 Scope of Alkylation Reaction with Mn Reductant

The scope of the heteroaryl imine coupling partner was investigated using benzyl bromide as the electrophile (Figure 3.5). Sterically diverse *N*-substitution on the imine was well tolerated, affording the products containing ^{n}Bu, ^{i}Pr, and ^{t}Bu groups in high yields (**273**–**275**). Imines bearing cyclopropyl and cyclobutyl groups, two increasingly popular fragments in drug development,[24] provided the coupled products in 67% yield (**276**) and 70% yield (**277**), respectively. Use of the chiral imine derived from (*R*)-1-phenylethylamine gave product **278** in good yield, albeit with poor diastereoselectivity. The use of a ketimine substrate did result in product formation (**279**); however, the yield was low, likely due to the increased steric hindrance at the site of C–C bond formation.

Figure 3.5. *Scope of α-iminopyridines.*

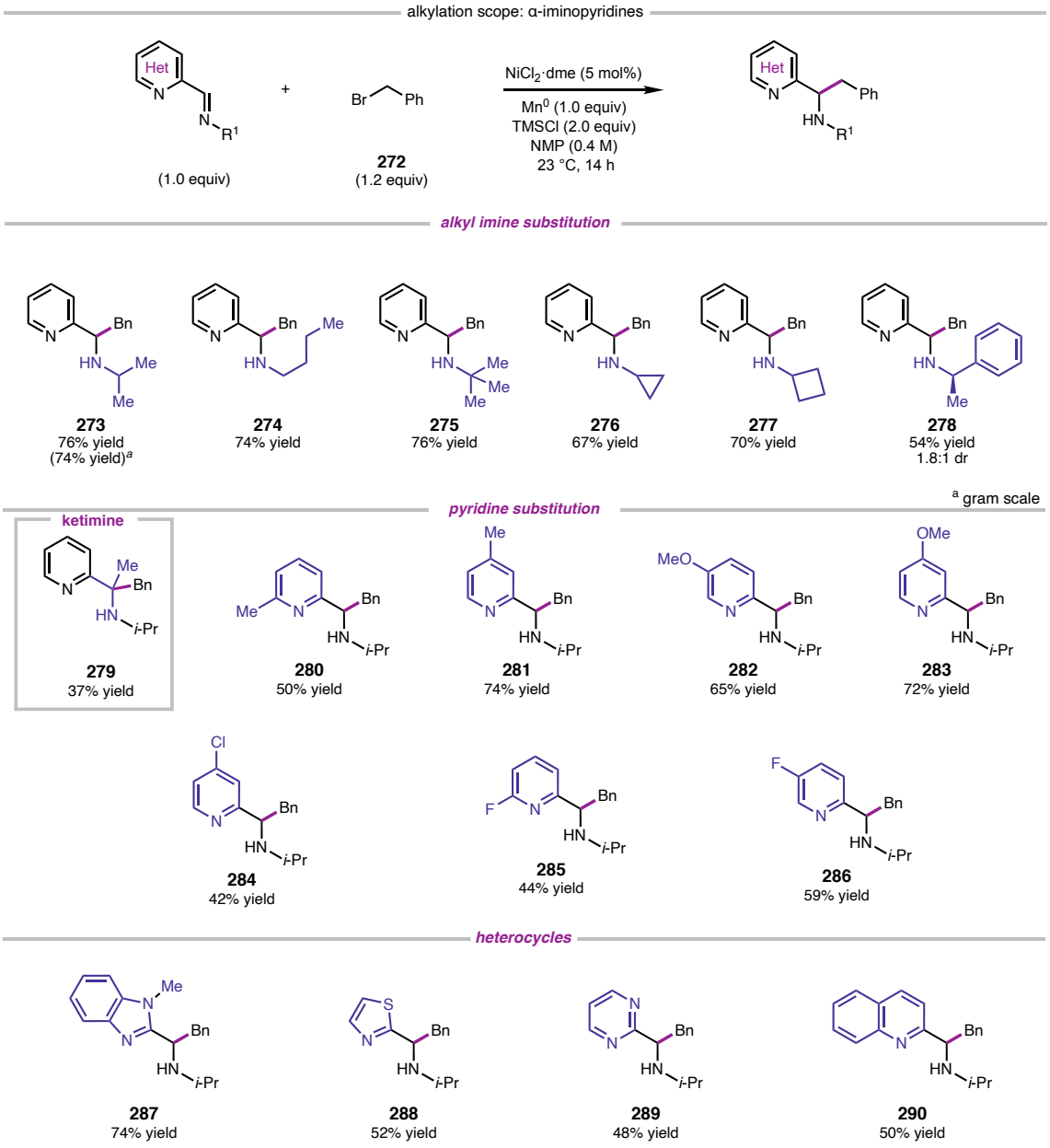

Electron-donating substituents at the 4- and 5-position of the pyridine were tolerated, furnishing the desired products in generally good yields (**281**–**283**). Substitution at the 6-position afforded the products in lower yields (**280** and **285**), possibly because the substituent hinders coordination of the imine to the Ni-catalyst. In general, substrates bearing electron withdrawing groups at the 5-position gave lower yields of the product

(Figure 3.13). In addition to 2-iminopyridines, several other heterocyclic imines can be employed, including the corresponding benzimidazole (**284**), thiazole (**288**), pyrimidine (**289**), and quinoline (**290**) (Figure 3.5).

Figure 3.6. *Scope of benzyl halide electrophiles.*

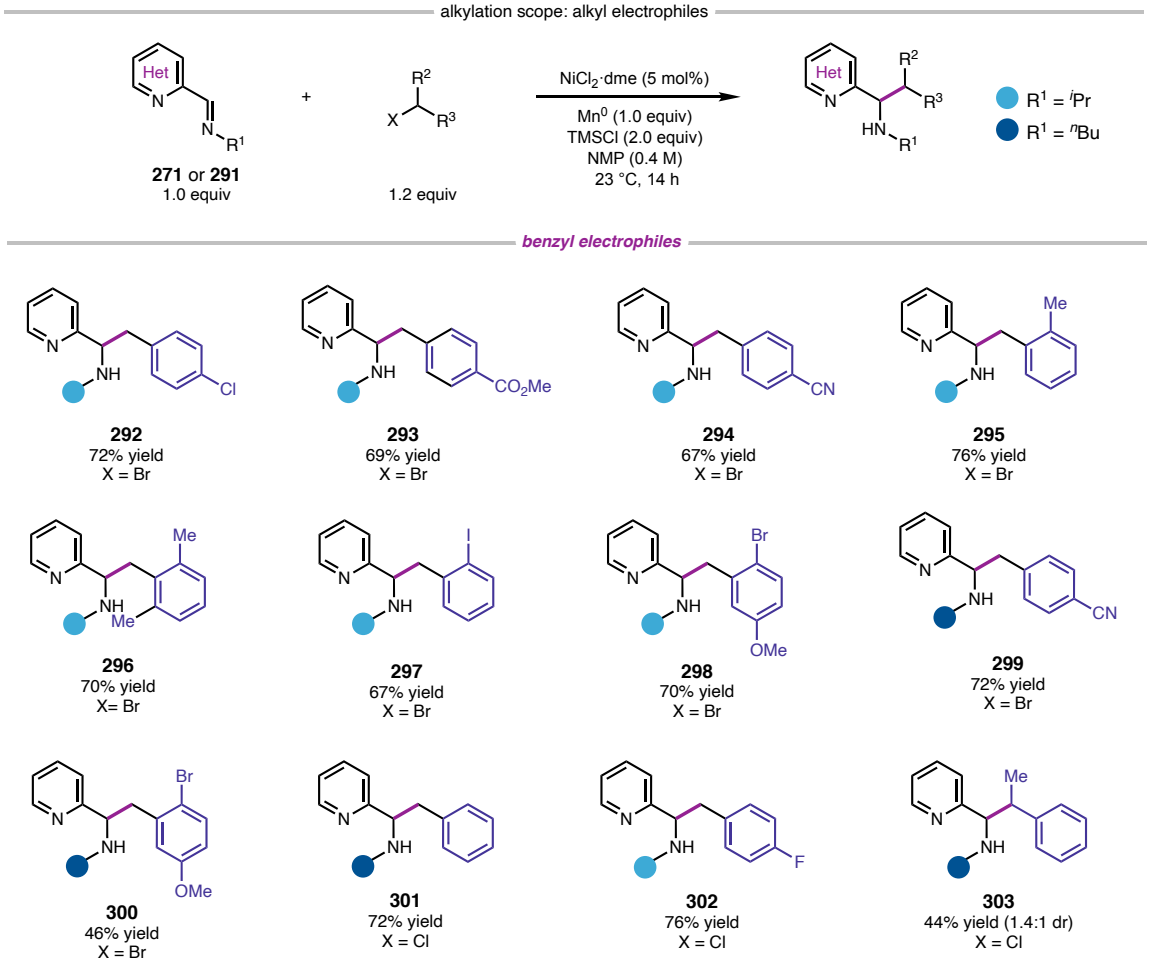

A range of substituted benzylic bromides could be coupled with imine **271**. *Ortho*-substituted benzylic bromides coupled smoothly, affording products **295**–**298** and in good yield. In addition, the reaction exhibits chemoselectivity for the benzylic halide in the presence of aryl iodides and bromides (**297** and **298**); these functionalities are frequently incompatible with standard organometallic reagents. Benzylic chlorides perform

comparably under standard reaction conditions (**301**-**303**). A secondary benzylic chloride also underwent the alkylation, although in reduced yield and with poor diastereoselectivity (**303**) (Figure 3.6).

Figure 3.7. *Scope of alkyl electrophiles.*

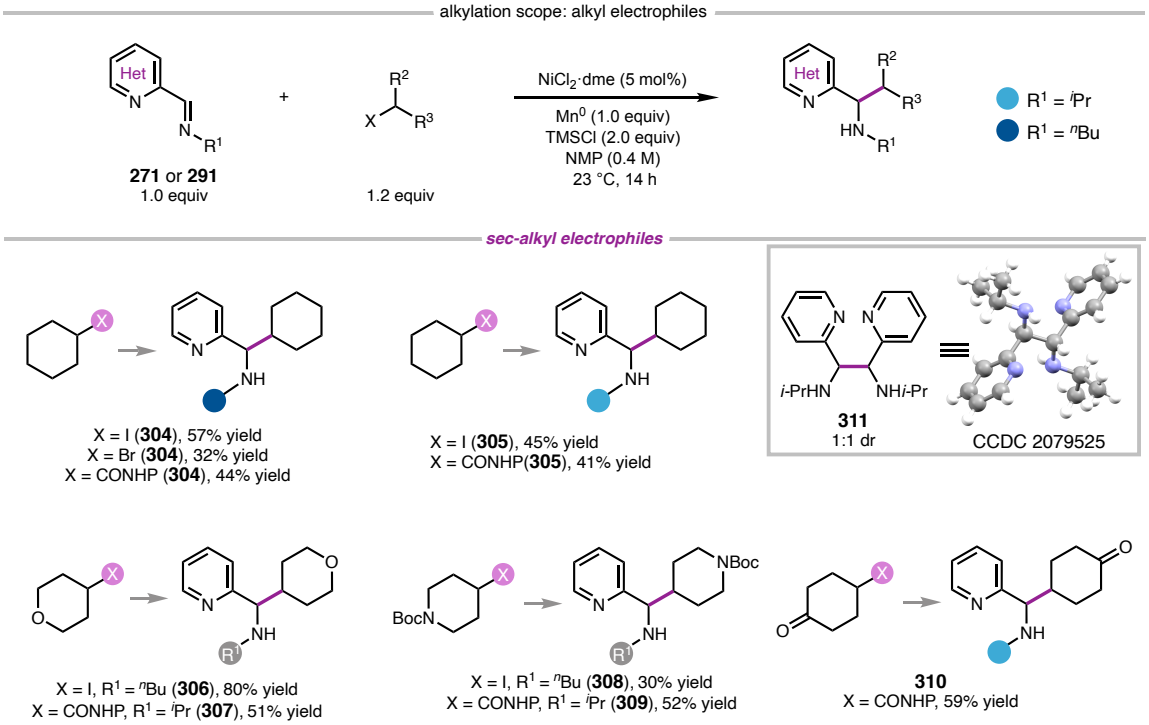

Non-benzylic alkyl halides were also investigated (Scheme 1), which revealed that the reaction yield is influenced by the identity of both the imine and the alkyl electrophile. *N*-^{n}Bu imine **291** could be coupled with cyclohexyl iodide and cyclohexyl bromide to furnish **304** in 57% yield and 32% yield, respectively. Coupling of the *N*-^{i}Pr imine (**271**) with cyclohexyl iodide gave **305** in 45% yield; however, it was accompanied by 50% yield of the imine homocoupling product **311**.[2526] In contrast, use of the corresponding *N*-hydroxyphthalimide (NHP) ester[27] gave **305** in 41% yield but with minimal formation of **311**. Reaction of **271** or **291** with pyranyl and piperdinyl electrophiles furnished products **306**–**309** in modest to good yields. Taken together, these scope studies demonstrate a

generally high tolerance for nitrile, ketone, ester, and halide functional groups, which are often incompatible with organomagnesium and organolithium reagents (Figure 3.7)

3.2.5 Optimization and Scope of Electroreductive Alkylation

Figure 3.8. *Electroreductive imine alkylation scope.*

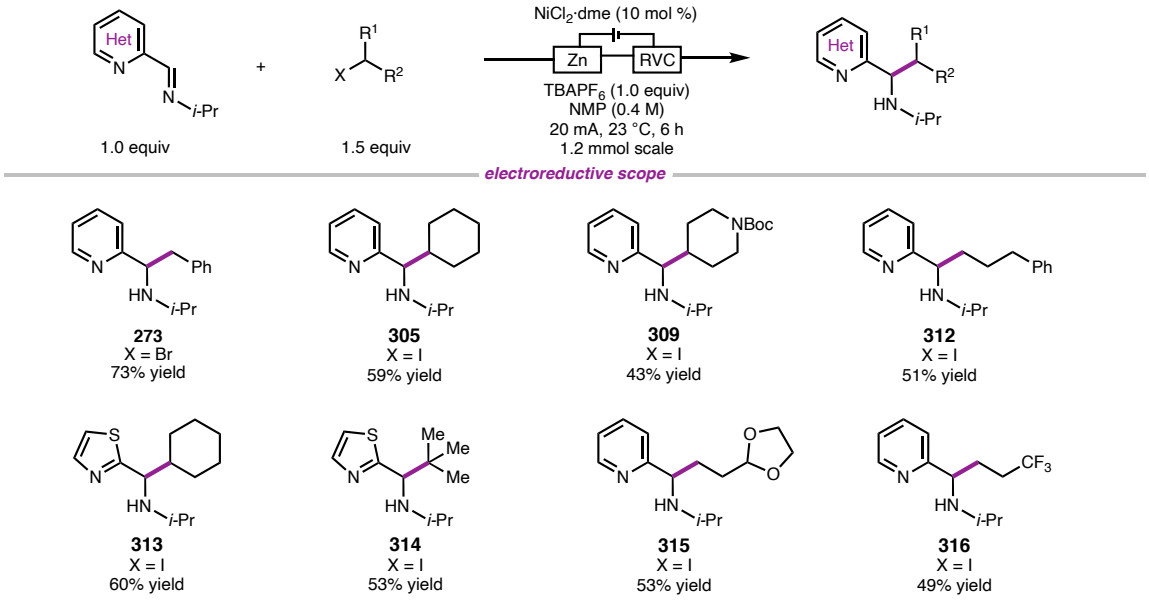

Given that deleterious imine homodimerization was observed in some reactions when Mn^0 was used as a reductant (Figure 3.14), we sought to drive the reaction electrochemically to eliminate the need for Mn^0. Moreover, an electroreductive system removes the mechanistic ambiguity about the identity of the active catalyst (Ni vs. Mn). Under constant current electrolysis using reticulated vitreous carbon (RVC) foam as the cathode and Zn^0 metal as a sacrificial anode, alkylation of **271** with **272** proceeded smoothly. We were pleased to find that several substrates that gave low yields under the Mn^0 conditions performed better under the electroreductive conditions. For example, when **271** was coupled with iodocyclohexane under standard conditions, product **305** was formed in 45% yield and was accompanied by 50% yield (see Figure S3.14) of imine dimer **311**

(Figure 3.7). Under the electroreductive conditions, **305** was produced in 59% yield on a 1.2 mmol scale; no **311** was observed. Alkylation products from primary (**312**, **315**, and **316**) and tertiary (**314**) iodides, could also be formed in good yield under the electroreductive conditions (Figure 3.8). Both reactions proceeded in <20% yield when Mn^0 was used as a reductant.

3.3 Mechanistic Studies

3.3.1 Investigating the Redox-Active Substrate-Catalyst Complex

Since the electroreductive coupling (Figure 3.8) demonstrates that Ni salts can catalyze the alkylation of 2-iminopyridines, we carried out a series of mechanistic experiments studying the Ni system. Initial mechanistic investigations focused on the substrate-catalyst complexes (like **270**, Figure 3.4) proposed to be key catalytic intermediates. Non-chelating substrates like benzaldehyde-derived imine **317** and isomeric pyridyl imine **318** failed to couple under standard conditions, demonstrating the importance of forming a bidentate substrate-metal complex (Scheme 3.3a). Bis(2-iminopyridine)·Ni complex **321** was prepared by the addition of imine **271** (2.0 equiv) to $Ni(cod)_2$ (1.0 equiv);[12] subsequent addition of benzyl bromide provided **273** in 53% yield, providing support for reduced Ni complex **321** as a competent species in the catalytic cycle (Scheme 3.3b).

Scheme 3.3. *Investigating the importance of the substrate acting as a ligand.*

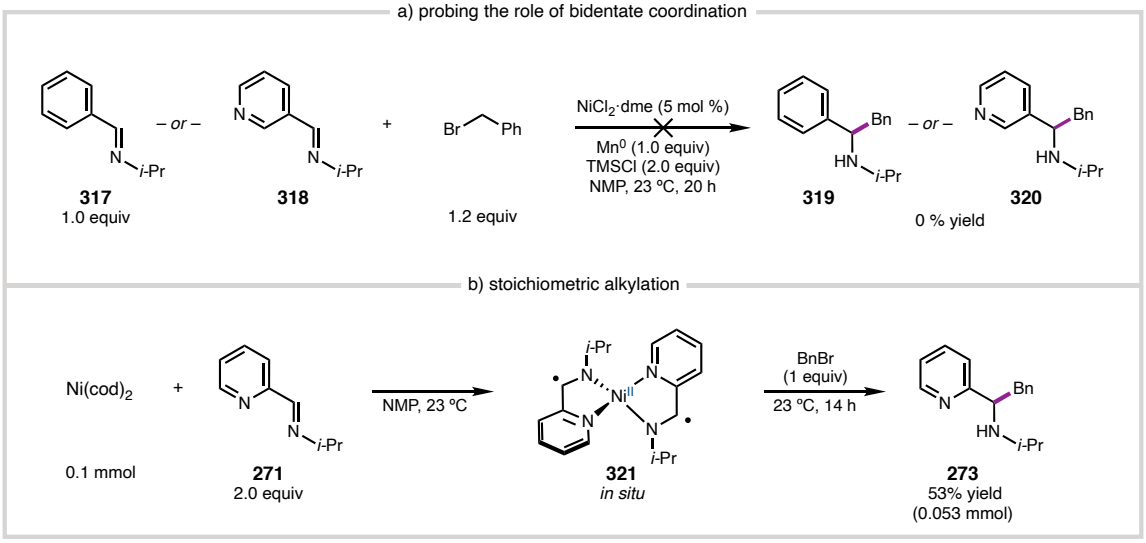

In agreement with Wieghardt and coworkers,[12] computational studies suggest that the electronic structure of the formally Ni^0 complex **321** is best described as a Ni^{II} center with antiferromagnetically coupled ligand-based radicals. DFT calculations of **321** at the B3LYP/def2-TZVP level of theory show the broken symmetry solution BS(2,2) being lower in energy than the closed-shell or high spin solutions (Figure 3.9a).[28,29] A qualitative molecular orbital diagram of the magnetic orbitals reveals seven orbitals with significant d contribution (Figure 3.40, section 3.5.17). Upon closer examination of the electronic structure, there are two ligand-based singly-occupied molecular orbitals (SOMOs) as the imine π^* orbitals (Scheme 3.9b). Using the Yamaguchi equation, the spin-spin coupling constant (J) between the metal-based SOMOs and the ligand-based SOMOs was calculated to be $J = -777$ cm^{-1}.[30] These data support our hypothesis that the ligand non-innocence of reduced catalyst-substrate complexes such as **321** allows for facile access to persistent α-amino radical intermediates (Figure 3.4b).

Figure 3.9. *Theoretical investigation of electronic structure of* ***321****.*

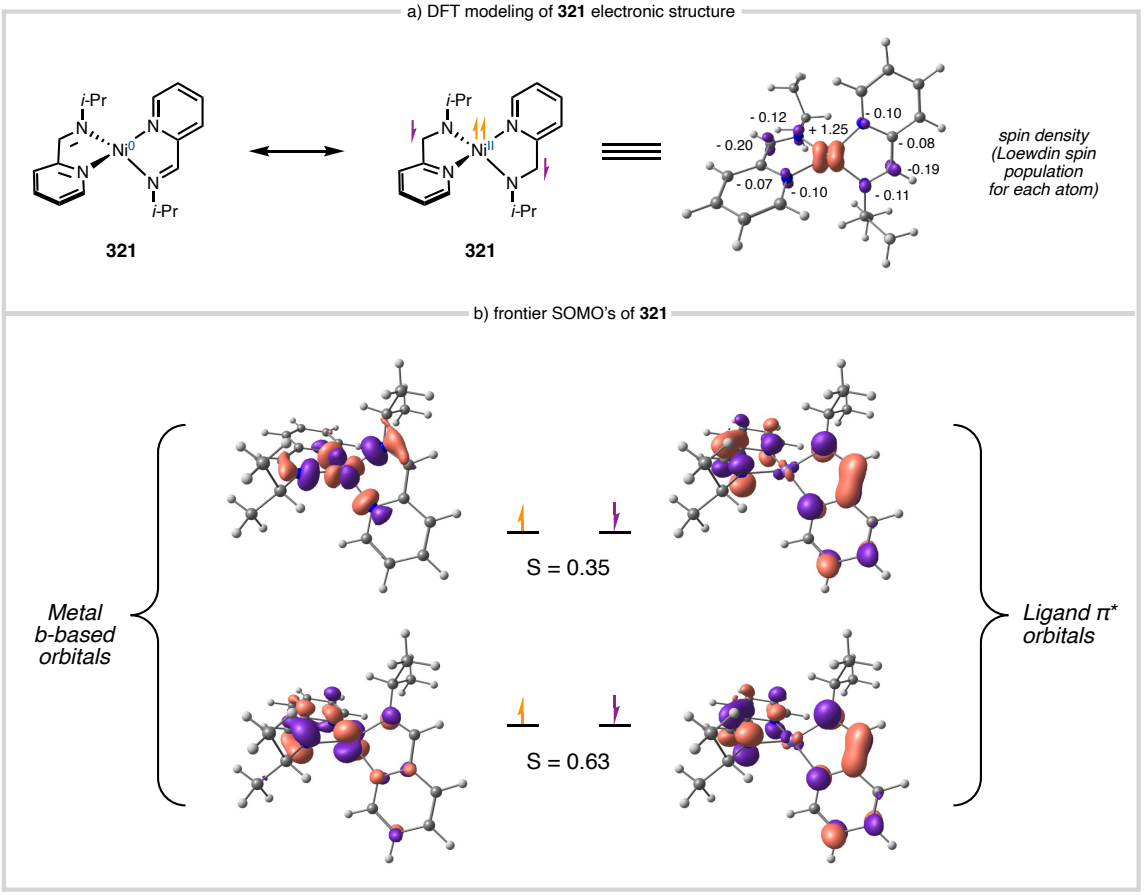

3.3.2 Redox Properties of Catalyst-Substrate Complex

We sought to investigate the redox properties of (**271**)$_2$NiCl$_2$ (**322**) to confirm that reduction to the low-valent complex **322** is possible under the reaction conditions. Using cyclic voltammetry (CV), the reduction potential of free **271** was compared to the reduction potentials of corresponding *in situ* generated complexes (**271**)$_2$NiCl$_2$ (**322**, purple) and (**271**)$_2$MnCl$_2$ (**323**, green) (Figure 3.10). Complex **323** ($E_{1/2}$ = –1.82 V vs. Fc/Fc$^+$ in NMP) is more challenging to reduce than Ni complex **322** ($E_{1/2}$ = –1.43 V vs. Fc/Fc$^+$ in NMP). The free imine **271** has a reduction potential ($E_{p/2}$) of –2.65 V vs. Fc/Fc$^+$ in NMP, which is significantly more negative than that of either complex **322** or **323**. Complexation of **271**

with a non-redox-active Lewis acid such as $MgBr_2$ does not significantly change the potential of imine reduction ($E_{p/2}$ = –2.55 V vs. Fc/Fc^+ in NMP) (Figure 3.10). The significant anodic shift of the reduction potentials and the increased reversibility of the redox events demonstrate that imine coordination to Ni and Mn facilitates reduction and stabilizes the ligand-centered radicals. We note that reduction of **322** is 420 mV more anodic than **323** indicating the formation of proposed intermediate **267** (or **321** when M = Ni) (Figure 3.4b) is more thermodynamically favorable, which may correlate with the improved product yields when catalytic Ni is included.

Figure 3.10. *Cyclic voltammetry of **271** and its catalytically relevant metal complexes.*

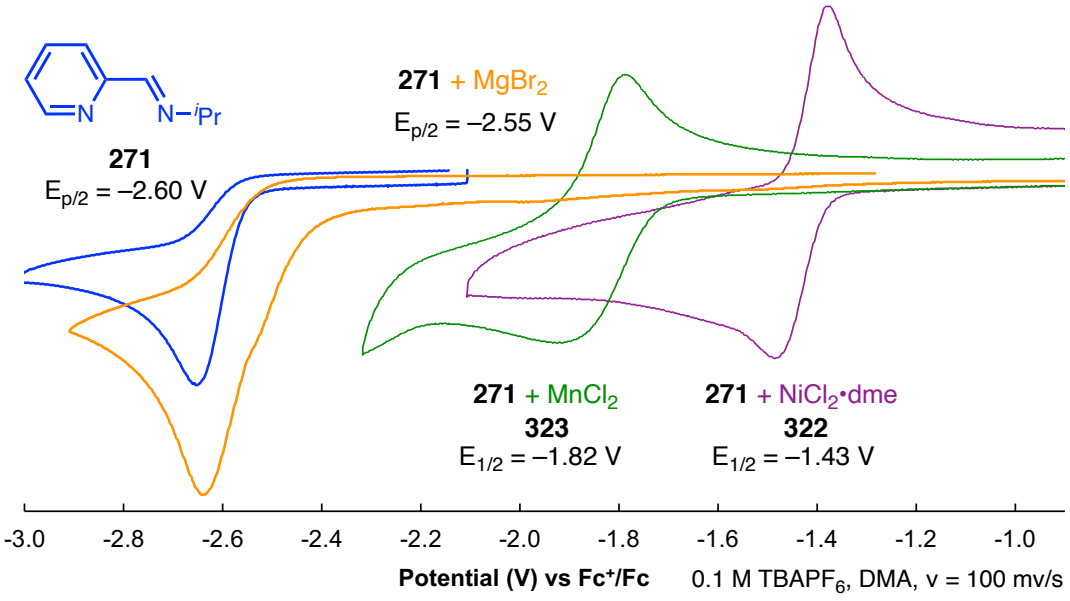

It was unclear from the CV alone whether the observed reduction of (**271**)$_2NiCl_2$ (**322**) corresponded to a one-electron or a two-electron process.[31] To investigate the identity of the species generated upon reduction, UV/Vis spectroelectrochemical analysis of **323** was performed at varying potentials (Figure 3.35, section 3.5.14). At –1.4 V vs. Fc/Fc^+, a

species develops with a UV/Vis spectrum that is consistent with that of an independently prepared sample of (**271**)$_2$Ni (**321**). Alternatively, mixing 1 equiv each of **322** and **321** results in comproportionation to the Ni^{I} complex (**324**); this species has a different spectroscopic profile, and consistent with Wieghardt's prior studies,[12] computational and EPR studies suggest that this complex does have not significant radical character on the ligand backbone (Section 3.5.16). These experiments suggest that at potentials accessible under the catalytic reaction conditions, complex **322** undergoes two electron reduction to generate **321** (Figure 3.11).[32,33]

Figure 3.11. *UV/vis comparison of electrochemically reduced* ***322*** *with independently prepared Ni complexes.*

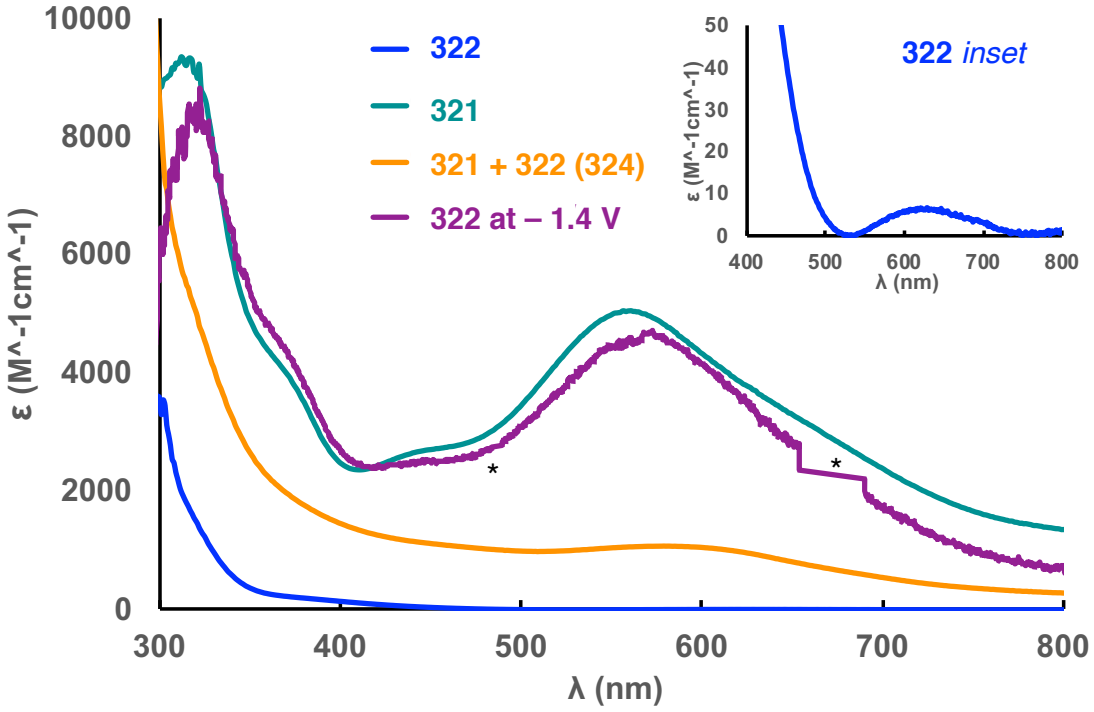

3.3.3 Electroanalytical Experiments

Figure 3.12. *Investigating the role of reaction components with CV.*

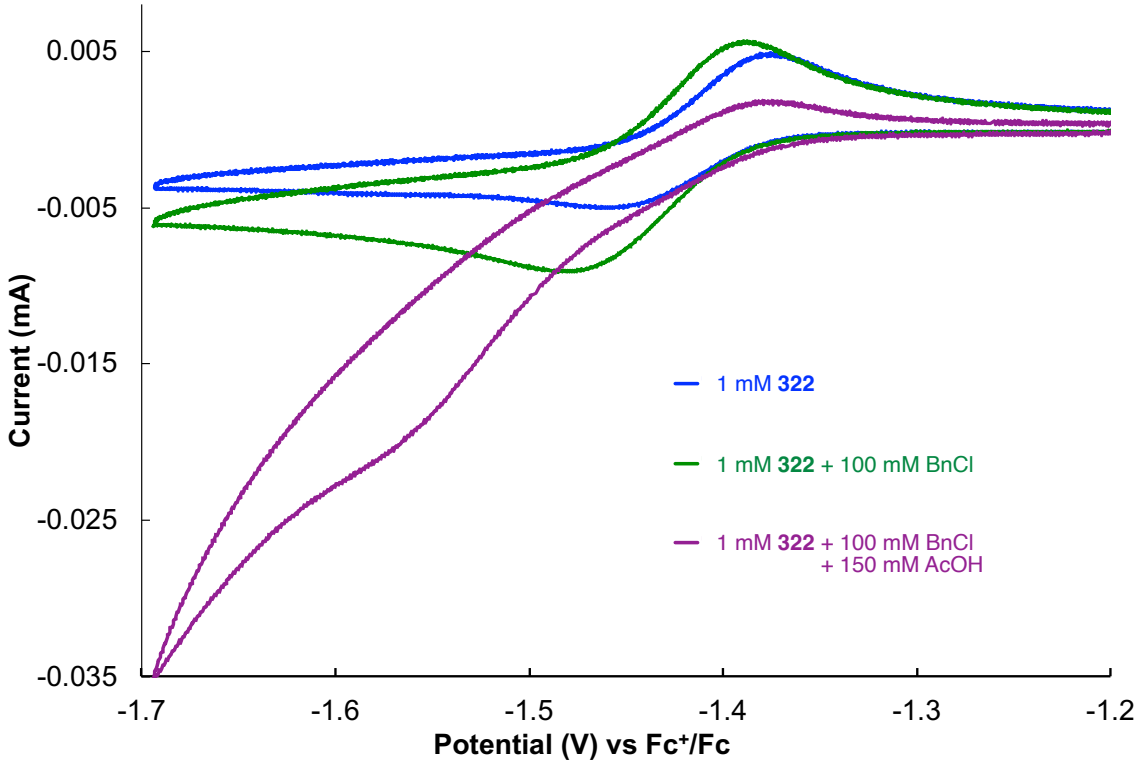

To probe whether reductively generated **321** can react with alkyl electrophiles, CVs of complex **322** in the presence of benzyl chloride were acquired. Scanning in the negative direction, the CV of a mixture of **322** (1 equiv) and benzyl chloride (100 equiv) shows a cathodic shift and increase in peak current relative to complex **322** alone (Figure 3.12). The cathodic shift indicates that, upon reduction, complex **322** does not react with benzyl chloride through a simple EC mechanism, but instead through a mechanism that likely involves intermediate chemicals steps such as loss of chloride ligands. Kinetic analysis of the reaction with benzyl chloride reveals a second order rate constant $k_{obs} = 1.8x10^{-1}$ $M^{-1}s^{-1}$ (Figures 3.26-30, section 3.5.12).[34] Addition of AcOH (150 equiv) and additional **271** (50 equiv) results in a catalytic wave (Figure 3.12) that is not observed in the absence of BnCl

or excess **271** (Figure 3.25). AcOH was used for these studies because it was found to give reasonable alkylation yields (Table 3.2, entry 3) and had greater stability than TMSCl in the electrochemical cell.

3.4 Conclusion and Future Directions

In conclusion, the Ni-catalyzed reductive cross-coupling of (2-imino)heterocycles with C(sp^3) alkyl electrophiles has been reported. The reaction occurs under mild conditions and is tolerant of a variety of functional groups, including *N*- and *S*-heterocyclic imine coupling partners. Mechanistic studies support the formation of low-valent bis(2-imino)pyridine·Ni complexes as persistent ligand-centered radical species that can react with alkyl electrophiles and be leveraged for catalytic C–C bond formation.

Future studies should be focused on extending this methodology to other functional groups that form redox-active complexes upon coordination to low-valent transitions metals. This would not only broaden the scope of this reactivity but also enable challenging radical additions into carbonyls, a functionality more challenging than imines. Additionally, an enantioselective variant would be powerful given the value of enantioenriched amines. Initial attempts at enantioinduction with chiral ligands have been unsuccessful, likely due to the fact that substrate coordination is essential for reactivity (Scheme 3.5).

3.5 EXPERIMENTAL SECTION

3.5.1 Materials and Methods

Unless otherwise stated, reactions were performed under a N_2 atmosphere using freshly dried solvents. All reagents were purchased from commercial suppliers (Sigma Aldrich, Combi- Blocks, TCI, Enamine, Strem) and used without further purification unless mentioned otherwise. Tetrahydrofuran (THF) and methylene chloride (CH_2Cl_2) were dried by passing through activated alumina columns. Anhydrous *N*-methylpyrrolidinone (NMP) was purchased from Aldrich and stored in a N_2-filled glovebox. $NiCl_2$·dme was purchased from Strem and stored in the glovebox. Manganese powder (~325 mesh, 99.3%) was purchased from Alfa Aesar. Zinc dust (97.5%) was purchased from Strem. Reactions were monitored by thin-layer chromatography using EMD/Merck silica gel 60 F254 pre-coated plates (0.25 mm) and were visualized by UV, *p*-Anisaldehyde, Ninhydrin, or $KMnO_4$ staining. Flash column chromatography was performed as described by Still et al. using silica gel (230-400 mesh, Silicycle).[35] Purified compounds were dried on a high vacuum line (0.2 torr) to remove trace solvent. ^1H and ^{13}C NMR spectra were recorded on a Bruker Avance III HD with Prodigy cryoprobe (at 400 MHz and 101 MHz, respectively), a Varian 400 MR (at 400 MHz and 101 MHz, respectively), or a Varian Inova 500 (at 500 MHz and 126 MHz, respectively). ^1H and ^{19}F NMR spectra were also recorded on a Varian Inova 300 (at 300 MHz and 282 MHz, respectively). NMR data is reported relative to internal $CHCl_3$ (^1H, δ = 7.26) and $CDCl_3$ (^{13}C, δ = 77.0). $CDCl_3$ for NMR spectra on amine-containing compounds was passed through basic alumina. Data for ^1H NMR spectra are reported as follows: chemical shift (δ ppm) (multiplicity, coupling constant (Hz),

integration). Multiplicity and qualifier abbreviations are as follows: s = singlet, d = doublet, t = triplet, q = quartet, m = multiplet, br = broad. IR spectra were recorded on a Perkin Elmer Paragon 1000 spectrometer and are reported in frequency of absorption (cm^{-1}). HRMS were acquired from the Caltech Mass Spectral Facility using fast-atom bombardment (FAB), electrospray ionization (ESI-TOF), Field Desorption (FD), or electron impact (EI). Elemental analysis (EA) with ICP-MS on a commercial manganese sample (mentioned above) was performed at the Resnick Sustainability Institute's Water and Environment Lab at the California Institute of Technology. X-ray diffraction was performed at the Caltech X-ray Crystal Facility. The computations presented here were conducted on the Resnick High Performance Cluster, a facility supported by the Resnick Sustainability Institute at the California Institute of Technology. Electroanalytical and spectroelectrochemical experiments were conducted in the Beckman Resource Laser Resource Center at the California Institute of Technology.

3.5.2 Optimization Experiments

General Procedure 3.1: To a 1-dram vial equipped with a stir bar (1.2 cm) was added 2-imino pyridine **271** (0.3 mmol), benzyl bromide **272** (0.36 mmol, 1.2 equiv), and reductant (Mn^0, 0.3 mmol, 1.0 equiv; Zn^0, 0.6 mmol, 2.0 equiv; TDAE, 0.45 mmol, 1.5 equiv) on the benchtop (or in the glovebox in the case of TDAE following the solvent addition). The vial was brought into a nitrogen-filled glovebox and a stock solution of metal catalyst in NMP (0.75 ml, 0.02 M, 0.05 equiv [M]) and additive (TMSCl, 0.6 mmol, 2.0 equiv; AcOH, 0.3 mmol, 1 equiv; HFIP, 1.5 mmol, 5 equiv) was added. The vial was sealed with a Teflon cap, removed from the glovebox, and stirred at ambient temperature for 14 hours at 600

rpm. The resulting suspension was diluted with CH_2Cl_2 (0.5 ml) and extracted 3x with 1 N HCl (0.5 ml). To the combined aqueous phases was added K_2CO_3 (s) until gas evolution ceased. The resulting aqueous solution was extracted 3x with EtOAc and the combined EtOAc layers were concentrated under reduced pressure then further concentrated at 30 °C until most of the NMP was removed and analyzed by ^{1}H NMR with 1,1,2,2-tetrachloroethane as an internal standard to obtain a quantitative NMR yield.

Impact of Stir Rate:

Scheme 3.4. *Control study showing minimal impact on alkylation yield across several stir rates. Yields determined by ^{1}HNMR with an internal standard.*

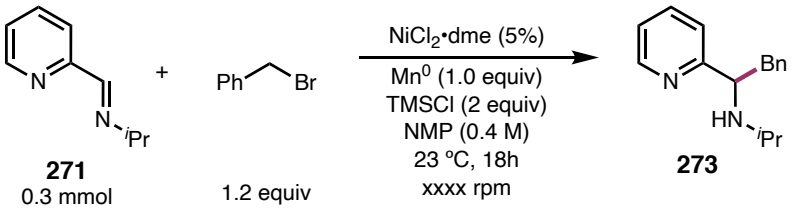

Stir rate (rpm)	*Yield (%)*
300	84
600	88
750	81
1200	81

Mediator or Electron Shuttle Additives:

The possibility that the role of the nickel catalyst is to act as an electron mediator that accelerates the Mn-mediated reaction was investigated through the addition of exogenous ligands and through the addition of known electron mediators (Scheme 3.5). Exogenous ligands we examed were bidentate nitrogen ligands (dtbbpy), tridentate nitrogen ligands (terpy), and bidentate phosphine ligands (dppe). All ligands or electron shuttles seemed to inhibit the reaction or shut down productive reactivity.

Scheme 3.5. *Using additional ligands and electron shuttles.*

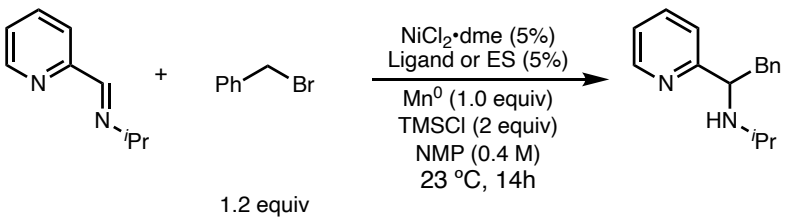

entry	ligand[b]/ES	yield (%)[a]
1	dtbbpy	65
2	terpy	< 5
3	dppe	< 5
4	$Ni(bpy)_3(BF_4)_2$	59
5	CoPc	25

3.5.3 Substrate Synthesis

Synthesis of Heteroaryl Imines

General Procedure 3.2: Heteroaryl Imine Synthesis using Volatile Amines

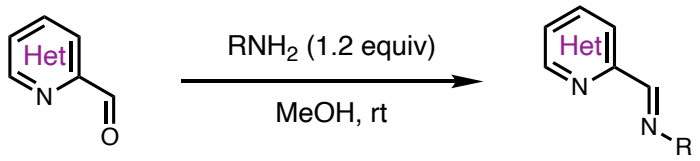

A 1-dram vial equipped with a stir bar was charged with MeOH (0.7 M), heteroaryl aldehyde (1.0 equiv), and primary amine RNH_2 (1.1-1.5 equiv). The resulting solution was stirred at room temperature for 2 hours, followed by concentration in vacuo. The resulting 2-imino-heteroarene was obtained in pure form and used without further purification.

b. General Procedure 3.3: Heteroaryl Imine Synthesis using Non-volatile Amines

A 1-dram vial equipped with a stir bar was charged with CH_2Cl_2 (0.7 M), heteroaryl aldehyde (1.05 equiv), $MgSO_4$ (1.5 equiv) and primary amine RNH_2 (1.0 equiv). The resulting solution was stirred at room temperature for 18 hours. The resulting suspension was filtered and concentrated in vacuo. The resulting 2-imino-heteroaryl was obtained in pure form and used without further purification.

(*E*)-*N*-isopropyl-1-(pyridin-2-yl)methanimine (271)

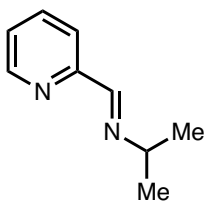

Prepared from 2-pyridine carboxaldehyde (2.30 g, 21.5 mmol) and isopropylamine (1.59 g, 26.8 mmol) following General Procedure 3.2. After concentration in vacuo, **271** (2.68 g, 18.1 mmol, 84%) was obtained as a yellow oil.

^{1}H NMR (500 MHz, $CDCl_3$): δ 8.63 (d, *J* = 3.1 Hz, 1H), 8.39 (s, 1H), 7.98 (d, *J* = 7.9 Hz, 1H), 7.73 (td, *J* = 7.9, 2.2 Hz, 1H), 7.29 (ddd, *J* = 7.5, 4.8, 1.2 Hz, 1H), 3.69 – 3.60 (m, 1H), 1.29 (d, *J* = 6.3 Hz, 6H).

^{13}C NMR (126 MHz, $CDCl_3$): δ 159.5, 155.0, 149.6, 136.7, 124.8, 121.6, 61.7, 24.2.

FTIR (NaCl, thin film, cm^{-1}): 3056, 2968, 2929, 2865, 1647, 1588, 1568, 1466, 1437, 1362, 1316, 1139, 993, 973, 945, 775, 744, 615.

HRMS (FAB, m/z): calc'd for $C_9H_{11}N_2$ $[M+H]^+ - H_2$: 147.0922; found 147.0922.

(*E*)-*N*-butyl-1-(pyridin-2-yl)methanimine (291)

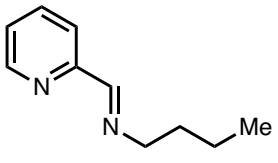

Prepared from 2-pyridine carboxaldehyde (1.07 g, 10.0 mmol) and *n*-butylamine (878 mg, 12.0 mmol) following General Procedure 3.2. After concentration in vacuo, **291**(1.30 g, 8.00 mmol, 80%) was obtained as a yellow oil.

^{1}H NMR (500 MHz, $CDCl_3$): δ 8.64 (d, *J* = 4.8 Hz, 1H), 8.37 (s, 1H), 7.97 (d, *J* = 7.9 Hz, 1H), 7.73 (td, *J* = 7.7, 1.7 Hz, 1H), 7.30 (dd, *J* = 7.5, 4.8 Hz, 1H), 3.68 (t, *J* = 6.8 Hz, 2H), 1.71 (p, *J* = 7.1 Hz, 2H), 1.40 (h, *J* = 7.4 Hz, 2H), 0.95 (t, *J* = 7.4 Hz, 3H).

^{13}C NMR (126 MHz, $CDCl_3$): δ 161.9, 154.8, 149.6, 136.8, 124.8, 121.4, 61.5, 33.0, 20.6, 14.1.

FTIR (NaCl, thin film, cm^{-1}): 3053, 3009, 2958, 2938, 2872, 1649, 1587, 1567, 1468, 1436, 1377, 1332, 1292, 1227, 1145, 1117, 1066, 1044, 992, 978, 939, 898, 864, 775, 743, 654, 617.

HRMS (FAB, m/z): calc'd for $C_{10}H_{15}N_2$ $[M+H]^+$: 163.1235; found 163.1256.

(*E*)-*N*-*tert*-butyl-1-(pyridin-2-yl)methanimine (325)

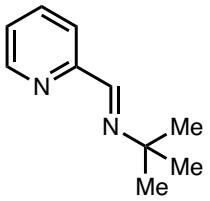

Prepared from 2-pyridine carboxaldehyde (225 mg, 2.10 mmol) and *tert*-butlyamine (185 mg, 2.52 mmol) following General Procedure 3.2. After concentration in vacuo, **325** (326 mg, 2.0 mmol, 95%) was obtained as a yellow oil.

^{1}H NMR (500 MHz, $CDCl_3$): δ 8.66 – 8.58 (m, 1H), 8.35 (s, 1H), 8.01 (dt, *J* = 7.9, 1.1 Hz, 1H), 7.76 – 7.67 (m, 1H), 7.28 (ddd, *J* = 7.5, 4.9, 1.3 Hz, 1H), 1.31 (s, 9H).

^{13}C NMR (126 MHz, $CDCl_3$): δ 156.6, 155.7, 149.5, 136.7, 124.6, 121.2, 58.0, 29.8.

FTIR (NaCl, thin film, cm^{-1}): 3056, 2969, 2931, 1646, 1588, 1568, 1467, 1436, 1228, 1209, 1044, 994, 972, 908, 860, 775, 744, 616.

HRMS (ESI-TOF, m/z): calc'd for $C_{10}H_{15}N_2$ $[M+H]^+$: 163.1235; found 163.1210.

(*E*)-*N*-cyclopropyl-1-(pyridin-2-yl)methanimine (357)

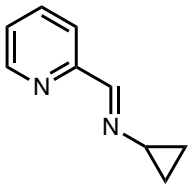

Prepared from 2-pyridine carboxaldehyde (225 mg, 2.10 mmol) and cyclopropylamine (144 mg, 2.52 mmol following General Procedure 3.2. After concentration in vacuo, **357** (200 mg, 1.37 mmol, 65%) was obtained as a yellow oil.

^{1}H NMR (500 MHz, $CDCl_3$): δ 8.63 (d, *J* = 4.9 Hz, 1H), 8.54 (s, 1H)7.88 (d, *J* = 9.0 Hz, 1H), 7.71 (td, *J* = 7.7, 1.7 Hz, 1H), 7.31 – 7.24 (m, 1H), 3.13 (hept, *J* = 6.8, 3.4 Hz, 1H), 1.09 – 1.04 (m, 2H), 1.03 – 0.97 (m, 2H).

^{13}C NMR (126 MHz, $CDCl_3$): δ 159.3, 154.8, 149.6, 136.6, 124.4, 121.3, 42.2, 9.5.

FTIR (NaCl, thin film, cm^{-1}): 3420, 3055, 3010, 2962, 2878, 1635, 1583, 1568, 1470, 1436, 1381, 1320, 1174, 1146, 1090, 1042, 956, 887, 812, 773, 743, 612.

HRMS (FAB, m/z): calc'd for $C_9H_{11}N_2$ $[M+H]^+$: 147.0922; found 147.0922.

(*E*)-*N*-cyclobutyl-1-(pyridin-2-yl)methanimine (326)

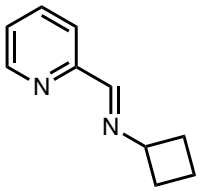

Prepared from 2-pyridine carboxaldehyde (225 mg, 2.10 mmol) and cyclobutylamine (179 mg, 2.52 mmol) following General Procedure 3.2. After concentration in vacuo, **326** (243 mg, 1.51 mmol, 72%) was obtained as a yellow oil.

^{1}H NMR (500 MHz, $CDCl_3$): δ 8.6 (d, *J* = 4.8 Hz, 1H), 8.3 (d, *J* = 1.7 Hz, 1H), 8.0 (d, *J* = 7.9 Hz, 1H), 7.7 (td, *J* = 7.7, 1.7 Hz, 1H), 7.3 (dd, *J* = 6.4, 4.8 Hz, 1H), 4.3 – 4.2 (m, 1H), 2.4 – 2.3 (m, 2H), 2.3 – 2.1 (m, 2H), 1.9 – 1.8 (m, 2H).

^{13}C NMR (126 MHz, $CDCl_3$): δ 159.4, 154.9, 149.6, 136.7, 124.8, 121.4, 62.9, 30.5, 15.8.

FTIR (NaCl, thin film, cm^{-1}): 3055, 2980, 2939, 2868, 1642, 1589, 1567, 1469, 1436, 1374, 1319, 1228, 1140, 1080, 1042, 992, 972, 861, 773, 743.

HRMS (FAB, m/z): calc'd for $C_{10}H_{13}N_2$ $[M+H]^+$: 161.1079; found 161.1086.

(*R*,*E*)-*N*-(1-phenylethyl)-1-(pyridin-2-yl)methanimine (327)

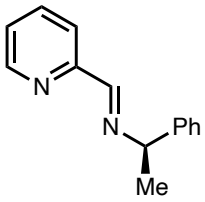

Prepared from 2-pyridine carboxaldehyde (176 mg, 1.65 mmol) and (*R*)-(+)-1-phenethylamine (190 mg, 1.57 mmol) following General Procedure 3.3. After concentration in vacuo, **327** (82.4 mg, 0.39 mmol, 25%) was obtained as tan solid.

^{1}H NMR (500 MHz, $CDCl_3$): δ 8.64 (ddd, *J* = 4.9, 1.7, 0.9 Hz, 1H), 8.47 (s, 1H), 8.10 (dt, *J* = 7.9, 1.1 Hz, 1H), 7.78 – 7.67 (m, 1H), 7.46 – 7.41 (m, 2H), 7.38 – 7.32 (m, 2H), 7.30 (ddd, *J* = 7.5, 4.8, 1.2 Hz, 1H), 7.28 – 7.22 (m, 1H), 4.65 (q, *J* = 6.4 Hz, 1H), 1.61 (d, *J* = 6.7 Hz, 3H).

^{13}C NMR (126 MHz, $CDCl_3$): δ 160.6, 155.0, 149.5, 144.8, 136.7, 128.7, 127.2, 126.9, 124.9, 121.7, 69.8, 24.8.

FTIR (NaCl, thin film, cm^{-1}): 3059, 3027, 2972, 2927, 2861, 1646, 1586, 1568, 1491, 1466, 1456, 1436, 1373, 1338, 1304, 1080, 993, 973, 908, 763, 700.

HRMS (FAB, m/z): calc'd for $C_{14}H_{15}N_2$ $[M+H]^+$: 211.1235; found 211.1217.

(*E*)-*N*-isopropyl-1-(pyridin-2-yl)ethan-1-imine (328)

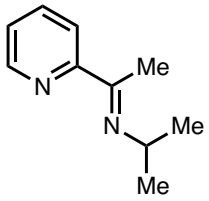

Prepared from 2-acetylpyridine (162 mg, 1.34 mmol) and isopropylamine (95.2 mg, 1.61 mmol following General Procedure 3.2 modified with the addition of 3Å molecular sieves (350mg, 2.2 mass equiv) to allow the reaction to run for 48 hours. After concentration in vacuo, **328** (126 mg, 0.78 mmol, 58%) was obtained as a yellow oil.

^{1}H NMR (400 MHz, CD_2Cl_2): δ 8.46 (ddd, J = 4.8, 1.8, 1.0 Hz, 1H), 7.98 (dt, J = 8.0, 1.1 Hz, 1H), 7.60 (ddd, J = 8.0, 7.4, 1.8 Hz, 1H), 7.18 (ddd, J = 7.4, 4.8, 1.3 Hz, 1H), 3.83 (hept, J = 6.3 Hz, 1H), 2.25 (s, 3H), 1.11 (d, J = 6.2 Hz, 6H).

^{13}C NMR (101 MHz, CD_2Cl_2): δ 163.19, 158.28, 148.07, 135.98, 123.76, 120.63, 51.46, 23.20, 12.98.

FTIR (NaCl, thin film, cm^{-1}): 3050, 2967, 2929, 2869, 1638, 1585, 1565, 1464, 1433, 1368, 1297, 1134, 1098, 1043, 991, 783, 743.

HRMS (FAB, m/z): calc'd for $C_{10}H_{15}N_2$ $[M+H]^+$: 163.1235; found: 163.1231.

(*E*)-*N*-isopropyl-1-(6-methylpyridin-2-yl)methanimine (329)

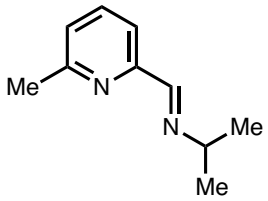

Prepared from 6-methylpicolinaldehyde (200 mg, 1.65 mmol) and isopropylamine (117 mg, 1.98 mmol) following General Procedure 3.2. After concentration in vacuo, **329** (174 mg, 1.07 mmol, 65%) was obtained as a yellow oil.

^{1}H NMR (500 MHz, $CDCl_3$): δ 8.37 (s, 1H), 7.81 (d, *J* = 7.7 Hz, 1H), 7.61 (t, *J* = 7.7 Hz, 1H), 7.16 (d, *J* = 7.6 Hz, 1H), 3.62 (hept, *J* = 6.3 Hz, 1H), 2.59 (s, 3H), 1.28 (d, *J* = 6.3 Hz, 6H).

^{13}C NMR (126 MHz, $CDCl_3$): δ 159.9, 158.2, 154.5, 137.0, 124.4, 118.5, 61.6, 24.6, 24.2.

FTIR (NaCl, thin film, cm^{-1}): 3061, 2968, 2927, 2863, 1646, 1591, 1574, 1455, 1378, 1361, 1308, 1250, 1224, 1141, 1086, 990, 967, 948, 9191, 863, 792, 762, 738, 636.

HRMS (FAB, m/z): calc'd for $C_{10}H_{15}N_2$ $[M+H]^+$: 163.1235; found 163.1236.

(*E*)-*N*-isopropyl-1-(4-methylpyridin-2-yl)methanimine (330)

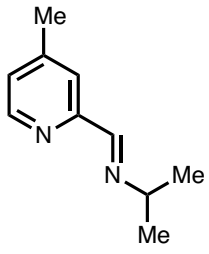

Prepared from 6-methylpicolinaldehyde (200 mg, 1.65 mmol) and isopropylamine (117 mg, 1.98 mmol) following General Procedure 3.2. After concentration in vacuo, **330** (224 mg, 1.37 mmol, 83%) was obtained as a yellow oil.

^{1}H NMR (500 MHz, $CDCl_3$): δ 8.48 (d, *J* = 5.0 Hz, 1H), 8.37 (s, 1H), 7.82 (s, 1H), 7.12 (d, *J* = 3.2 Hz, 1H), 3.63 (hept, *J* = 6.3 Hz, 1H), 2.38 (s, 3H), 1.29 (d, *J* = 6.3 Hz, 6H).

^{13}C NMR (126 MHz, $CDCl_3$): δ 159.8, 154.7, 149.4, 148.0, 125.8, 122.1, 61.7, 24.2, 21.2.

FTIR (NaCl, thin film, cm^{-1}): 2968, 2925, 2864, 1647, 1602, 1558, 1466, 1380, 1362, 1315, 1155, 994, 945, 850, 826, 768, 650.

HRMS (FAB, m/z): calc'd for $C_{10}H_{15}N_2$ $[M+H]^+$: 163.1235; found 163.1257.

(*E*)-*N*-isopropyl-1-(5-methoxypyridin-2-yl)methanimine (331)

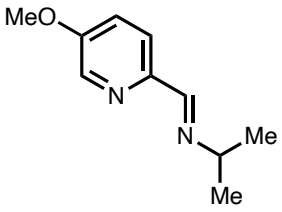

Prepared from 5-methoxypicolinaldehyde (250 mg, 1.82 mmol) and isopropylamine (129 mg, 2.19 mmol) following General Procedure 3.2 After concentration in vacuo, **331** (195 mg, 1.09 mmol, 60%) was obtained as a yellow oil.

^{1}H NMR (500 MHz, $CDCl_3$): δ 8.34 (s, 1H), 8.30 (d, *J* = 2.9 Hz, 1H), 7.93 (d, *J* = 8.7 Hz, 1H), 7.22 (dd, *J* = 8.7, 2.9 Hz, 1H), 3.89 (s, 3H), 3.60 (hept, *J* = 6.3 Hz, 1H), 1.27 (d, *J* = 6.3 Hz, 6H).

^{13}C NMR (126 MHz, $CDCl_3$): δ 158.8, 156.7, 147.9, 137.2, 122.4, 120.9, 61.6, 55.9, 24.3.

FTIR (NaCl, thin film, cm^{-1}): 2967, 2867, 1644, 1588, 1571, 1491, 1379, 1363, 1302, 1278, 1251, 1217, 1142, 1030, 1142, 1030, 972, 886, 838.

HRMS (FAB, m/z): calc'd for $C_{10}H_{15}N_2O$ $[M+H]^+$: 179.1184; found 179.1187.

(*E*)-*N*-isopropyl-1-(4-methoxypyridin-2-yl)methanimine (332)

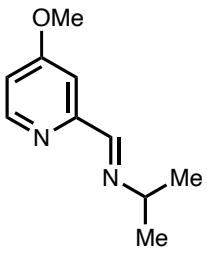

Prepared from 4-methoxypicolinaldehyde (250 mg, 1.82 mmol) and isopropylamine (129 mg, 2.19 mmol) following General Procedure 3.2. After concentration in vacuo, **332** (310 mg, 1.73 mmol, 95%) was obtained as a yellow oil.

^{1}H NMR (500 MHz, $CDCl_3$): δ 8.41 (d, *J* = 5.8 Hz, 1H), 8.33 (s, 1H), 7.49 (s, 1H), 6.81 (d, *J* = 5.9 Hz, 1H), 3.88 (s, 3H), 3.62 (hept, *J* = 6.5 Hz, 1H), 1.27 (d, *J* = 4.9 Hz, 6H).

^{13}C NMR (126 MHz, $CDCl_3$): δ 166.4, 159.4, 156.9, 150.6, 112.1, 106.1, 61.5, 55.5, 24.1.

FTIR (NaCl, thin film, cm^{-1}): 2968, 2866, 1648, 1592, 1560, 1477, 1364, 1303, 1252, 1142, 1037, 993, 969, 944, 850, 767.

HRMS (FAB, m/z): calc'd for $C_{10}H_{15}N_2O$ $[M+H]^+$: 179.1184; found 179.1181.

(*E*)-1-(4-chloropyridin-2-yl)-*N*-isopropylmethanimine (333)

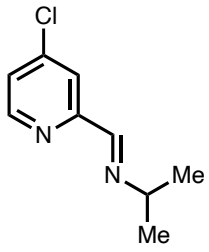

Prepared from 4-chloropicolinaldehyde (200 mg, 1.41 mmol) and isopropylamine (100.0 mg, 1.70 mmol) following General Procedure 3.2. After concentration in vacuo, **333** (224 mg, 1.22 mmol, 87%) was obtained as a yellow oil.

^{1}H NMR (500 MHz, $CDCl_3$): δ 8.51 (d, *J* = 7.0 Hz, 1H), 8.35 (s, 1H), 8.02 (s, 1H), 7.30 (d, *J* = 5.4 Hz, 1H), 3.65 (hept, *J* = 6.2 Hz, 1H), 1.28 (d, *J* = 5.7 Hz, 6H).

^{13}C NMR (126 MHz, $CDCl_3$): δ 158.3, 156.5, 150.4, 145.1, 125.0, 121.7, 61.6, 24.1.

FTIR (NaCl, thin film, cm^{-1}): 2969, 2924, 2864, 1648, 1575, 1553, 1458, 1398, 1362, 1313, 1264, 1230, 1145, 1090, 945, 827, 709.

HRMS (FAB, m/z): calc'd for $C_9H_{12}N_2Cl$ $[M+H]^+$: 183.0689; found 183.0662.

(*E*)-1-(6-fluoropyridin-2-yl)-*N*-isopropylmethanimine (334)

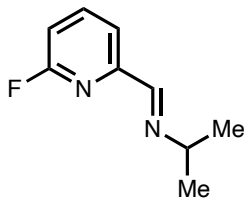

Prepared from 6-fluoropicolinaldehyde (177 mg, 1.41 mmol) and isopropylamine (100.0 mg, 1.70 mmol) following General Procedure 3.2. After concentration in vacuo, **334** (202 mg, 1.21 mmol, 86%) was obtained as a yellow oil.

^{1}H NMR (500 MHz, $CDCl_3$): δ 8.25 (s, 1H), 7.88 (d, *J* = 7.3 Hz, 1H), 7.85 – 7.78 (m, 1H), 6.95 (d, *J* = 8.0 Hz, 1H), 3.63 (hept, *J* = 6.3 Hz, 1H), 1.27 (d, *J* = 6.4 Hz, 6H).

^{13}C NMR (126 MHz, $CDCl_3$): δ 163.4 (d, *J* = 240.1 Hz), 158.0, 153.7 (d, *J* = 12.5 Hz), 141.6 (d, *J* = 7.4 Hz), 118.6 (d, *J* = 4.1 Hz), 110.7 (d, *J* = 36.9 Hz), 61.6, 24.1.

^{19}F NMR (282 MHz, $CDCl_3$) δ -67.84.

FTIR (NaCl, thin film, cm^{-1}): 2970, 2930, 2868, 1650, 1598, 1578, 1455, 1380, 1362, 1309, 1262, 1228, 1139, 1071, 994, 974, 937, 865, 804, 771, 731, 630.

HRMS (FAB, m/z): calc'd for $C_9H_{12}N_2F$ $[M+H]^+$: 167.0985; found 167.0963.

(*E*)-1-(5-fluoropyridin-2-yl)-*N*-isopropylmethanimine (335)

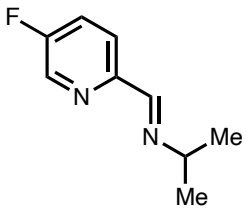

Prepared from 5-fluoropicolinaldehyde (177 mg, 1.41 mmol) and isopropylamine (100.0 mg, 1.70 mmol) following General Procedure 3.2. After concentration in vacuo, **335** (162 mg, 0.98 mmol, 69%) was obtained as a yellow oil.

^{1}H NMR (500 MHz, $CDCl_3$): δ 8.46 (s, 1H), 8.35 (s, 1H), 8.02 (dd, *J* = 8.5, 4.9 Hz, 1H), 7.43 (t, *J* = 8.4 Hz, 1H), 3.62 (hept, *J* = 7.1 Hz, 1H), 1.27 (d, *J* = 6.5 Hz, 6H).

^{13}C NMR (126 MHz, $CDCl_3$): δ 160.2 (d, *J* = 259.2 Hz), 158.0, 151.5 (d, *J* = 3.9 Hz), 137.8 (d, *J* = 24.1 Hz), 123.6 (d, *J* = 18.5 Hz), 122.8 (d, *J* = 5.0 Hz), 61.6, 24.2.

^{19}F NMR (282 MHz, $CDCl_3$) δ -124.70.

FTIR (NaCl, thin film, cm^{-1}): 2970, 2933, 2865, 1647, 1593, 1579, 1478, 1380, 1363, 1312, 1253, 1232, 1143, 1281, 1232, 1143, 1019, 961, 886, 841.

HRMS (FAB, m/z): calc'd for $C_9H_{12}FN_2$ $[M+H]^+$: 167.0985; found 167.0980.

(*E*)-*N*-isopropyl-1-(1-methyl-1H-benzo[d]imidazol-2-yl)methanimine (336)

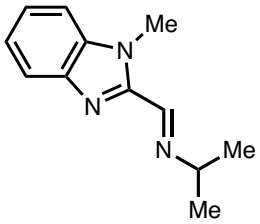

Prepared from 1-methyl-1H-benzo[d]imidazole-2-carbaldehyde (200 mg, 1.25 mmol) and isopropylamine (88.5 mg, 1.50 mmol) following General Procedure 3.2. After concentration in vacuo, **336** (227 mg, 1.13 mmol, 91%) was obtained as a yellow oil.

^{1}H NMR (500 MHz, $CDCl_3$): δ 8.53 (s, 1H), 7.80 (d, *J* = 8.0 Hz, 1H), 7.40 (d, *J* = 8.0 Hz, 1H), 7.38 – 7.32 (m, 1H), 7.29 (t, *J* = 7.5 Hz, 1H), 4.18 (s, 3H), 3.65 – 3.56 (m, 1H), 1.30 (d, *J* = 8.1 Hz, 6H).

^{13}C NMR (126 MHz, $CDCl_3$): δ 151.6, 147.8, 142.6, 137.0, 124.2, 122.7, 120.6, 109.8, 62.4, 31.9, 24.1.

FTIR (NaCl, thin film, cm^{-1}): 2968, 2861, 1471, 1405, 1359, 1336, 1143, 931, 882, 748.

HRMS (ESI-TOF, m/z): calc'd for $C_{12}H_{16}N_3$ $[M+H]^+$: 202.1344; found 202.1315.

(*E*)-*N*-isopropyl-1-(thiazol-2-yl)methanimine (337)

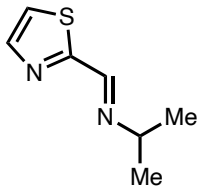

Prepared from thiazole-2-carbaldehyde (200 mg, 1.77 mmol) and isopropylamine (115 mg, 1.94 mmol) following General Procedure 3.2. After concentration in vacuo, **337** (251 mg, 1.63 mmol, 92%) was obtained as a yellow oil.

^{1}H NMR (500 MHz, $CDCl_3$): δ 8.46 (s, 1H), 7.89 (d, *J* = 3.5 Hz, 1H), 7.38 (s, 1H), 3.65 (hept, *J* = 6.4 Hz, 1H), 1.28 (d, *J* = 6.3 Hz, 6H).

^{13}C NMR (126 MHz, $CDCl_3$): δ 167.7, 152.6, 144.0, 121.4, 61.4, 23.9.

FTIR (NaCl, thin film, cm^{-1}): 3080, 2969, 2966, 1636, 1507, 1490, 1458, 1418, 1362, 1294, 1235, 1132, 1058, 945, 853, 775, 733, 691, 629.

HRMS (FAB, m/z): calc'd for $C_7H_{11}N_2S$ $[M+H]^+$: 155.0643; found 155.0652.

(*E*)-*N*-isopropyl-1-(pyrimidin-2-yl)methanimine (338)

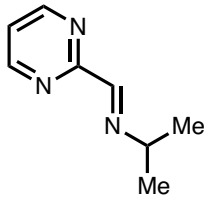

Prepared from pyrimidine-2-carbaldehyde (120 mg, 1.11 mmol) and isopropylamine (72.2 mg, 1.22 mmol) following General Procedure 3.2. After concentration in vacuo, **338** (75.1 mg, 0.50 mmol, 45%) was obtained as a yellow oil.

^{1}H NMR (500 MHz, $CDCl_3$): δ 8.84 (d, *J* = 4.9 Hz, 1H), 8.43 (s, 1H), 7.29 (t, *J* = 5.4 Hz, 2H), 3.72 (hept, *J* = 6.4 Hz, 1H), 1.33 (d, *J* = 6.9 Hz, 6H).

^{13}C NMR (126 MHz, $CDCl_3$): δ 162.3, 158.3, 157.8, 121.2, 62.0, 24.0.

FTIR (NaCl, thin film, cm^{-1}): 3041, 2969, 3938, 3867, 1651, 1561, 1423, 1382, 1365, 1319, 1246, 1144, 994, 964, 944, 898, 818, 793, 634.

HRMS (FAB, m/z): calc'd for $C_8H_{12}N_3$ $[M+H]^+$: 150.1031; found 150.1043.

(*E*)-N-isopropyl-1-(quinolin-2-yl)methanimine (339)

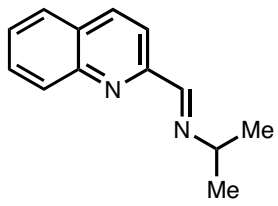

Prepared from quinoline-2-carbaldehyde (250 mg, 1.59 mmol) and isopropylamine (113 mg, 1.91 mmol) following General Procedure 3.2. After concentration in vacuo, **339** (296 mg, 1.50 mmol, 94%) was obtained as a yellow oil.

^{1}H NMR (500 MHz, $CDCl_3$): δ 8.56 (s, 1H), 8.17 (s, 2H), 8.12 (d, *J* = 8.5 Hz, 1H), 7.83 (d, *J* = 8.1 Hz, 1H), 7.73 (t, *J* = 7.7 Hz, 1H), 7.57 (t, *J* = 7.6 Hz, 1H), 3.73 (hept, *J* = 6.2 Hz, 1H), 1.33 (d, *J* = 6.4 Hz, 6H).

^{13}C NMR (126 MHz, $CDCl_3$): δ 160.1, 155.3, 148.0, 136.7, 130.0, 129.7, 128.9, 127.9, 127.5, 118.7, 61.7, 24.2.

FTIR (NaCl, thin film, cm^{-1}): 3061, 2968, 2929, 2865, 1716, 1939, 1596, 1559, 1540, 1505, 1457, 1363, 1338, 1302, 1142, 966, 893, 833, 752, 620.

HRMS (FAB, m/z): calc'd for $C_{13}H_{15}N_2$ $[M+H]^+$: 199.1235; found 199.1210.

(*E*)-*N*-isopropyl-1-phenylmethanimine (317)

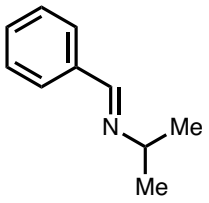

Prepared from benzaldehyde (157 mg, 1.48 mmol) and isopropylamine (105 mg, 1.77 mmol) following General Procedure 3.2. After concentration in vacuo, **317** (215 mg, 1.46 mmol, 99%) was obtained as a yellow oil.

^{1}H NMR (500 MHz, $CDCl_3$): δ 8.31 (s, 1H), 7.77 – 7.69 (m, 2H), 7.40 (t, *J* = 3.9 Hz, 3H), 3.55 (hept, *J* = 6.3 Hz, 1H), 1.28 (d, *J* = 6.3 Hz, 6H).

^{13}C NMR (126 MHz, $CDCl_3$): δ 158.5, 136.7, 130.6, 128.7, 128.2, 61.9, 24.4.

FTIR (NaCl, thin film, cm^{-1}): 3061, 3026, 2967, 2931, 2836, 1647, 1581, 1450, 1382, 1306, 1159, 1141, 967, 881, 755, 693.

HRMS (FAB, m/z): calc'd for $C_{10}H_{14}N$ $[M+H]^+$: 148.1126; found 148.1125

(*E*)-*N*-isopropyl-1-(pyridin-3-yl)methanimine (318)

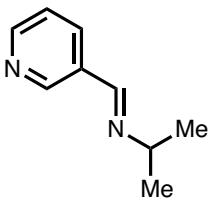

Prepared from nicotinaldehyde (151 mg, 1.41 mmol) and isopropylamine (91.9 mg, 1.55 mmol) following General Procedure 3.2. After concentration in vacuo, **318** (199 mg, 1.34 mmol, 95%) was obtained as a yellow oil.

^{1}H NMR (500 MHz, $CDCl_3$): δ 8.83 (s, 1H), 8.62 (d, *J* = 4.7 Hz, 1H), 8.33 (s, 1H), 8.11 (d, *J* = 5.9 Hz, 1H), 7.36 – 7.29 (m, 1H), 3.57 (hept, *J* = 12.6, 6.3 Hz, 1H), 1.27 (d, *J* = 6.4 Hz, 6H).

^{13}C NMR (126 MHz, $CDCl_3$): δ 155.6, 151.5, 150.4, 134.6, 132.2, 123.8, 62.0, 24.2.

FTIR (NaCl, thin film, cm^{-1}): 2969, 2931, 2864, 1646, 1591, 1575, 1558, 1419, 1385, 1315, 1188, 1142, 1026, 975, 944, 882, 806, 708.

HRMS (FAB, m/z): calc'd for $C_9H_{13}N_2$ $[M+H]^+$: 149.1079; found 149.1086.

((*E*)-N-isopropyl-1-(6-methoxypyridin-2-yl)methanimine (340)

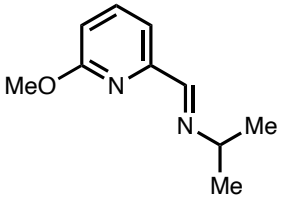

Prepared from 6-methoxypicolinaldehyde (250 mg, 1.82 mmol) and isopropylamine (129 mg, 2.19 mmol) following General Procedure 3.2. After concentration in vacuo, **340** (246 mg, 1.38 mmol, 76%) was obtained as a yellow oil.

^{1}H NMR (500 MHz, $CDCl_3$): δ 8.28 (s, 1H), 7.64 – 7.56 (m, 2H), 6.75 (dd, *J* = 6.0, 3.0 Hz, 1H), 3.97 (s, 3H), 3.62 (p, *J* = 6.3 Hz, 1H), 1.28 (d, *J* = 6.3 Hz, 6H).

^{13}C NMR (126 MHz, $CDCl_3$): δ 164.0, 159.7, 152.7, 139.1, 114.1, 112.0, 61.6, 53.6, 24.2.

FTIR (NaCl, thin film, cm^{-1}): 2968, 2862, 1648, 1592, 1574, 1469, 1434, 1414, 1362, 1324, 1305, 1266, 1139, 1073, 1034, 988, 966, 866, 805, 765, 734, 631.

HRMS (FAB, m/z): calc'd for $C_{10}H_{15}N_2O$ $[M+H]^+$: 179.1184; found 179.1155.

Methyl (*E*)-6-((isopropylimino)methyl)nicotinate (341)

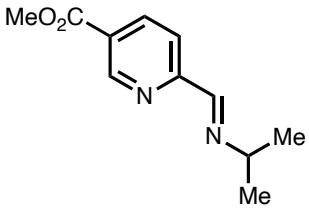

Prepared from methyl-6-formylnicotinate (237 mg, 1.43 mmol) and isopropylamine (127 mg, 2.15 mmol) following General Procedure 3.2. After concentration in vacuo, **341** (294 mg, 1.43 mmol, 99%) was obtained as a brown solid.

^{1}H NMR (500 MHz, $CDCl_3$): δ 9.22 (s, 1H), 8.43 (s, 1H), 8.32 (d, *J* = 8.2 Hz, 1H), 8.08 (d, *J* = 9.7 Hz, 1H), 3.97 (s, 3H), 3.68 (hept, *J* = 6.4 Hz, 1H), 1.30 (d, *J* = 6.4 Hz, 6H).

^{13}C NMR (126 MHz, $CDCl_3$): δ 165.8, 158.7, 158.2, 150.8, 137.8, 126.6, 121.1, 61.9, 52.7, 24.1.

FTIR (NaCl, thin film, cm^{-1}): 2968, 2863, 1721, 1596, 1456, 1388, 1360, 1287, 1194, 1112, 1021, 965, 862, 776.

HRMS (FAB, m/z): calc'd for $C_{11}H_{15}N_2O_2$ $[M+H]^+$: 207.1134; found 207.1131.

(*E*)-1-(5-bromopyridin-2-yl)-*N*-isopropylmethanimine (342)

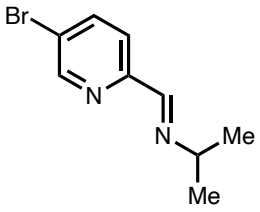

Prepared from 5-bromopicolinaldehyde (247 mg, 1.33 mmol) and isopropylamine (118 mg, 2.00 mmol) following General Procedure 3.2. After concentration in vacuo, **342** (282 mg, 1.24 mmol, 93%) was obtained as a colorless oil.

^{1}H NMR (400 MHz, $CDCl_3$): δ 8.69 (dd, J = 2.2, 0.8 Hz, 1H), 8.33 (d, J = 0.7 Hz, 1H), 7.94 – 7.80 (m, 2H), 3.64 (pd, J = 6.3, 0.8 Hz, 1H), 1.27 (d, J = 6.3 Hz, 6H).

^{13}C NMR (101 MHz, $CDCl_3$): δ 158.34, 153.43, 150.59, 139.34, 122.61, 122.08, 61.60, 24.05.

FTIR (NaCl, thin film, cm^{-1}): 3046, 2969, 2926, 2867, 1645, 1570, 1553, 1462, 1380, 1363, 1314, 1141, 1087, 1006, 963, 945, 881, 837, 630.

HRMS (FAB, m/z): calc'd for $C_9H_{12}N_2Br$ $[M+H]^+$: 227.0184; found 227.0201.

(*E*)-N-isopropyl-1-(isoquinolin-3-yl)methanimine (343)

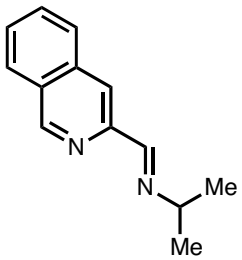

Prepared from isoquinoline-2-carbaldehyde (300 mg, 1.91 mmol) and isopropylamine (135 mg, 2.29 mmol) following General Procedure 3.2. After concentration in vacuo, **343** (370 mg, 1.87 mmol, 98%) was obtained as a yellow oil.

^{1}H NMR (500 MHz, $CDCl_3$): δ 9.28 (s, 1H), 8.57 (s, 1H), 8.26 (s, 1H), 7.98 (d, *J* = 8.1 Hz, 1H), 7.89 (d, *J* = 8.2 Hz, 1H), 7.70 (t, *J* = 7.6 Hz, 1H), 7.63 (t, *J* = 8.3 Hz, 1H), 3.69 (hept, *J* = 5.9 Hz, 1H), 1.34 (d, *J* = 4.8 Hz, 6H).

^{13}C NMR (126 MHz, $CDCl_3$): δ 159.5, 152.8, 148.5, 136.2, 130.9, 129.3, 128.3, 127.8, 127.7, 119.5, 61.9, 24.3.

FTIR (NaCl, thin film, cm^{-1}): 2967, 2924, 2864, 1646, 1624, 1508, 1490, 1379, 1362, 1309, 1272, 1148, 970, 945, 894, 751.

HRMS (FAB, m/z): calc'd for $C_{13}H_{15}N_2$ $[M+H]^+$: 199.1235; found 199.1245.

(*E*)-N-isopropyl-1-(1-methyl-1H-indazol-3-yl)methanimine (344)

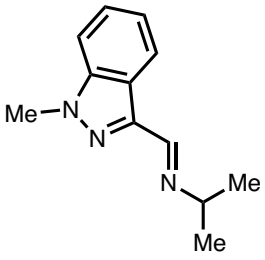

Prepared from 1-methyl-1H-indazole-3-carbaldehyde (200 mg, 1.25 mmol) and isopropylamine (88.6 mg, 1.50 mmol) following General Procedure 3.2. After concentration in vacuo, **344** (208 mg, 1.03 mmol, 83%) was obtained as a yellow oil.

^{1}H NMR (500 MHz, $CDCl_3$): δ 8.63 (d, *J* = 0.8 Hz, 1H), 8.39 (dt, *J* = 8.1, 1.0 Hz, 1H), 7.47 – 7.34 (m, 2H), 7.28 – 7.20 (m, 1H), 4.10 (s, 3H), 3.66 – 3.51 (m, 1H), 1.31 (d, *J* = 6.3 Hz, 6H).

^{13}C NMR (126 MHz, $CDCl_3$): δ 152.4, 142.1, 141.2, 126.8, 123.2, 122.3, 121.9, 108.8, 62.1, 35.8, 24.4.

FTIR (NaCl, thin film, cm^{-1}): 3056, 2966, 2936, 2852, 1644, 1618, 1576, 1487, 1456, 1401, 1377, 1360, 1346, 1294, 1247, 1142, 1062, 1004, 961, 944, 864, 795, 768, 746, 660.

HRMS (FAB, m/z): calc'd for $C_{12}H_{16}N_3$ $[M+H]^+$: 202.1344; found 202.1320.

(*E*)-1-(1H-imidazol-2-yl)-N-isopropylmethanimine (345)

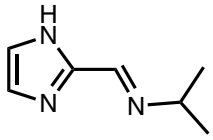

Prepared from 1*H*-imidazole-2-carbaldehyde (1.44 g, 15 mmol) and isopropylamine (1.11 g, 18.8 mmol) following General Procedure 3.2. After concentration in vacuo, **345** (1.87 g, 13.7 mmol, 91%) was obtained as a brown solid.

^{1}H NMR (500 MHz, $CDCl_3$): δ 8.16 (d, *J* = 0.7 Hz, 1H), 7.13 (d, *J* = 1.2 Hz, 1H), 7.06 – 6.98 (m, 1H), 3.52 (pd, *J* = 6.3, 0.8 Hz, 1H), 1.16 (d, *J* = 6.3 Hz, 6H).

^{13}C NMR (126 MHz, $CDCl_3$): δ 149.15, 145.18, 130.58, 117.59, 60.88, 24.00.

FTIR (NaCl, thin film, cm^{-1}): 2963, 1646, 1558, 1446, 1387, 1108, 998, 755, 683.

HRMS (ESI, m/z): calc'd for $C_{17}H_{12}N_3$ $[M+H]^+$: 138.1026; found 138.026.

Synthesis of *N*-hydroxyphthalimide (NHP) Ester Substrates

NHP esters **346-349** were prepared according to procedure reported and referenced by Reisman and coworkers.[36] The NMR spectra of **346** [37], **347** [38], **348** [39], and **349** [39] matched those reported in the literature.

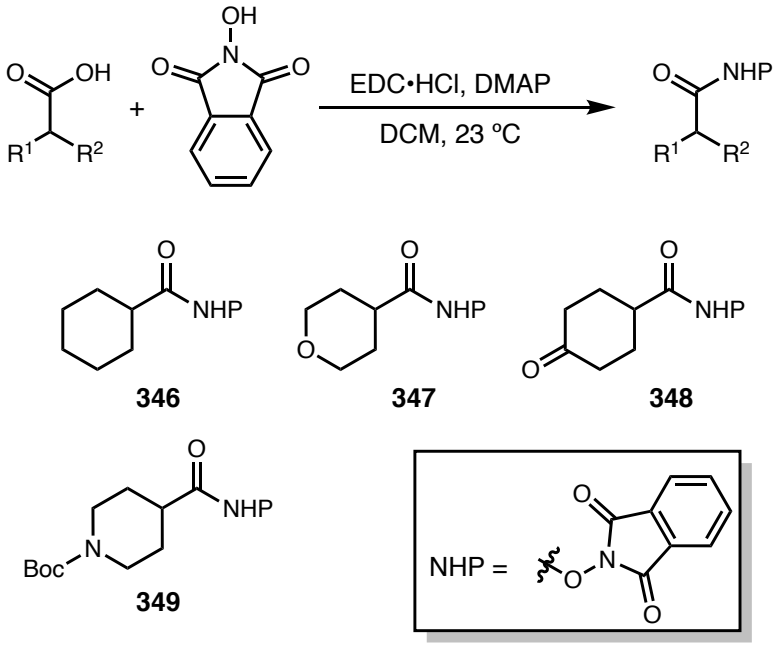

3.5.4 Nickel-Catalyzed Alkylation of Heteroaryl Imines

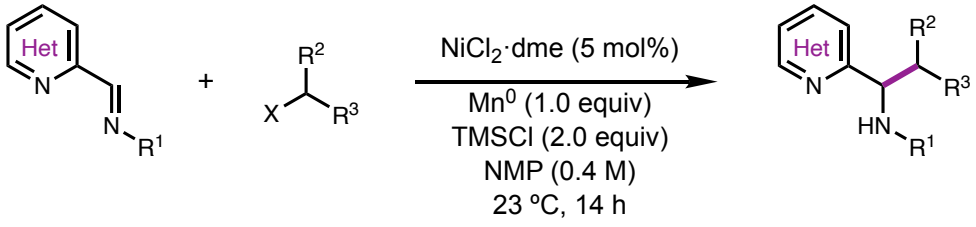

General procedure 3.4: Reaction on 0.3 mmol scale

On the bench-top, an oven-dried 1 dram vial, equipped with a stir bar, was charged with heteroarylimine (0.3 mmol, 1.0 equiv), alkyl halide (if non-volatile, 0.36 mmol, 1.2 equiv),

and Mn^0 (16.5 mg, 0.3 mmol, 1.0 equiv). The vial was brought into a N_2-filled glovebox and a stock-solution of $NiCl_2$·dme in NMP (0.75 ml, 0.02 M, 0.05 equiv [Ni]), TMSCl (76 µl, 0.6 mmol, 2.0 equiv) and alkyl halide (if volatile, 0.36 mmol, 1.2 equiv) was added consecutively. The vial was sealed with a Teflon cap and taken out of the glove box. The vial was sealed with electrical tape and stirred at room temperature for 14 hours at 600 rpm. The resulting suspension was diluted with CH_2Cl_2 (0.5 ml) and extracted 3x with 1N HCl (0.5 ml). To the combined aqueous phases was added K_2CO_3 (s) until gas evolution ceased. The resulting aqueous solution was extracted 3x with EtOAc and the combined organic phases were concentrated under reduced pressure. The crude material was purified by column chromatography to afford the desired product.

Substrates here are not featured in the main text and undergo alkylation under the optimized conditions in poor yields. Products **350-356** were prepared from imines **340-345** reacted under General Procedure 3.2 with 1.2 equivalents of benzyl bromide. Product **353** was prepared from reacting **291** under standard reaction conditions with 1.2 equivalents of 4-iodo-1-tosylpiperidine. Yields are reported as the average of 2 runs based on isolated product on 0.3 mmol scale.

Figure 3.13. *Unsuccessful or challenging substrates under the optimized conditions.*

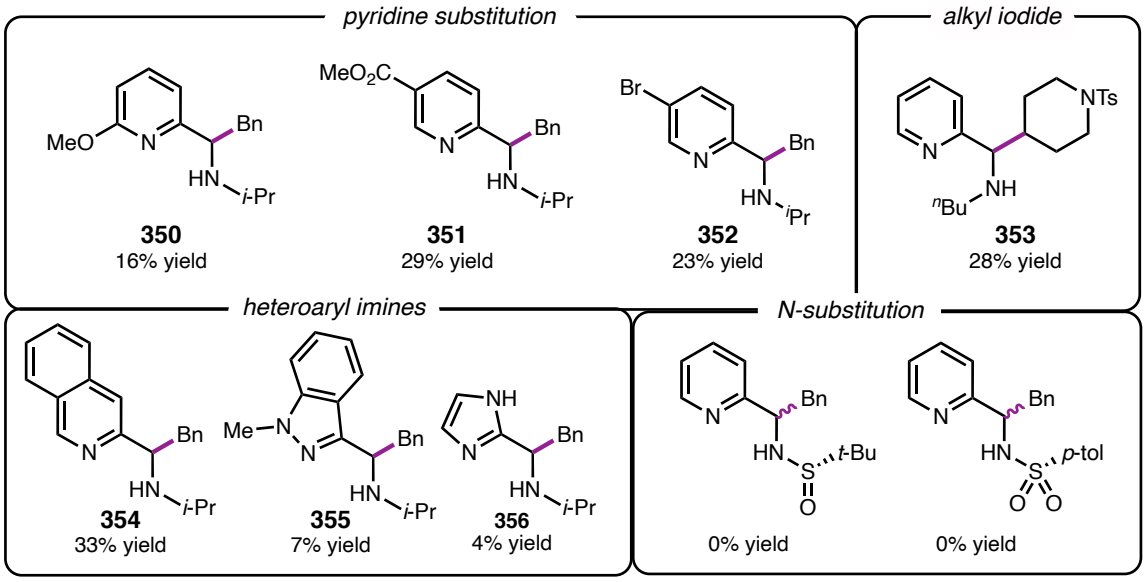

Product Distribution for Reactions with 271 and 2º Alkyl Halides

General Details: All reaction were carried out according to General Procedure 3.4 on a 0.3 mmol scale. Yields determined from quantitative ^{1}H NMR measurements against 1,3,5-trimeoxybenzene or 1,1,2,2-tetrachloroethane. Yields of **311** are reported out of 0.15 mmol theoretical yield of **311**.

Figure 3.14. *Distribution of desired alkylation versus homocoupling across several alkyl electrophiles. Yields of **311** are based on a 0.15 mmol theoretical yield.*

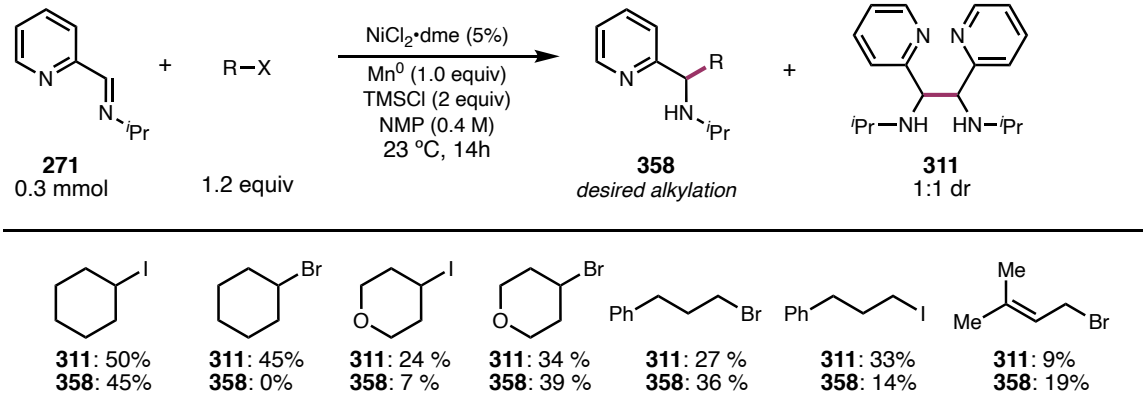

3.5.5 Characterization of Reaction Products:

_N_-(2-phenyl-1-(pyridin-2-yl)ethyl)propan-2-amine (273)

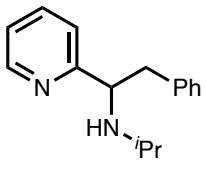

Prepared from imine **271** (44.5 mg, 0.3 mmol) and benzyl bromide (42.8 μL, 0.36 mmol, 1.2 equiv) following General Procedure 3.4. Purification of the crude residue by silica gel column chromatography (Hex/EtOAc 1:1 w/ 1% Et_3N) afforded **273** (56.0 mg, 0.23 mmol, 78%) as a colorless oil. Yield for duplicate run: 54.0 mg, 0.23 mmol, 75% – 76 % average yield.

Reaction was also performed on 1.0 mmol scale to afford **273** (184 mg, 0.77 mmol, 77 %). Yield for duplicate run: 168 mg, 0.70 mmol, 70% – 74% average yield.

R_f = 0.27 (silica, Hex/EtOAc 1:1 w/ 1% Et_3N, UV).

^{1}H NMR (500 MHz, $CDCl_3$): δ 8.58 (d, *J* = 4.7 Hz, 1H), 7.51 (t, *J* = 7.6 Hz, 1H), 7.20 (t, *J* = 7.3 Hz, 2H), 7.18 – 7.08 (m, 2H), 7.05 (dd, *J* = 17.7, 7.6 Hz, 3H), 4.06 (t, *J* = 7.2 Hz, 1H), 3.04 (dd, *J* = 13.2, 7.2 Hz, 1H), 2.98 (dd, *J* = 13.2, 7.2 Hz, 1H), 2.57 (hept, *J* = 6.3 Hz, 1H), 1.77 (s, 1H), 0.96 (d, *J* = 6.2 Hz, 6H).

^{13}C NMR (126 MHz, $CDCl_3$): δ 163.5, 149.6, 139.0, 136.2, 129.4, 128.4, 126.4, 122.8, 122.1, 63.2, 46.2, 43.9, 24.2, 22.2.

FTIR (NaCl, thin film, cm^{-1}): 3328, 3062, 3038, 3005, 2964, 2928, 2868, 1682, 1590, 1572, 1556, 1494, 1470, 1454, 1434, 1379, 1368, 1337, 1295, 1266, 1175, 1148, 1126, 1083, 1049, 1030, 996, 775, 748, 701.

HRMS (ESI-TOF, m/z): calc'd for $C_{16}H_{21}N_2$ $[M+H]^+$: 241.1705; found 241.1693.

_N_-(2-phenyl-1-(pyridin-2-yl)ethyl)butan-1-amine (274)

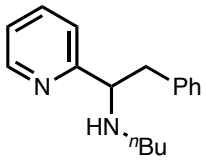

Prepared from imine **291** (48.7 mg, 0.3 mmol) and benzyl bromide (42.8 μL, 0.36 mmol, 1.2 equiv) following General Procedure 3.4. Purification of the crude residue by silica gel column chromatography (Hex/EtOAc 1:1 w/ 1% Et_3N) afforded **274** (56.0 mg, 0.22 mmol, 73%) as a colorless oil. Yield for duplicate run: 57.5 mg, 0.23 mmol, 75% – 74% average yield.

Also prepared from imine **291** (48.7 mg, 0.3 mmol) and benzyl chloride (41.4 μL, 0.36 mmol, 1.2 equiv) following General Procedure 3.4. Purification of the crude residue by silica gel column chromatography (Hex/EtOAc 1:1 w/ 1% Et_3N) afforded **274** (54.6 mg, 0.21 mmol, 72%) as a colorless oil. Yield for duplicate run: 53.9 mg, 0.21 mmol, 71% – 72% average yield.

R_f = 0.30 (silica, Hex/EtOAc 1:1 w/ 1% Et_3N, UV).

^{1}H NMR (500 MHz, $CDCl_3$): δ 8.58 (d, *J* = 4.9 Hz, 1H), 7.56 (td, *J* = 7.6, 1.8 Hz, 1H), 7.22 (t, *J* = 7.3 Hz, 2H), 7.20 – 7.10 (m, 3H), 7.09 (d, *J* = 7.0 Hz, 2H), 3.95 (d, *J* = 7.4 Hz, 1H), 3.07 (dd, *J* = 13.3, 6.5 Hz, 1H), 2.95 (dd, *J* = 13.3, 7.8 Hz, 1H), 2.45 – 2.32 (m, 2H), 1.83 (s, 1H), 1.42 – 1.32 (m, 2H), 1.27 – 1.14 (m, 2H), 0.81 (t, *J* = 7.3 Hz, 3H).

^{13}C NMR (126 MHz, $CDCl_3$): δ 163.3, 149.5, 139.0, 136.4, 129.5, 128.5, 126.5, 122.4, 122.2, 66.1, 47.8, 43.7, 32.4, 20.5, 14.1.

FTIR (NaCl, thin film, cm^{-1}): 3062, 3027, 2956, 2927, 2859, 1589, 1570, 1495, 1456, 1433, 1120, 996, 774, 748, 700, 668.

HRMS (ESI-TOF, m/z): calc'd for $C_{17}H_{23}N_2$ $[M+H]^+$: 255.1861; found 255.1859.

2-methyl-*N*-(2-phenyl-1-(pyridin-2-yl)ethyl)propan-2-amine (275)

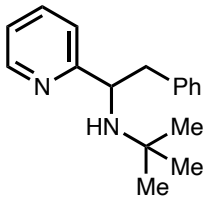

Prepared from imine **325** (48.7 mg, 0.3 mmol) and benzyl bromide (42.8 μL, 0.36 mmol, 1.2 equiv) following General Procedure 3.4. Purification of the crude residue by silica gel column chromatography (Hex/EtOAc 1:1 w/ 1% Et_3N) afforded **275** (60.0 mg, 0.24 mmol, 79%) as a colorless oil. Yield for duplicate run: 55.0 mg, 0.22 mmol, 72% – 76% average yield.

R_f = 0.42 (silica, Hex/EtOAc 1:1 w/ 1% Et_3N, UV).

^{1}H NMR (500 MHz, $CDCl_3$): δ 8.56 (d, *J* = 4.8 Hz, 1H), 7.58 (td, *J* = 7.6, 1.8 Hz, 1H), 7.39 (d, *J* = 8.0 Hz, 1H), 7.31 – 7.24 (m, 2H), 7.25 – 7.18 (m, 1H), 7.17 (d, *J* = 6.9 Hz, 2H), 7.12 (dd, *J* = 6.3, 4.9 Hz, 1H), 4.13 (dd, *J* = 8.9, 5.7 Hz, 1H), 3.06 (dd, *J* = 13.3, 5.7 Hz, 1H), 2.76 (dd, *J* = 13.3, 8.9 Hz, 1H), 1.84 (s, 1H), 0.86 (s, 9H).

^{13}C NMR (126 MHz, $CDCl_3$): δ 166.6, 149.0, 139.2, 136.2, 129.6, 128.5, 126.5, 122.3, 121.7, 60.6, 51.3, 45.6, 29.6.

FTIR (NaCl, thin film, cm^{-1}): 3063, 3027, 2961, 2928, 1590, 1570, 1495, 1472, 1456, 1434, 1388, 1364, 1229, 1108, 1030, 995, 774, 746, 700.

HRMS (ESI-TOF, m/z): calc'd for $C_{17}H_{23}N_2$ $[M+H]^+$: 255.1861; found 255.1848.

***N*-(2-phenyl-1-(pyridin-2-yl)ethyl)cyclopropanamine (276)**

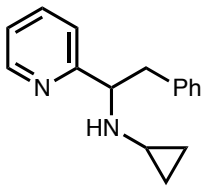

Prepared from imine **357** (43.9 mg, 0.3 mmol) and benzyl bromide (42.8 μL, 0.36 mmol, 1.2 equiv) following General Procedure 3.4. Purification of the crude residue by silica gel column chromatography (Hex/EtOAc 1:1 w/ 1% Et_3N) afforded **276** (50.0 mg, 0.21 mmol, 70%) as a colorless oil. Yield for duplicate run: 46.0 mg, 0.19 mmol, 64% – 67% average yield.

R_f = 0.27 (silica, Hex/EtOAc 1:1 w/ 1% Et_3N, UV).

^{1}H NMR (500 MHz, $CDCl_3$): δ 8.60 (d, *J* = 5.0 Hz, 1H), 7.52 (td, *J* = 7.6, 1.8 Hz, 1H), 7.19 (t, *J* = 7.2 Hz, 2H), 7.17 – 7.10 (m, 2H), 7.06 – 7.00 (m, 3H), 4.05 (t, *J* = 7.2 Hz, 1H), 3.10 – 2.97 (m, 2H), 2.20 (s, 1H), 1.96 – 1.88 (m, 1H), 0.35 – 0.25 (m, 3H), 0.25 – 0.19 (m, 1H).

^{13}C NMR (126 MHz, $CDCl_3$): δ 163.2, 149.6, 139.0, 136.1, 129.5, 128.4, 126.3, 123.1, 122.2, 66.1, 43.2, 29.3, 7.1, 6.1.

FTIR (NaCl, thin film, cm^{-1}): 3325, 2084, 3006, 2928, 1684, 1590, 1570, 1496, 1472, 1455, 1434, 1369, 1338, 1216, 1148, 1088, 1015, 773, 747, 700.

HRMS (FAB, m/z): calc'd for $C_{16}H_{19}N_2$ $[M+H]^+$: 239.1548; found 239.1555.

***N*-(2-phenyl-1-(pyridin-2-yl)ethyl)cyclobutanamine (277)**

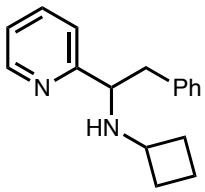

Prepared from imine **326** (48.1 mg, 0.3 mmol) and benzyl bromide (42.8 μL, 0.36 mmol, 1.2 equiv) following General Procedure 3.4. Purification of the crude residue by silica gel column chromatography (Hex/EtOAc 1:1 w/ 1% Et_3N) afforded **277** (54.0 mg, 0.21 mmol, 71%) as a colorless oil. Yield for duplicate run: 52.0 mg, 0.21 mmol, 69% – 70% average yield.

R_f = 0.21 (silica, Hex/EtOAc 1:1 w/ 1% Et_3N, UV).

^{1}H NMR (500 MHz, $CDCl_3$): δ 8.57 (d, *J* = 3.4 Hz, 1H), 7.55 (td, *J* = 7.7, 1.8 Hz, 1H), 7.23 (t, *J* = 7.3 Hz, 2H), 7.20 – 7.10 (m, 3H), 7.09 (d, *J* = 7.0 Hz, 2H), 3.95 (dt, *J* = 1627.0, 7.3 Hz, 1H), 3.12 – 3.02 (m, 2H), 2.93 (dd, *J* = 13.3, 8.0 Hz, 1H), 2.15 – 2.07 (m, 1H), 2.02 (s, 1H), 1.91 – 1.79 (m, 1H), 1.58 – 1.39 (m, 4H).

^{13}C NMR (126 MHz, $CDCl_3$): δ 163.3, 149.4, 138.9, 129.4, 128.5, 126.5, 122.4, 122.2, 63.8, 52.6, 43.6, 31.6, 31.6, 14.8.

FTIR (NaCl, thin film, cm^{-1}): 3321, 3061, 3026, 2968, 2932, 2853, 1590, 1570, 1495, 1472, 1455, 1434, 1340, 1237, 1161, 1119, 1076, 1049, 996, 774, 747, 700.

HRMS (FAB, m/z): calc'd for $C_{17}H_{21}N_2$ $[M+H]^+$: 253.1705; found 253.1691.

2-phenyl-*N*-((*S*)-1-phenylethyl)-1-(pyridin-2-yl)ethan-1-amine (278)

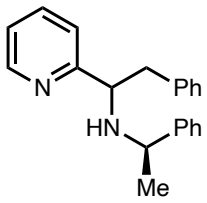

Prepared from imine **327** (63.1 mg, 0.3 mmol) and benzyl bromide (42.8 μL, 0.36 mmol, 1.2 equiv) following General Procedure 3.4. Purification of the crude residue by silica gel column chromatography (Hex/EtOAc 1:1 w/ 1% Et_3N) afforded a 1.8:1 mixture of diastereomers of **278** (55.0 mg, 0.18 mmol, 61%) as a colorless oil. Yield for duplicate run: 43.0 mg, 0.14 mmol, 47% – 54% average yield.

R_f = 0.39 (silica, Hex/EtOAc 1:1 w/ 1% Et_3N, UV).

^{1}H NMR (500 MHz, $CDCl_3$): δ 8.66 (d, *J* = 6.5 Hz, 1H, *minor*), 8.59 (d, *J* = 4.9 Hz, 1H, *major*), 7.57 (td, *J* = 7.6, 1.8 Hz, 1H, *minor*), 7.46 (td, *J* = 7.6, 1.8 Hz, 1H, *major*), 7.28 – 7.16 (m, 17H), 7.11 (dd, *J* = 7.6, 4.8 Hz, 1H, *major*), 7.01 (q, *J* = 9.9, 8.7 Hz, 5H, *major*), 6.93 (d, *J* = 6.6 Hz, 1H, *major*), 4.03 (t, *J* = 7.0 Hz, 1H, *major*), 3.77 (q, *J* = 6.5 Hz, 1H, *major*), 3.71 (dd, *J* = 8.2, 6.4 Hz, 1H, *minor*), 3.46 (q, *J* = 6.6 Hz, 1H, *minor*), 3.15 (dd, *J* = 13.2, 6.6 Hz, 1H, *major*), 3.08 (dd, *J* = 13.2, 7.4 Hz, 1H, *major*), 3.03 (dd, *J* = 13.4, 6.4 Hz, 1H, *minor*), 2.94 (dd, *J* = 13.4, 8.3 Hz, 1H, *minor*), 1.98 (s, 2H), 1.34 (d, *J* = 6.5 Hz, 6H, *major*), 1.27 (d, *J* = 6.6 Hz, 6H, *minor*).

^{13}C NMR (126 MHz, $CDCl_3$): δ 163.4 (*minor*), 163.0 (*major*), 149.8 (*minor*), 149.4 (*major*), 145.9 (*major*), 145.5 (*minor*), 138.99 (*major*), 138.96 (*minor*), 136.2 (*minor*), 136.1 (*major*), 129.54 (*minor*), 129.50 (*major*), 128.49 (*minor*), 128.45 (*major*), 128.35 (*major*), 128.32 (*minor*), 126.93 (*minor*), 126.91 (*major*), 126.8, 126.32 (*minor*), 126.29 (*major*), 122.9 (*minor*), 122.8 (*major*), 122.1 (*minor*), 122.0 (*major*), 63.4 (*major*), 62.6 (*minor*), 55.7, 43.9 (*minor*), 42.9 (*major*), 25.4 (*minor*), 23.2 (*major*).

FTIR (NaCl, thin film, cm^{-1}): 3060, 3026, 3963, 2922, 2860, 1589, 1570, 1493, 1472, 1455, 1435, 1369, 1207, 1127, 748, 700.

HRMS (FAB, m/z): calc'd for $C_{21}H_{23}N_2$ $[M+H]^+$: 303.1861; found 303.1848.

***N*-isopropyl-1-phenyl-2-(pyridin-2-yl)propan-2-amine (279)**

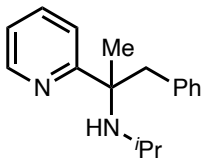

Prepared from imine **328** (48.7 mg, 0.3 mmol) and benzyl bromide (42.8 μL, 0.36 mmol, 1.2 equiv) following General Procedure 3.4. Purification of the crude residue by silica gel column chromatography (Hex/EtOAc 1:1 w/ 1% Et_3N) afforded **279** (28.0 mg, 0.11 mmol, 37%) as a colorless oil. Yield for duplicate run: 28.0 mg, 0.11 mmol, 37% – 37% average yield.

R_f = 0.19 (silica, Hex/EtOAc 1:1 w/ 1% Et_3N, UV).

^{1}H NMR (500 MHz, $CDCl_3$): δ 8.65 (d, *J* = 4.7 Hz, 1H), 7.48 (t, *J* = 7.7 Hz, 1H), 7.15 – 7.09 (m, 1H), 7.06 (dt, *J* = 14.6, 7.6 Hz, 4H), 6.65 (d, *J* = 6.9 Hz, 2H), 3.17 (d, *J* = 12.7 Hz, 1H), 2.95 (d, *J* = 12.7 Hz, 1H), 2.66 (hept, *J* = 6.4 Hz, 1H), 1.50 (s, 3H), 1.08 (d, *J* = 6.1 Hz, 3H), 0.84 (d, *J* = 6.3 Hz, 3H).

^{13}C NMR (126 MHz, $CDCl_3$): δ 165.8, 148.8, 137.9, 135.7, 130.6, 127.7, 126.2, 121.9, 121.6, 62.1, 50.6, 44.4, 26.3, 25.3, 22.4.

FTIR (NaCl, thin film, cm^{-1}): 3337, 3061, 3028, 2960, 2866, 1698, 1587, 1570, 1496, 1456, 1431, 1376, 1339, 1168, 1093, 993, 794, 749, 703, 633.

HRMS (FAB, m/z): calc'd for $C_{17}H_{23}N_2$ $[M+H]^+$: 255.1861; found 255.1843.

***N*-(1-(6-methylpyridin-2-yl)-2-phenylethyl)propan-2-amine (280)**

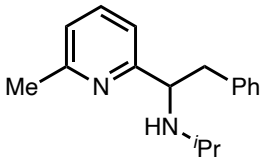

Prepared from imine **329** (48.7 mg, 0.3 mmol) and benzyl bromide (42.8 μL, 0.36 mmol, 1.2 equiv) following General Procedure 3.4. Purification of the crude residue by silica gel column chromatography (Hex/EtOAc 1:1 w/ 1% Et_3N) afforded **280** (39.0 mg, 0.15 mmol, 51%) as a colorless oil. Yield for duplicate run: 38.0 mg, 0.15 mmol, 50% – 50% average yield.

R_f = 0.19 (silica, Hex/EtOAc 1:1 w/ 1% Et_3N, UV).

^{1}H NMR (500 MHz, $CDCl_3$): δ 7.41 (t, *J* = 7.6 Hz, 1H), 7.23 – 7.18 (m, 2H), 7.17 – 7.13 (m, 1H), 7.08 – 7.02 (m, 2H), 6.97 (d, *J* = 7.6 Hz, 1H), 6.88 (d, *J* = 7.6 Hz, 1H), 4.05 (t, *J* = 7.1 Hz, 1H), 3.06 (dd, *J* = 13.3, 7.0 Hz, 1H), 2.96 (dd, *J* = 13.6, 7.2 Hz, 1H), 2.63 – 2.57 (m, 1H), 2.56 (s, 3H), 0.97 (dd, *J* = 6.2, 1.8 Hz, 6H).

^{13}C NMR (126 MHz, $CDCl_3$): δ 162.9, 158.1, 139.1, 136.3, 129.5, 128.4, 126.3, 121.6, 119.5, 63.1, 46.2, 43.8, 24.8, 24.2, 22.3.

FTIR (NaCl, thin film, cm^{-1}): 3325, 3061, 3026, 2961, 2927, 2866, 1592, 1576, 1559, 1456, 1377, 1339, 1170, 1085, 1031, 996, 792, 746, 700.

HRMS (FAB, m/z): calc'd for $C_{17}H_{23}N_2$ $[M+H]^+$: 255.1861; found 255.1865.

_N_-(1-(4-methylpyridin-2-yl)-2-phenylethyl)propan-2-amine (281)

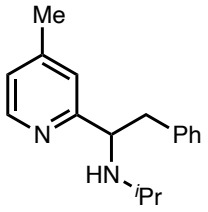

Prepared from imine **330** (48.7 mg, 0.3 mmol) and benzyl bromide (42.8 μL, 0.36 mmol, 1.2 equiv) following General Procedure 3.4. Purification of the crude residue by silica gel column chromatography (Hex/EtOAc 1:1 w/ 1% Et_3N) afforded **281**(57.0 mg, 0.23 mmol, 75%) as a colorless oil. Yield for duplicate run: 55.0 mg, 0.14 mmol, 72% – 74% average yield.

R_f = 0.16 (silica, Hex/EtOAc 1:1 w/ 1% Et_3N, UV).

^{1}H NMR (500 MHz, $CDCl_3$): δ 8.42 (d, *J* = 5.0 Hz, 1H), 7.20 (dd, *J* = 8.0, 6.4 Hz, 2H), 7.15 (t, *J* = 7.3 Hz, 1H), 7.05 (d, *J* = 7.1 Hz, 2H), 6.94 (d, *J* = 5.1 Hz, 1H), 6.91 (s, 1H), 4.02 (t, *J* = 7.2 Hz, 1H), 3.04 (dd, *J* = 13.3, 7.0 Hz, 1H), 2.94 (dd, *J* = 13.3, 7.4 Hz, 1H), 2.57 (p, *J* = 6.2 Hz, 1H), 2.26 (s, 3H), 0.95 (t, *J* = 6.6 Hz, 6H).

^{13}C NMR (126 MHz, $CDCl_3$): δ 163.2, 149.2, 147.3, 139.1, 129.4, 128.4, 126.3, 123.5, 123.1, 63.1, 46.2, 43.8, 24.2, 22.2, 21.2.

FTIR (NaCl, thin film, cm^{-1}): 3307, 3059, 3026, 2962, 2924, 2865, 1604, 1559, 1455, 1378, 1339, 1174, 1084, 1030, 998, 823, 743, 700.

HRMS (FAB, m/z): calc'd for $C_{17}H_{23}N_2$ $[M+H]^+$: 255.1861; found 255.1859.

_N_-(1-(5-methoxypyridin-2-yl)-2-phenylethyl)propan-2-amine (282)

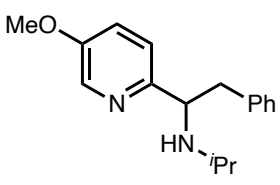

Prepared from imine **331** (53.5 mg, 0.3 mmol) and benzyl bromide (42.8 μL, 0.36 mmol, 1.2 equiv) following General Procedure 3.4. Purification of the crude residue by silica gel column chromatography (Hex/EtOAc 1:1 w/ 1% Et_3N) afforded **282** (54.0 mg, 0.20 mmol, 67%) as a colorless oil. Yield for duplicate run: 51.0 mg, 0.019 mmol, 63% – 65% average yield.

R_f = 0.16 (silica, Hex/EtOAc 1:1 w/ 1% Et_3N, UV).

^{1}H NMR (500 MHz, $CDCl_3$): δ 8.28 (d, *J* = 2.9 Hz, 1H), 7.23 – 7.16 (m, 2H), 7.17 – 7.11 (m, 1H), 7.07 – 7.00 (m, 3H), 6.97 (d, *J* = 8.5 Hz, 1H), 4.02 (t, *J* = 7.2 Hz, 1H), 3.84 (s, 3H), 3.05 – 2.93 (m, 2H), 2.55 (hept, *J* = 6.2 Hz, 1H), 1.83 (s, 1H), 0.95 (dd, *J* = 6.2, 2.6 Hz, 6H).

^{13}C NMR (126 MHz, $CDCl_3$): δ 155.3, 154.6, 139.1, 137.1, 129.4, 128.4, 126.3, 122.9, 120.6, 62.4, 55.8, 46.1, 43.9, 24.2, 22.2.

FTIR (NaCl, thin film, cm^{-1}): 3026, 2961, 2837, 1574, 1491, 1475, 1396, 1339, 1266, 1176, 1125, 1078, 1032, 831, 749, 700.

HRMS (FAB, m/z): calc'd for $C_{17}H_{23}N_2O$ $[M+H]^+$: 271.1810; found 271.1804.

***N*-(1-(4-methoxypyridin-2-yl)-2-phenylethyl)propan-2-amine (283)**

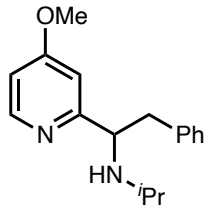

Prepared from imine **332** (53.5 mg, 0.3 mmol) and benzyl bromide (42.8 μL, 0.36 mmol, 1.2 equiv) following General Procedure 3.4. Purification of the crude residue by silica gel column chromatography (Hex/EtOAc 1:1 w/ 1% Et_3N) afforded **283** (60.0 mg, 0.22 mmol, 74%) as a colorless oil. Yield for duplicate run: 56.0 mg, 0.21 mmol, 69% – 72% average yield.

R_f = 0.13 (silica, Hex/EtOAc 1:1 w/ 1% Et_3N, UV).

^{1}H NMR (500 MHz, $CDCl_3$): δ 8.41 – 8.36 (m, 1H), 7.24 – 7.18 (m, 2H), 7.18 – 7.12 (m, 1H), 7.07 (d, *J* = 7.0 Hz, 2H), 6.68 – 6.62 (m, 2H), 4.01 (t, *J* = 7.2 Hz, 1H), 3.75 (s, 3H), 3.04 (dd, *J* = 13.3, 6.9 Hz, 1H), 2.92 (dd, *J* = 13.3, 7.5 Hz, 1H), 2.57 (hept, *J* = 6.2 Hz, 1H), 1.92 (s, 1H), 0.96 (d, *J* = 6.3 Hz, 3H), 0.94 (d, *J* = 6.1 Hz, 3H).

^{13}C NMR (126 MHz, $CDCl_3$): δ 166.0, 165.5, 150.6, 139.0, 129.4, 128.4, 126.4, 108.6, 108.2, 63.3, 55.2, 46.3, 43.7, 24.2, 22.2.

FTIR (NaCl, thin film, cm^{-1}): δ 3025, 2963, 1596, 1569, 1479, 1457, 1367, 1302, 1166, 1039, 994, 820, 742, 700.

HRMS (FAB, m/z): calc'd for $C_{17}H_{23}N_2O$ $[M+H]^+$: 271.1810; found 271.1796.

***N*-(1-(4-chloropyridin-2-yl)-2-phenylethyl)propan-2-amine (284)**

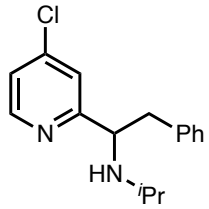

Prepared from imine **333**(54.8 mg, 0.3 mmol) and benzyl bromide (42.8 μL, 0.36 mmol, 1.2 equiv) following General Procedure 3.4. Purification of the crude residue by silica gel column chromatography (Hex/EtOAc 1:1 w/ 1% Et_3N) afforded **284** (35.0 mg, 0.13 mmol, 42%) as a colorless oil. Yield for duplicate run: 34.0 mg, 0.12 mmol, 41% – 42% average yield.

R_f = 0.32 (silica, Hex/EtOAc 1:1 w/ 1% Et_3N, UV).

^{1}H NMR (500 MHz, $CDCl_3$): δ 8.46 (d, *J* = 5.3 Hz, 1H), 7.26 – 7.16 (m, 4H), 7.14 (dd, *J* = 5.3, 2.0 Hz, 1H), 7.09 – 7.04 (m, 2H), 4.09 – 4.02 (m, 1H), 3.04 (dd, *J* = 13.4, 6.6 Hz, 1H), 2.90 (dd, *J* = 13.4, 7.7 Hz, 1H), 2.55 (hept, *J* = 6.3 Hz, 1H), 1.71 (s, 1H), 0.94 (dd, *J* = 10.9, 6.2 Hz, 6H).

^{13}C NMR (126 MHz, $CDCl_3$): δ 165.9, 150.3, 144.4, 138.5, 129.4, 128.6, 126.6, 122.8, 122.5, 63.1, 46.5, 43.7, 24.2, 22.2.

FTIR (NaCl, thin film, cm^{-1}): 3027, 2963, 2928, 2865, 1697, 1574, 1557, 1457, 1389, 1367, 1339, 1174, 1127, 1096, 826, 745, 700.

HRMS (FAB, m/z): calc'd for $C_{16}H_{20}N_2Cl$ $[M+H]^+$: 275.1315; found 275.1330.

***N*-(1-(6-fluoropyridin-2-yl)-2-phenylethyl)propan-2-amine (285)**

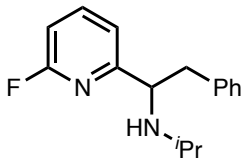

Prepared from imine **334** (49.9 mg, 0.3 mmol) and benzyl bromide (42.8 μL, 0.36 mmol, 1.2 equiv) following General Procedure 3.4. Purification of the crude residue by silica gel column chromatography (Hex/EtOAc 1:1 w/ 1% Et_3N) afforded **285** (35.0 mg, 0.14 mmol, 45%) as a colorless oil. Yield for duplicate run: 34.0 mg, 0.13 mmol, 44% – 44% average yield.

R_f = 0.35 (silica, Hex/EtOAc 1:1 w/ 1% Et_3N, UV).

^{1}H NMR (500 MHz, $CDCl_3$): δ 7.59 (q, *J* = 7.9 Hz, 1H), 7.23 – 7.11 (m, 3H), 7.02 (d, *J* = 6.7 Hz, 2H), 6.92 (dd, *J* = 7.3, 2.5 Hz, 1H), 6.75 (dd, *J* = 8.0, 2.8 Hz, 1H), 4.00 (t, *J* = 7.2 Hz, 1H), 3.00 (qd, *J* = 13.3, 7.2 Hz, 2H), 2.56 (hept, *J* = 6.2 Hz, 1H), 1.85 (s, 1H), 0.97 (dd, *J* = 11.7, 6.2 Hz, 6H).

^{13}C NMR (126 MHz, $CDCl_3$): δ 163.8 (d, *J* = 216.9 Hz), 162.8 (d, *J* = 10.6 Hz), 141.1 (d, *J* = 7.7 Hz), 138.6, 129.4, 128.5, 126.5, 120.0 (d, *J* = 3.9 Hz), 107.6 (d, *J* = 37.1 Hz), 62.5, 46.2, 43.4, 24.2, 22.1.

^{19}F NMR (282 MHz, $CDCl_3$): δ -67.71.

FTIR (NaCl, thin film, cm^{-1}): 3322, 3063, 3028, 2964, 2926, 2866, 1603, 1575, 1494, 1445, 1380, 1368, 1338, 1269, 1222, 1174, 1147, 1070, 995, 943, 916, 894, 845, 802, 744, 701.

HRMS (FAB, m/z): calc'd for $C_{16}H_{20}N_2F$ $[M+H]^+$: 259.1611; found 259.1598.

***N*-(1-(5-fluoropyridin-2-yl)-2-phenylethyl)propan-2-amine (286)**

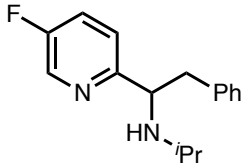

Prepared from imine **335** (49.9 mg, 0.3 mmol) and benzyl bromide (42.8 μL, 0.36 mmol, 1.2 equiv) following General Procedure 3.4.

Purification of the crude residue by silica gel column chromatography (Hex/EtOAc 1:1 w/ 1% Et_3N) afforded **286** (48.9 mg, 0.19 mmol, 63%) as a colorless oil. Yield for duplicate run: 43.0 mg, 0.17 mmol, 55% – 59% average yield.

R_f = 0.29 (silica, Hex/EtOAc 1:1 w/ 1% Et_3N, UV).

^{1}H NMR (500 MHz, $CDCl_3$): δ 8.43 (s, 1H), 7.26 – 7.12 (m, 4H), 7.07 (dd, *J* = 8.7, 4.5 Hz, 1H), 7.02 (d, *J* = 7.3 Hz, 2H), 4.08 (t, *J* = 7.2 Hz, 1H), 3.03 – 2.92 (m, 2H), 2.55 (hept, *J* = 6.3 Hz, 1H), 1.85 (s, 1H), 0.95 (d, *J* = 6.1 Hz, 6H).

^{13}C NMR (126 MHz, $CDCl_3$): δ 159.48 (d, *J* = 3.7 Hz), 158.5 (d, *J* = 254 Hz), 157.5, 138.7, 137.6 (d, *J* = 23.5 Hz), 129.4, 128.5, 126.5, 123.4 (d, *J* = 3.9 Hz), 122.9 (d, *J* = 17.8 Hz), 62.6, 46.3, 43.9, 24.2, 22.2.

^{19}F NMR (282 MHz, $CDCl_3$): δ -130.02.

FTIR (NaCl, thin film, cm^{-1}): 3062, 3027, 2963, 3928, 2867, 1683, 1584, 1480, 1455, 1388, 1368, 1340, 1225, 1171, 1112, 1020, 956, 909, 838, 750, 700.

HRMS (FAB, m/z): calc'd for $C_{16}H_{20}N_2F$ $[M+H]^+$: 259.1611; found 259.1610.

***N*-(1-(1-methyl-1H-benzo[d]imidazol-2-yl)-2-phenylethyl)propan-2-amine (287)**

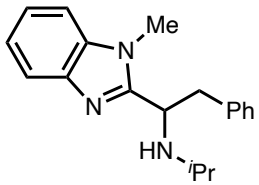

Prepared from imine **336** (60.4 mg, 0.3 mmol) and benzyl bromide (42.8 μL, 0.36 mmol, 1.2 equiv) following General Procedure 3.4. Purification of the crude residue by silica gel column chromatography (Hex/EtOAc 1:1 w/ 1% Et_3N) afforded **287** (67.0 mg, 0.23 mmol, 76%) as a colorless oil. Yield for duplicate run: 64.0 mg, 0.22 mmol, 73% – 74% average yield.

R_f = 0.09 (silica, Hex/EtOAc 1:1 w/ 1% Et_3N, UV).

^{1}H NMR (500 MHz, $CDCl_3$): δ 7.79 (d, *J* = 7.5 Hz, 1H), 7.32 – 7.13 (m, 6H), 6.98 (d, *J* = 4.6 Hz, 2H), 4.30 (dd, *J* = 9.1, 5.9 Hz, 1H), 3.33 (dd, *J* = 12.9, 5.7 Hz, 1H), 3.27 (s, 3H), 3.19 – 3.11 (m, 1H), 2.72 (hept, *J* = 6.0 Hz, 1H), 2.20 (s, 1H), 1.04 (dd, *J* = 14.3, 6.2 Hz, 6H).

^{13}C NMR (126 MHz, $CDCl_3$): δ 156.8, 142.6, 138.1, 135.7, 129.4, 128.6, 126.8, 122.3, 122.1, 119.5, 109.4, 55.5, 46.2, 43.2, 29.3, 23.9, 22.2.

FTIR (NaCl, thin film, cm^{-1}): 3322, 3028, 2963, 1670, 1472, 1406, 1338, 1281, 1239, 1175, 1084, 1007, 852, 745, 702, 681.

HRMS (FAB, m/z): calc'd for $C_{19}H_{24}N_3$ $[M+H]^+$: 294.1970; found 294.1973.

***N*-(2-phenyl-1-(thiazol-2-yl)ethyl)propan-2-amine (288)**

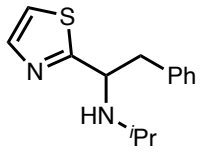

Prepared from imine **337** (61.6 mg, 0.3 mmol) and benzyl bromide (42.8 μL, 0.36 mmol, 1.2 equiv) following General Procedure 3.4. Purification of the crude residue by silica gel column chromatography (Hex/EtOAc 1:1 w/ 1% Et_3N) afforded **288** (40.0 mg, 0.16 mmol, 54%) as a colorless oil. Yield for duplicate run: 37.0 mg, 0.15 mmol, 50% – 52% average yield.

R_f = 0.41 (silica, Hex/EtOAc 1:1 w/ 1% Et_3N, UV).

^{1}H NMR (500 MHz, $CDCl_3$): δ 7.76 (d, *J* = 3.3 Hz, 1H), 7.35 – 7.28 (m, 2H), 7.28 – 7.23 (m, 2H), 7.23 – 7.19 (m, 2H), 4.41 (dd, *J* = 9.0, 5.1 Hz, 1H), 3.28 (dd, *J* = 13.6, 5.1 Hz, 1H), 2.91 (dd, *J* = 13.6, 9.0 Hz, 1H), 2.71 (hept, *J* = 6.3 Hz, 1H), 1.64 (s, 1H), 1.01 (d, *J* = 6.4 Hz, 3H), 0.89 (d, *J* = 6.1 Hz, 3H).

^{13}C NMR (126 MHz, $CDCl_3$): δ 178.1, 142.7, 137.8, 129.4, 128.8, 127.0, 118.9, 59.8, 47.3, 44.3, 24.1, 22.2.

FTIR (NaCl, thin film, cm^{-1}): 3064, 3028, 2961, 2925, 2864, 1698, 1497, 1473, 1456, 1381, 1368, 1319, 1177, 1124, 1056, 773, 726, 700.

HRMS (FAB, m/z): calc'd for $C_{16}H_{21}N_2$ $[M+H]^+$: 247.1269; found 247.1244.

***N*-(2-phenyl-1-(pyrimidin-2-yl)ethyl)propan-2-amine (289)**

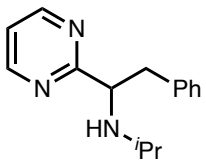

Prepared from imine **338** (44.8 mg, 0.3 mmol) and benzyl bromide (42.8 μL, 0.36 mmol, 1.2 equiv) following General Procedure 3.4. Purification of the crude residue by silica gel column chromatography (Hex/EtOAc 1:1 w/ 1% Et_3N) afforded **289** (36.0 mg, 0.15 mmol, 50%) as a colorless oil. Yield for duplicate run: 34.0 mg, 0.14 mmol, 47% – 48% average yield.

R_f = 0.10 (silica, Hex/EtOAc 1:1 w/ 1% Et_3N, UV).

^{1}H NMR (500 MHz, $CDCl_3$): δ 8.63 (d, *J* = 6.7 Hz, 2H), 7.20 – 7.07 (m, 4H), 7.01 (d, *J* = 7.2 Hz, 2H), 4.27 (t, *J* = 7.2 Hz, 2H), 3.15 (dd, *J* = 13.4, 6.6 Hz, 1H), 3.06 (dd, *J* = 13.4, 7.7 Hz, 1H), 2.58 (hept, *J* = 6.1 Hz, 1H), 1.94 (s, 1H), 1.01 (d, *J* = 6.2 Hz, 3H), 0.96 (d, *J* = 6.2 Hz, 3H).

^{13}C NMR (126 MHz, $CDCl_3$): δ 172.8, 157.0, 138.4, 129.3, 128.4, 126.3, 119.2, 63.8, 46.5, 42.9, 24.0, 22.4.

FTIR (NaCl, thin film, cm^{-1}): 3420, 3029, 2965, 2866, 1561, 1541, 1496, 1455, 1437, 1418, 1380, 1339, 1174, 1085, 1030, 995, 805, 751, 700.

HRMS (FAB, m/z): calc'd for $C_{15}H_{20}N_3$ $[M+H]^+$: 242.1657; found 242.1662.

***N*-(2-phenyl-1-(quinolin-2-yl)ethyl)propan-2-amine (290)**

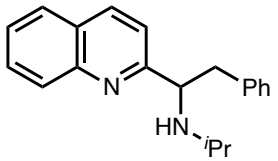

Prepared from imine **339** (59.5 mg, 0.3 mmol) and benzyl bromide (42.8 μL, 0.36 mmol, 1.2 equiv) following General Procedure 3.4. Purification of the crude residue by silica gel column chromatography (Hex/EtOAc 1:1 w/ 1% Et_3N) afforded **290** (44.0 mg, 0.15 mmol, 51%) as a colorless oil. Yield for duplicate run: 43.5 mg, 0.15 mmol, 50% – 50% average yield.

R_f = 0.31 (silica, Hex/EtOAc 1:1 w/ 1% Et_3N, UV).

^{1}H NMR (500 MHz, $CDCl_3$): δ 8.10 (d, *J* = 8.4 Hz, 1H), 8.04 (d, *J* = 9.2 Hz, 1H), 7.79 (d, *J* = 8.1 Hz, 1H), 7.70 (t, *J* = 7.7 Hz, 1H), 7.51 (t, *J* = 7.5 Hz, 1H), 7.37 (d, *J* = 8.4 Hz, 1H), 7.25 – 7.11 (m, 5H), 4.31 (t, *J* = 7.2 Hz, 1H), 3.15 (dd, *J* = 13.5, 6.4 Hz, 1H), 3.00 (dd, *J* = 13.5, 8.0 Hz, 1H), 2.61 (hept, *J* = 5.9 Hz, 1H), 1.80 (s, 1H), 0.96 (dd, *J* = 14.4, 4.7 Hz, 6H).

^{13}C NMR (126 MHz, $CDCl_3$): δ 164.8, 148.0, 138.8, 136.2, 129.5, 129.4, 129.3, 128.5, 127.8, 127.7, 126.5, 126.1, 120.6, 64.0, 46.8, 43.9, 24.3, 22.4.

FTIR (NaCl, thin film, cm^{-1}): 3028, 2961, 2928, 1618, 1600, 1558, 1540, 1506, 1473, 1456, 1379, 1169, 826, 750, 700.

HRMS (FAB, m/z): calc'd for $C_{20}H_{23}N_2$ $[M+H]^+$: 291.1861; found 291.1876.

***N*-(2-(4-chlorophenyl)-1-(pyridin-2-yl)ethyl)propan-2-amine (292)**

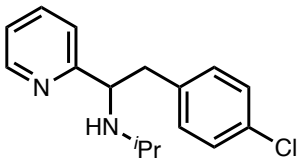

Prepared from imine **271** (44.5 mg, 0.3 mmol) and 1-(bromomethyl)-4-chlorobenzene (74.0 mg, 0.36 mmol) and following General Procedure 3.4. Purification of the crude residue by silica gel column chromatography (Hex/EtOAc 1:1 w/ 1% Et_3N) afforded **292**

(64.1 mg, 0.23 mmol, 78%) as a colorless oil. Yield for duplicate run: 53.3 mg, 0.20 mmol, 65% – 72% average yield.

R_f = 0.24 (silica, Hex/EtOAc 1:1 w/ 1% Et_3N, UV).

^{1}H NMR (400 MHz, $CDCl_3$): 8.50 (ddd, J = 4.8, 1.8, 0.9 Hz, 1H), 7.44 (td, J = 7.6, 1.8 Hz, 1H), 7.11 – 7.01 (m, 3H), 6.95 (dt, J = 7.8, 1.1 Hz, 1H), 6.89 – 6.83 (m, 2H), 3.93 (t, J = 7.2 Hz, 1H), 2.90 (dd, J = 7.2, 1.6 Hz, 2H), 2.48 (p, J = 6.3 Hz, 1H), 1.84 (s, 1H), 0.88 (dd, J = 6.2, 1.3 Hz, 6H).

^{13}C NMR (101 MHz, $CDCl_3$): δ 162.83, 149.46, 137.30, 136.03, 131.91, 130.57, 128.28, 122.64, 122.00, 62.81, 45.94, 42.90, 23.99, 22.04.

FTIR (NaCl, thin film, cm^{-1}): 3309, 3005, 2962, 2925, 2865, 1589, 1570, 1490, 1469, 1433, 1379, 1367, 1338, 1174, 1092, 1015, 812, 776, 748.

HRMS (FAB, m/z): calc'd for $C_{16}H_{20}N_2Cl$ $[M+H]^+$: 275.1315; found: 275.1328.

Methyl 4-(2-(isopropylamino)-2-(pyridin-2-yl)ethyl)benzoate (293)

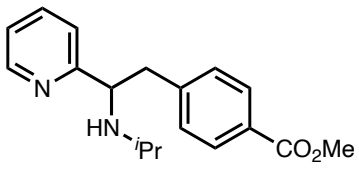

Prepared from imine **271** (44.5 mg, 0.3 mmol) and methyl 4-(bromomethyl)benzoate (82.5 mg, 0.36 mmol) following General Procedure 3.4. Purification of the crude residue by silica gel column chromatography (Hex/EtOAc 1:1 w/ 1% Et_3N) afforded **293** (68.1 mg, 0.23 mmol, 76%) as a white solid. Yield for duplicate run: 55.7 mg, 0.19 mmol, 62% – 69% average yield.

R_f = 0.21 (silica, Hex/EtOAc 1:1 w/ 1% Et_3N, UV).

^{1}H NMR (400 MHz, $CDCl_3$): 8.48 (ddd, J = 4.8, 1.8, 0.9 Hz, 1H), 7.88 – 7.66 (m, 2H), 7.39 (td, J = 7.6, 1.8 Hz, 1H), 7.09 – 6.93 (m, 3H), 6.89 (dt, J = 7.8, 1.1 Hz, 1H), 3.95 (t, J

= 7.2 Hz, 1H), 3.77 (s, 3H), 2.96 (d, J = 7.2 Hz, 2H), 2.46 (p, J = 6.2 Hz, 1H), 1.86 (s, 2H), 0.85 (d, J = 6.3 Hz, 7H).

^{13}C NMR (101 MHz, $CDCl_3$): 162.22, 149.64, 144.73, 136.12, 131.91, 130.04, 122.62, 122.20, 119.02, 109.97, 62.46, 45.84, 43.61, 23.96, 22.05.

FTIR (NaCl, thin film, cm^{-1}): 3311**,** 2960, 2867, 1721, 1609, 1589, 1570, 1469, 1434, 1414, 1309, 1280, 1178, 1111, 765, 749, 706.

HRMS (FAB, m/z): calc'd for $C_{18}H_{23}N_2O_2$ $[M+H]^+$: 299.1760; found: 299.1767.

4-(2-(isopropylamino)-2-(pyridin-2-yl)ethyl)benzonitrile (294)

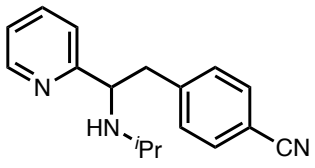

Prepared from imine **271** (44.5 mg, 0.3 mmol) and 4-(bromomethyl)benzonitrile (70.6 mg, 0.36 mmol) following General Procedure 3.4. Purification of the crude residue by silica gel column chromatography (Hex/EtOAc 1:1 w/ 1% Et_3N) afforded **294** (55.2mg, 0.21 mmol, 69%) as a white solid. Yield for duplicate run: 51.4 mg, 0.20 mmol, 65% – 67% average yield.

R_f = 0.15 (silica, EtOAc, UV).

^{1}H NMR (500 MHz, $CDCl_3$): δ 8.67 – 8.51 (m, 1H), 7.52 (td, *J* = 7.6, 1.8 Hz, 1H), 7.49 – 7.43 (m, 2H), 7.14 (ddd, *J* = 7.6, 4.8, 1.2 Hz, 1H), 7.10 (d, *J* = 8.0 Hz, 2H), 6.97 (d, *J* = 7.7 Hz, 1H), 4.02 (t, *J* = 7.2 Hz, 1H), 3.15 – 2.95 (m, 2H), 2.56 (hept, *J* = 6.1 Hz, 1H), 1.26 (d, *J* = 3.1 Hz, 1H), 0.98 (d, *J* = 6.2 Hz, 6H).

^{13}C NMR (101 MHz, $CDCl_3$):δ 162.22, 149.64, 144.73, 136.12, 131.91, 130.04, 122.62, 122.20, 119.02, 109.97, 62.46, 45.84, 43.61, 23.96, 22.05.

FTIR (NaCl, thin film, cm^{-1}): 3316, 3049, 2962, 2929, 2866, 2226, 1606, 1589, 1570, 1505, 1470, 1433, 1379, 1337, 1175, 1147, 996, 823, 780, 751.

HRMS (FAB, m/z): calc'd for $C_{17}H_{20}N_3$ $[M+H]^+$: 266.1657; found: 266.1677.

***N*-(1-(pyridin-2-yl)-2-(*o*-tolyl)ethyl)propan-2-amine (295)**

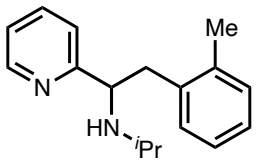

Prepared from imine **271** (44.5 mg, 0.3 mmol) and 1-(bromomethyl)-2-methylbenzene (66.6 mg, 0.36 mmol) following General Procedure 3.4. Purification of the crude residue by silica gel column chromatography (Hex/EtOAc 1:1 w/ 1% Et_3N) afforded **295** (60.0 mg, 0.24 mmol, 79%) as a white solid. Yield for duplicate run: 56.3 mg, 0.22 mmol, 74% – 76% average yield.

R_f = 0.18 (silica, Hex/EtOAc 1:1 w/ 1% Et_3N, UV).

^{1}H NMR (400 MHz, $CDCl_3$): δ 8.47 (ddd, *J* = 4.8, 1.9, 1.0 Hz, 1H), 7.35 (td, *J* = 7.6, 1.8 Hz, 1H), 7.02 – 6.92 (m, 3H), 6.92 – 6.86 (m, 1H), 6.83 (dt, *J* = 7.8, 1.1 Hz, 1H), 6.81 – 6.76 (m, 1H), 3.93 (dd, *J* = 8.0, 6.5 Hz, 1H), 3.04 – 2.77 (m, 2H), 2.46 (p, *J* = 6.2 Hz, 1H), 2.08 (s, 3H), 2.03 – 1.90 (s, 1H), 0.96 – 0.79 (m, 6H).

^{13}C NMR (101 MHz, $CDCl_3$): δ 163.33, 149.40, 137.07, 136.54, 135.83, 130.15, 129.95, 126.21, 125.62, 122.74, 121.89, 61.89, 46.03, 40.99, 24.04, 22.12, 19.42.

FTIR (NaCl, thin film, cm^{-1}): 3317, 3061, 3009, 2961, 2928, 2864, 1681, 1589, 1569, 1468, 1432, 1378, 1365, 1339, 1169, 1147, 1125, 1049, 995, 841, 781, 741.

HRMS (FAB, m/z): calc'd for $C_{17}H_{23}N_2$ $[M+H]^+$: 255.1861; found: 255.1864.

***N*-(2-(2,6-dimethylphenyl)-1-(pyridin-2-yl)ethyl)propan-2-amine (296)**

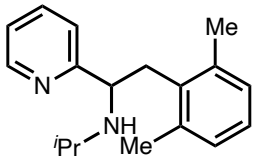

Prepared from imine **271** (44.5 mg, 0.3 mmol) and 2-(bromomethyl)-1,3-dimethylbenzene (71.6 mg, 0.36 mmol) following General

Procedure 3.4. Purification of the crude residue by silica gel column chromatography (Hex/EtOAc 1:1 w/ 1% Et_3N) afforded **296** (58.5 mg, 0.22 mmol, 73 %) as a white solid. Yield for duplicate run: 55.0 mg, 0.20 mmol, 68% – 70% average yield.

R_f = 0.16 (silica, Hex/EtOAc 1:1 w/ 1% Et_3N, UV).

^{1}H NMR (500 MHz, $CDCl_3$): δ 8.56 (ddd, *J* = 4.8, 1.8, 0.9 Hz, 1H), 7.40 (td, *J* = 7.6, 1.8 Hz, 1H), 7.09 (ddd, *J* = 7.5, 4.8, 1.2 Hz, 1H), 6.94 (dd, *J* = 8.3, 6.5 Hz, 1H), 6.88 (d, *J* = 7.4 Hz, 2H), 6.69 (dt, *J* = 7.7, 1.1 Hz, 1H), 3.95 (dd, *J* = 9.2, 5.3 Hz, 1H), 3.10 (dd, *J* = 13.4, 5.3 Hz, 1H), 2.96 (dd, *J* = 13.5, 9.3 Hz, 1H), 2.53 (hept, *J* = 6.2 Hz, 1H), 2.04 (s, 6H), 1.95 (brs, 4H), 0.99 (dd, *J* = 11.6, 6.2 Hz, 6H).

^{13}C NMR (101 MHz, $CDCl_3$): δ 163.06, 149.42, 137.13, 135.74, 128.04, 125.97, 123.07, 121.97, 60.95, 45.97, 37.92, 24.10, 22.07, 20.02.

FTIR (NaCl, thin film, cm^{-1}): 3308, 3065, 3007, 2961, 2867, 1687, 1588, 1569, 1468, 1432, 1378, 1366, 1171, 1146, 1096, 995, 769, 749.

HRMS (FAB, m/z): calc'd for $C_{18}H_{25}N_2$ $[M+H]^+$: 269.2018; found: 269.2020.

***N*-(2-(2-iodophenyl)-1-(pyridin-2-yl)ethyl)propan-2-amine (297)**

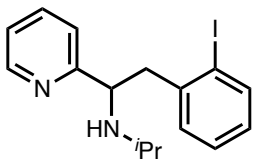

Prepared from imine **271** (44.5 mg, 0.3 mmol) and 1-(bromomethyl)-2-iodobenzene (107 mg, 0.36 mmol) following General Procedure 3.4. Purification of the crude residue by silica gel column chromatography (Hex/EtOAc 1:1 w/ 1% Et_3N) afforded **297** (77.3 mg, 0.21 mmol, 70%) as a pale yellow oil.

R_f = 0.22 (silica, Hex/EtOAc 1:1, UV w/ 1% Et_3N). Yield for duplicate run: 69.6 mg, 0.19 mmol, 63% – 67% average yield.

^{1}H NMR (500 MHz, $CDCl_3$): δ 8.62 (ddd, *J* = 4.9, 1.8, 0.9 Hz, 1H), 7.79 (dd, *J* = 7.8, 1.3 Hz, 1H), 7.47 (td, *J* = 7.6, 1.8 Hz, 1H), 7.13 (ddd, *J* = 7.5, 4.8, 1.2 Hz, 1H), 7.07 (td, *J* = 7.4, 1.3 Hz, 1H), 6.93 (dt, *J* = 7.7, 1.1 Hz, 1H), 6.83 (td, *J* = 7.6, 1.7 Hz, 1H), 6.78 (dd, *J* = 7.6, 1.7 Hz, 1H), 4.19 (dd, *J* = 8.5, 6.2 Hz, 1H), 3.25 (dd, *J* = 13.2, 6.2 Hz, 1H), 3.12 – 3.06 (m, 1H), 2.64 (hept, *J* = 6.3 Hz, 1H), 2.09 (s, 2H), 1.04 (dd, *J* = 7.1, 6.2 Hz, 6H).

^{13}C NMR (101 MHz, $CDCl_3$): δ 162.60, 149.55, 141.71, 139.39, 135.81, 130.95, 127.91, 127.78, 123.05, 121.99, 100.90, 60.83, 48.04, 46.02, 24.00, 22.40.

FTIR (NaCl, thin film, cm^{-1}): 3051, 2960, 1693, 1588, 1568, 1466, 1433, 1366, 1170, 1010, 748.

HRMS (FAB, m/z): calc'd for $C_{16}H_{20}N_2I$ $[M+H]^+$: 367.0671; found: 367.0677.

***N*-(2-(2-bromo-5-methoxyphenyl)-1-(pyridin-2-yl)ethyl)propan-2-amine (298)**

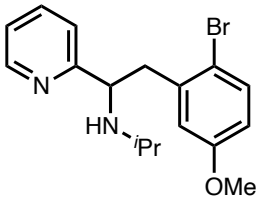

Prepared from imine **271** (44.5 mg, 0.3 mmol) and 1-bromo-2-(bromomethyl)-4-methoxybenzene (101 mg, 0.36 mmol) following General Procedure 3.4. Purification of the crude residue by silica gel column chromatography (Hex/EtOAc 1:1 w/ 1% Et_3N) afforded **298** (77.2 mg, 0.22 mmol, 74 %) as an off-white solid. Yield for duplicate run: 68.1 mg, 0.19 mmol, 65% – 70% average yield.

R_f = 0.19 (silica, Hex/EtOAc 1:1, UV w/ 1% Et_3N).

^{1}H NMR (400 MHz, $CDCl_3$): δ 8.53 (ddd, *J* = 4.8, 1.8, 0.9 Hz, 1H), 7.41 (td, *J* = 7.6, 1.8 Hz, 1H), 7.29 (d, *J* = 8.7 Hz, 1H), 7.05 (ddd, *J* = 7.5, 4.9, 1.2 Hz, 1H), 6.88 (dt, *J* = 7.7, 1.1 Hz, 1H), 6.50 (dd, *J* = 8.8, 3.1 Hz, 1H), 6.27 (d, *J* = 3.1 Hz, 1H), 4.10 (dd, *J* = 8.4, 6.3 Hz,

1H), 3.52 (s, 3H), 3.18 (dd, *J* = 13.1, 6.3 Hz, 1H), 2.91 (dd, *J* = 13.1, 8.4 Hz, 1H), 2.57 (p, *J* = 6.2 Hz, 1H), 1.70 (brs, 3H), 0.94 (t, *J* = 6.2 Hz, 6H).

^{13}C NMR (101 MHz, $CDCl_3$): δ 162.75, 158.41, 149.49, 139.30, 135.93, 133.09, 123.08, 121.99, 116.62, 115.22, 114.22, 60.65, 55.30, 46.01, 43.87, 23.88, 22.38.

FTIR (NaCl, thin film, cm^{-1}): 3069, 3003, 2960, 1589, 1570,1471, 1433, 1378, 1292, 1278, 1241, 1164, 1129, 1056, 1015, 996, 801, 749.

HRMS (FAB, m/z): HRMS (ESI-TOF, m/z): calc'd for $C_{17}H_{22}N_2OBr$ $[M+H]^+$: 349.0915; found: 349.0917.

4-(2-(butylamino)-2-(pyridin-2-yl)ethyl)benzonitrile (299)

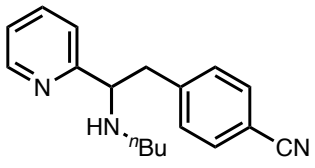

Prepared from imine **291** (48.7 mg, 0.3 mmol) and 4-(bromomethyl)benzonitrile (70.6 mg, 0.36 mmol) following General Procedure 3.4. Purification of the crude residue by silica gel column chromatography (Hex/EtOAc 1:1 w/ 1% Et_3N) afforded **299** (61.4 mg, 0.22 mmol, 73%) as a yellow-orange solid. Yield for duplicate run: 59.0 mg, 0.18 mmol, 70% – 72% average yield.

R_f = 0.22 (silica, Hex/EtOAc 1:1, UV w/ 1% Et_3N).

^{1}H NMR (400 MHz, $CDCl_3$): δ 8.60 – 8.50 (m, 1H), 7.53 (td, J = 7.6, 1.8 Hz, 1H), 7.49 – 7.42 (m, 2H), 7.13 (ddd, J = 7.7, 4.9, 1.2 Hz, 3H), 7.02 (dt, J = 7.8, 1.1 Hz, 1H), 3.90 (t, J = 7.1 Hz, 1H), 3.07 (d, J = 7.1 Hz, 2H), 2.50 – 2.30 (m, 2H), 2.00 – 1.77 (m, 2H), 1.43 – 1.31 (m, 2H), 1.27 – 1.15 (m, 2H), 0.80 (t, J = 7.3 Hz, 3H).

^{13}C NMR (101 MHz, $CDCl_3$): δ 161.83, 149.36, 144.45, 136.00, 131.74, 129.82, 122.21, 122.04, 118.78, 109.81, 65.16, 47.21, 43.18, 32.03, 20.10, 13.67.

FTIR (NaCl, thin film, cm^{-1}): 2955, 2926, 2869, 2226, 1606, 1589, 1570, 1504, 1469, 1433, 1121, 995, 824, 779, 750.

HRMS (FAB, m/z): calc'd for $C_{18}H_{22}N_3$ $[M+H]^+$: 280.1814; found: 280.1822.

4-(2-(butylamino)-2-(pyridin-2-yl)ethyl)benzonitrileN-(2-(2-bromo-5-methoxyphenyl)-1-(pyridin-2-yl)ethyl)butan-1-amine (300)

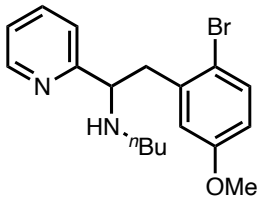

Prepared from imine **291** (48.7 mg, 0.3 mmol) and 1-bromo-2-(bromomethyl)-4-methoxybenzene (101 mg, 0.36 mmol) following General Procedure 3.4. Purification of the crude residue by silica gel column chromatography (Hex/EtOAc 1:1 w/ 1% Et_3N) afforded **300** (51.2 mg, 0.14 mmol, 47%) as a yellow oil. Yield for duplicate run: 49.5 mg, 0.14 mmol, 45% – 46% average yield.

R_f = 0.19 (silica, Hex/EtOAc 1:1, UV w/ 1% Et_3N).

^{1}H NMR (400 MHz, $CDCl_3$): δ 8.60 (ddd, J = 4.8, 1.8, 0.9 Hz, 1H), 7.52 (td, J = 7.6, 1.8 Hz, 1H), 7.37 (d, J = 8.8 Hz, 1H), 7.13 (ddd, J = 7.5, 4.8, 1.2 Hz, 1H), 7.05 (dt, J = 7.7, 1.1 Hz, 1H), 6.58 (dd, J = 8.8, 3.1 Hz, 1H), 6.45 (d, J = 3.1 Hz, 1H), 4.05 (t, J = 7.2 Hz, 1H), 3.62 (s, 3H), 3.21 (dd, J = 13.3, 6.9 Hz, 1H), 3.03 (dd, J = 13.3, 7.5 Hz, 1H), 2.57 – 2.33 (m, 2H), 1.52 – 1.30 (m, 2H), 1.30 – 1.16 (m, 2H), 0.83 (t, J = 7.3 Hz, 3H).

^{13}C NMR (101 MHz, $CDCl_3$): δ 163.08, 158.95, 149.92, 139.69, 136.52, 133.62, 123.27, 122.51, 117.08, 115.74, 114.70, 64.10, 55.77, 47.96, 44.04, 32.73, 20.81, 14.39.

FTIR (NaCl, thin film, cm^{-1}): 3004, 2955, 2927, 2857, 1589, 1570, 1471, 1433, 1291, 1240, 1163, 1112, 1048, 1015, 995, 782, 749.

HRMS (FAB, m/z): calc'd for $C_{18}H_{24}N_2OBr$ $[M+H]^+$: 363.1072; found: 363.1083.

***N*-(2-(4-fluorophenyl)-1-(pyridin-2-yl)ethyl)propan-2-amine (302)**

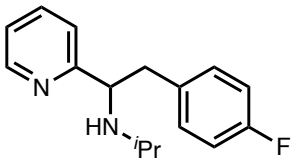

Prepared from imine **271** (44.5 mg, 0.3 mmol) and 1-(chloromethyl)-4-fluorobenzene (52.0 mg, 0.36 mmol) following General Procedure 3.4. Purification of the crude residue by silica gel column chromatography (Hex/EtOAc 1:1 w/ 1% Et_3N) afforded **302** (61.5 mg, 0.24 mmol, 79%) as a pale yellow oil. Yield for duplicate run: 57.2 mg, 0.22 mmol, 74% – 76% average yield.

R_f = 0.13 (silica, Hex/EtOAc 1:1 w/ 1% Et_3N, UV).

^{1}H NMR (500 MHz, $CDCl_3$): δ 8.56 (ddd, *J* = 4.9, 1.8, 0.9 Hz, 1H), 7.50 (td, *J* = 7.6, 1.8 Hz, 1H), 7.10 (ddd, *J* = 7.6, 4.8, 1.2 Hz, 1H), 7.00 (dt, *J* = 7.8, 1.1 Hz, 1H), 6.96 – 6.91 (m, 2H), 6.89 – 6.82 (m, 2H), 3.99 (t, *J* = 7.2 Hz, 1H), 3.02 – 2.91 (m, 2H), 2.54 (hept, *J* = 6.2 Hz, 1H), 1.80 – 1.69 (m, 3H), 0.95 (dd, *J* = 6.2, 1.4 Hz, 6H).

^{13}C NMR (101 MHz, $CDCl_3$): δ 163.00, 160.24, 149.44, 136.02, 134.47, 130.64, 122.65, 121.97, 115.07, 114.86, 63.02, 45.98, 42.76, 24.02, 22.03.

^{19}F NMR (282 MHz, $CDCl_3$): δ -117.15

FTIR (NaCl, thin film, cm^{-1}): 3046, 3005, 2962, 2927, 2865, 1684, 1589, 1570, 1508, 1469, 1433, 1379, 1367, 1338, 1221, 1168, 1157, 1094, 830, 748.

HRMS (FAB, m/z): calc'd for $C_{16}H_{20}N_2F$ $[M+H]^+$: 259.1611; found 259.1622.

***N*-(2-phenyl-1-(pyridin-2-yl)propyl)butan-1-amine (303)**

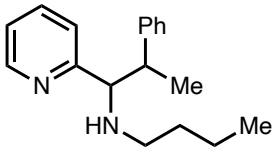

Prepared from imine **291** (48.7 mg, 0.3 mmol) and (1-chloroethyl)benzene (50.6 mg, 0.36 mmol) following General Procedure 3.4. Purification of the crude residue by silica gel column chromatography (Hex/EtOAc 1:1 w/ 1% Et_3N) afforded **303** (36.4 mg, 0.14 mmol,

46%) as a 1.4:1 mixture of diastereomers as a brown oil. Yield for duplicate run: 34.4 mg, 0.13 mmol, 43% – 44% average yield.

R_f = 0.39 (silica, Hex/EtOAc 1:1, UV w/ 1% Et_3N).

^{1}H NMR (500 MHz, $CDCl_3$): δ 8.57 (d, *J* = 4.9 Hz, 1H, *major*), 8.51 – 8.46 (d, *J* = 4.6 Hz,, 1H, *minor*), 7.61 (td, *J* = 7.6, 1.8 Hz, 1H, *major*), 7.41 (td, *J* = 7.6, 1.8 Hz, 1H, *major*), 7.33 (d, *J* = 8.4 Hz, 2H, *minor*), 7.29 (d, *J* = 7.3 Hz, 2H, *major*), 7.24 (m, *J* = 4.6 Hz, 1H, *major*), 7.21 (t, *J* = 7.1 Hz, 1H, *minor*), 7.15 (t, *J* = 7.6 Hz, 3H, *major*), 7.10 – 7.04 (m, 3H, *minor*), 7.01 (dd, *J* = 7.5, 4.9 Hz, 1H, *minor*), 6.95 (d, *J* = 7.8 Hz, 1H, *minor*), 3.81 (d, *J* = 9.3 Hz, 1H, *minor*), 3.79 – 3.73 (m, 1H, *major*), 3.17 (p, *J* = 7.1 Hz, 1H, *minor*), 3.01 (p, *J* = 7.1 Hz, 1H, *major*), 2.37 – 2.27 (m, 2H, *minor*), 2.27 – 2.17 (m, 2H, *major*), 1.64 (br s, 2H), 1.39 – 1.33 (m, 2H, *minor*), 1.31 (d, *J* = 7.1 Hz, 3H, *minor*), 1.20 (m, 4H, *major*+*minor*), 1.04 (dt, *J* = 14.9, 7.4 Hz, 2H, *major*), 0.98 (d, *J* = 7.1 Hz, 3H, *major*), 0.79 (t, *J* = 7.3 Hz, 3H, *minor*), 0.70 (t, *J* = 7.3 Hz, 3H, *major*).

^{13}C NMR (126 MHz, $CDCl_3$): δ 163.22 (*major)*, 162.71 (*minor)*, 149.15 (*minor)*, 149.02 (*major)*, 144.65 (*major)*, 144.52 (*minor)*, 136.35 (*major)*, 135.54 (*minor)*, 128.71 (*major)*, 128.11 (*minor)*, 127.94 (*minor)*, 127.83 (*major)*, 126.74 (*major)*, 126.15 (*minor)*, 123.13 (*minor)*, 122.64 (*major)*, 122.19 (*major)*, 121.62 (*minor)*, 70.68 (*major)*, 70.09 (*minor)*, 47.88 (*minor)*, 47.71 (*major)*, 46.51 (*major)*, 45.47 (*minor)*, 32.34 (*minor)*, 31.91 (*major)*, 20.41 (*minor)*, 20.21 (*major)*, 19.34 (*major)*, 16.63 (*minor)*, 14.04 (*minor)*, 13.91 (*major)*.

FTIR (NaCl, thin film, cm^{-1}): 3026, 2957, 2926, 2871, 1589, 1569, 1453, 1432, 1376, 1125, 994, 763,748, 700.

HRMS (FAB, m/z): calc'd for $C_{18}H_{25}N_2$ $[M+H]^+$: 269.2018; found: 269.2028.

_N_-(cyclohexyl(pyridin-2-yl)methyl)butan-1-amine (304)

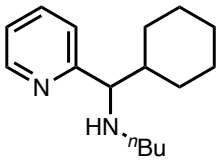

Prepared from imine **291** (48.7 mg, 0.3 mmol) and iodocyclohexane (75.6 mg, 0.36 mmol) following General Procedure 3.4. Purification of the crude residue by silica gel column chromatography (Hex/EtOAc 1:1 w/ 1% Et_3N) afforded **304** (42.9 mg, 0.17 mmol, 58%) as a yellow oil. Yield for duplicate run: 41.3 mg, 0.17 mmol, 56% – 57% average yield.

Also prepared from imine **291** (48.7 mg, 0.3 mmol) and bromocyclohexane (58.7 mg, 0.36 mmol) following General Procedure 3.4. Purification of the crude residue by silica gel column chromatography (Hex/EtOAc 1:1 w/ 1% Et_3N) afforded **304** (25.6 mg, 0.10 mmol, 35%) as a yellow oil. Yield for duplicate run: 21.5 mg, 0.087 mmol, 29% – 32% average yield.

Also prepared from imine **291** (48.7 mg, 0.3 mmol) and **346** (98.4 mg, 0.36 mmol) following General Procedure 3.4. Purification of the crude residue by silica gel column chromatography (Hex/EtOAc 1:1 w/ 1% Et_3N) afforded **304** (32.7 mg, 0.13 mmol, 44%) as a yellow oil. Yield for duplicate run: 21.7 mg, 0.11 mmol, 37% – 41% average yield.

R_f = 0.26 (silica, Hex/EtOAc 1:1, UV w/ 1% Et_3N).

^{1}H NMR (400 MHz, $CDCl_3$):δ 8.54 (ddd, J = 4.9, 1.8, 0.9 Hz, 1H), 7.59 (td, J = 7.6, 1.8 Hz, 1H), 7.22 (dt, J = 7.8, 1.1 Hz, 1H), 7.11 (ddd, J = 7.5, 4.8, 1.2 Hz, 1H), 3.42 (d, J = 6.9 Hz, 1H), 2.42 – 2.23 (m, 2H), 1.91 (ddq, J = 12.3, 4.0, 2.1 Hz, 2H), 1.83 (d, J = 7.5 Hz, 1H), 1.74 – 1.53 (m, 2H), 1.47 – 1.01 (m, 6H), 1.01 – 0.89 (m, 2H), 0.83 (t, J = 7.3 Hz, 3H).

^{13}C NMR (101 MHz, $CDCl_3$): δ 163.28, 148.87, 135.50, 122.68, 121.37, 69.50, 47.67, 43.50, 32.22, 29.80, 29.72, 26.36, 26.15, 26.11, 20.24, 13.78.

FTIR (NaCl, thin film, cm^{-1}): 3311,3068, 2923, 2851, 1588, 1569, 1467, 1431, 1375, 1342, 1117, 994, 838, 777, 747.

HRMS (FAB, m/z): calc'd for $C_{16}H_{27}N_2$ $[M+H]^+$: 247.2174; found: 247.2186.

***N*-(cyclohexyl(pyridin-2-yl)methyl)propan-2-amine (305)**

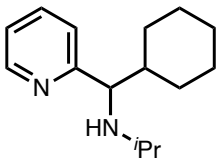

Prepared from imine **271** (44.5 mg, 0.3 mmol) and **346** (98.4 mg, 0.36 mmol) following General Procedure 3.4. Purification of the crude residue by silica gel column chromatography (Hex/EtOAc 1:1 w/ 1% Et_3N) afforded **305** (34.2 mg, 0.15 mmol, 49%) as a colorless oil. Yield for duplicate run: 28.0 mg, 0.12 mmol, 40% – 44% average yield.

R_f = 0.26 (silica, Hex/EtOAc 1:1 w/ 1% Et_3N, UV).

^{1}H NMR (400 MHz, $CDCl_3$): δ 8.70 (ddd, J = 4.9, 1.8, 0.9 Hz, 1H), 7.73 (td, J = 7.6, 1.8 Hz, 1H), 7.35 (dt, J = 7.8, 1.1 Hz, 1H), 7.25 (ddd, J = 7.5, 4.8, 1.2 Hz, 1H), 3.66 (d, J = 6.8 Hz, 1H), 2.60 (hept, J = 6.2 Hz, 1H), 2.08 (dtt, J = 12.1, 3.6, 1.7 Hz, 1H), 1.95 – 1.82 (m, 3H), 1.75 (dddd, J = 13.4, 11.5, 6.7, 3.3 Hz, 3H), 1.54 – 1.42 (m, 1H), 1.37 – 1.19 (m, 2H), 1.17 – 1.02 (m, 6H).

^{13}C NMR (101 MHz, $CDCl_3$): δ 163.81, 149.09, 135.61, 123.04, 121.50, 66.70, 46.26, 43.80, 30.08, 29.96, 26.59, 26.37, 26.32, 24.27, 22.18.

FTIR (NaCl, thin film, cm^{-1}): 2920, 2851, 1693, 1588, 1432, 1364, 1174, 749.

HRMS (FAB, m/z): calc'd for $C_{15}H_{25}N_2$ $[M+H]^+$: 233.2018; found: 233.2027.

***tert*-butyl 4-((butylamino)(pyridin-2-yl)methyl)piperidine-1-carboxylate (308)**

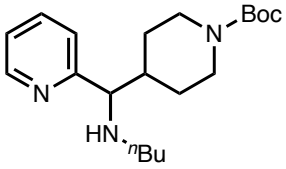

Prepared from imine **291** (48.7 mg, 0.3 mmol) and tert-butyl 4-iodopiperidine-1-carboxylate (112 mg, 0.36 mmol) following General Procedure 3.4. Purification of the crude residue by silica gel column chromatography (Hex/EtOAc 1:1 w/ 1% Et_3N) afforded **308** (33.8 mg, 0.10 mmol, 32%) as a yellow oil. Yield for duplicate run: 28.9 mg, 0.083 mmol, 29% – 30% average yield.

R_f = 0.18 (silica, Hex/EtOAc 1:1, UV w/ 1% Et_3N).

^{1}H NMR (400 MHz, $CDCl_3$): δ 8.56 (ddd, J = 4.9, 1.8, 0.9 Hz, 1H), 7.60 (td, J = 7.6, 1.8 Hz, 1H), 7.21 – 7.09 (m, 2H), 4.04 (d, J = 38.7 Hz, 2H), 3.39 (d, J = 7.4 Hz, 1H), 2.59 (dt, J = 25.7, 11.8 Hz, 2H), 2.40 – 2.25 (m, 2H), 2.03 – 1.86 (m, 1H), 1.77 (ddt, J = 19.0, 11.3, 3.1 Hz, 3H), 1.41 (s, 9H), 1.39 – 0.98 (m, 1H), 0.82 (t, J = 7.3 Hz, 3H).

^{13}C NMR (101 MHz, $CDCl_3$): δ 162.96, 155.23, 149.89, 136.31, 123.55, 122.33, 79.60, 69.17, 48.14, 42.46, 32.80, 28.86, 20.80, 14.37.

FTIR (NaCl, thin film, cm^{-1}): 2954, 2929, 2853, 1732, 1692, 1651, 1588, 1424, 1365, 1276, 1247, 1171, 872, 750.

HRMS (FAB, m/z): calc'd for $C_{20}H_{34}N_3O_2$ $[M+H]^+$: 348.2651; found: 348.2646.

***tert*-butyl 4-((isopropylamino)(pyridin-2-yl)methyl)piperidine-1-carboxylate (309)**

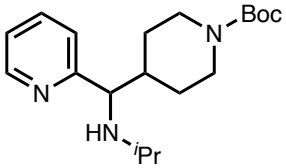

Prepared from imine **271** (44.5 mg, 0.3 mmol) and 1-(tert-butyl) 4-(1,3-dioxoisoindolin-2-yl) piperidine-1,4-dicarboxylate (135 mg, 0.36 mmol) following General Procedure 3.4. Purification of the crude residue by silica gel column chromatography (Hex/EtOAc 1:1 w/ 1% Et_3N)

afforded **309** (55.9 mg, 0.17 mmol, 56%) as a white solid. Yield for duplicate run: 47.7 mg, 0.14 mmol, 48% – 52% average yield.

R_f = 0.19 (silica, Hex/EtOAc 1:1 w/ 1% Et_3N, UV).

^{1}H NMR (400 MHz, $CDCl_3$): δ δ 8.56 (ddd, J = 4.8, 1.8, 0.9 Hz, 1H), 7.59 (td, J = 7.6, 1.8 Hz, 1H), 7.21 – 7.01 (m, 2H), 4.04 (d, J = 37.9 Hz, 2H), 3.46 (d, J = 7.4 Hz, 1H), 2.71 – 2.49 (m, 2H), 2.44 (p, J = 6.2 Hz, 1H), 2.02 – 1.91 (m, 2H), 1.73 (tdt, J = 11.3, 7.4, 3.7 Hz, 1H), 1.40 (s, 9H), 1.22 – 1.03 (m, 3H), 0.94 (dd, J = 18.2, 6.2 Hz, 6H).

^{13}C NMR (101 MHz, $CDCl_3$): δ 162.98, 154.92, 149.61, 135.91, 123.29, 121.94, 79.27, 65.89, 46.21, 42.26, 29.23, 28.56, 24.38, 22.23.

FTIR (NaCl, thin film, cm^{-1}): 2964, 1861, 2724, 1772, 1735, 1689, 1589, 1569, 1469, 1424, 1365, 1278, 1250, 1168, 1119, 1050, 871, 750, 718.

HRMS (FAB, m/z): calc'd for $C_{19}H_{32}N_3O_2$ $[M+H]^+$: 334.2495; found: 334.2469.

***N*-(pyridin-2-yl(tetrahydro-2H-pyran-4-yl)methyl)butan-1-amine (306)**

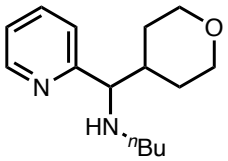

Prepared from imine **291** (48.7 mg, 0.3 mmol) and 4-iodotetrahydro-2H-pyran (76.3 mg, 0.36 mmol) following General Procedure 3.4. Purification of the crude residue by silica gel column chromatography (Hex/EtOAc 1:1 w/ 1% Et_3N) afforded **306** (63.9 mg, 0.26 mmol, 86%) as a yellow oil. Yield for duplicate run: 54.3 mg, 0.22 mmol, 73% – 80% average yield.

R_f = 0.19 (silica, Hex/EtOAc 1:1, UV w/ 1% Et_3N).

^{1}H NMR (400 MHz, $CDCl_3$): δ 8.56 (ddd, J = 4.9, 1.8, 0.9 Hz, 1H), 7.60 (td, J = 7.6, 1.9 Hz, 1H), 7.18 (dt, J = 7.8, 1.1 Hz, 1H), 7.12 (ddd, J = 7.5, 4.8, 1.2 Hz, 1H), 3.90 (dddd, J

= 47.4, 11.5, 4.5, 2.5 Hz, 2H), 3.38 (d, J = 7.4 Hz, 1H), 3.29 (dtd, J = 33.0, 11.9, 2.1 Hz, 2H), 2.43 – 2.23 (m, 2H), 1.96 – 1.72 (m, 4H), 1.48 – 1.17 (m, 6H), 1.10 (ddq, J = 13.2, 4.3, 2.3 Hz, 1H), 0.82 (t, J = 7.3 Hz, 3H).

^{13}C NMR (101 MHz, $CDCl_3$): δ 162.96, 149.89, 136.27, 123.58, 122.30, 69.52, 68.59, 68.31, 48.10, 41.39, 32.82, 30.74, 30.42, 20.81, 14.37.

FTIR (NaCl, thin film, cm^{-1}): 3317, 3067, 3004, 2928, 2839, 2755, 1588, 1569, 1468, 1432, 1385, 1264, 1237, 1122, 1093, 1015, 994, 983, 876, 782, 749.

HRMS (FAB, m/z): calc'd for $C_{15}H_{25}N_2O$ $[M+H]^+$: 249.1967; found: 249.1973.

***N*-(pyridin-2-yl(tetrahydro-2H-pyran-4-yl)methyl)propan-2-amine (307)**

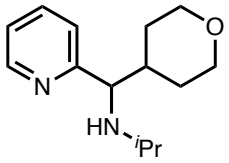

Prepared from imine **271** (44.5 mg, 0.3 mmol) and 1,3-dioxoisoindolin-2-yl tetrahydro-2H-pyran-4-carboxylate (99.1 mg, 0.36 mmol) following General Procedure 3.4. Purification of the crude residue by silica gel column chromatography (Hex/EtOAc 1:1 w/ 1% Et_3N) afforded **307** (36.2 mg, 0.15 mmol, 51%) as a yellow oil. Yield for duplicate run: 36.1 mg, 0.15 mmol, 51% – 51% average yield.

R_f = 0.23 (silica, Hex/EtOAc 1:1, UV w/ 1% Et_3N).

^{1}H NMR (300 MHz, $CDCl_3$): δ 8.58 (dt, J = 4.7, 1.2 Hz, 1H), 7.60 (td, J = 7.6, 1.8 Hz, 1H), 7.23 – 7.08 (m, 2H), 4.04 – 3.78 (m, 2H), 3.48 (d, J = 7.5 Hz, 1H), 3.30 (dtd, J = 25.5, 11.8, 2.1 Hz, 2H), 2.46 (p, J = 6.2 Hz, 1H), 1.98 – 1.75 (m, 4H), 1.41 – 1.22 (m, 2H), 1.15 – 1.03 (m, 1H), 0.96 (dd, J = 15.9, 6.2 Hz, 6H).

^{13}C NMR (101 MHz, $CDCl_3$): δ 163.30, 149.95, 136.22, 123.68, 122.26, 68.67, 68.34, 66.57, 46.53, 41.54, 30.93, 30.48, 24.73, 22.59.

FTIR (NaCl, thin film, cm^{-1}): 3315, 2957, 2929, 2841, 1588,1569, 1469, 1433, 1366,1262, 1236, 1176, 1127, 1093, 877, 750.

HRMS (FAB, m/z): calc'd for $C_{14}H_{23}N_2O$ $[M+H]^+$: 235.1810; found: 235.1805.

4-((isopropylamino)(pyridin-2-yl)methyl)cyclohexan-1-one (310)

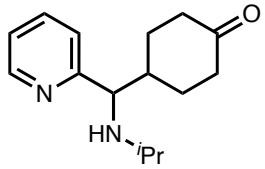

Prepared from imine **291** (44.5 mg, 0.3 mmol) and 1,3-dioxoisoindolin-2-yl 4-oxocyclohexane-1-carboxylate (103 mg, 0.36 mmol) following General Procedure 3.4. Purification of the crude residue by silica gel column chromatography (Hex/EtOAc 1:1 w/ 1% Et_3N) afforded **310** (49.0 mg, 0.20 mmol, 66%) as a yellow oil. Yield for duplicate run: 38.2 mg, 0.16 mmol, 52% – 59% average yield.

R_f = 0.20 (silica, Hex/EtOAc 1:1, UV w/ 1% Et_3N).

^{1}H NMR (400 MHz, $CDCl_3$): δ 8.57 (ddd, J = 4.8, 1.8, 1.0 Hz, 1H), 7.60 (td, J = 7.6, 1.9 Hz, 1H), 7.22 – 7.06 (m, 2H), 3.55 (d, J = 7.3 Hz, 1H), 2.45 (p, J = 6.2 Hz, 1H), 2.40 – 2.18 (m, 4H), 2.06 (dddd, J = 14.6, 11.5, 6.6, 3.2 Hz, 1H), 1.95 (s, 2H), 1.64 (ddq, J = 12.4, 6.4, 3.2 Hz, 1H), 1.56 – 1.32 (m, 2H), 0.96 (dd, J = 18.3, 6.2 Hz, 6H).

^{13}C NMR (101 MHz, CD_2Cl_2): δ 212.10, 149.99, 136.30, 123.59, 122.38, 65.34, 46.77, 42.53, 41.29, 30.12, 24.56, 22.42.

FTIR (NaCl, thin film, cm^{-1}): 3314, 2960, 2866, 1714, 1589, 1469, 1432, 1378, 1337, 1168, 753.

HRMS (FAB, m/z): calc'd for $C_{15}H_{23}N_2O$ $[M+H]^+$: 247.1810; found: 247.1805.

_N_-(1-(6-methoxypyridin-2-yl)-2-phenylethyl)propan-2-amine (350)

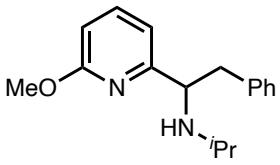

Prepared from imine **340** (53.5 mg, 0.3 mmol) and benzyl bromide (42.8 μL, 0.36 mmol, 1.2 equiv) following General Procedure 3.4. Purification of the crude residue by silica gel column chromatography (Hex/EtOAc 1:1 w/ 1% Et_3N) afforded **350** (14.0 mg, 0.051 mmol, 17%) as a colorless oil. Yield for duplicate run: 12.0 mg, 0.044 mmol, 15% – 16% average yield.

R_f = 0.29 (silica, Hex/EtOAc 1:1 w/ 1% Et_3N, UV).

^{1}H NMR (500 MHz, $CDCl_3$): δ 7.35 (t, *J* = 7.7 Hz, 1H), 7.20 – 7.09 (m, 3H), 6.97 (d, *J* = 7.4 Hz, 2H), 6.55 (d, *J* = 7.4 Hz, 1H), 6.48 (d, *J* = 7.1 Hz, 1H), 3.95 – 3.86 (m, 4H), 3.02 (t, *J* = 6.3 Hz, 2H), 2.58 (hept, *J* = 6.3 Hz, 1H), 1.89 (s, 1H), 1.00 (s, 6H).

^{13}C NMR (126 MHz, $CDCl_3$): δ 164.1, 160.5, 139.3, 138.5, 129.5, 128.2, 126.2, 115.8, 108.7, 62.5, 45.9, 43.5, 24.3, 22.1.

FTIR (NaCl, thin film, cm^{-1}): 3063, 3026, 2962, 2857, 1599, 1578, 1466, 1436, 1416, 1310, 1288, 1173, 1147, 1073, 1032, 988, 803, 770, 743, 699.

HRMS (FAB, m/z): calc'd for $C_{17}H_{23}N_2O$ $[M+H]^+$: 271.1810; found 271.1806.

Methyl 6-(1-(isopropylamino)-2-phenylethyl)nicotinate (351)

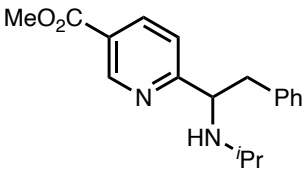

Prepared from imine **341** 61.9 mg, 0.3 mmol) and benzyl bromide (42.8 μL, 0.36 mmol, 1.2 equiv) following General Procedure 3.4. Purification of the crude residue by silica gel column chromatography (Hex/EtOAc 1:1 w/ 1% Et_3N) afforded **351** (26.0 mg, 0.087 mmol, 29%) as a colorless oil. Yield for duplicate run: 26.0 mg, 0.087 mmol, 29% – 29% average yield.

R_f = 0.23 (silica, Hex/EtOAc 1:1 w/ 1% Et_3N, UV).

^{1}H NMR (500 MHz, $CDCl_3$): δ 9.17 (d, *J* = 2.1 Hz, 1H), 8.12 (dd, *J* = 8.1, 2.2 Hz, 1H), 7.23 – 7.13 (m, 4H), 7.02 (d, *J* = 6.8 Hz, 2H), 4.13 (t, *J* = 7.2 Hz, 1H), 3.94 (s, 3H), 3.04 (dd, *J* = 13.3, 7.2 Hz, 1H), 2.98 (dd, *J* = 13.3, 7.2 Hz, 1H), 2.58 – 2.49 (m, 1H), 1.78 (s, 1H), 0.95 (d, *J* = 6.3 Hz, 6H).

^{13}C NMR (126 MHz, $CDCl_3$): δ 168.5, 166.1, 157.1, 150.9, 138.4, 137.3, 129.4, 128.5, 126.6, 124.5, 122.3, 63.3, 52.5, 46.5, 43.7, 24.2, 22.2.

FTIR (NaCl, thin film, cm^{-1}): 3063, 3027, 2960, 2866, 1729, 1597, 1586, 1456, 1436, 1381, 1339, 1289, 1194, 1176, 1118, 1024, 960, 777, 738, 701.

HRMS (FAB, m/z): calc'd for $C_{18}H_{23}N_2O_2$ $[M+H]^+$: 299.1760; found 299.1755.

***N*-(1-(5-bromopyridin-2-yl)-2-phenylethyl)propan-2-amine (352)**

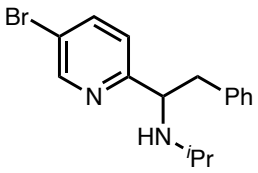

Prepared from imine **342** (68.1 mg, 0.3 mmol) and benzyl bromide (42.8 μL, 0.36 mmol, 1.2 equiv) following General Procedure 3.4. Purification of the crude residue by silica gel column chromatography (Hex/EtOAc 1:1 w/ 1% Et_3N) afforded **352** (22.0 mg, 0.069 mmol, 23%) as a colorless oil. Yield for duplicate run: 22.0 mg, 0.069 mmol, 23% – 23% average yield.

R_f = 0.35 (silica, Hex/EtOAc 1:1 w/ 1% Et_3N, UV).

^{1}H NMR (500 MHz, $CDCl_3$): δ 8.63 (dd, *J* = 2.4, 0.7 Hz, 1H), 7.64 (dd, *J* = 8.3, 2.4 Hz, 1H), 7.26 – 7.12 (m, 3H), 7.07 – 6.94 (m, 3H), 4.05 (t, *J* = 7.2 Hz, 1H), 3.05 – 2.90 (m, 2H), 2.54 (hept, *J* = 6.3 Hz, 1H), 2.07 (s, 1H), 0.95 (dd, *J* = 6.3, 2.9 Hz, 6H).

^{13}C NMR (126 MHz, $CDCl_3$): δ 162.2, 150.6, 138.8, 138.5, 129.4, 128.6, 126.6, 124.0, 118.8, 62.8, 46.5, 43.7, 24.1, 22.1.

FTIR (NaCl, thin film, cm^{-1}): 3083, 3027, 2925, 1863, 1710, 1602, 1572, 1494, 1463, 1367, 1173, 1091, 1006, 839, 744, 628.

HRMS (FAB, m/z): calc'd for $C_{16}H_{20}N_2Br$ $[M+H]^+$: 319.0810; found 319.0825.

N-(1-(isoquinolin-3-yl)-2-phenylethyl)propan-2-amine (354)

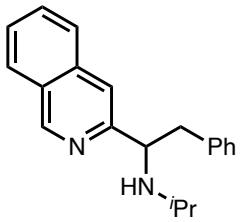

Prepared from imine **343** (59.5 mg, 0.3 mmol) and benzyl bromide (42.8 μL, 0.36 mmol, 1.2 equiv) following General Procedure 3.4. Purification of the crude residue by silica gel column chromatography (Hex/EtOAc 1:1 w/ 1% Et_3N) afforded **354** (30.5 mg, 0.11 mmol, 35%) as a colorless oil. Yield for duplicate run: 27.0 mg, 0.093 mmol, 31% – 33% average yield.

R_f = 0.19 (silica, Hex/EtOAc 1:1 w/ 1% Et_3N, UV).

^{1}H NMR (500 MHz, $CDCl_3$): δ 9.27 (s, 1H), 7.95 (d, *J* = 8.2 Hz, 1H), 7.69 (d, *J* = 9.5 Hz, 1H), 7.64 (ddd, *J* = 8.2, 6.7, 1.2 Hz, 1H), 7.55 (ddd, *J* = 8.1, 6.7, 1.3 Hz, 1H), 7.38 (s, 1H), 7.20 – 7.09 (m, 3H), 7.04 (d, *J* = 4.5 Hz, 2H), 4.19 (t, *J* = 7.1 Hz, 1H), 3.20 (dd, *J* = 13.3, 7.5 Hz, 1H), 3.08 (dd, *J* = 13.3, 6.8 Hz, 1H), 2.58 (hept, *J* = 6.2 Hz, 1H), 2.09 (s, 1H), 0.99 (d, *J* = 6.2 Hz, 6H).

^{13}C NMR (126 MHz, $CDCl_3$): δ 156.0, 152.7, 139.2, 136.2, 130.5, 129.4, 128.4, 128.0, 127.7, 126.9, 126.7, 126.3, 118.8, 63.0, 46.1, 43.6, 24.3, 22.1.

FTIR (NaCl, thin film, cm^{-1}): 3308, 3057, 3026, 2963, 2927, 2862, 1684, 1647, 1628, 1582, 1558, 1490, 1456, 1379, 1339, 1271, 1174, 1127, 1080, 945, 883, 750, 689, 668.

HRMS (FAB, m/z): calc'd for $C_{20}H_{23}N_2$ $[M+H]^+$: 291.1861; found 291.1858.

N-(1-(1-methyl-1H-indazol-3-yl)-2-phenylethyl)propan-2-amine (355)

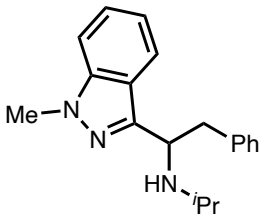

Prepared from imine **344** (60.4 mg, 0.3 mmol) and benzyl bromide (42.8 μL, 0.36 mmol, 1.2 equiv) following General Procedure 3.4. Purification of the crude residue by silica gel column chromatography (Hex/EtOAc 1:1 w/ 1% Et_3N) afforded **355** (6.0 mg, 0.021 mmol, 7%) as a colorless oil.

R_f = 0.19 (silica, Hex/EtOAc 1:1 w/ 1% Et_3N, UV).

^{1}H NMR (500 MHz, $CDCl_3$): δ 7.78 (d, *J* = 8.2 Hz, 1H), 7.38 – 7.30 (m, 2H), 7.23 – 7.11 (m, 5H), 7.11 – 7.03 (m, 1H), 4.53 (t, *J* = 7.1 Hz, 1H), 4.01 (s, 3H), 3.18 (dd, *J* = 7.1, 2.7 Hz, 2H), 2.68 (hept, *J* = 6.3 Hz, 1H), 1.71 (s, 1H), 0.96 (dd, *J* = 10.7, 6.2 Hz, 6H).

^{13}C NMR (126 MHz, $CDCl_3$): δ 141.0, 138.8, 129.3, 128.2, 126.2, 126.1, 121.1, 119.7, 108.9, 55.7, 46.1, 43.3, 35.3, 23.9, 22.0.

FTIR (NaCl, thin film, cm^{-1}): 3444, 3025, 2956, 2928, 2864, 1684, 1615, 1506, 1456, 1369, 1294, 1236, 1171, 768, 746, 702.

HRMS (FAB, m/z): calc'd for $C_{19}H_{24}N_3$ $[M+H]^+$: 294.1970; found 294.1961.

***N*-(pyridin-2-yl(1-tosylpiperidin-4-yl)methyl)butan-1-amine (353)**

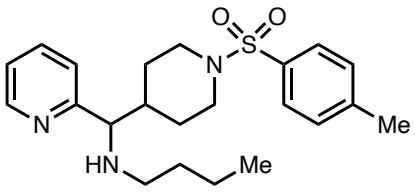

Prepared from imine **291** (48.7 mg, 0.3 mmol) and tert-butyl 4-iodo-1-tosylpiperidine (131 mg, 0.36 mmol) following General Procedure 3.4. Purification of the crude residue by silica gel column chromatography (Hex/EtOAc 1:1 w/ 1% Et_3N) afforded **353** (36.2 mg, 0.090 mmol, 30%) as a white solid. Yield for duplicate run: 31.1 mg, 0.077 mmol, 26% – 28% average yield.

R_f = 0.22 (silica, Hex/EtOAc 1:1, UV w/ 1% Et_3N).

^{1}H NMR (500 MHz, $CDCl_3$): δ 8.54 (d, J = 4.8 Hz, 1H), 7.60 (m, 3H), 7.28 (d, J = 7.9 Hz, 2H), 7.14 (m, 2H), 3.81 (d, J = 11.6 Hz, 1H), 3.70 (d, J = 11.4 Hz, 1H), 3.37 (d, J = 14.4 Hz, 1H), 2.42 (s, 3H), 2.40 – 2.25 (m, 1H), 2.18 (td, J = 11.9, 2.6 Hz, 1H), 2.11 (td, J = 11.3, 7.2 Hz, 1H), 2.05 (dd, J = 13.5, 3.2 Hz, 1H), 1.47 – 1.34 (m, 3H), 1.34 – 1.18 (m, 8H), 0.84 (t, J = 7.3 Hz, 3H).

^{13}C NMR (126 MHz, $CDCl_3$): δ 149.63, 143.35, 135.94, 133.00, 129.52, 127.72, 123.25, 122.05, 68.21, 47.64, 46.63, 46.40, 41.08, 32.32, 28.65, 28.40, 21.52, 20.36, 13.94.

FTIR (NaCl, thin film, cm^{-1}): 3323, 2952, 2921, 2856, 2361, 1588, 1467, 1351, 1338, 1163, 1093, 929, 752, 728.

HRMS (FAB, m/z): calc'd for $C_{22}H_{32}N_3O_2S$ $[M+H]^+$: 402.2215; found: 402.2218.

***N*-(1-(1*H*-imidazol-2-yl)-2-phenylethyl)propan-2-amine (356)**

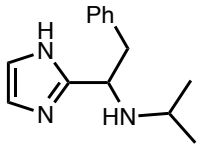

Prepared from imine **345** (41.2 mg, 0.3 mmol) and benzyl bromide (42.8 μL, 0.36 mmol, 1.2 equiv) following General Procedure 3.4. Purification of the crude residue by silica gel column chromatography (Hex/EtOAc 1:1 w/ 1% Et_3N) afforded **356** (3.3 mg, 0.014 mmol, 5%) as a yellow oil.

R_f = 0.21 (silica, Hex/EtOAc 1:1 w/ 1% Et_3N, UV).

^{1}H NMR (400 MHz, $CDCl_3$): δ 7.26 – 7.18 (m, 5H), 6.94 (d, J = 1.4 Hz, 1H), 6.75 (d, J = 1.4 Hz, 1H), 5.07 (s, 1H), 3.70 (s, 1H), 3.53 (s, 1H), 2.94 (p, J = 6.6 Hz, 1H), 1.69 (d, J = 29.6 Hz, 1H), 1.07 (d, J = 6.6 Hz, 6H).

^{13}C NMR (100 MHz, $CDCl_3$): δ 135.71, 129.47, 129.16, 128.63, 128.08, 127.25, 121.25, 53.65, 30.25, 28.60 17.80.

FTIR (NaCl, thin film, cm^{-1}): 3355, 2953, 2914, 1733, 1716, 1558, 1506, 1456, 1167, 910

HRMS (ESI, m/z): calc'd for $C_{14}H_{20}N_3$ $[M+H]^+$: 230.1652; found: 230.1648.

3.5.6 Investigation into Imine Homocoupling

N1,N2-diisopropyl-1,2-di(pyridin-2-yl)ethane-1,2-diamine (311)

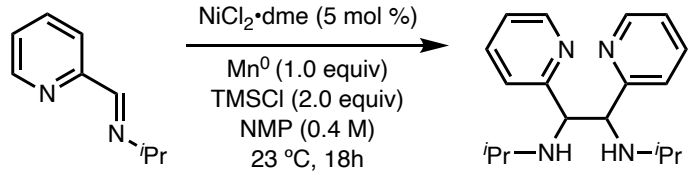

Independent synthesis of **311**: On the bench-top, to a 1 dram vial, equipped with a stir bar, was charged with (*E*)-*N*-isopropyl-1-(pyridin-2-yl)methanimine **271** (44.5 mg 0.3 mmol, 1.0 equiv) and Mn^0 (16.5 mg, 0.3 mmol, 1.0 equiv). The vial was brought into a N_2-filled glovebox and a stock-solution of $NiCl_2$·dme in NMP (0.75 ml, 0.02 M, 0.05 equiv [Ni]) and TMSCl (76 μl, 0.6 mmol, 2.0 equiv) was added consecutively. The vial was sealed with a Teflon cap and electrical tape and stirred at room temperature for 18 hours at 600 rpm. The resulting suspension was diluted with CH_2Cl_2 (0.5 ml) and extracted 3x with 1N HCl (0.5 ml). To the combined aqueous phases was added K_2CO_3 (s) until gas evolution ceased. The resulting aqueous solution was extracted 3x with EtOAc and the combined organic phases were concentrated under reduced pressure at 40 °C until most of the NMP was removed. The crude material was purified by column chromatography (Hex/EtOAc 1:1 w/ 1% Et_3N) to afford **311** (11.2 mg, 0.038 mmol, 25%) as a colorless crystalline solid.

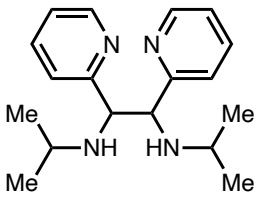

R_f = 0.26 (silica, Hex/EtOAc 1:1, UV).

^{1}H NMR (400 MHz, $CDCl_3$): δ 8.44 (dddd, J = 5.0, 3.3, 1.8, 0.9 Hz, 4H), 7.46 (td, J = 7.6, 1.8 Hz, 2H), 7.33 (td, J = 7.6, 1.8 Hz, 2H), 7.05 (ddd, J = 7.5, 4.9, 1.2 Hz, 2H), 7.01 – 6.93 (m, 4H), 6.88 (dt, J = 7.8, 1.1 Hz, 2H), 4.16 (s, 2H), 3.93 (s, 2H), 2.52 (dh, J = 25.0, 6.2 Hz, 4H), 0.97 (d, J = 6.2 Hz, 2H), 0.94 – 0.82 (m, 18H).

^{13}C NMR (101 MHz, $CDCl_3$): δ 206.96, 162.16, 161.91, 149.03, 148.74, 135.59, 135.39, 123.32, 123.10, 121.64, 121.54, 67.00, 65.85, 65.09, 46.91, 46.13, 30.93, 24.28, 23.86, 22.45, 22.41.

FTIR (NaCl, thin film, cm^{-1}): 3298, 3051, 2960, 2926, 2866, 1693, 1589, 1568, 1469, 1433, 1379, 1337, 1173, 1146, 995, 748.

HRMS (FAB, m/z): calc'd for $C_{18}H_{27}N_4$ $[M+H]^+$: 348.2651; found: 348.2646.

Investigating Conditions that Result in Imine Homocoupling

Table 3.4. *Investigating **271** homocoupling under various conditions.*

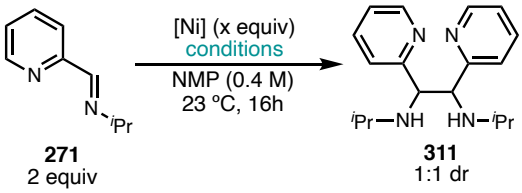

entry	[Ni] (equiv)	conditions (equiv)	yield **311** (%)
1	$Ni(COD)_2$ (1)	–	0
2	$Ni(COD)_2$ (1)	Mn^0 (1)	0
3	$Ni(COD)_2$ (1)	TMSCl (2)	0
4	$Ni(COD)_2$ (1)	Mn^0 (1), TMSCl (2)	0
5	$Ni(COD)_2$ (0.05)	Mn^0 (1)	0
6	$Ni(COD)_2$ (0.05)	TMSCl (2)	trace
7	$Ni(COD)_2$ (0.05)	Mn^0 (1), TMSCl (2)	30
8	$NiCl_2$•dme (0.05)	Mn^0 (1), TMSCl (2)	55
9	–	Mn^0 (1)	0
10	–	TMSCl (2)	0
11	–	Mn^0 (1), TMSCl (2)	74

3.5.7 Probing the Intermediacy of an Organomanganese Intermediate:

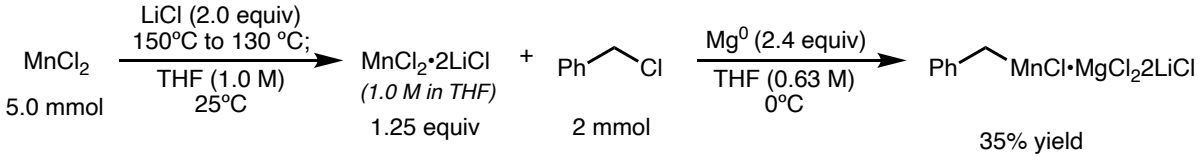

Benzyl organomanganese reagent **6** was prepared according to a procedure from Knochel and coworkers.[40]

Preparation of $MnCl_2$•2LiCl: To an oven-dried 10 mL Schlenk flask charged with a stir bar and cooled under an atmosphere of N_2 was added LiCl (424 mg, 10.0 mmol). The flask was then placed under vacuum (~0.2 mmHg) and heated to 150 ºC in an oil bath for 3 hours. The flask was then backfilled with N_2 and removed from the oil bath. After cooling to room temperature, $MnCl_2$ (629 mg, 5.0 mmol) was added. The flask was then resealed and the mixture of solids was reheated under vacuum at 130 ºC for 3 hours. The flask was then refilled with N_2 and cooled to room temperature followed by the addition of 5 mL of THF was added to the flask. The solution was then stirred for 24 hours at 25 ºC to give a transparent, light-yellow solution of 1.0 M $MnCl_2$•2LiCl in THF.

Preparation of Benzylmanganese chloride: A 50 mL round-bottom flask charged with a stir bar was flame-dried under vacuum and allow to cool to 25 ºC under an atmosphere of N_2 then charged with activated Mg^0 turnings (117 mg, 4.80 mmol, 2.4 equiv). The flask was then evacuated and backfilled with N_2 three times before 0.67 mL of THF was added to the flask followed by 2.5 mL of the $MnCl_2$•2LiCl solution (1.0 M in THF, 2.50 mmol). The mixture was then cooled to 0 ºC in an ice bath and stirred. Once cooled, benzyl chloride (253 mg, 2.0 mmol) was added neat to the reaction and the solution was allowed to stir at

0 ºC for 1.5 hours. The solution was then transferred to a flame-dried Schlenk flask with a filter cannula. The resulting solution was then titrated with I_2 in triplicate to give an average concentration of 0.22 M of **6** in THF (35% yield).

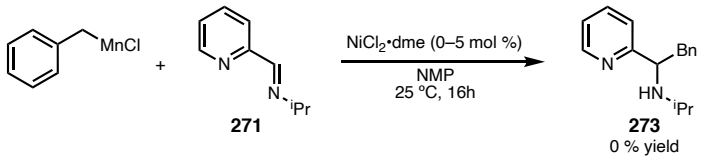

1,2-addition with Organomanganese Reagent: To an oven-dried 1 dram vial with a stir bar was added **271** (14.8 mg, 0.10 mmol). The vial was then pumped into a N_2-filled glovebox where (if applicable) $NiCl_2$•dme (1.1 mg, 5 μmol, 5 mol %) was added and dissolved in 750 μL of NMP. This solution was allowed to stir for 15 min at 27 ºC causing it to turn green (in the presence of Ni). To the solution was then added 545 μL 0.22 M solution of organomanganese reagent via syringe. The vial was then sealed with a teflon-lined cap and isolation tape then removed from the glovebox and stirred on the bench at 600 rpm for 16 hours. The resulting suspension was diluted with CH_2Cl_2 (0.5 ml) and extracted 3x with 1N HCl (0.5 ml). To the combined aqueous phases was added K_2CO_3 (s) until gas evolution ceased. The resulting aqueous solution was extracted 3x with EtOAc and the combined organic phases were concentrated under reduced pressure and analyzed by ^{1}H NMR to obtain the reaction yield. In the case of 0 % Nickel catalyst only starting material was recovered with no product formed. Likewise with 5 mol % $NiCl_2$•dme no product **273** was formed but a significant amount of **311** (57% yield) was recovered.

3.5.8 Stoichiometric Ni^0 Alkylation:

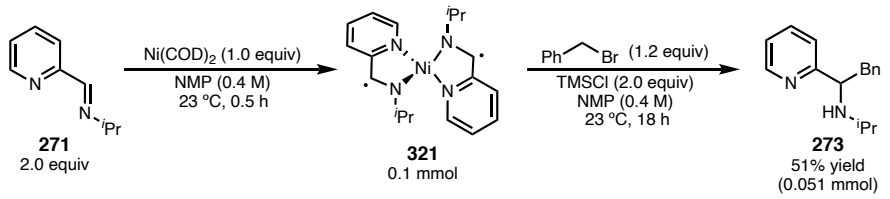

An oven-dried 1-dram vial equipped with a stir bar was charged with 2-imino pyridine **271** (29.6 mg, 0.20 mmol) in a nitrogen-filled glovebox. To the vial was then added $Ni(COD)_2$ (27.5 mg, 0.10 mmol) which immediately turned dark violet as it made contact with the **271** in the vial. The residue was then dissolved in NMP (250 µL, 0.4 M) to give an opaque, royal purple solution. This was then stirred for 30 minutes to ensure complete complexation followed by addition of benzyl bromide (20.5 mg, 0.12 mmol). The vial was then sealed with a Teflon cap, removed from the glovebox, and stirred for 18 hours at 600 rpm. The resulting suspension was diluted with CH_2Cl_2 (0.5 ml) and extracted 3x with 1N HCl (0.5 ml). To the combined aqueous phases was added K_2CO_3 (s) until gas evolution ceased. The resulting aqueous solution was extracted 3x with EtOAc and the combined organic phases were concentrated under reduced pressure and analyzed by ^1H NMR to obtain the reaction yield. Average yield of **273** over 2 runs: 53 % yield (0.053 mmol).

3.5.9 Synthesis of $(271)_2MCl_2$ Complexes 322 and 323:

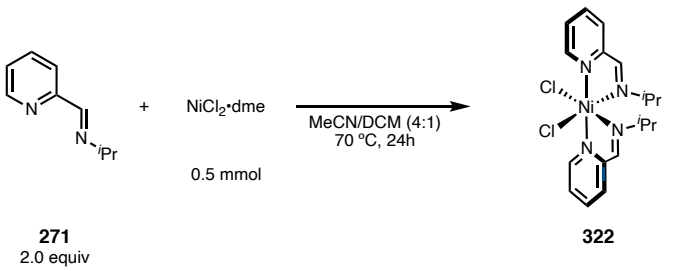

Synthesis of 322: Procedure adapted from method described by Andrade-Lopez and coworkers[41]. In a nitrogen-filled glovebox an oven-dried 1 dram vial with a stir bar was charged with $NiCl_2$•dme (110mg, 0.5 mmol, 1 equiv) and suspended in 2mL MeCN then sealed with a septa cap. To a separate 1 dram vial was added 0.5mL DCM and imine **271** (148mg, 1.0 mmol, 2 equiv) then sealed with a septa cap. The vials were then removed from the glovebox and placed under a flow of N_2. The stirring acetonitrile solution was then heated to 70 ºC where the DCM solution of **271** was added causing the mixture to become a homogenous green solution. After 5 hours a green precipitate started to form. After 24 hours the solution was cooled to room temperature and filtered. The green powder was washed with cold MeCN two times then dried under high vacuum to give **322** (173 mg, 0.41 mmol, 81% yield) as a green powder. The crude powder could be recrystallized from a minimal amount of 4:1 MeCN:$CHCl_3$ and cooled to –20 ºC to give green rhombic crystals.

FTIR (NaCl, thin film, cm^{-1}): 2969, 1976, 1596, 1442, 1390, 1331, 1300, 1167, 1018, 780, 729, 509.

HRMS (FD, m/z): calc'd for $C_{18}H_{24}N_4ClNi$ $[M\text{-}Cl^-]^+$: 389.10375; found: 389.10334.

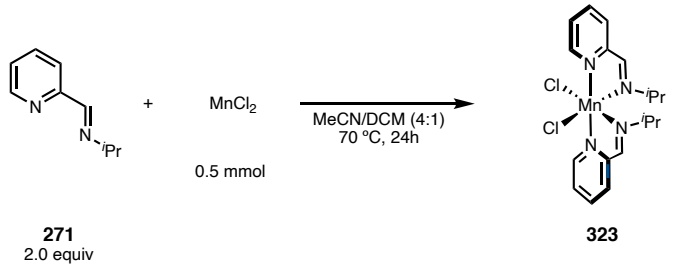

Synthesis of 323: Procedure adapted from method described by Andrade-Lopez and coworkers.[41] In a nitrogen-filled glovebox an oven-dried 1 dram vial with a stir bar was

charged with $MnCl_2$ (62.9 mg, 0.5 mmol, 1 equiv) and suspended in 2mL MeCN then sealed with a septa cap. To a separate 1 dram vial was added 0.5 mL DCM and imine **271** (148 mg, 1.0 mmol, 2 equiv) then sealed with a septa cap. The vials were then removed from the glovebox and placed under a flow of N_2. The stirring acetonitrile solution was then heated to 70 ºC where the DCM solution of **271** was added causing the mixture to become a cloudy orange solution. After 1 hour an orange precipitate started to form. After 24 hours the solution was cooled to room temperature and filtered. The orange powder was washed with cold MeCN two times then dried under high vacuum to give **323** (194 mg, 0.46 mmol, 92% yield) as an orange solid. The crude powder could be recrystallized from a minimal amount of 4:1 MeCN:$CHCl_3$ and was lightly capped so the solvent can slowly evaporate and allowed to sit for to give orange rhombic crystals.

FTIR (NaCl, thin film, cm^{-1}): 2966, 2929, 1645, 1593, 1461, 1440, 1394, 1363, 1305, 1166, 1012, 874, 784, 749, 637, 506.

3.5.10 Preparation of $(271)_2Ni^{I}$ complex 324 :

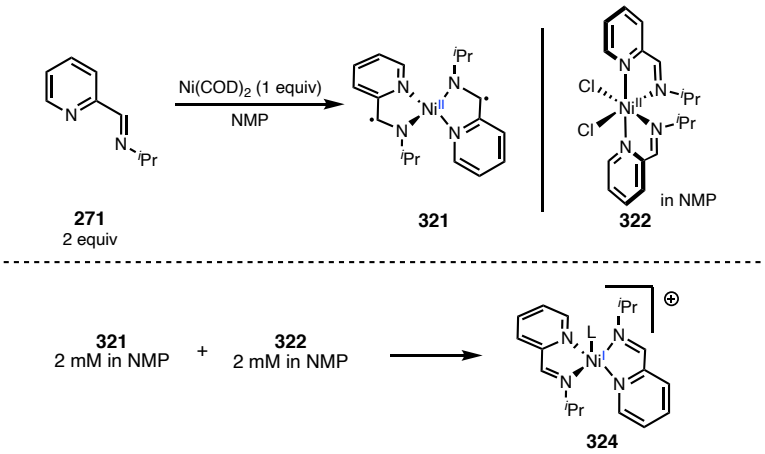

UV/VIS sample Preparation: In a N_2-filled glovebox, an oven-dried 20 mL scintillation vial with a stir bar was charged with $Ni(COD)_2$ (2.2 mg, 8 μmol, 0.8 equiv) and 2.5 mL of NMP. To the stirring suspension was added **271** (2.4 mg, 16 μmol, 1.6 equiv) causing the solution to turn a deep royal purple and was allowed to stir for 15 minutes to form **321**. Concurrently, an oven-dried 1 dram vial with a stir bar was charged with **322** (4.3 mg, 10 μmol, 1 equiv). To the vial was added 2.5 mL of NMP to give a green solution. After 15 minutes the NMP solution of **322** was transferred to the solution of **321** in NMP causing the solution to turn black. The solution was stirred for 2 hours then transferred to a quartz cuvette (1 cm pathlength) for UV/VIS analysis.

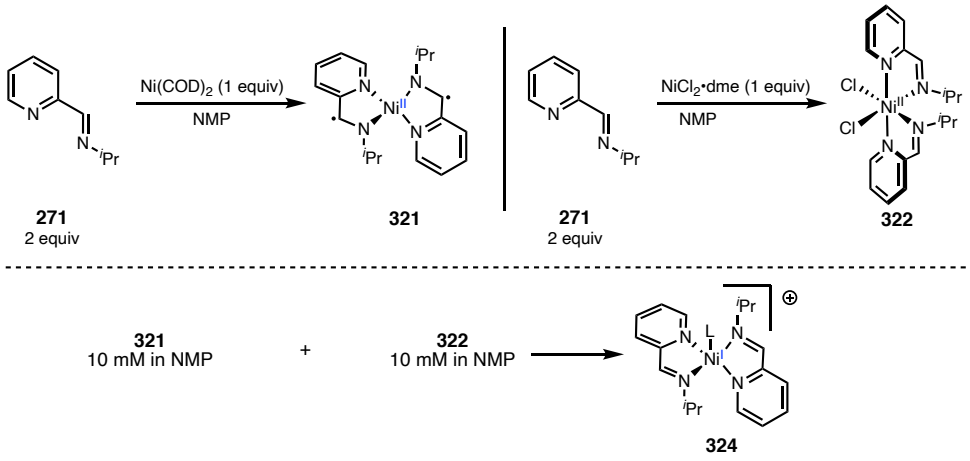

EPR sample Preparation: In a N_2-filled glovebox, an oven-dried 20 mL scintillation vial with a stir bar was charged with $Ni(COD)_2$ (13.7 mg, 50 μmol, 1 equiv) and 1 mL of NMP. To the stirring suspension was added **271** (14.8 mg, 100 μmol, 2 equiv) causing the solution to turn a deep royal purple and was allowed to stir for 15 minutes to form **321**. Concurrently, an oven-dried 1 dram vial with a stir bar was charged with $NiCl_2$•dme (11.0 mg, 50 μmol, 1 equiv). To the vial was added 1 mL of NMP to give a blue solution followed by **271** (14.8 mg, 100 μmol, 2 equiv) causing the solution to turn light green to form **322**

After 15 minutes the NMP solution of **322** was transferred to the solution of **321** in NMP. The 1 dram vial was then rinsed with 3 mL of NMP (final concentration 10 mM) to ensure quantitative transfer. This solution was then stirred for 15 minutes and turned from dark purple to black. An aliquot of this solution was then transferred to an EPR tube which was then rapidly frozen at 77 K in a liquid N_2 dewar and was analyzed by EPR.

General EPR Details: X-Band EPR spectra (9.4 Hz, continuous wave) using a Bruker EMX spectrometer with Bruker Win-EPR software. Samples were collected at 77 K using a vacuum-insulated quartz liquid N_2 dewar. For maximum sensitivity, several microwave frequencies were scanned between 20 mW to 20 μW where 2 mW was found to be optimal. EPR data was simulated in MATLAB with Easyspin. Key parameters: Temperature = 77 K, solvent = NMP, microwave frequency = 9.36 GHz, power = 2.181 mW, modulation amplitude = 1200.00 G.: EPR was simulated as two S=1/2 Ni^{I} isomeric species (based on optimal fitting parameters and related work from Wieghardt.[45] Fitting parameters for species 1 (plum): $g_1 = 2.25$, $g_2 = 2.16$, $g_3 = 2.03$, linewidth = 4.4 mT, $\Gamma_1 = 70$, $\Gamma_2 = 47$, $\Gamma_3 = 85$ MHz, weighting factor = 1.0. Fitting parameters for species 2 (teal): $g_1 = 2.30$, $g_2 = 2.20$, $g_3 = 2.07$, linewidth = 3.5 mT, $\Gamma_1 = 106$, $\Gamma_2 = 2$, $\Gamma_3 = 123$ MHz, weighting factor = 0.56.

EPR Data of 324:

Figure 3.15. *Experimental and simulated EPR spectrum of comproportionation reaction.*

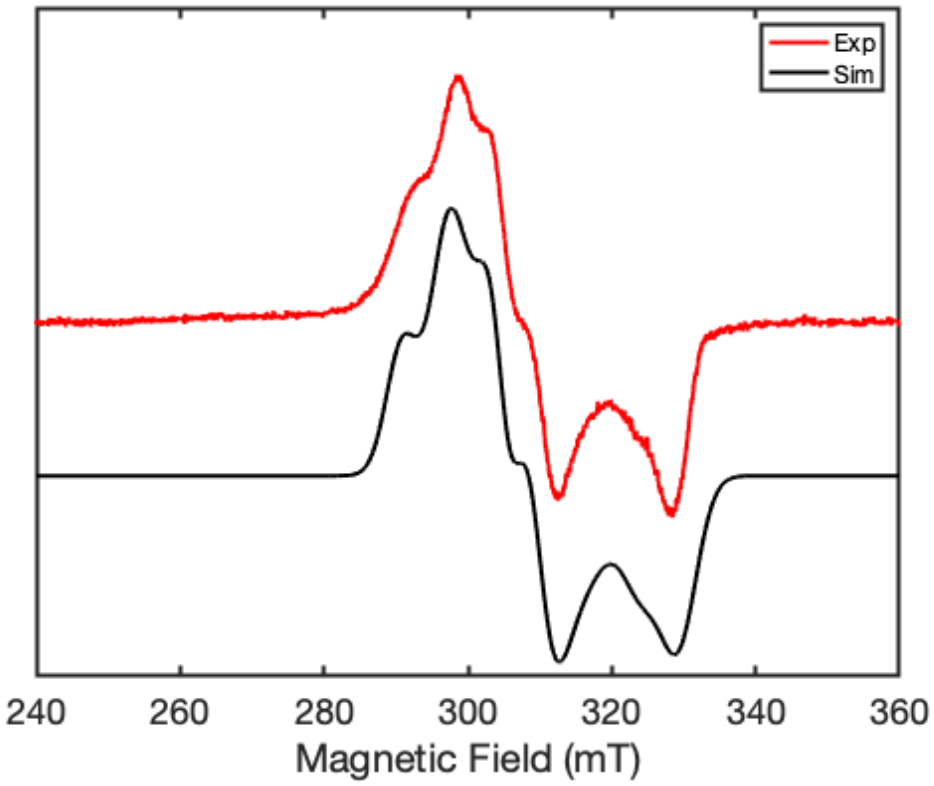

Figure 3.16. *EPR of each simulated species shown separately.*

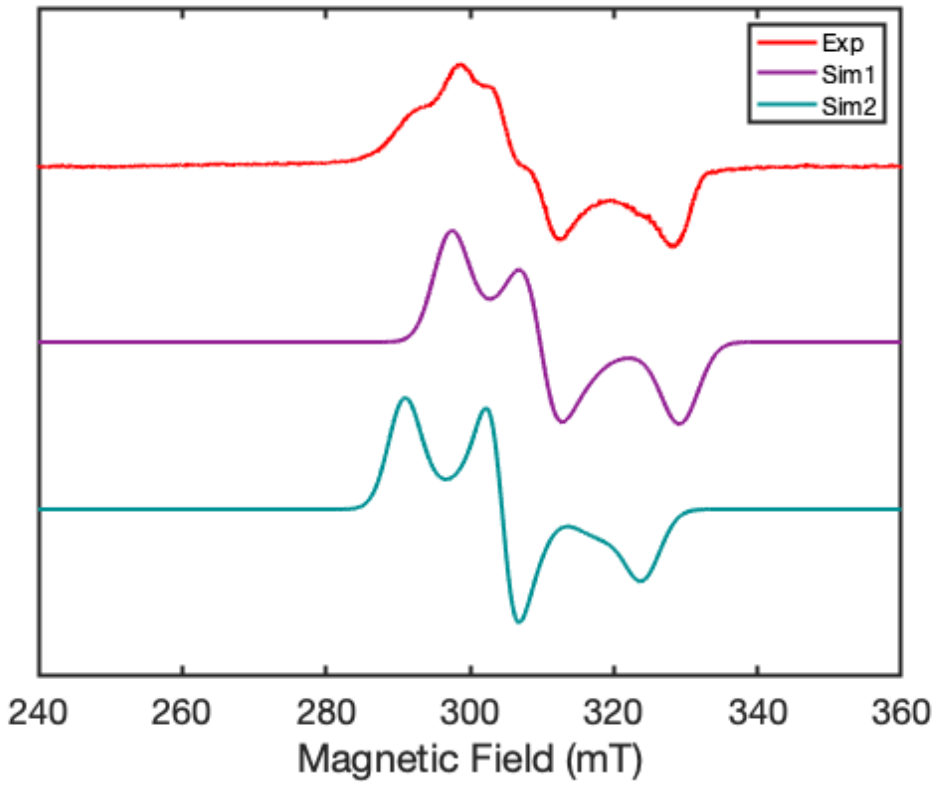

3.5.11 Alternative Radical Generation Approaches for Alkylation

Lewis and Brønsted acids were evaluated as alternative catalysts to facilitate radical addition into heteroaryl imines. Using Lewis acids under otherwise optimized conditions in place of $NiCl_2$•dme did not provide the same yield boost or improve the yield beyond the Mn-mediated background reaction. Yields determined by ^{1}HNMR with an internal standard. (Table S3.5).

Table 3.5. *Alkylation reaction with alternative, non redox-active, metal catalysts.*

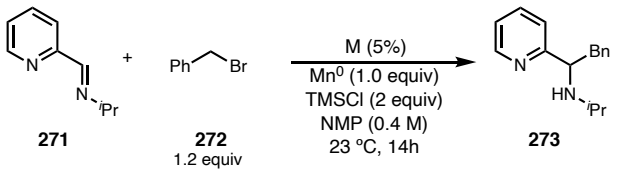

entry	M	yield **273** (%)
1	–	66
2	$MgBr_2$	58
3	BPh_3	48
4	AcOH	53
5	$AlCl_3$	44

Radical generation under thermal AIBN/$^{n}Bu_3SnH$ conditions in the absense of Mn^0 did not result in product formation whereas the optimized conditions performed at 80ºC gave alkylated product in 42% yield (Scheme 3.6).

Scheme 3.6. *Thermal radical generation conditions for a redox-neutral imine alkylation (top) and control experiment of the optimized reaction conditions run at 80ºC (bottom).*

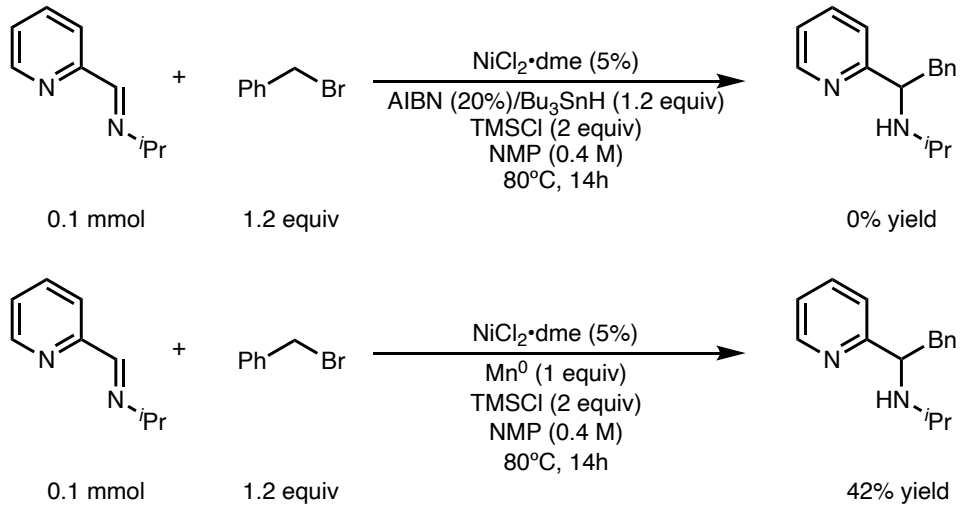

Genration of benzylic radicals through the reduction of NHP esters in the presence of TMSCl and TDAE as a reductant. Across several metal catalysts we observe significant levels of benzyl homocoupled product indicating radical formation and trace levels of alkated products (Scheme 3.7).

Scheme 3.7. *Radical generation under mild reductive conditions employing NHP esters as radical precursors and several metal catalysts*

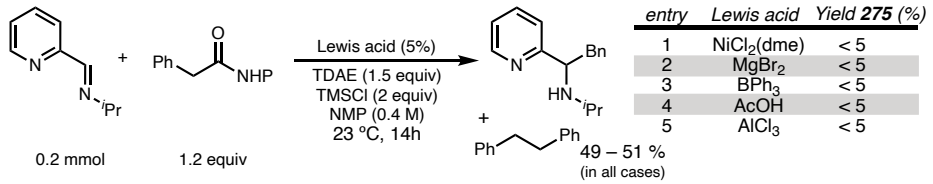

entry	*Lewis acid*	*Yield **275** (%)*
1	$NiCl_2$(dme)	< 5
2	$MgBr_2$	< 5
3	BPh_3	< 5
4	AcOH	< 5
5	$AlCl_3$	< 5

3.5.12 Electroanalytical Experiments

General Details: Cyclic voltammograms were obtained in a N_2-filled glovebox using a standard three electrode cell consisting of a freshly polished (0.3 μm then 0.05 μm alumina) glassy carbon working electrode, platinum counter electrode, and a silver wire non aqueous reference electrode in 10mM $AgNO_3$ (MeCN). Data were collected using a Biologic SP-300 potentiostat and analyzed in EC-Lab. All cyclic voltammograms were measured in NMP with 0.1M $TBAPF_6$ supporting electrolyte and then referenced to freshly sublimed ferrocene (Fc). All voltammagrams were background corrected against blank solvent/electrolyte unless specified. Peak currents were calculated from linear baseline-corrected "peak analysis" feature in EC-Lab. The reduction potentials are reported versus the reduction potential of the Fc/Fc^+ peak. Ohmic drop compensation was done with all samples before each scan using positive-feedback iR-compensation at 85% of uncompensated resistance (R_u) measured from potentio electrochemical impedence spectroscopy (PEIS). All CVs shown are first scan in 0.1 M $TBAPF_6$ electrolyte in NMP at 25 ºC, ν = 100 mv/s unless otherwise specified.

Cyclic Voltammetry of Heteroaryl Imines and Metal Complexes:

Figure 3.17. *CV of* ***271*** *(1 mM).*

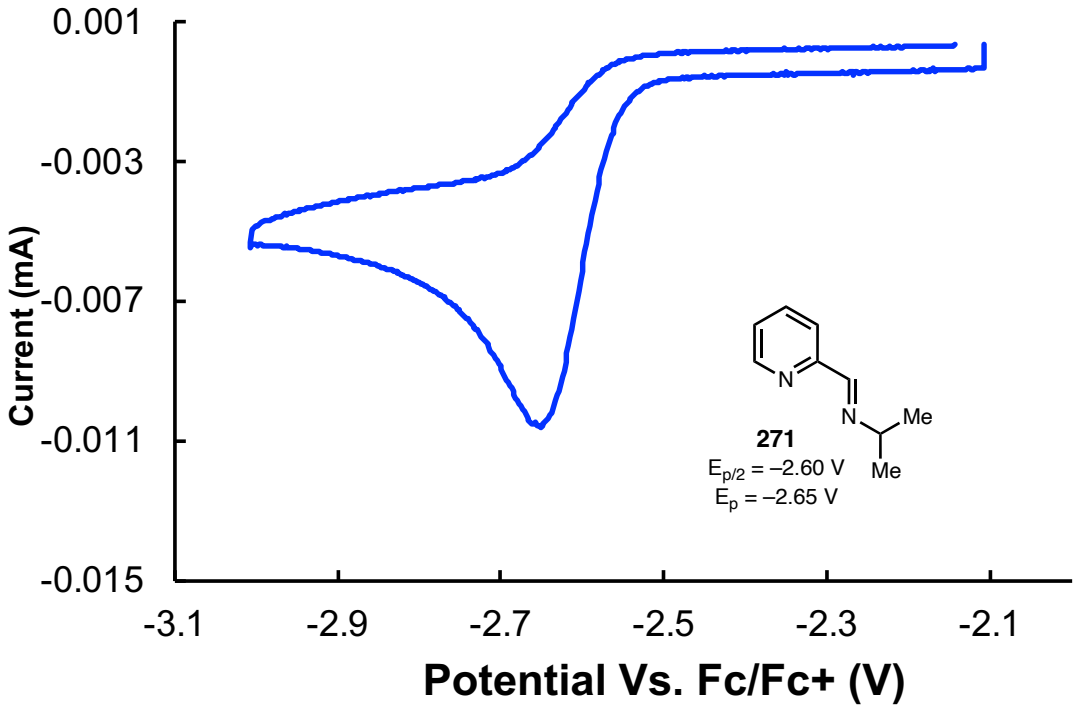

Figure 3.18. *CV of* ***322*** *(1 mM) that was independently synthesized.*

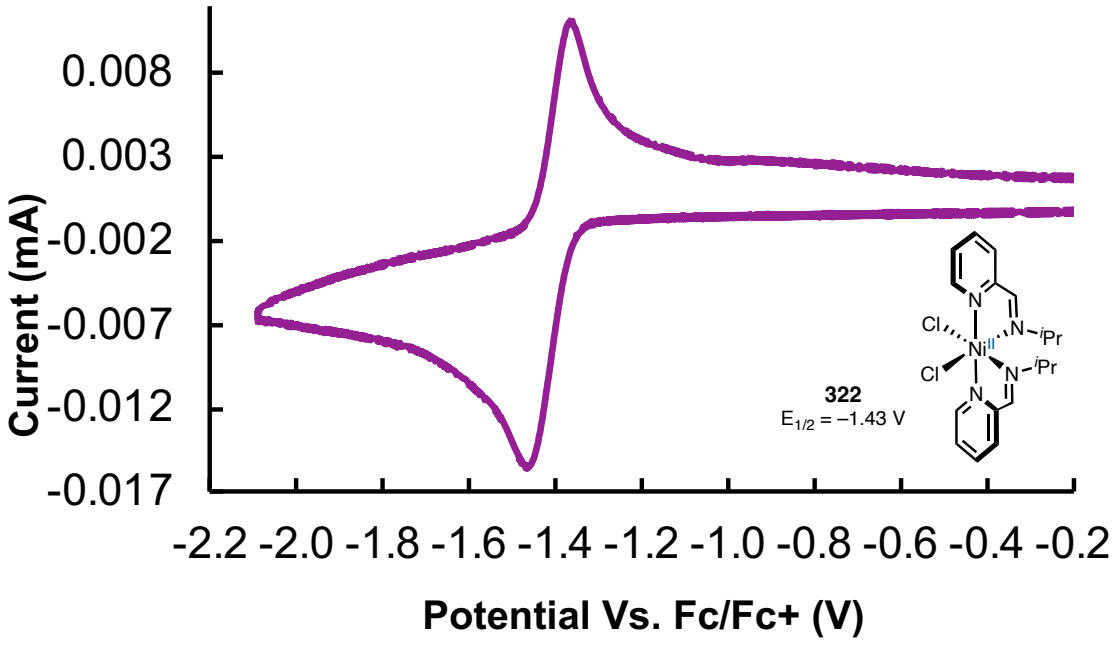

Figure 3.19. *CV of* ***322*** *(1 mM) prepared in situ from $NiCl_2$·dme. The second reduction peak is likely small amounts of the Ni complex with three* ***271*** *ligands.*[42]

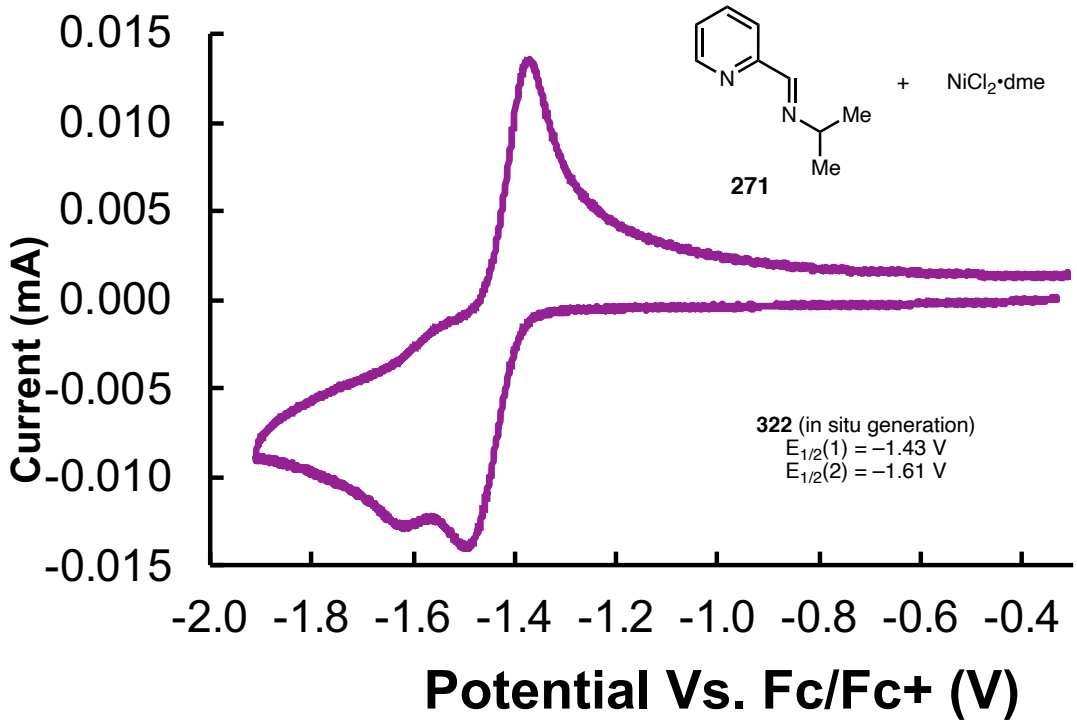

Figure 3.20. *CV of* ***321*** *(1 mM) prepared in situ from $Ni(COD)_2$.*

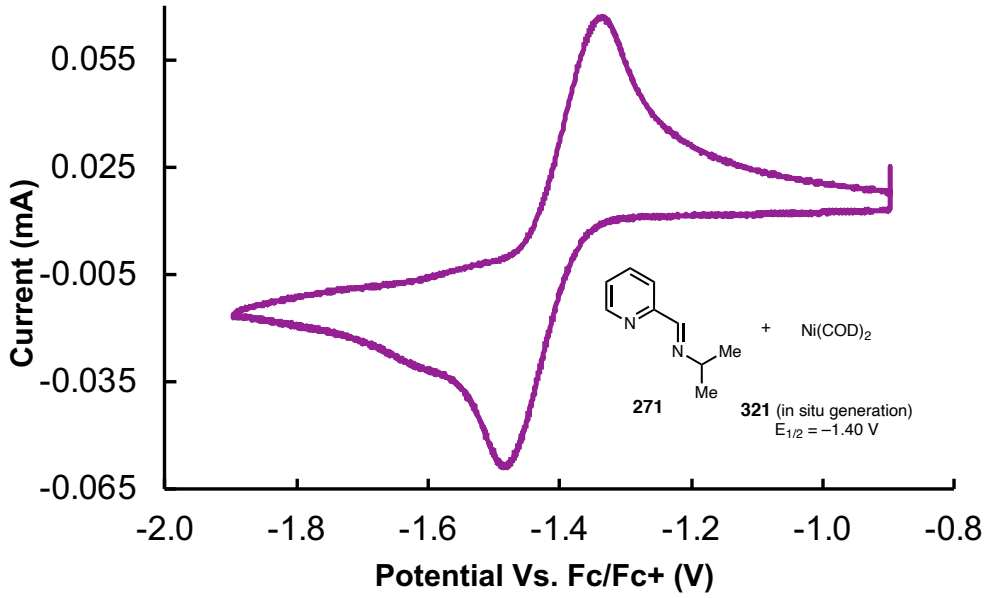

Figure 3.21. *CV of* ***323*** *(2 mM) prepared in situ from* $MnCl_2$.

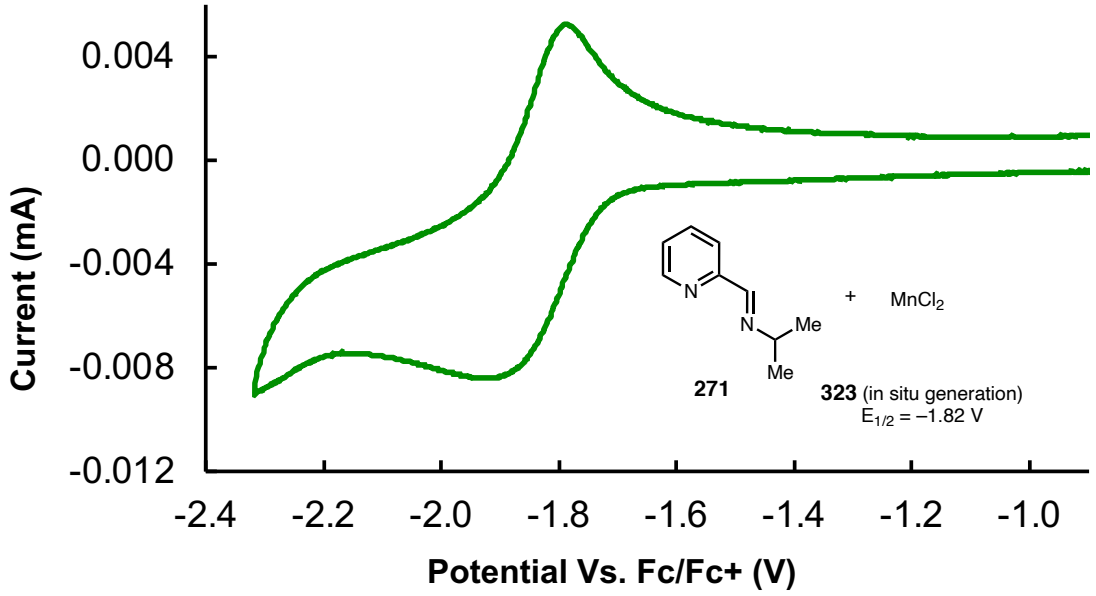

Figure 3.22. *CV of* ***271***–$MgBr_2$ *prepared in situ from* $MgBr_2$.

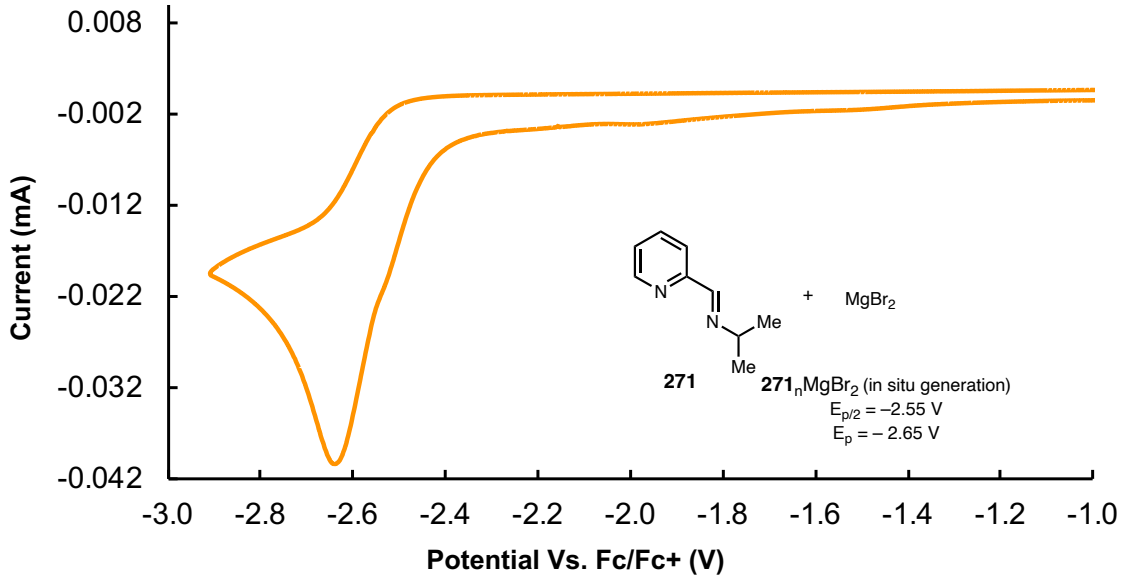

3.5.13 Effect of Reaction Components on 322

Figure 3.23. *Cyclic voltammograms of* ***322*** *(1 mM, purple) followed by the addition of 10 mM BnCl (green) and 90 mM BnCl (100 mM total, blue).*

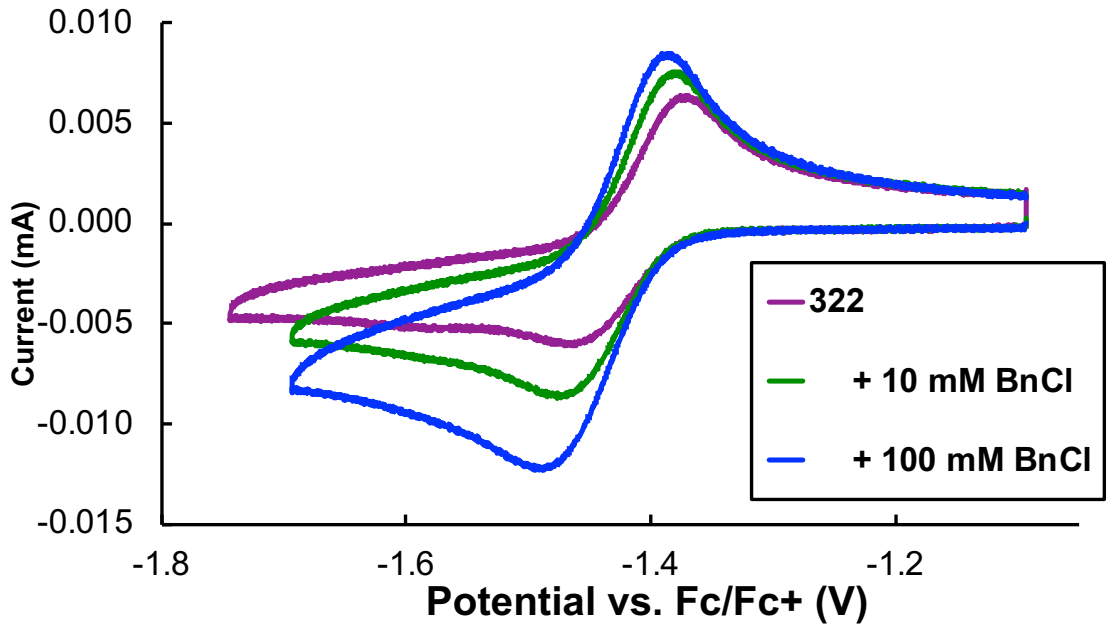

Figure 3.24. *Cyclic voltammograms of* ***322*** *(1 mM, purple) followed by the addition of 100 mM BnCl (green). Addition of 40 mM* ***271*** *to allow for turnover for additive studies (blue). Addition of 50 mM AcOH additive (teal) followed by an additional 100 mM AcOH to the same cell (150 mM total, orange).*

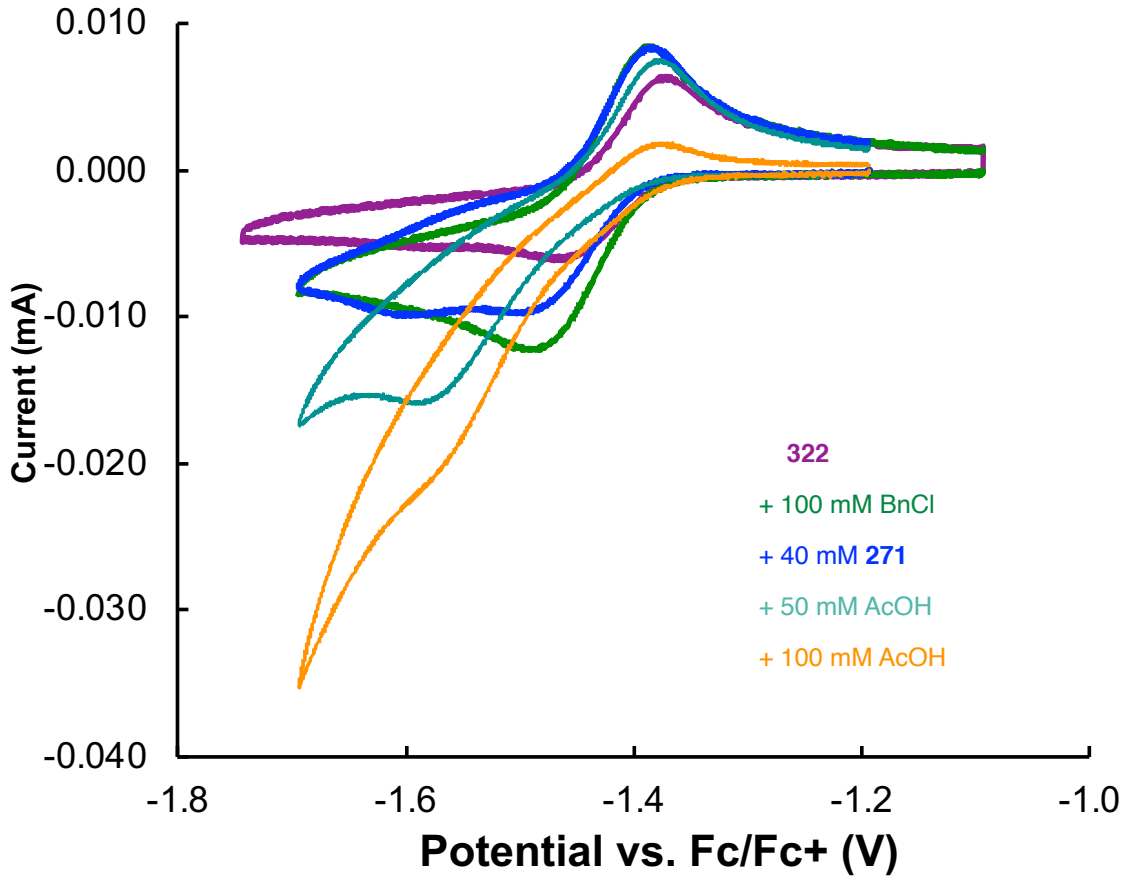

Figure 3.25. *Control experiment for Figure 3.24 showing voltammetry for different order of addition of reaction components. Cyclic voltammograms of* ***322*** *(1 mM, purple) with 20mM excess* ***271****. Reaction component addition order: 2 mM AcOH (green), addition of 98 mM AcOH (blue), then 100mM BnCl to the cell.*

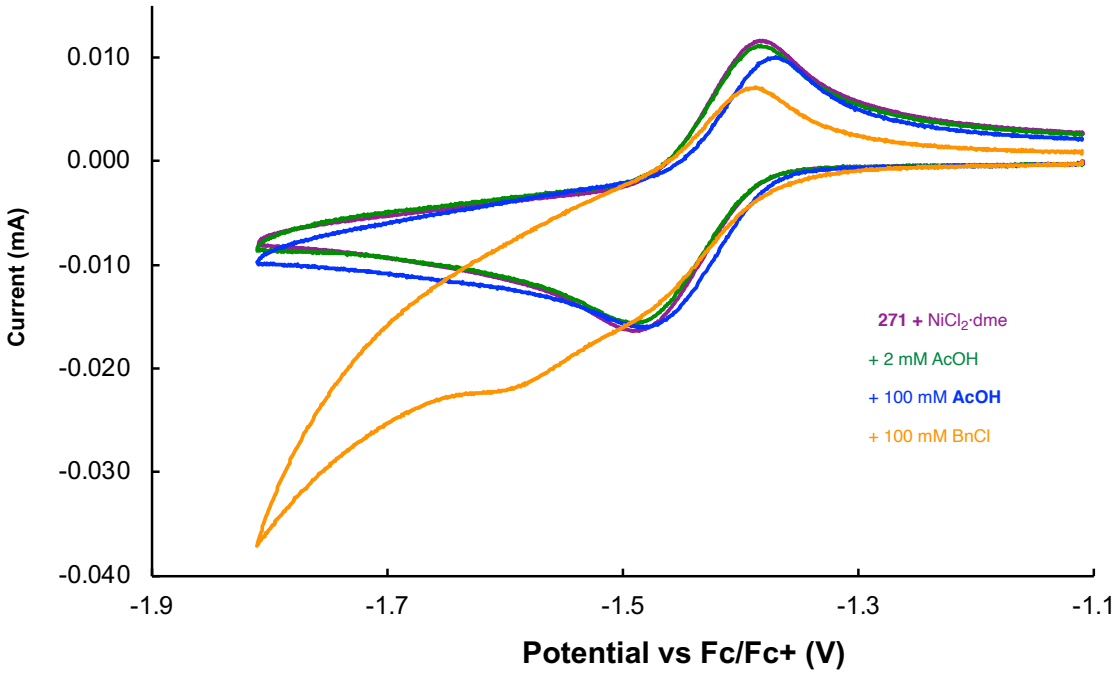

Kinetics of Reaction of Reduced 322 (322^{red}) and Benzyl Chloride:

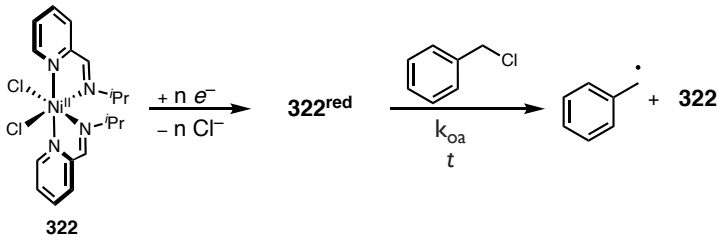

To calculate the reaction rate constant between reduced **322** (**322^{red}**) with benzyl chloride) a procedure described by Sigman and Minteer was used.[43] This reaction could be studied by mixing **322** with a large excess of benzyl chloride and measuring the cathodic and

anodic peak currents (i_{pc} and i_{pa}) of the **322** redox wave at varying scan rates (ν) from 2 V/s to 3 mV/s. Varying the scan rate changes the time it takes to go from E_{pc}, where **322^{red}** is generated, to the E_{pa}, where any remaining **322^{red}** is reoxidized to **322**, enabling us to calculate the amount of **322^{red}** remaining after it reacts with benzyl chloride at various time points. In the case of a CV potential window $E_i \rightarrow E_r$ (± 0.25 V to $E_{1/2}$ here) then the reaction time (t) can be calcualted as:

$$t = \frac{\left|E_r - E_{pc}\right| + \left|E_r - E_{pa}\right|}{\nu}$$

where E_{pc} is the potential of the peak cathodic current and E_{pa} is the potential of the peak anodic current. From the Randles-Sevcik equation, the amount of **322^{red}** remaining at time t can be detemined from the baseline-corrected peak height ratios (i_{pa}/i_{pc}):

$$\frac{i_{pa}}{i_{pc}} = \frac{\left[\mathbf{322}^{red}\right]_t \sqrt{D_{\mathbf{322}red}}}{\left[\mathbf{322}^{red}\right]_0 \sqrt{D_{\mathbf{322}}}}$$

We can simplify this by assuming that the difussion coefficents for the reduced species **322^{red}** and **322** ($D_{\mathbf{322}}{}^{red}$ and $D_{\mathbf{322}}$ respectively) are approximately the same:

$$\frac{i_{pa}}{i_{pc}} = \frac{\left[\mathbf{322}^{red}\right]_t}{\left[\mathbf{322}^{red}\right]_0}$$

Multiplying the fraction by the known initial concetration of **322** (1 mM) will give us the concentration of **322^{red}** at t allowing us to extract a time course. This time course can then be treated as a pseudo-1st order reaction due to large excess of benzyl chloride (100 mM) or be simulated as a second order reaction and analyzed in the COPASI[44] kinetics simulation software.

Figure 3.26. *Voltammograms of the reaction of* ***322*** *(1 mM) with BnCl (100 mM) with scan rates 3-80 mV/s.*

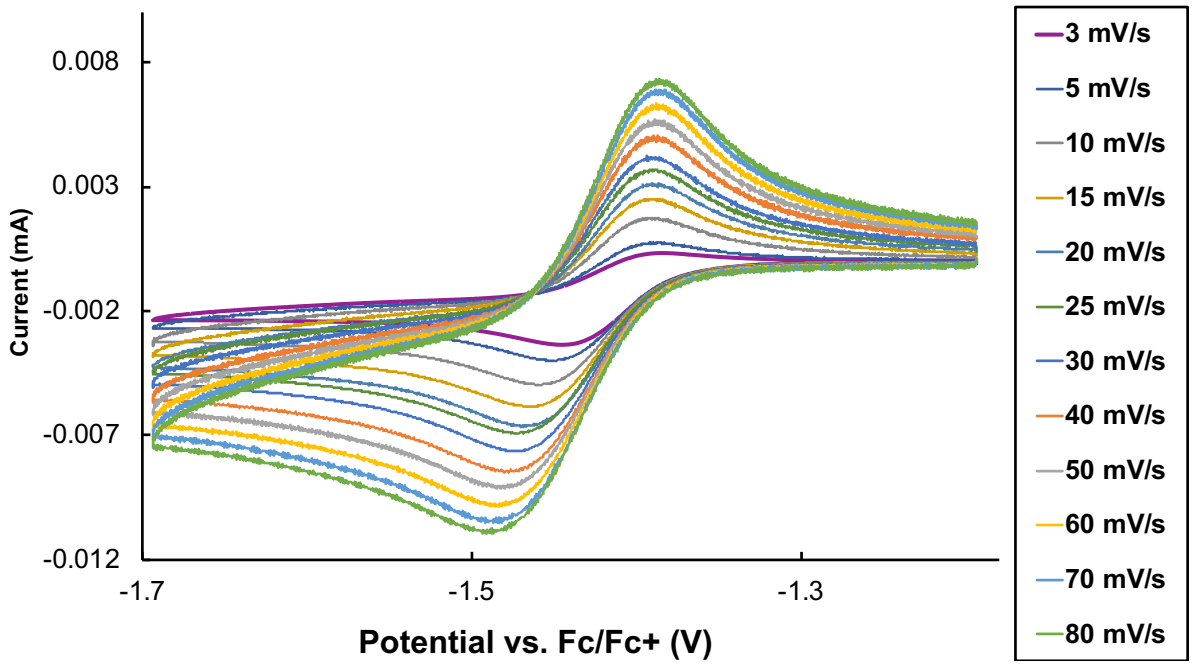

Figure 3.27. *Voltammograms of the reaction of* ***322*** *(1 mM) with BnCl (100 mM) with scan rates 100-2000 mV/s.*

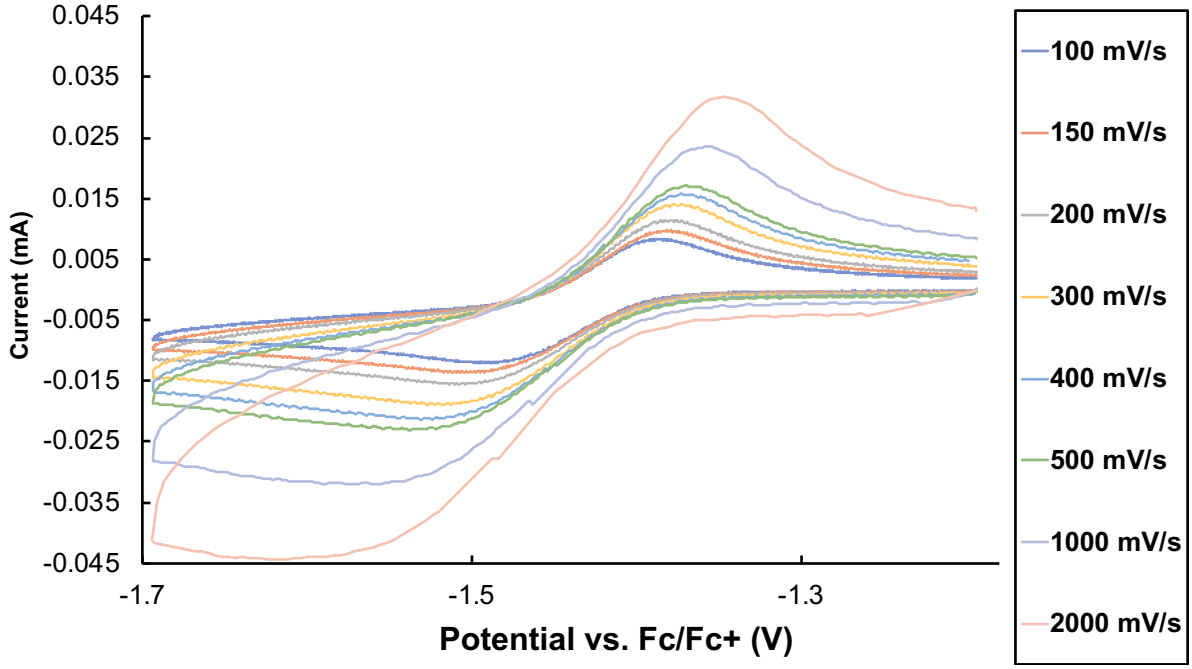

Figure 3.28. *Time course of calculated* ***322***^{red} *remaining over time after reacting with BnCl.*

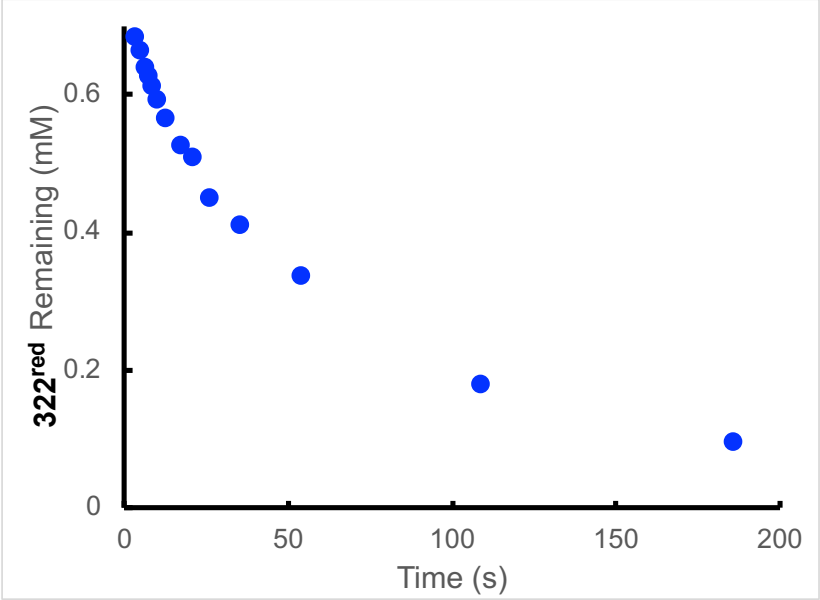

Kinetic Analysis: The net reaction between **322**^{red} and benzyl chloride follows the second order rate equation:

$$rate = k_{oa}[BnCl][322^{red}]$$

Given the large excess of BnCl added, the reaction can be treated as a pseudo-1st order reaction with the rate law:

$$rate = k_{app}[322^{red}]$$

$$k_{app} = k_{oa}[BnCl]$$

For the pseudo-1st order treatment the rate constant k_{app} can be determined from the slope of a plot of ln([**322**^{red}]) vs. time (Figure 3.29) which can then be used to determine k_{oa} with the known amount of benzyl chloride added ($[BnCl]_0$). From the measured $k_{app} = 0.018$ s^{-1} we determine the corresponding 2nd order rate constant $k_{oa} = 0.18$ M^{-1}s^{-1}.

Figure 3.29. *First order treatment of time course data from reaction of* ***322***^{red} *and benzyl chloride.*

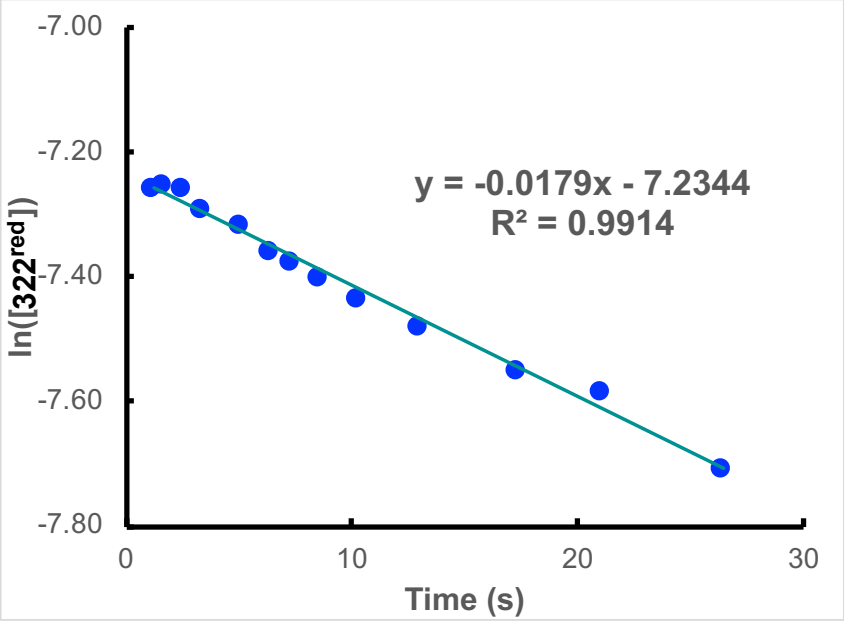

A complementary approach utilizing kinetic modeling software was also done with the time course data. The reaction was modeled as a second order process and gave a $k_{oa} = 0.17$ $M^{-1}s^{-1}$ (Figure 3.30).

Figure 3.30. *Experimental time course and simulated reaction fit. Fit was used for first entire time course measured.*

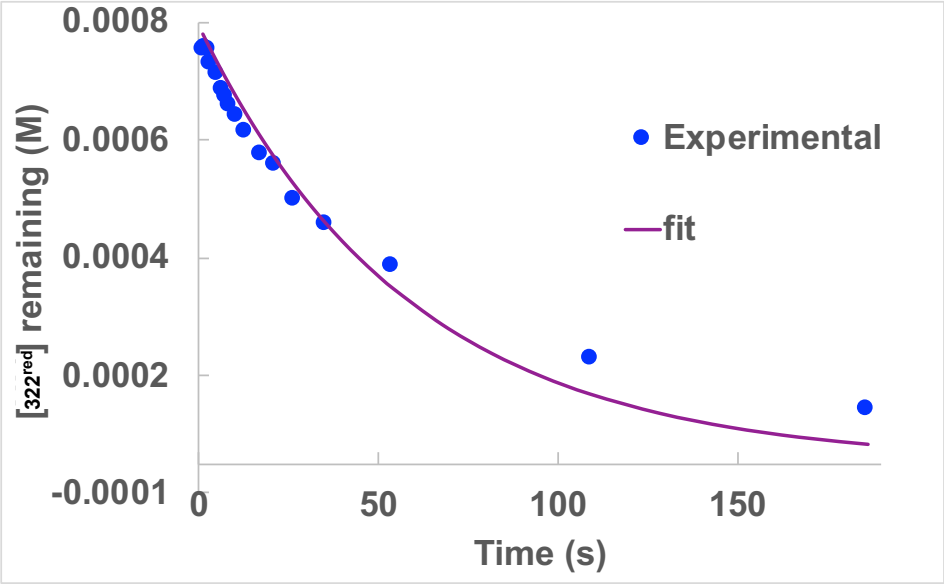

3.5.14 UV/Vis and Spectroelectrochemistry

General Details of UV/Vis studies: All UV/Vis measurements were performed on a Cary 50 spectrophotometer with Cary WinUV software. Samples were prepared in a nitrogen filled glovebox and sealed in a 1 cm quartz cuvette for analysis. Background correction was done against an NMP blank and samples were scanned from 1100 nm to 300 nm. ε values were calculated from the prepared concentration in the case of **321** and **322** and in the case of the Ni^{I} the reaction (section 3.5.10) to make the Ni^{I} sample was assumed to be quantitative. This assumption appears to be valid based on the lack of spectral features resembling **321** in the sample and similarities in the known ε values for the analogous Ni^{I} and formally Ni^{0} complexes studied by Wieghardt and Coworkers.[45]

UV/Vis of Independently Prepared Complexes

Figure 3.31. *UV/Vis spectrum of* ***322*** *(1mM) in NMP. Inset: Close up of 400-1100 nm region to show transitions.*

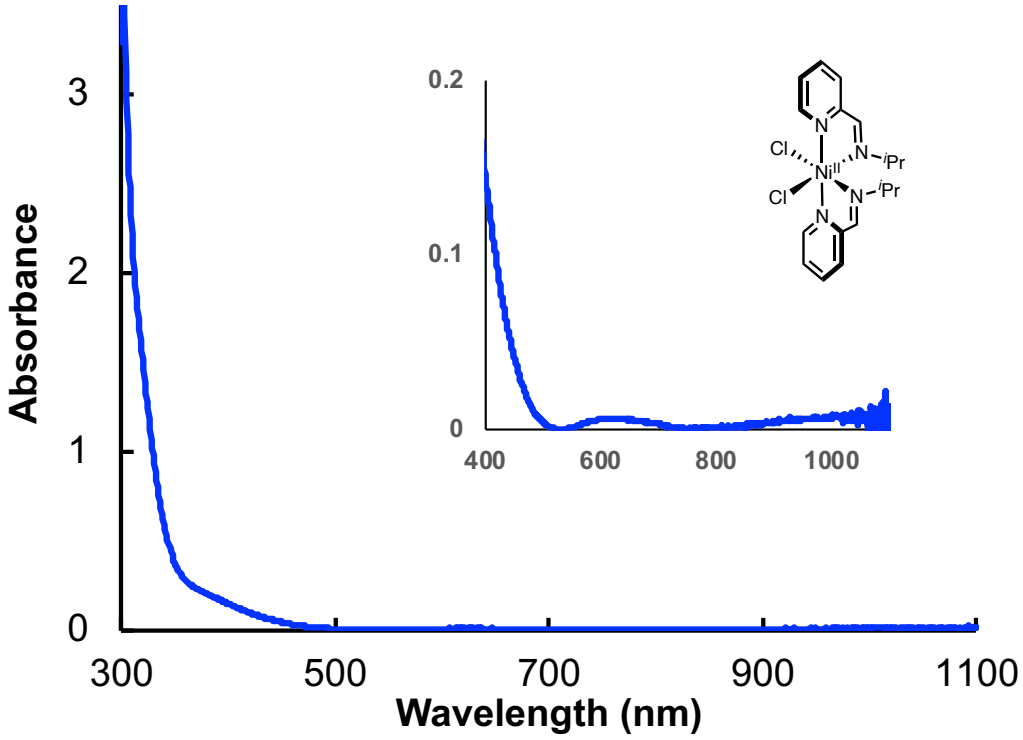

Figure 3.32. *UV/Vis spectrum of* ***321*** *(0.26 mM) prepared from* ***271*** *(0.52 mM) and* $Ni(COD)_2$.

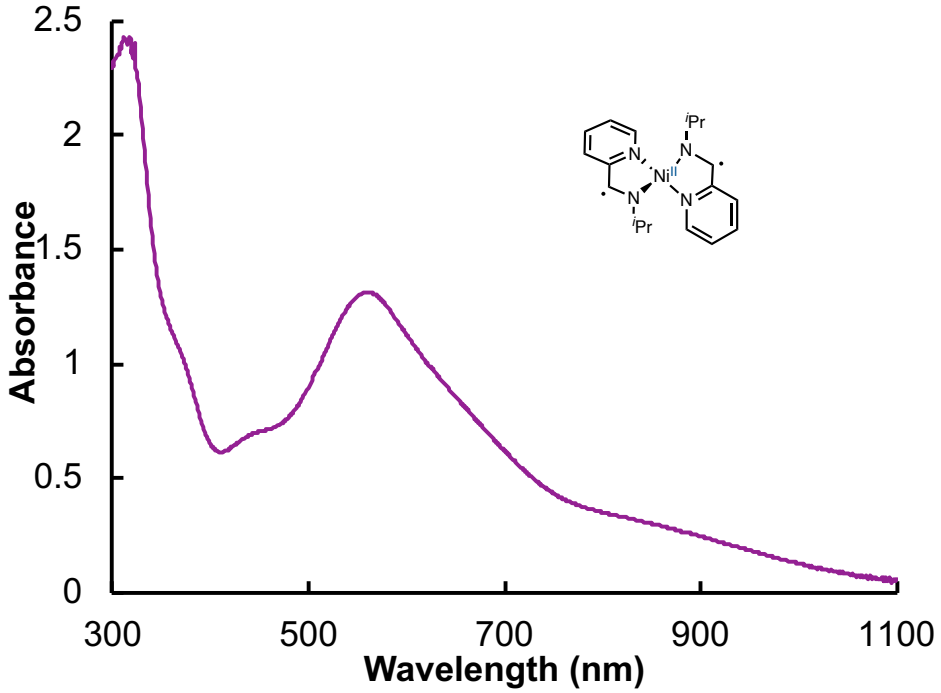

Figure 3.33. *UV/Vis spectrum of* $(\mathbf{271})_2Ni^{I}$ *(0.32 mM) prepared from reacting* ***321*** *and* ***322*** *after 2 hours to ensure complete disproportionation.*

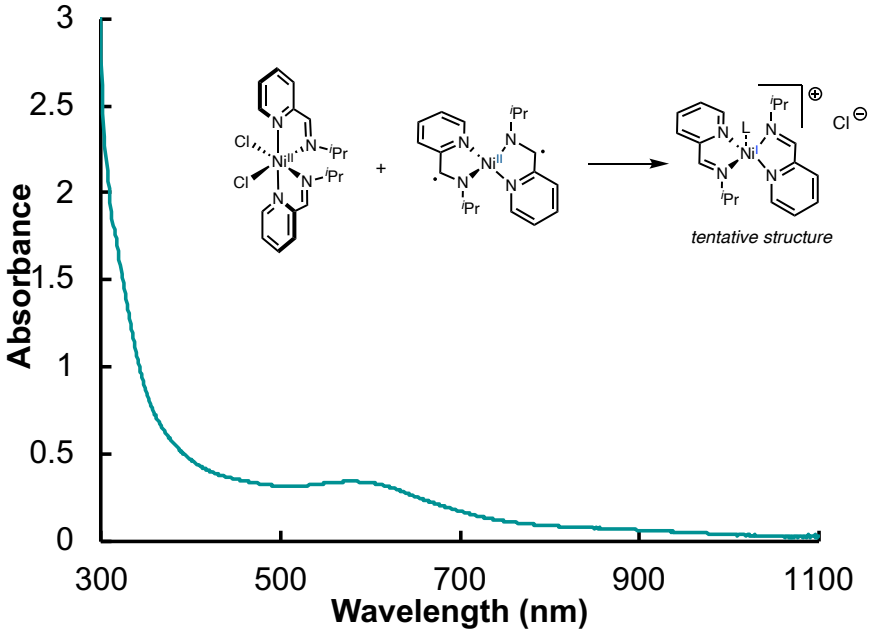

Spectroelectrochemistry of 322

General Details: Spectroelectrochemistry studies were conducted in a nitrogen-filled glovebox. Spectroelectrochemistry kit from Pine Research (AKSTCKIT3) was used with measurements done in a quartz spectroelectrochemical cell with 0.17 cm path length. A three electrode setup composed of a honeycomb electrode containing Pt working and Pt counter electrodes was used along with a silver wire, $Ag/AgNO_3$ (10 mM MeCN), non-aqueous reference electrode. The cell was placed in a Ocean Optics CUV–UV cuvette holder connected to the light source and spectrophotometer with 600 μm core optical fibers. UV/Vis measurements were done with an Hamamatsu L1179 deuterium light source coupled to an Ocean Optics USB4000-UV-Vis-ES detector.

Spectroelectrochemistry Measurement Procedure: An initial cyclic voltammagram was taken of the 1 mM solution of **321** (0.1 M $TBAPF_6$ in NMP to identify redox peaks. For spectroelectrochemistry measurements the cell was held at a constant voltage for 3 minutes where after 2.5 minutes of elecrolysis the spectrum was saved to ensure that the majority of electroactive species were reduced at the electrode despite most of the current passing within the first 5 seconds once sufficiently reducing potentials were reached (Figure 3.34). Starting at -1.04 V vs. Fc/Fc^+ the potential was then decreased stepwise by 0.1 V increments until significant current started to pass at which point the step sizes decreased to 0.05 V. This was done until the spectrum remained unchanged indicating reduction was complete (–1.94 V vs. Fc/Fc^+). After this the procedure was repeated in the oxidative direction to ensure the reversibility of the process. All spectra were basline corrected at 860 nm and plotted as the 5-point moving average.

Calculating ε in Figure 3.11: The UV/Vis spectra remained largely unchanged in intensity and absorbance features at -1.74 V (vs. Fc/Fc^+) suggesting all of **322** at the electrode had been reduced. Assuming this is true the ε was calculated from an assumed concentration of 1 mM of reduced species at each measured wavelength. From these values, the concentration of **321** can be calculated at lower potentials containing <1 mM of **321**. The concentration was calculated by averaging the concentration calculated for each wavelength by A/(ε*0.17 cm) between 320 nm and 630 nm. The average concentration calculated at the $E_{1/2}$ (-1.44 V) was 0.54 ± 0.04 mM.

Figure 3.34. *Representative current of electrochemical cell over time under constant potential electrolysis (-1.54 V vs Fc/Fc^+ here). By the time the UV/Vis spectrum was recorded most of the current had passed to generate the reduced species.*

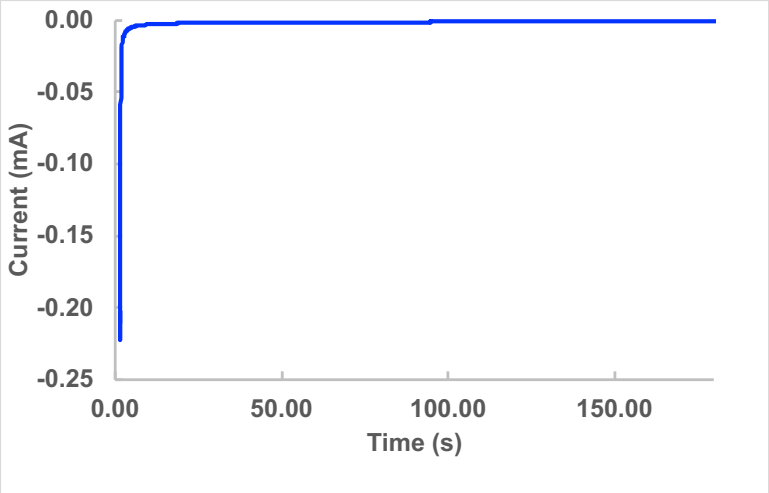

Figure 3.35. *UV/Vis spectroelectrochemical absorbance spectra during stepwise potential scan. Potentials listed are relative to Fc/Fc⁺. Shown spectra are taken after 2.5 minutes of electrolysis. * Indicates signal saturation inherent to light source and detector used for experiment.*

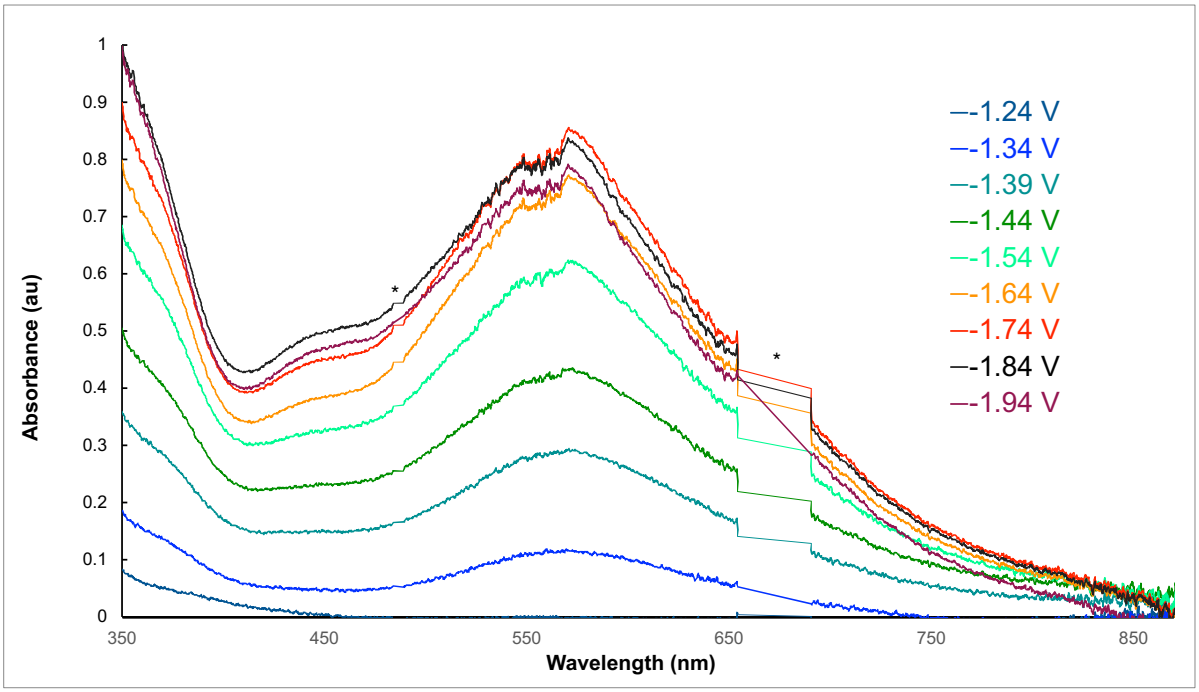

3.5.15 Optimization of Electrocatalytic Imine Alkylation

General Details: All reactions were performed according to General Procedure 3.5 (*vide infra*) on a 1.2 mmol scale unless specified otherwise. Reaction yields were determined by ^{1}H NMR using 1,1,2,2-tetrachloroethylene as an internal standard added after workup.

Table 3.6. *Optimization table and control experiments for electroreductive alkylation. * indicates voltage overload due to the high resistance of the divided cell (94% yield based on amount of current passed).*

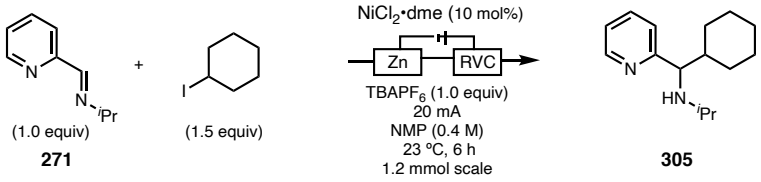

Deviation from Standard Conditions	*Yield %*
None	63
0.2 M, 10 mA	28
10 mA, 12h	59
30 mA, 1h	58
TMSCl (2 equiv)	58
3.2h (2 equiv of e^-)	63
Mg^0 sacrificial anode	43
Al^0 sacrificial anode	35
TBACl (0.2 M) as electrolyte	51
No $NiCl_2$•dme	0
0 mA	44
Divided Cell, 11.11 mA	37*
Ni^0 sacrifical anode, No $NiCl_2$•dme	50
$CoCl_2$ (10 mol%) as catalyst	53
$MnCl_2$ (10 mol%) as catalyst	7

Divided Cell Experiment: Divided cell electrolysis was performed on an H-Cell type electrochemical cell on a 2.0 mmol scale. Due to the high resistance of the divided cell setup, the reaction reached its safety voltage limit after 3.75 h corresponding limiting the reaction to a 39% theoretical yield based on the amount of electrons passed. Each cell was analyzed individually to ensure there was not significant substrate diffusion over the course

of the reaction which was confirmed by finding the anodic cell had <5% of **271** and no **305** could be detected.

General Procedure 4: Electrolysis on 1.2 mmol Scale:

In a N_2-filled glovebox, to an oven-dried standard 5 mL ElectraSyn vial charged with a stir bar was added $NiCl_2$·dme (26.4 mg, 0.12 mmol, 0.1 equiv) and $TBAPF_6$ (456 mg, 1.2 mmol, 1 equiv). The solids were then dissolved in 3mL of NMP (0.4 M) and stirred for 10 minutes. To the blue solution was then added heteroaryl imine (1.2 mmol, 1 equiv) causing the solution to turn light green followed by alkyl halide (1.5 equiv, 1.8 mmol). The threading of the vial was then lined with teflon tape and the vial cap fitted with Zn^0 anode (counter electrode) and RVC cathode (working electrode) was attached. The cell was then removed from the glovebox and attached to the Electrasyn 2.0 where the following setup was employed: *New exp. -> Constant current -> -20 mA -> no ref. electrode -> no alternating polarity -> start.* The reaction was stirred at room temperature for 6 hours. The resulting dark solution was diluted with CH_2Cl_2 (30 ml) and extracted 3x with 1N HCl (30 ml). To the combined aqueous phases was added K_2CO_3 (s) until gas evolution ceased and the pH ~9. The resulting aqueous solution was extracted 3x with EtOAc (50 mL) and the combined organic phases were dried with Na_2SO_4, filtered through celite and then concentrated under reduced pressure. The crude material was purified by column chromatography to afford the desired products.

_N_-(2-phenyl-1-(pyridin-2-yl)ethyl)propan-2-amine (273)

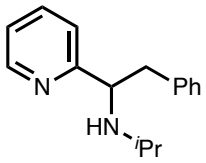

Prepared from imine **271** (178 mg, 1.2 mmol, 1 equiv) and benzyl bromide (214 μL, 1.8 mmol, 1.5 equiv) and following General Procedure 3.5. Purification of the crude residue by silica gel column chromatography (Hex/EtOAc 3:2 w/ 1% Et_3N) afforded **273** (210 mg, 0.88 mmol, 73%) as a colorless oil.

_N_-(cyclohexyl(pyridin-2-yl)methyl)propan-2-amine (305)

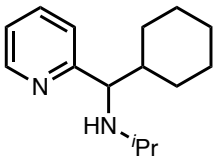

Prepared from imine **271** (178 mg, 1.2 mmol, 1 equiv) and cyclohexyliodide (233 μL, 1.8 mmol, 1.5 equiv) following General Procedure 3.5. Purification of the crude residue by silica gel column chromatography (Hex/EtOAc 3:2 w/ 1% Et_3N) afforded **305** (165 mg, 0.71 mmol, 59%) as a yellow oil.

_N_-isopropyl-4-phenyl-1-(pyridin-2-yl)butan-1-amine (312)

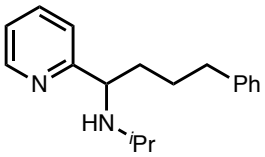

Prepared from imine **271** (178 mg, 1.2 mmol, 1 equiv) and 1-iodo-3-phenylpropane (290 μL, 1.8 mmol, 1.5 equiv) following General Procedure 3.5. Purification of the crude residue by silica gel column chromatography (Hex/EtOAc 3:2 w/ 1% Et_3N) afforded **312** (164 mg, 0.61 mmol, 51%) as a yellow oil.

R_f = 0.32 (silica, Hex/EtOAc 3:2 w/ 1% Et_3N, UV).

^{1}H NMR (500 MHz, $CDCl_3$): δ 8.56 (ddd, J = 4.8, 1.8, 0.9 Hz, 1H), 7.60 (td, J = 7.6, 1.8 Hz, 1H), 7.25 – 7.19 (m, 2H), 7.17 – 7.09 (m, 5H), 3.79 (dd, J = 7.5, 6.3 Hz, 1H), 2.57 (t, J = 7.7 Hz, 2H), 2.52 (p, J = 6.2 Hz, 1H), 1.83 – 1.68 (m, 3H), 1.67 – 1.55 (m, 1H), 1.51 – 1.39 (m, 1H), 1.02 (d, J = 6.1 Hz, 3H), 0.96 (d, J = 6.3 Hz, 3H).

^{13}C NMR (101 MHz, $CDCl_3$): δ 164.66, 149.94, 142.87, 136.53, 128.85, 128.68, 126.10, 122.71, 122.21, 61.69, 46.24, 37.51, 36.40, 28.71, 24.59, 22.64.

FTIR (NaCl, thin film, cm^{-1}): 2960, 2858, 1588, 1432, 1367, 747, 698

HRMS (FD, m/z): calc'd for $C_{18}H_{24}N_2$ $[M]^+$: 268.19340; found: 268.19358.

tert-butyl 4-((isopropylamino)(pyridin-2-yl)methyl)piperidine-1-carboxylate (309)

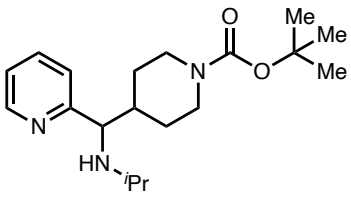

Prepared from imine **271** (178 mg, 1.2 mmol, 1 equiv) and 1-boc-4-iodo-piperidine (560 mg, 1.8 mmol, 1.5 equiv) following General Procedure 3.5. Purification of the crude residue by silica gel column chromatography (Hex/EtOAc 3:2 w/ 1% Et_3N) afforded **309** (173 mg, 0.52 mmol, 43%) as a white solid.

N-isopropyl-4-phenyl-1-(pyridin-2-yl)butan-1-amine (313)

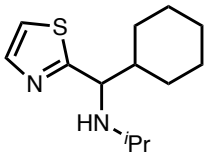

Prepared from imine **337** (185 mg, 1.2 mmol, 1 equiv) and cyclohexyliodide (233 μL, 1.8 mmol, 1.5 equiv) following General Procedure 3.5. Purification of the crude residue by silica gel column chromatography (Hex/EtOAc 4:1 w/ 1% Et_3N) afforded **313** (172 mg, 0.72 mmol, 60%) as a yellow oil.

R_f = 0.67 (silica, Hex/EtOAc 1:1 w/ 1% Et_3N, UV).

^{1}H NMR (400 MHz, $CDCl_3$): δ 7.70 (d, J = 3.4 Hz, 1H), 7.22 (d, J = 3.3 Hz, 1H), 3.89 (d, J = 6.0 Hz, 1H), 2.67 (hept, J = 6.3 Hz, 1H), 1.85 – 1.57 (m, 5H), 1.57 – 1.43 (m, 2H), 1.29 – 1.06 (m, 4H), 1.04 (d, J = 6.2 Hz, 3H), 1.02 (d, J = 6.2 Hz, 3H).

^{13}C NMR (101 MHz, $CDCl_3$): δ 178.12, 142.63, 118.76, 63.95, 47.68, 45.04, 30.29, 29.76, 26.86, 26.68, 24.54, 22.75.

FTIR (NaCl, thin film, cm^{-1}): 2958, 2924, 2851, 1497, 1448, 1379, 1365, 1316, 1176, 1121, 1052, 776, 720.

HRMS (FD, m/z): calc'd for $C_{13}H_{22}N_2S$ $[M]^+$: 238.14982; found: 238.15067.

_N_-isopropyl-2,2-dimethyl-1-(thiazol-2-yl)propan-1-amine (314)

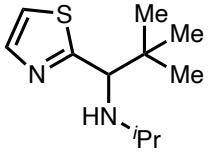

Prepared from imine **337** (185 mg, 1.2 mmol, 1 equiv) and 2-iodo-2-methylpropane (215 µL, 1.8 mmol, 1.5 equiv) following General Procedure 3.5. Purification of the crude residue by silica gel column chromatography (Hex/EtOAc 4:1 w/ 1% Et_3N) afforded **314** (136 mg, 0.64 mmol, 53%) as a yellow oil.

R_f = 0.56 (silica, Hex/EtOAc 1:1 w/ 1% Et_3N, UV).

^{1}H NMR (400 MHz, $CDCl_3$): δ 7.71 (d, J = 3.3 Hz, 1H), 7.23 (d, J = 3.2 Hz, 1H), 3.77 (s, 1H), 2.57 (hept, J = 6.2 Hz, 1H), 1.01 (d, J = 6.1 Hz, 3H), 0.98 (m, 3H), 0.97 (s, 9H).

^{13}C NMR (101 MHz, $CDCl_3$): δ 176.43, 142.29, 118.77, 67.79, 47.62, 35.23, 27.41, 24.61, 22.46.

FTIR (NaCl, thin film, cm^{-1}): 2960, 2866, 1495, 1475, 1367, 1175, 1120, 1089, 1053, 854, 722.

HRMS (FD, m/z): calc'd for $C_{11}H_{20}N_2S$ $[M]^+$: 212.13417; found: 212.13459.

3-(1,3-dioxolan-2-yl)-_N_-isopropyl-1-(pyridin-2-yl)propan-1-amine (315)

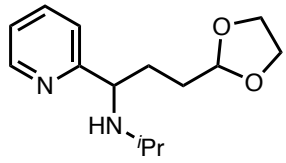

Prepared from imine **271** (178 mg, 1.2 mmol, 1 equiv) and 2-(2-iodoethyl)-1,3-dioxolane (410 mg, 1.8 mmol, 1.5 equiv) following General Procedure 3.5. Purification of the crude residue by silica gel column chromatography (Hex/EtOAc 3:2 w/ 1% Et_3N) afforded **315** (158.7 mg, 0.64 mmol, 53%) as a yellow oil.

R_f = 0.24 (silica, Hex/EtOAc 3:2 w/ 1% Et_3N, UV).

^{1}H NMR (400 MHz, $CDCl_3$): δ 8.56 (ddd, J = 4.9, 1.8, 0.9 Hz, 1H), 7.65 – 7.56 (m, 1H), 7.25 – 7.22 (m, 1H), 7.18 – 7.05 (m, 1H), 4.82 (t, J = 4.6 Hz, 1H), 3.97 – 3.89 (m, 2H), 3.86 (ddd, J = 12.1, 4.6, 0.7 Hz, 1H), 3.81 – 3.76 (m, 2H), 2.56 (hept, J = 6.2 Hz, 1H), 1.90

– 1.72 (m, 3H), 1.73 – 1.60 (m, 1H), 1.57 – 1.43 (m, 1H), 1.02 (d, J = 6.1 Hz, 3H), 0.96 (d, J = 6.3 Hz, 3H).

^{13}C NMR (101 MHz, $CDCl_3$): δ 164.05, 149.61, 136.25, 122.41, 121.94, 104.58, 65.01, 64.98, 61.12, 45.97, 31.50, 30.76, 24.17, 22.44.

FTIR (NaCl, thin film, cm^{-1}): 2960, 2929, 1589, 1569, 1464, 1432, 1365, 1137, 1036, 747.

HRMS (ESI, m/z): calc'd for $C_{14}H_{23}N_2O_2$ [M+H]: 251.1754; found: 251.1857.

4,4,4-trifluoro-*N*-isopropyl-1-(pyridin-2-yl)butan-1-amine (316)

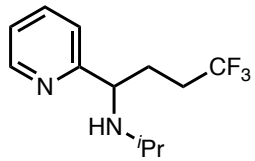

Prepared from imine **271** (178 mg, 1.2 mmol, 1 equiv) and 1,1,1-trifluoro-3-iodopropane (211 μL, 1.8 mmol, 1.5 equiv) following General Procedure 3.5. Purification of the crude residue by silica gel column chromatography (Hex/EtOAc 3:2 w/ 1% Et_3N) afforded **316** (145 mg, 0.59 mmol, 49%) as a yellow oil.

R_f = 0.53 (silica, Hex/EtOAc 3:2 w/ 1% Et_3N, UV).

^{1}H NMR (400 MHz, $CDCl_3$): δ 8.58 (ddd, J = 4.8, 1.8, 1.0 Hz, 1H), 7.64 (td, J = 7.6, 1.8 Hz, 1H), 7.21 (dt, J = 7.8, 1.1 Hz, 1H), 7.17 (ddd, J = 7.5, 4.8, 1.2 Hz, 1H), 3.77 (t, J = 6.8 Hz, 1H), 2.54 (hept, J = 6.2 Hz, 1H), 2.35 – 2.11 (m, 1H), 2.11 – 1.96 (m, 1H), 1.96 – 1.84 (m, 2H), 1.75 (s, 1H), 1.01 (d, J = 6.1 Hz, 3H), 0.96 (d, J = 6.3 Hz, 3H).

^{13}C NMR (101 MHz, $CDCl_3$): δ 162.97, 149.91, 136.52, 127.73 (q, J = 277.4 Hz), 122.35, 122.28, 59.88, 45.84, 30.86 (q, J = 28.6 Hz), 29.46 (q, J = 2.8 Hz), 24.18, 22.34.

^{19}F NMR (282 MHz, $CDCl_3$): -66.2 (t, J = 10.8 Hz).

FTIR (NaCl, thin film, cm^{-1}): 3309, 2996, 2964, 1590, 1571, 1471, 1452, 1434, 1382, 1337, 1289, 1251, 1134, 1091, 1023, 787, 749

HRMS (ESI, m/z): calc'd for $C_{12}H_{18}N_2F_3$ [M+H]: 247.1417; found: 247.1851

3.5.16 DFT Calculations of Substrate-Catalyst Complex

General Computational Details: All density functional theory (DFT) calculations were carried out using the ORCA 4.2 software package.[46] Geometry optimizations and numerical frequency calculations were carried out using the B3LYP hybrid functional.[47] All atoms were described with the def2-TZVP basis set.[Error! Bookmark not defined.] For all calculations, the resolution of identity (RI) approximation was used to calculate the coulomb integrals and the chain-of-spheres[48] approximation was used for the exchange integrals (RIJCOSX). Weigend's coulomb fitting auxiliary basis set[49] (Def2/J) was also employed for all calculations. Calculations were converged to tight SCF criteria ($\Delta E <= 1*10^{-8}$ Eh). All stationary points were confirmed as local minima by the absence of imaginary vibrational modes. Fine integration grids were used with the GRID7 and NOFINALGRID keywords. Broken symmetry calculations were performed using the method described by Ginsberg[50] and Noodleman *et al*[51]. The broken symmetry notation (*m,n*)[52] is employed where the m (n) is the number of spin up (or spin-down) electrons on each fragment. All graphical representations shown were rendered with the program CYLview[53] and orbital/density surfaces with the program *ChemCraft*.[54]

DFT Input Files and Coordinates

Input File – $(271)_2$Ni BS(0,0) (Low Spin)

```
! UKS B3LYP def2-TZVP def2/J RIJCOSX Grid7 TightSCF NoFinalGrid LargePrint
! Opt NumFreq

% pal nprocs 16 # num of processors
end
%maxcore 9000
%method
Z_solver DIIS
end

*xyz 0 1
C       -0.08651      -3.70002       2.07639
N        0.69789      -2.47950       1.83316
C        0.45604      -1.41247       2.58729
C        1.15663      -0.22934       2.24501
N        2.09886      -0.42527       1.24915
Ni       2.04979      -2.19969       0.50253
N        2.45194      -1.83399      -1.34168
C        3.13733      -2.86225      -1.96491
C        3.33308      -3.98983      -1.12655
N        2.93217      -3.86804       0.13320
C        3.19296      -4.96161       1.07941
C        3.57466      -2.73898      -3.30672
C        3.30958      -1.58023      -4.01101
C        2.59063      -0.54055      -3.36863
C        2.19485      -0.71236      -2.05385
C        2.81676       0.64458       0.83213
C        2.64151       1.92122       1.33545
C        1.66315       2.13562       2.34167
C        0.93376       1.05530       2.79805
H       -0.27266      -1.41630       3.40535
H        3.81281      -4.89507      -1.51148
H        4.12399      -3.56650      -3.76334
H        3.64903      -1.46440      -5.04343
H        2.32663       0.37753      -3.89757
H        1.63104       0.06630      -1.53457
H        3.57044       0.44479       0.06589
H        3.26672       2.73740       0.96648
H        1.48984       3.13524       2.74925
H        0.16921       1.17461       3.57027
C       -0.03364      -4.19572       3.53004
```

H	1.00544	-4.33915	3.86696
H	-0.56364	-5.15742	3.62494
H	-0.51769	-3.48699	4.22121
C	-1.53722	-3.50164	1.60390
H	0.36420	-4.47372	1.43644
H	-2.05826	-2.75609	2.22660
H	-2.10053	-4.44694	1.66624
H	-1.56038	-3.14500	0.56234
C	4.60357	-4.81493	1.67543
H	5.37225	-5.00132	0.90649
H	4.75967	-5.53717	2.49305
H	4.75317	-3.80003	2.07403
C	2.97945	-6.37338	0.51074
H	2.47651	-4.81532	1.90217
H	3.74189	-6.64022	-0.23805
H	1.98994	-6.47302	0.03599
H	3.05516	-7.11503	1.32198

*

Optimized coordinates – $(271)_2$Ni (321) (Low Spin)

C	-0.07139688048135	-3.68994745690584	2.12487431847914
N	0.69457607470368	-2.46847311460371	1.82154805145691
C	0.46230487368270	-1.40579204444689	2.56862153431397
C	1.14434009100596	-0.22144322634441	2.22294863299765
N	2.08908020452348	-0.39907719496350	1.23289295160638
Ni	2.05405208904355	-2.18531967202371	0.47923647332427
N	2.49643854225418	-1.81468121815090	-1.36865285410353
C	3.16446186466836	-2.85339073012088	-1.97920690295865
C	3.31760272384933	-3.98920040401533	-1.15196806361930
N	2.91187147934083	-3.87930406652301	0.09674659500334
C	3.11663739078330	-5.01105774748437	1.01483205871569
C	3.63666674260574	-2.74228514674203	-3.29998010570616
C	3.42987520482683	-1.58194872471534	-4.00569252858579
C	2.73521978741020	-0.52733337208899	-3.38020051761558
C	2.30198321662912	-0.68703717184991	-2.08427020650156
C	2.75926602868113	0.69616869616506	0.80989558621606
C	2.53408645796020	1.96185256089880	1.29845706195641
C	1.55641364281730	2.14840111450956	2.29977193544369
C	0.87764936094192	1.04924644715982	2.76459391405816
H	-0.24436539587200	-1.41220981699462	3.39183929255147
H	3.76267991173966	-4.89465032843539	-1.54733269752619
H	4.16585461087004	-3.57878731768715	-3.73981093627253
H	3.79354917566678	-1.47697113063354	-5.01976970038894

H	2.51804955554337	0.39203256272523	-3.90693723882010
H	1.75340643056829	0.10123739387726	-1.58632148319338
H	3.51580560597679	0.52604040965820	0.05503786662332
H	3.11988717088641	2.79058844620730	0.92377829313703
H	1.34556487197089	3.13471108498792	2.69286025990739
H	0.11585794297099	1.14176537769507	3.52896357533661
C	0.11074053819156	-4.19024906155441	3.56442148756822
H	1.16673948233884	-4.32106394706288	3.80795291978854
H	-0.39364895576934	-5.15035231697145	3.69451235474330
H	-0.31777214323576	-3.49409255492280	4.28805617503585
C	-1.55674571487992	-3.48493452800464	1.79467332974312
H	0.31030707160697	-4.45376368456651	1.44663185168743
H	-2.01062574174205	-2.74917438642245	2.46167437112740
H	-2.10423254973763	-4.42282511073171	1.91061235597269
H	-1.67776764610482	-3.13044557318379	0.76984802654670
C	4.47205228314121	-4.86997104291255	1.72112741662872
H	5.29010903289212	-5.05281554296529	1.01952885957022
H	4.55529007731697	-5.59451606866376	2.53456036697896
H	4.58876080603594	-3.86839722947529	2.13538087580025
C	2.97595111228601	-6.40027658488880	0.38279121384763
H	2.34359858105154	-4.91169080470743	1.77668397354347
H	3.79366684408679	-6.62646057336273	-0.30412720758781
H	2.03542278018867	-6.50090537390851	-0.16244896055192
H	3.00275536676520	-7.15809982484962	1.16880542372144

Final Single point energy = -2427.4312451 Eh

Input File – $(271)_2$Ni BS(0,0) (321) (High Spin)

```
! UKS B3LYP def2-TZVP def2/J RIJCOSX Grid7 TightSCF NoFinalGrid Slowconv
! Opt

%scf
maxiter 1000
end

%output
Print[P_basis] 2
Print[P_MOs] 1
Print[P_ReducedOrbPop_L] 1
Print[P_BondOrder_L] 1
```

```
Print[P_FragBondOrder_L] 1
Print[P_OrbPopMO_L] 1
Print[P_ReducedOrbPopMO_L] 1
end


% pal nprocs 16 # num of processors
end

%maxcore 9000
%method
Z_solver DIIS
end

*xyz 0 5
 C     -0.951965    -2.779945     0.804853
  N     0.259699    -2.102834     1.291891
  C     0.163355    -1.290541     2.329373
  C     1.350443    -0.685445     2.793235
  N     2.463620    -0.955323     2.021895
  Ni    2.053936    -2.206995     0.539021
  N     1.742323    -2.523282    -1.369608
  C     2.678467    -3.365674    -1.930862
  C     3.726973    -3.721126    -1.055626
  N     3.657444    -3.292665     0.193550
  C     4.729961    -3.669707     1.127692
  C     2.550432    -3.801319    -3.265637
  C     1.486983    -3.378194    -4.023452
  C     0.544277    -2.500162    -3.446775
  C     0.714281    -2.114017    -2.137559
  C     3.636564    -0.413382     2.404333
  C     3.780399     0.382584     3.518903
  C     2.647019     0.657126     4.313447
  C     1.438701     0.124188     3.943490
  H    -0.780918    -1.086001     2.824841
  H     4.551035    -4.324971    -1.419412
  H     3.297312    -4.471572    -3.673059
  H     1.371032    -3.710044    -5.047326
  H    -0.291167    -2.118372    -4.016995
  H     0.018994    -1.432443    -1.667480
  H     4.484679    -0.624744     1.764898
  H     4.747774     0.798084     3.765959
  H     2.730258     1.277822     5.196037
  H     0.541774     0.312628     4.521249
  C    -1.455537    -3.820099     1.814489
  H    -0.645229    -4.482391     2.122697
```

H	-2.245541	-4.426493	1.365088
H	-1.863838	-3.341612	2.707932
C	-2.071478	-1.810464	0.402491
H	-0.643524	-3.321370	-0.090273
H	-2.502866	-1.304444	1.269126
H	-2.876169	-2.354760	-0.097181
H	-1.703037	-1.044378	-0.280688
C	6.144799	-3.487931	0.559935
H	6.361578	-4.207074	-0.232116
H	6.881618	-3.649528	1.350048
H	6.285166	-2.484870	0.151832
C	4.534816	-5.105218	1.637839
H	4.625304	-3.001741	1.984372
H	4.717330	-5.829427	0.840031
H	3.520480	-5.251628	2.011436
H	5.234461	-5.317148	2.449504

Optimized coordinates – $(271)_2$Ni (321) (High Spin)

C	-0.67546185593229	-3.01194225132354	0.92708152761451
N	0.42185027785309	-2.14512275088691	1.35709043685846
C	0.27564528000301	-1.31235792858595	2.38383064783419
C	1.37589458224275	-0.53820945874821	2.80674309984266
N	2.55366162706074	-0.72430748576660	2.09817672072619
Ni	2.20468422617664	-1.90443895458006	0.47692934150778
N	1.77952259766498	-2.29063061590460	-1.46521155960331
C	2.55888972003137	-3.32553819770884	-1.94712921159489
C	3.48133275460832	-3.86633290826890	-1.02959788003236
N	3.54603526470520	-3.37824541431330	0.21011174374495
C	4.54799023363377	-3.91417448488668	1.13750299156853
C	2.40078613021566	-3.75701305275399	-3.28640821131654
C	1.47988829073571	-3.14798893768625	-4.09894613837900
C	0.70545783110605	-2.07659559763725	-3.59339277021777
C	0.89995869127111	-1.69731482795463	-2.28356029587924
C	3.64682896609949	-0.03975167619023	2.47042703095854
C	3.67040603206030	0.84501486773517	3.52626249042815
C	2.47001490049755	1.06401314045836	4.24394358441745
C	1.33796771803904	0.38380815391404	3.88069174346983
H	-0.67015343136389	-1.21172307967440	2.90927433326902
H	4.14020678172387	-4.66434306401669	-1.35901269956403
H	3.01434682121694	-4.57186533811043	-3.65097000188068
H	1.34312538238766	-3.48308378167296	-5.11962790927482
H	-0.02429527181179	-1.56689936367529	-4.20587410603150
H	0.32460334196373	-0.88574080162952	-1.85233421673640

H	4.54182071776966	-0.22705303128079	1.88674700027297
H	4.58570328144591	1.35471913858034	3.79146892748243
H	2.44695341891206	1.76388857215933	5.06956499811675
H	0.40280869534655	0.53895332715564	4.40535018097080
C	-1.12386070295983	-3.98233590569120	2.02889670659211
H	-0.26918651137828	-4.51420948783956	2.45026931425936
H	-1.81982242832530	-4.71758085398521	1.61803551282206
H	-1.63264918222916	-3.45852403537860	2.84184804464185
C	-1.86926459359883	-2.22494633961223	0.36735387872994
H	-0.26656389676660	-3.61097962558761	0.11018584818412
H	-2.35533346271860	-1.63177861865786	1.14602425214132
H	-2.61364803209557	-2.90751673609144	-0.04911651188103
H	-1.55088880888699	-1.54730414961070	-0.42498168358554
C	5.98047210835223	-3.76814126952864	0.60074281549449
H	6.14772409012766	-4.40647269955022	-0.26939446276233
H	6.70291629159882	-4.06158047195875	1.36583302140057
H	6.18667568751465	-2.73789488205202	0.30389133657664
C	4.26691101614032	-5.37147314218721	1.53487640008259
H	4.46763781644977	-3.30527628775653	2.04108670449169
H	4.40728607395273	-6.04573261803369	0.68651383314665
H	3.24560313840414	-5.48761539513916	1.90098397237021
H	4.95153639075551	-5.68726367808600	2.32525721872257

Final Single point energy = -2427.425281762070 Eh

Input File – $(271)_2$Ni (321) BS(2,2)

```
! UKS B3LYP def2-TZVP def2/J RIJCOSX Grid7 TightSCF NoFinalGrid Slowconv
! Opt NumFreq

%scf
maxiter 500
brokensym 2,2
end

%output
Print[P_basis] 2
Print[P_MOs] 1
Print[P_ReducedOrbPop_L] 1
Print[P_BondOrder_L] 1
Print[P_FragBondOrder_L] 1
Print[P_OrbPopMO_L] 1
Print[P_ReducedOrbPopMO_L] 1
end
```

```
% pal nprocs 16 # num of processors
end

%maxcore 9000
%method
Z_solver DIIS
 end

 *xyz 0 1
 C  (2) -0.67546185593229    -3.01194225132354     0.92708152761451
 N  (2) 0.42185027785309     -2.14512275088691     1.35709043685846
 C  (2) 0.27564528000301     -1.31235792858595     2.38383064783419
 C  (2) 1.37589458224275     -0.53820945874821     2.80674309984266
 N  (2) 2.55366162706074     -0.72430748576660     2.09817672072619
 Ni (1) 2.20468422617664     -1.90443895458006     0.47692934150778
 N  (2) 1.77952259766498     -2.29063061590460    -1.46521155960331
 C  (2) 2.55888972003137     -3.32553819770884    -1.94712921159489
 C  (2) 3.48133275460832     -3.86633290826890    -1.02959788003236
 N  (2) 3.54603526470520     -3.37824541431330     0.21011174374495
 C  (2) 4.54799023363377     -3.91417448488668     1.13750299156853
 C  (2) 2.40078613021566     -3.75701305275399    -3.28640821131654
 C  (2) 1.47988829073571     -3.14798893768625    -4.09894613837900
 C  (2) 0.70545783110605     -2.07659559763725    -3.59339277021777
 C  (2) 0.89995869127111     -1.69731482795463    -2.28356029587924
 C  (2) 3.64682896609949     -0.03975167619023     2.47042703095854
 C  (2) 3.67040603206030      0.84501486773517     3.52626249042815
 C  (2) 2.47001490049755      1.06401314045836     4.24394358441745
 C  (2) 1.33796771803904      0.38380815391404     3.88069174346983
 H  (2) -0.67015343136389    -1.21172307967440     2.90927433326902
 H  (2) 4.14020678172387     -4.66434306401669    -1.35901269956403
 H  (2) 3.01434682121694     -4.57186533811043    -3.65097000188068
 H  (2) 1.34312538238766     -3.48308378167296    -5.11962790927482
 H  (2) -0.02429527181179    -1.56689936367529    -4.20587410603150
 H  (2) 0.32460334196373     -0.88574080162952    -1.85233421673640
 H  (2) 4.54182071776966     -0.22705303128079     1.88674700027297
 H  (2) 4.58570328144591      1.35471913858034     3.79146892748243
 H  (2) 2.44695341891206      1.76388857215933     5.06956499811675
 H  (2) 0.40280869534655      0.53895332715564     4.40535018097080
 C  (2) -1.12386070295983    -3.98233590569120     2.02889670659211
 H  (2) -0.26918651137828    -4.51420948783956     2.45026931425936
 H  (2) -1.81982242832530    -4.71758085398521     1.61803551282206
 H  (2) -1.63264918222916    -3.45852403537860     2.84184804464185
 C  (2) -1.86926459359883    -2.22494633961223     0.36735387872994
 H  (2) -0.26656389676660    -3.61097962558761     0.11018584818412
 H  (2) -2.35533346271860    -1.63177861865786     1.14602425214132
```

H	(2) -2.61364803209557	-2.90751673609144	-0.04911651188103
H	(2) -1.55088880888699	-1.54730414961070	-0.42498168358554
C	(2) 5.98047210835223	-3.76814126952864	0.60074281549449
H	(2) 6.14772409012766	-4.40647269955022	-0.26939446276233
H	(2) 6.70291629159882	-4.06158047195875	1.36583302140057
H	(2) 6.18667568751465	-2.73789488205202	0.30389133657664
C	(2) 4.26691101614032	-5.37147314218721	1.53487640008259
H	(2) 4.46763781644977	-3.30527628775653	2.04108670449169
H	(2) 4.40728607395273	-6.04573261803369	0.68651383314665
H	(2) 3.24560313840414	-5.48761539513916	1.90098397237021
H	(2) 4.95153639075551	-5.68726367808600	2.32525721872257

*Optimized coordinates – $(271)_2$Ni BS(2,2)

C	-0.82966725295907	-2.97306713556467	0.98391231232957
N	0.31564234965178	-2.15527474656864	1.40782141871046
C	0.18661233428015	-1.33365819506513	2.42525572669296
C	1.32336723113946	-0.57496948947910	2.81296607198333
N	2.45429284502804	-0.80784045035236	2.06392406346494
Ni	2.11753418788747	-2.18194211647260	0.59157108406639
N	1.80730737748709	-2.38982914395920	-1.40140706855030
C	2.66651854234869	-3.30142609460453	-1.96359592895860
C	3.63871133700863	-3.82578467504436	-1.07114459864131
N	3.63406068386660	-3.40203483160523	0.17808972585921
C	4.65664348682686	-3.93044270469426	1.09807499949608
C	2.56123406887550	-3.65040384601567	-3.32424709364504
C	1.59405290476536	-3.06390578955357	-4.10564791322658
C	0.73247912049560	-2.11135073207650	-3.52593502716818
C	0.88201265069838	-1.81674660505081	-2.18780151942203
C	3.56414020275364	-0.11371601738159	2.37404419350835
C	3.62863002751118	0.80548319982150	3.40042012551173
C	2.47421252842772	1.04528959947848	4.17137853294205
C	1.32541467023087	0.35382753235277	3.87111665751198
H	-0.74588001742733	-1.21556780975476	2.97154102682376
H	4.36121280100347	-4.54818633399696	-1.43956806609851
H	3.24853369356283	-4.37906660171230	-3.73659968489463
H	1.49340461786156	-3.32930051696091	-5.15051795826389
H	-0.03220987487715	-1.61562434895246	-4.10767980364031
H	0.23844146902882	-1.09163645342390	-1.70488962134146
H	4.43422482929762	-0.32033657840444	1.76167551809855
H	4.55448653054053	1.32556247694397	3.60510426880362
H	2.49152854072316	1.76261765538979	4.98170850251515
H	0.41282833897479	0.51533399946811	4.43254171105362
C	-1.29663195204607	-3.94015376684175	2.07947861570671
H	-0.45555934592671	-4.50803479167501	2.48105002423090
H	-2.02357114475044	-4.64470896680287	1.66867936084098

H	-1.77506831063915	-3.40942228204270	2.90613888016039
C	-1.99346728089541	-2.12185590998760	0.46081942566359
H	-0.46036283971450	-3.57423842264255	0.15078687748887
H	-2.46073753745544	-1.54583541991035	1.26324088180872
H	-2.75926448757613	-2.76183013597538	0.01663442695652
H	-1.65056205108871	-1.42191592936799	-0.30126124978734
C	6.08382252180126	-3.78607083923497	0.55105479119808
H	6.26233964219568	-4.45088125340704	-0.29636774561966
H	6.80716089441652	-4.04808921722188	1.32656496589356
H	6.27933532732471	-2.76314241839612	0.22368482975174
C	4.37677434030353	-5.38454233057516	1.50308869809208
H	4.58176804085155	-3.31690715271850	1.99841875882622
H	4.51608674562748	-6.06140174982159	0.65663405032687
H	3.35657157902320	-5.49943129834275	1.87275900108364
H	5.06361363353594	-5.69444336179592	2.29392175185709

Final Single point energy = -2427.44810734845 Eh

Input File – $(271)_2Ni^{I}$ cation 324

```
! UKS B3LYP def2-TZVP def2/J RIJCOSX Grid7 TightSCF NoFinalGrid
! Opt NumFreq

%scf
maxiter 5000
end

% pal nprocs 16 # num of processors
end

%maxcore 9000
%method
Z_solver DIIS
end

*xyz 1 2
Ni       0.51596      2.09723     -0.02143
N        1.81002      1.51809      1.33417
C        2.35675      2.17322      2.41468
C        3.32582      1.54135      3.24432
C        3.72963      0.22863      2.98842
C        3.21863     -0.41494      1.87415
```

C	2.31312	0.27836	1.04395
C	1.94083	-0.21588	-0.09597
N	1.18628	0.67240	-0.89632
C	0.38934	0.16841	-1.99026
N	-0.16644	3.48433	0.94890
C	-0.65038	3.32205	2.30746
C	-0.74338	4.51006	0.15069
C	-0.44499	4.48045	-1.09272
N	0.30543	3.41515	-1.45021
C	0.81731	3.41399	-2.71424
C	0.48725	4.41011	-3.65458
C	-0.38946	5.43407	-3.30178
C	-0.85928	5.48487	-1.99617
H	2.10844	3.19485	2.62629
H	3.77585	2.05881	4.08381
H	4.46582	-0.27545	3.61731
H	3.57251	-1.41803	1.63193
H	0.91009	4.37908	-4.65095
H	-0.66834	6.19923	-4.02091
H	-1.50924	6.30673	-1.69242
H	1.50976	2.68711	-2.99876
H	-1.38555	5.28894	0.52767
H	2.24614	-1.20527	-0.42055
C	-0.50344	4.64554	2.99402
H	0.55043	4.91314	2.78345
H	-0.69834	4.60717	4.07343
H	-1.21392	5.37289	2.56605
C	-2.11500	2.87816	2.13570
H	-0.18599	2.54663	2.95985
H	-2.63824	3.42984	1.31716
H	-2.70846	3.05330	3.04734
H	-2.09435	1.80994	1.81735
C	-0.34142	-1.12207	-1.60208
H	0.38288	-1.90666	-1.30508
H	-0.88086	-1.52782	-2.48417
H	-1.03995	-0.91156	-0.76664
C	1.27951	-0.13300	-3.12592
H	-0.39797	0.90573	-2.27466
H	2.03737	-0.85363	-2.76667
H	1.77314	0.78459	-3.40276
H	0.66321	-0.51383	-3.95883

*

Optimized coordinates – $(271)_2Ni^I$ cation 274

Ni	0.86668948178079	2.34373126908244	-0.05349092107067
N	2.19137284337807	1.66568639702621	1.25013265054364
C	2.73636546055795	2.28845641823813	2.31284464235365
C	3.70981418252361	1.69773435388661	3.11749493212786
C	4.14110400547722	0.40050451215240	2.82417205572819
C	3.59418559913333	-0.25193996855542	1.72045203604887
C	2.63206477682334	0.40489374023037	0.94691274963695
C	2.02287804079151	-0.15826991062898	-0.24321813339487
N	1.16464547689342	0.58344628819015	-0.87713438438844
C	0.44534573642135	0.07829861155353	-2.06798486041708
N	-0.34710864531494	3.54982224150299	0.91648319139516
C	-0.81863848907384	3.33436847276040	2.30267671266730
C	-0.77156901744477	4.55317275743465	0.20827184668137
C	-0.29453440050272	4.64722568698935	-1.15872117188268
N	0.54509764315184	3.62827973444604	-1.52263035764586
C	1.07737241822241	3.65738327343779	-2.75958614819228
C	0.79561596144076	4.66630212769202	-3.67977989965004
C	-0.08209378272296	5.69277984011979	-3.31808996661902
C	-0.63154644312627	5.68177039813570	-2.03708517801509
H	2.38092178248726	3.30012744195258	2.51337458727689
H	4.11996351047010	2.25292018284593	3.96051766864292
H	4.89436037435653	-0.08901222539984	3.44129931407601
H	3.90802086243901	-1.26031327171365	1.44807310081955
H	1.26172165641352	4.64164633662294	-4.66429719523258
H	-0.32695624593520	6.48949490496955	-4.02033994762582
H	-1.31266810036221	6.46749026369357	-1.70810377509851
H	1.76028207075683	2.84435534872303	-3.00987365934374
H	-1.46265590081787	5.30749391544666	0.59539527448741
H	2.29123696370020	-1.16863531605443	-0.56504844719297
C	-1.59775625724950	4.49488118365771	2.92071254262963
H	-1.03237729909225	5.43736899512491	2.89109457639443
H	-1.80238209158107	4.26522569150410	3.97477770736791
H	-2.56984009927747	4.64871576059044	2.42901203183016
C	-1.61599590885385	2.02187428869902	2.34264378489570
H	0.10109967383892	3.18031017374853	2.89233398380984
H	-2.55357768718930	2.12318831011814	1.77727536048871
H	-1.86464865340668	1.76584733429559	3.38123641876040
H	-1.03626526994738	1.19545976522246	1.90974124195912
C	-1.04971244662453	-0.01154535184039	-1.72582957612469
H	-1.22734897611980	-0.79864017700929	-0.97893119511815
H	-1.62661523941233	-0.25449936899212	-2.62815940684242
H	-1.41911531029175	0.94087900573238	-1.32224721834388
C	0.97711686293287	-1.23001016700869	-2.65214290136927
H	0.56370383748324	0.87104699392680	-2.82610713623952

H	0.81218759623364	-2.08207531289966	-1.97600226461422
H	2.04800665374394	-1.17200576049644	-2.89434691053008
H	0.43875279289497	-1.44892518915429	-3.58375775566983

Final Single Point Energy = –2427.283556656272

EPR g-tensor values

g(tot) = 2.0498914 2.1114845 2.2104202 iso = 2.1239320

Input File – $(271)_2Ni^{I}Cl$ – Structure 323-Cl (not shown in text)

```
! UKS B3LYP def2-SVP def2/J RIJCOSX Grid7 TightSCF NoFinalGrid
! Opt NumFreq

% pal nprocs 16 # num of processors
end

%maxcore 9000
%method
Z_solver DIIS
end


* xyz 0 2
28      1.820504000     2.710304000    -0.462278000
7       1.422289000     1.090697000     0.764874000
6       0.401372000     0.921321000     1.621705000
6       0.058226000    -0.297284000     2.189291000
6       0.821599000    -1.436538000     1.831022000
6       1.869925000    -1.289572000     0.943384000
6       2.175578000    -0.010785000     0.400603000
6       3.241551000     0.241976000    -0.535267000
7       3.314755000     1.482274000    -1.009712000
6       4.399285000     1.933652000    -1.871706000
7       0.466660000     4.144535000     0.430781000
6       0.969791000     5.074446000     1.436590000
6      -0.587175594     4.338434098    -0.251245236
6      -0.871256000     3.368339000    -1.353266000
7       0.128340000     2.503397000    -1.621594000
6       0.003177000     1.612616000    -2.606858000
6      -1.145336000     1.530870000    -3.398371000
```

6	-2.189476000	2.420140000	-3.141325000
6	-2.051919000	3.353557000	-2.110629000
1	-0.169211000	1.822996000	1.867731000
1	-0.775611000	-0.366476000	2.890336000
1	0.578813000	-2.417735000	2.248399000
1	2.465272000	-2.155223000	0.648204000
1	-1.209968000	0.792107000	-4.199662000
1	-3.104976000	2.389510000	-3.737219000
1	-2.856508000	4.058659000	-1.900939000
1	0.858411000	0.949393000	-2.766945000
6	0.684235000	4.619732000	2.868991000
1	-0.395971000	4.617329000	3.091718000
1	1.171787000	5.307345000	3.577609000
1	1.079913000	3.609316000	3.054810000
6	5.538328000	2.563691000	-1.062708000
1	6.004233000	1.836413000	-0.376084000
1	6.319969000	2.956801000	-1.734309000
1	5.134877000	3.404343000	-0.479095000
1	0.580898000	6.094449000	1.281388000
1	2.053707000	5.129474000	1.255847000
1	4.789275000	1.122418000	-2.513043000
1	3.985874000	2.712384000	-2.528071000
17	2.720062000	4.694190000	-1.397898000
1	-1.163679128	5.232292730	-0.003459350
1	3.872757602	-0.666009171	-0.718639988

*

Optimized coordinates – $(271)_2Ni^ICl$ 324-Cl

Ni	1.773684	2.748519	-0.441386
N	1.337728	1.115032	0.794175
C	0.313973	0.926189	1.644589
C	-0.017682	-0.304618	2.192577
C	0.752012	-1.436281	1.819386
C	1.802422	-1.269308	0.937534
C	2.098978	0.021781	0.428770
C	3.166806	0.304448	-0.476342
N	3.287567	1.533500	-0.941481
C	4.443347	1.888833	-1.750263
N	0.375015	4.147715	0.439693
C	0.758428	5.139418	1.431384
C	-0.676130	4.285697	-0.270952
C	-0.911218	3.352378	-1.388620
N	0.100366	2.495808	-1.647986
C	-0.012489	1.622576	-2.650317
C	-1.152679	1.555742	-3.457084
C	-2.202748	2.443014	-3.206670

C	-2.080135	3.360202	-2.159500
H	-0.264999	1.819488	1.902259
H	-0.850959	-0.390422	2.892710
H	0.510469	-2.423155	2.223599
H	2.415849	-2.115864	0.616208
H	-1.206201	0.826591	-4.268152
H	-3.106373	2.419559	-3.820645
H	-2.876379	4.073949	-1.934926
H	0.842679	0.959411	-2.812783
C	1.211784	4.512194	2.748120
H	0.386885	3.996644	3.265927
H	1.602040	5.292785	3.419879
H	2.016377	3.781942	2.571738
C	5.518788	2.581909	-0.908155
H	5.898840	1.914360	-0.116697
H	6.368541	2.889934	-1.540079
H	5.085824	3.481742	-0.446254
H	-0.054651	5.873087	1.594287
H	1.607365	5.669665	0.963652
H	4.865271	0.990035	-2.244192
H	4.109586	2.591413	-2.528759
Cl	2.691700	4.703564	-1.375914
H	-1.394397	5.109548	-0.117481
H	3.875094	-0.489246	-0.758889

EPR g-tensor values

g(tot) =2.1899638 2.2366671 2.2529868 iso = 2.2262059

Calculated Geometries of 321 and 324

Figure 3.36. *BS(0,0) low spin optimized geometry of* ***321****.*

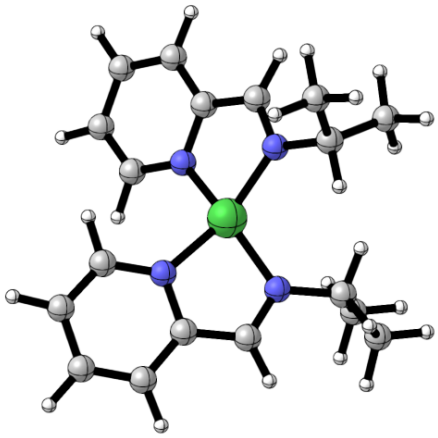

Figure 3.37. *BS(0,0) high spin optimized geometry of* ***321****.*

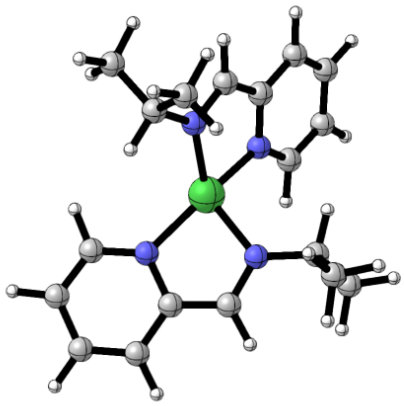

Figure 3.38. *BS(2,2) optimized geometry of* ***321****.*

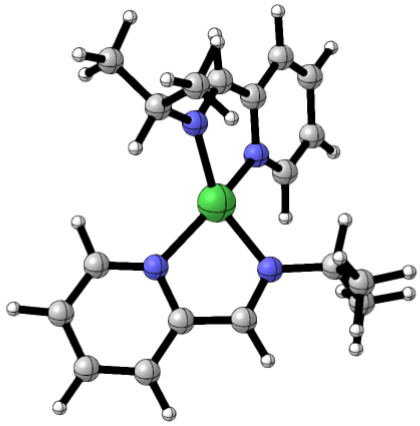

Figure 3.39. *Optimized geometry of cationic* ***324****.*

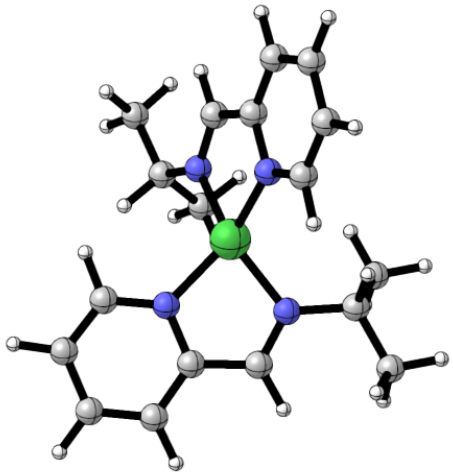

3.5.17 Qualitative MO Diagram of 321 BS(2,2)

Figure 3.40. *Qualitative MO diagram of BS(2,2)* ***321*** *with spatial overlap values for S<0.999. Assignments of M (metal-based) or L (ligand-based) are made based on Ni d character or the corresponding orbital.*

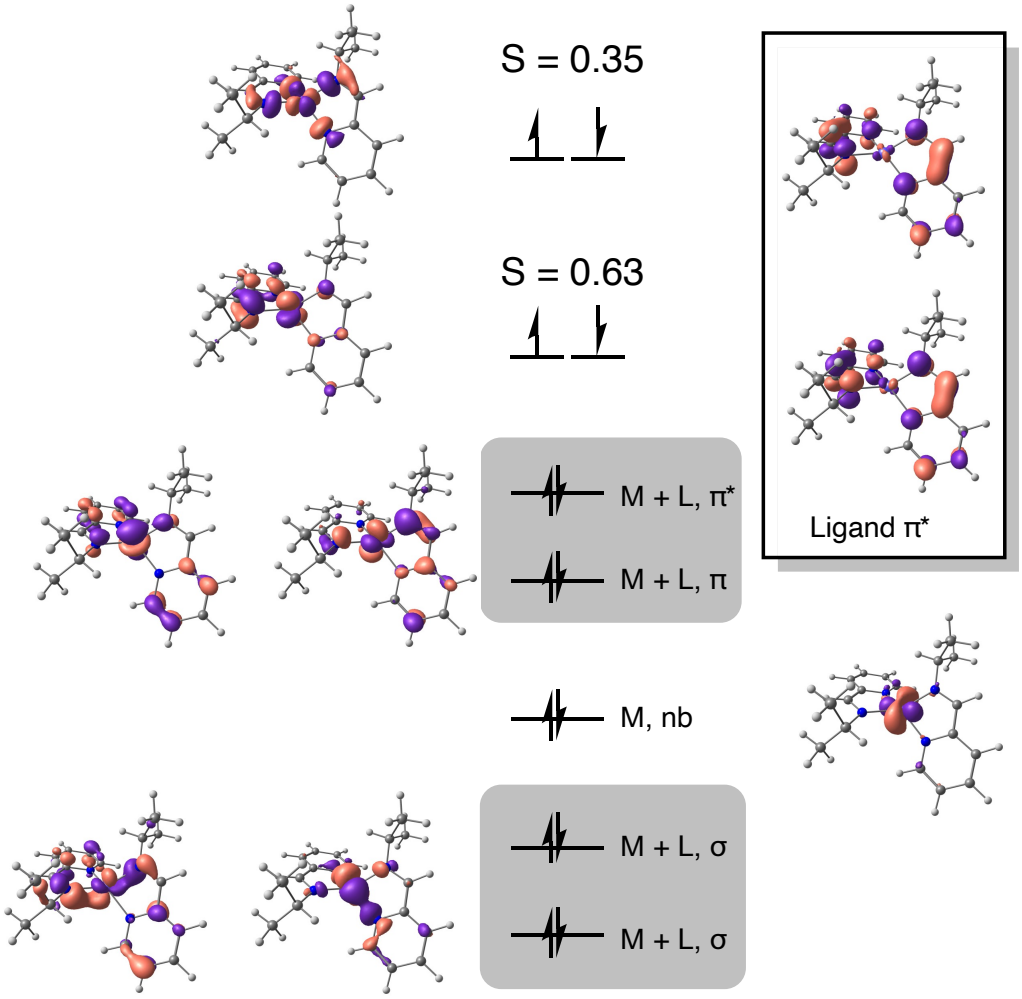

3.5.18 X-Ray Crystallography

General Details: Low-temperature diffraction data (φ- and ω-scans) were collected on a Bruker AXS D8 VENTURE KAPPA diffractometer coupled to a PHOTON II CPAD detector with Cu K_α radiation (λ = 1.54178 Å) from a IμS HB micro-focus sealed X-ray tube. All diffractometer manipulations, including data collection, integration, and scaling were carried out using the Bruker APEXII software.[55] Absorption corrections were applied using SADABS. The structure was solved by intrinsic phasing using SHELXT[56] and refined against F2 on all data by full-matrix least squares with SHELXL-2017[57] using established refinement techniques.[58] All non-hydrogen atoms were refined anisotropically. Unless otherwise noted, all hydrogen atoms were included into the model at geometrically calculated positions and refined using a riding model. The isotropic displacement parameters of all hydrogen atoms were fixed to 1.2 times the U value of the atoms they are linked to (1.5 times for methyl groups). Crystallographic data for **311**, **322**, and **323** can be obtained free of charge from The Cambridge Crystallographic Data Centre (CCDC) via www.ccdc.cam.ac.uk/data_request/cif under CCDC deposition numbers CCDC 2079525. Graphical representation of the structures with 50% probability thermal ellipsoids was generated using Mercury visualization software.[59]

Table 3.7. *Crystal and Refinement data for* ***311****.*

CCDC Number	2079525
Formula	$C_{18}H_{26}N_4$
Formula Weight	298.43
Crystal System	Triclinic
Space Group	P–1
a, Å	5.859(3)
b, Å	8.709(6)
c, Å	8.720(5)
α, °	95.09(2)
β, °	103.38(3)
γ, °	100.86(4)
Volume, Å	421.0(4)
T (K)	100
d_{calc}, g/cm ^{3}	1.082
Z	1
R_1,[a] *w*R_2,[b] [I>2σ(I)]	0.0506, 0.1679
GOF	1.05

[a]$R_1 = \Sigma||Fo|-|Fc||/\Sigma|Fo|$. [b]$wR2 = [\Sigma[w(F_o^2 - F_c^2)^2]/\Sigma[w(Fo^2)^2]]^{1/2}$.

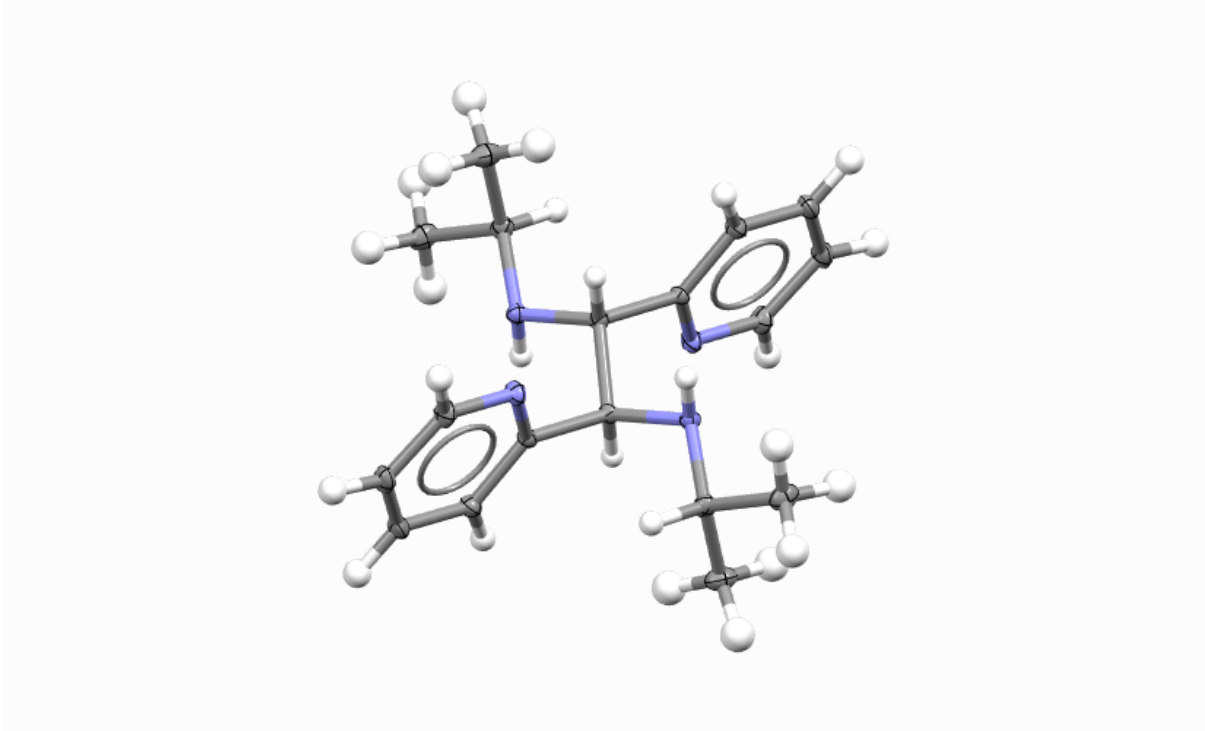

Table 3.8. *Crystal and Refinement data for* ***322****.*

CCDC Number	2117478
Formula	$C_{18}H_{24}N_4Cl_2Ni$
Formula Weight	426.02
Crystal System	monoclinic
Space Group	$P2_1/c$
a, Å	14.142(5)
b, Å	25.845(7)
c, Å	11.136(4)
α, °	90
β, °	91.374(17)
γ, °	90
Volume, Å	4069(2)
T (K)	100
d_{calc}, g/cm ^{3}	1.391
Z	8
R_1,[a] wR_2,[b] [I>2σ(I)]	0.0549, 0.1487
GOF	1.033

[a]$R_1 = \Sigma||Fo|-|Fc||/\Sigma|Fo|$. [b]$wR2 = [\Sigma[w(F_o^2 - F_c^2)^2]/\Sigma[w(Fo^2)^2]]^{1/2}$.

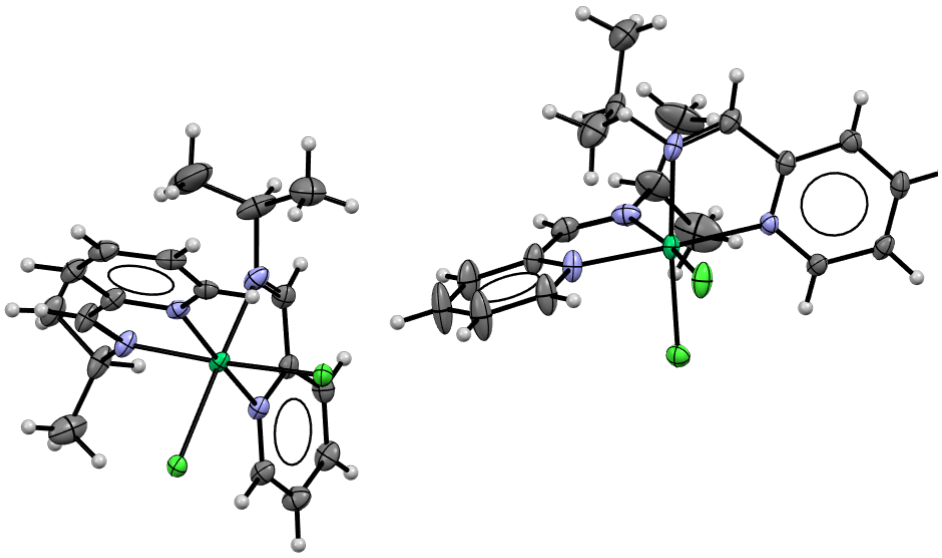

Table 3.9. *Crystal and Refinement data for* ***323****.*

CCDC Number	2117477
Formula	$C_{18}H_{24}N_4Cl_2Mn$
Formula Weight	422.261
Crystal System	Orthorhombic
Space Group	$P2_12_12_1$
a, Å	11.185(6)
b, Å	13.024(7)
c, Å	13.725(11)
α, °	90
β, °	90
γ, °	90
Volume, Å	1999(2)
T (K)	100
d_{calc}, g/cm ^{3}	1.403
Z	4
R_1,[a] wR_2,[b] [I>2σ(I)]	0.0486, 0.0819
GOF	1.010

[a] $R_1 = \Sigma||Fo|-|Fc||/\Sigma|Fo|$. [b] $wR2 = [\Sigma[w(F_o^2 - F_c^2)^2]/\Sigma[w(Fo^2)^2]]^{1/2}$.

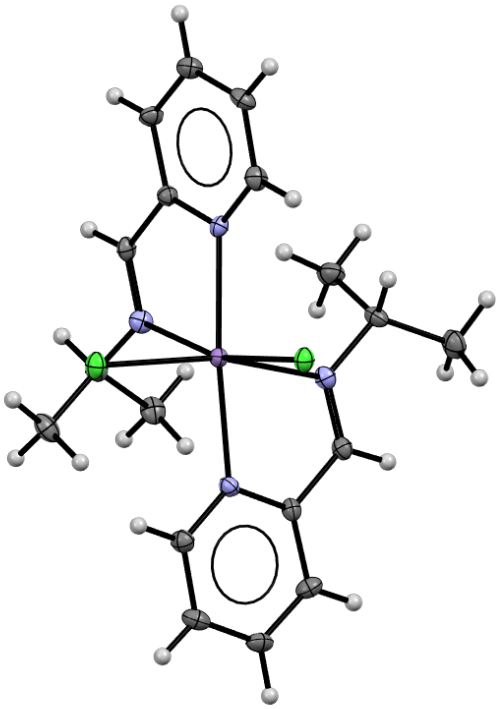

3.5.19 Elemental Analysis of Commercial Mn^0

Samples were measured on an Agilent 8800 ICP-MS instrument. ICP-MS was used to quantify trace Ni impurities in the commercial Mn^0 metal powder sample that was used throughout this publication. Three samples were prepared where sample A is the commercial metal, sample B is a procedural digestion blank to establish a background response, and sample C which is the commercial sample that was spiked with a transition metal analytical standard containing 500 ppb Ni. Sample data was quantified against a calibration curve (Figure **S34**) and amount of trace Ni in sample A was corrected for matrix/digestion effects determined by samples B and C.

Figure 3.41. *Ni calibration curve of measured counts/s against concentration in ppb.*

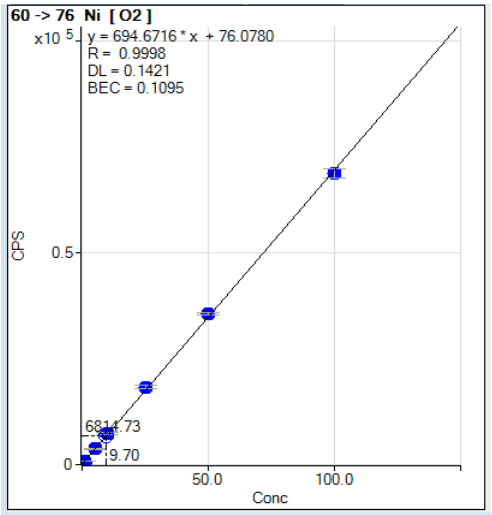

Sample preparation: To a 50 mL PTFE digestion tube was added Mn^0 metal powder (108.2 mg) followed by 2 mL of conc. HNO_3 (sample A). To the procedural blank tube (sample B) was also added 2 mL of conc. HNO_3, then all samples were refluxed under a watch glass for 2h at 80 ºC. The homogenous solutions were then diluted to 50 mL with conc. HNO_3. These solutions were then diluted again by diluting 1 mL to 50 mL in conc.

HNO_3 to make the instrument ready samples. Another Mn-containing sample (sample C) was prepared the same as sample A except 1 mL of a transition metal standard containing 500 ppb Ni was added. The standard adds a net 10 ppb Ni to the sample C over the unspiked sample A in the instrument ready samples.

Table 3.10. *Average concentration of Ni measured in each sample with relative standard deviation (RSD).*

Sample Name	Avg Conc. (ppb)	Conc. RSD (%)
Sample **A**	2.3	18.6
Sample **B**	0.6	46.5
Sample **C** (**A** +10ppb Ni)	9.6	6.4

Calculation of Trace Ni in Mn sample:

$$\frac{[Ni]_C - [Ni]_A}{[Ni]_{Std}} \times 100\% = \frac{9.6\ ppb - \ 2.3\ ppb}{10\ ppb} \times 100\% = 73\%$$

From the digestion recovery and procedural blank (sample B) the measured concentration of Ni can be corrected by taking the difference of the concentration in sample A (2.3 ppb) and the background from sample B (0.6 ppb) giving 1.7 ppb Ni. This value is then further corrected by dividing by the recovery, 73% (equation above) to give a final corrected concentration of 2.3 ppb Ni. A 2.3 ppb concentration from the 108.2 mg sample corresponds to a final concentration of **54.1 ppm**. This corresponds to 54.1 μg of total Ni per gram of Mn metal added. As a consequence, each reaction on a 0.3 mmol scale described by general procedure 3.4 has ~900 ng of nickel species (0.005 mol%) added through the addition of our Mn^0 reductant.

3.6 NOTES AND REFERENCES

(1) Turro, R. F.; Brandstätter, M.; Reisman, S. E. Nickel-Catalyzed Reductive Alkylation of Heteroaryl Imines. *Angew. Chem. Int. Ed.* **2022**, *61*, e202207597.

(2) a) S. A. Lawrence, *Amines : Synthesis, Properties and Applications.*, Cambridge University Press, **2004**; b) J. R. Lewis, *Nat. Prod. Rep.* **2001**, *18*, 95–128; c) J. S. Carey, D. Laffan, C. Thomson, M. T. Williams, *Org. Biomol. Chem*. **2006**, 4, 2337–2347; d) R. Hili, A. K. Yudin, *Nat Chem Biol.* **2006**, 2, 284–287.

(3) J. O. Link, M. S. Rhee, W. C. Tse, J. Zheng, J. R. Somoza, W. Rowe, R. Begley, A. Chiu, A. Mulato, D. Hansen, E. Singer, L. K. Tsai, R. A. Bam, C.-H. Chou, E. Canales, G. Brizgys, J. R. Zhang, J. Li, M. Graupe, P. Morganelli, Q. Liu, Q. Wu, R. L. Halcomb, R. D. Saito, S. D. Schroeder, S. E. Lazerwith, S. Bondy, D. Jin, M. Hung, N. Novikov, X. Liu, A. G. Villaseñor, C. E. Cannizzaro, E. Y. Hu, R. L. Anderson, T. C. Appleby, B. Lu, J. Mwangi, A. Liclican, A. Niedziela-Majka, G. A. Papalia, M. H. Wong, S. A. Leavitt, Y. Xu, D. Koditek, G. J. Stepan, H. Yu, N. Pagratis, S. Clancy, S. Ahmadyar, T. Z. Cai, S. Sellers, S. A. Wolckenhauer, J. Ling, C. Callebaut, N. Margot, R. R. Ram, Y.-P. Liu, R. Hyland, G. I. Sinclair, P. J. Ruane, G. E. Crofoot, C. K. McDonald, D. M. Brainard, L. Lad, S. Swaminathan, W. I. Sundquist, R. Sakowicz, A. E. Chester, W. E. Lee, E. S. Daar, S. R. Yant, T. Cihlar, *Nature* **2020**, 584, 614–618.

(4) M. J. Munchhof, Q. Li, A. Shavnya, G. V. Borzillo, T. L. Boyden, C. S. Jones, S. D. LaGreca, L. Martinez-Alsina, N. Patel, K. Pelletier, L. A. Reiter, M. D. Robbins, G. T. Tkalcevic, *ACS Med. Chem. Lett*. **2012**, 3, 106–111.

(5) a) R. Bloch, *Chem. Rev*. **1998**, 98, 1407–1438; b) E. Marcantoni, M. Petrini, in *Comprehensive Organic Synthesis* (Second Edition) (Ed.: P. Knochel), Elsevier, Amsterdam, **2014**, pp. 344–364.

(6) For reviews on radical additions to imines under thermal conditions, see: a) G. K. Friestad, *Tetrahedron* **2001**, 57, 5461–5496; b) H. Miyabe, E. Yoshioka, S. Kohtani, *Current Organic Chemistry* **2010**, 14, 1254–1264. (c) J. Tauber, D. Imbri, T. Opatz, *Molecules* **2014**, *19*, 16190–16222.

(7) For reviews on addition to imines under photoredox catalysis, see: a) S. T. J. Cullen, G. K. Friestad, *Synthesis* **2021**, *53*, 2319–2341; b) J.-J. Zhao, H.-H. Zhang, S. Yu, *Synthesis* **2021**, *53*, 1706–1718.

(8) For a recent method involving free radical addition to *N*-alkyliminium ions, see: R. Kumar, N. J. Flodén, W. G. Whitehurst, M. J. Gaunt, *Nature* **2020**, *581*, 415–420.

(9) For a review on the use of photoredox catalysis to generate α-amino radicals from imines, see: J. A. Leitch, T. Rossolini, T. Rogova, J. A. P. Maitland, D. J. Dixon, *ACS Catal.* **2020**, *10*, 2009–2025.

(10) Halland, N.; Jørgensen, K. A. Intermolecular Addition of Alkyl Radicals to Imines in the Absence and in the Presence of a Lewis Acid. *J. Chem. Soc., Perkin Trans. 1* **2001**, No. 11, 1290–1295.

(11) Ni, S.; Garrido-Castro, A. F.; Merchant, R. R.; de Gruyter, J. N.; Schmitt, D. C.; Mousseau, J. J.; Gallego, G. M.; Yang, S.; Collins, M. R.; Qiao, J. X.; Yeung, K.-S.; Langley, D. R.; Poss, M. A.; Scola, P. M.; Qin, T.; Baran, P. S. A General Amino Acid Synthesis Enabled by Innate Radical Cross-Coupling. *Angew. Chem. Int. Ed.* **2018**, *57*, 14560–14565.

(12) Yamada, K.; Fujihara, H.; Yamamoto, Y.; Miwa, Y.; Taga, T.; Tomioka, K. Radical Addition of Ethers to Imines Initiated by Dimethylzinc. *Org. Lett.* **2002**, *4*, 3509–3511.

(13) Friestad, G. K.; Qin, J. Highly Stereoselective Intermolecular Radical Addition to Aldehyde Hydrazones from a Chiral 3-Amino-2-Oxazolidinone. *J. Am. Chem. Soc.* **2000**, *122*, 8329–8330.

(14) Leitch, J. A.; Rossolini, T.; Rogova, T.; Maitland, J. A. P.; Dixon, D. J. α-Amino Radicals via Photocatalytic Single-Electron Reduction of Imine Derivatives. *ACS Catal.* **2020**, *10*, 2009–2025.

(15) For representative examples see: (a) Jeffrey, J. L.; Petronijević, F. R.; MacMillan, D. W. C. Selective Radical–Radical Cross-Couplings: Design of a Formal β-Mannich Reaction. *J. Am. Chem. Soc.* **2015**, *137*, 8404–8407. (b) Hager, D.; MacMillan, D. W. C. Activation of C–H Bonds via the Merger of Photoredox and Organocatalysis: A Coupling of Benzylic Ethers with Schiff Bases. *J. Am. Chem. Soc.* **2014**, *136*, 16986–16989. (c) Fava, E.; Millet, A.; Nakajima, M.; Loescher, S.; Rueping, M. Reductive Umpolung of Carbonyl Derivatives with Visible-Light Photoredox Catalysis: Direct Access to Vicinal Diamines and Amino Alcohols via

α-Amino Radicals and Ketyl Radicals. *Angew. Chem. Int. Ed.* **2016**, *55*, 6776–6779. (d) Zhang, H.-H.; Yu, S. Visible-Light-Induced Radical Acylation of Imines with α-Ketoacids Enabled by Electron-Donor–Acceptor Complexes. *Org. Lett.* **2019**, *21*, 3711–3715.

(16) For a complementary Ni-catalyzed imine alkylation, see C. Heinz, J. P. Lutz, E. M. Simmons, M. M. Miller, W. R. Ewing, A. G. Doyle, *J. Am. Chem. Soc.* **2018**, *140*, 2292–2300.

(17) For a Ni-catalyzed addition of free radicals to glyoxylate-derived sulfinnimines, see: S. Ni, A. F. Garrido-Castro, R. R. Merchant, J. N. de Gruyter, D. C. Schmitt, J. J. Mousseau, G. M. Gallego, S. Yang, M. R. Collins, J. X. Qiao, K.-S. Yeung, D. R. Langley, M. A. Poss, P. M. Scola, T. Qin, P. S. Baran, *Angew. Chem. Int. Ed.***2018**, *57*, 14560–14565.

(18) (a) J. Jacquet, M. Desage-El Murr, L. Fensterbank, *ChemCatChem* **2016**, *8*, 3310–3316; b) O. R. Luca, R. H. Crabtree, *Chem. Soc. Rev.* **2013**, *42*, 1440–1459; c) V. K. K. Praneeth, M. R. Ringenberg, T. R. Ward, *Angew. Chem. Int. Ed.* **2012**, *51*, 10228–10234; d) V. Lyaskovskyy, B. de Bruin, *ACS Catal.* **2012**, *2*, 270–279; e) P. J. Chirik, K. Wieghardt, *Science* **2010**, *327*, 794–795.

(19) C. C. Lu, E. Bill, T. Weyhermüller, E. Bothe, K. Wieghardt, *J. Am. Chem. Soc.* **2008**, *130*, 3181–3197.

(20) a) P. J. Bailey, C. M. Dick, S. Fabre, S. Parsons, L. J. Yellowlees, *Dalton Trans.* **2006**, 1602–1610; b) V. Riollet, C. Copéret, J.-M. Basset, L. Rousset, D. Bouchu, L. Grosvalet, M. Perrin, *Angew. Chem. Int. Ed.* **2002**, *41*, 3025–3027; c) M. Kaupp,

H. Stoll, H. Preuss, W. Kaim, T. Stahl, G. Van Koten, E. Wissing, W. J. J. Smeets, A. L. Spek, *J. Am. Chem. Soc.* **1991**, *113*, 5606–5618.

(21) (a) M. B. Solomon, B. Chan, C. P. Kubiak, K. A. Jolliffe, D. M. D'Alessandro, *Dalton Trans.* **2019**, *48*, 3704–3713; b) M. M. Morrison, D. T. Sawyer, *Inorg. Chem.* **1978**, *17*, 333–337; c) J. M. Rao, M. C. Hughes, D. J. Macero, *Inorg. Chim. Acta* **1976**, *18*, 127–131.

(22) Trace metal analysis by ICP-MS found that the Mn^0 source contains 54 ppm total Ni species. However, this would represent a very low concentration of Ni catalyst (<0.005 mol %). See Supporting Information section 3.5.19 for ICP-MS sample preparation and calculations.

(23) Alternative additives such as phenol, acetic anhydride, trifluoroacetic anhydride, and benzoic acid led to no further improvement.

(24) T. T. Talele, *J. Med. Chem.* **2016**, *59*, 8712–8756.

(25) Less reactive alkyl halides with hindered imines produce varying quantities of **311** (see Figure 3.14 for **311** production across several substrates). Using a radical precursor that is more facile to reduce, like NHP esters, enhances the rate of alkyl radical generation and favors cross-coupling over sp^2–sp^2 homocoupling. For examples, see: a) V. Faugeroux, Y. Genisson, *Current Organic Chemistry* **2008**, *12*, 751–773; b) E. B. Hulley, P. T. Wolczanski, E. B. Lobkovsky, *J. Am. Chem. Soc.* **2011**, *133*, 18058–18061; c) S. Inoue, Y.-N. Yan, K. Yamanishi, Y. Kataoka, T. Kawamoto, *Chem. Commun.* **2020**, *56*, 2829–2832; d) D. Pokhriyal, S. P. Heins,

R. J. Sifri, D. T. Gentekos, R. E. Coleman, P. T. Wolczanski, T. R. Cundari, B. P. Fors, K. M. Lancaster, S. N. MacMillan, *Inorg. Chem.* **2021**, *60*, 18662–18673.

(26) All data for X-ray crystal structures have been deposited in the CCDC, under the following deposition numbers: **311** = 2079525, **322** = 2117478, **323** = 2117477

(27) a) K. M. M. Huihui, J. A. Caputo, Z. Melchor, A. M. Olivares, A. M. Spiewak, K. A. Johnson, T. A. DiBenedetto, S. Kim, L. K. G. Ackerman, D. J. Weix, *J. Am. Chem. Soc.* **2016**, *138*, 5016–5019; b) N. Suzuki, J. L. Hofstra, K. E. Poremba, S. E. Reisman, *Org. Lett.* **2017**, *19*, 2150–2153;. For a recent review of Ni-catalyzed cross-couplings with NHP esters, see: M. O. Konev, E. R. Jarvo, *Angew. Chem. Int. Ed.* **2016**, *55*, 11340–11342.

(28) For additional investigations into the electronic structure of redox-active first-row transition metal bis-iminopyridine complexes, see reference 13 as well as: a) C. C. Lu, E. Bill, T. Weyhermüller, E. Bothe, K. Wieghardt, *Inorg. Chem.* **2007**, *46*, 7880–7889; b) A. Mondal, T. Weyhermüller, K. Wieghardt, *Chem. Commun.* **2009**, 6098–6100; c) N. P. Tsvetkov, C.-H. Chen, J. G. Andino, R. L. Lord, M. Pink, R. W. Buell, K. G. Caulton, *Inorg. Chem.* **2013**, *52*, 9511–9521; d) D. Sengupta, P. Ghosh, T. Chatterjee, H. Datta, N. D. Paul, S. Goswami, *Inorg. Chem.* **2014**, *53*, 12002–12013.

(29) DFT calculations were performed using the ORCA software package at the B3LYP/def2-TZVP level of theory. See Supporting Information for optimization, frequency, broken symmetry, and property calculations.

(30) T. Soda, Y. Kitagawa, T. Onishi, Y. Takano, Y. Shigeta, H. Nagao, Y. Yoshioka, K. Yamaguchi, *Chem. Phys. Lett.* **2000**, *319*, 223–230.

(31) The peak-to-peak separation was determined to be ~106 mV for **322**. Given this deviation from theoretical, we cannot draw a conclusion from the CV alone about whether the reduction is a one or two electron process.

(32) $Mn^{0}_{(S)}$ -> $Mn^{II}_{(NMP)}$ is estimated to be ~ –1.8 V vs. Fc/Fc^{+} by converting the known value of –1.185 V vs. SHE for Mn to Mn^{II}. The reduction of **322** was found to occur at –1.4 V vs. Fc/Fc^{+}, and therefore should be in the reducing window of Mn^{0}. (a) For standard reduction potential values, see: W. M. Haynes, *CRC Handbook of Chemistry and Physics. [Electronic Resource] : A Ready-Reference Book of Chemical and Physical Data.*, CRC Press, **2018**. b) For converting SCE potentials to 0.1 M $TBAPF_6$ in DMF vs. Fc/Fc^{+}, see: Q. Lin, G. Dawson, T. Diao, *Synlett* **2021**, *32*, 1606–1620.

(33) The facile two electron reduction of **322** is in contrast to recent studies of $(Phen)NiBr_2$ complexes, which undergo one electron reduction at similar potentials: Q. Lin, T. Diao, *J. Am. Chem. Soc.* **2019**, *141*, 17937–17948.

(34) C. Sandford, L. R. Fries, T. E. Ball, S. D. Minteer, M. S. Sigman, *J. Am. Chem. Soc.* **2019**, *141*, 18877–18889.

(35) W. C. Still, M. Kahn, A. Mitra, *J. Org. Chem.* **1978**, *43*, 2923–2925.

(36) N. Suzuki, J. L. Hofstra, K. E. Poremba, S. E. Reisman, *Org. Lett.* **2017**, *19*, 2150–2153.

(37) L. M. Kammer, A. Rahman, T. Opatz, *Molecules* **2018**, *23*, 764.

(38) Y. Jiang, J. Pan, T. Yang, Y. Zhao, M. J. Koh, *Chem* **2021**, *7*, 993–1005.

(39) L. R. Mills, C. Zhou, E. Fung, S. A. L. Rousseaux, *Org. Lett.* **2019**, *21*, 8805–8809.

(40) Z. Peng, P. Knochel, *Org. Lett.* **2011**, *13*, 3198–3201.

(41]) J. Roberto Pioquinto-Mendoza, D. Martínez-Otero, N. Andrade-López, J. G. Alvarado-Rodríguez, V. Salazar-Pereda, G. Sánchez-Cabrera, F. J. Zuno-Cruz, *Polyhedron* **2013**, *50*, 289–296.

(42) S. Daniele, M. Martelli, G. Bontempelli, *Inorganica Chimica Acta* **1991**, *179*, 105–111.

(43) C. Sandford, L. R. Fries, T. E. Ball, S. D. Minteer, M. S. Sigman, *J. Am. Chem. Soc.* **2019**, *141*, 18877–18889.

(44) S. Hoops, S. Sahle, R. Gauges, C. Lee, J. Pahle, N. Simus, M. Singhal, L. Xu, P. Mendes, U. Kummer, *Bioinformatics* **2006**, *22*, 3067–3074.

(45) C. C. Lu, E. Bill, T. Weyhermüller, E. Bothe, K. Wieghardt, *J. Am. Chem. Soc.* **2008**, *130*, 3181–3197.

(46) F. Neese, *WIREs Computational Molecular Science* **2012**, *2*, 73–78; b) F. Neese, *WIREs Computational Molecular Science* **2018**, *8*, e1327.

(47) A. D. Becke, *J. Chem. Phys.* **1993**, *98*, 5648–5652.

(48) F. Neese, F. Wennmohs, A. Hansen, U. Becker, *Chemical Physics* **2009**, *356*, 98–109.

(49) F. Weigend, *Phys. Chem. Chem. Phys.* **2006**, *8*, 1057–1065.

(50) A. P. Ginsberg, *J. Am. Chem. Soc.* **1980**, *102*, 111–117.

(51) L. Noodleman, C. Y. Peng, D. A. Case, J.-M. Mouesca, *Coordination Chemistry Reviews* **1995**, *144*, 199–244.

(52) B. Kirchner, F. Wennmohs, S. Ye, F. Neese, *Current Opinion in Chemical Biology* **2007**, *11*, 134–141.

(53) C. Y. Legault, CYLview, 1.0b; Université de Sherbrooke: Québec, Montreal, Canada, **2009**; http://www.cylview.org

(54) Chemcraft - graphical software for visualization of quantum chemistry computations. https://www.chemcraftprog.com

(55) G. M. Sheldrick, "SADABS (version 2008/1): Program for Absorption Correction for Data from Area Detector Frames", University of Göttingen, **2008.**

(56) G. M. Sheldrick, **2008** *Acta Cryst*., 64, 112-122.

(57) G. M. Sheldrick, **2015**, *Acta Cryst.,* A71, 3–8.

(58) P. Müller, *Crystallography Reviews* **2009**, *15*, 57–83.

(59) C. F. Macrae, I. Sovago, S. J. Cottrell, P. T. A. Galek, P. McCabe, E. Pidcock, M. Platings, G. P. Shields, J. S. Stevens, M. Towler, P. A. Wood, **2020**. *J. Appl. Cryst*. 53, 226-235.

Appendix 1

Spectra Relevant to Chapter 3:

Nickel-Catalyzed Reductive Alkylation of Heteroaryl Imines

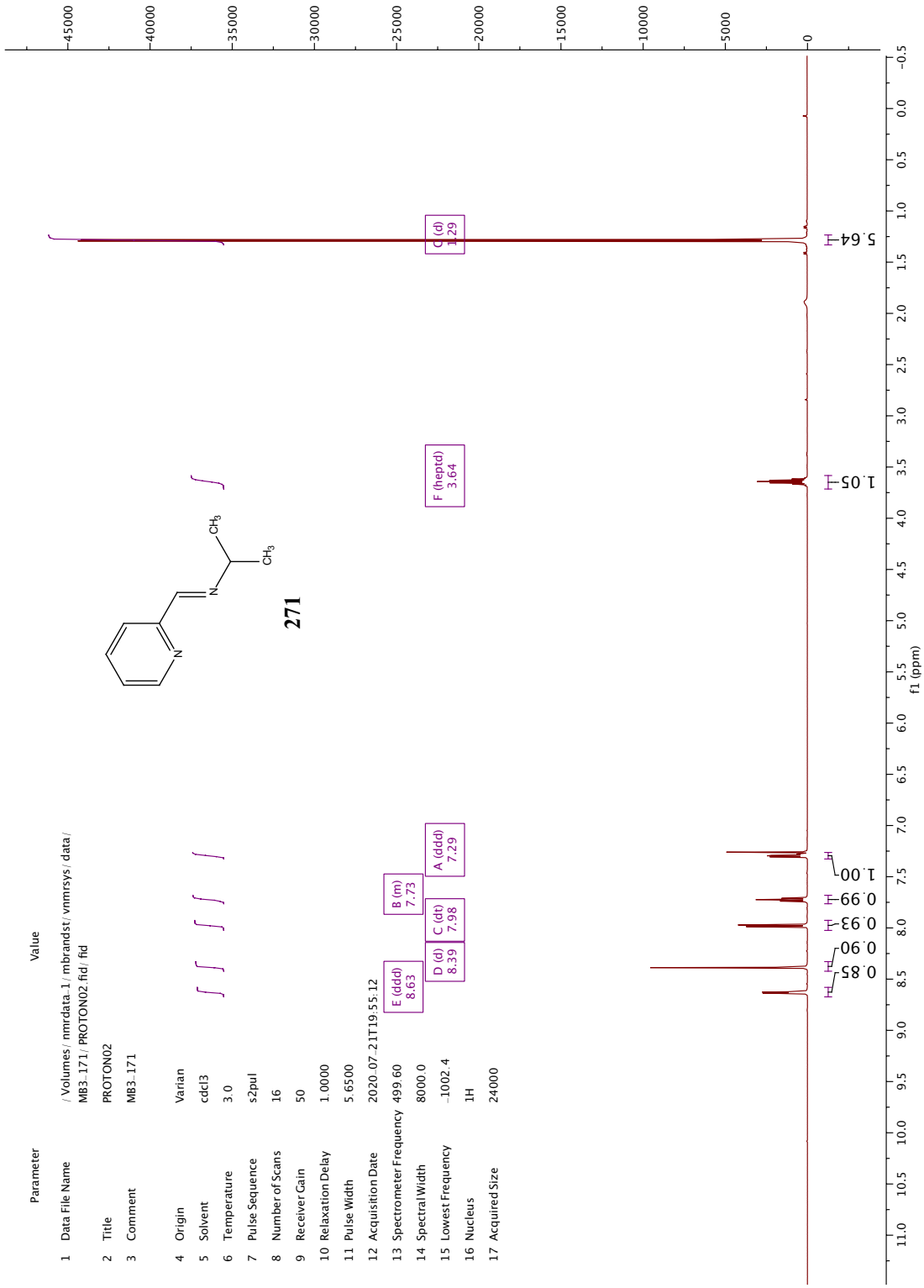
Parameter
Value
1 Data File Name / Volumes/ nmrdata_1/ mbrandst/ vnmrsys/ data / MB3_171/ PROTON02.fid/ fid
2 Title PROTON02
3 Comment MB3_171
4 Origin Varian
5 Solvent cdcl3
6 Temperature 3.0
7 Pulse Sequence s2pul
8 Number of Scans 16
9 Receiver Gain 50
10 Relaxation Delay 1.0000
11 Pulse Width 5.6500
12 Acquisition Date 2020-07-21T19:55:12
13 Spectrometer Frequency 499.60
14 Spectral Width 8000.0
15 Lowest Frequency -1002.4
16 Nucleus 1H
17 Acquired Size 24000
271
E (ddd) 8.63
D (d) 8.39
C (dt) 7.98
B (m) 7.73
A (dddd) 7.29
F (heptd) 3.64
C (d) 1.29
0.85
0.90
0.93
0.99
1.00
1.05
5.64
f1 (ppm)

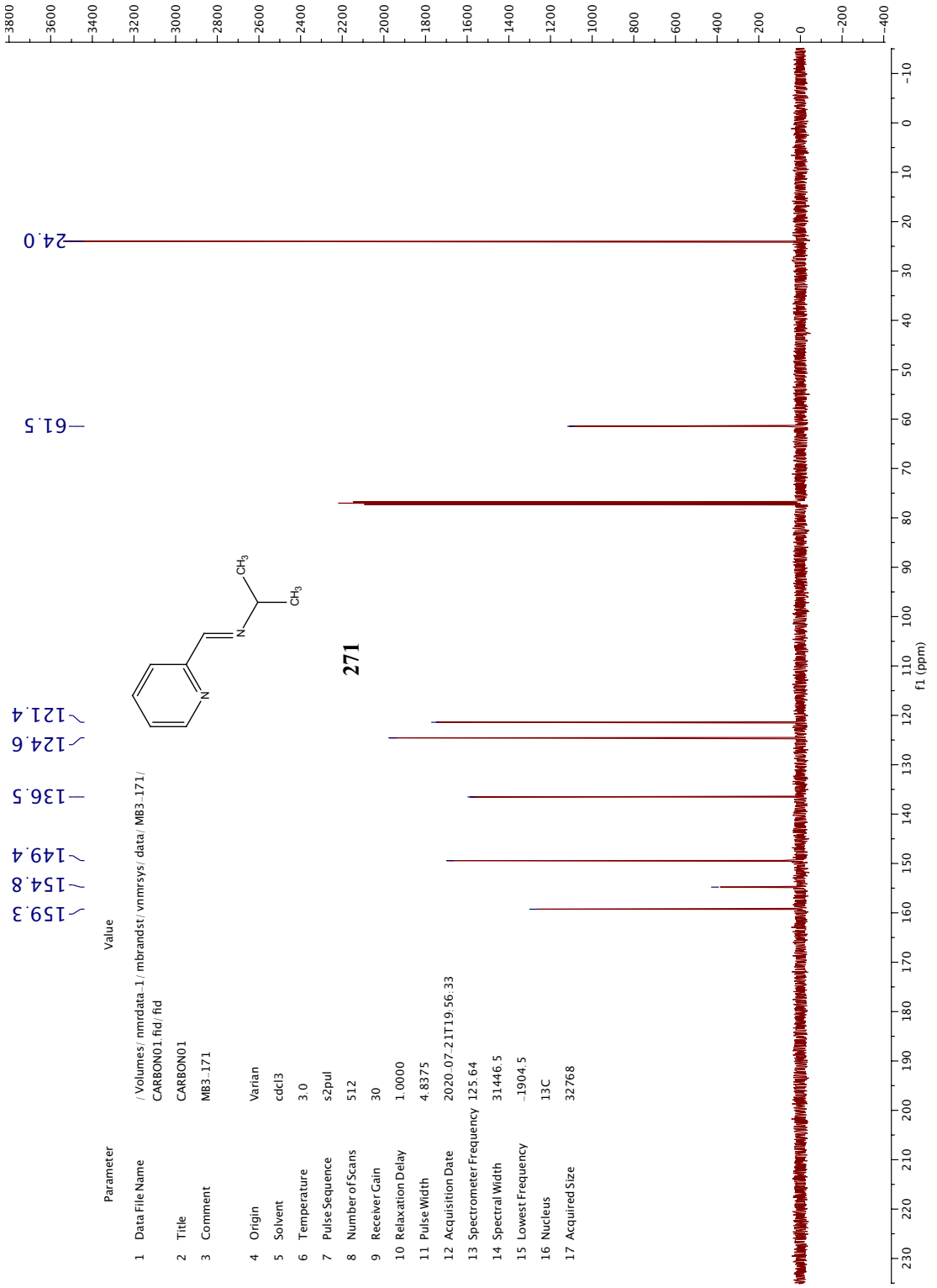

	Parameter	Value
1	Data File Name	/Volumes/nmrdata_1/mbrandst/vnmrsys/data/MB3_171/CARBON01.fid/fid
2	Title	CARBON01
3	Comment	MB3_171
4	Origin	Varian
5	Solvent	cdcl3
6	Temperature	3.0
7	Pulse Sequence	s2pul
8	Number of Scans	512
9	Receiver Gain	30
10	Relaxation Delay	1.0000
11	Pulse Width	4.8375
12	Acquisition Date	2020_07_21T19:56:33
13	Spectrometer Frequency	125.64
14	Spectral Width	31446.5
15	Lowest Frequency	-1904.5
16	Nucleus	13C
17	Acquired Size	32768

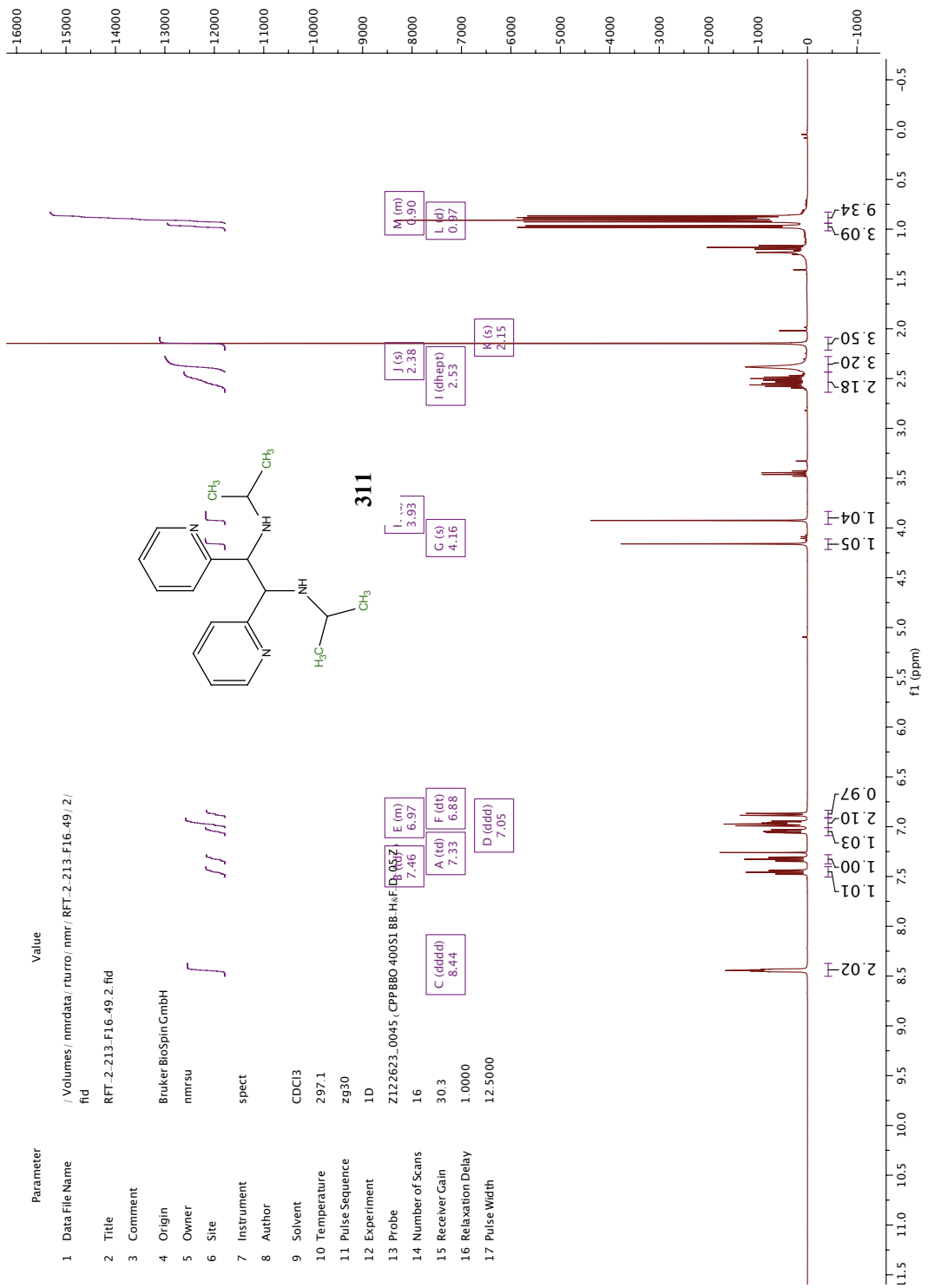
311
Parameter
Value
1 Data File Name / Volumes / nmrdata / rturro / nmr / RFT_2_213_F16_49 / 2 / fid
2 Title RFT_2_213_F16_49 2 fid
3 Comment
4 Origin Bruker BioSpin GmbH
5 Owner nmrsu
6 Site
7 Instrument spect
8 Author
9 Solvent CDCl3
10 Temperature 297.1
11 Pulse Sequence zg30
12 Experiment 1D
13 Probe Z122623_0045_CPPBBO 400S1 BB H&F D Z
14 Number of Scans 16
15 Receiver Gain 30.3
16 Relaxation Delay 1.0000
17 Pulse Width 12.5000
C (dddd) 8.44
A (td) 7.33
B (td) 7.46
F (dt) 6.88
E (m) 6.97
D (ddd) 7.05
I, ... 3.93
G (s) 4.16
J (s) 2.38
I (dhept) 2.53
K (s) 2.15
M (m) 0.90
L (dd) 0.97
2.02
1.01
1.00
1.03
2.10
0.97
1.04
1.05
2.18
3.20
3.50
3.09
9.34
f1 (ppm)

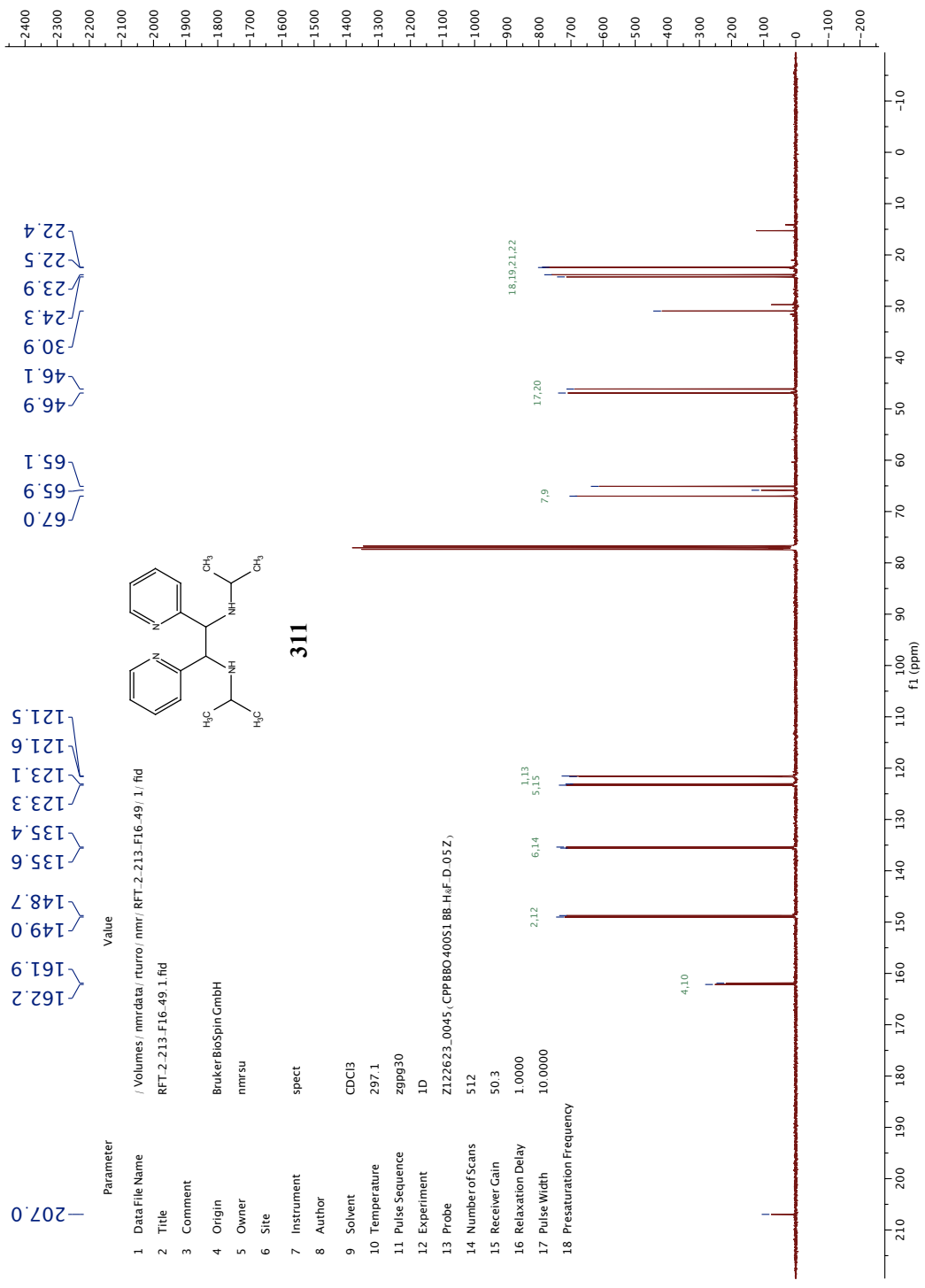
311
f1 (ppm)
207.0
162.2
161.9
149.0
148.7
135.6
135.4
123.3
123.1
121.6
121.5
67.0
65.9
65.1
46.9
46.1
30.9
24.3
23.9
22.5
22.4
Parameter
Value
1 Data File Name / Volumes / nmrdata / rturro / nmr / RFT-2-213-F16.49 / 1 / fid
2 Title RFT-2-213-F16.49.1.fid
3 Comment
4 Origin Bruker BioSpin GmbH
5 Owner nmrsu
6 Site
7 Instrument spect
8 Author
9 Solvent CDCl3
10 Temperature 297.1
11 Pulse Sequence zgpg30
12 Experiment 1D
13 Probe Z122623_0045 (CPPBBO 400S1 BB-H&F-D-05Z)
14 Number of Scans 512
15 Receiver Gain 50.3
16 Relaxation Delay 1.0000
17 Pulse Width 10.0000
18 Presaturation Frequency

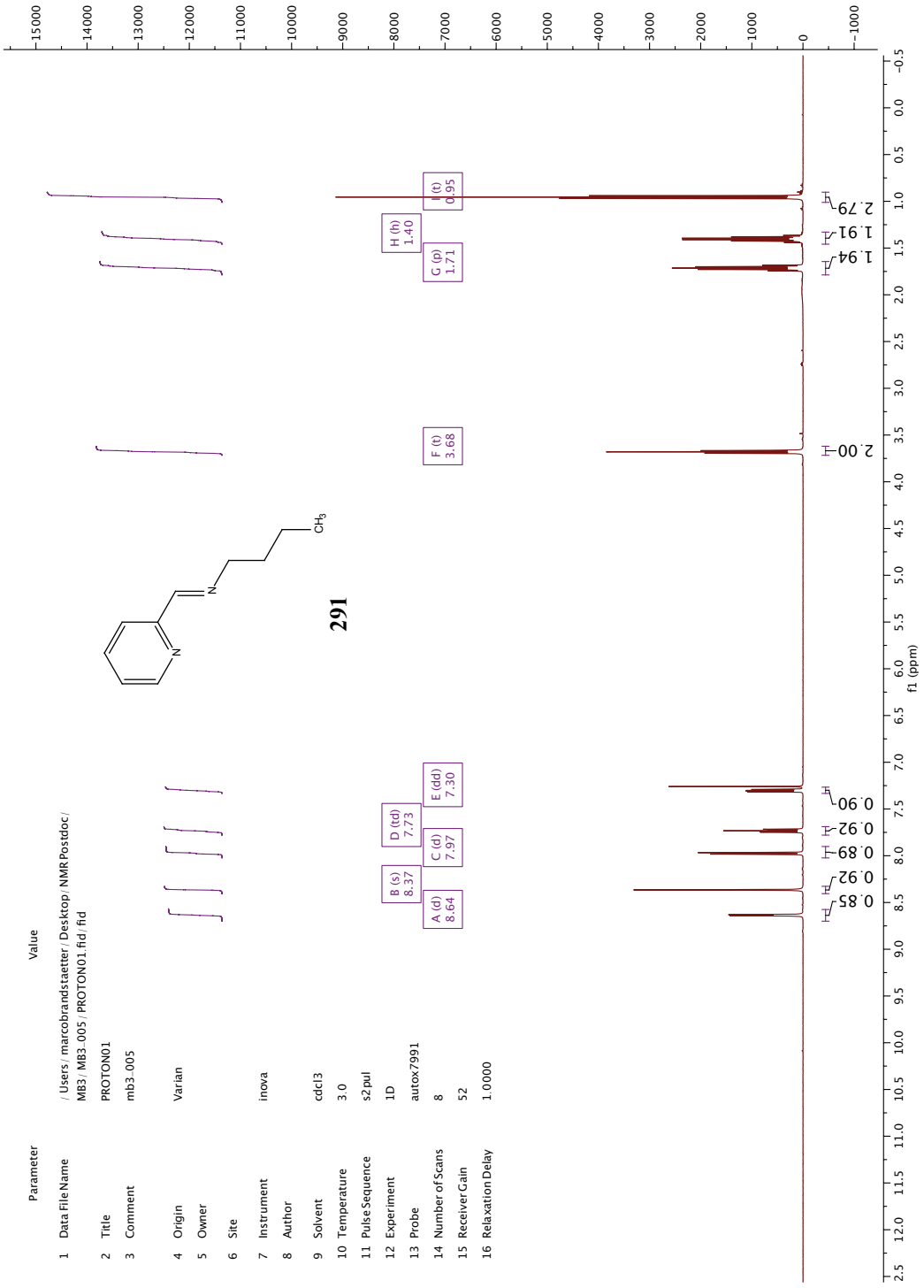
Parameter
Value
1 Data File Name / Users / marcobrandstaetter / Desktop / NMR Postdoc / MB3 / MB3-005 / PROTON01.fid / fid
2 Title PROTON01
3 Comment mb3-005
4 Origin Varian
5 Owner
6 Site
7 Instrument inova
8 Author
9 Solvent cdcl3
10 Temperature 3.0
11 Pulse Sequence s2pul
12 Experiment 1D
13 Probe autox7991
14 Number of Scans 8
15 Receiver Gain 52
16 Relaxation Delay 1.0000
A (d) 8.64
B (s) 8.37
C (d) 7.97
D (td) 7.73
E (dd) 7.30
F (t) 3.68
G (p) 1.71
H (h) 1.40
I (t) 0.95
291
CH3
N
N
0.85
0.92
0.89
0.92
0.90
2.00
1.94
1.91
2.79
f1 (ppm)

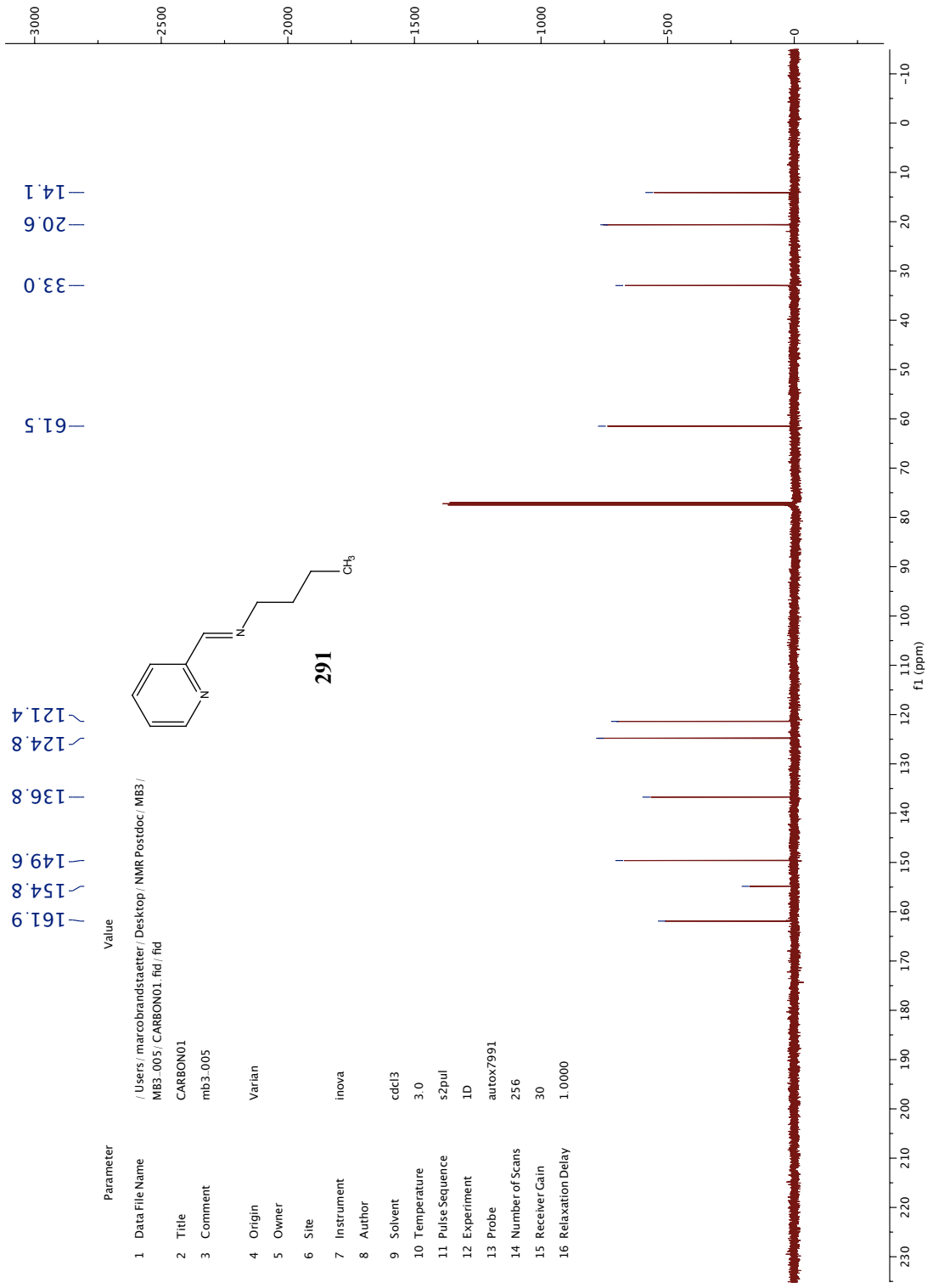

Parameter		Value
1	Data File Name	/Users/marcobrandstaetter/Desktop/NMR Postdoc/MB3/MB3_005/CARBON01.fid/fid
2	Title	CARBON01
3	Comment	mb3_005
4	Origin	Varian
5	Owner	
6	Site	
7	Instrument	inova
8	Author	
9	Solvent	cdcl3
10	Temperature	3.0
11	Pulse Sequence	s2pul
12	Experiment	1D
13	Probe	autox7991
14	Number of Scans	256
15	Receiver Gain	30
16	Relaxation Delay	1.0000

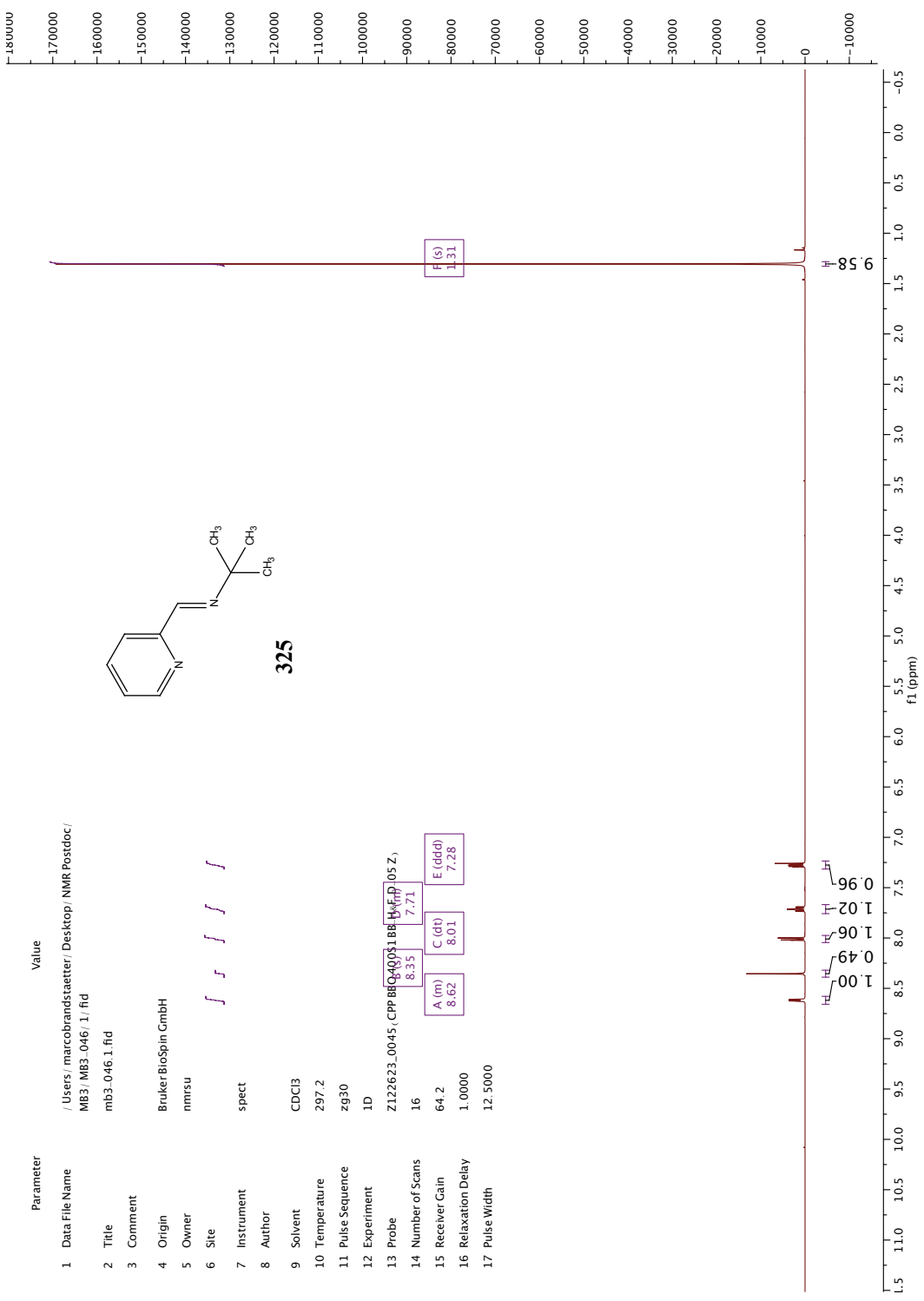
325
Parameter
Value
1 Data File Name /Users/marcobrandstaetter/Desktop/NMR Postdoc/MB3/MB3_046/1/fid
2 Title mb3_046_1.fid
3 Comment
4 Origin Bruker BioSpin GmbH
5 Owner nmrsu
6 Site
7 Instrument spect
8 Author
9 Solvent CDCl3
10 Temperature 297.2
11 Pulse Sequence zg30
12 Experiment 1D
13 Probe Z122623_0045, CPP BBO 400S1 BB-H-D-05 Z
14 Number of Scans 16
15 Receiver Gain 64.2
16 Relaxation Delay 1.0000
17 Pulse Width 12.5000
A (m) 8.62
B (m) 8.35
C (dd) 8.01
D (m) 7.71
E (ddd) 7.28
F (s) 1.31
9.58
1.00
0.49
1.06
1.02
0.96
f1 (ppm)

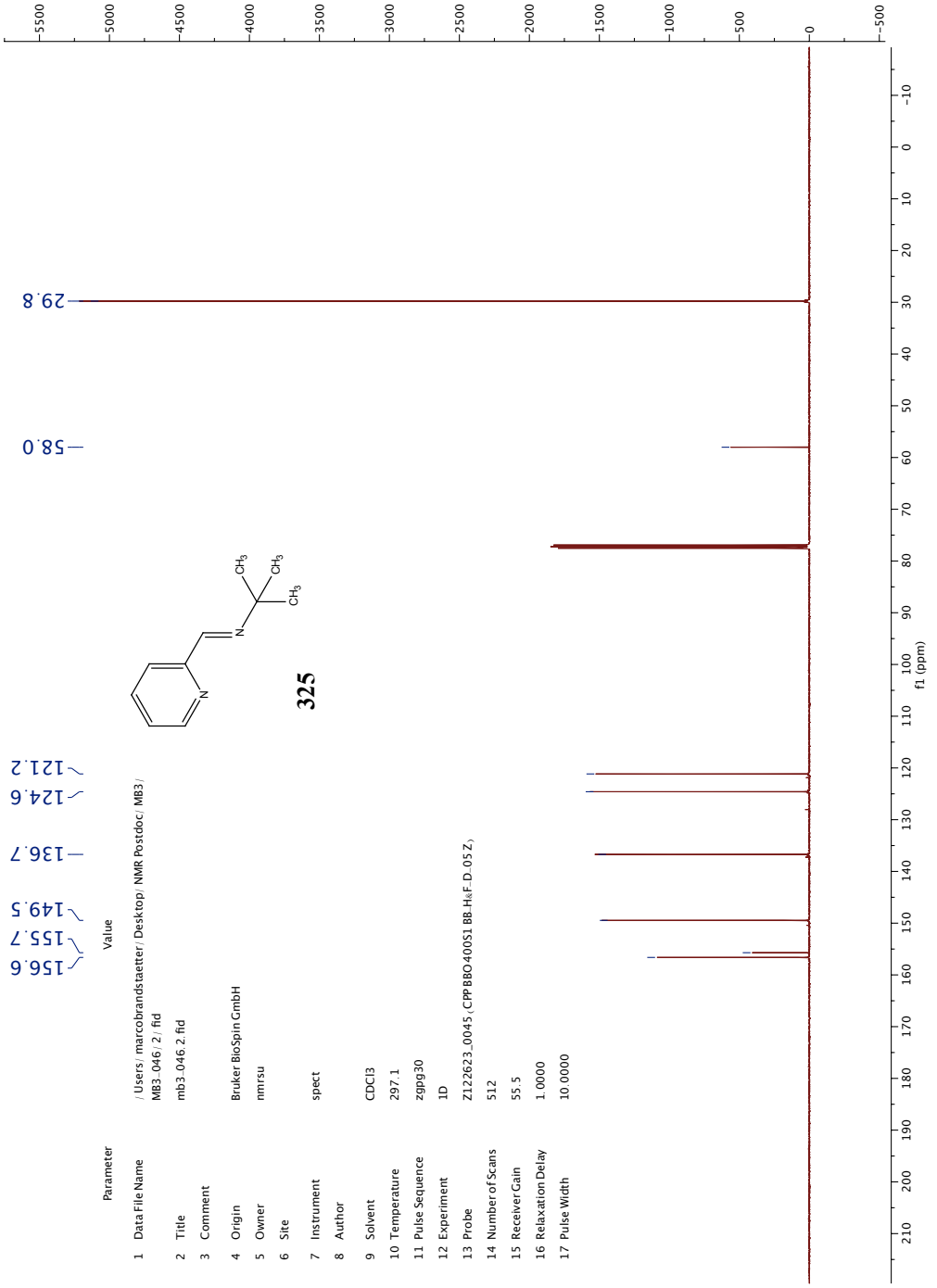

Parameter	Value
1 Data File Name	/Users/marcobrandstaetter/Desktop/NMR Postdoc/MB3/MB3_046/2/fid
2 Title	mb3_046_2.fid
3 Comment	
4 Origin	Bruker BioSpin GmbH
5 Owner	nmrsu
6 Site	
7 Instrument	spect
8 Author	
9 Solvent	CDCl3
10 Temperature	297.1
11 Pulse Sequence	zgpg30
12 Experiment	1D
13 Probe	Z122623_0045_CPPBBO400S1 BB-H&F-D-05 Z
14 Number of Scans	512
15 Receiver Gain	55.5
16 Relaxation Delay	1.0000
17 Pulse Width	10.0000

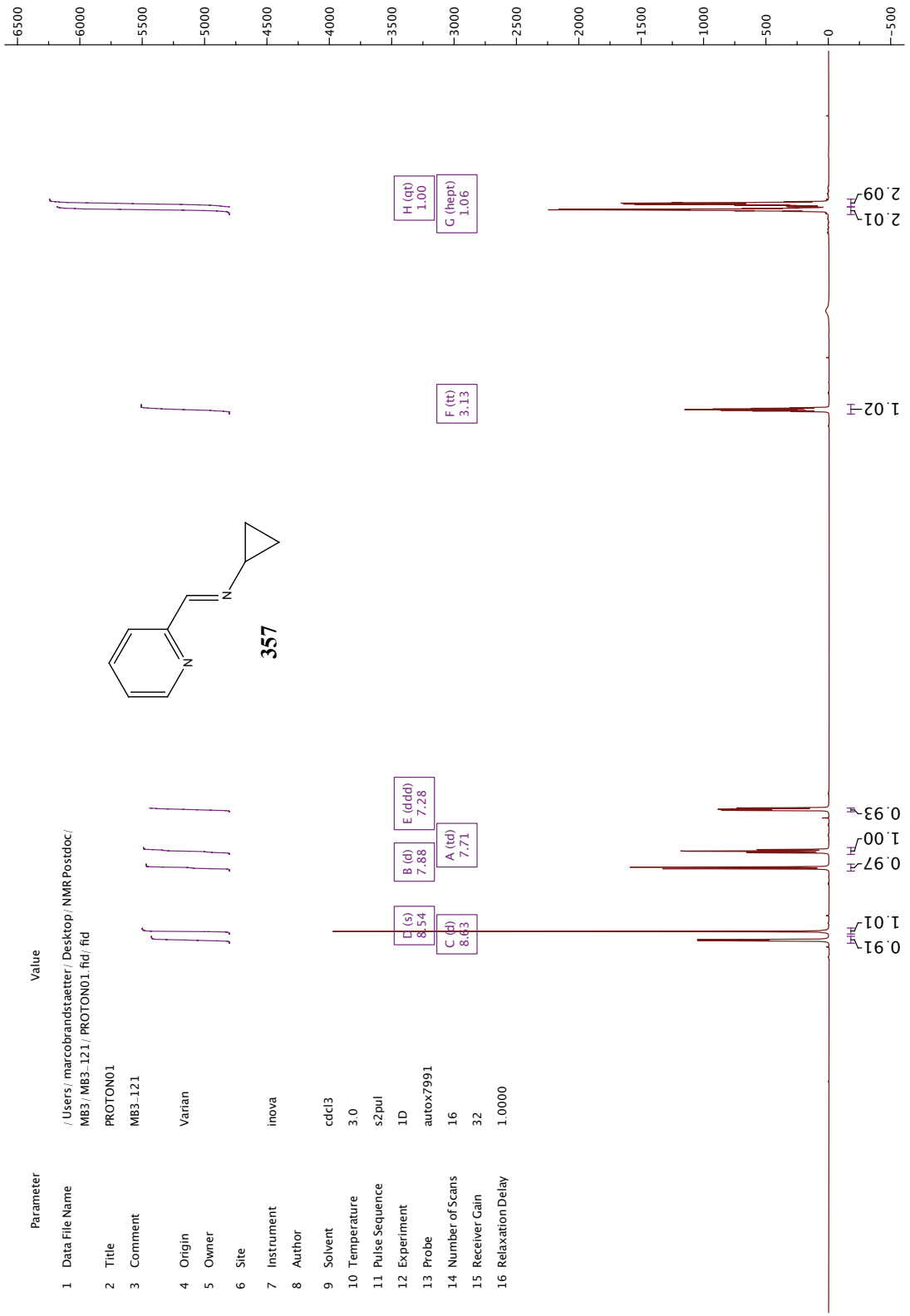
Parameter
Value
1 Data File Name
/ Users/ marcobrandstaetter/ Desktop/ NMR Postdoc/ MB3/ MB3_121/ PROTON01.fid/ fid
2 Title
PROTON01
3 Comment
MB3_121
4 Origin
Varian
5 Owner
6 Site
7 Instrument
inova
8 Author
9 Solvent
cdcl3
10 Temperature
3.0
11 Pulse Sequence
s2pul
12 Experiment
1D
13 Probe
autox7991
14 Number of Scans
16
15 Receiver Gain
32
16 Relaxation Delay
1.0000
D (s) 8.54
C (d) 8.63
B (d) 7.88
A (td) 7.71
E (ddd) 7.28
F (tt) 3.13
H (qt) 1.00
G (hept) 1.06
357
0.91
1.01
0.97
1.00
0.93
1.02
2.01
2.09
f1 (ppm)

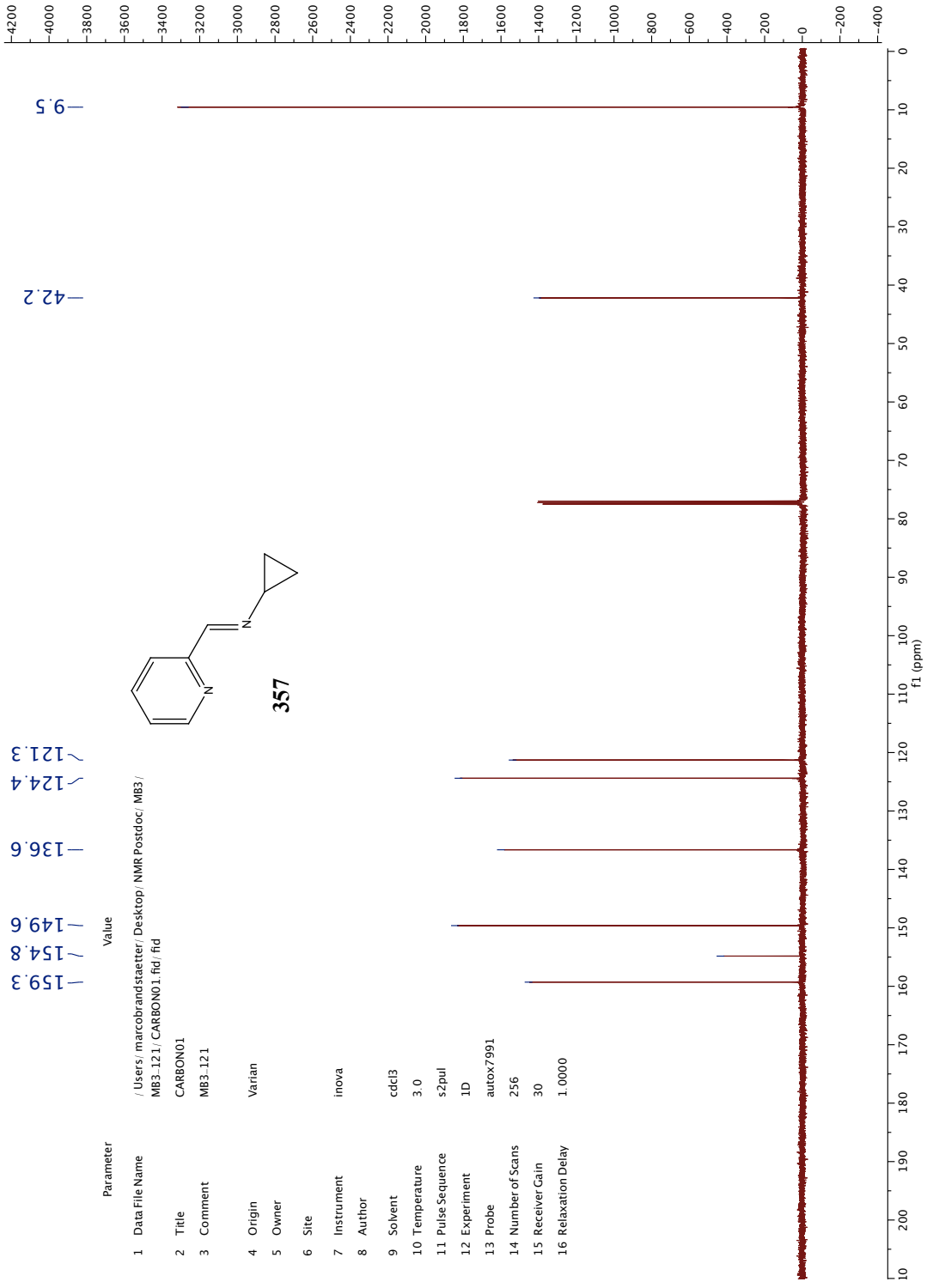

Parameter	Value
1 Data File Name	/Users/marcobrandstaetter/Desktop/NMR Postdoc/MB3/MB3_121/CARBON01.fid/fid
2 Title	CARBON01
3 Comment	MB3_121
4 Origin	Varian
5 Owner	
6 Site	
7 Instrument	inova
8 Author	
9 Solvent	cdcl3
10 Temperature	3.0
11 Pulse Sequence	s2pul
12 Experiment	1D
13 Probe	autox7991
14 Number of Scans	256
15 Receiver Gain	30
16 Relaxation Delay	1.0000

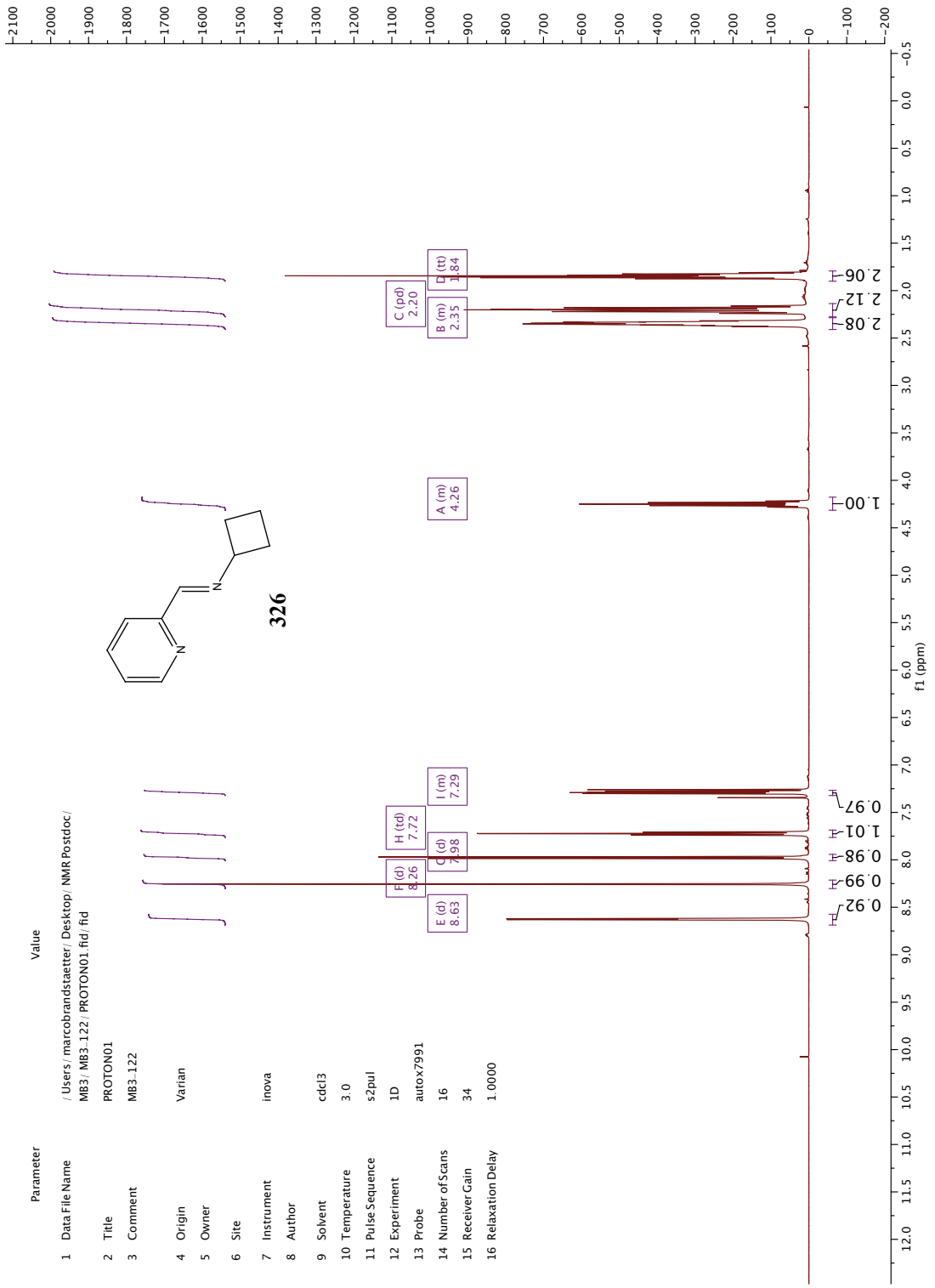
Parameter
Value
1 Data File Name
/ Users / marcobrandstaetter / Desktop / NMR Postdoc / MB3 / MB3_122 / PROTON01.fid / fid
2 Title
PROTON01
3 Comment
MB3_122
4 Origin
Varian
5 Owner
6 Site
7 Instrument
inova
8 Author
9 Solvent
cdcl3
10 Temperature
3.0
11 Pulse Sequence
s2pul
12 Experiment
1D
13 Probe
autox7991
14 Number of Scans
16
15 Receiver Gain
34
16 Relaxation Delay
1.0000
326
A (m) 4.26
B (m) 2.35
C (pd) 2.20
D (tt) 1.84
E (d) 8.63
F (d) 8.26
G (d) 7.98
H (td) 7.72
I (m) 7.29
2.06
2.12
2.08
1.00
0.97
1.01
0.98
0.99
0.92
f1 (ppm)

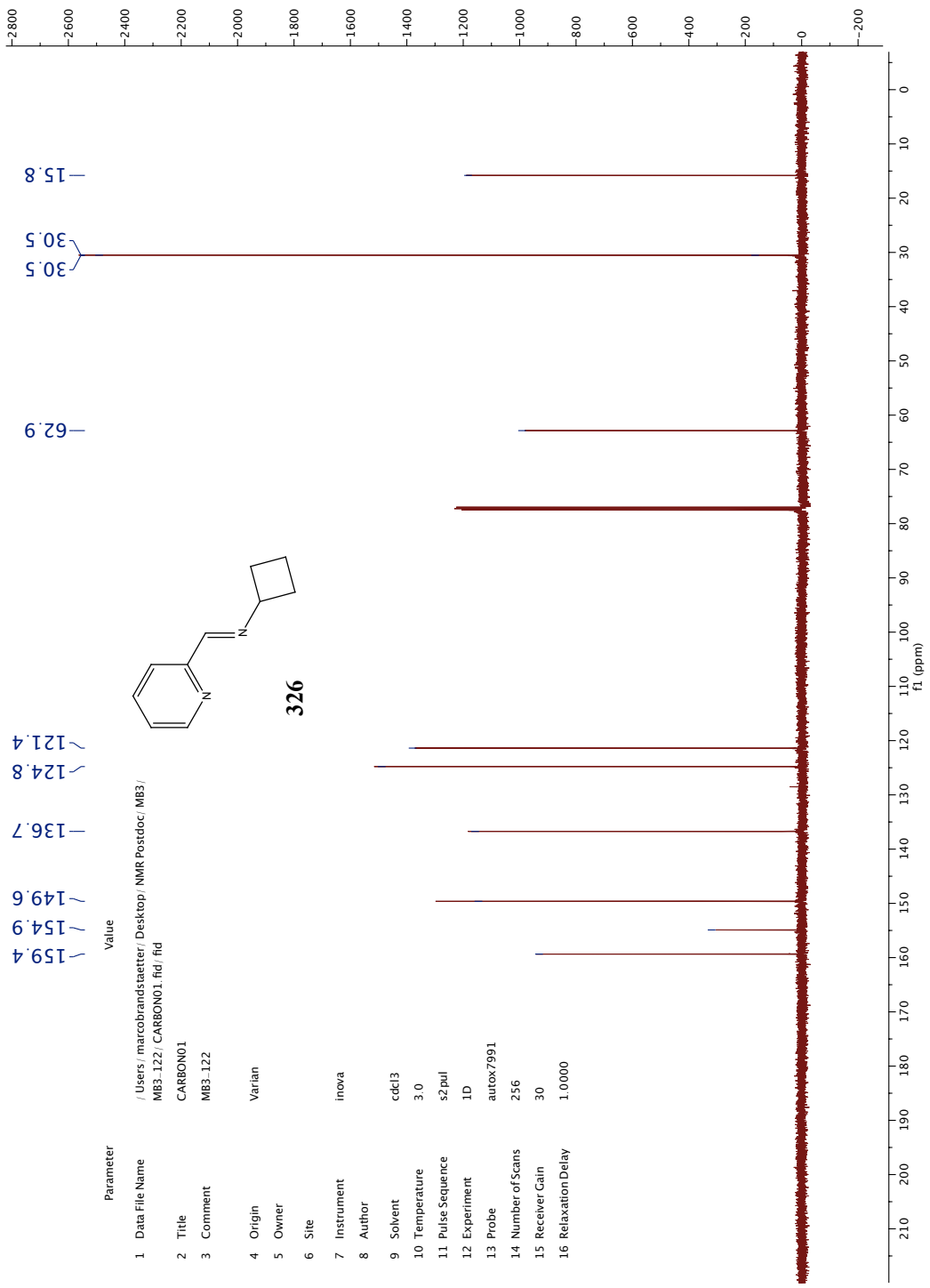
15.8
30.5
30.5
62.9
121.4
124.8
136.7
149.6
154.9
159.4
326
f1 (ppm)
Parameter
Value
1 Data File Name
/ Users / marcobrandstaetter / Desktop / NMR Postdoc / MB3 / MB3_122 / CARBON01.fid / fid
2 Title
CARBON01
3 Comment
MB3_122
4 Origin
Varian
5 Owner
6 Site
7 Instrument
inova
8 Author
9 Solvent
cdcl3
10 Temperature
3.0
11 Pulse Sequence
s2pul
12 Experiment
1D
13 Probe
autox7991
14 Number of Scans
256
15 Receiver Gain
30
16 Relaxation Delay
1.0000

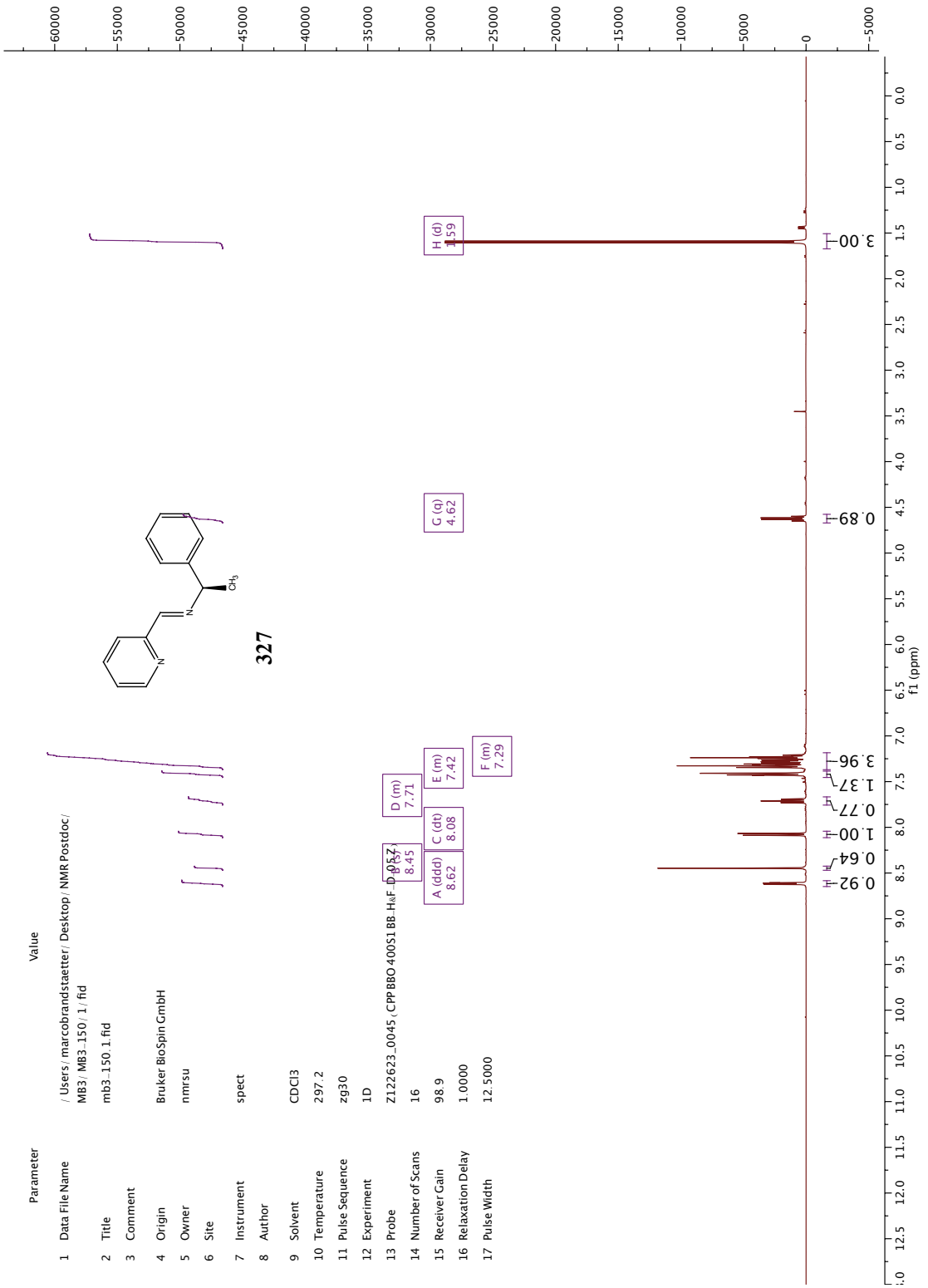
Parameter
Value
1 Data File Name / Users / marcobrandstaetter / Desktop / NMR Postdoc / MB3 / MB3_150 / 1 / fid
2 Title mb3_150_1.fid
3 Comment
4 Origin Bruker BioSpin GmbH
5 Owner nmrsu
6 Site
7 Instrument spect
8 Author
9 Solvent CDCl3
10 Temperature 297.2
11 Pulse Sequence zg30
12 Experiment 1D
13 Probe Z122623_0045_CPP BBO 400S1 BB-H&F-D-05Z
14 Number of Scans 16
15 Receiver Gain 98.9
16 Relaxation Delay 1.0000
17 Pulse Width 12.5000
A (ddd) 8.62
B (s) 8.45
C (dt) 8.08
D (m) 7.71
E (m) 7.42
F (m) 7.29
G (q) 4.62
H (d) 1.59
327
3.00
0.89
3.96
1.37
0.77
1.00
0.64
0.92
f1 (ppm)

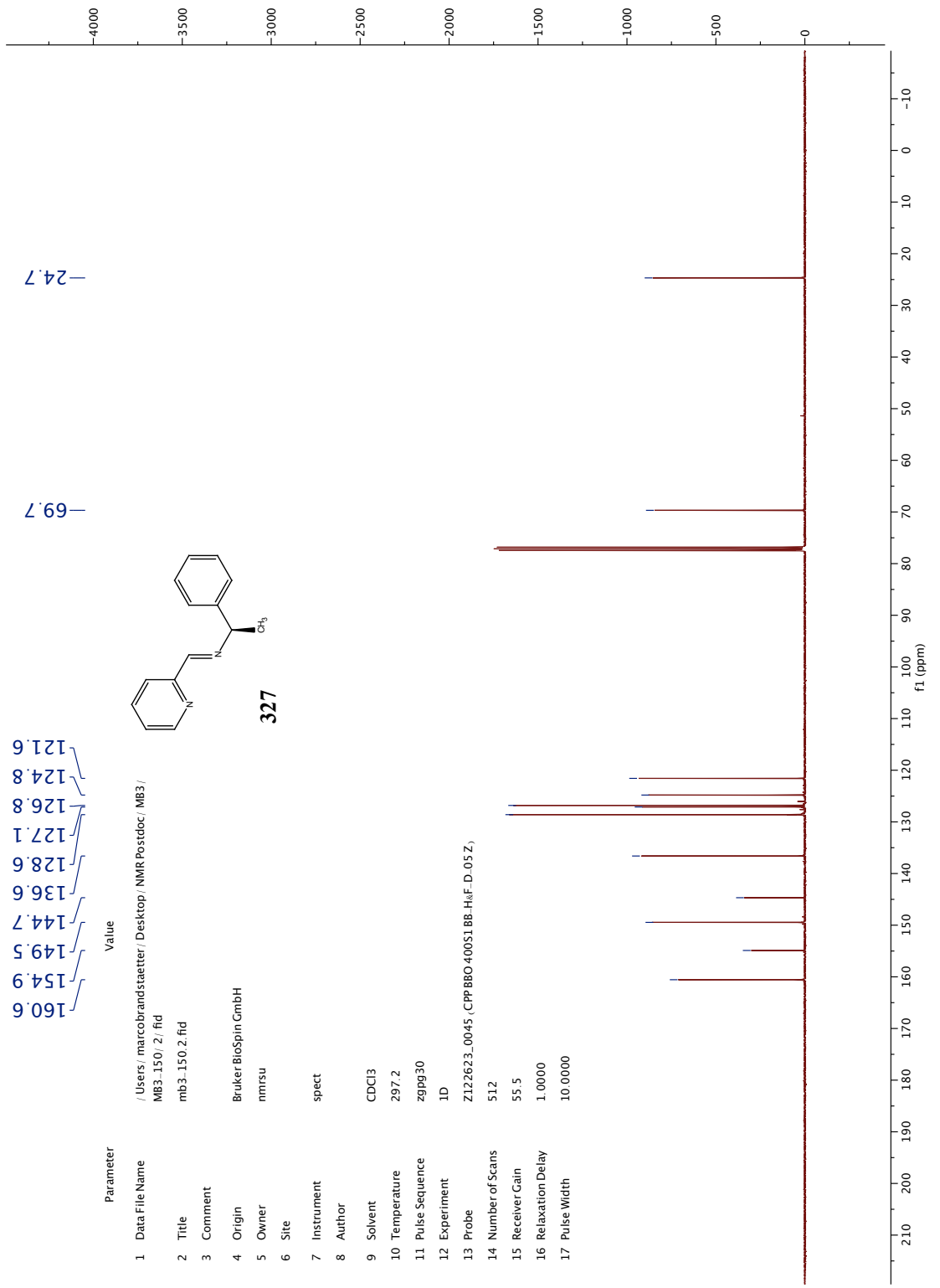

	Parameter	Value
1	Data File Name	/Users/marcobrandstaetter/Desktop/NMR Postdoc/MB3/MB3_150/2/fid
2	Title	mb3_150_2.fid
3	Comment	
4	Origin	Bruker BioSpin GmbH
5	Owner	nmrsu
6	Site	
7	Instrument	spect
8	Author	
9	Solvent	CDCl3
10	Temperature	297.2
11	Pulse Sequence	zgpg30
12	Experiment	1D
13	Probe	Z122623_0045 (CPP BBO 400S1 BB-H&F-D-05 Z)
14	Number of Scans	512
15	Receiver Gain	55.5
16	Relaxation Delay	1.0000
17	Pulse Width	10.0000

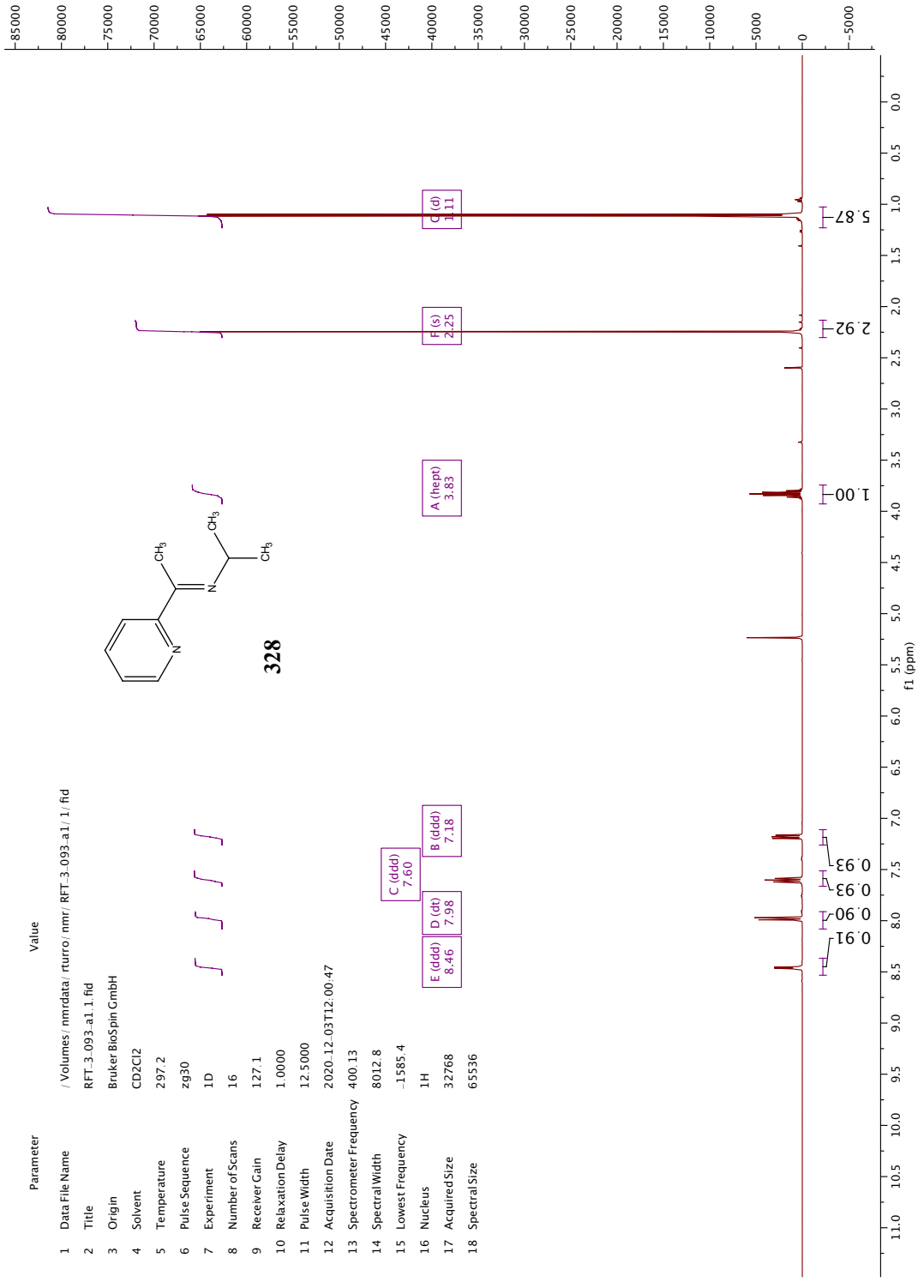
Parameter
Value
1 Data File Name / Volumes/ nmrdata/ rturro/ nmr/ RFT_3_093_a1/ 1/ fid
2 Title RFT_3_093_a1_1.fid
3 Origin Bruker BioSpin GmbH
4 Solvent CD2Cl2
5 Temperature 297.2
6 Pulse Sequence zg30
7 Experiment 1D
8 Number of Scans 16
9 Receiver Gain 127.1
10 Relaxation Delay 1.0000
11 Pulse Width 12.5000
12 Acquisition Date 2020-12-03T12:00:47
13 Spectrometer Frequency 400.13
14 Spectral Width 8012.8
15 Lowest Frequency -1585.4
16 Nucleus 1H
17 Acquired Size 32768
18 Spectral Size 65536
328
A (hept) 3.83
B (ddd) 7.18
C (ddd) 7.60
D (dt) 7.98
E (ddd) 8.46
F (s) 2.25
G (d) 1.11
5.87
2.92
1.00
0.93
0.93
0.90
0.91
f1 (ppm)

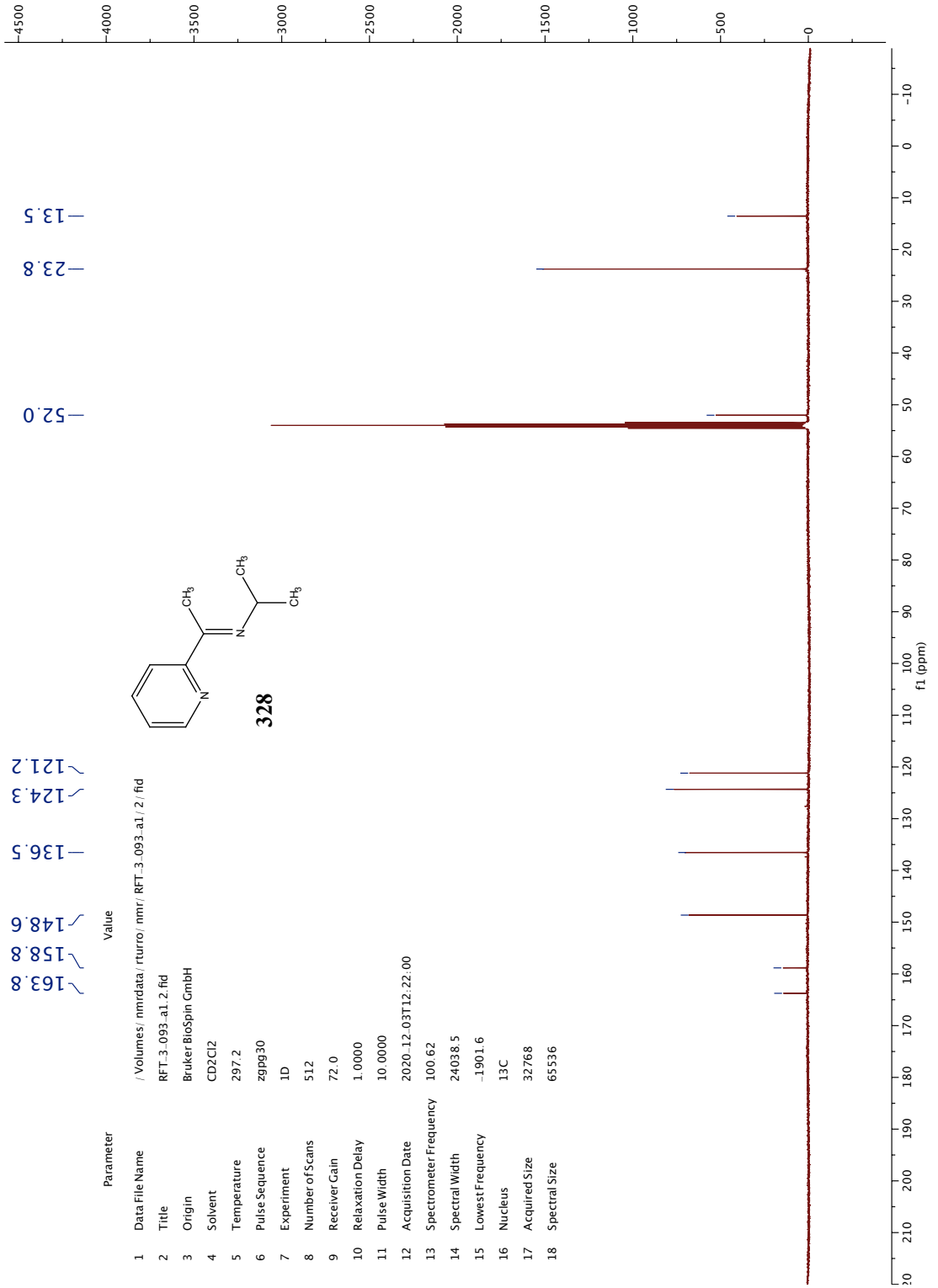

	Parameter	Value
1	Data File Name	/Volumes/nmrdata/rturro/nmr/RFT_3_093_a1/2/fid
2	Title	RFT_3_093_a1_2.fid
3	Origin	Bruker BioSpin GmbH
4	Solvent	CD2Cl2
5	Temperature	297.2
6	Pulse Sequence	zgpg30
7	Experiment	1D
8	Number of Scans	512
9	Receiver Gain	72.0
10	Relaxation Delay	1.0000
11	Pulse Width	10.0000
12	Acquisition Date	2020_12_03T12_22_00
13	Spectrometer Frequency	100.62
14	Spectral Width	24038.5
15	Lowest Frequency	-1901.6
16	Nucleus	13C
17	Acquired Size	32768
18	Spectral Size	65536

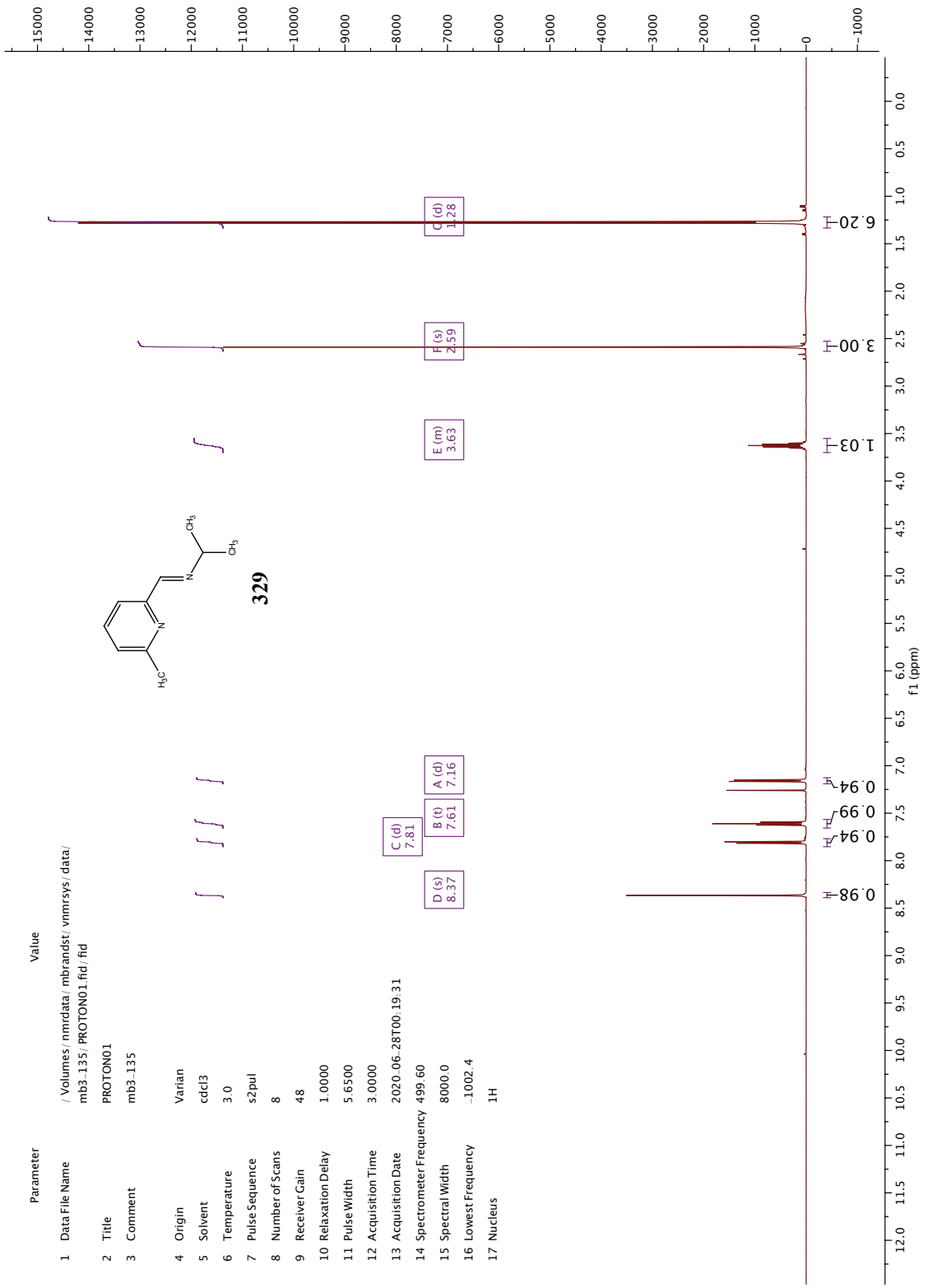
Parameter
Value
1 Data File Name / Volumes/ nmrdata/ mbrandst/ vnmrsys/ data/ mb3_135/ PROTON01.fid/ fid
2 Title PROTON01
3 Comment mb3_135
4 Origin Varian
5 Solvent cdcl3
6 Temperature 3.0
7 Pulse Sequence s2pul
8 Number of Scans 8
9 Receiver Gain 48
10 Relaxation Delay 1.0000
11 Pulse Width 5.6500
12 Acquisition Time 3.0000
13 Acquisition Date 2020_06_28T00:19:31
14 Spectrometer Frequency 499.60
15 Spectral Width 8000.0
16 Lowest Frequency -1002.4
17 Nucleus 1H
329
D (s) 8.37
C (d) 7.81
B (t) 7.61
A (d) 7.16
E (m) 3.63
F (s) 2.59
C (d) 1.28
6.20
3.00
1.03
0.98
0.94
0.99
0.94
f1 (ppm)

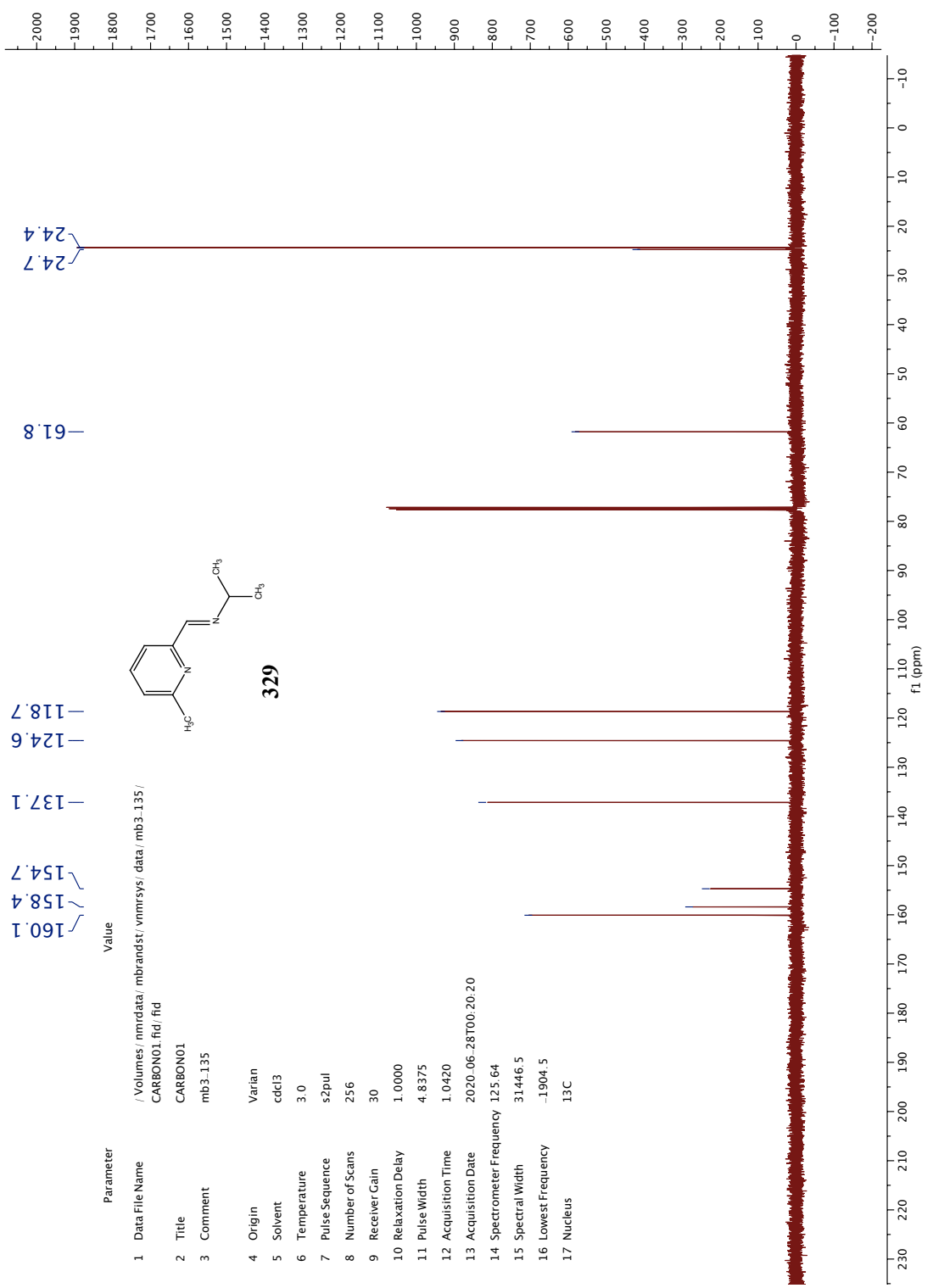

	Parameter	Value
1	Data File Name	/Volumes/nmrdata/mbrandst/vnmrsys/data/mb3-135/CARBON01.fid/fid
2	Title	CARBON01
3	Comment	mb3-135
4	Origin	Varian
5	Solvent	cdcl3
6	Temperature	3.0
7	Pulse Sequence	s2pul
8	Number of Scans	256
9	Receiver Gain	30
10	Relaxation Delay	1.0000
11	Pulse Width	4.8375
12	Acquisition Time	1.0420
13	Acquisition Date	2020-06-28T00:20:20
14	Spectrometer Frequency	125.64
15	Spectral Width	31446.5
16	Lowest Frequency	-1904.5
17	Nucleus	13C

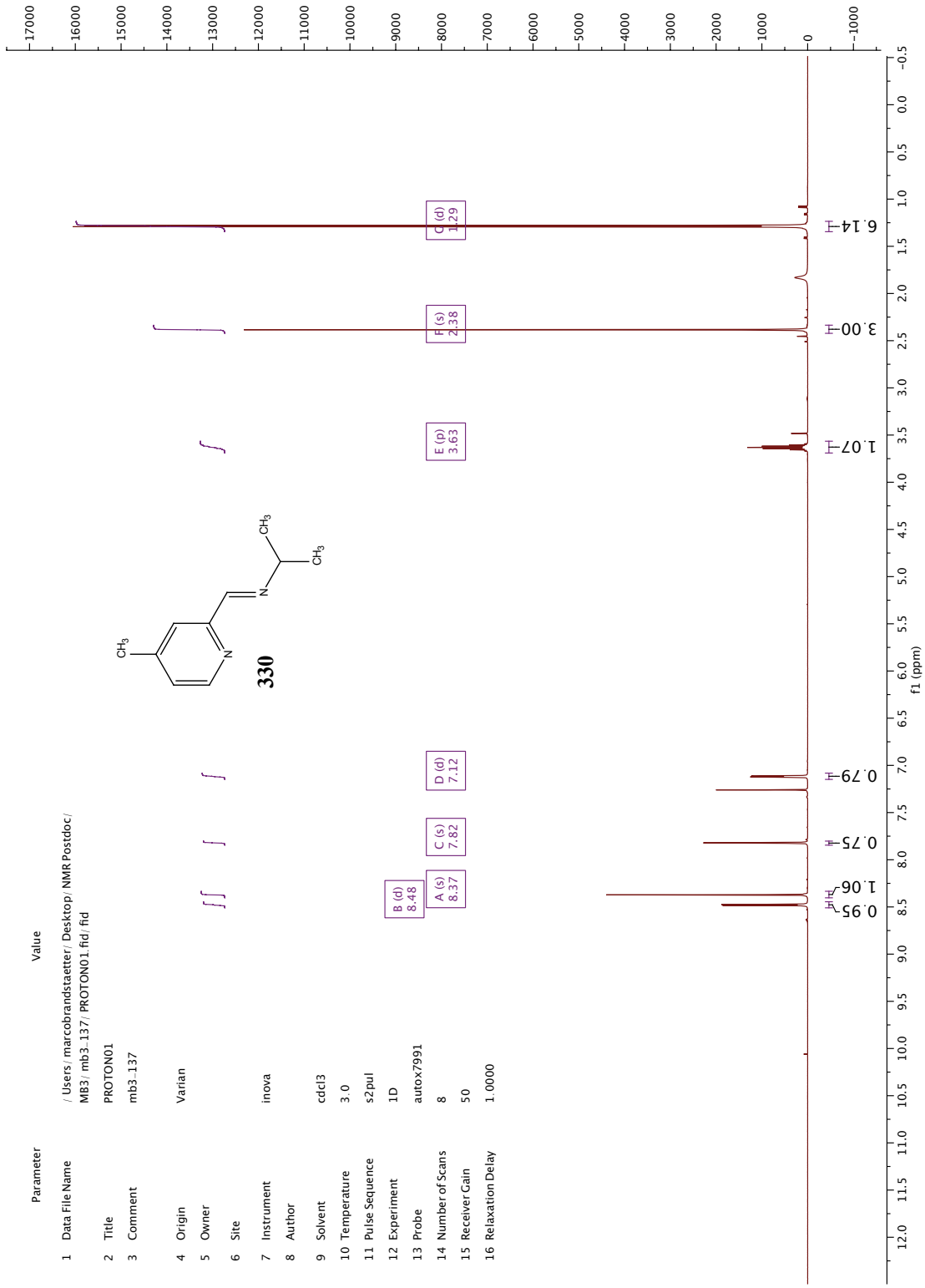
Parameter
Value
1 Data File Name
/ Users/ marcobrandstaetter/ Desktop/ NMR Postdoc/ MB3/ mb3_137/ PROTON01.fid/ fid
2 Title
PROTON01
3 Comment
mb3_137
4 Origin
Varian
5 Owner
6 Site
7 Instrument
inova
8 Author
9 Solvent
cdcl3
10 Temperature
3 0
11 Pulse Sequence
s2pul
12 Experiment
1D
13 Probe
autox7991
14 Number of Scans
8
15 Receiver Gain
50
16 Relaxation Delay
1 0000
330
A (s) 8.37
B (d) 8.48
C (s) 7.82
D (d) 7.12
E (p) 3.63
F (s) 2.38
G (d) 1.29
6.14
3.00
1.07
0.79
0.75
1.06
0.95
f1 (ppm)

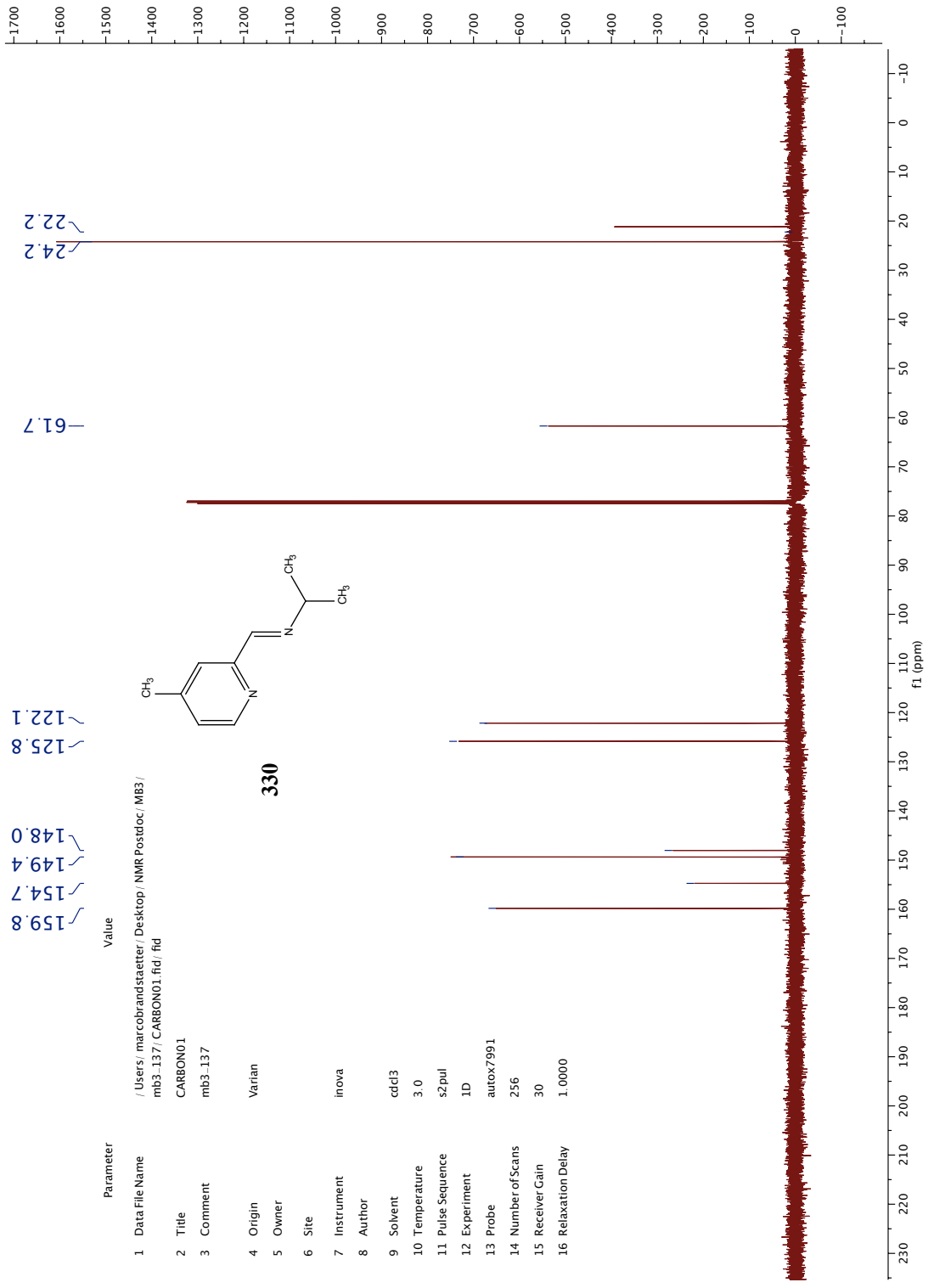

Parameter	Value
1 Data File Name	/Users/marcobrandstaetter/Desktop/NMR Postdoc/MB3/mb3-137/CARBON01.fid/fid
2 Title	CARBON01
3 Comment	mb3-137
4 Origin	Varian
5 Owner	
6 Site	
7 Instrument	inova
8 Author	
9 Solvent	cdcl3
10 Temperature	3.0
11 Pulse Sequence	s2pul
12 Experiment	1D
13 Probe	autox7991
14 Number of Scans	256
15 Receiver Gain	30
16 Relaxation Delay	1.0000

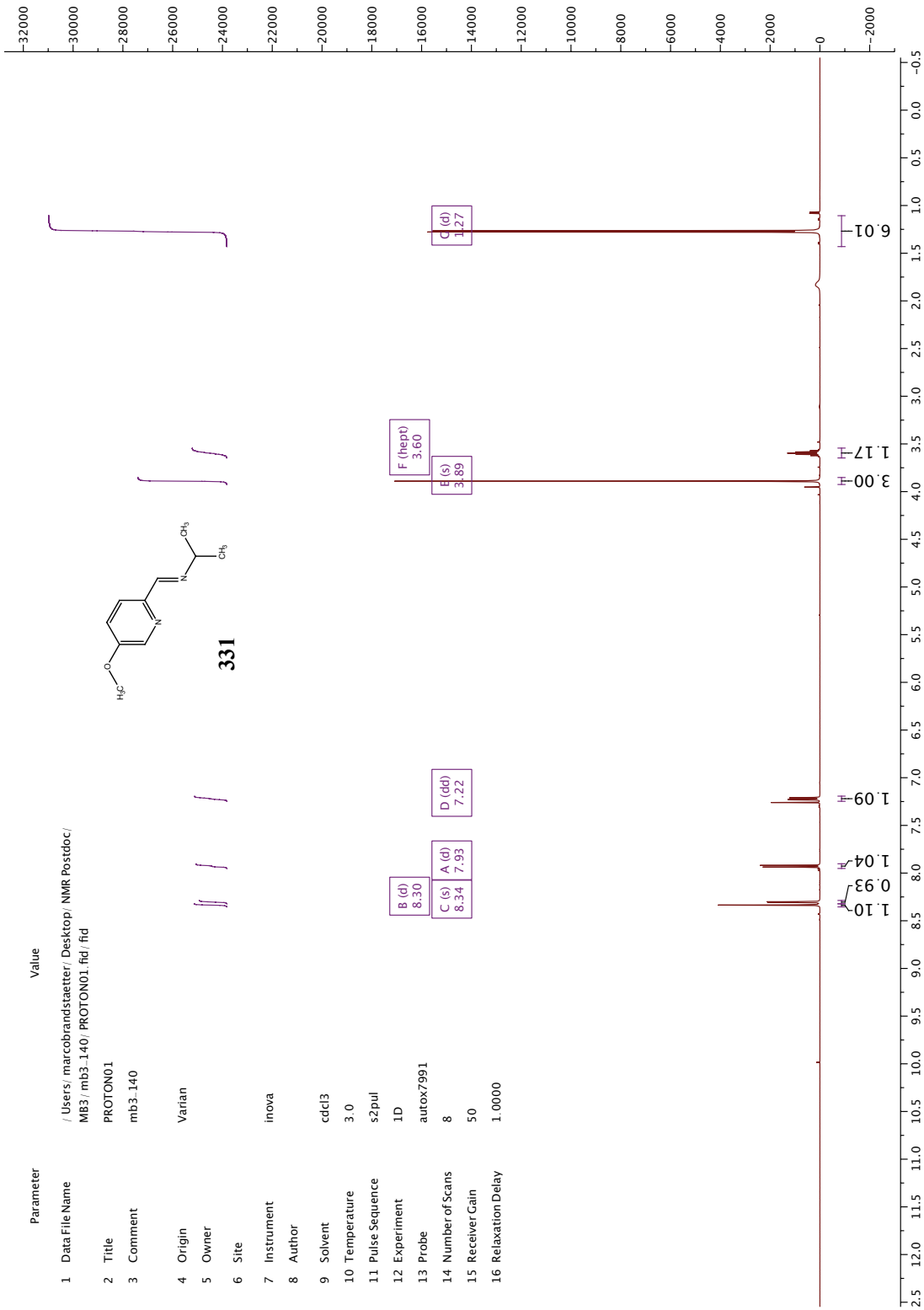
Parameter
Value
1 Data File Name / Users/ marcobrandstaetter/ Desktop/ NMR Postdoc/ MB3/ mb3_140/ PROTON01 fid/ fid
2 Title PROTON01
3 Comment mb3_140
4 Origin Varian
5 Owner
6 Site
7 Instrument inova
8 Author
9 Solvent cdcl3
10 Temperature 3.0
11 Pulse Sequence s2pul
12 Experiment 1D
13 Probe autox7991
14 Number of Scans 8
15 Receiver Gain 50
16 Relaxation Delay 1.0000
331
B (d) 8.30
C (s) 8.34
A (d) 7.93
D (dd) 7.22
F (hept) 3.60
E (s) 3.89
G (d) 1.27
6.01
1.17
3.00
1.09
1.04
0.93
1.10
f1 (ppm)

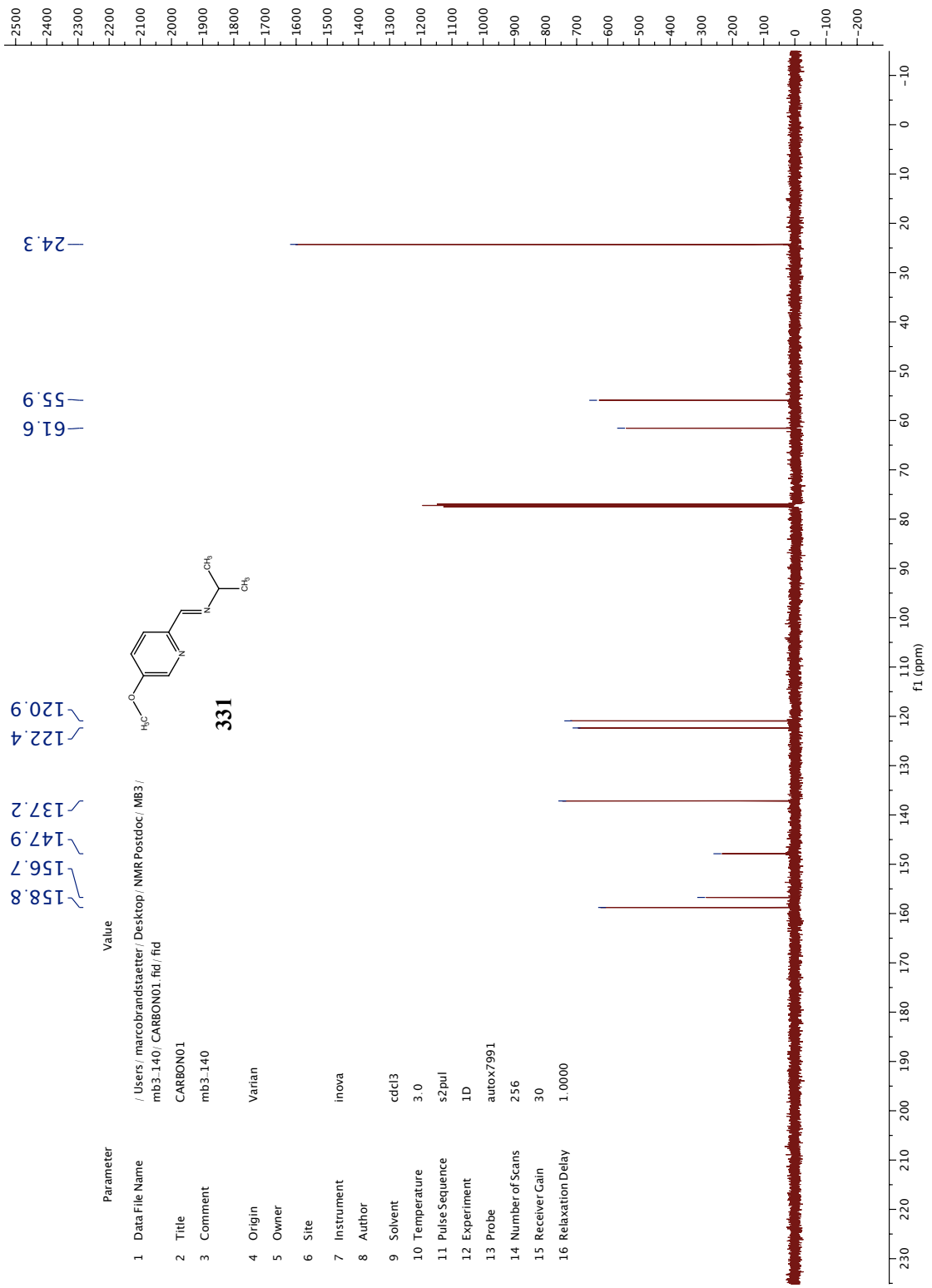

Parameter	Value
1 Data File Name	/ Users / marcobrandstaetter / Desktop / NMR Postdoc / MB3 / mb3-140 / CARBON01.fid / fid
2 Title	CARBON01
3 Comment	mb3-140
4 Origin	Varian
5 Owner	
6 Site	
7 Instrument	inova
8 Author	
9 Solvent	cdcl3
10 Temperature	3.0
11 Pulse Sequence	s2pul
12 Experiment	1D
13 Probe	autox7991
14 Number of Scans	256
15 Receiver Gain	30
16 Relaxation Delay	1.0000

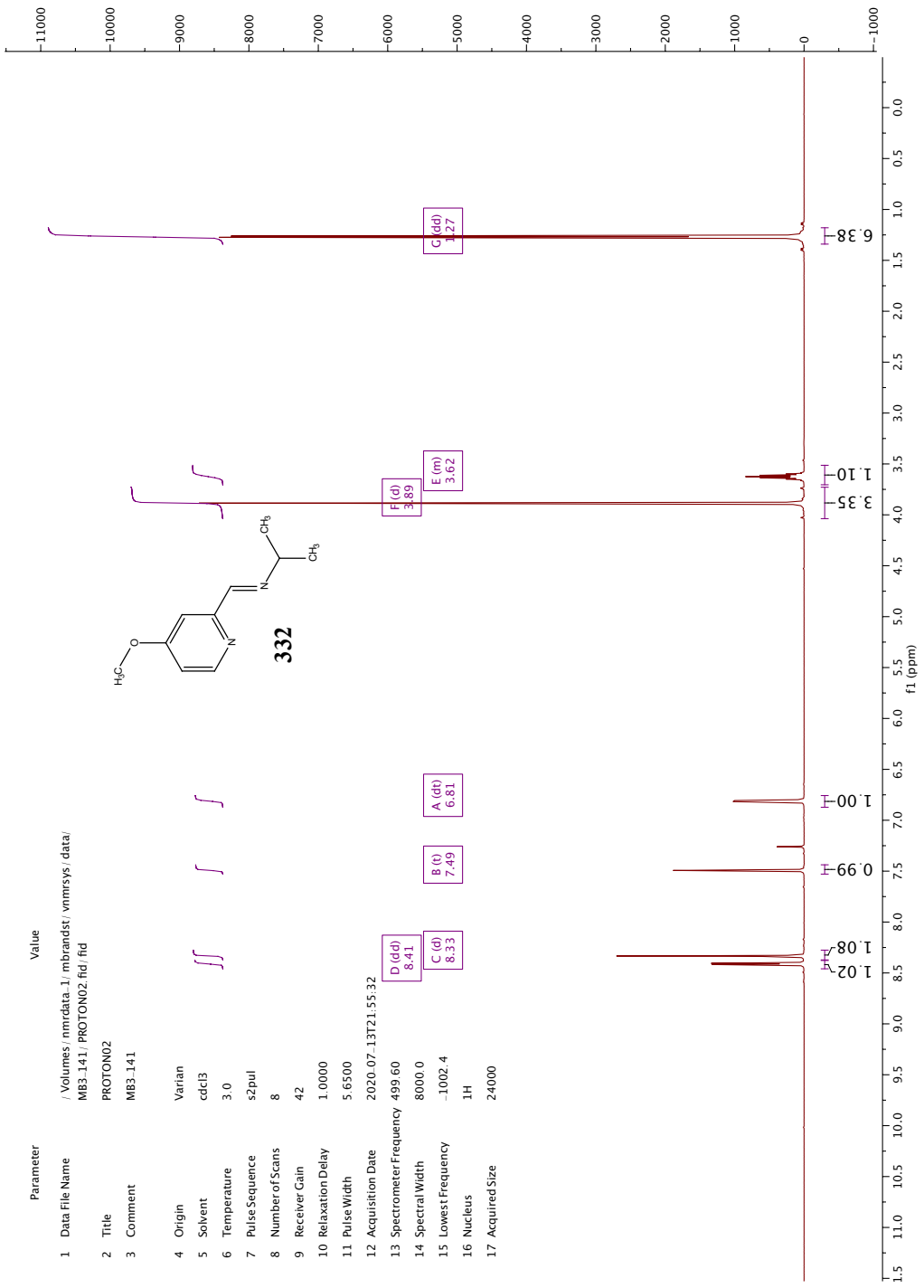
Parameter
Value
1 Data File Name / Volumes / nmrdata_1 / mbrandst / vnmrsys / data / MB3_141 / PROTON02.fid / fid
2 Title PROTON02
3 Comment MB3_141
4 Origin Varian
5 Solvent cdcl3
6 Temperature 3.0
7 Pulse Sequence s2pul
8 Number of Scans 8
9 Receiver Gain 42
10 Relaxation Delay 1.0000
11 Pulse Width 5.6500
12 Acquisition Date 2020-07-13T21:55:32
13 Spectrometer Frequency 499.60
14 Spectral Width 8000.0
15 Lowest Frequency -1002.4
16 Nucleus 1H
17 Acquired Size 24000
D (dd) 8.41
C (d) 8.33
B (t) 7.49
A (dt) 6.81
F (d) 3.89
E (m) 3.62
G (dd) 1.27
332
1.02
1.08
0.99
1.00
1.10
3.35
6.38
f1 (ppm)

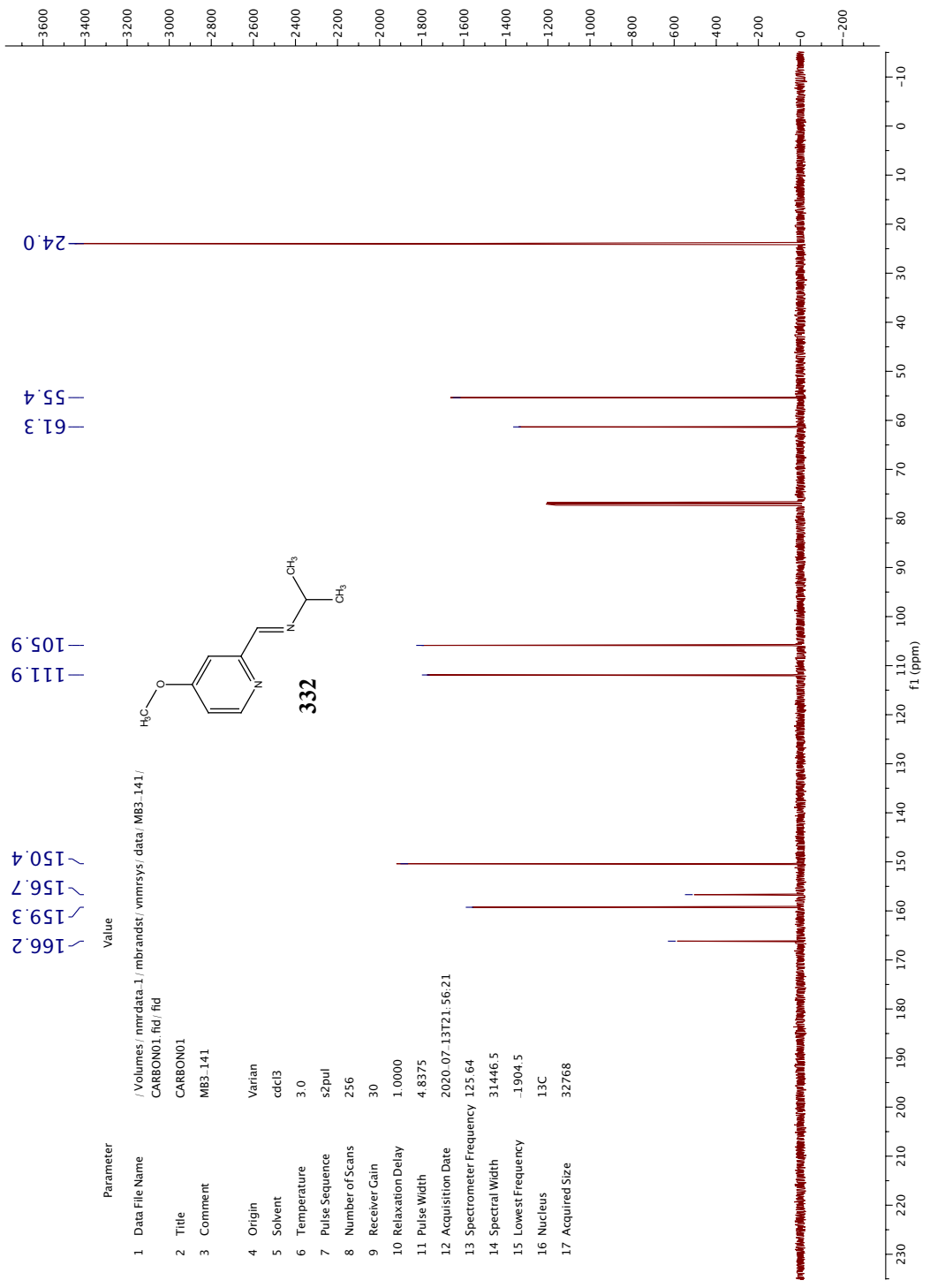

	Parameter	Value
1	Data File Name	/Volumes/nmrdata.1/mbrandst/vnmrsys/data/MB3_141/CARBON01.fid/fid
2	Title	CARBON01
3	Comment	MB3_141
4	Origin	Varian
5	Solvent	cdcl3
6	Temperature	3.0
7	Pulse Sequence	s2pul
8	Number of Scans	256
9	Receiver Gain	30
10	Relaxation Delay	1.0000
11	Pulse Width	4.8375
12	Acquisition Date	2020_07_13T21:56:21
13	Spectrometer Frequency	125.64
14	Spectral Width	31446.5
15	Lowest Frequency	-1904.5
16	Nucleus	13C
17	Acquired Size	32768

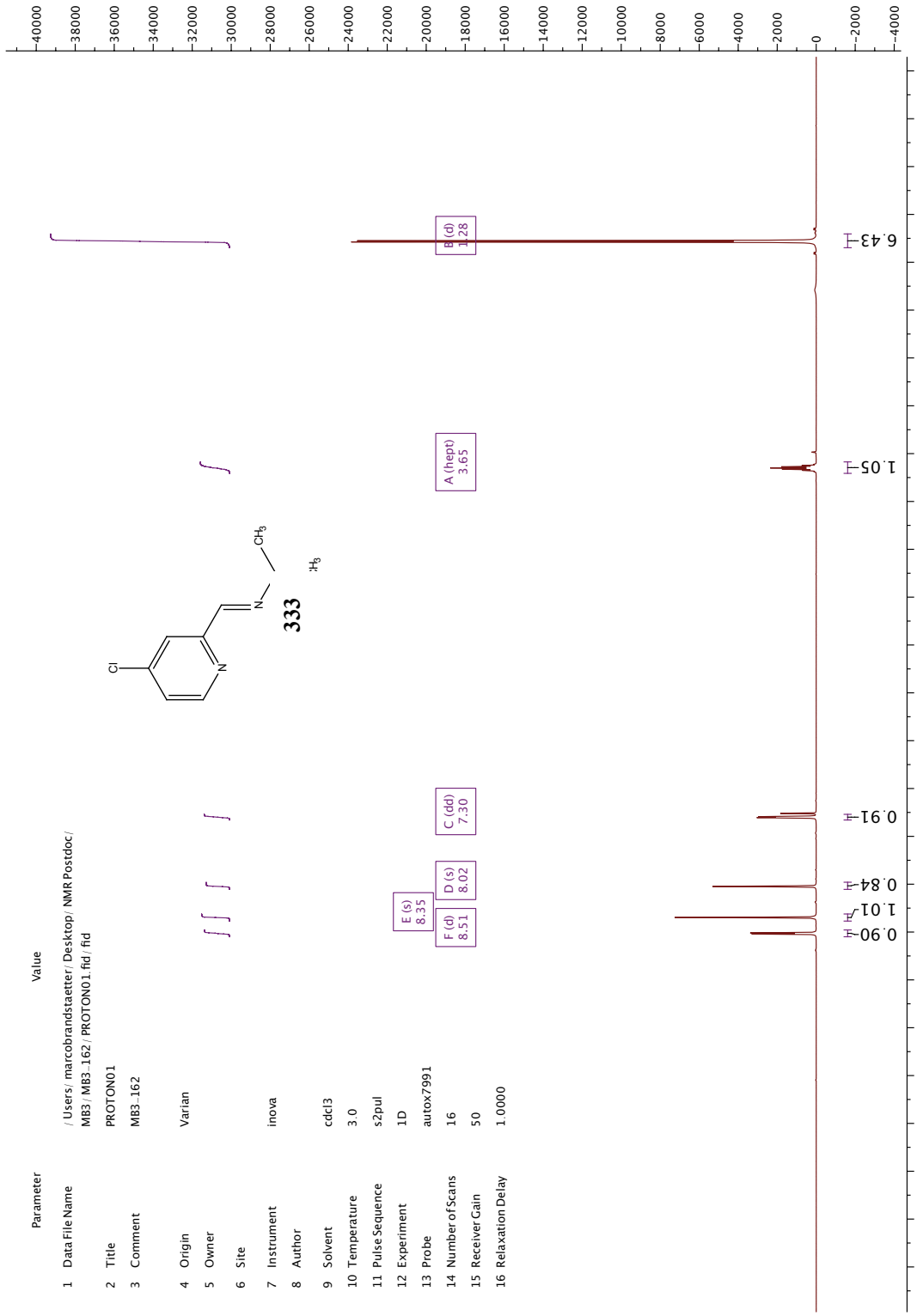
Parameter
Value
1 Data File Name
/ Users/ marcobrandstaetter/ Desktop/ NMR Postdoc/ MB3 / MB3_162 / PROTON01.fid / fid
2 Title
PROTON01
3 Comment
MB3_162
4 Origin
Varian
5 Owner
6 Site
7 Instrument
inova
8 Author
9 Solvent
cdcl3
10 Temperature
3.0
11 Pulse Sequence
s2pul
12 Experiment
1D
13 Probe
autox7991
14 Number of Scans
16
15 Receiver Gain
50
16 Relaxation Delay
1.0000
333
E (s) 8.35
F (d) 8.51
D (s) 8.02
C (dd) 7.30
A (hept) 3.65
B (d) 1.28
6.43
1.05
0.91
0.84
1.01
0.90
f1 (ppm)

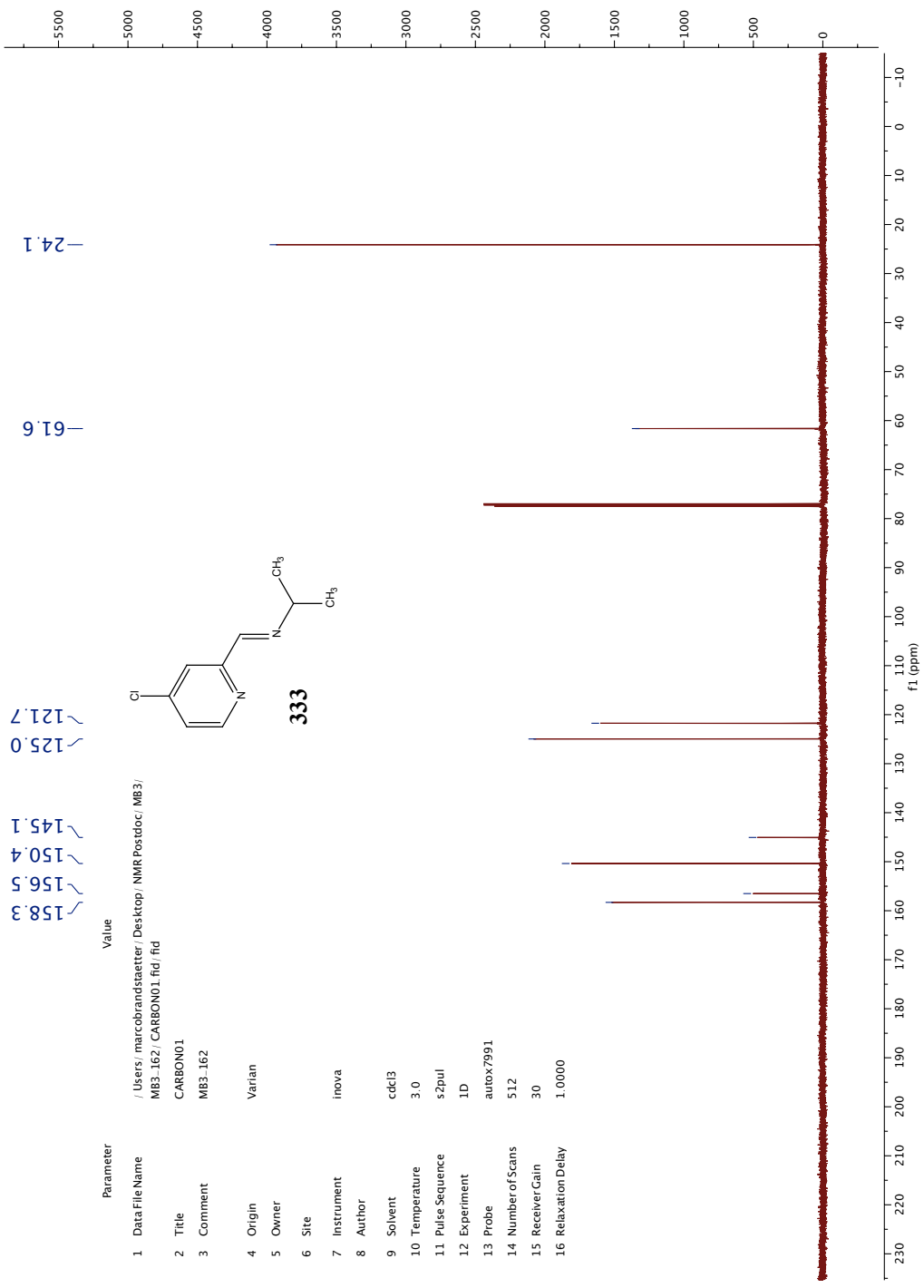

Parameter	Value
1 Data File Name	/_Users/_marcobrandstaetter/_Desktop/_NMR Postdoc/_MB3/MB3_162/_CARBON01.fid/_fid
2 Title	CARBON01
3 Comment	MB3_162
4 Origin	Varian
5 Owner	
6 Site	
7 Instrument	inova
8 Author	
9 Solvent	cdcl3
10 Temperature	3.0
11 Pulse Sequence	s2pul
12 Experiment	1D
13 Probe	autox7991
14 Number of Scans	512
15 Receiver Gain	30
16 Relaxation Delay	1.0000

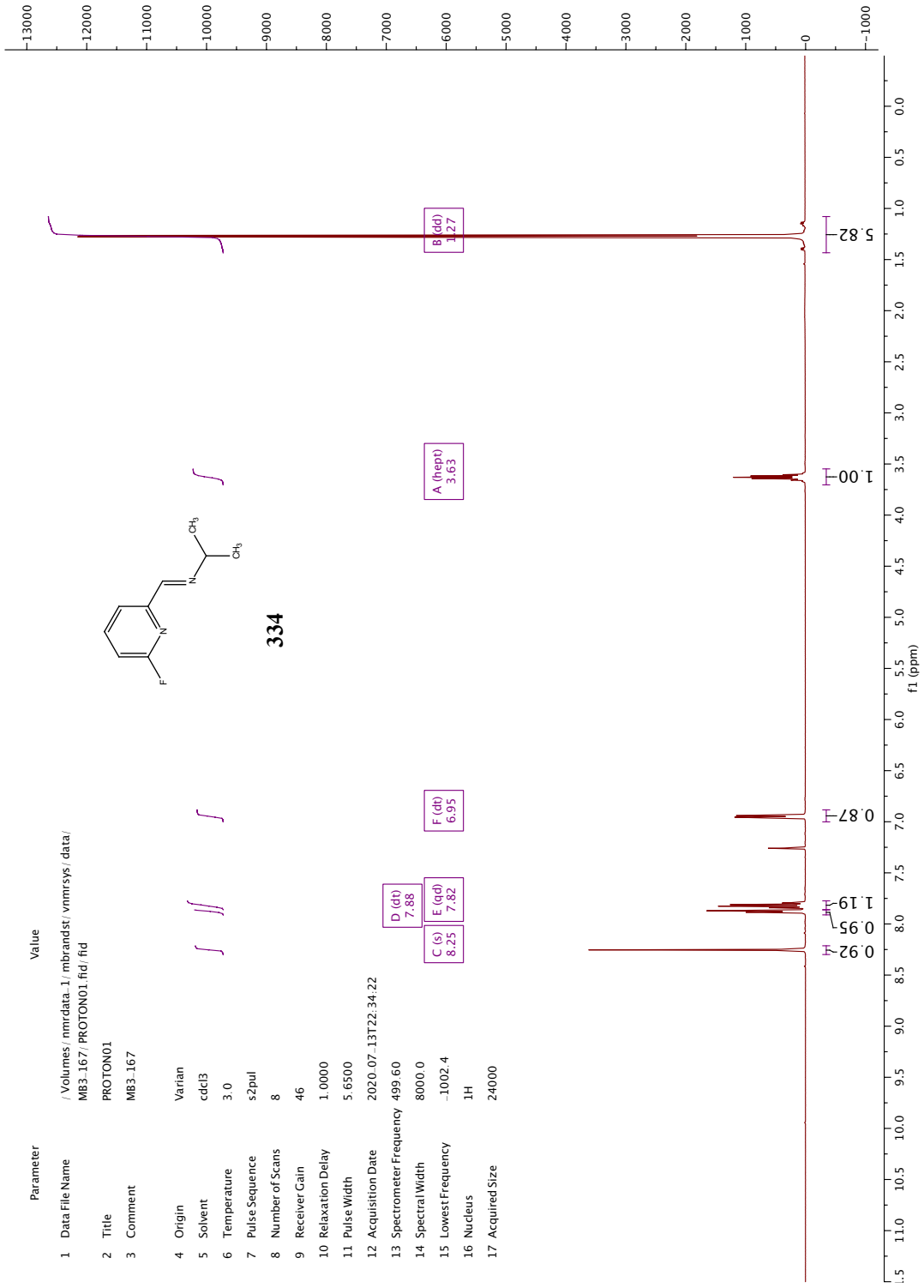
334
Parameter
Value
1 Data File Name
/ Volumes/ nmrdata_1/ mbrandst/ vnmrsys/ data/ MB3_167/ PROTON01.fid/ fid
2 Title
PROTON01
3 Comment
MB3_167
4 Origin
Varian
5 Solvent
cdcl3
6 Temperature
3.0
7 Pulse Sequence
s2pul
8 Number of Scans
8
9 Receiver Gain
46
10 Relaxation Delay
1.0000
11 Pulse Width
5.6500
12 Acquisition Date
2020_07_13T22:34:22
13 Spectrometer Frequency
499.60
14 Spectral Width
8000.0
15 Lowest Frequency
-1002.4
16 Nucleus
1H
17 Acquired Size
24000
A (hept) 3.63
B (dd) 1.27
C (s) 8.25
D (dt) 7.88
E (qd) 7.82
F (dt) 6.95
5.82
1.00
0.87
1.19
0.95
0.92
f1 (ppm)

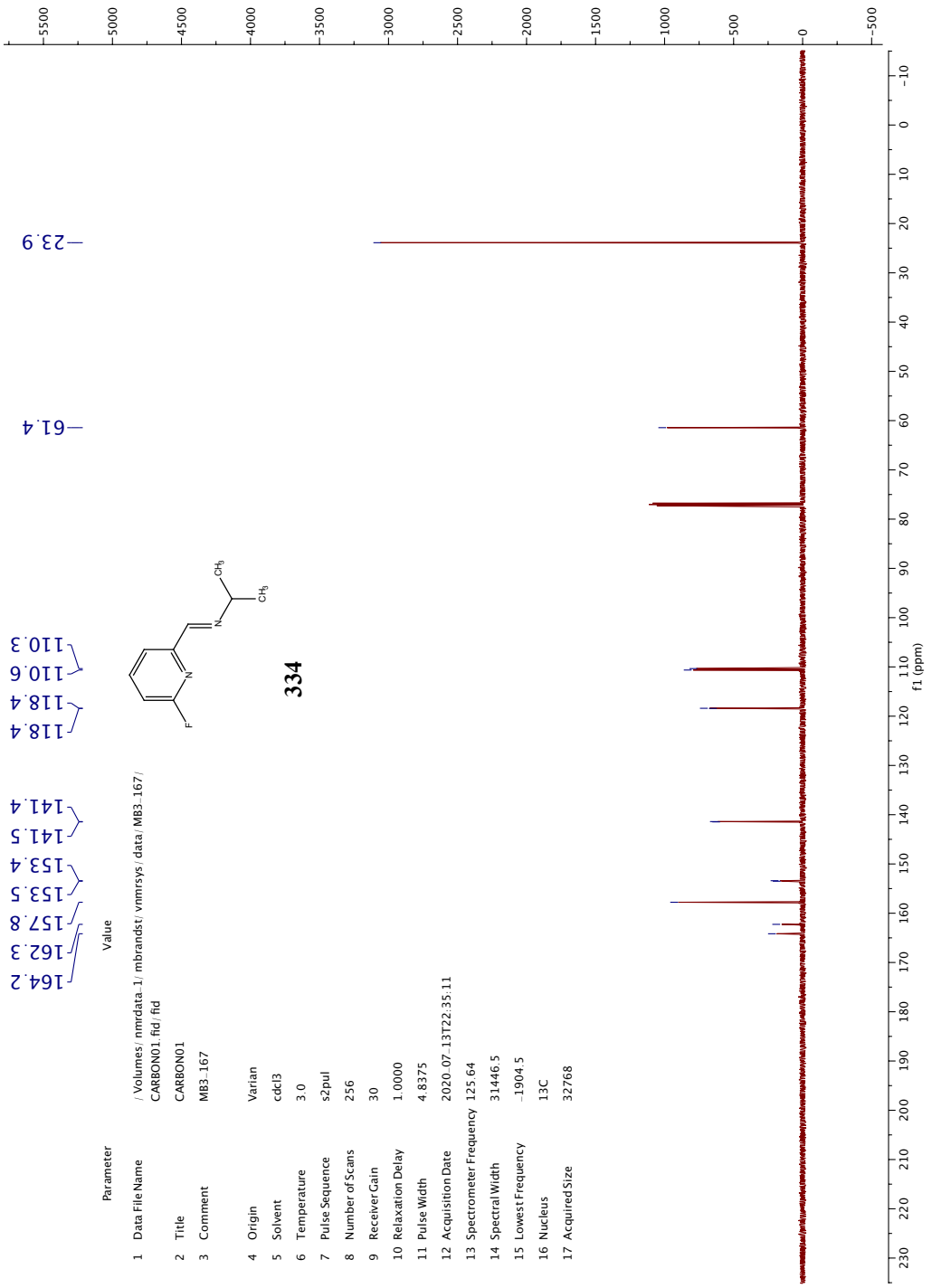

	Parameter	Value
1	Data File Name	/Volumes/nmrdata_1/mbrandst/vnmrsys/data/MB3_167/CARBON01.fid/fid
2	Title	CARBON01
3	Comment	MB3_167
4	Origin	Varian
5	Solvent	cdcl3
6	Temperature	3.0
7	Pulse Sequence	s2pul
8	Number of Scans	256
9	Receiver Gain	30
10	Relaxation Delay	1.0000
11	Pulse Width	4.8375
12	Acquisition Date	2020_07_13T22:35:11
13	Spectrometer Frequency	125.64
14	Spectral Width	31446.5
15	Lowest Frequency	-1904.5
16	Nucleus	13C
17	Acquired Size	32768

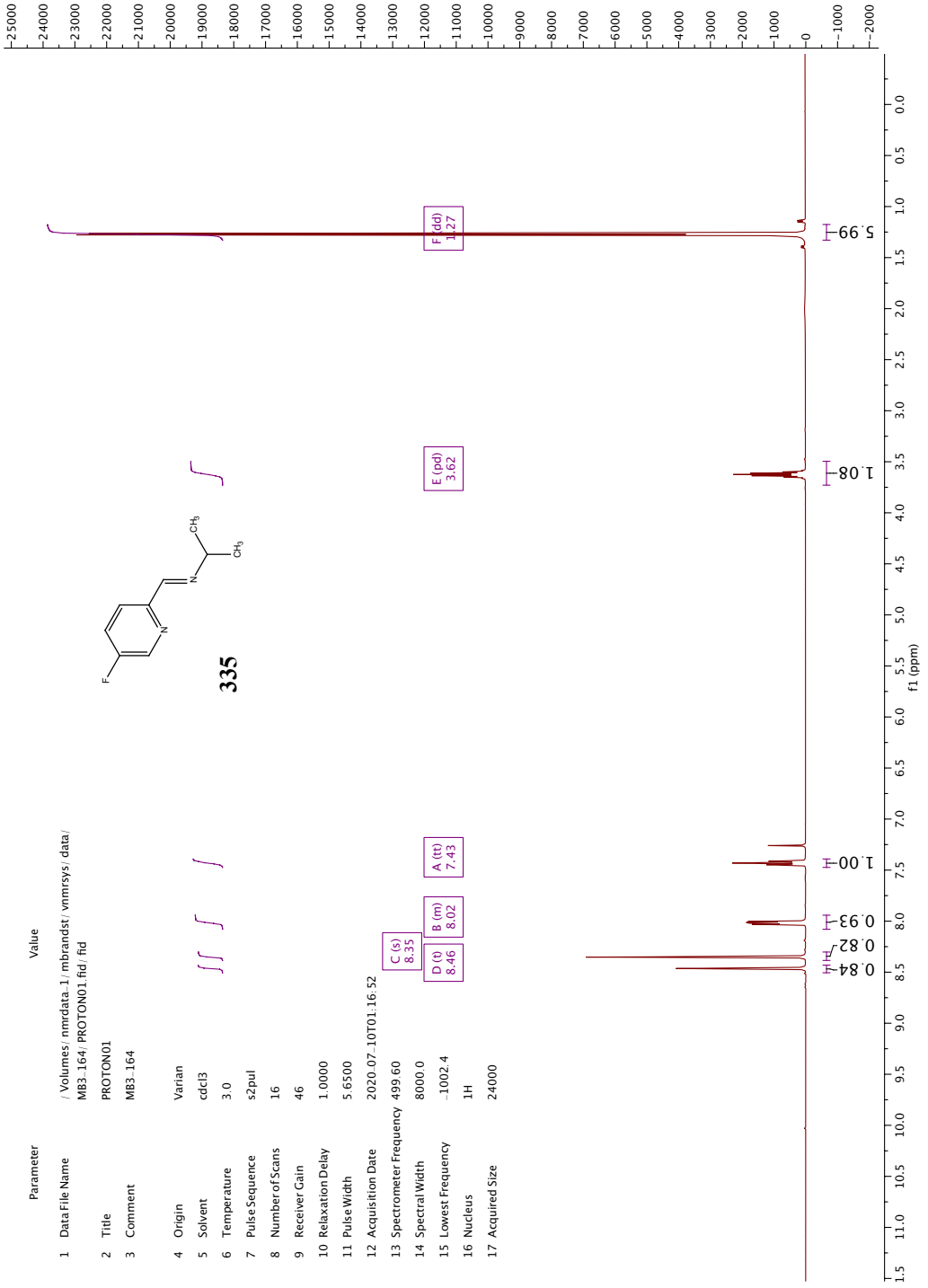
Parameter
Value
1 Data File Name
/ Volumes/ nmrdata_1/ mbrandst/ vnmrsys/ data/ MB3_164/ PROTON01.fid/ fid
2 Title
PROTON01
3 Comment
MB3_164
4 Origin
Varian
5 Solvent
cdcl3
6 Temperature
3.0
7 Pulse Sequence
s2pul
8 Number of Scans
16
9 Receiver Gain
46
10 Relaxation Delay
1.0000
11 Pulse Width
5.6500
12 Acquisition Date
2020-07-10T01:16:52
13 Spectrometer Frequency
499.60
14 Spectral Width
8000.0
15 Lowest Frequency
-1002.4
16 Nucleus
1H
17 Acquired Size
24000
335
C (s) 8.35
D (t) 8.46
B (m) 8.02
A (tt) 7.43
E (pd) 3.62
F (dd) 1.27
5.99
1.08
1.00
0.93
0.82
0.84
f1 (ppm)

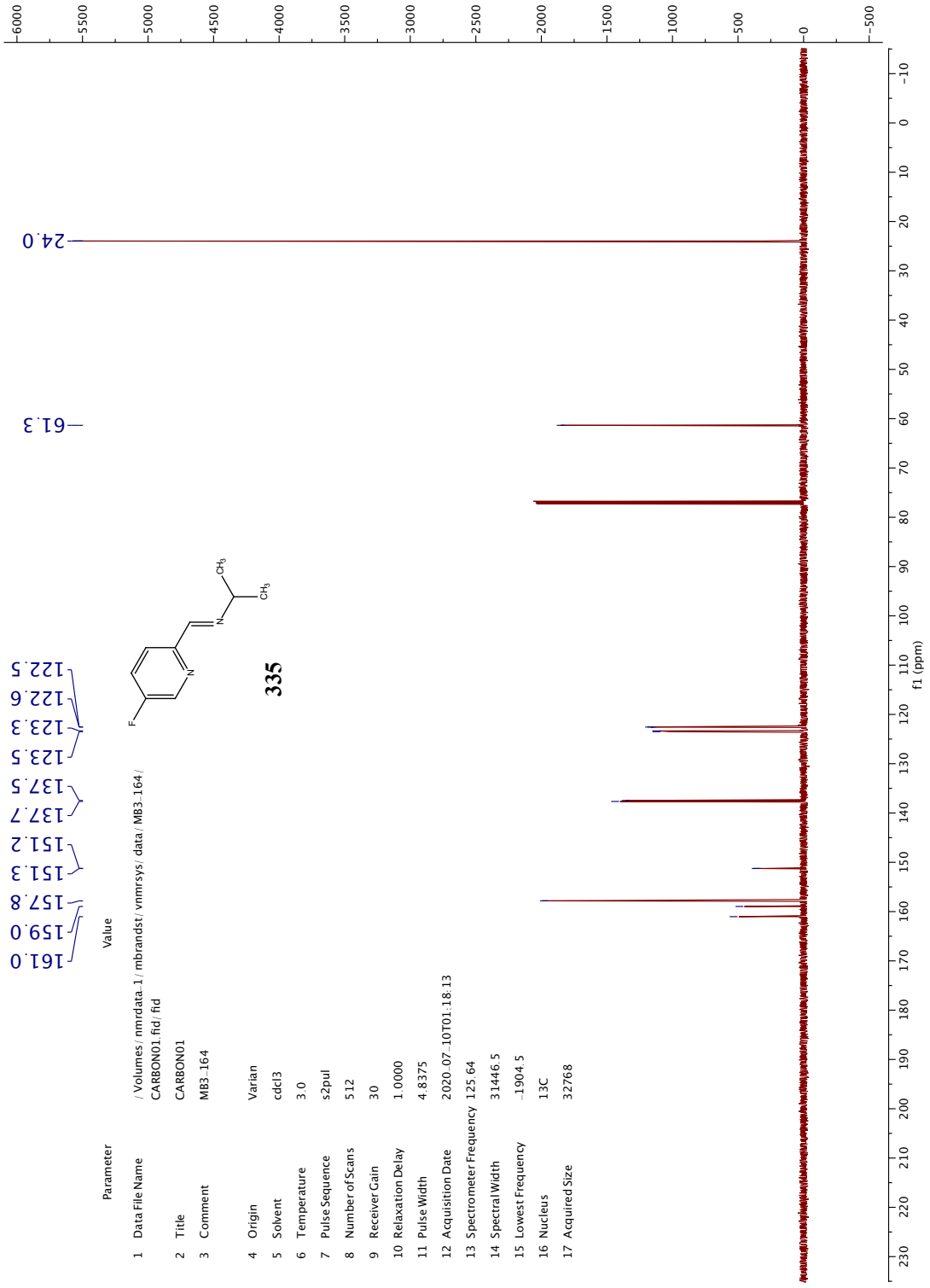

	Parameter	Value
1	Data File Name	/Volumes/nmrdata_1/mbrandst/vnmrsys/data/MB3_164/CARBON01.fid/fid
2	Title	CARBON01
3	Comment	MB3_164
4	Origin	Varian
5	Solvent	cdcl3
6	Temperature	3.0
7	Pulse Sequence	s2pul
8	Number of Scans	512
9	Receiver Gain	30
10	Relaxation Delay	1.0000
11	Pulse Width	4.8375
12	Acquisition Date	2020_07_10T01:18:13
13	Spectrometer Frequency	125.64
14	Spectral Width	31446.5
15	Lowest Frequency	-1904.5
16	Nucleus	13C
17	Acquired Size	32768

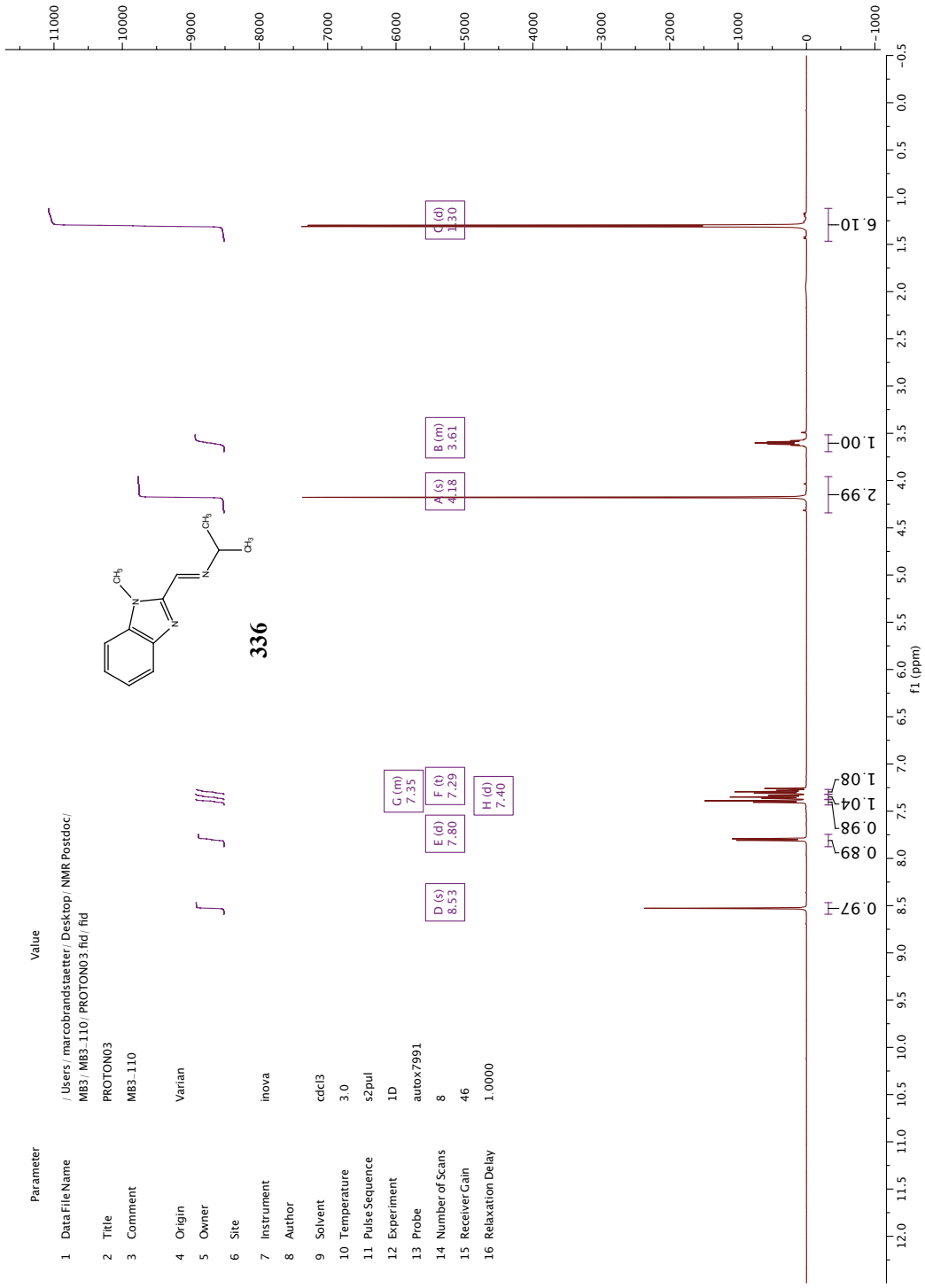
Parameter
Value
1 DataFileName
/ Users / marcobrandstaetter / Desktop / NMR Postdoc / MB3 / MB3_110 / PROTON03.fid / fid
2 Title
PROTON03
3 Comment
MB3_110
4 Origin
Varian
5 Owner
6 Site
7 Instrument
inova
8 Author
9 Solvent
cdcl3
10 Temperature
3 0
11 PulseSequence
s2pul
12 Experiment
1D
13 Probe
autox7991
14 Number of Scans
8
15 ReceiverGain
46
16 RelaxationDelay
1.0000
D (s) 8.53
E (d) 7.80
F (t) 7.29
G (m) 7.35
H (d) 7.40
A (s) 4.18
B (m) 3.61
C (d) 1.30
6.10
1.00
2.99
0.97
0.89
0.98
1.04
1.08
336
f1 (ppm)

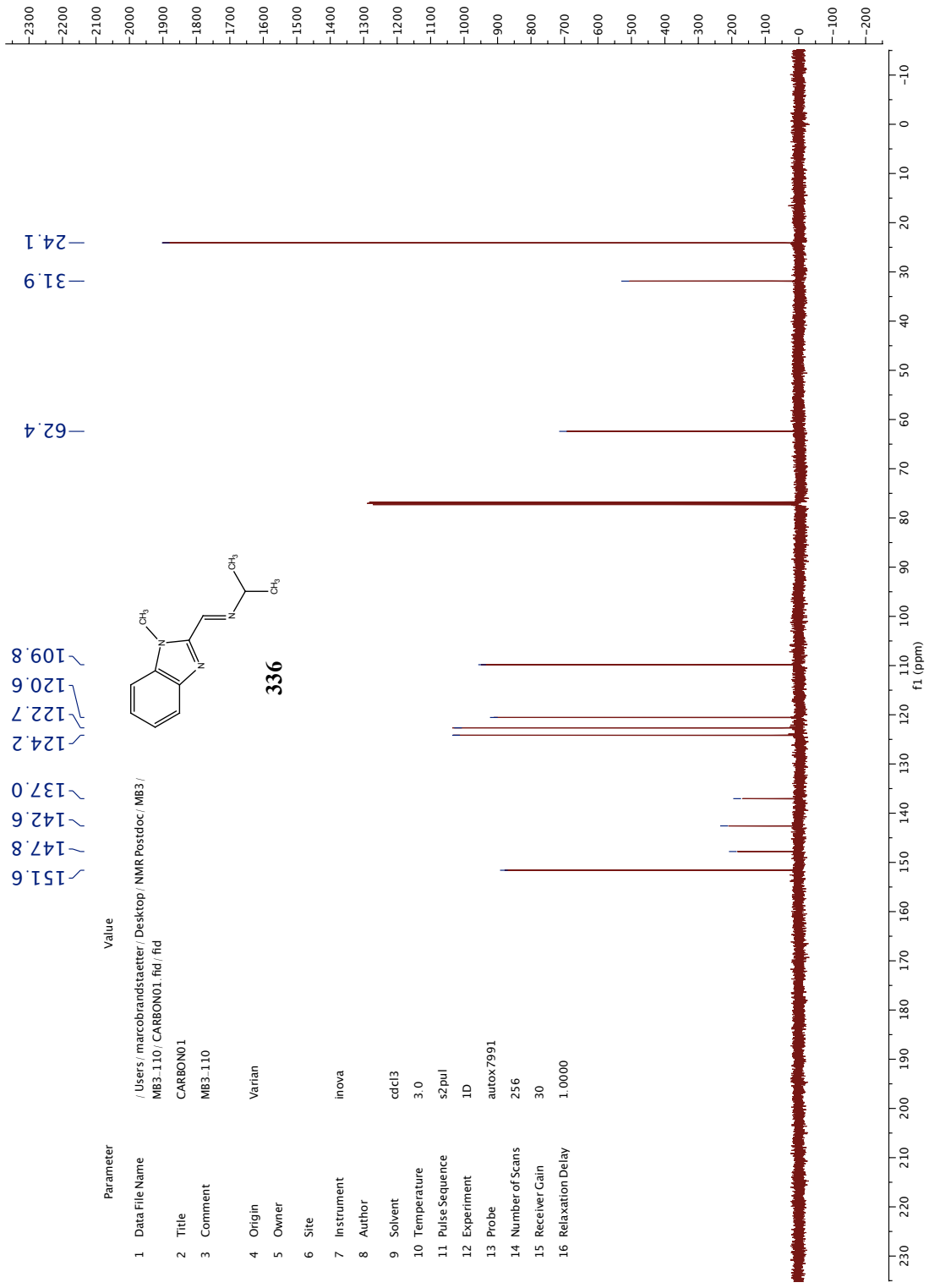

Parameter	Value
1 Data File Name	/ Users / marcobrandstaetter / Desktop / NMR Postdoc / MB3 / MB3_110 / CARBON01 fid / fid
2 Title	CARBON01
3 Comment	MB3_110
4 Origin	Varian
5 Owner	
6 Site	
7 Instrument	inova
8 Author	
9 Solvent	cdcl3
10 Temperature	3.0
11 Pulse Sequence	s2pul
12 Experiment	1D
13 Probe	autox7991
14 Number of Scans	256
15 Receiver Gain	30
16 Relaxation Delay	1.0000

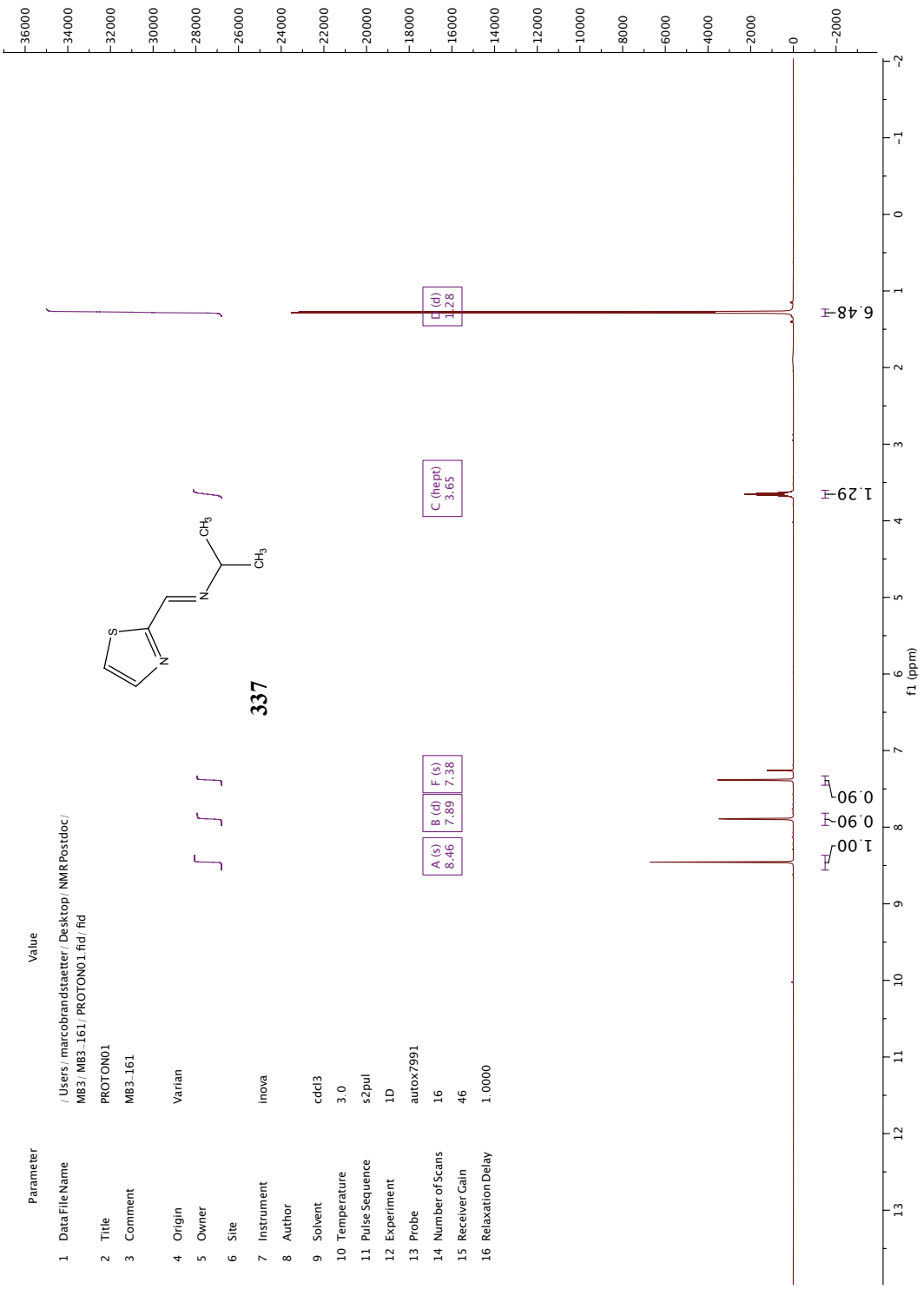
Parameter
Value
1 DataFileName / Users / marcobrandstaetter / Desktop / NMRPostdoc / MB3 / MB3_161 / PROTON01.fid / fid
2 Title PROTON01
3 Comment MB3_161
4 Origin Varian
5 Owner
6 Site
7 Instrument inova
8 Author
9 Solvent cdcl3
10 Temperature 3.0
11 PulseSequence s2pul
12 Experiment 1D
13 Probe autox7991
14 NumberofScans 16
15 ReceiverGain 46
16 RelaxationDelay 1.0000
337
A (s) 8.46
B (d) 7.89
F (s) 7.38
C (hept) 3.65
D (d) 1.28
6.48
1.29
1.00
0.90
0.90
f1 (ppm)

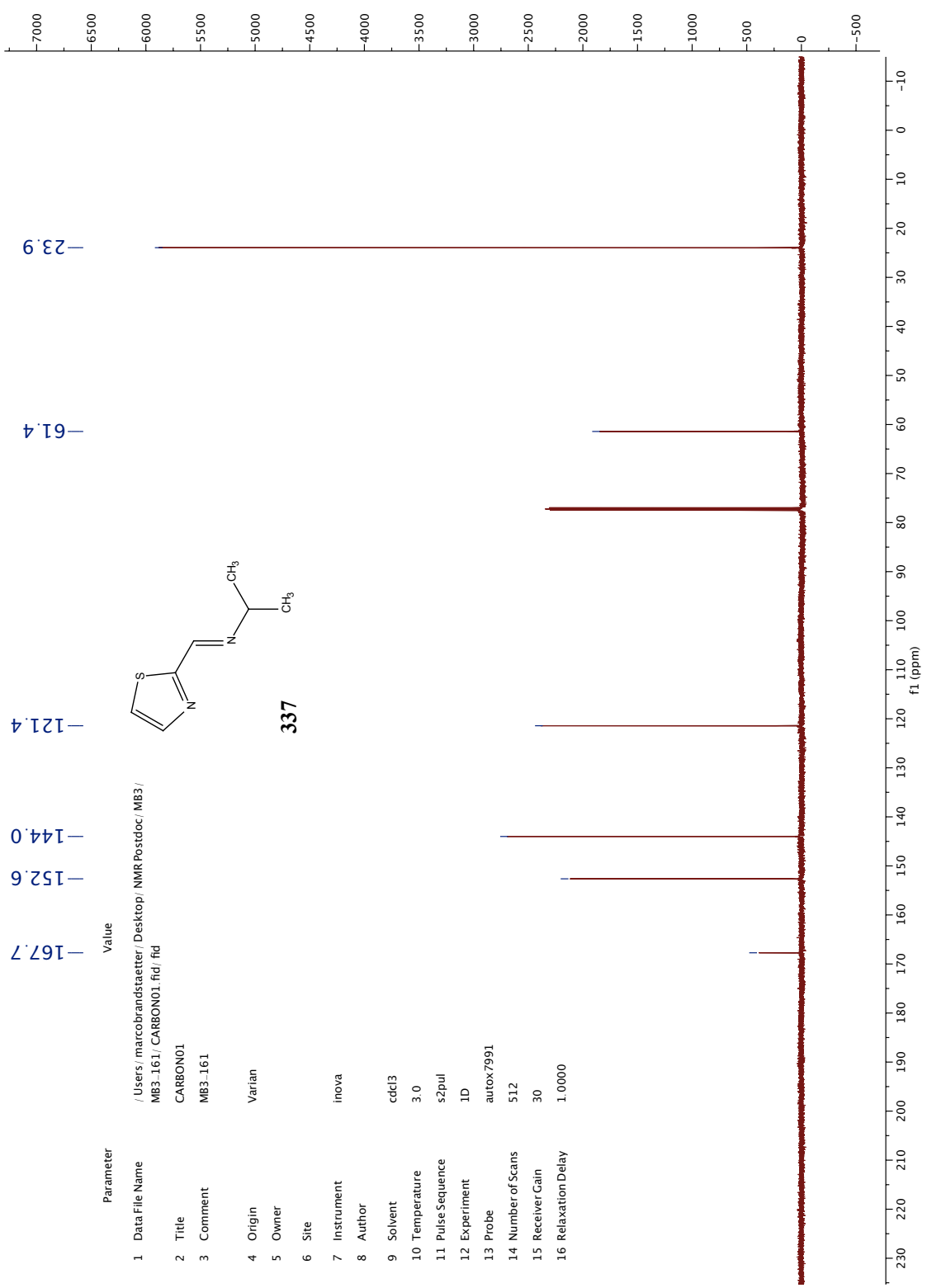

Parameter	Value
1 Data File Name	/Users/marcobrandstaetter/Desktop/NMR Postdoc/MB3/MB3_161/CARBON01.fid/fid
2 Title	CARBON01
3 Comment	MB3_161
4 Origin	Varian
5 Owner	
6 Site	
7 Instrument	inova
8 Author	
9 Solvent	cdcl3
10 Temperature	3.0
11 Pulse Sequence	s2pul
12 Experiment	1D
13 Probe	autox7991
14 Number of Scans	512
15 Receiver Gain	30
16 Relaxation Delay	1.0000

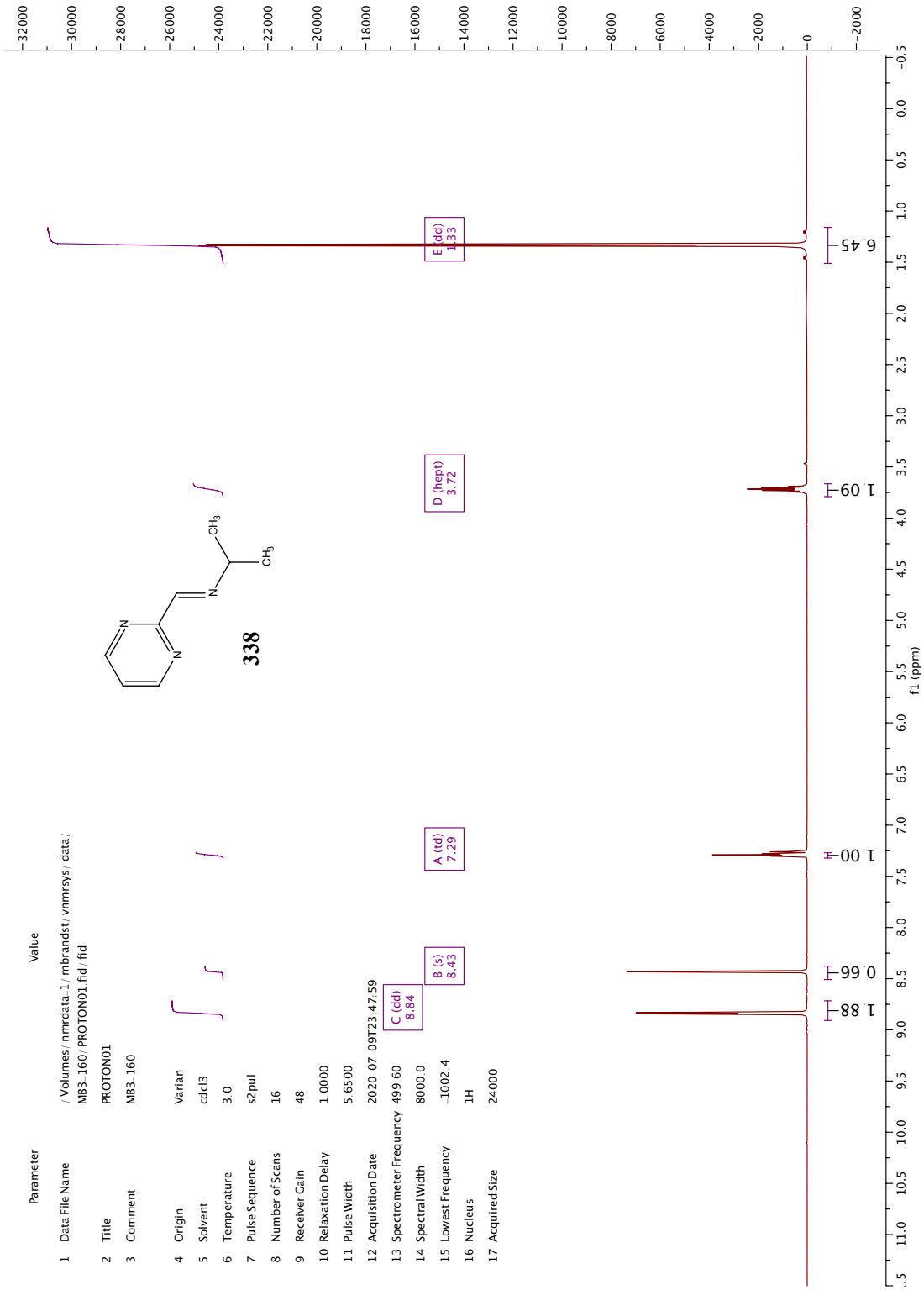
Parameter
Value
1 Data File Name / Volumes / nmrdata_1 / mbrandst / vnmrsys / data / MB3_160 / PROTON01.fid / fid
2 Title PROTON01
3 Comment MB3_160
4 Origin Varian
5 Solvent cdcl3
6 Temperature 3.0
7 Pulse Sequence s2pul
8 Number of Scans 16
9 Receiver Gain 48
10 Relaxation Delay 1.0000
11 Pulse Width 5.6500
12 Acquisition Date 2020-07-09T23:47:59
13 Spectrometer Frequency 499.60
14 Spectral Width 8000.0
15 Lowest Frequency -1002.4
16 Nucleus 1H
17 Acquired Size 24000
C (dd) 8.84
B (s) 8.43
A (td) 7.29
D (hept) 3.72
E (dd) 1.33
338
6.45
1.09
1.00
0.96
1.88
f1 (ppm)

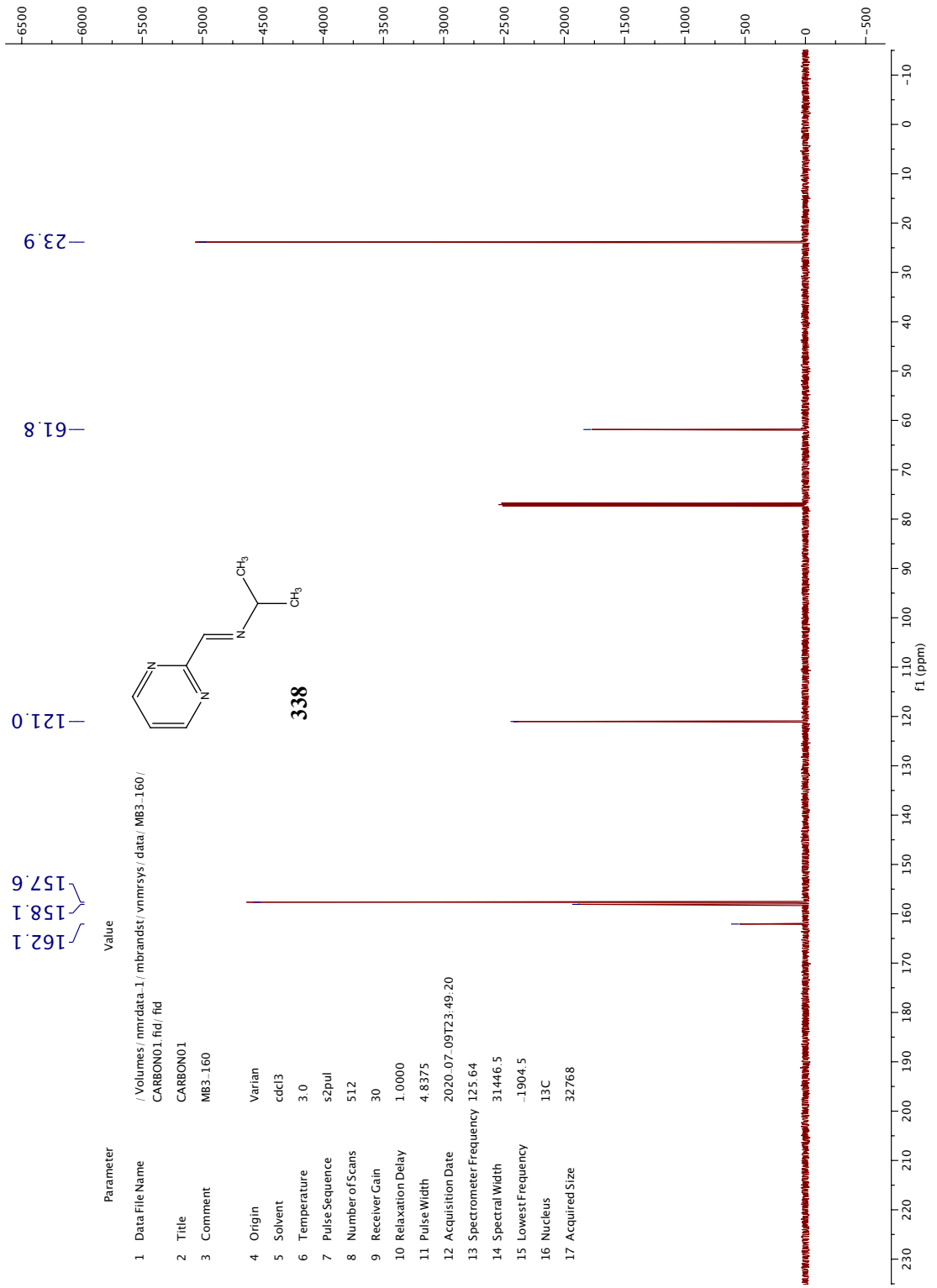

Parameter	Value
1 Data File Name	/Volumes/nmrdata_1/mbrandst/vnmrsys/data/MB3_160/CARBON01.fid/fid
2 Title	CARBON01
3 Comment	MB3_160
4 Origin	Varian
5 Solvent	cdcl3
6 Temperature	3.0
7 Pulse Sequence	s2pul
8 Number of Scans	512
9 Receiver Gain	30
10 Relaxation Delay	1.0000
11 Pulse Width	4.8375
12 Acquisition Date	2020_07_09T23:49:20
13 Spectrometer Frequency	125.64
14 Spectral Width	31446.5
15 Lowest Frequency	-1904.5
16 Nucleus	13C
17 Acquired Size	32768

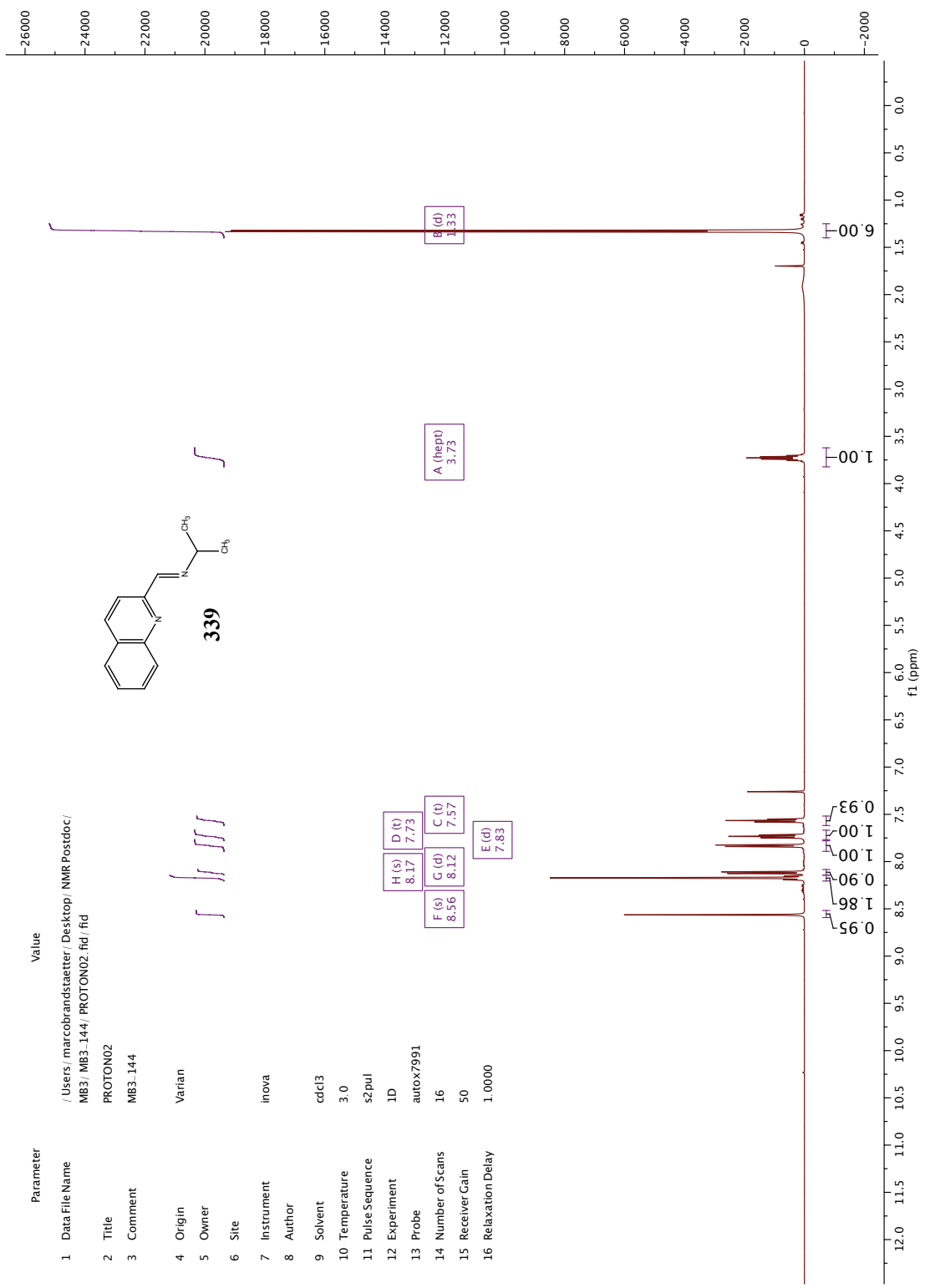

	Parameter	Value
1	Data File Name	/Users/marcobrandstaetter/Desktop/NMR Postdoc/MB3/MB3_144/PROTON02.fid/fid
2	Title	PROTON02
3	Comment	MB3_144
4	Origin	Varian
5	Owner	
6	Site	
7	Instrument	inova
8	Author	
9	Solvent	cdcl3
10	Temperature	3.0
11	Pulse Sequence	s2pul
12	Experiment	1D
13	Probe	autox7991
14	Number of Scans	16
15	Receiver Gain	50
16	Relaxation Delay	1.0000

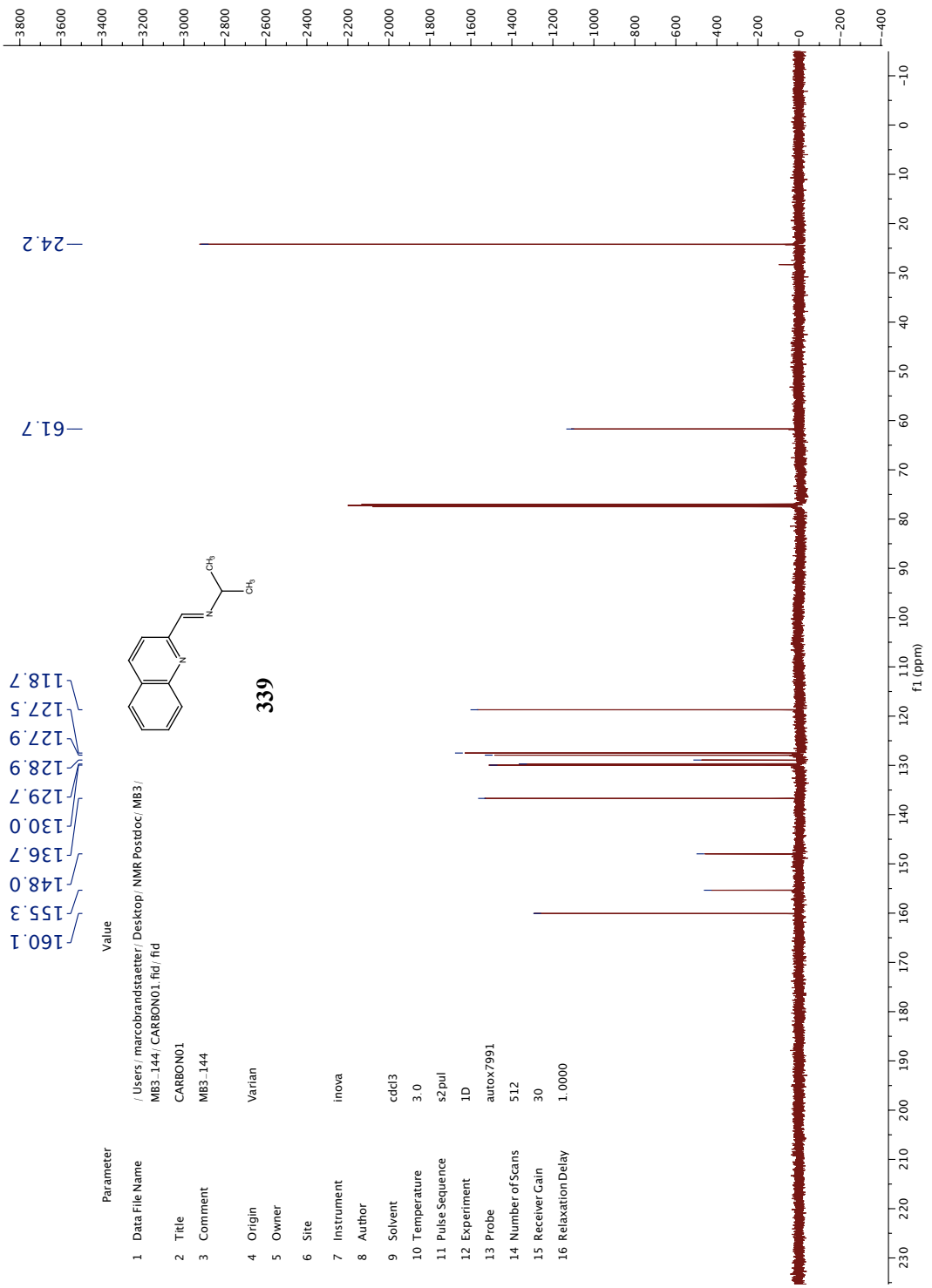

Parameter	Value
1 Data File Name	/Users/marcobrandstaetter/Desktop/NMR Postdoc/MB3/MB3_144/CARBON01.fid/fid
2 Title	CARBON01
3 Comment	MB3_144
4 Origin	Varian
5 Owner	
6 Site	
7 Instrument	inova
8 Author	
9 Solvent	cdcl3
10 Temperature	3.0
11 Pulse Sequence	s2pul
12 Experiment	1D
13 Probe	autox7991
14 Number of Scans	512
15 Receiver Gain	30
16 Relaxation Delay	1.0000

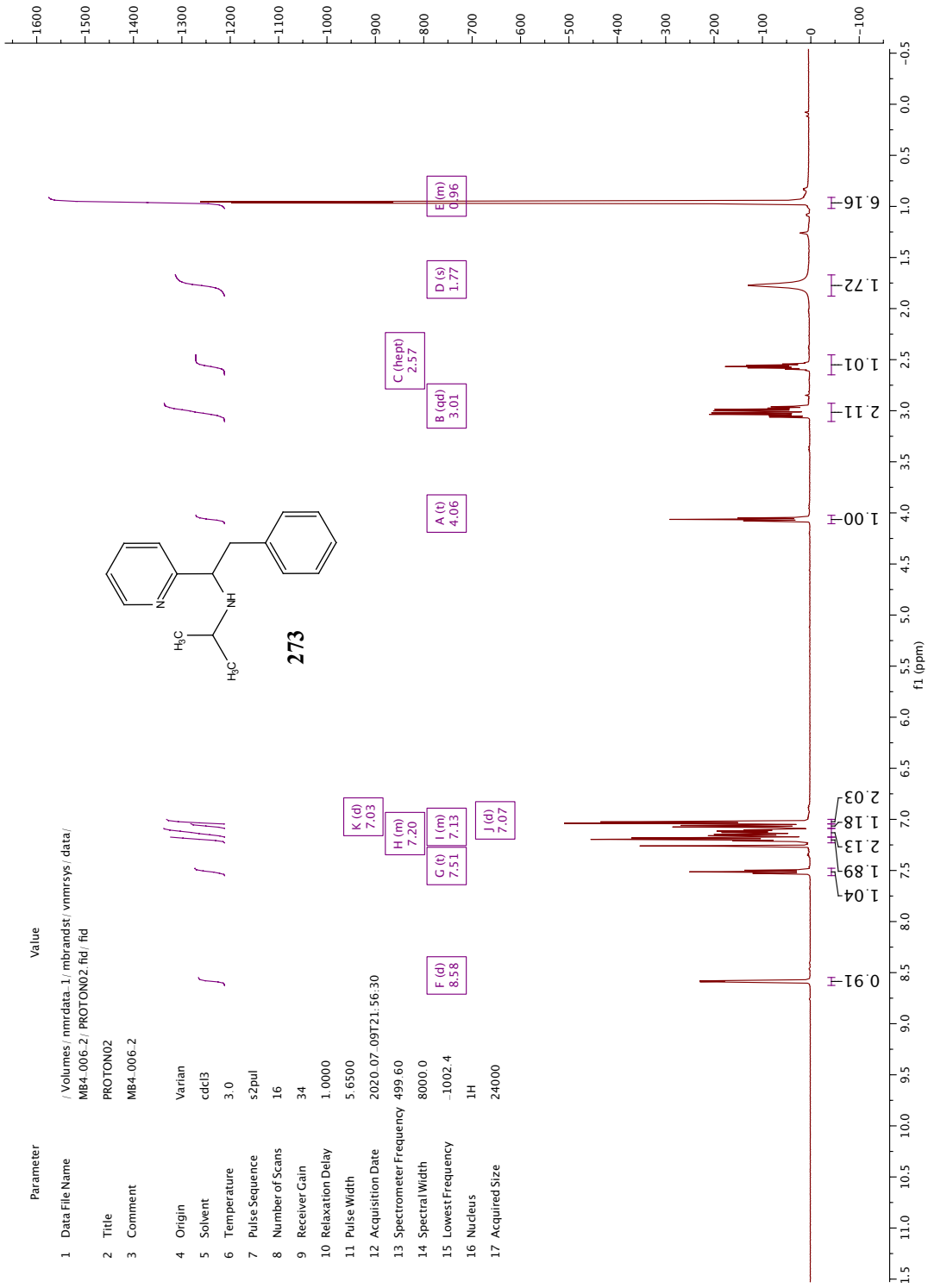
Parameter
Value
1 Data File Name / Volumes/ nmrdata_1/ mbrandst/ vnmrsys/ data/ MB4_006_2/ PROTON02.fid/ fid
2 Title PROTON02
3 Comment MB4_006_2
4 Origin Varian
5 Solvent cdcl3
6 Temperature 3.0
7 Pulse Sequence s2pul
8 Number of Scans 16
9 Receiver Gain 34
10 Relaxation Delay 1.0000
11 Pulse Width 5.6500
12 Acquisition Date 2020_07_09T21:56:30
13 Spectrometer Frequency 499.60
14 Spectral Width 8000.0
15 Lowest Frequency -1002.4
16 Nucleus 1H
17 Acquired Size 24000
273
A (t) 4.06
B (qd) 3.01
C (hept) 2.57
D (s) 1.77
E (m) 0.96
F (d) 8.58
G (t) 7.51
H (m) 7.20
I (m) 7.13
J (d) 7.07
K (d) 7.03
0.91
1.04
1.89
2.13
1.18
2.03
1.00
2.11
1.01
1.72
6.16
f1 (ppm)

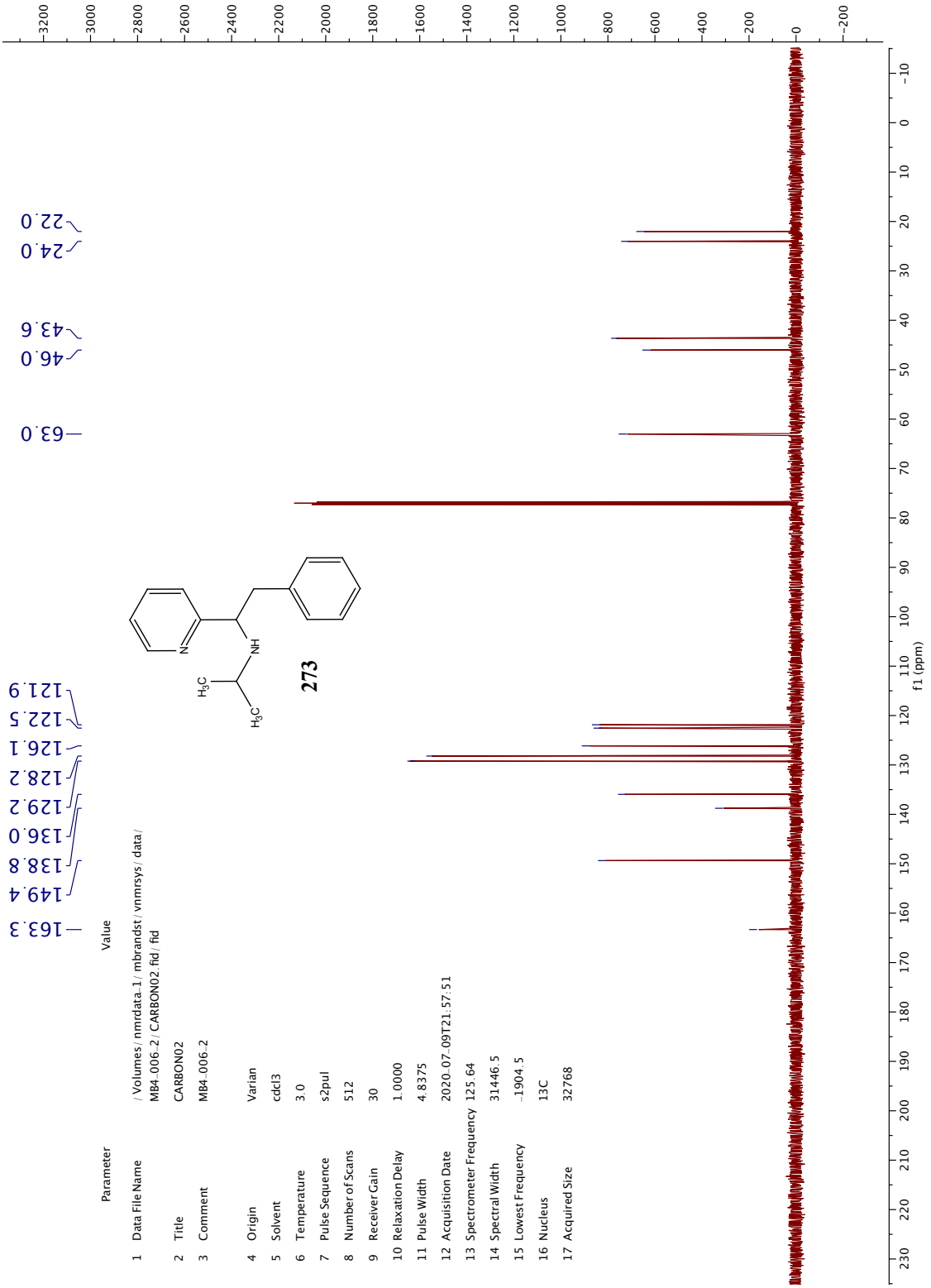

Parameter	Value
1 Data File Name	/Volumes/nmrdata_1/mbrandst/vnmrsys/data/MB4_006_2/CARBON02.fid/fid
2 Title	CARBON02
3 Comment	MB4_006_2
4 Origin	Varian
5 Solvent	cdcl3
6 Temperature	3.0
7 Pulse Sequence	s2pul
8 Number of Scans	512
9 Receiver Gain	30
10 Relaxation Delay	1.0000
11 Pulse Width	4.8375
12 Acquisition Date	2020-07-09T21:57:51
13 Spectrometer Frequency	125.64
14 Spectral Width	31446.5
15 Lowest Frequency	-1904.5
16 Nucleus	13C
17 Acquired Size	32768

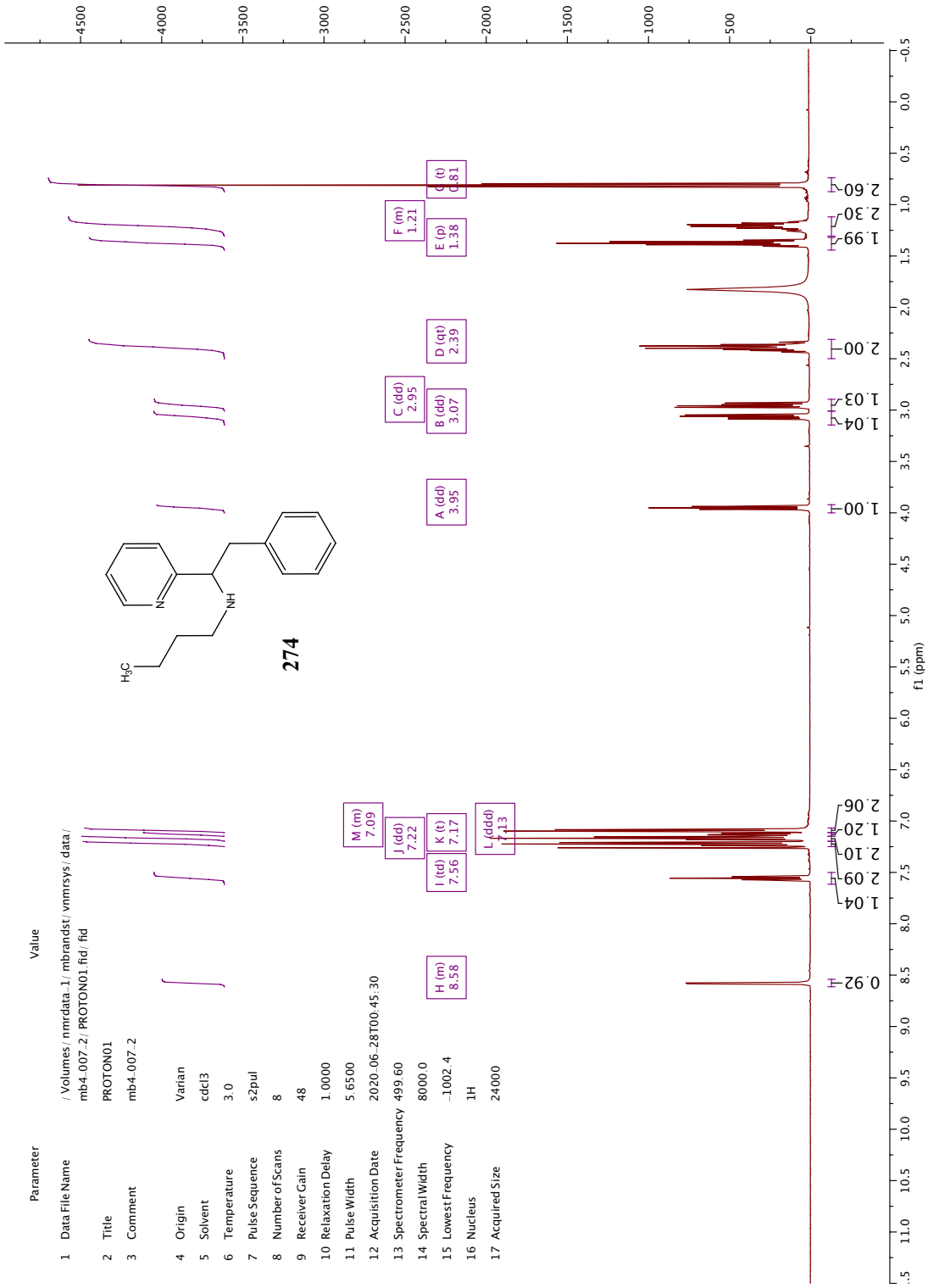
Parameter
Value
1 Data File Name / Volumes/ nmrdata_1/ mbrandst/ vnmrsys/ data/ mb4_007_2/ PROTON01.fid/ fid
2 Title PROTON01
3 Comment mb4_007_2
4 Origin Varian
5 Solvent cdcl3
6 Temperature 3.0
7 Pulse Sequence s2pul
8 Number of Scans 8
9 Receiver Gain 48
10 Relaxation Delay 1.0000
11 Pulse Width 5.6500
12 Acquisition Date 2020_06_28T00.45.30
13 Spectrometer Frequency 499.60
14 Spectral Width 8000.0
15 Lowest Frequency -1002.4
16 Nucleus 1H
17 Acquired Size 24000
H (m) 8.58
I (td) 7.56
K (t) 7.17
J (dd) 7.22
M (m) 7.09
L (ddd) 7.13
A (dd) 3.95
B (dd) 3.07
C (dd) 2.95
D (qt) 2.39
E (p) 1.38
F (m) 1.21
G (t) 0.81
0.92
2.04
2.09
2.10
1.20
2.06
1.00
1.04
1.03
2.00
1.99
2.30
2.60
N
NH
H3C
274
f1 (ppm)

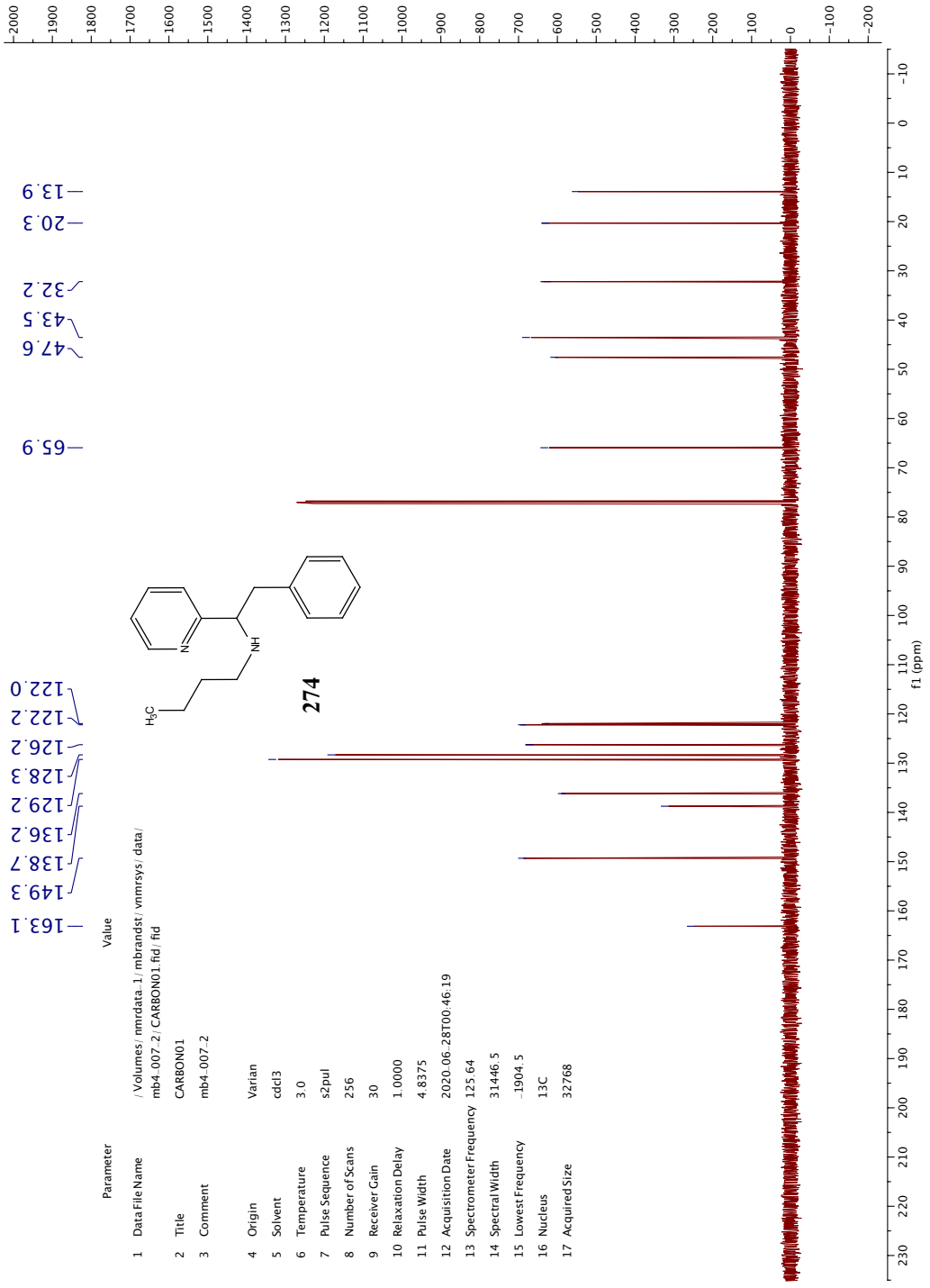

	Parameter	Value
1	Data File Name	/Volumes/mmrdata_1/mbrandst/vnmrsys/data/mb4_007_2/CARBON01.fid/fid
2	Title	CARBON01
3	Comment	mb4_007_2
4	Origin	Varian
5	Solvent	cdcl3
6	Temperature	3.0
7	Pulse Sequence	s2pul
8	Number of Scans	256
9	Receiver Gain	30
10	Relaxation Delay	1.0000
11	Pulse Width	4.8375
12	Acquisition Date	2020_06_28T00:46:19
13	Spectrometer Frequency	125.64
14	Spectral Width	31446.5
15	Lowest Frequency	-1904.5
16	Nucleus	13C
17	Acquired Size	32768

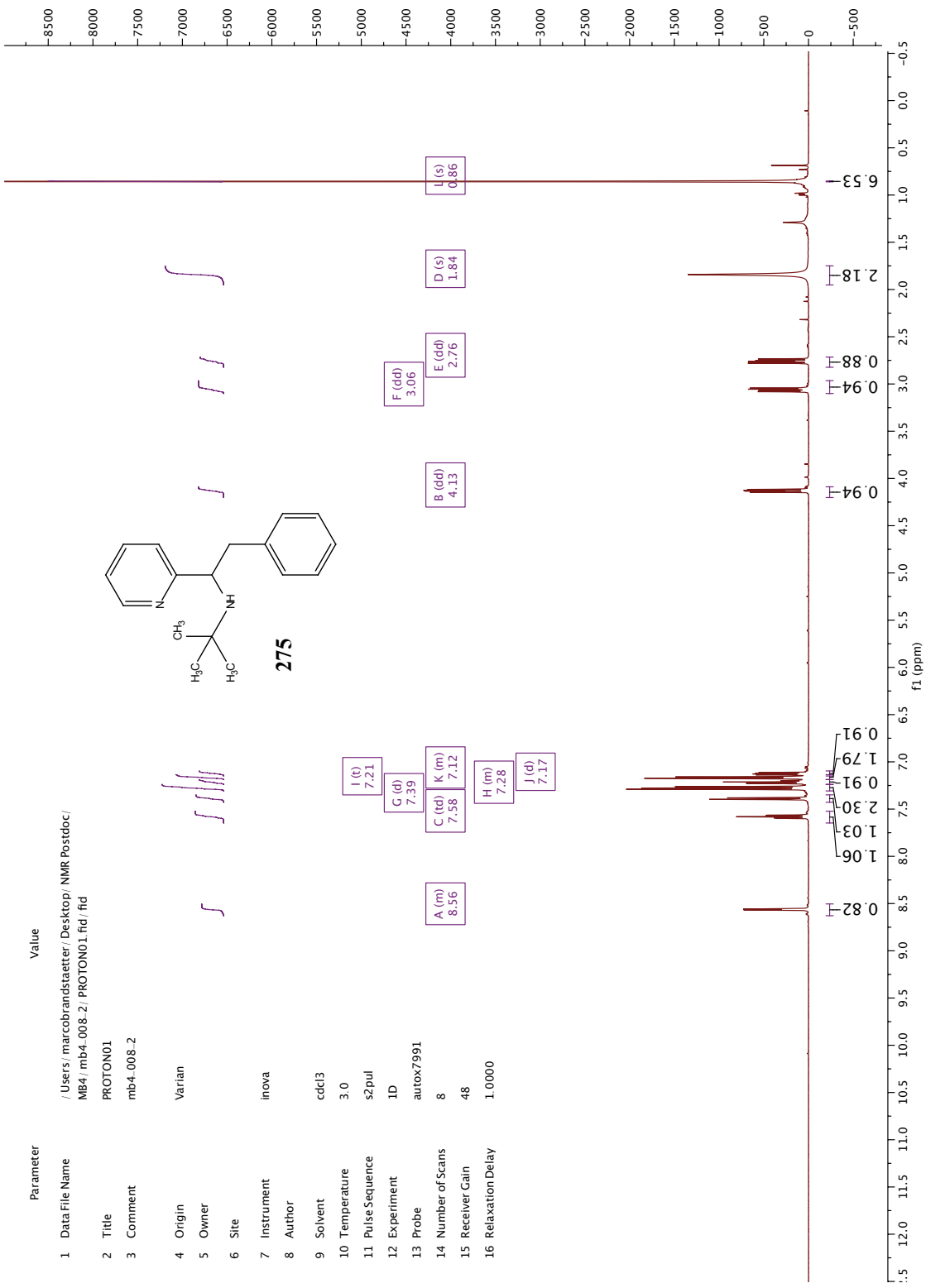
Parameter
Value
1 Data File Name / Users/ marcobrandstaetter/ Desktop/ NMR Postdoc/ MB4/ mb4_008.2/ PROTON01.fid/ fid
2 Title PROTON01
3 Comment mb4_008.2
4 Origin Varian
5 Owner
6 Site
7 Instrument inova
8 Author
9 Solvent cdcl3
10 Temperature 3.0
11 Pulse Sequence s2pul
12 Experiment 1D
13 Probe autox7991
14 Number of Scans 8
15 Receiver Gain 48
16 Relaxation Delay 1.0000
A (m) 8.56
C (td) 7.58
K (m) 7.12
I (t) 7.21
G (d) 7.39
H (m) 7.28
J (d) 7.17
F (dd) 3.06
E (dd) 2.76
B (dd) 4.13
D (s) 1.84
L (s) 0.86
275
6.53
2.18
0.88
0.94
0.94
0.82
1.06
2.30
1.03
0.91
1.79
0.91
f1 (ppm)

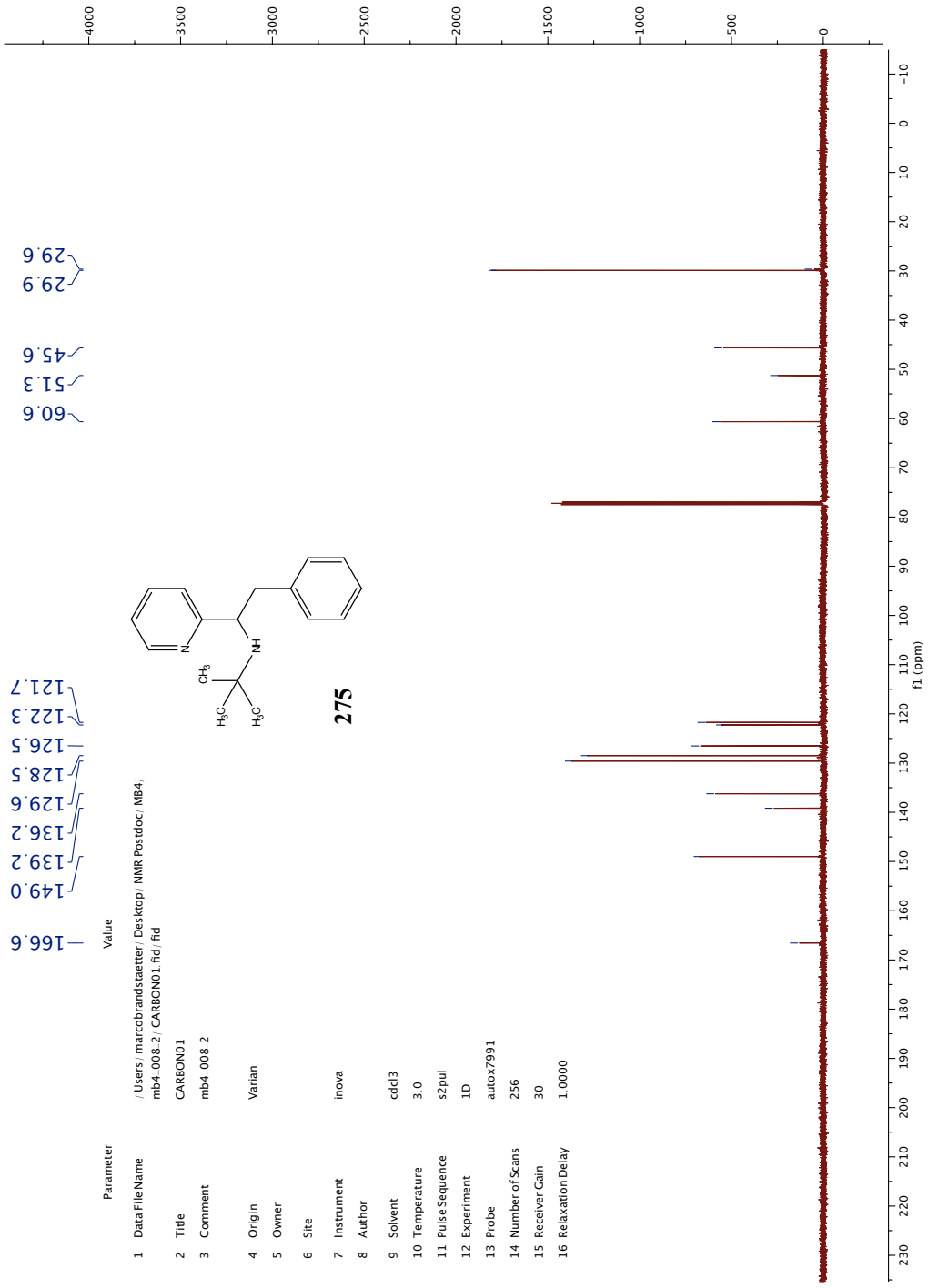
29.9
29.6
45.6
51.3
60.6
121.7
122.3
126.5
128.5
129.6
136.2
139.2
149.0
166.6
275
Parameter
Value
1 Data File Name / Users / marcobrandstaetter / Desktop / NMR Postdoc / MB4 / mb4-008-2 / CARBON01.fid / fid
2 Title CARBON01
3 Comment mb4-008-2
4 Origin Varian
5 Owner
6 Site
7 Instrument inova
8 Author
9 Solvent cdcl3
10 Temperature 3.0
11 Pulse Sequence s2pul
12 Experiment 1D
13 Probe autox7991
14 Number of Scans 256
15 Receiver Gain 30
16 Relaxation Delay 1.0000
f1 (ppm)

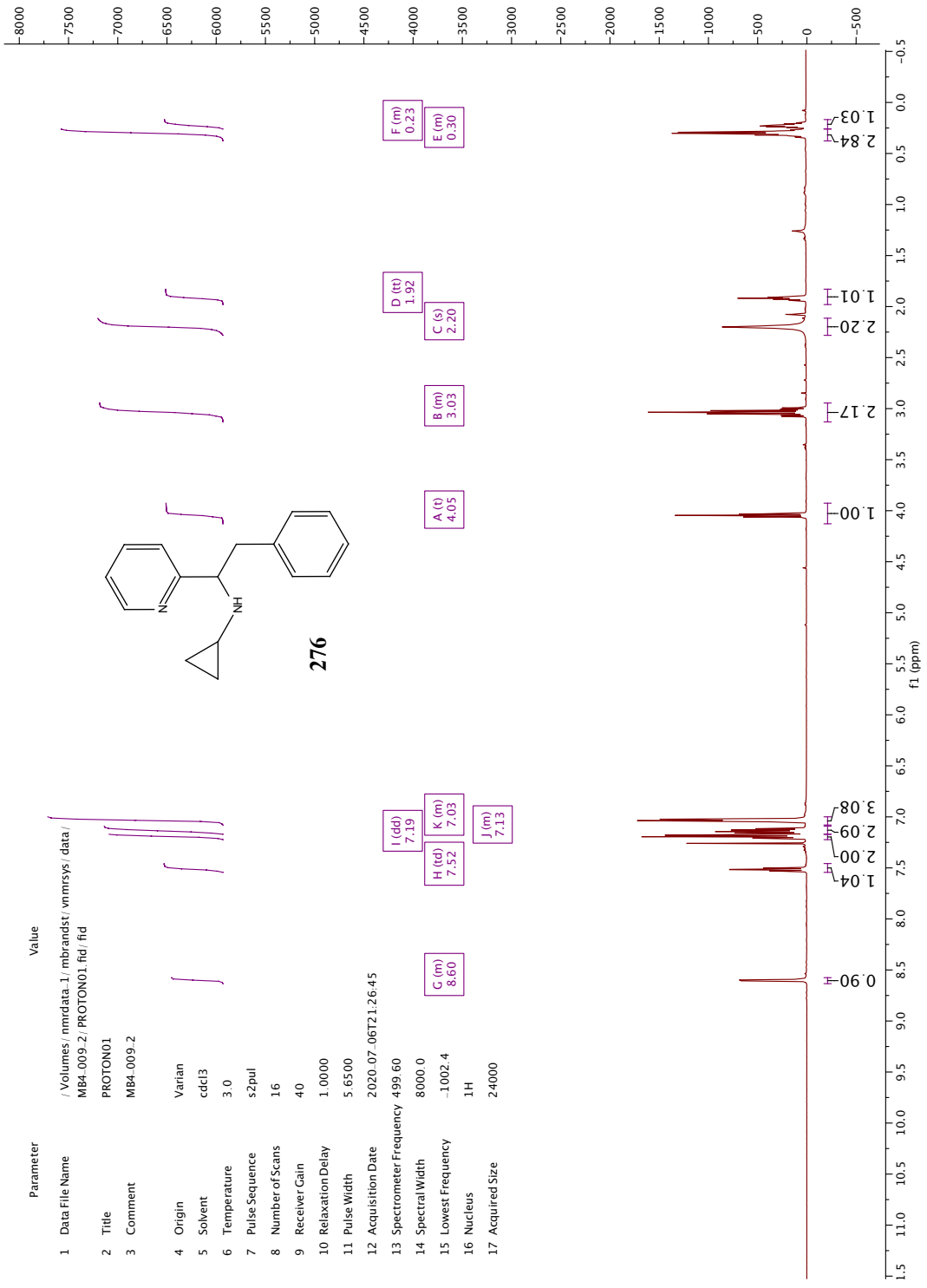

	Parameter	Value
1	Data File Name	/Volumes/nmrdata_1/mbrandst/vnmrsys/data/MB4.009.2/PROTON01.fid/fid
2	Title	PROTON01
3	Comment	MB4.009.2
4	Origin	Varian
5	Solvent	cdcl3
6	Temperature	3.0
7	Pulse Sequence	s2pul
8	Number of Scans	16
9	Receiver Gain	40
10	Relaxation Delay	1.0000
11	Pulse Width	5.6500
12	Acquisition Date	2020_07_06T21:26:45
13	Spectrometer Frequency	499.60
14	Spectral Width	8000.0
15	Lowest Frequency	-1002.4
16	Nucleus	1H
17	Acquired Size	24000

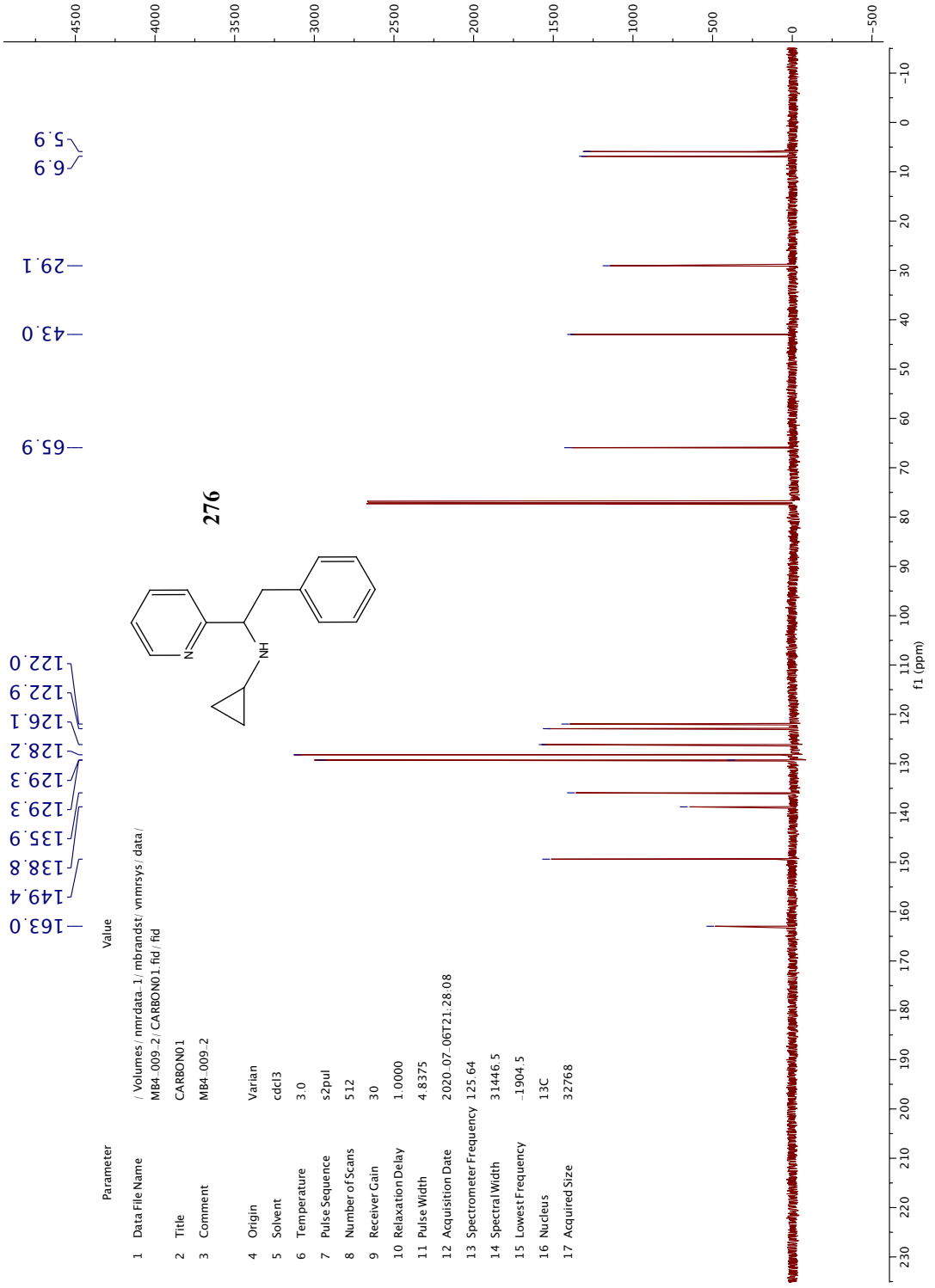

	Parameter	Value
1	Data File Name	/Volumes/nmrdata_1/mbrandst/vnmrsys/data/MB4_009_2/CARBON01.fid/fid
2	Title	CARBON01
3	Comment	MB4_009_2
4	Origin	Varian
5	Solvent	cdcl3
6	Temperature	3.0
7	Pulse Sequence	s2pul
8	Number of Scans	512
9	Receiver Gain	30
10	Relaxation Delay	1.0000
11	Pulse Width	4.8375
12	Acquisition Date	2020_07_06T21:28:08
13	Spectrometer Frequency	125.64
14	Spectral Width	31446.5
15	Lowest Frequency	-1904.5
16	Nucleus	13C
17	Acquired Size	32768

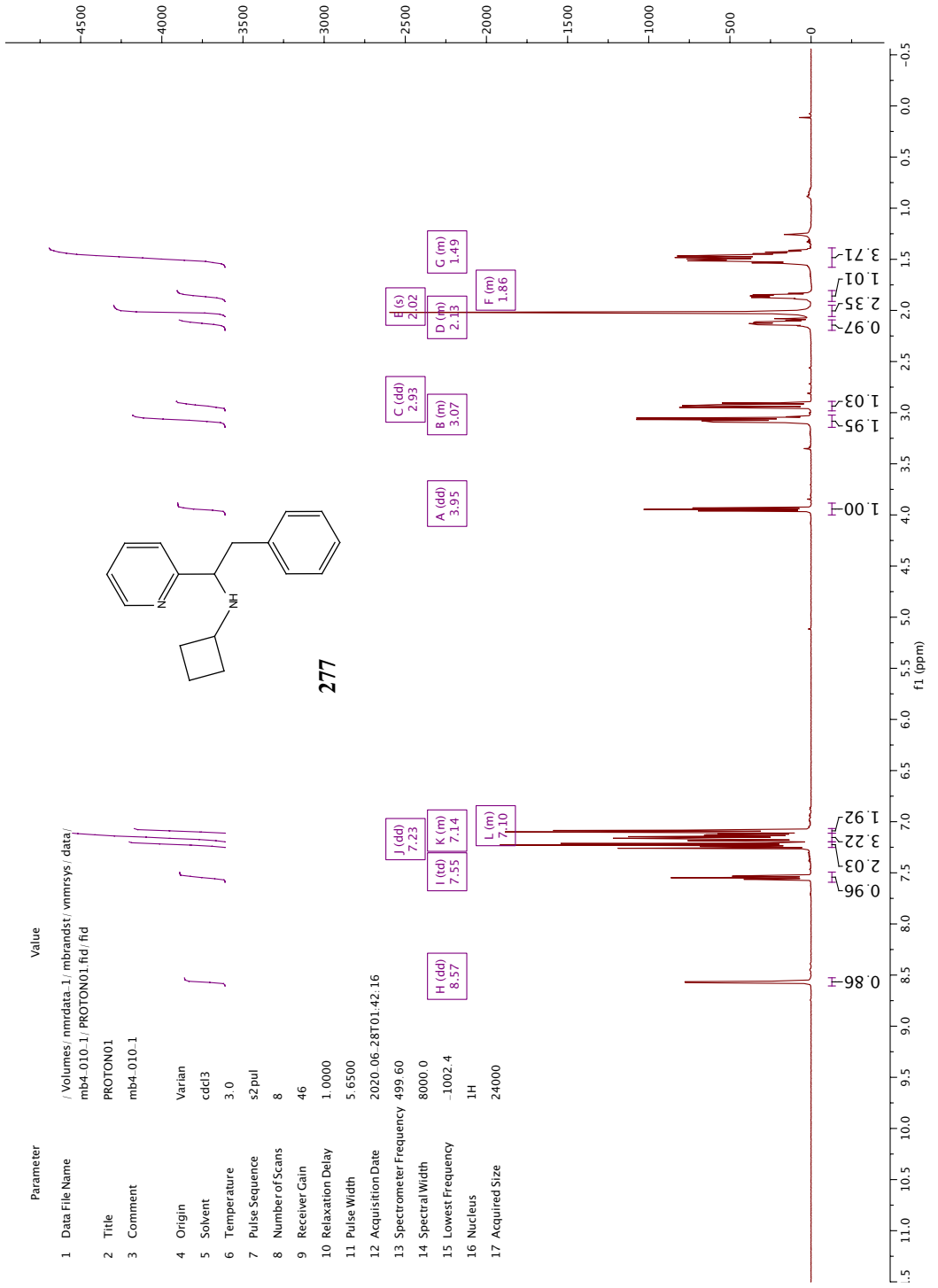
277
Parameter
Value
1 Data File Name
/ Volumes/ nmrdata_1/ mbrandst/ vnmrsys/ data/ mb4-010-1/ PROTON01.fid/ fid
2 Title
PROTON01
3 Comment
mb4-010-1
4 Origin
Varian
5 Solvent
cdcl3
6 Temperature
3 0
7 Pulse Sequence
s2pul
8 Number of Scans
8
9 Receiver Gain
46
10 Relaxation Delay
1 0000
11 Pulse Width
5 6500
12 Acquisition Date
2020-06-28T01:42:16
13 Spectrometer Frequency
499 60
14 Spectral Width
8000 0
15 Lowest Frequency
-1002 4
16 Nucleus
1H
17 Acquired Size
24000
H (dd) 8.57
I (td) 7.55
J (dd) 7.23
K (m) 7.14
L (m) 7.10
A (dd) 3.95
B (m) 3.07
C (dd) 2.93
E (s) 2.02
D (m) 2.13
F (m) 1.86
G (m) 1.49
0.86
0.96
2.03
3.22
1.92
1.00
1.95
1.03
0.97
2.35
1.01
3.71
f1 (ppm)

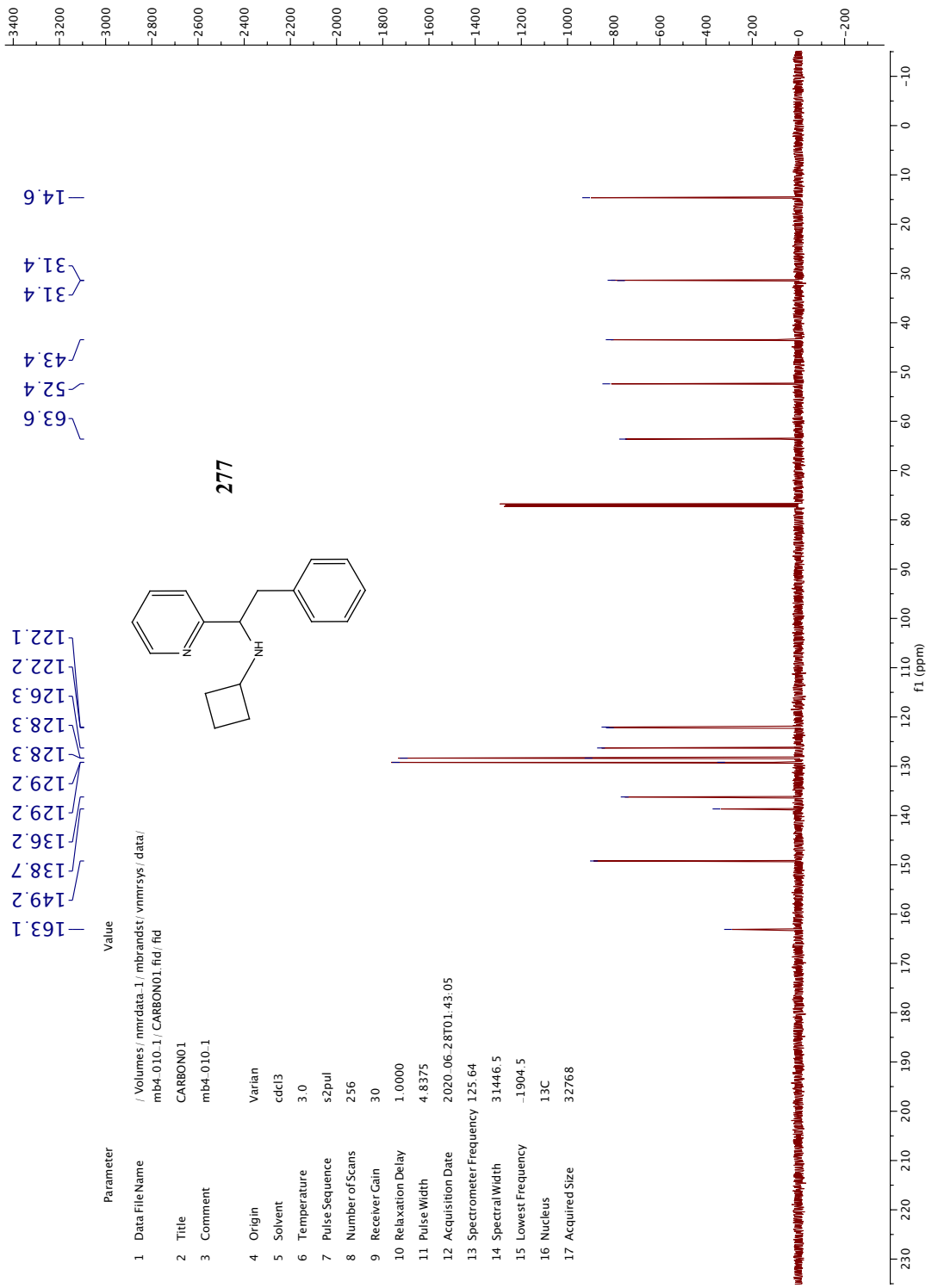

	Parameter	Value
1	Data File Name	/Volumes/nmrdata_1/mbrandst/vnmrsys/data/mb4.010.1/CARBON01.fid/fid
2	Title	CARBON01
3	Comment	mb4.010.1
4	Origin	Varian
5	Solvent	cdcl3
6	Temperature	3.0
7	Pulse Sequence	s2pul
8	Number of Scans	256
9	Receiver Gain	30
10	Relaxation Delay	1.0000
11	Pulse Width	4.8375
12	Acquisition Date	2020_06_28T01:43:05
13	Spectrometer Frequency	125.64
14	Spectral Width	31446.5
15	Lowest Frequency	-1904.5
16	Nucleus	13C
17	Acquired Size	32768

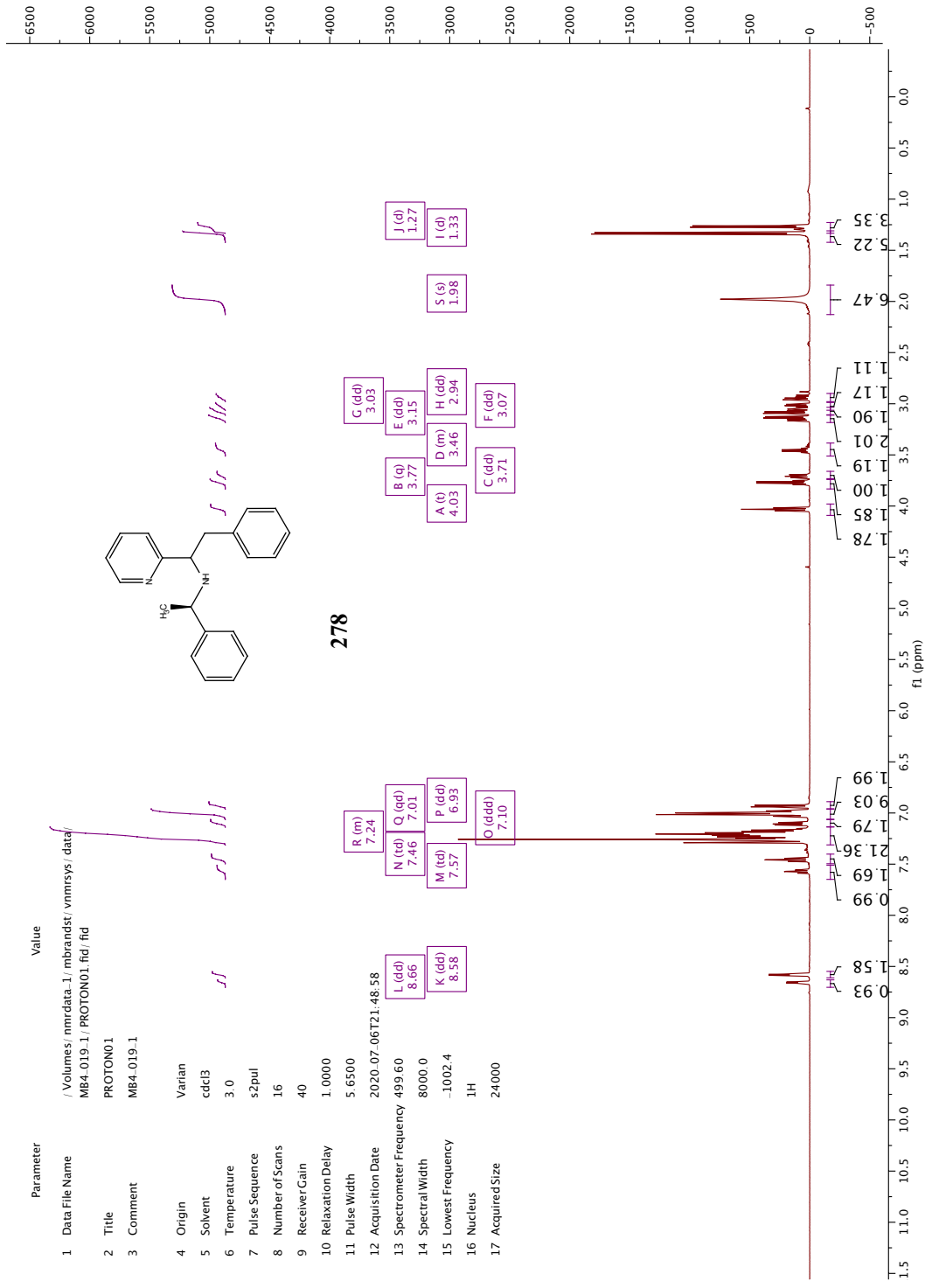
278
A (t) 4.03
B (q) 3.77
C (dd) 3.71
D (m) 3.46
E (dd) 3.15
F (dd) 3.07
G (dd) 3.03
H (dd) 2.94
I (d) 1.33
J (d) 1.27
K (dd) 8.58
L (dd) 8.66
M (td) 7.57
N (td) 7.46
O (ddd) 7.10
P (dd) 6.93
Q (qd) 7.01
R (m) 7.24
S (s) 1.98
Parameter
Value
1 Data File Name / Volumes/ nmrdata_1/ mbrandst/ vnmrsys/ data/ MB4_019_1/ PROTON01.fid/ fid
2 Title PROTON01
3 Comment MB4_019_1
4 Origin Varian
5 Solvent cdcl3
6 Temperature 3.0
7 Pulse Sequence s2pul
8 Number of Scans 16
9 Receiver Gain 40
10 Relaxation Delay 1.0000
11 Pulse Width 5.6500
12 Acquisition Date 2020-07-06T21:48:58
13 Spectrometer Frequency 499.60
14 Spectral Width 8000.0
15 Lowest Frequency -1002.4
16 Nucleus 1H
17 Acquired Size 24000
f1 (ppm)

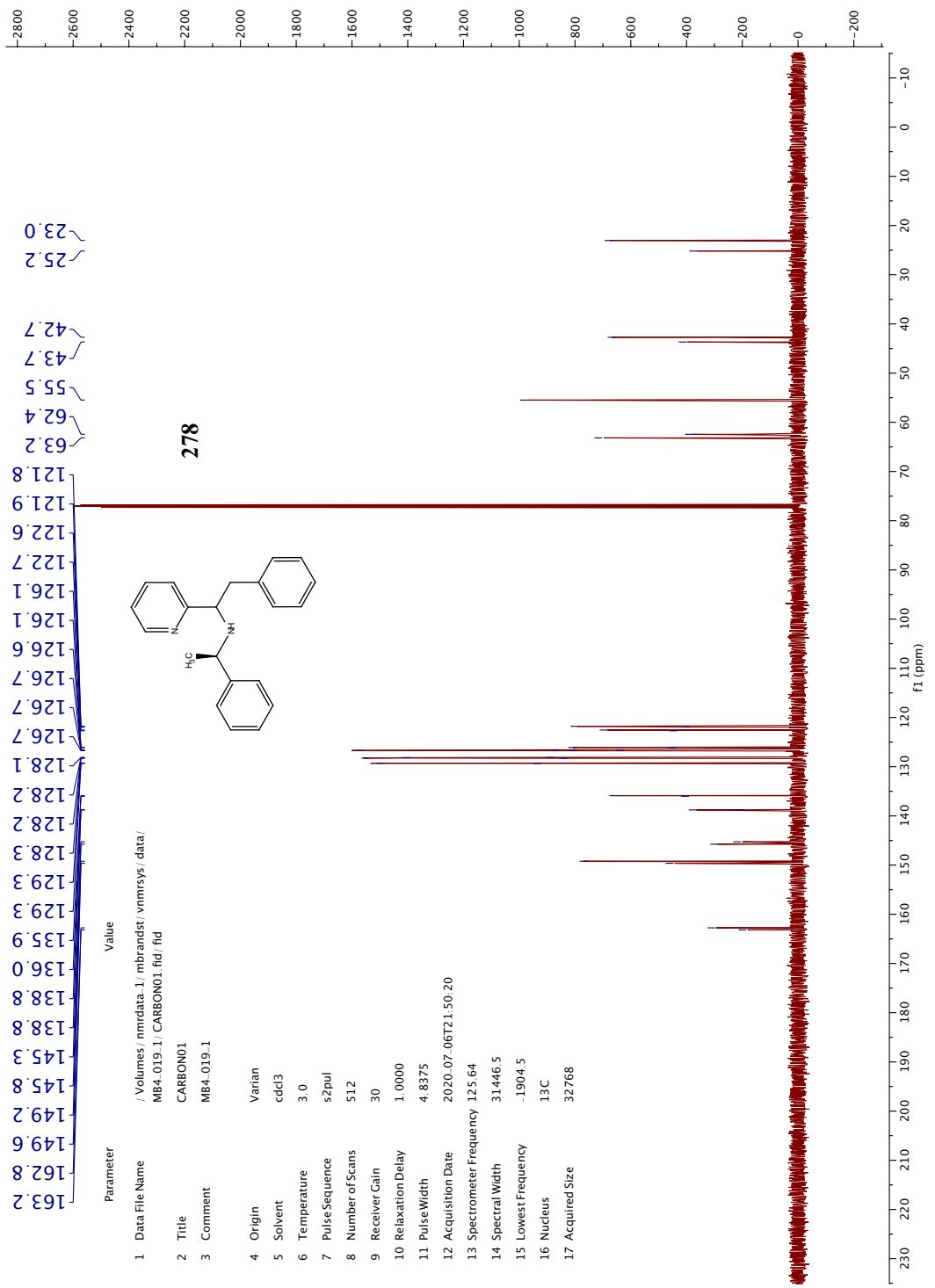
278
f1 (ppm)
Parameter
Value
1 Data File Name / Volumes / nmrdata_1 / mbrandst / vnmrsys / data / MB4.019_1 / CARBON01.fid / fid
2 Title CARBON01
3 Comment MB4.019_1
4 Origin Varian
5 Solvent cdcl3
6 Temperature 3.0
7 PulseSequence s2pul
8 Number of Scans 512
9 Receiver Gain 30
10 Relaxation Delay 1.0000
11 PulseWidth 4.8375
12 Acquisition Date 2020_07_06T21:50:20
13 Spectrometer Frequency 125.64
14 Spectral Width 31446.5
15 Lowest Frequency -1904.5
16 Nucleus 13C
17 Acquired Size 32768

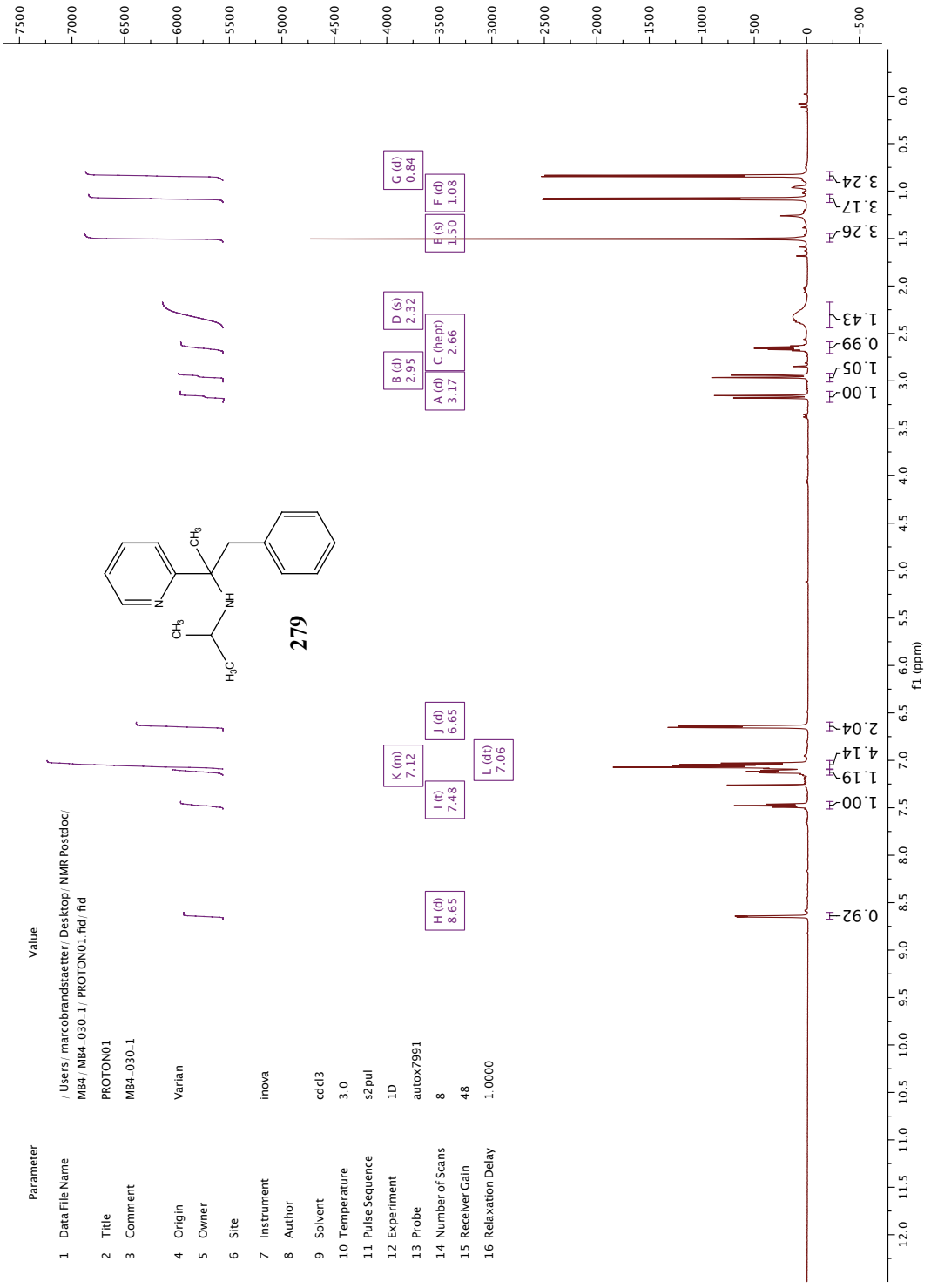
Parameter
Value
1 Data File Name /Users/marcobrandstaetter/Desktop/NMR Postdoc/MB4/MB4_030_1/PROTON01.fid/fid
2 Title PROTON01
3 Comment MB4_030_1
4 Origin Varian
5 Owner
6 Site
7 Instrument inova
8 Author
9 Solvent cdcl3
10 Temperature 3.0
11 Pulse Sequence s2pul
12 Experiment 1D
13 Probe autox7991
14 Number of Scans 8
15 Receiver Gain 48
16 Relaxation Delay 1.0000
279
H (d) 8.65
I (t) 7.48
J (d) 6.65
K (m) 7.12
L (dt) 7.06
A (d) 3.17
B (d) 2.95
C (hept) 2.66
D (s) 2.32
E (s) 1.50
F (d) 1.08
G (d) 0.84
0.92
1.00
1.19
4.14
2.04
3.26
3.17
3.24
1.00
1.05
0.99
1.43
f1 (ppm)

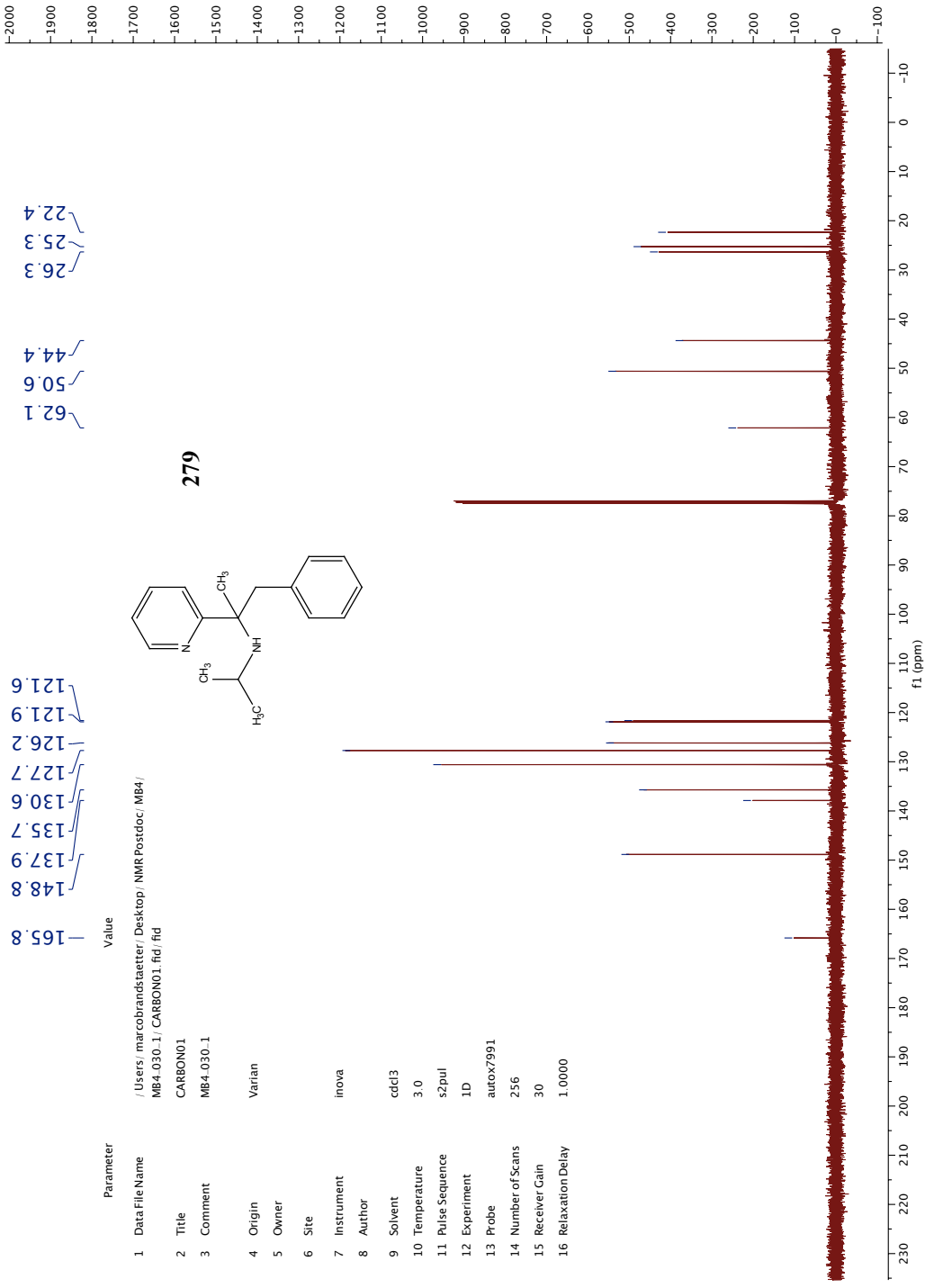
279
22.4
25.3
26.3
44.4
50.6
62.1
121.6
121.9
126.2
127.7
130.6
135.7
137.9
148.8
165.8
Parameter
Value
1 Data File Name
/Users/marcobrandstaetter/Desktop/NMR Postdoc/MB4/MB4-030-1/CARBON01.fid/fid
2 Title
CARBON01
3 Comment
MB4-030-1
4 Origin
Varian
5 Owner
6 Site
7 Instrument
inova
8 Author
9 Solvent
cdcl3
10 Temperature
3.0
11 Pulse Sequence
s2pul
12 Experiment
1D
13 Probe
autox7991
14 Number of Scans
256
15 Receiver Gain
30
16 Relaxation Delay
1.0000
f1 (ppm)

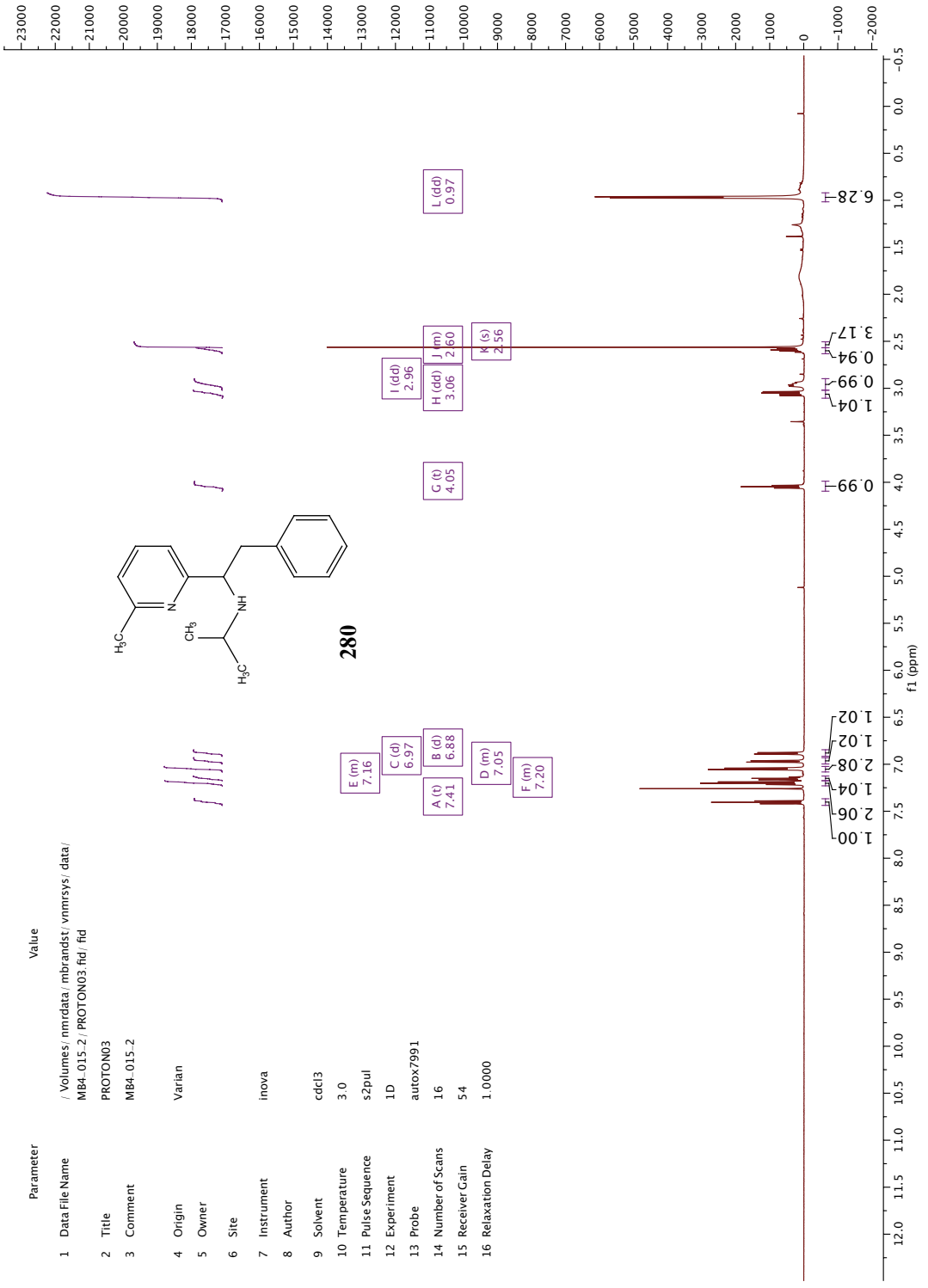
Parameter
Value
1 Data File Name / Volumes/ nmrdata/ mbrandst/ vnmrsys/ data/ MB4_015_2/ PROTON03.fid/ fid
2 Title PROTON03
3 Comment MB4_015_2
4 Origin Varian
5 Owner
6 Site
7 Instrument inova
8 Author
9 Solvent cdcl3
10 Temperature 3.0
11 Pulse Sequence s2pul
12 Experiment 1D
13 Probe autox7991
14 Number of Scans 16
15 Receiver Gain 54
16 Relaxation Delay 1.0000
280
A (t) 7.41
B (d) 6.88
C (d) 6.97
D (m) 7.05
E (m) 7.16
F (m) 7.20
G (t) 4.05
H (dd) 3.06
I (dd) 2.96
J (m) 2.60
K (s) 2.56
L (dd) 0.97
6.28
3.17
0.94
0.99
1.04
0.99
1.00
2.06
1.04
2.08
1.02
1.02
f1 (ppm)

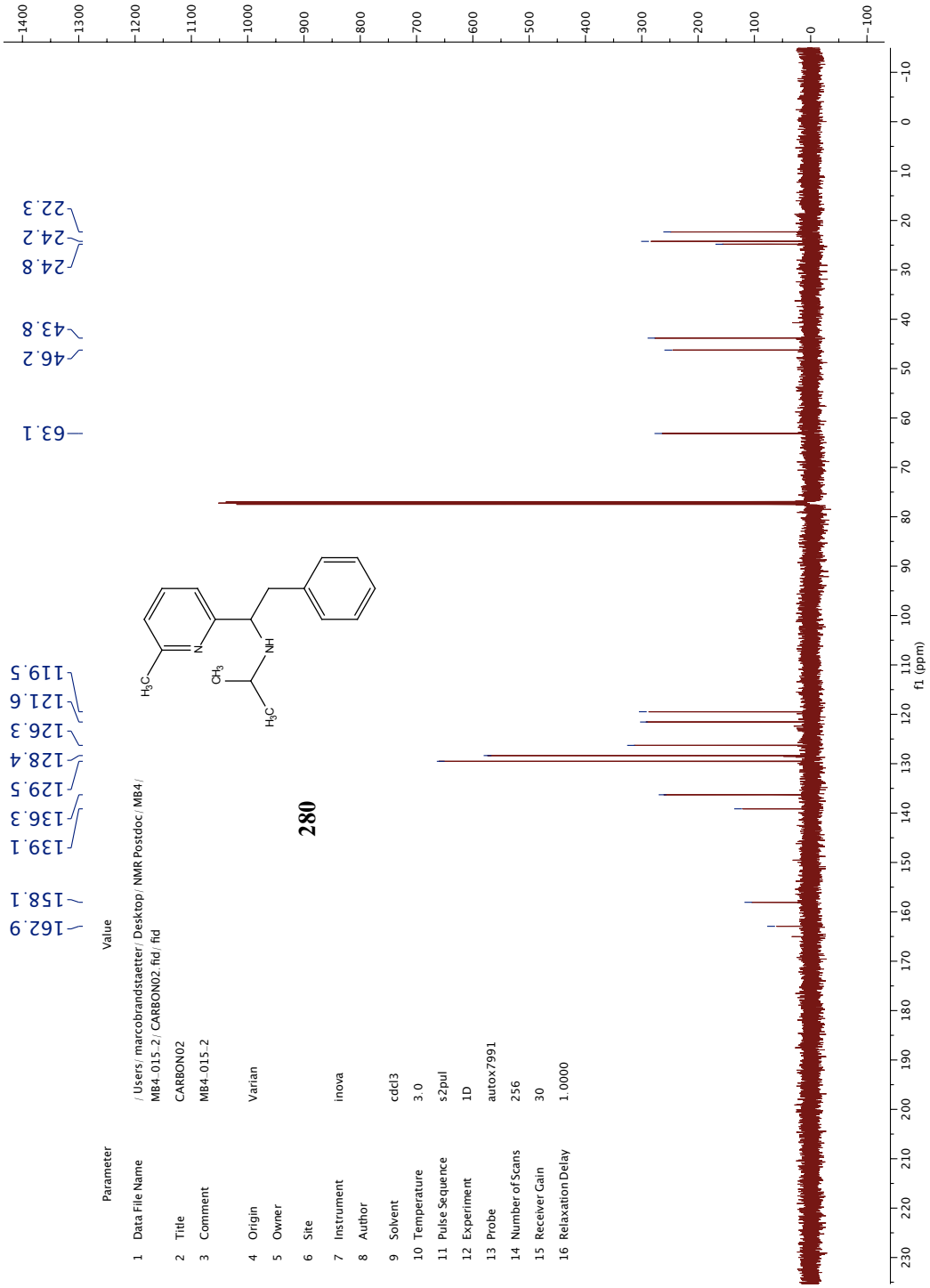

	Parameter	Value
1	Data File Name	/Users/marcobrandstaetter/Desktop/NMR Postdoc/MB4/MB4_015_2/CARBON02.fid/fid
2	Title	CARBON02
3	Comment	MB4_015_2
4	Origin	Varian
5	Owner	
6	Site	
7	Instrument	inova
8	Author	
9	Solvent	cdcl3
10	Temperature	3.0
11	Pulse Sequence	s2pul
12	Experiment	1D
13	Probe	autox7991
14	Number of Scans	256
15	Receiver Gain	30
16	Relaxation Delay	1.0000

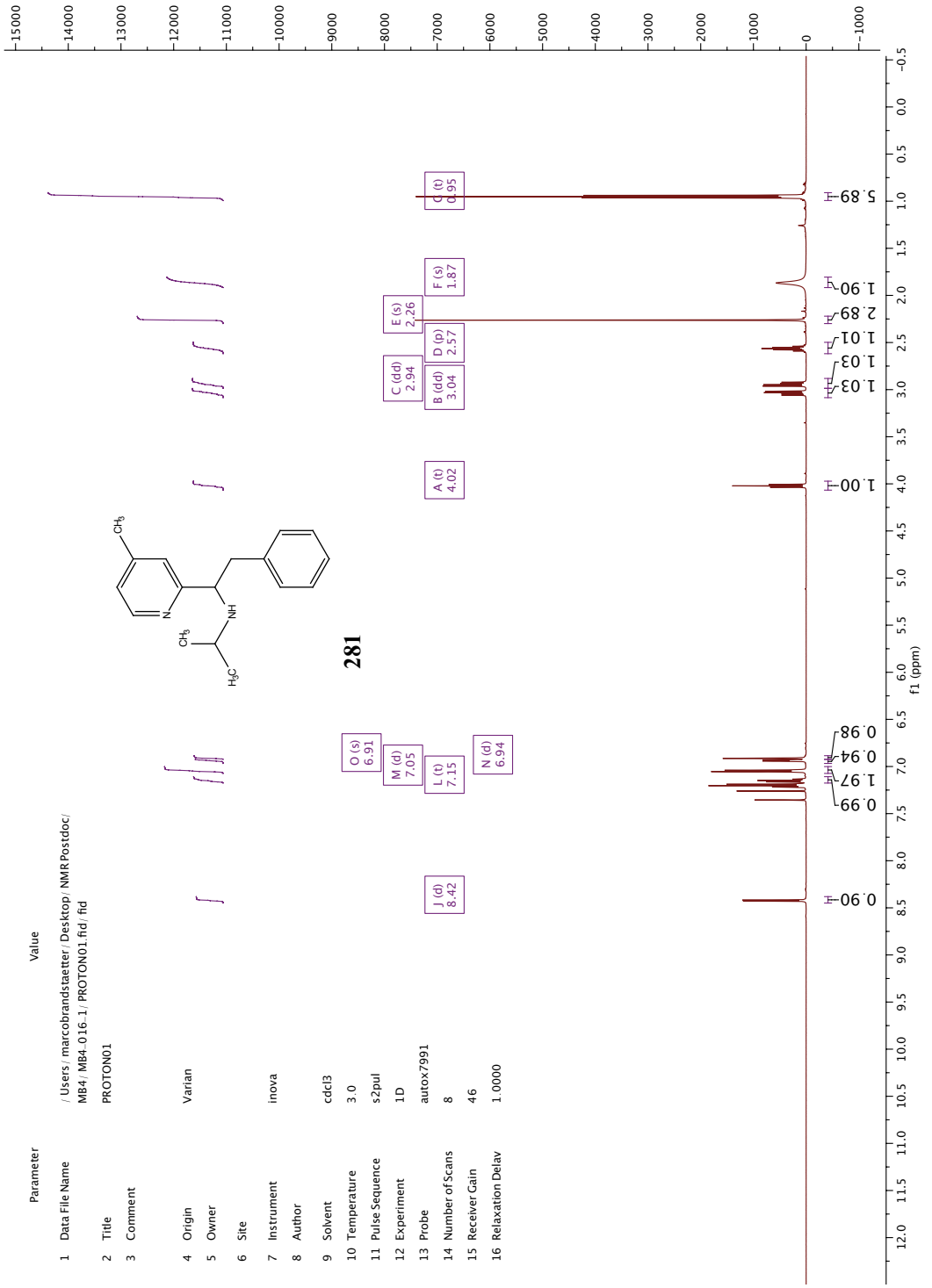
Parameter
Value
1 Data File Name
/ Users / marcobrandstaetter / Desktop / NMR Postdoc / MB4 / MB4-016-1 / PROTON01.fid / fid
2 Title
PROTON01
3 Comment
4 Origin
Varian
5 Owner
6 Site
7 Instrument
inova
8 Author
9 Solvent
cdcl3
10 Temperature
3.0
11 Pulse Sequence
s2pul
12 Experiment
1D
13 Probe
autox7991
14 Number of Scans
8
15 Receiver Gain
46
16 Relaxation Delay
1.0000
281
A (t) 4.02
B (dd) 3.04
C (dd) 2.94
D (p) 2.57
E (s) 2.26
F (s) 1.87
G (t) 0.95
J (d) 8.42
L (t) 7.15
M (d) 7.05
N (d) 6.94
O (s) 6.91
5.89
1.90
2.89
1.01
1.03
1.03
1.00
0.90
0.99
1.97
0.94
0.98
f1 (ppm)

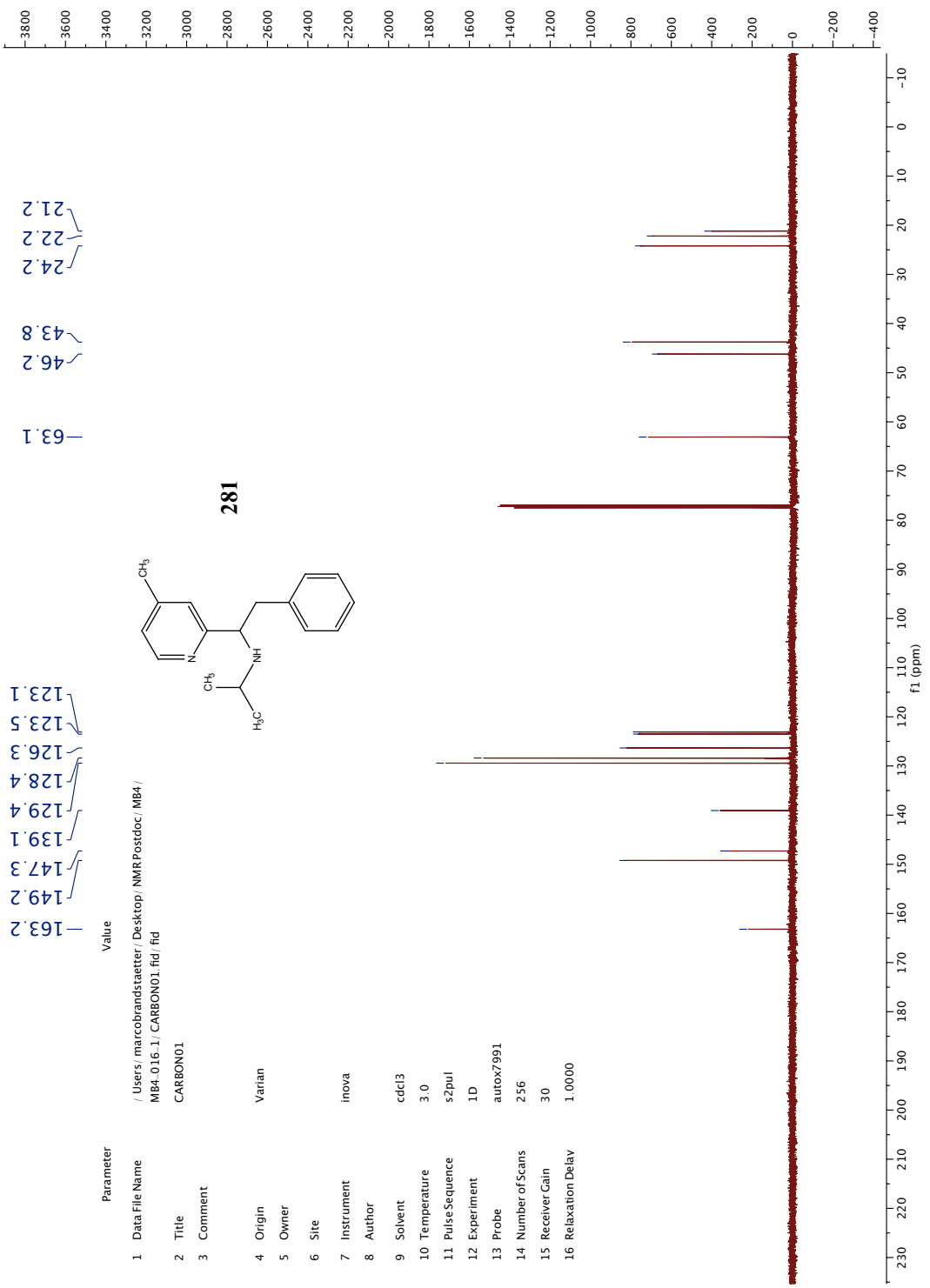

Parameter	Value
1 Data File Name	/Users/marcobrandstaetter/Desktop/NMR Postdoc/MB4/MB4-016-1/CARBON01.fid/fid
2 Title	CARBON01
3 Comment	
4 Origin	Varian
5 Owner	
6 Site	
7 Instrument	inova
8 Author	
9 Solvent	cdcl3
10 Temperature	3.0
11 Pulse Sequence	s2pul
12 Experiment	1D
13 Probe	autox7991
14 Number of Scans	256
15 Receiver Gain	30
16 Relaxation Delay	1.0000

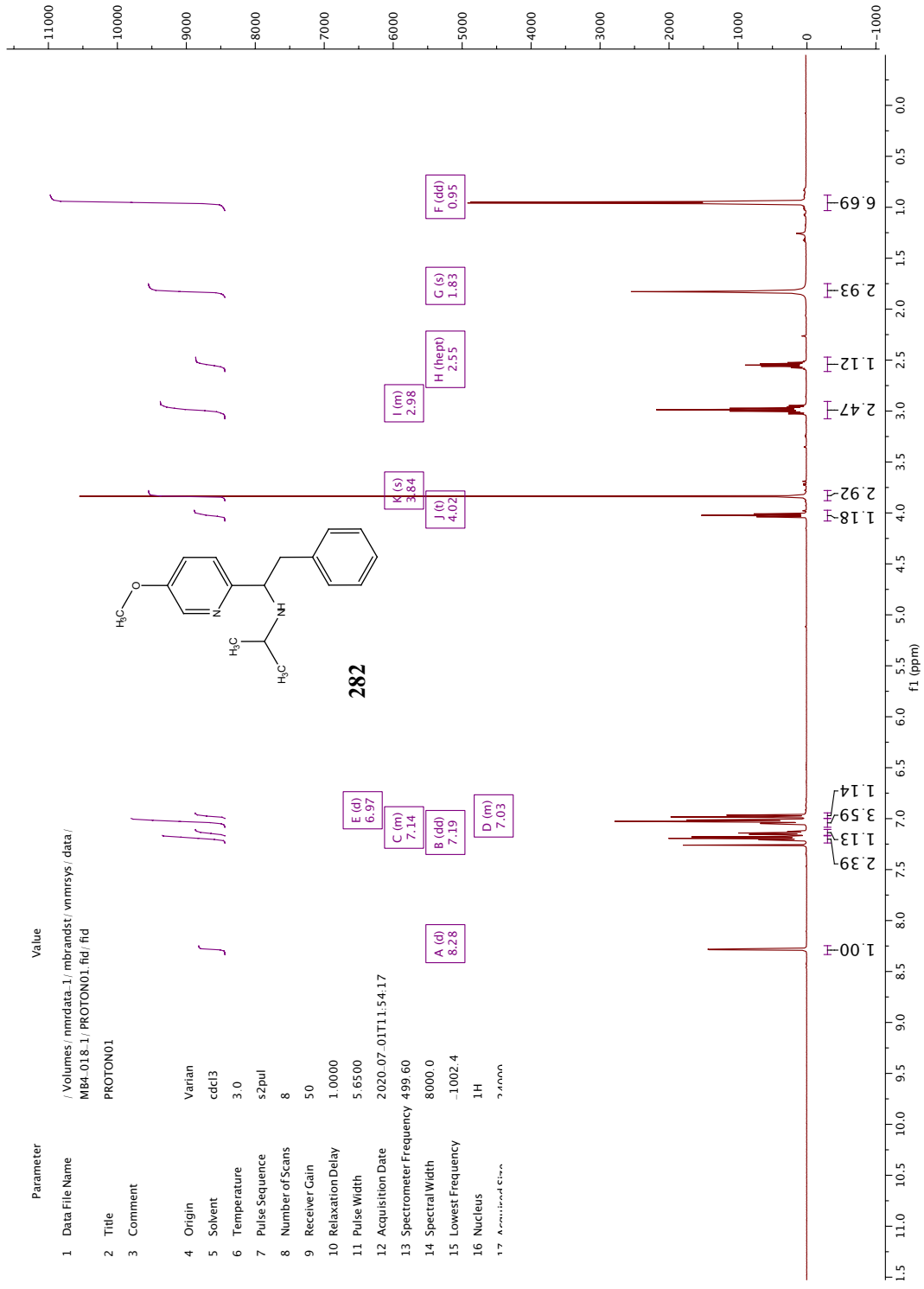
Parameter
Value
1 Data File Name /Volumes/nmrdata_1/mbrandst/vnmrsys/data/MB4-018-1/PROTON01.fid/fid
2 Title PROTON01
3 Comment
4 Origin Varian
5 Solvent cdcl3
6 Temperature 3.0
7 Pulse Sequence s2pul
8 Number of Scans 8
9 Receiver Gain 50
10 Relaxation Delay 1.0000
11 Pulse Width 5.6500
12 Acquisition Date 2020-07-01T11:54:17
13 Spectrometer Frequency 499.60
14 Spectral Width 8000.0
15 Lowest Frequency -1002.4
16 Nucleus 1H
A (d) 8.28
B (dd) 7.19
C (m) 7.14
D (m) 7.03
E (d) 6.97
F (dd) 0.95
G (s) 1.83
H (hept) 2.55
I (m) 2.98
J (t) 4.02
K (s) 3.84
282
1.00
2.39
1.13
3.59
1.14
1.18
2.92
2.47
1.12
2.93
6.69
f1 (ppm)

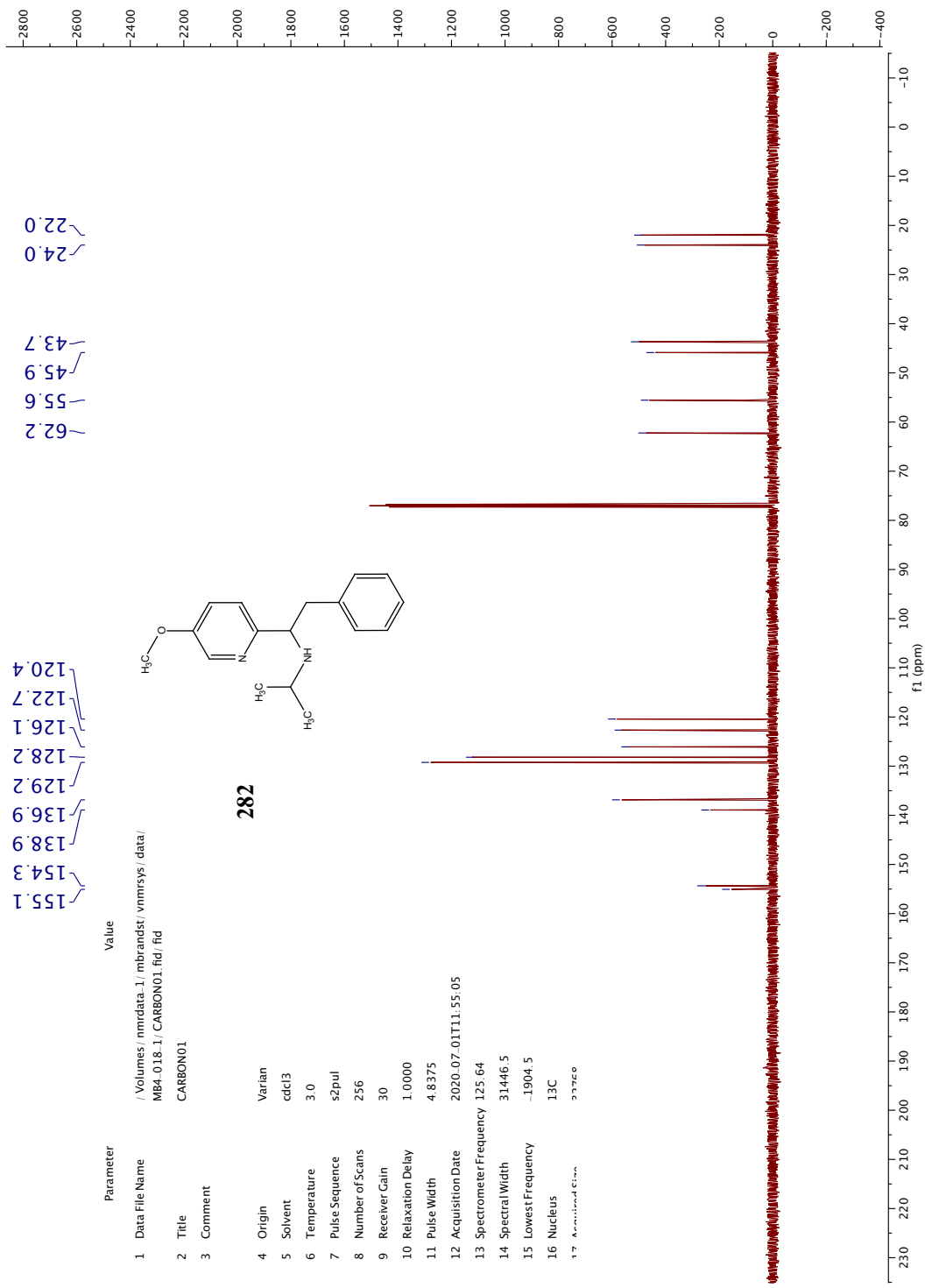
22.0
24.0
43.7
45.9
55.6
62.2
120.4
122.7
126.1
128.2
129.2
136.9
138.9
154.3
155.1
282
Parameter
Value
1 Data File Name
/ Volumes / nmrdata_1 / mbrandst / vnmrsys / data / MB4_018_1 / CARBON01.fid / fid
2 Title
3 Comment
CARBON01
4 Origin
Varian
5 Solvent
cdcl3
6 Temperature
3.0
7 Pulse Sequence
s2pul
8 Number of Scans
256
9 Receiver Gain
30
10 Relaxation Delay
1.0000
11 Pulse Width
4.8375
12 Acquisition Date
2020-07-01T11:55:05
13 Spectrometer Frequency
125.64
14 Spectral Width
31446.5
15 Lowest Frequency
-1904.5
16 Nucleus
13C
f1 (ppm)

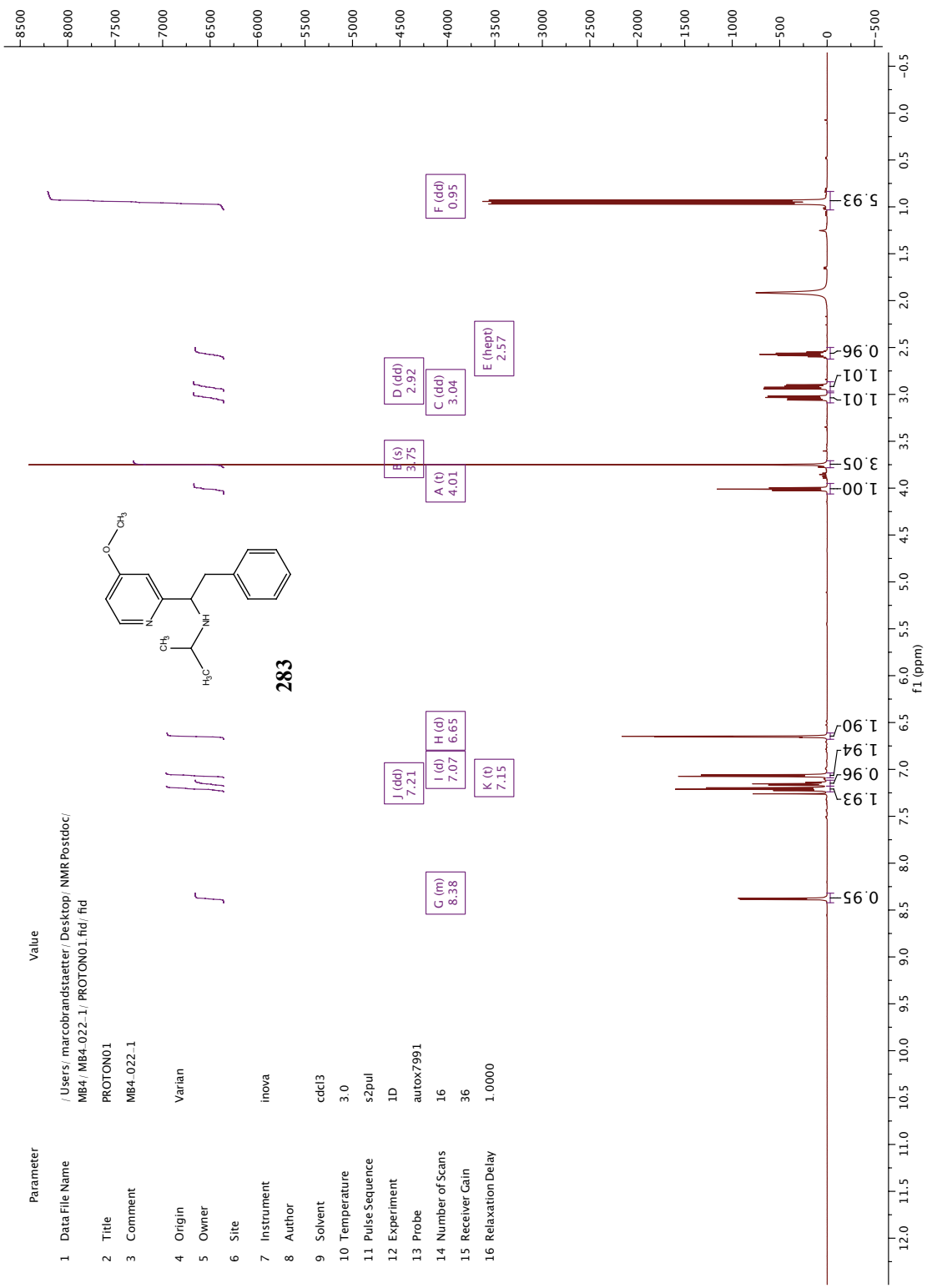
283
Parameter
Value
1 Data File Name
/ Users/ marcobrandstaetter/ Desktop/ NMR Postdoc/ MB4/ MB4.022.1/ PROTON01.fid/ fid
2 Title
PROTON01
3 Comment
MB4_022_1
4 Origin
Varian
5 Owner
6 Site
7 Instrument
inova
8 Author
9 Solvent
cdcl3
10 Temperature
3 0
11 Pulse Sequence
s2pul
12 Experiment
1D
13 Probe
autox7991
14 Number of Scans
16
15 Receiver Gain
36
16 Relaxation Delay
1.0000
G (m) 8.38
J (dd) 7.21
I (d) 7.07
H (d) 6.65
K (t) 7.15
B (s) 3.75
A (t) 4.01
D (dd) 2.92
C (dd) 3.04
E (hept) 2.57
F (dd) 0.95
5.93
0.96
1.01
1.01
3.05
1.00
1.90
1.94
0.96
1.93
0.95
f1 (ppm)

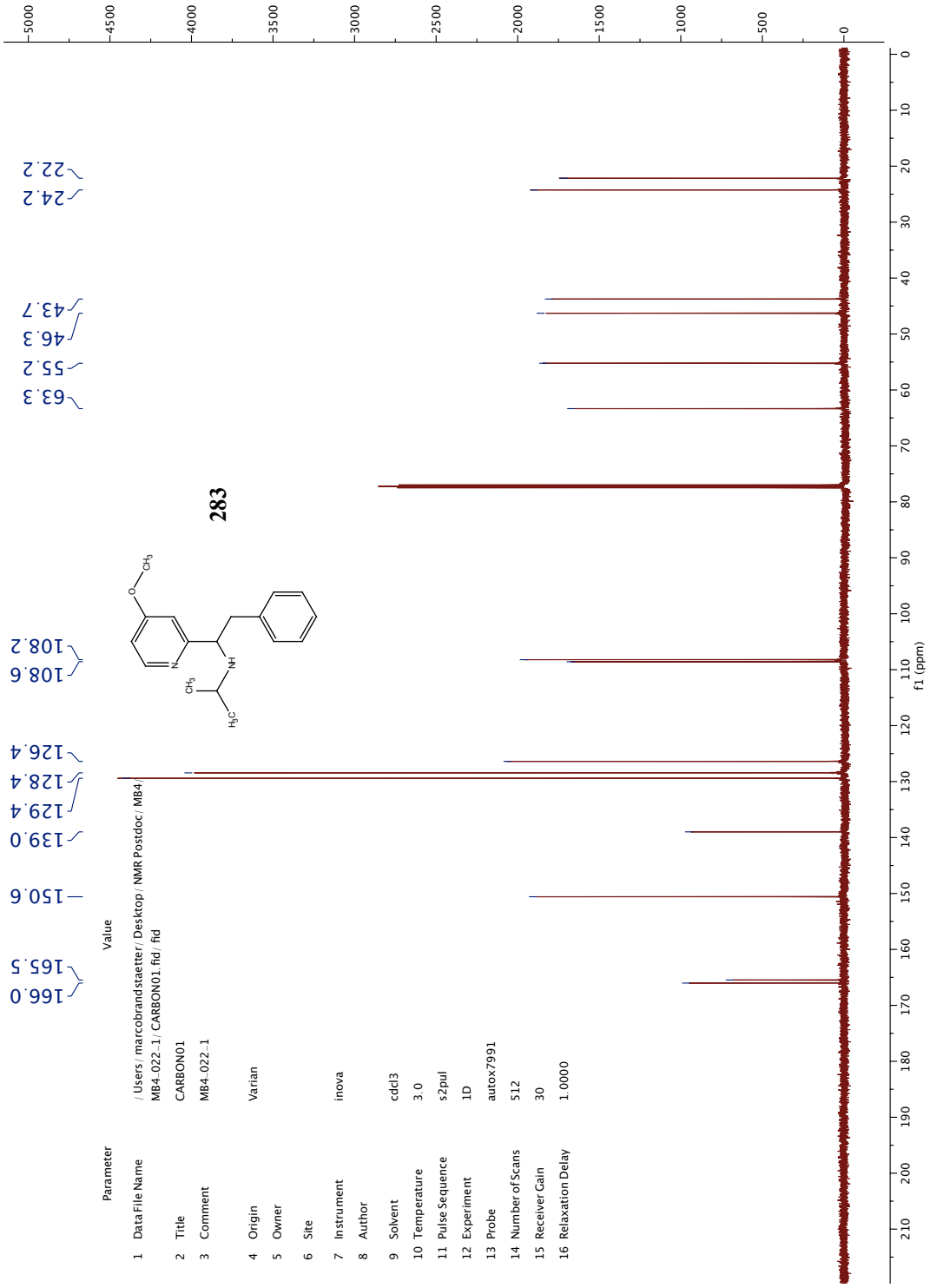
283
22.2
24.2
43.7
46.3
55.2
63.3
108.2
108.6
126.4
128.4
129.4
139.0
150.6
165.5
166.0
f1 (ppm)
Parameter
Value
1 DataFile Name / Users / marcobrandstaetter / Desktop / NMR Postdoc / MB4 / MB4-022-1 / CARBON01.fid / fid
2 Title CARBON01
3 Comment MB4-022-1
4 Origin Varian
5 Owner
6 Site
7 Instrument inova
8 Author
9 Solvent cdd3
10 Temperature 3.0
11 Pulse Sequence s2pul
12 Experiment 1D
13 Probe autox7991
14 Number of Scans 512
15 Receiver Gain 30
16 Relaxation Delay 1.0000

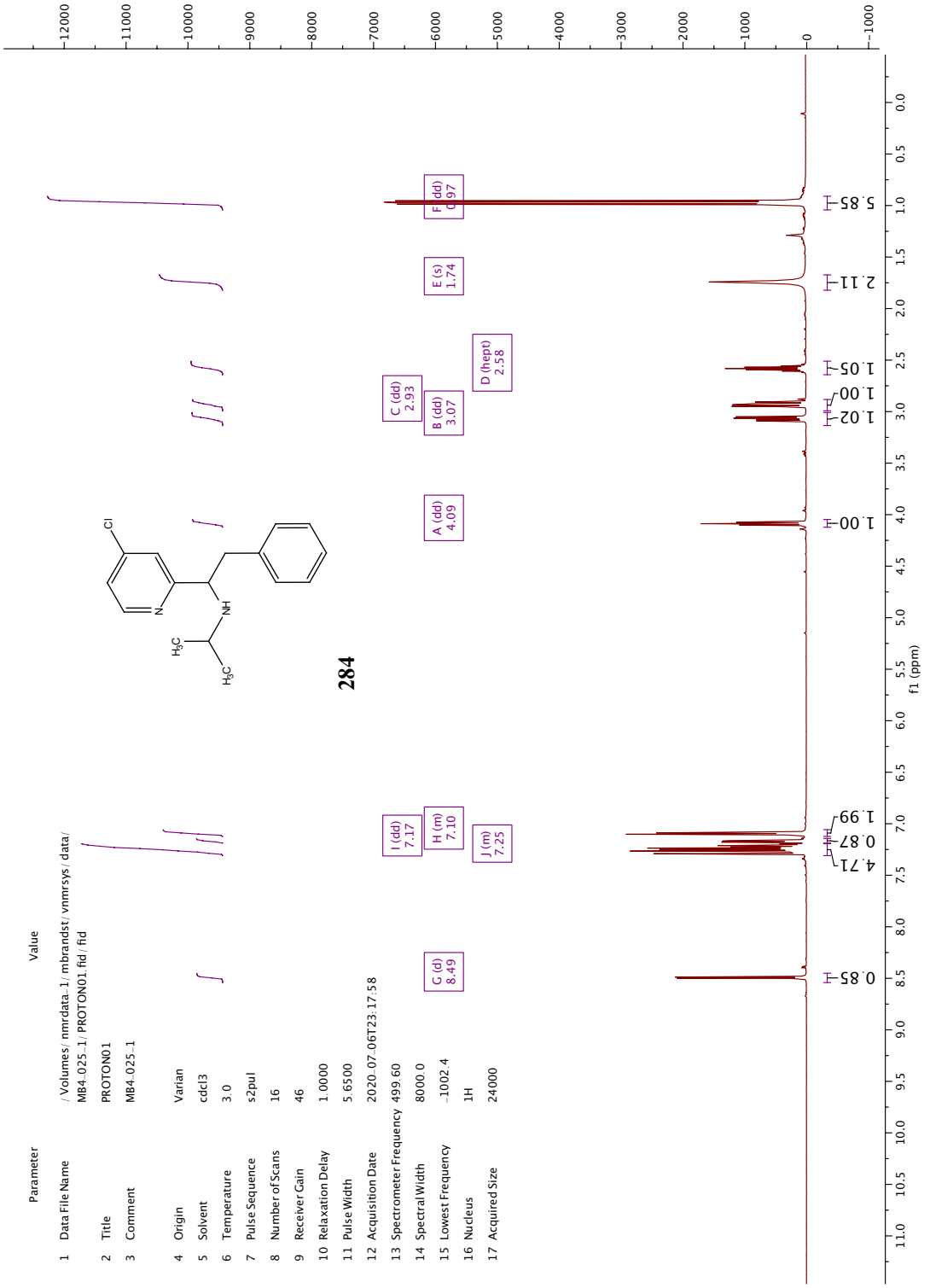
Parameter
Value
1 Data File Name /Volumes/nmrdata_1/mbrandst/vnmrsys/data/MB4.025-1/PROTON01.fid/fid
2 Title PROTON01
3 Comment MB4.025-1
4 Origin Varian
5 Solvent cdcl3
6 Temperature 3.0
7 Pulse Sequence s2pul
8 Number of Scans 16
9 Receiver Gain 46
10 Relaxation Delay 1.0000
11 Pulse Width 5.6500
12 Acquisition Date 2020-07-06T23:17:58
13 Spectrometer Frequency 499.60
14 Spectral Width 8000.0
15 Lowest Frequency -1002.4
16 Nucleus 1H
17 Acquired Size 24000
284
G (d) 8.49
I (dd) 7.17
H (m) 7.10
J (m) 7.25
A (dd) 4.09
C (dd) 2.93
B (dd) 3.07
D (hept) 2.58
E (s) 1.74
F (dd) 0.97
0.85
4.71
0.87
1.99
1.00
1.02
1.00
1.05
2.11
5.85
f1 (ppm)

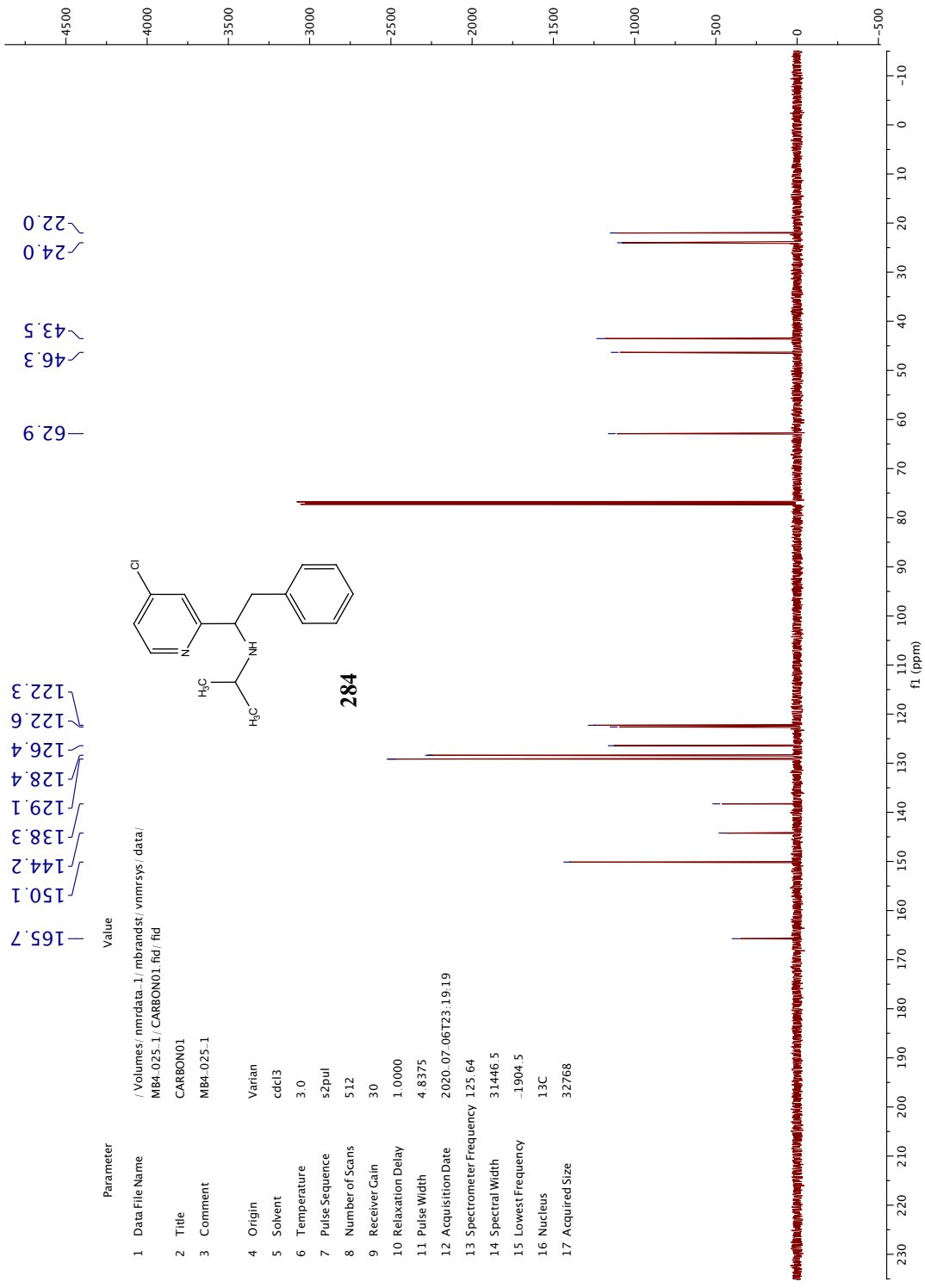

	Parameter	Value
1	Data File Name	/ Volumes/ nmrdata_1/ mbrandst/ vnmrsys/ data/ MB4.025_1/ CARBON01.fid/ fid
2	Title	CARBON01
3	Comment	MB4.025_1
4	Origin	Varian
5	Solvent	cdcl3
6	Temperature	3.0
7	Pulse Sequence	s2pul
8	Number of Scans	512
9	Receiver Gain	30
10	Relaxation Delay	1.0000
11	Pulse Width	4.8375
12	Acquisition Date	2020_07_06T23:19:19
13	Spectrometer Frequency	125.64
14	Spectral Width	31446.5
15	Lowest Frequency	-1904.5
16	Nucleus	13C
17	Acquired Size	32768

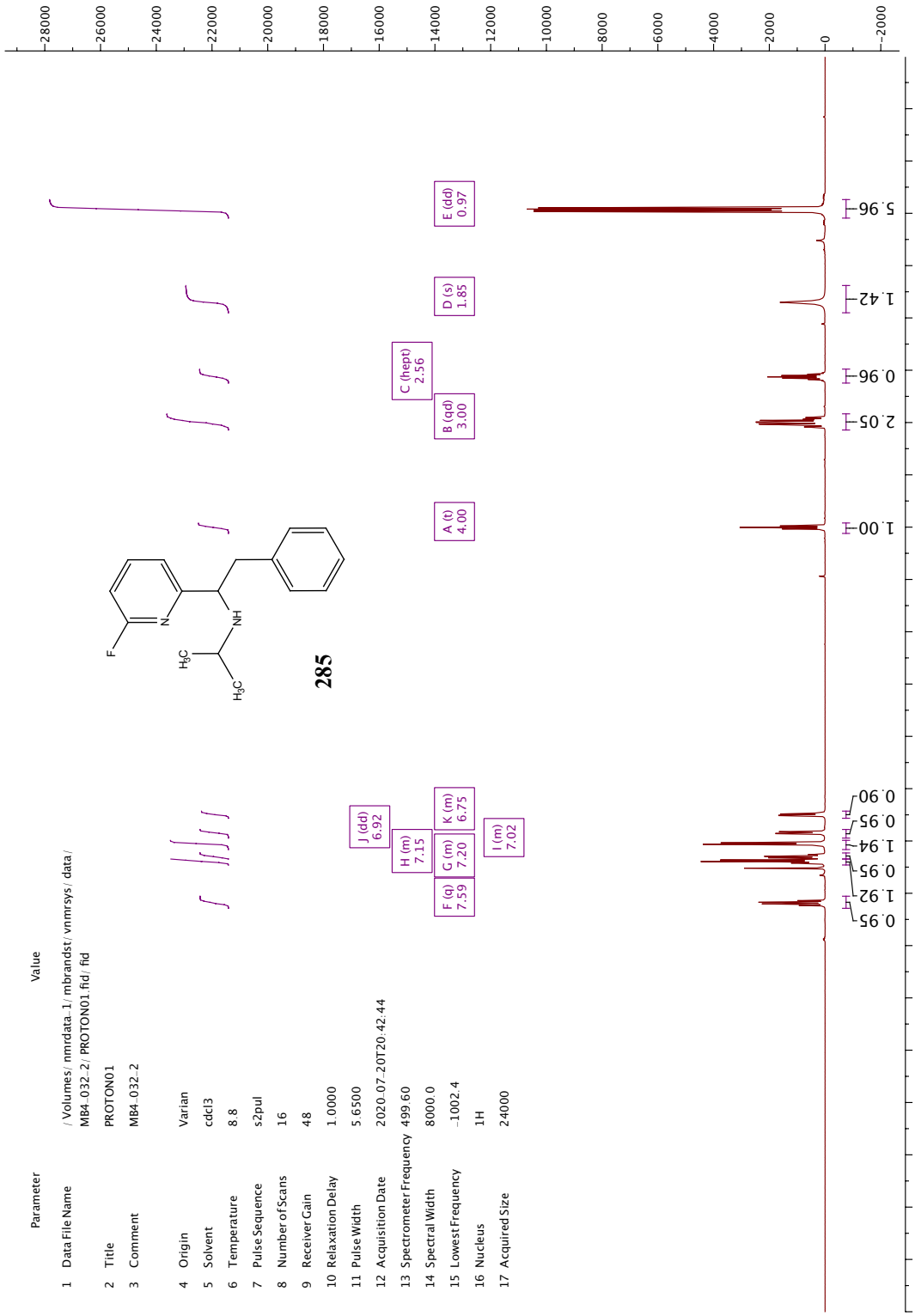
Parameter
Value
1 Data File Name / Volumes/ nmrdata_1/ mbrandst/ vnmrsys/ data / MB4-032-2/ PROTON01.fid/ fid
2 Title PROTON01
3 Comment MB4-032-2
4 Origin Varian
5 Solvent cdcl3
6 Temperature 8.8
7 Pulse Sequence s2pul
8 Number of Scans 16
9 Receiver Gain 48
10 Relaxation Delay 1.0000
11 Pulse Width 5.6500
12 Acquisition Date 2020-07-20T20:42:44
13 Spectrometer Frequency 499.60
14 Spectral Width 8000.0
15 Lowest Frequency -1002.4
16 Nucleus 1H
17 Acquired Size 24000
285
F (q) 7.59
G (m) 7.20
H (m) 7.15
J (dd) 6.92
K (m) 6.75
I (m) 7.02
A (t) 4.00
B (qd) 3.00
C (hept) 2.56
D (s) 1.85
E (dd) 0.97
5.96
1.42
0.96
2.05
1.00
0.90
0.95
1.94
0.95
1.92
0.95
f1 (ppm)

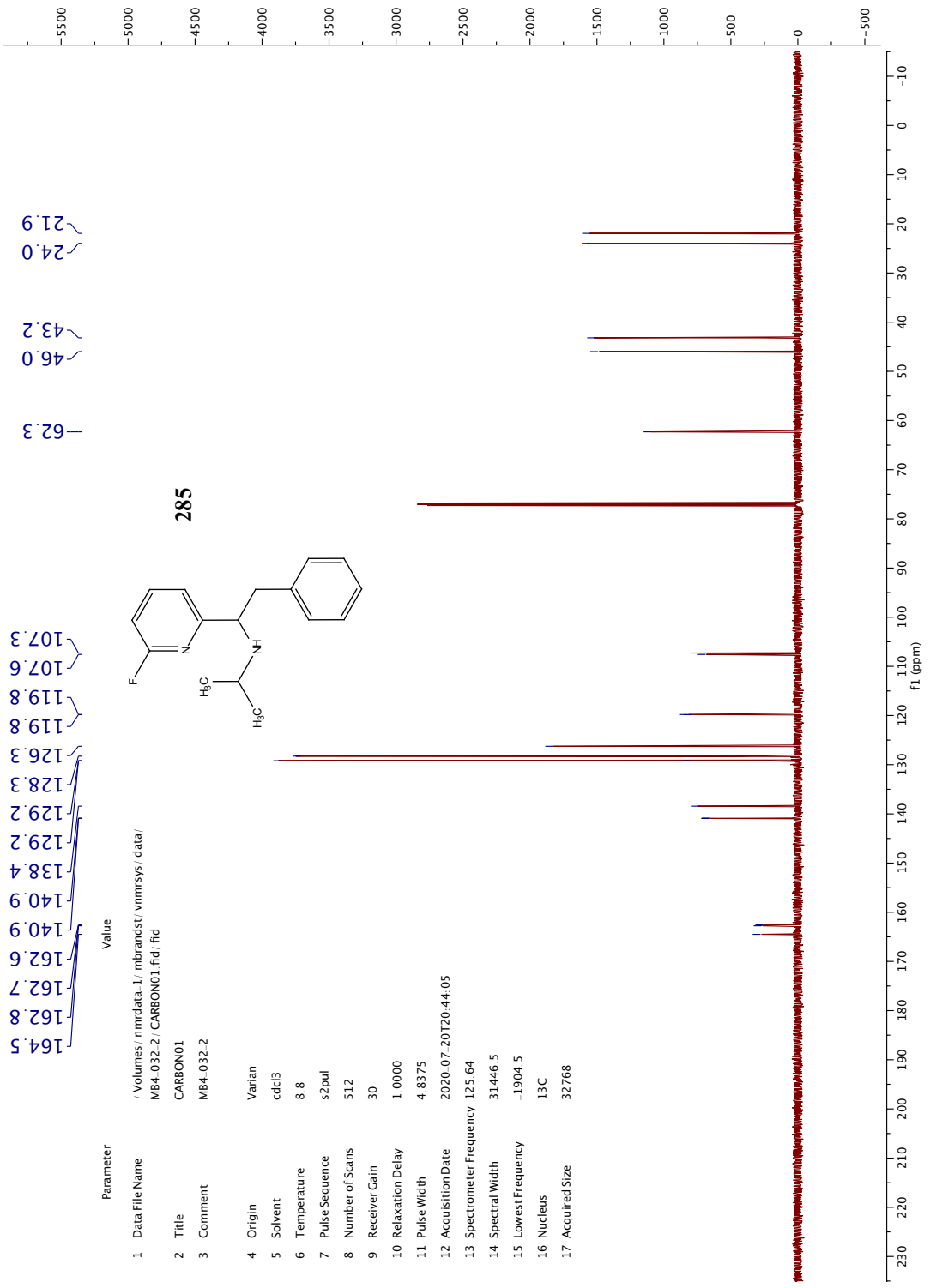

	Parameter	Value
1	Data File Name	/Volumes/nmrdata_1/mbrandst/vnmrsys/data/MB4-032-2/CARBON01.fid/fid
2	Title	CARBON01
3	Comment	MB4-032-2
4	Origin	Varian
5	Solvent	cdcl3
6	Temperature	8.8
7	Pulse Sequence	s2pul
8	Number of Scans	512
9	Receiver Gain	30
10	Relaxation Delay	1.0000
11	Pulse Width	4.8375
12	Acquisition Date	2020-07-20T20:44:05
13	Spectrometer Frequency	125.64
14	Spectral Width	31446.5
15	Lowest Frequency	-1904.5
16	Nucleus	13C
17	Acquired Size	32768

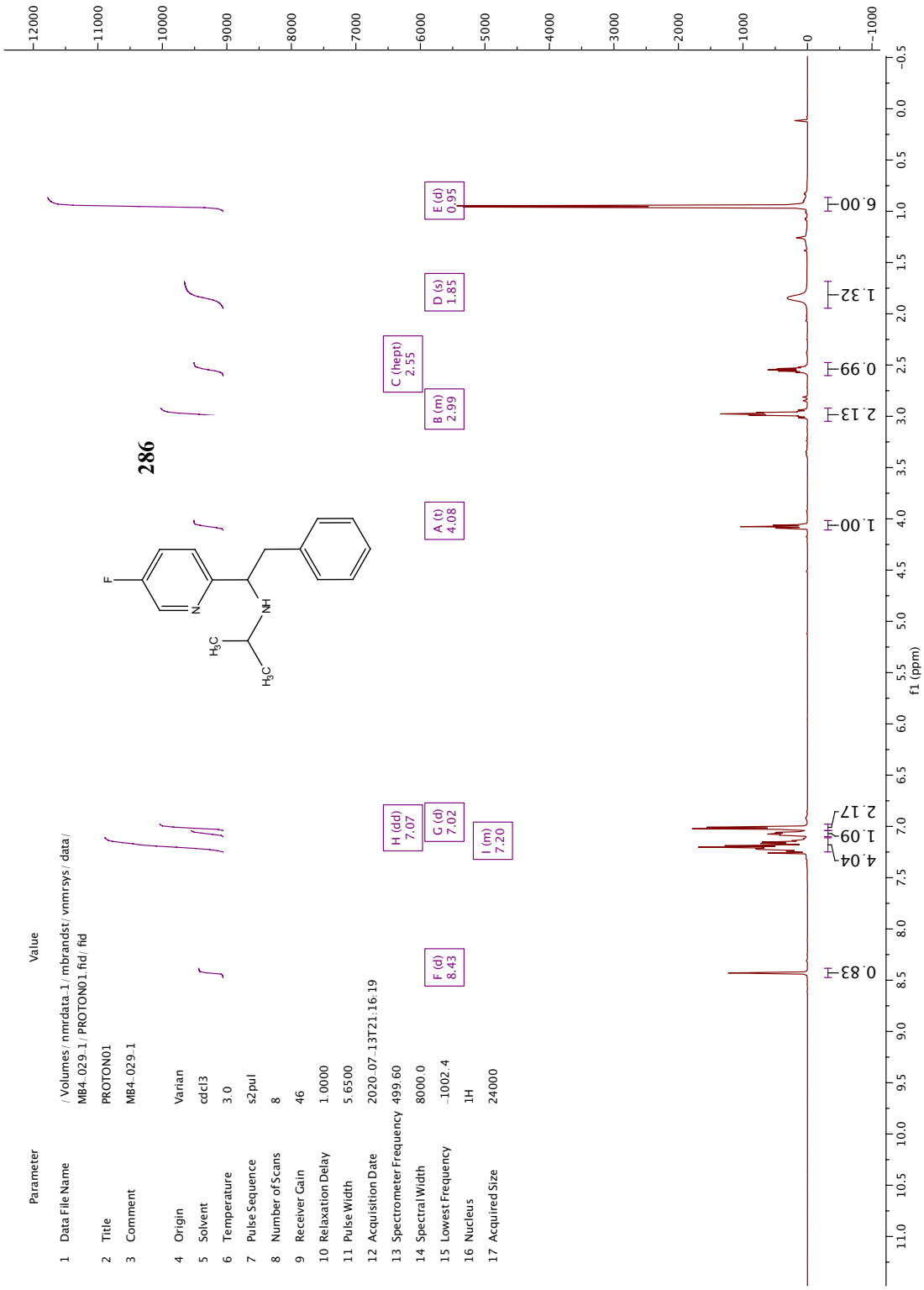

	Parameter	Value
1	Data File Name	/Volumes/nmrdata_1/mbrandst/vnmrsys/data/MB4_029_1/PROTON01.fid/fid
2	Title	PROTON01
3	Comment	MB4_029_1
4	Origin	Varian
5	Solvent	cdcl3
6	Temperature	3.0
7	Pulse Sequence	s2pul
8	Number of Scans	8
9	Receiver Gain	46
10	Relaxation Delay	1.0000
11	Pulse Width	5.6500
12	Acquisition Date	2020_07_13T21:16:19
13	Spectrometer Frequency	499.60
14	Spectral Width	8000.0
15	Lowest Frequency	-1002.4
16	Nucleus	1H
17	Acquired Size	24000

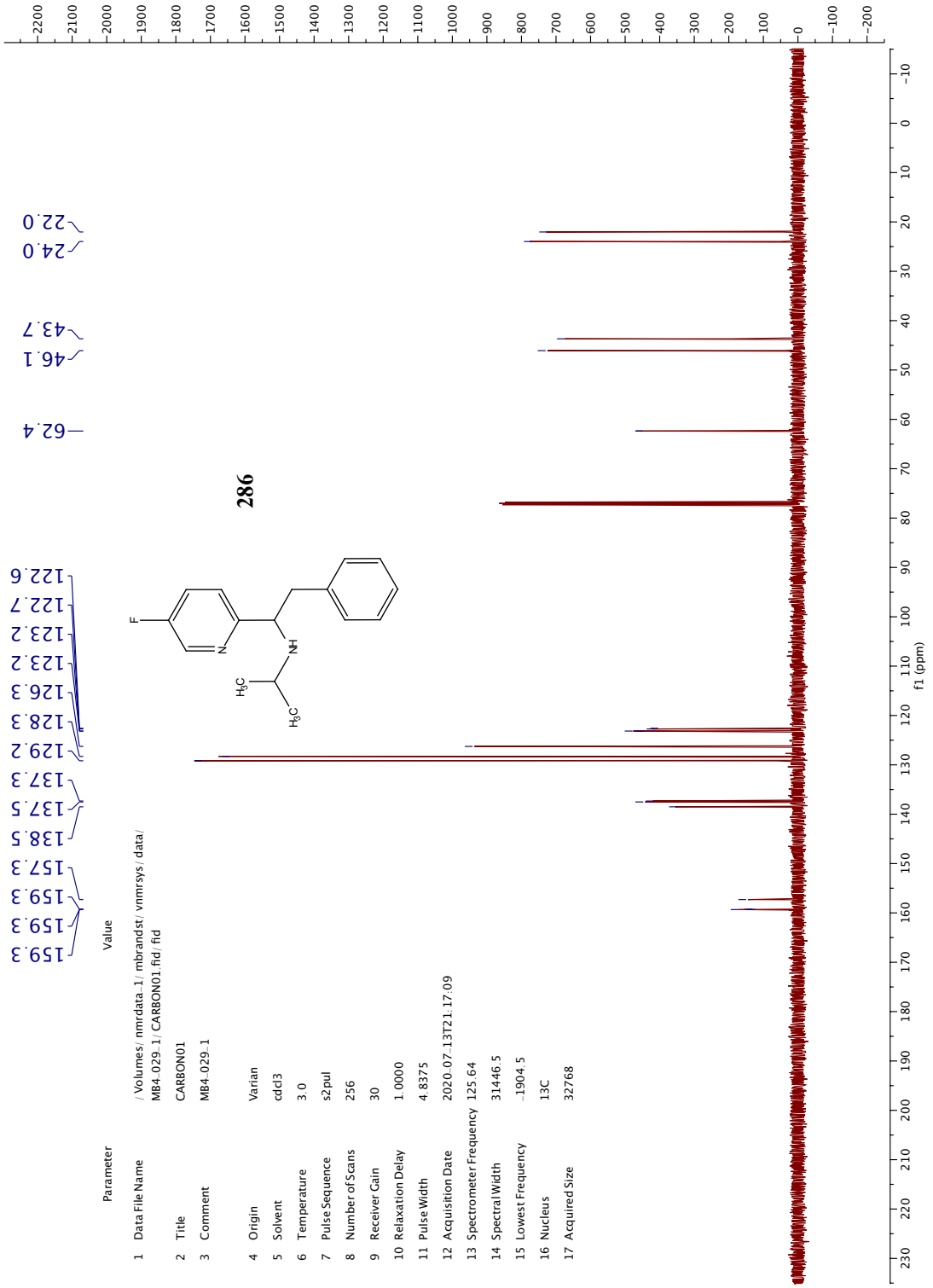

	Parameter	Value
1	Data File Name	/Volumes/nmrdata_1/mbrandst/vnmrsys/data/MB4.029.1/CARBON01.fid/fid
2	Title	CARBON01
3	Comment	MB4.029.1
4	Origin	Varian
5	Solvent	cdcl3
6	Temperature	3.0
7	Pulse Sequence	s2pul
8	Number of Scans	256
9	Receiver Gain	30
10	Relaxation Delay	1.0000
11	Pulse Width	4.8375
12	Acquisition Date	2020-07-13T21:17:09
13	Spectrometer Frequency	125.64
14	Spectral Width	31446.5
15	Lowest Frequency	-1904.5
16	Nucleus	13C
17	Acquired Size	32768

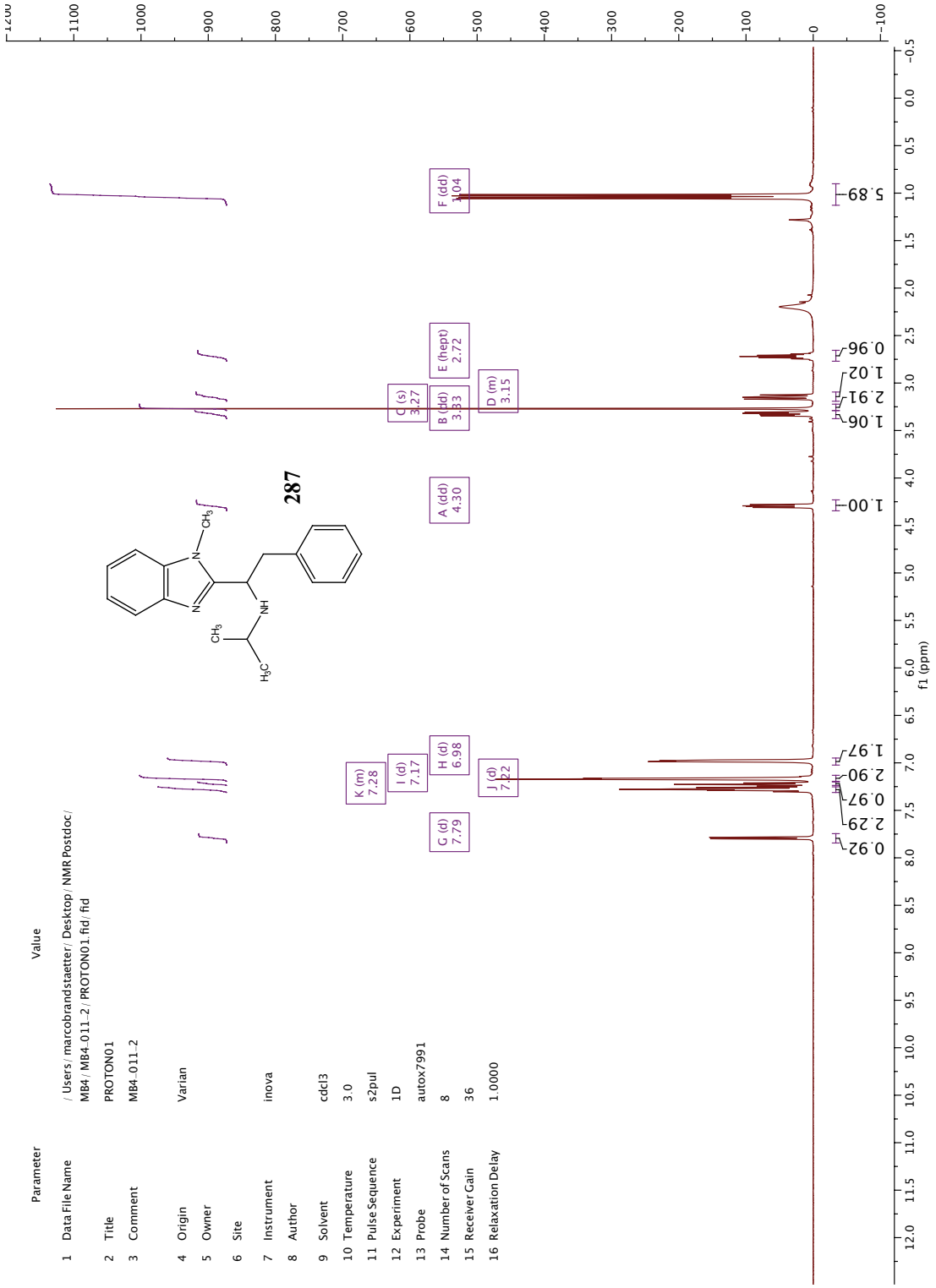
287
A (dd) 4.30
B (dd) 3.33
C (s) 3.27
D (m) 3.15
E (hept) 2.72
F (dd) 1.04
G (d) 7.79
H (d) 6.98
I (d) 7.17
J (d) 7.22
K (m) 7.28
5.89
1.00
0.96
1.02
2.91
1.06
0.92
2.29
0.97
2.90
1.97
f1 (ppm)
Parameter
Value
1 Data File Name / Users / marcobrandstaetter / Desktop / NMR Postdoc / MB4 / MB4-011-2 / PROTON01.fid / fid
2 Title PROTON01
3 Comment MB4-011-2
4 Origin Varian
5 Owner
6 Site
7 Instrument inova
8 Author
9 Solvent cdcl3
10 Temperature 3.0
11 Pulse Sequence s2pul
12 Experiment 1D
13 Probe autox7991
14 Number of Scans 8
15 Receiver Gain 36
16 Relaxation Delay 1.0000

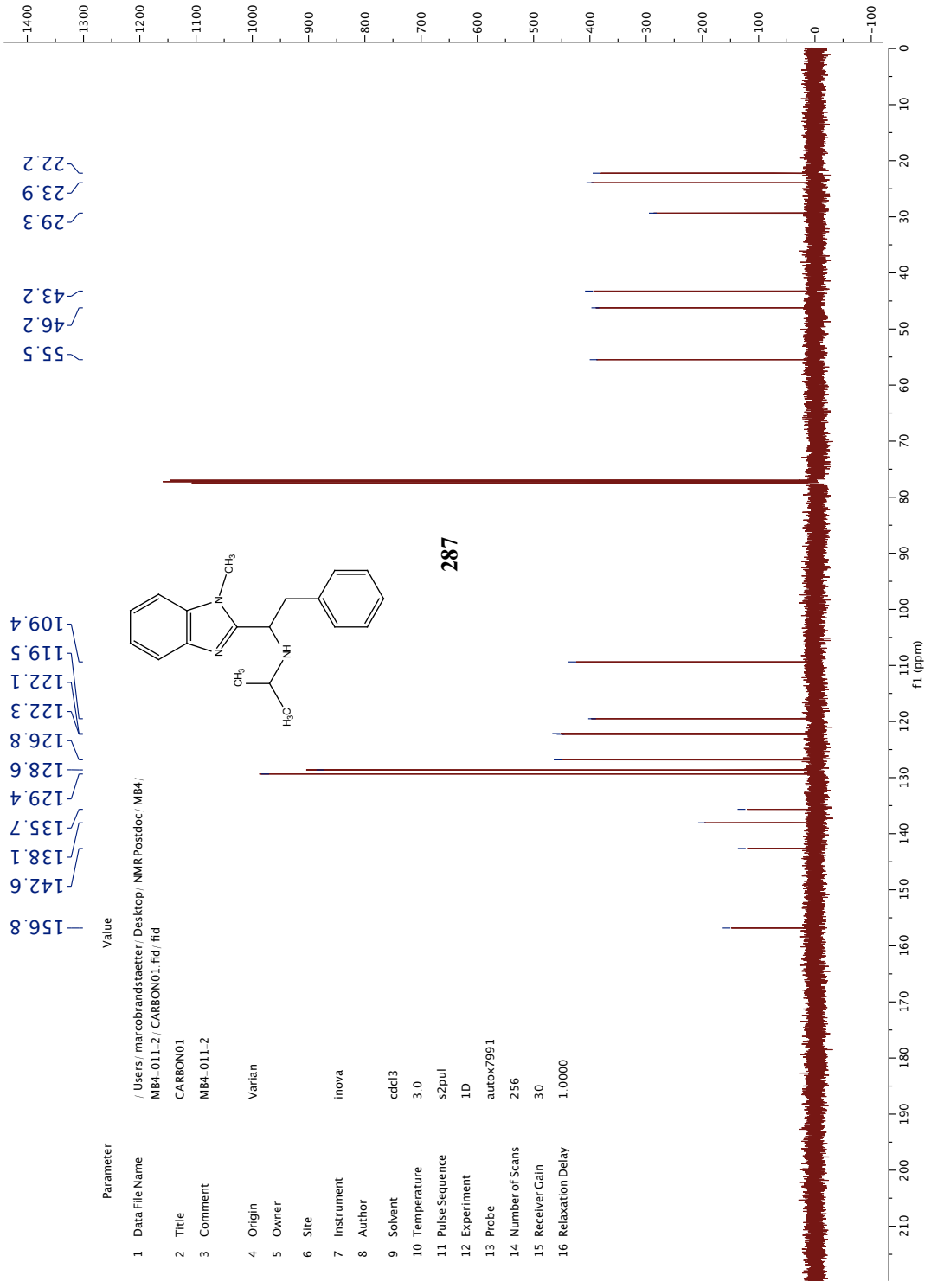
22.2
23.9
29.3
43.2
46.2
55.5
109.4
119.5
122.1
122.3
126.8
128.6
129.4
135.7
138.1
142.6
156.8
287
Parameter
Value
1 Data File Name / Users/ marcobrandstaetter/ Desktop/ NMR Postdoc/ MB4/ MB4-011-2/ CARBON01.fid/ fid
2 Title CARBON01
3 Comment MB4-011-2
4 Origin Varian
5 Owner
6 Site
7 Instrument inova
8 Author
9 Solvent cdcl3
10 Temperature 3.0
11 Pulse Sequence s2pul
12 Experiment 1D
13 Probe autox7991
14 Number of Scans 256
15 Receiver Gain 30
16 Relaxation Delay 1.0000
f1 (ppm)

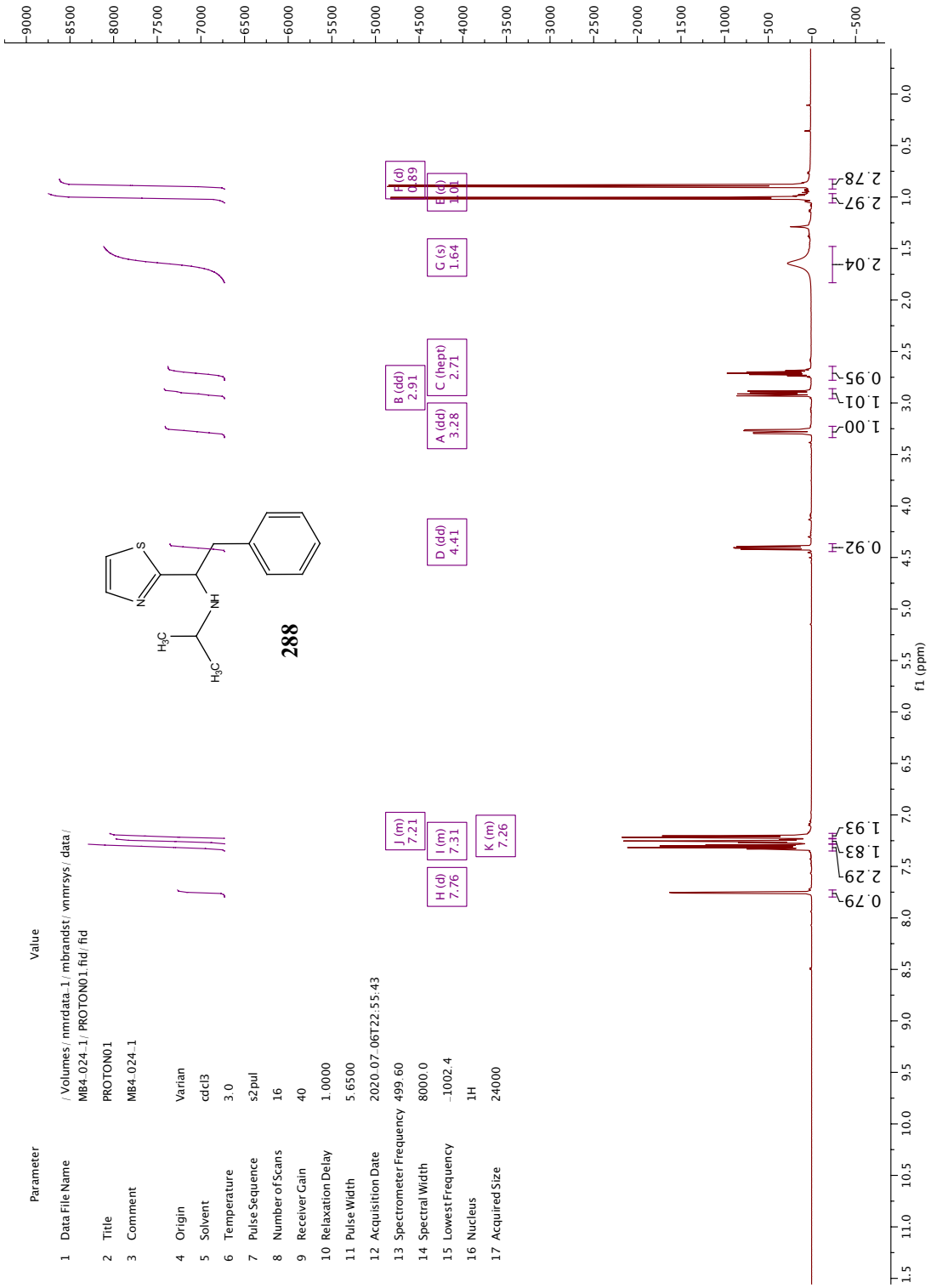

	Parameter	Value
1	Data File Name	/ Volumes / nmrdata_1 / mbrandst / vnmrsys / data / MB4_024_1 / PROTON01.fid / fid
2	Title	PROTON01
3	Comment	MB4_024_1
4	Origin	Varian
5	Solvent	cdcl3
6	Temperature	3.0
7	Pulse Sequence	s2pul
8	Number of Scans	16
9	Receiver Gain	40
10	Relaxation Delay	1.0000
11	Pulse Width	5.6500
12	Acquisition Date	2020-07-06T22:55:43
13	Spectrometer Frequency	499.60
14	Spectral Width	8000.0
15	Lowest Frequency	-1002.4
16	Nucleus	1H
17	Acquired Size	24000

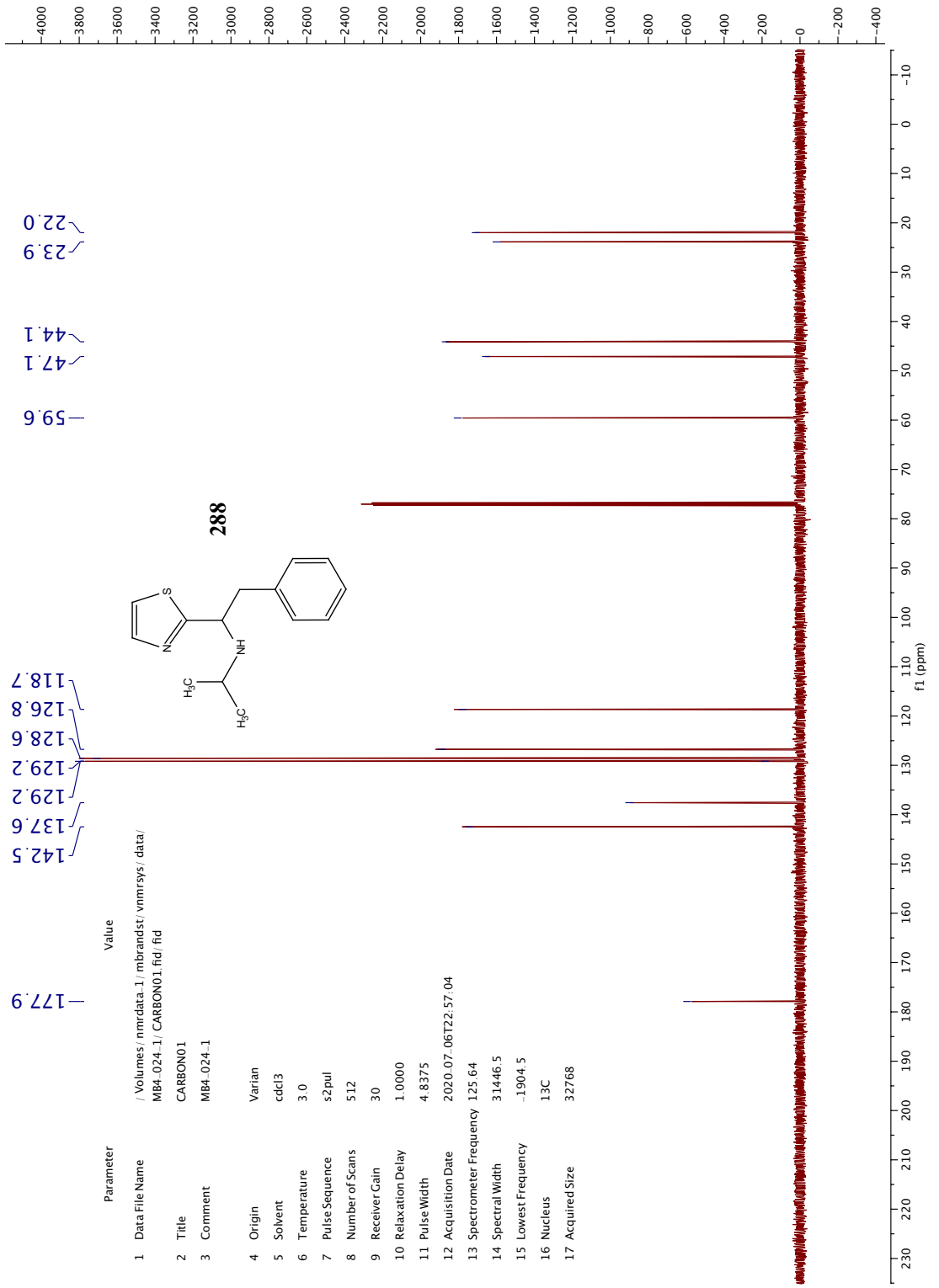
288
177.9
142.5
137.6
129.2
129.2
129.2
128.6
126.8
118.7
59.6
47.1
44.1
23.9
22.0
f1 (ppm)
Parameter Value
1 Data File Name /Volumes/nmrdata_1/mbrandst/vnmrsys/data/MB4_024_1/CARBON01.fid/fid
2 Title CARBON01
3 Comment MB4_024_1
4 Origin Varian
5 Solvent cdcl3
6 Temperature 3.0
7 Pulse Sequence s2pul
8 Number of Scans 512
9 Receiver Gain 30
10 Relaxation Delay 1.0000
11 Pulse Width 4.8375
12 Acquisition Date 2020-07-06T22:57:04
13 Spectrometer Frequency 125.64
14 Spectral Width 31446.5
15 Lower Frequency -1904.5
16 Nucleus 13C
17 Acquired Size 32768

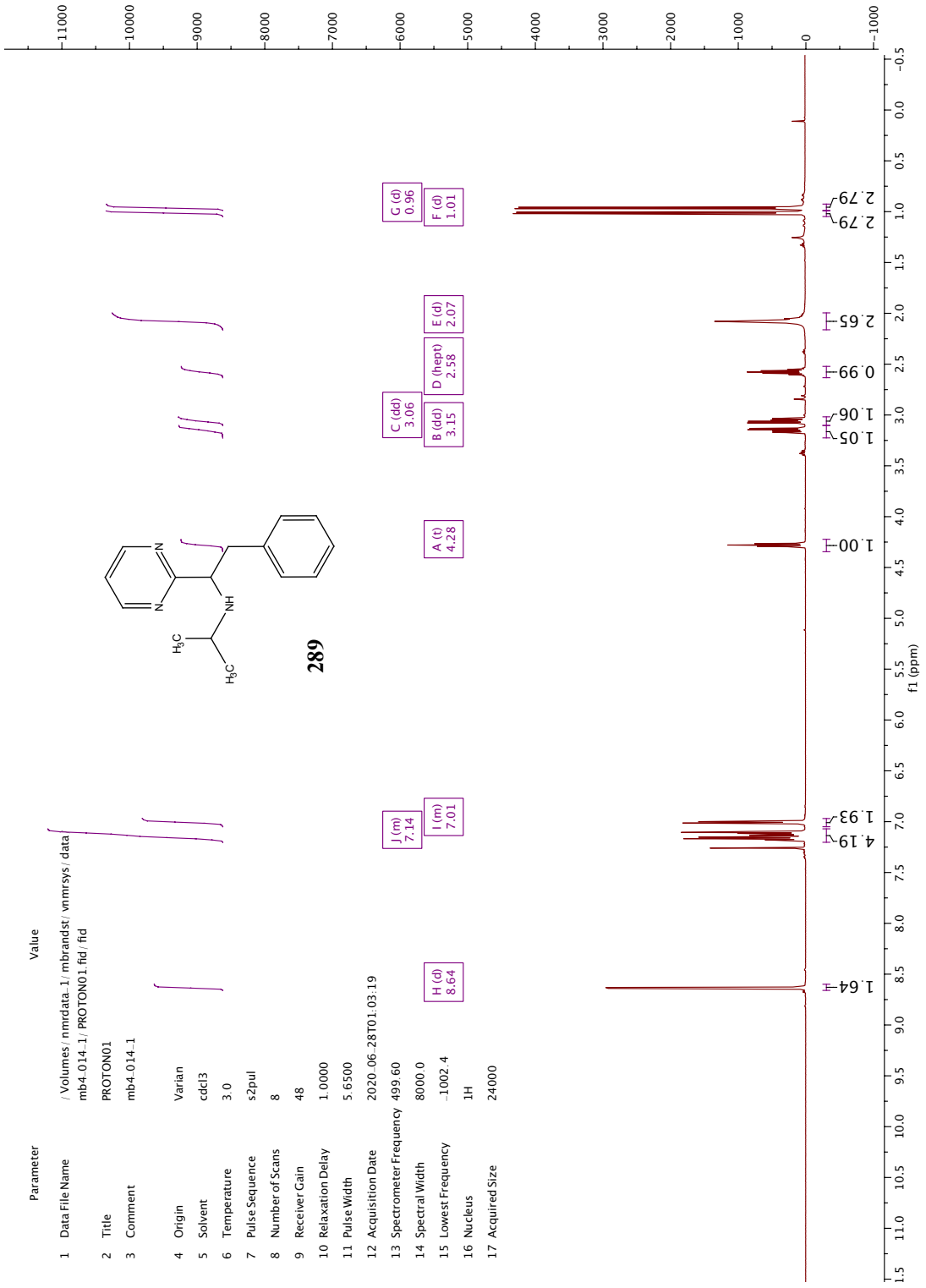
Parameter
Value
1 Data File Name /Volumes/nmrdata_1/mbrandst/vnmrsys/data/mb4_014_1/PROTON01.fid/fid
2 Title PROTON01
3 Comment mb4_014_1
4 Origin Varian
5 Solvent cdcl3
6 Temperature 3.0
7 Pulse Sequence s2pul
8 Number of Scans 8
9 Receiver Gain 48
10 Relaxation Delay 1.0000
11 Pulse Width 5.6500
12 Acquisition Date 2020_06_28T01:03:19
13 Spectrometer Frequency 499.60
14 Spectral Width 8000.0
15 Lowest Frequency -1002.4
16 Nucleus 1H
17 Acquired Size 24000
H (d) 8.64
I (m) 7.01
J (m) 7.14
A (t) 4.28
B (dd) 3.15
C (dd) 3.06
D (hept) 2.58
E (d) 2.07
F (d) 1.01
G (d) 0.96
289
1.64
4.19
1.93
1.00
1.05
1.06
0.99
2.65
2.79
2.79
f1 (ppm)

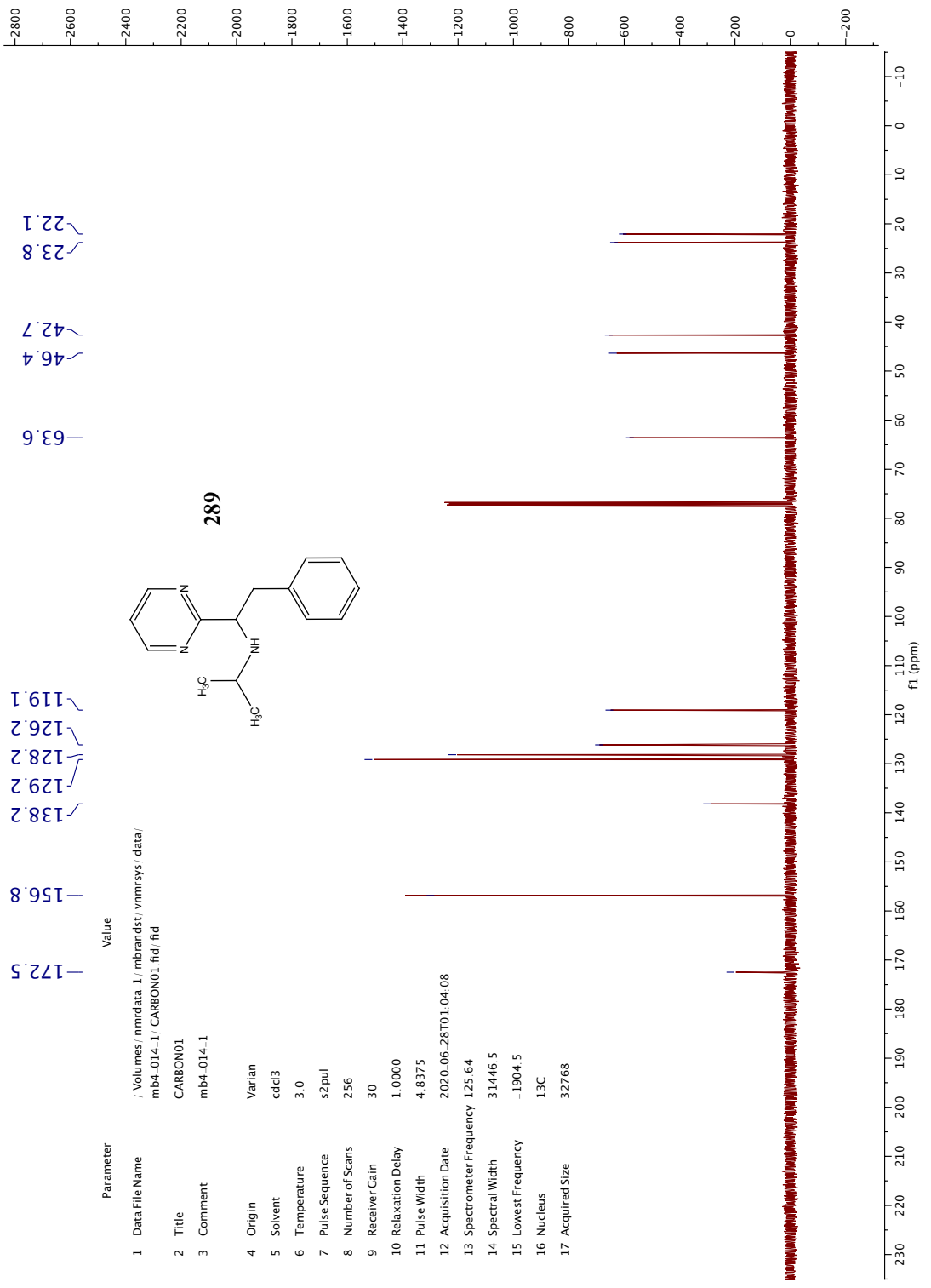

Parameter	Value
1 Data File Name	/ Volumes / nmrdata_1 / mbrandst / vnmrsys / data / mb4_014_1 / CARBON01.fid / fid
2 Title	CARBON01
3 Comment	mb4_014_1
4 Origin	Varian
5 Solvent	cdcl3
6 Temperature	30
7 Pulse Sequence	s2pul
8 Number of Scans	256
9 Receiver Gain	30
10 Relaxation Delay	1.0000
11 Pulse Width	4.8375
12 Acquisition Date	2020-06-28T01:04:08
13 Spectrometer Frequency	125.64
14 Spectral Width	31446.5
15 Lowest Frequency	-1904.5
16 Nucleus	13C
17 Acquired Size	32768

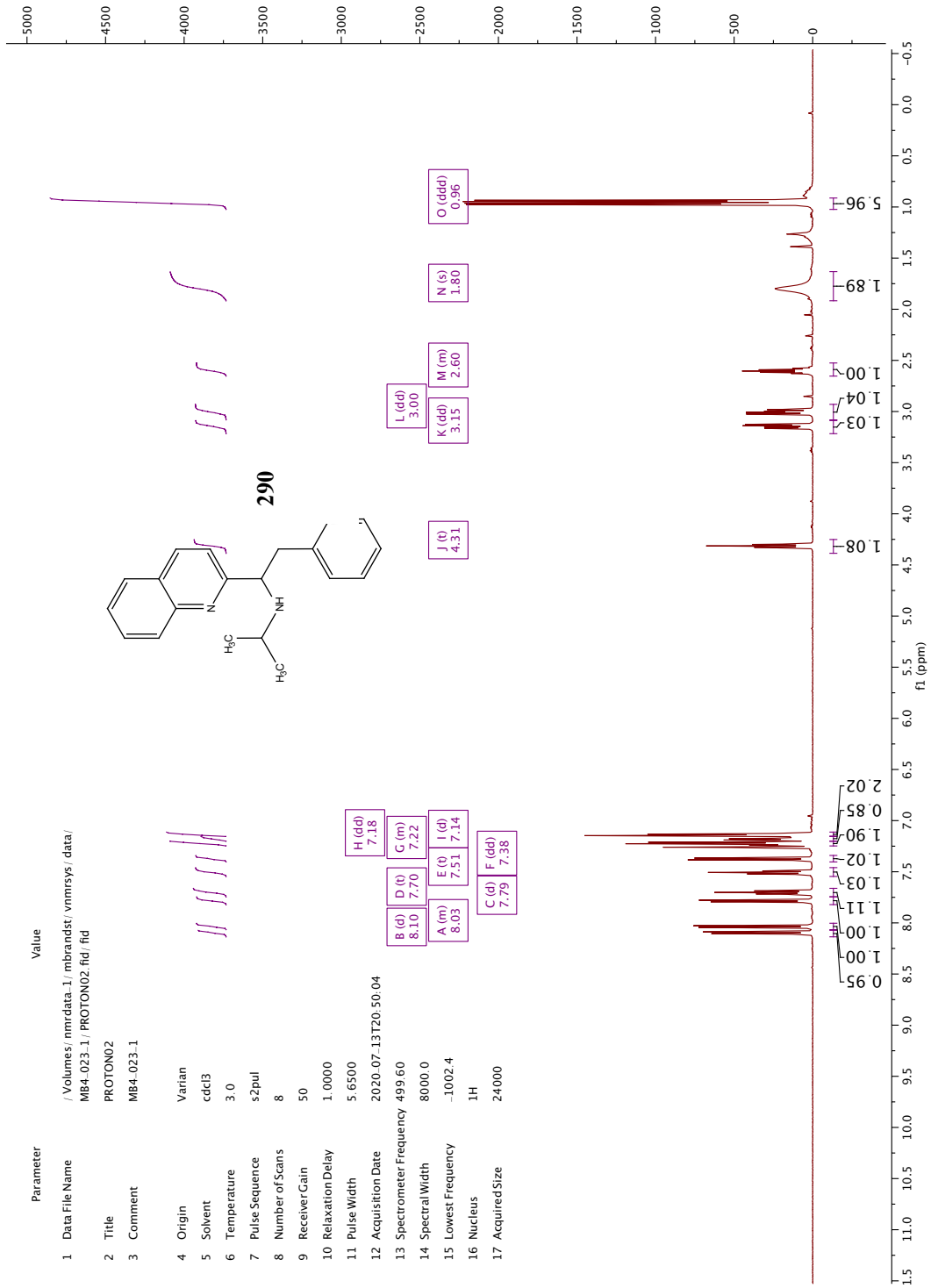
290
Parameter
Value
1 Data File Name / Volumes/ nmrdata_1/ mbrandst/ vnmrsys/ data/ MB4_023_1 / PROTON02 fid/ fid
2 Title PROTON02
3 Comment MB4_023_1
4 Origin Varian
5 Solvent cdcl3
6 Temperature 3.0
7 Pulse Sequence s2pul
8 Number of Scans 8
9 Receiver Gain 50
10 Relaxation Delay 1.0000
11 Pulse Width 5.6500
12 Acquisition Date 2020-07-13T20:50:04
13 Spectrometer Frequency 499.60
14 Spectral Width 8000.0
15 Lowest Frequency -1002.4
16 Nucleus 1H
17 Acquired Size 24000
B (d) 8.10
D (t) 7.70
G (m) 7.22
H (dd) 7.18
A (m) 8.03
E (t) 7.51
I (d) 7.14
C (d) 7.79
F (dd) 7.38
J (t) 4.31
L (dd) 3.00
K (dd) 3.15
M (m) 2.60
N (s) 1.80
O (ddd) 0.96
5.96
1.89
1.00
1.04
1.03
1.08
0.95
1.00
1.00
1.11
1.03
1.02
1.90
0.85
2.02
f1 (ppm)

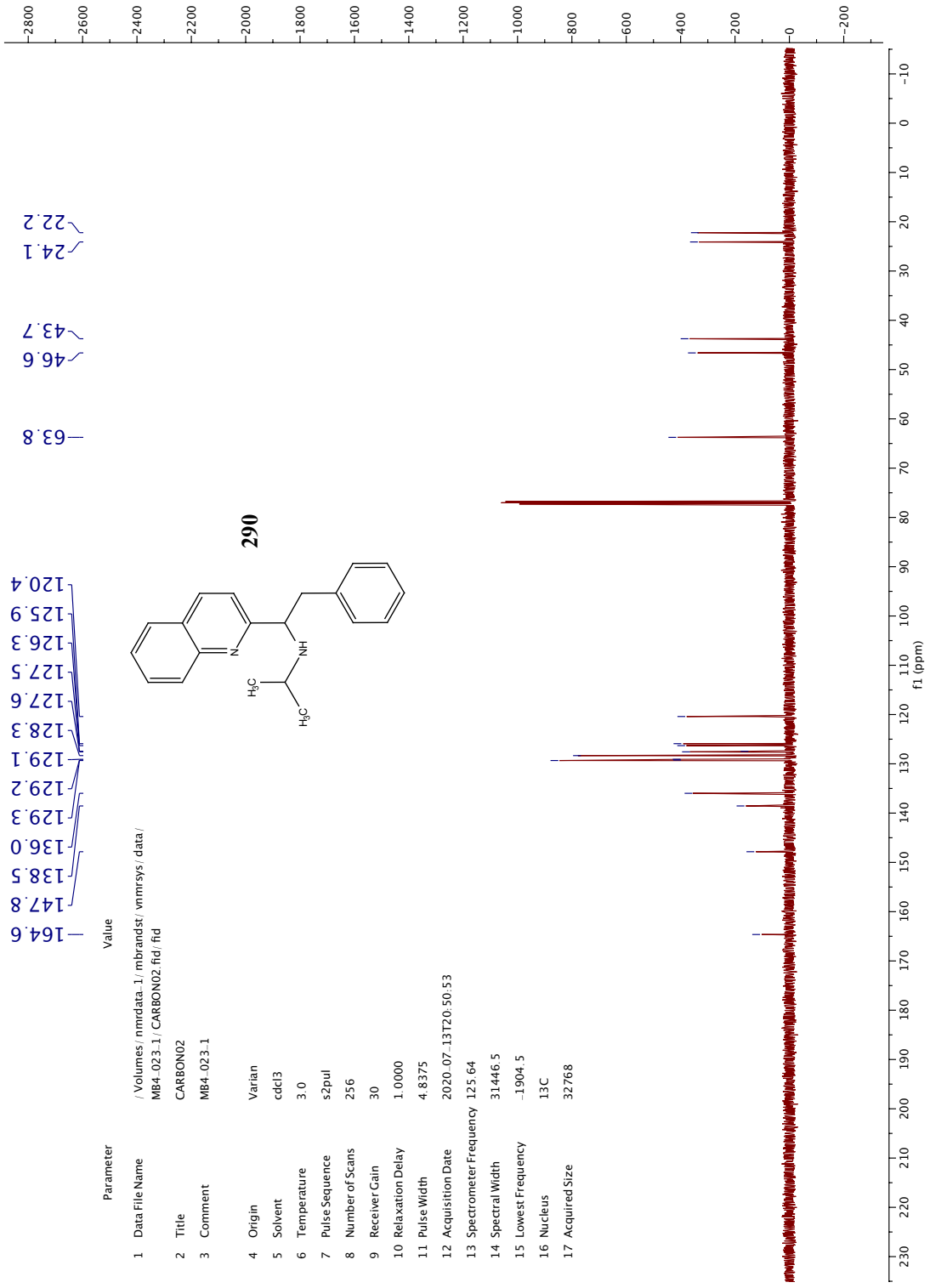

	Parameter	Value
1	Data File Name	/Volumes/nmrdata_1/mbrandst/vnmrsys/data/MB4_023_1/CARBON02.fid/fid
2	Title	CARBON02
3	Comment	MB4_023_1
4	Origin	Varian
5	Solvent	cdcl3
6	Temperature	3.0
7	Pulse Sequence	s2pul
8	Number of Scans	256
9	Receiver Gain	30
10	Relaxation Delay	1.0000
11	Pulse Width	4.8375
12	Acquisition Date	2020_07_13T20:50:53
13	Spectrometer Frequency	125.64
14	Spectral Width	31446.5
15	Lowest Frequency	-1904.5
16	Nucleus	13C
17	Acquired Size	32768

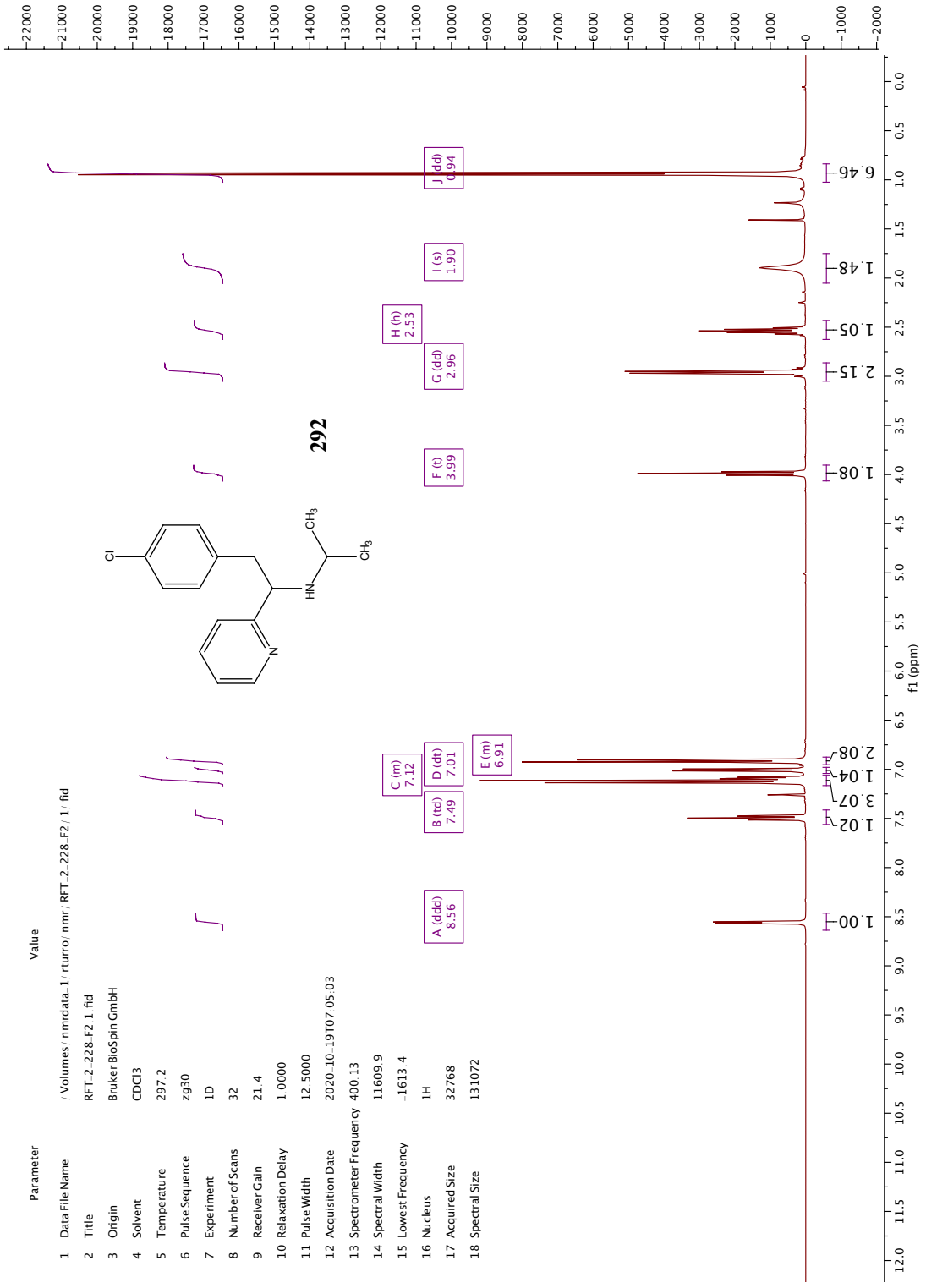

Parameter	Value
1 Data File Name	/Volumes/nmrdata_1/rturro/nmr/RFT_2_228_F2/1/fid
2 Title	RFT_2_228_F2_1.fid
3 Origin	Bruker BioSpin GmbH
4 Solvent	CDCl3
5 Temperature	297.2
6 Pulse Sequence	zg30
7 Experiment	1D
8 Number of Scans	32
9 Receiver Gain	21.4
10 Relaxation Delay	1.0000
11 Pulse Width	12.5000
12 Acquisition Date	2020_10_19T07.05.03
13 Spectrometer Frequency	400.13
14 Spectral Width	11609.9
15 Lowest Frequency	-1613.4
16 Nucleus	1H
17 Acquired Size	32768
18 Spectral Size	131072

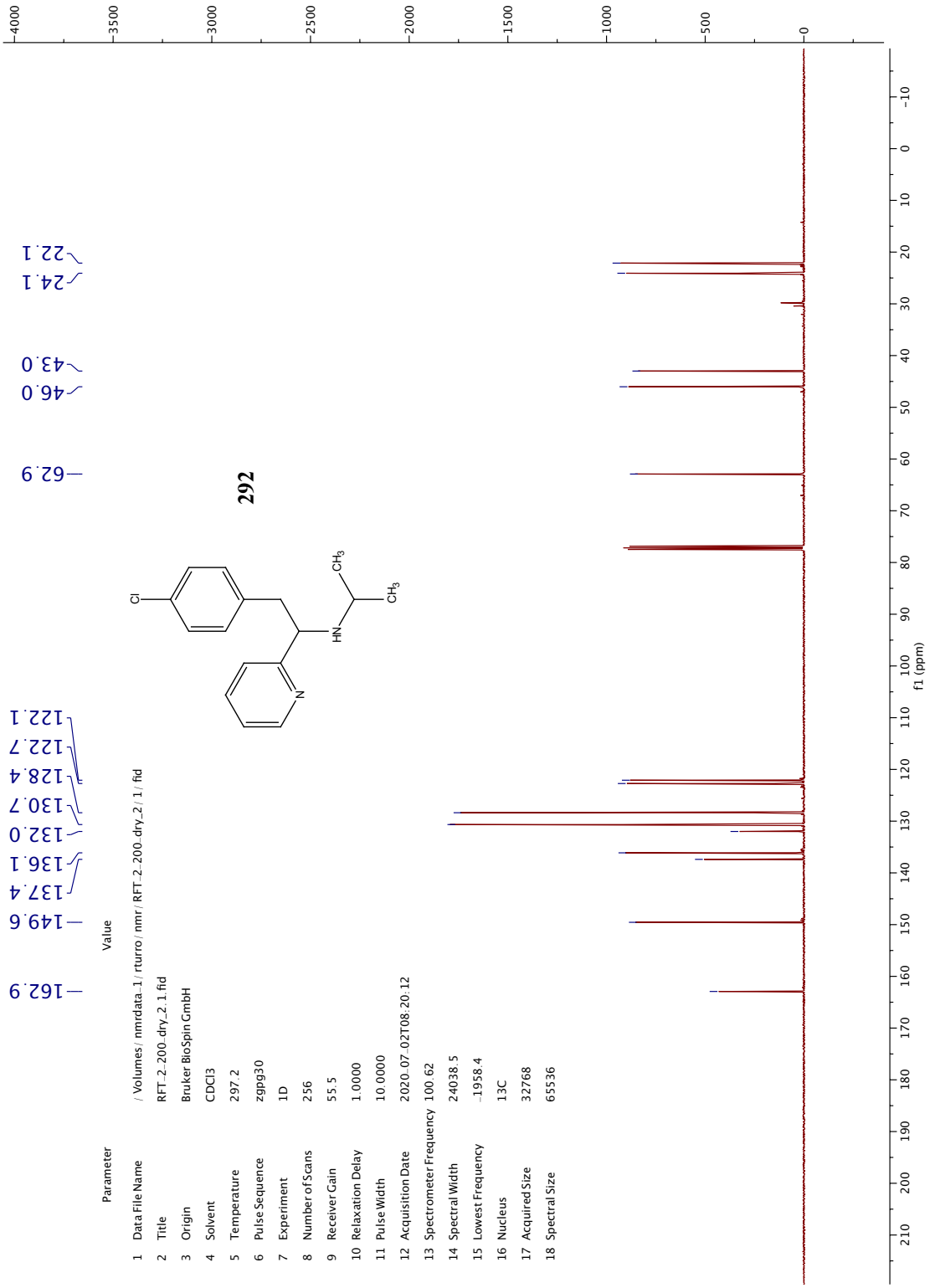

Parameter	Value
1 Data File Name	/ Volumes / nmrdata_1 / rturro / nmr / RFT_2_200_dry_2 / 1 / fid
2 Title	RFT_2_200_dry_2_1.fid
3 Origin	Bruker BioSpin GmbH
4 Solvent	CDCl3
5 Temperature	297.2
6 Pulse Sequence	zgpg30
7 Experiment	1D
8 Number of Scans	256
9 Receiver Gain	55.5
10 Relaxation Delay	1.0000
11 Pulse Width	10.0000
12 Acquisition Date	2020_07_02T08:20:12
13 Spectrometer Frequency	100.62
14 Spectral Width	24038.5
15 Lowest Frequency	-1958.4
16 Nucleus	13C
17 Acquired Size	32768
18 Spectral Size	65536

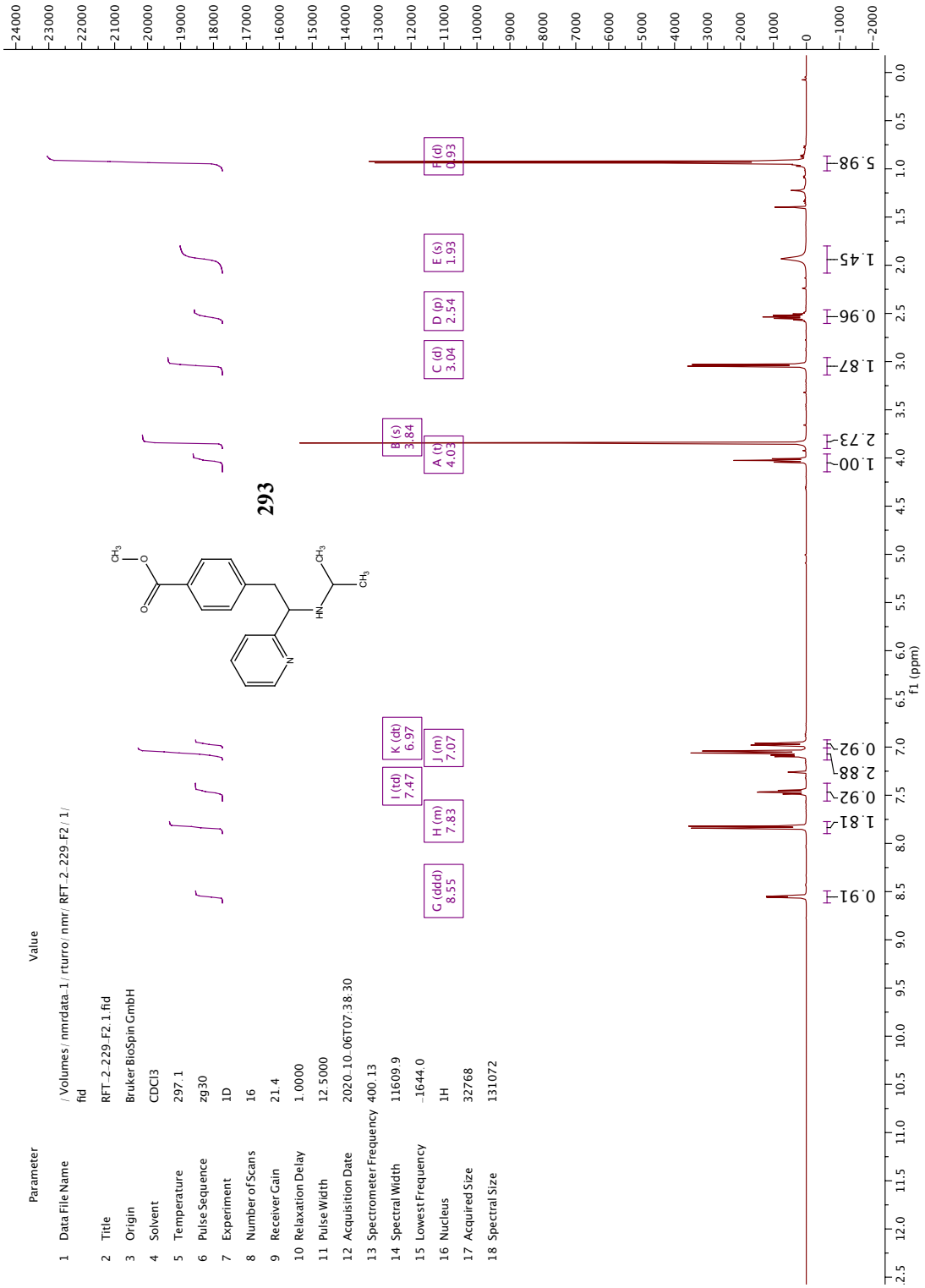

Parameter		Value
1	Data File Name	/ Volumes / nmrdata_1 / rturro / nmr / RFT_2_229_F2 / 1 / fid
2	Title	RFT_2_229_F2_1.fid
3	Origin	Bruker BioSpin GmbH
4	Solvent	CDCl3
5	Temperature	297.1
6	Pulse Sequence	zg30
7	Experiment	1D
8	Number of Scans	16
9	Receiver Gain	21.4
10	Relaxation Delay	1.0000
11	Pulse Width	12.5000
12	Acquisition Date	2020_10_06T07:38:30
13	Spectrometer Frequency	400.13
14	Spectral Width	11609.9
15	Lowest Frequency	-1644.0
16	Nucleus	1H
17	Acquired Size	32768
18	Spectral Size	131072

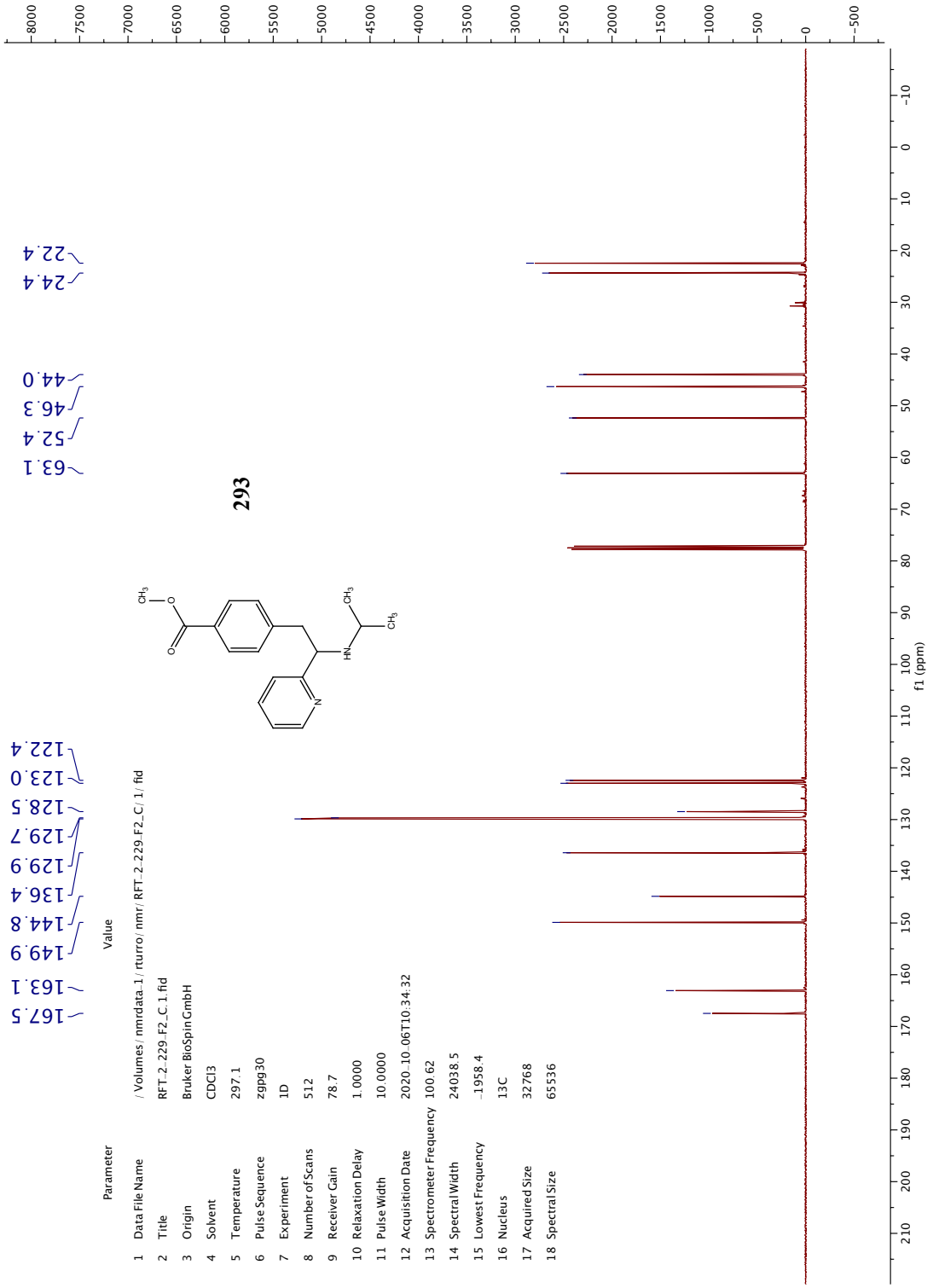

	Parameter	Value
1	Data File Name	/ Volumes/ nmrdata_1/ rturro/ nmr/ RFT_2_229_F2_C/ 1/ fid
2	Title	RFT_2_229_F2_C_1.fid
3	Origin	Bruker BioSpin GmbH
4	Solvent	CDCl3
5	Temperature	297.1
6	Pulse Sequence	zgpg30
7	Experiment	1D
8	Number of Scans	512
9	Receiver Gain	78.7
10	Relaxation Delay	1.0000
11	Pulse Width	10.0000
12	Acquisition Date	2020_10_06T10:34:32
13	Spectrometer Frequency	100.62
14	Spectral Width	24038.5
15	Lowest Frequency	-1958.4
16	Nucleus	13C
17	Acquired Size	32768
18	Spectral Size	65536

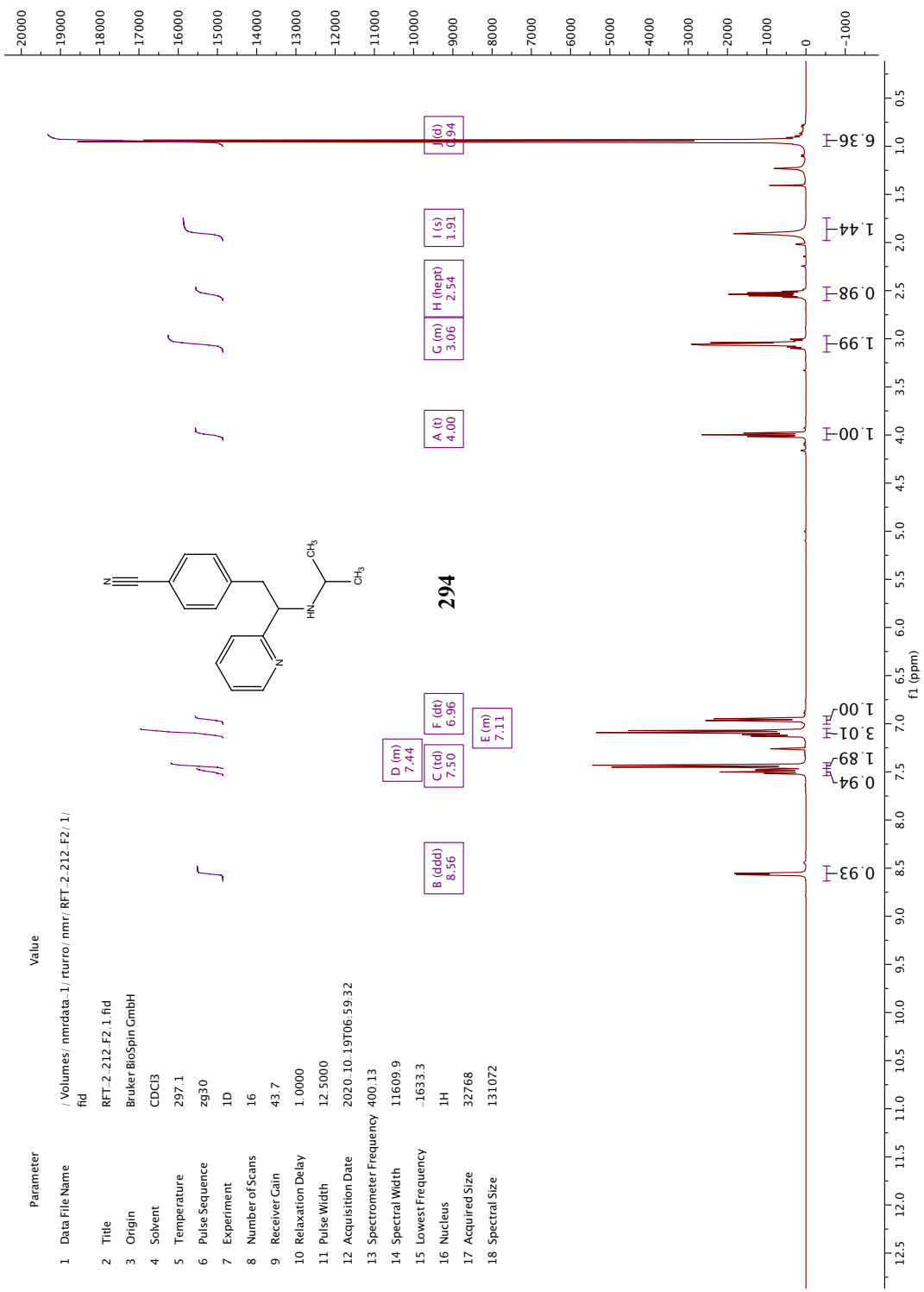
Parameter
Value
1 Data File Name /.Volumes/.nmrdata_1/.rturro/.nmr/.RFT_2_212_F2/.1/fid
2 Title RFT_2_212_F2.1.fid
3 Origin Bruker BioSpin GmbH
4 Solvent CDCl3
5 Temperature 297.1
6 Pulse Sequence zg30
7 Experiment 1D
8 Number of Scans 16
9 Receiver Gain 43.7
10 Relaxation Delay 1.0000
11 Pulse Width 12.5000
12 Acquisition Date 2020-10-19T06:59:32
13 Spectrometer Frequency 400.13
14 Spectral Width 11609.9
15 Lowest Frequency -1633.3
16 Nucleus 1H
17 Acquired Size 32768
18 Spectral Size 131072
294
B (ddd) 8.56
C (td) 7.50
D (m) 7.44
E (m) 7.11
F (dt) 6.96
A (t) 4.00
G (m) 3.06
H (hept) 2.54
I (s) 1.91
J (d) 0.94
6.36
1.44
0.98
1.99
1.00
0.93
0.94
1.89
3.01
1.00
f1 (ppm)

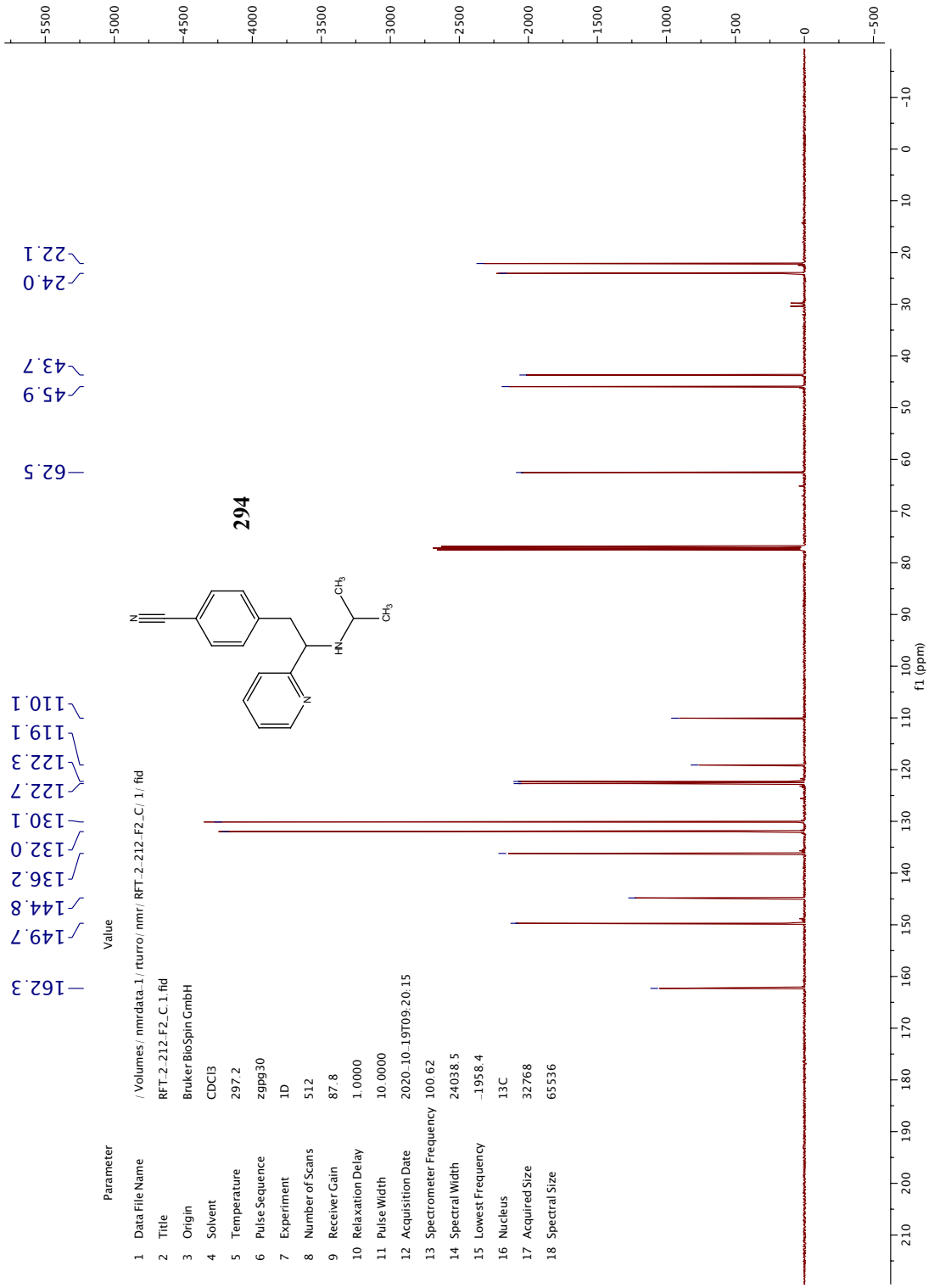

Parameter	Value
1 Data File Name	/Volumes/nmrdata.1/rturro/nmr/RFT-2-212-F2_C/1/fid
2 Title	RFT-2-212-F2_C 1 fid
3 Origin	Bruker BioSpin GmbH
4 Solvent	CDCl3
5 Temperature	297.2
6 Pulse Sequence	zgpg30
7 Experiment	1D
8 Number of Scans	512
9 Receiver Gain	87.8
10 Relaxation Delay	1.0000
11 Pulse Width	10.0000
12 Acquisition Date	2020_10_19T09:20:15
13 Spectrometer Frequency	100.62
14 Spectral Width	24038.5
15 Lowest Frequency	-1958.4
16 Nucleus	13C
17 Acquired Size	32768
18 Spectral Size	65536

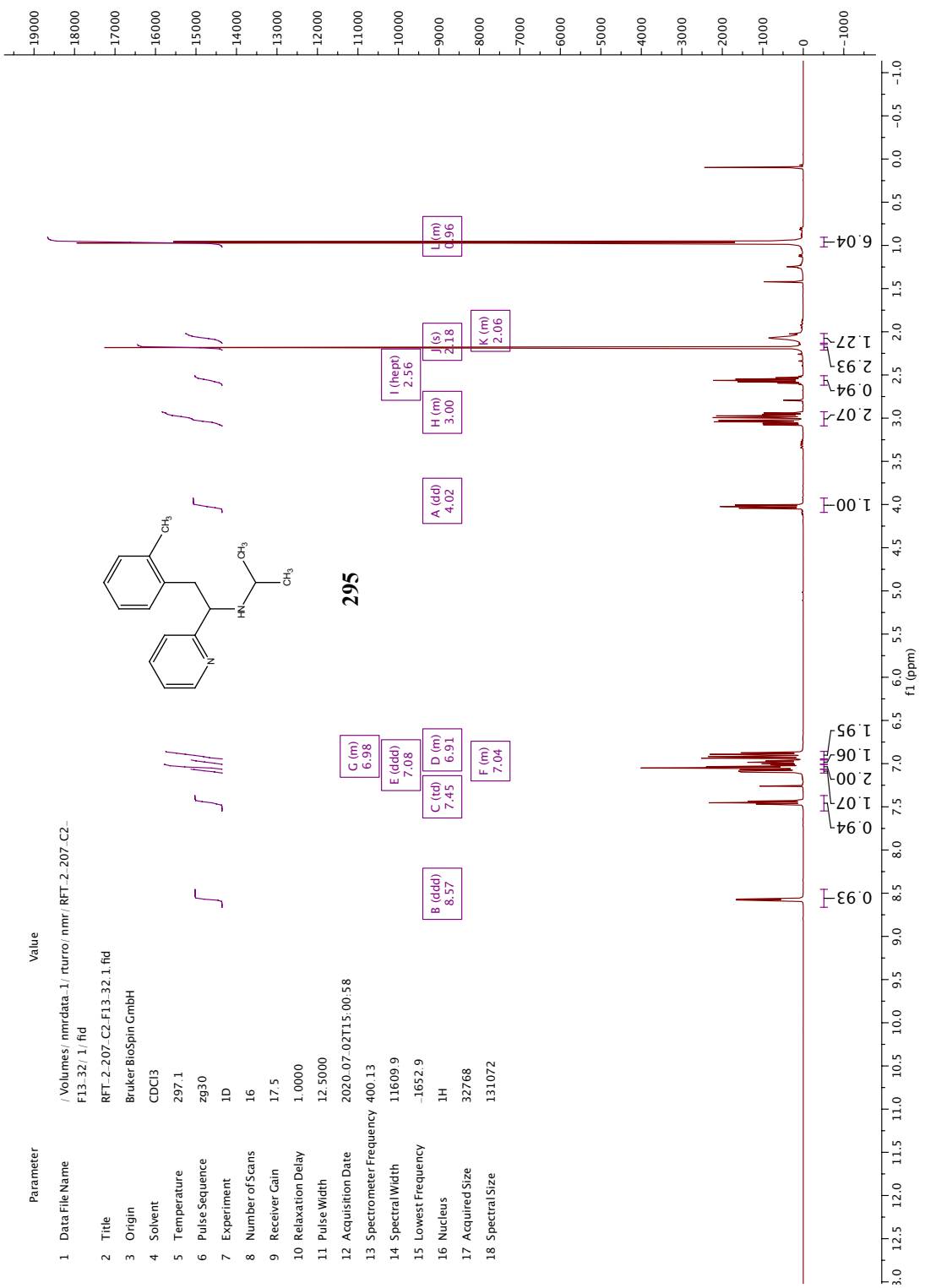
Parameter
Value
1 Data File Name / Volumes/ nmrdata_1/ rturro/ nmr/ RFT_2_207_C2_F13_32/ 1/ fid
2 Title RFT_2_207_C2_F13_32 1.fid
3 Origin Bruker BioSpin GmbH
4 Solvent CDCl3
5 Temperature 297.1
6 Pulse Sequence zg30
7 Experiment 1D
8 Number of Scans 16
9 Receiver Gain 17.5
10 Relaxation Delay 1.0000
11 Pulse Width 12.5000
12 Acquisition Date 2020-07-02T15:00:58
13 Spectrometer Frequency 400.13
14 Spectral Width 11609.9
15 Lowest Frequency -1652.9
16 Nucleus 1H
17 Acquired Size 32768
18 Spectral Size 131072
295
B (ddd) 8.57
C (td) 7.45
D (m) 6.91
E (ddd) 7.08
F (m) 7.04
G (m) 6.98
A (dd) 4.02
I (hept) 2.56
H (m) 3.00
J (s) 2.18
K (m) 2.06
L (m) 0.96
0.93
0.94
1.07
2.00
1.06
1.95
1.00
2.07
0.94
2.93
1.27
6.04
f1 (ppm)

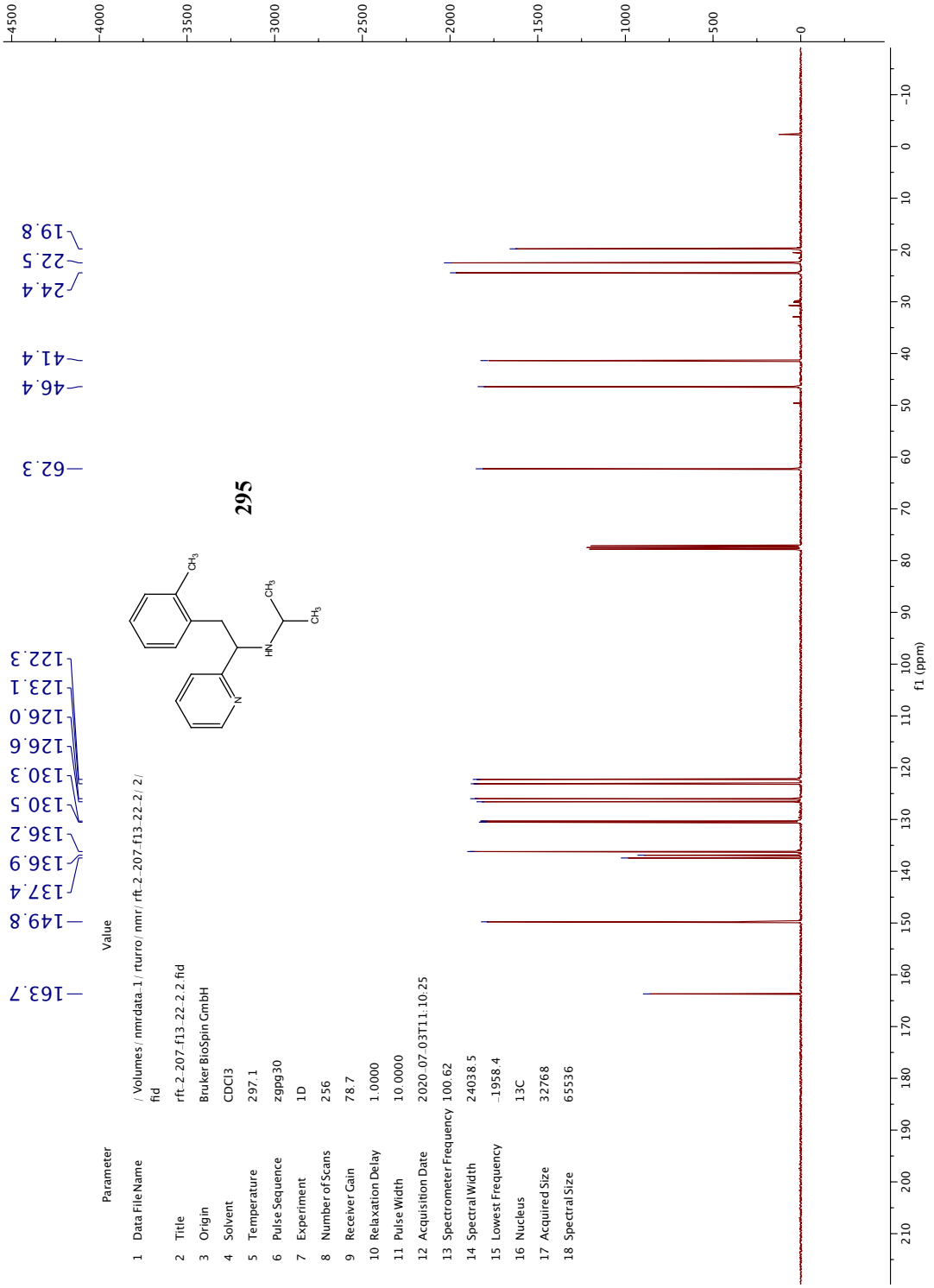

Parameter	Value
1 Data File Name	/Volumes/nmrdata_1/rturro/nmr/rft_2_207_f13_22_2/2/fid
2 Title	rft_2_207_f13_22_2_2.fid
3 Origin	Bruker BioSpin GmbH
4 Solvent	CDCl3
5 Temperature	297.1
6 Pulse Sequence	zgpg30
7 Experiment	1D
8 Number of Scans	256
9 Receiver Gain	78.7
10 Relaxation Delay	1.0000
11 Pulse Width	10.0000
12 Acquisition Date	2020_07_03T11:10:25
13 Spectrometer Frequency	100.62
14 Spectral Width	24038.5
15 Lowest Frequency	-1958.4
16 Nucleus	13C
17 Acquired Size	32768
18 Spectral Size	65536

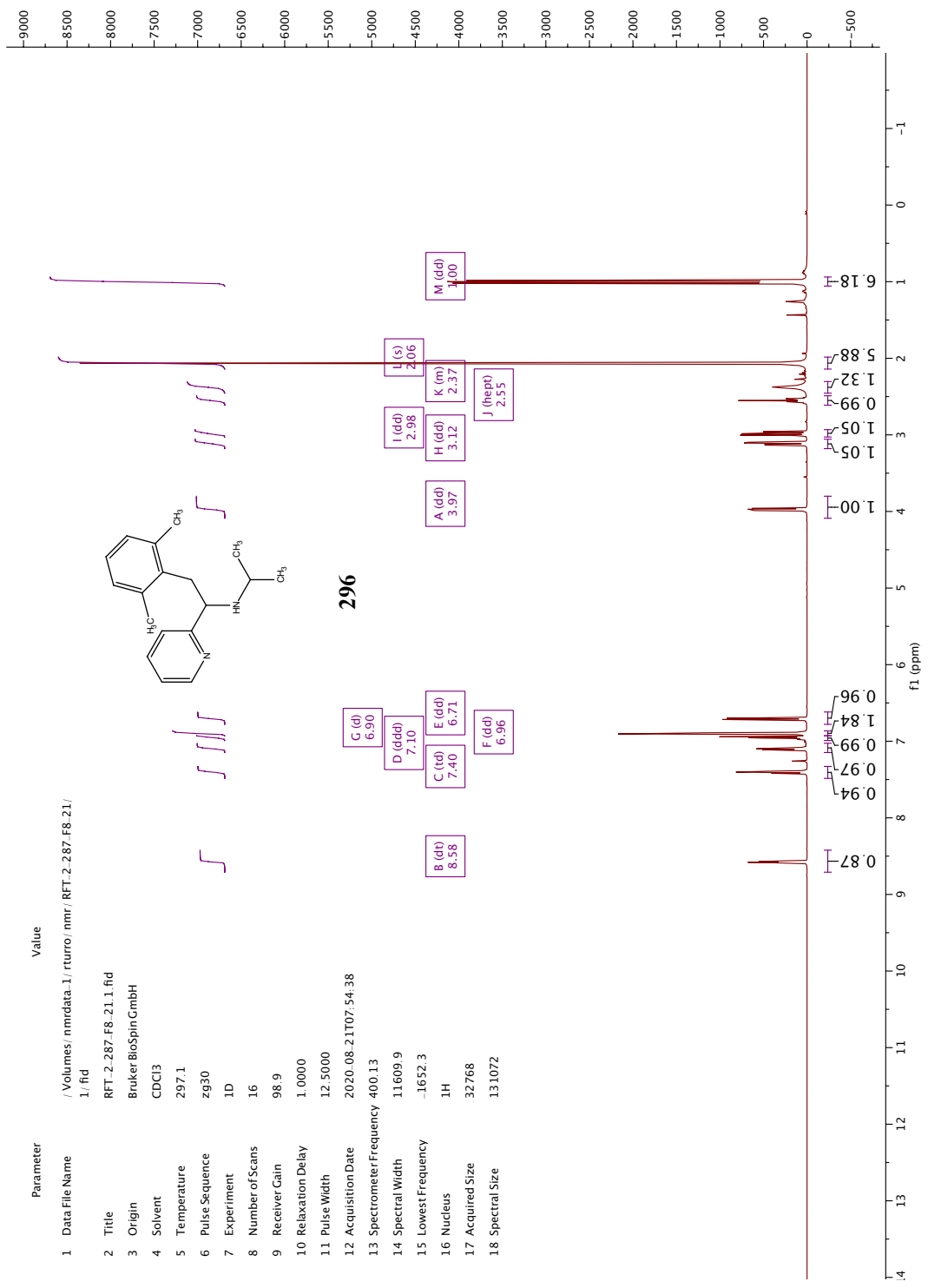
Parameter
Value
1 Data File Name /Volumes/nmrdata.1/rturro/nmr/RFT-2-287-F8-21/1/fid
2 Title RFT-2-287-F8-21-1.fid
3 Origin Bruker BioSpin GmbH
4 Solvent CDCl3
5 Temperature 297.1
6 Pulse Sequence zg30
7 Experiment 1D
8 Number of Scans 16
9 Receiver Gain 98.9
10 Relaxation Delay 1.0000
11 Pulse Width 12.5000
12 Acquisition Date 2020-08-21T07:54:38
13 Spectrometer Frequency 400.13
14 Spectral Width 11609.9
15 Lowest Frequency -1652.3
16 Nucleus 1H
17 Acquired Size 32768
18 Spectral Size 131072
296
A (dd) 3.97
B (dt) 8.58
C (td) 7.40
D (ddd) 7.10
E (dd) 6.71
F (dd) 6.96
G (d) 6.90
H (dd) 3.12
I (dd) 2.98
J (hept) 2.55
K (m) 2.37
L (s) 2.06
M (dd) 4.00
6.18
5.88
1.32
0.99
1.05
1.05
1.00
0.96
1.84
0.99
0.97
0.94
0.87
f1 (ppm)

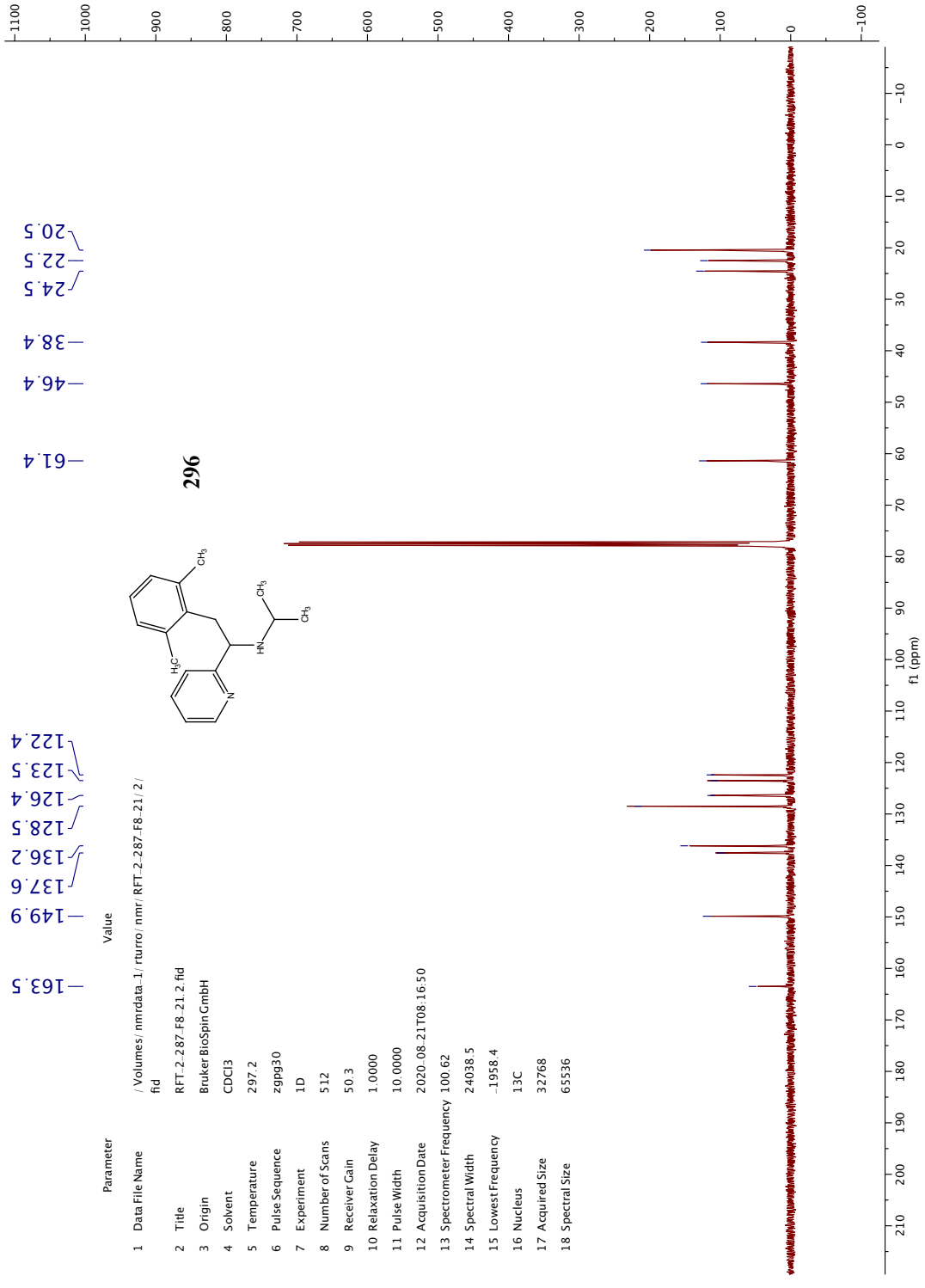

Parameter	Value
1 Data File Name	/Volumes/nmrdata_1/rturro/nmr/RFT_2_287_F8_21/2/fid
2 Title	RFT_2_287_F8_21_2.fid
3 Origin	Bruker BioSpin GmbH
4 Solvent	CDCl3
5 Temperature	297.2
6 Pulse Sequence	zgpg30
7 Experiment	1D
8 Number of Scans	512
9 Receiver Gain	50.3
10 Relaxation Delay	1.0000
11 Pulse Width	10.0000
12 Acquisition Date	2020_08_21T08:16:50
13 Spectrometer Frequency	100.62
14 Spectral Width	24038.5
15 Lowest Frequency	-1958.4
16 Nucleus	13C
17 Acquired Size	32768
18 Spectral Size	65536

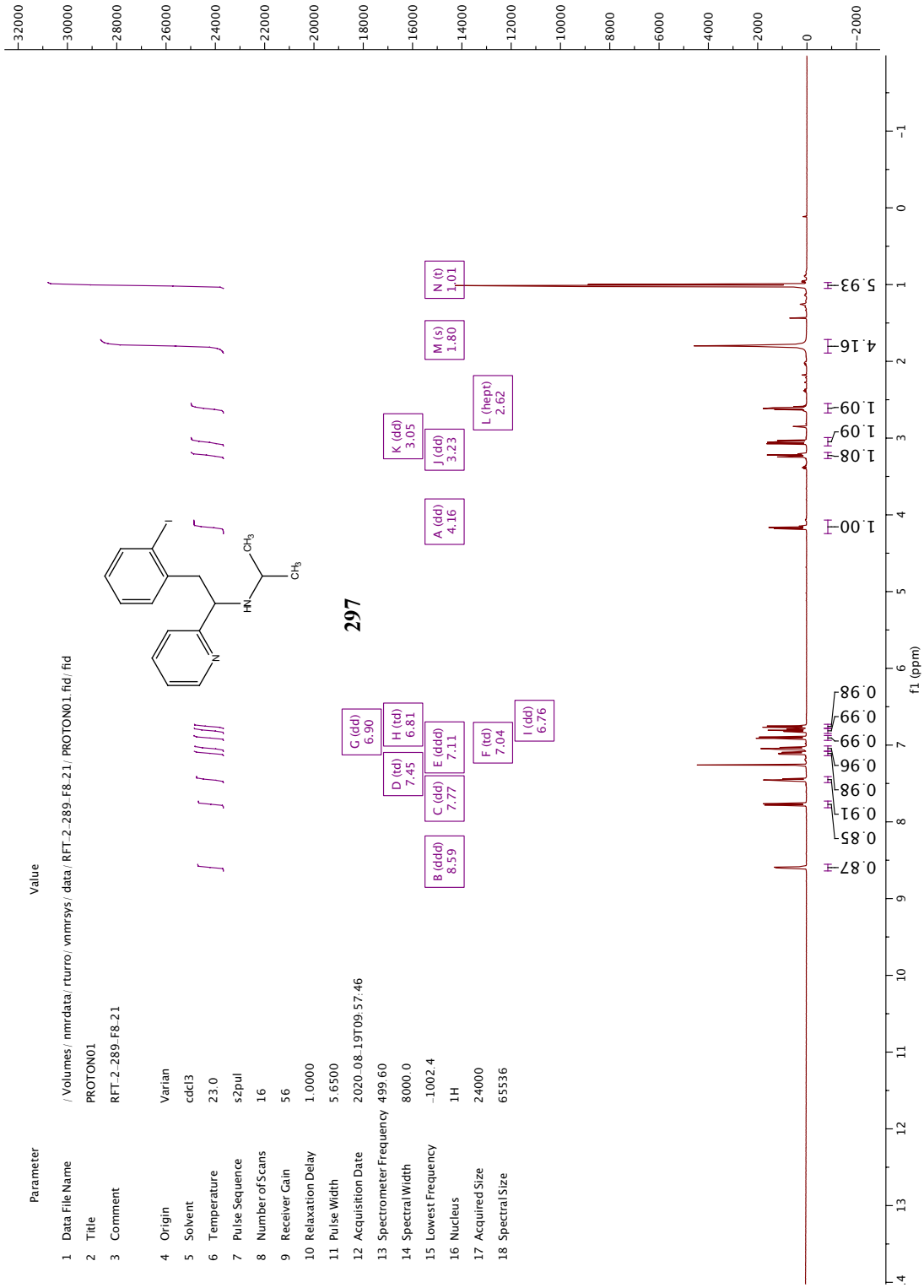
Parameter
Value
1 Data File Name /Volumes/nmrdata/rturro/vnmrsys/data/RFT-2-289-F8-21/PROTON01.fid/fid
2 Title PROTON01
3 Comment RFT-2-289-F8-21
4 Origin Varian
5 Solvent cdcl3
6 Temperature 23.0
7 Pulse Sequence s2pul
8 Number of Scans 16
9 Receiver Gain 56
10 Relaxation Delay 1.0000
11 Pulse Width 5.6500
12 Acquisition Date 2020-08-19T09:57:46
13 Spectrometer Frequency 499.60
14 Spectral Width 8000.0
15 Lowest Frequency -1002.4
16 Nucleus 1H
17 Acquired Size 24000
18 Spectral Size 65536
297
A (dd) 4.16
B (ddd) 8.59
C (dd) 7.77
D (td) 7.45
E (ddd) 7.11
F (td) 7.04
G (dd) 6.90
H (td) 6.81
I (dd) 6.76
J (dd) 3.23
K (dd) 3.05
L (hept) 2.62
M (s) 1.80
N (t) 1.01
f1 (ppm)

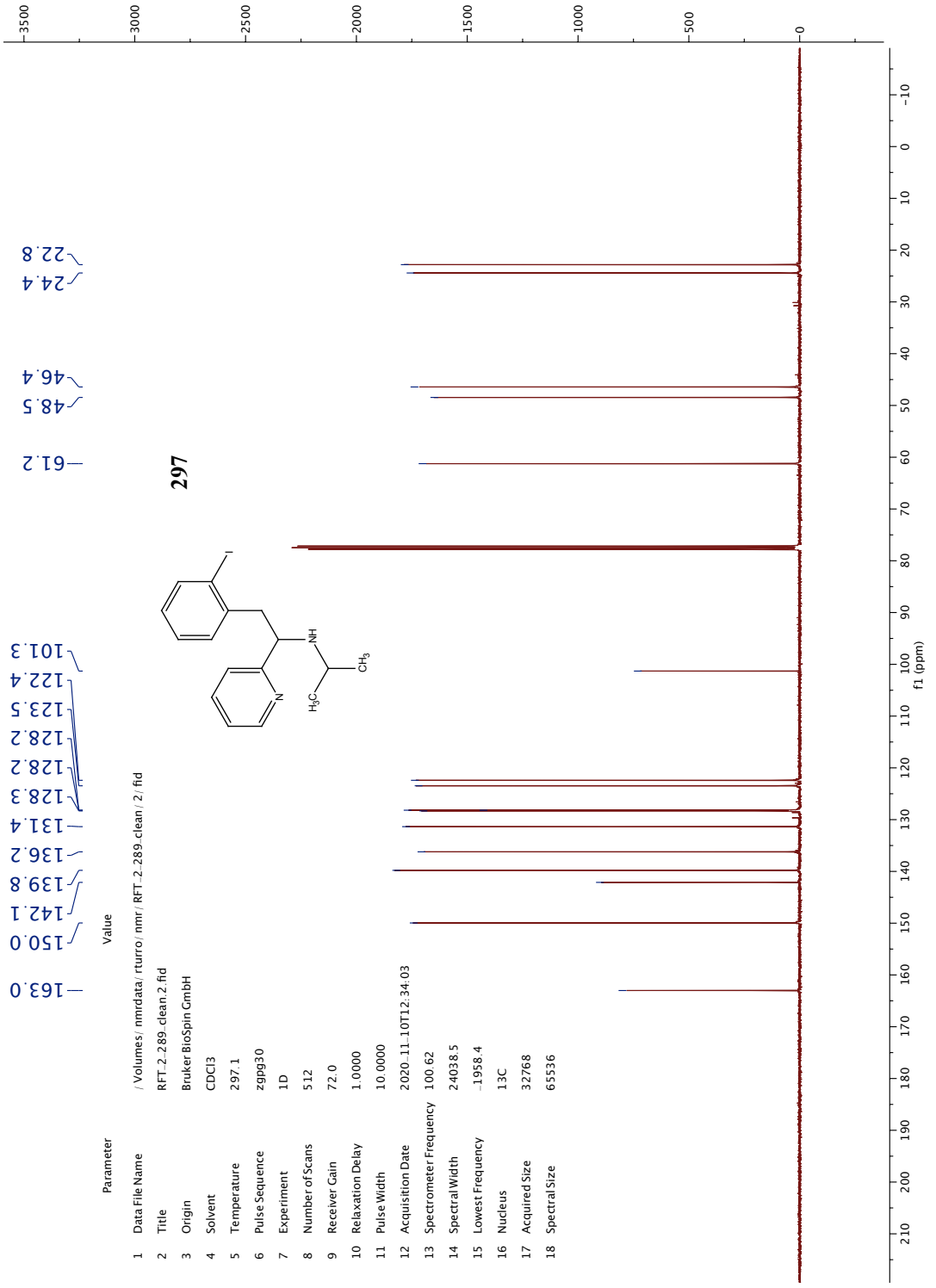
297
22.8
24.4
46.4
48.5
61.2
101.3
122.4
123.5
128.2
128.2
128.3
131.4
136.2
139.8
142.1
150.0
163.0
Parameter
Value
1 Data File Name / Volumes/ nmrdata/ rturro/ nmr/ RFT_2_289_clean/ 2/ fid
2 Title RFT_2_289_clean 2 fid
3 Origin Bruker BioSpin GmbH
4 Solvent CDCl3
5 Temperature 297.1
6 Pulse Sequence zgpg30
7 Experiment 1D
8 Number of Scans 512
9 Receiver Gain 72.0
10 Relaxation Delay 1.0000
11 Pulse Width 10.0000
12 Acquisition Date 2020_11_10T12:34:03
13 Spectrometer Frequency 100.62
14 Spectral Width 24038.5
15 Lowest Frequency -1958.4
16 Nucleus 13C
17 Acquired Size 32768
18 Spectral Size 65536
f1 (ppm)

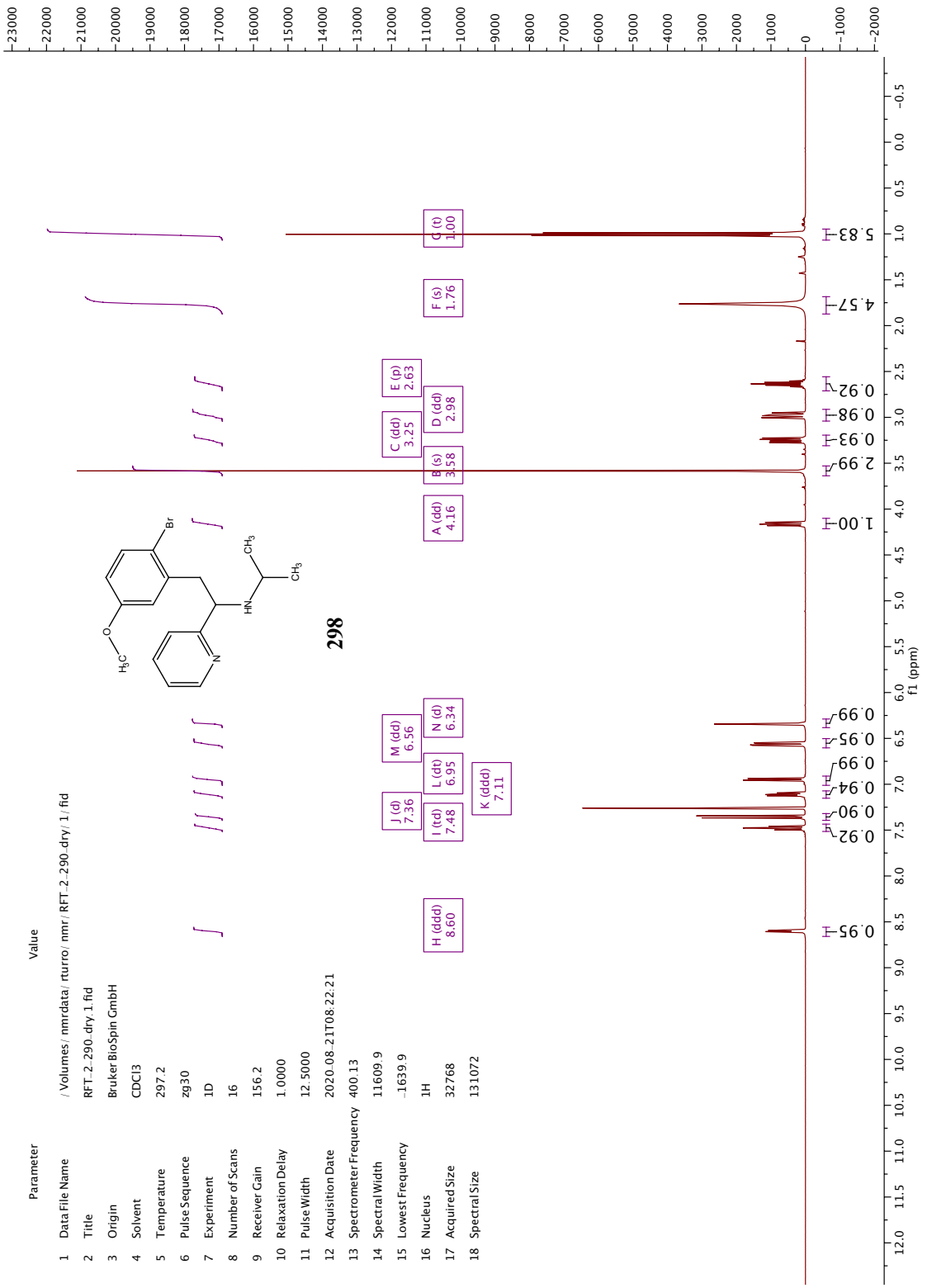
Parameter
Value
1 Data File Name / Volumes / nmrdata / rturro / nmr / RFT_2_290_dry / 1 / fid
2 Title RFT_2_290_dry_1.fid
3 Origin Bruker BioSpin GmbH
4 Solvent CDCl3
5 Temperature 297.2
6 Pulse Sequence zg30
7 Experiment 1D
8 Number of Scans 16
9 Receiver Gain 156.2
10 Relaxation Delay 1.0000
11 Pulse Width 12.5000
12 Acquisition Date 2020.08.21T08.22.21
13 Spectrometer Frequency 400.13
14 Spectral Width 11609.9
15 Lowest Frequency -1639.9
16 Nucleus 1H
17 Acquired Size 32768
18 Spectral Size 131072
298
H (ddd) 8.60
I (td) 7.48
J (d) 7.36
K (ddd) 7.11
L (dt) 6.95
M (dd) 6.56
N (d) 6.34
A (dd) 4.16
B (s) 3.58
C (dd) 3.25
D (dd) 2.98
E (p) 2.63
F (s) 1.76
G (t) 1.00
0.95
0.92
0.90
0.94
0.99
0.95
0.99
1.00
2.99
0.93
0.98
0.92
4.57
5.83
f1 (ppm)

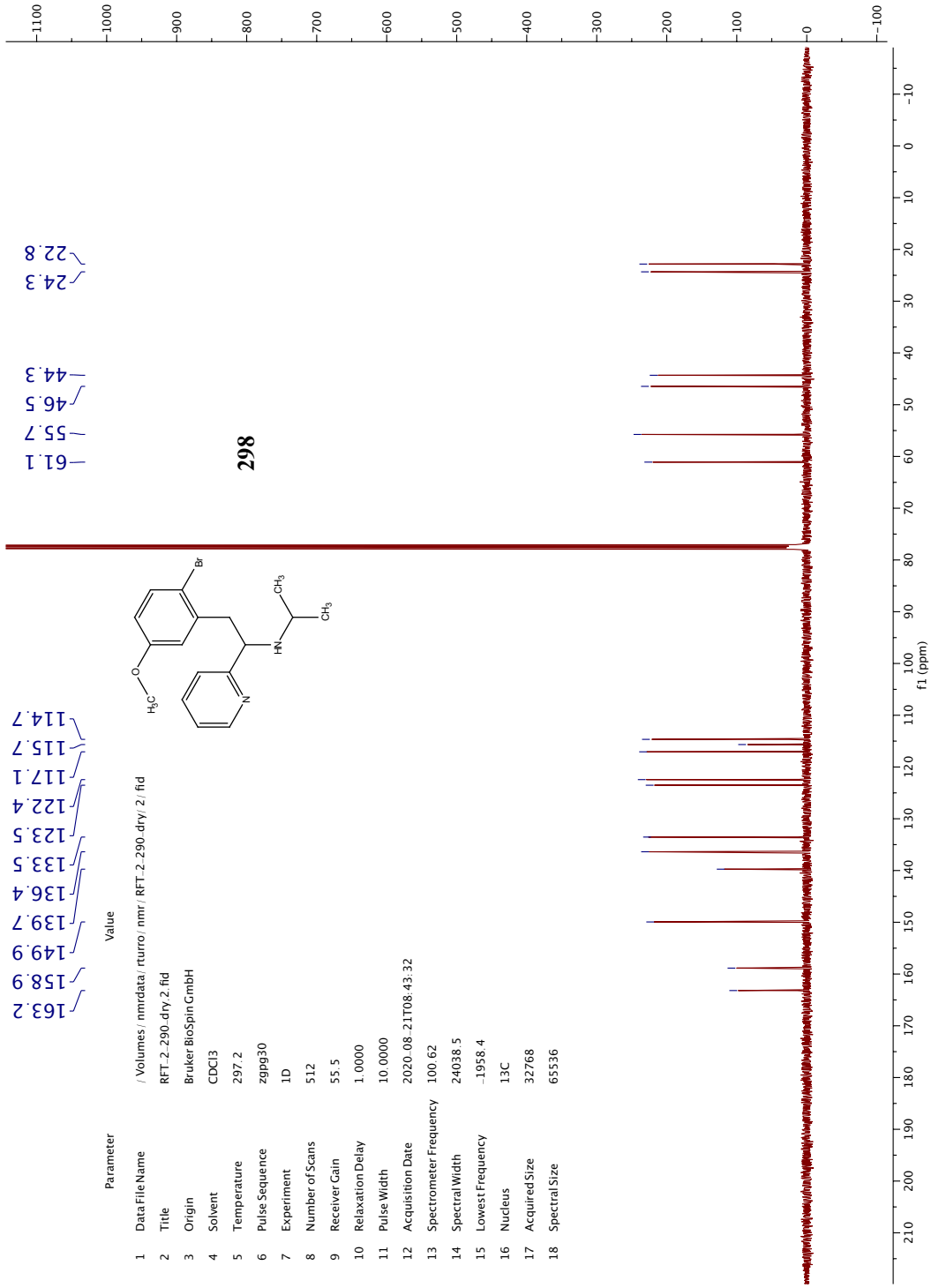

	Parameter	Value
1	Data File Name	/Volumes/nmrdata/rturro/nmr/RFT_2_290_dry/2/fid
2	Title	RFT_2_290_dry_2.fid
3	Origin	Bruker BioSpin GmbH
4	Solvent	CDCl3
5	Temperature	297.2
6	Pulse Sequence	zgpg30
7	Experiment	1D
8	Number of Scans	512
9	Receiver Gain	55.5
10	Relaxation Delay	1.0000
11	Pulse Width	10.0000
12	Acquisition Date	2020.08.21T08.43.32
13	Spectrometer Frequency	100.62
14	Spectral Width	24038.5
15	Lowest Frequency	-1958.4
16	Nucleus	13C
17	Acquired Size	32768
18	Spectral Size	65536

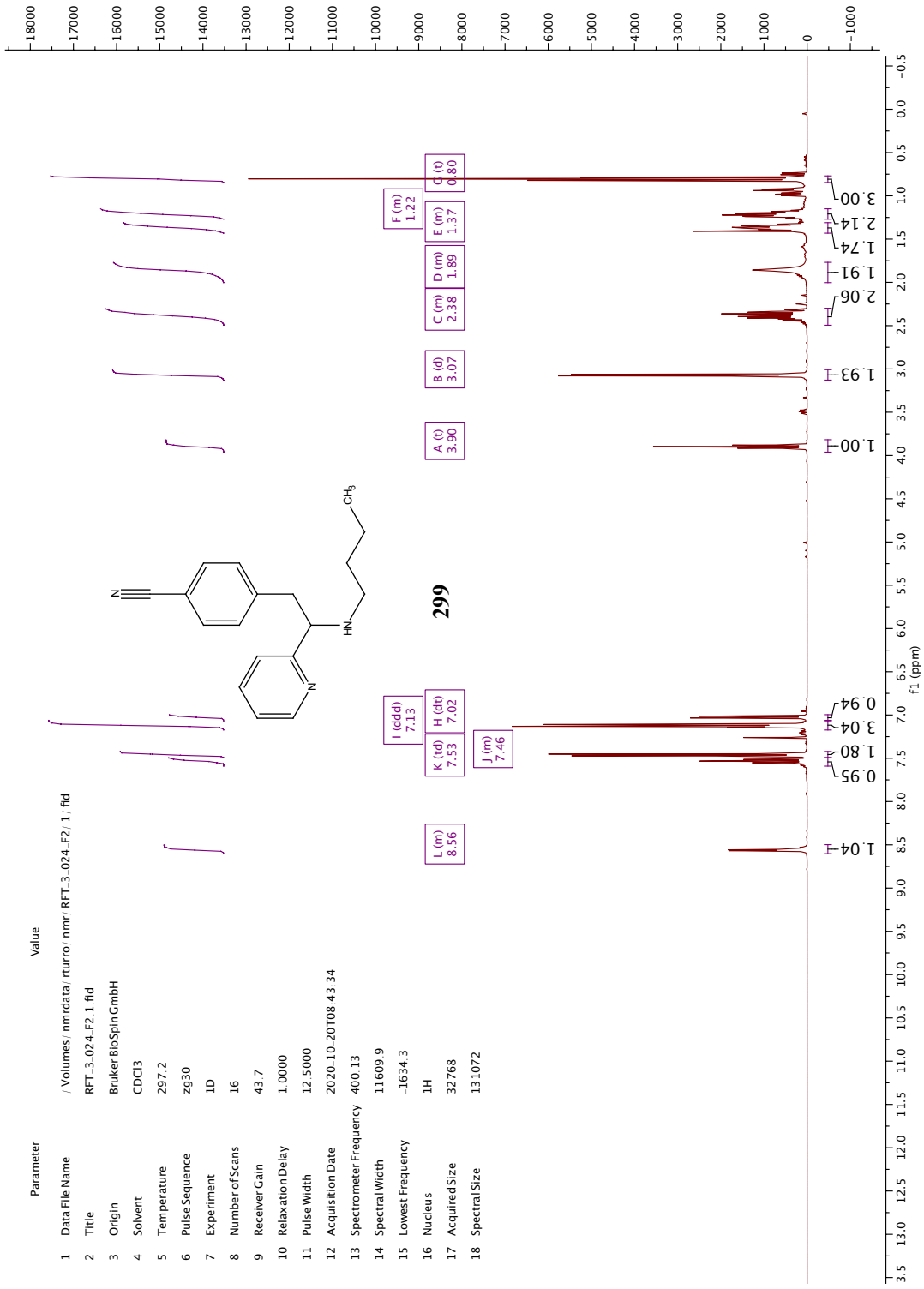
Parameter
Value
1 Data File Name / Volumes / nmrdata / rturro / nmr / RFT_3_024_F2 / 1 / fid
2 Title RFT_3_024_F2_1.fid
3 Origin Bruker BioSpin GmbH
4 Solvent CDCl3
5 Temperature 297.2
6 Pulse Sequence zg30
7 Experiment 1D
8 Number of Scans 16
9 Receiver Gain 43.7
10 Relaxation Delay 1.0000
11 Pulse Width 12.5000
12 Acquisition Date 2020_10_20T08.43.34
13 Spectrometer Frequency 400.13
14 Spectral Width 11609.9
15 Lowest Frequency -1634.3
16 Nucleus 1H
17 Acquired Size 32768
18 Spectral Size 131072
299
A (t) 3.90
B (d) 3.07
C (m) 2.38
D (m) 1.89
E (m) 1.37
F (m) 1.22
G (t) 0.80
H (dt) 7.02
I (ddd) 7.13
J (m) 7.46
K (td) 7.53
L (m) 8.56
1.04
0.95
1.80
3.04
0.94
1.00
1.93
2.06
1.91
1.74
2.14
3.00
f1 (ppm)

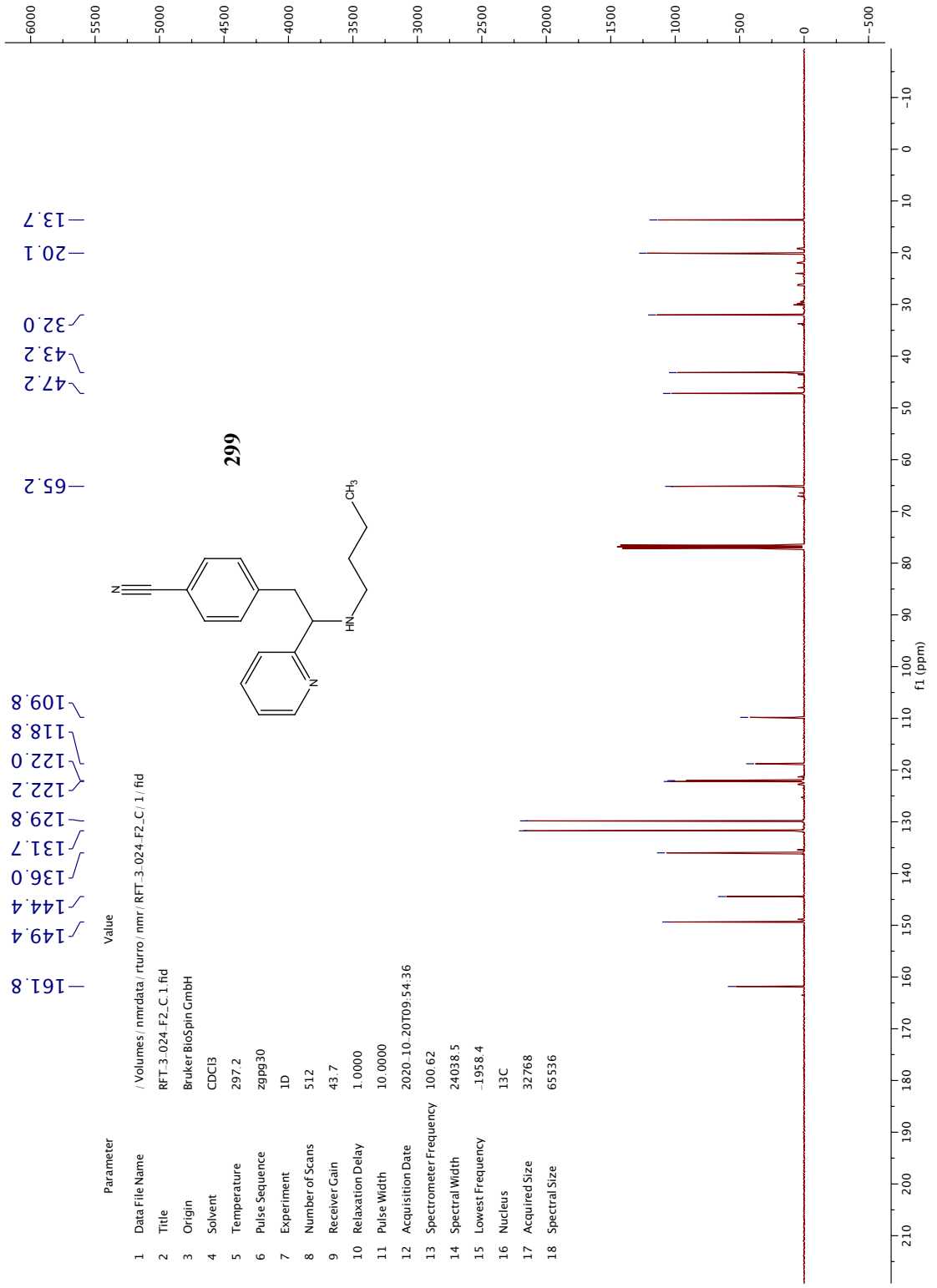

	Parameter	Value
1	Data File Name	/Volumes/nmrdata/rturro/nmr/RFT-3_024-F2_C/1/fid
2	Title	RFT-3_024-F2_C 1 fid
3	Origin	Bruker BioSpin GmbH
4	Solvent	CDCl3
5	Temperature	297.2
6	Pulse Sequence	zgpg30
7	Experiment	1D
8	Number of Scans	512
9	Receiver Gain	43.7
10	Relaxation Delay	1.0000
11	Pulse Width	10.0000
12	Acquisition Date	2020_10_20T09:54:36
13	Spectrometer Frequency	100.62
14	Spectral Width	24038.5
15	Lowest Frequency	-1958.4
16	Nucleus	13C
17	Acquired Size	32768
18	Spectral Size	65536

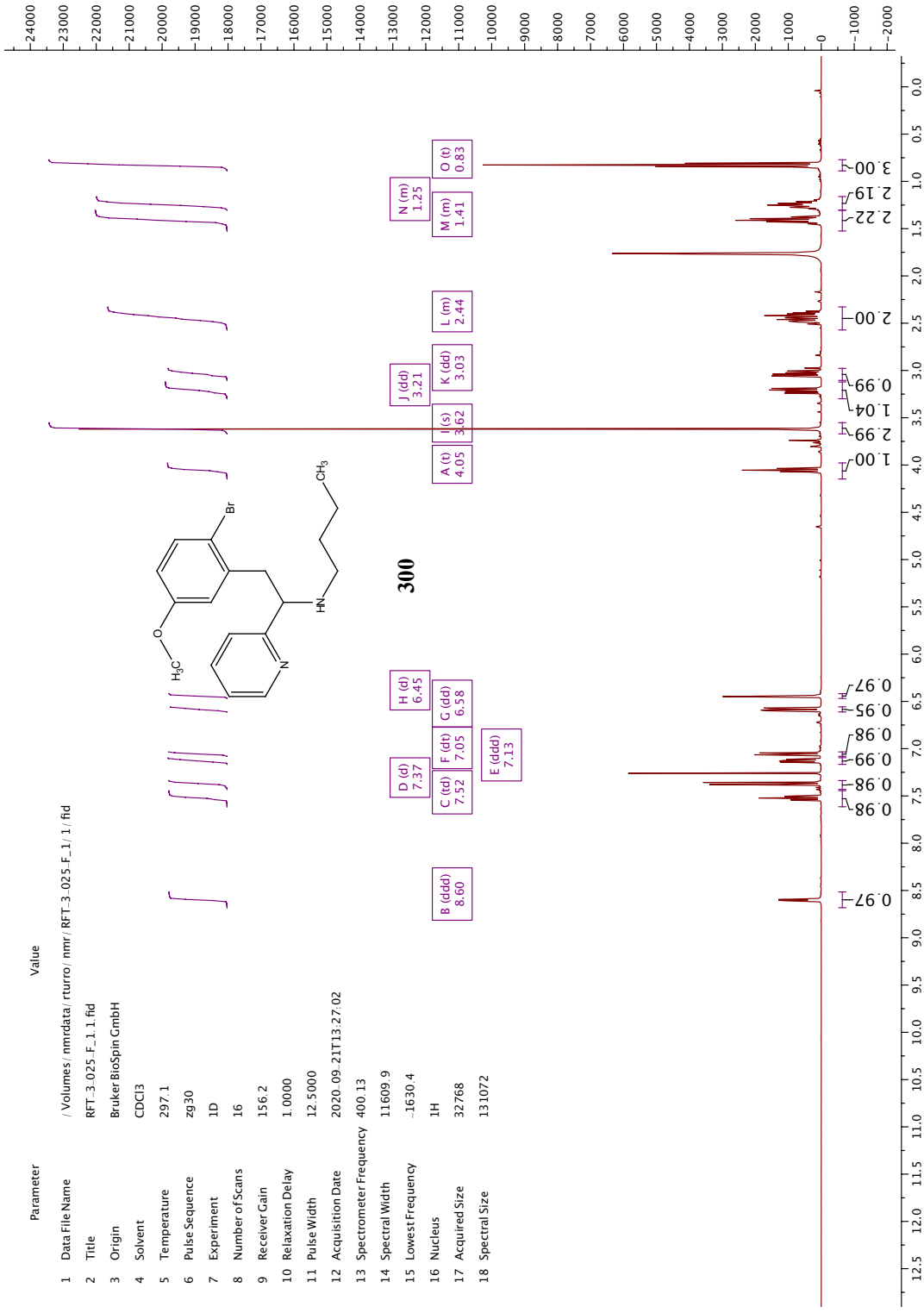
Parameter
Value
1 Data File Name / Volumes/ nmrdata/ rturro/ nmr/ RFT_3_025_F_1/ 1/ fid
2 Title RFT_3_025_F_1_1.fid
3 Origin Bruker BioSpin GmbH
4 Solvent CDCl3
5 Temperature 297.1
6 Pulse Sequence zg30
7 Experiment 1D
8 Number of Scans 16
9 Receiver Gain 156.2
10 Relaxation Delay 1.0000
11 Pulse Width 12.5000
12 Acquisition Date 2020_09_21T13:27:02
13 Spectrometer Frequency 400.13
14 Spectral Width 11609.9
15 Lowest Frequency -1630.4
16 Nucleus 1H
17 Acquired Size 32768
18 Spectral Size 131072
300
B (ddd) 8.60
C (td) 7.52
D (d) 7.37
E (ddd) 7.13
F (dt) 7.05
G (dd) 6.58
H (d) 6.45
A (t) 4.05
I (s) 3.62
J (dd) 3.21
K (dd) 3.03
L (m) 2.44
M (m) 1.41
N (m) 1.25
O (t) 0.83
3.00
2.19
2.22
2.00
0.99
1.04
2.99
1.00
0.97
0.95
0.98
0.99
0.98
0.98
0.97
f1 (ppm)

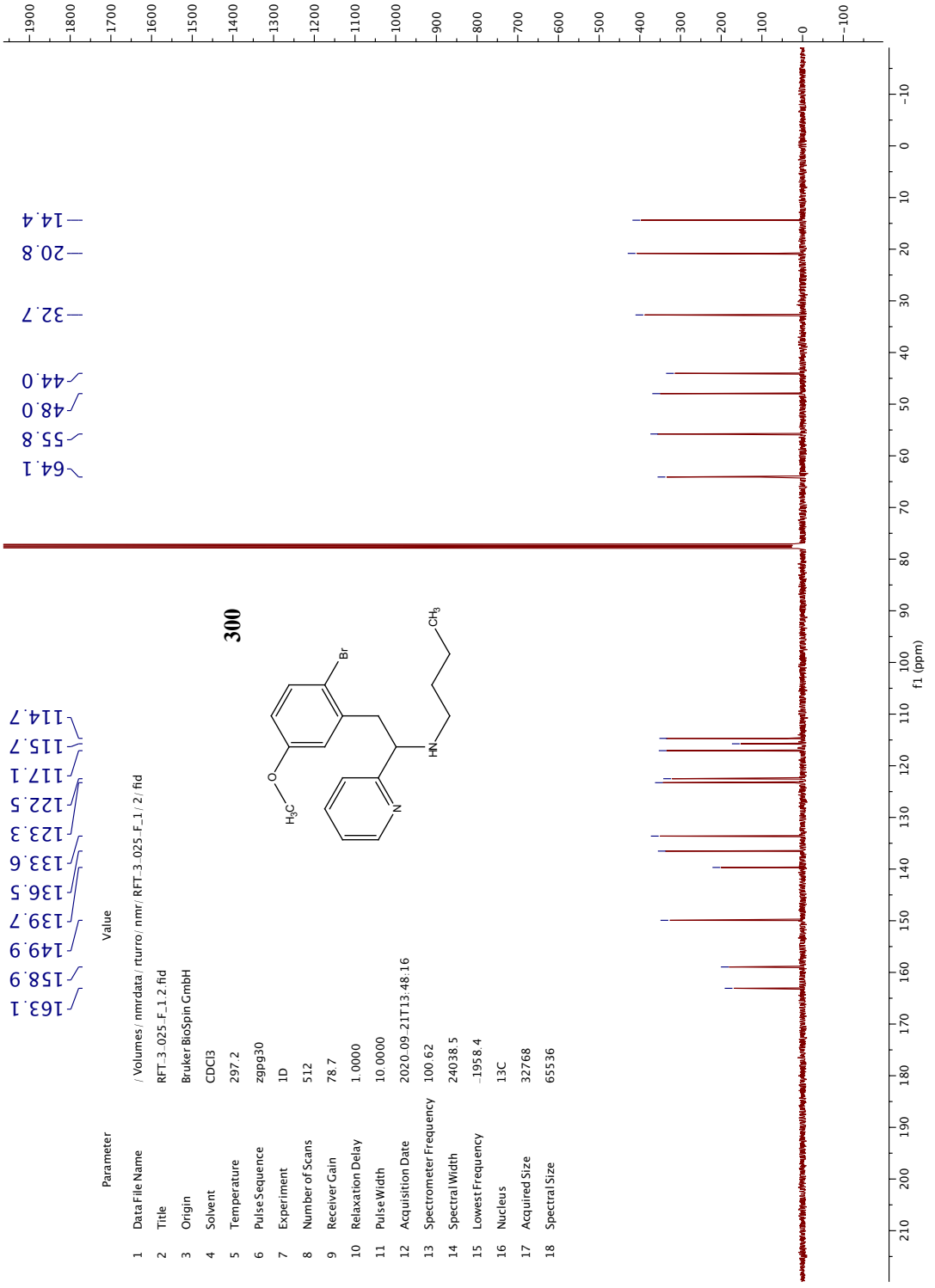

	Parameter	Value
1	Data File Name	/Volumes/nmrdata/rturro/nmr/RFT-3_025_F_1/2/fid
2	Title	RFT_3_025_F_1_2.fid
3	Origin	Bruker BioSpin GmbH
4	Solvent	CDCl3
5	Temperature	297.2
6	Pulse Sequence	zgpg30
7	Experiment	1D
8	Number of Scans	512
9	Receiver Gain	78.7
10	Relaxation Delay	1.0000
11	Pulse Width	10.0000
12	Acquisition Date	2020_09_21T13:48:16
13	Spectrometer Frequency	100.62
14	Spectral Width	24038.5
15	Lowest Frequency	-1958.4
16	Nucleus	13C
17	Acquired Size	32768
18	Spectral Size	65536

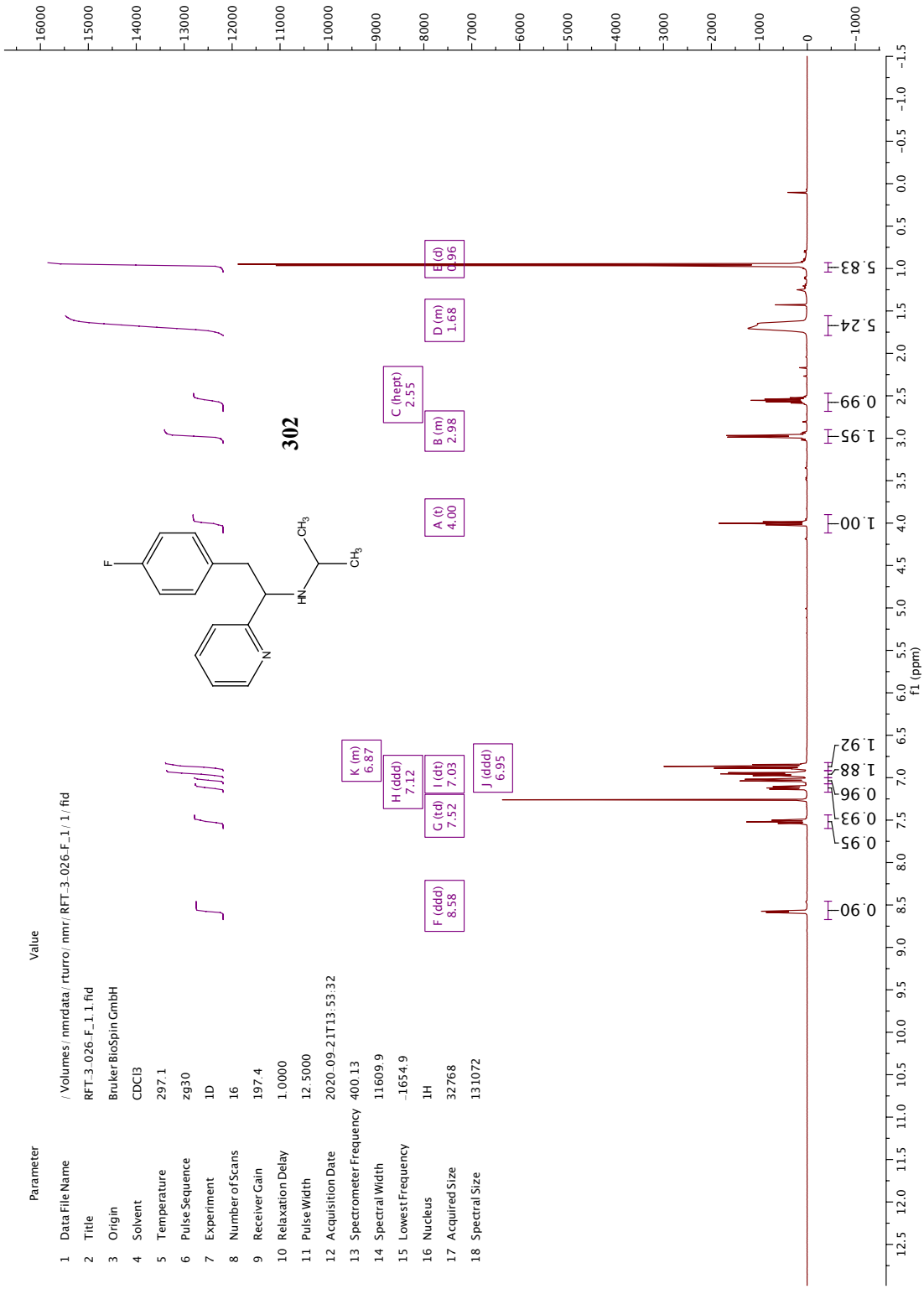

Parameter		Value
1	Data File Name	/Volumes/nmrdata/rturro/nmr/RFT-3_026-F_1/1/fid
2	Title	RFT-3_026-F_1 1.fid
3	Origin	Bruker BioSpin GmbH
4	Solvent	CDCl3
5	Temperature	297.1
6	Pulse Sequence	zg30
7	Experiment	1D
8	Number of Scans	16
9	Receiver Gain	197.4
10	Relaxation Delay	1.0000
11	Pulse Width	12.5000
12	Acquisition Date	2020_09_21T13:53:32
13	Spectrometer Frequency	400.13
14	Spectral Width	11609.9
15	Lowest Frequency	-1654.9
16	Nucleus	1H
17	Acquired Size	32768
18	Spectral Size	131072

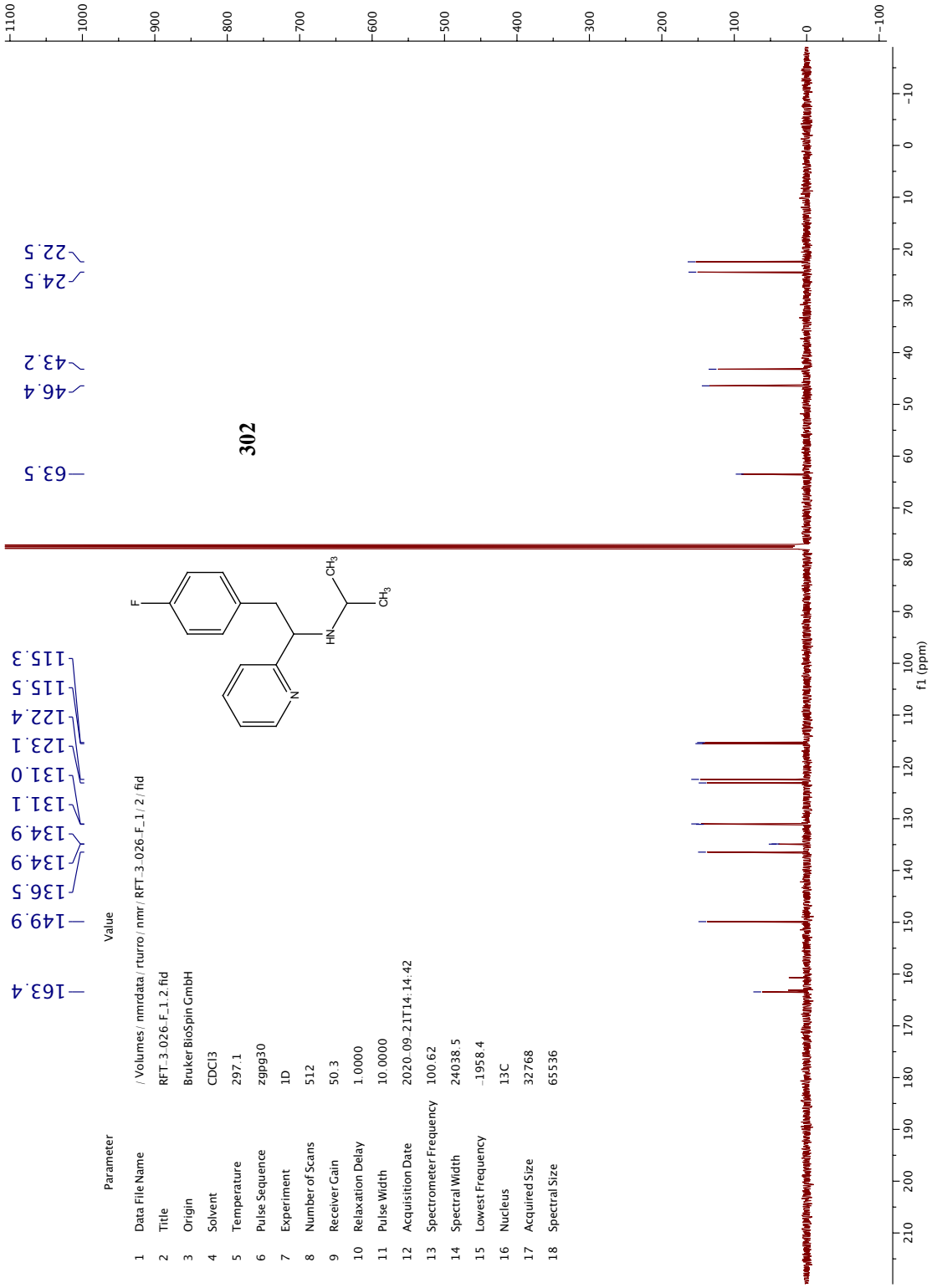

	Parameter	Value
1	Data File Name	/ Volumes / nmrdata / rturro / nmr / RFT_3_026_F_1 / 2 / fid
2	Title	RFT_3_026_F_1_2.fid
3	Origin	Bruker BioSpin GmbH
4	Solvent	CDCl3
5	Temperature	297.1
6	Pulse Sequence	zgpg30
7	Experiment	1D
8	Number of Scans	512
9	Receiver Gain	50.3
10	Relaxation Delay	1.0000
11	Pulse Width	10.0000
12	Acquisition Date	2020_09_21T14:14:42
13	Spectrometer Frequency	100.62
14	Spectral Width	24038.5
15	Lowest Frequency	-1958.4
16	Nucleus	13C
17	Acquired Size	32768
18	Spectral Size	65536

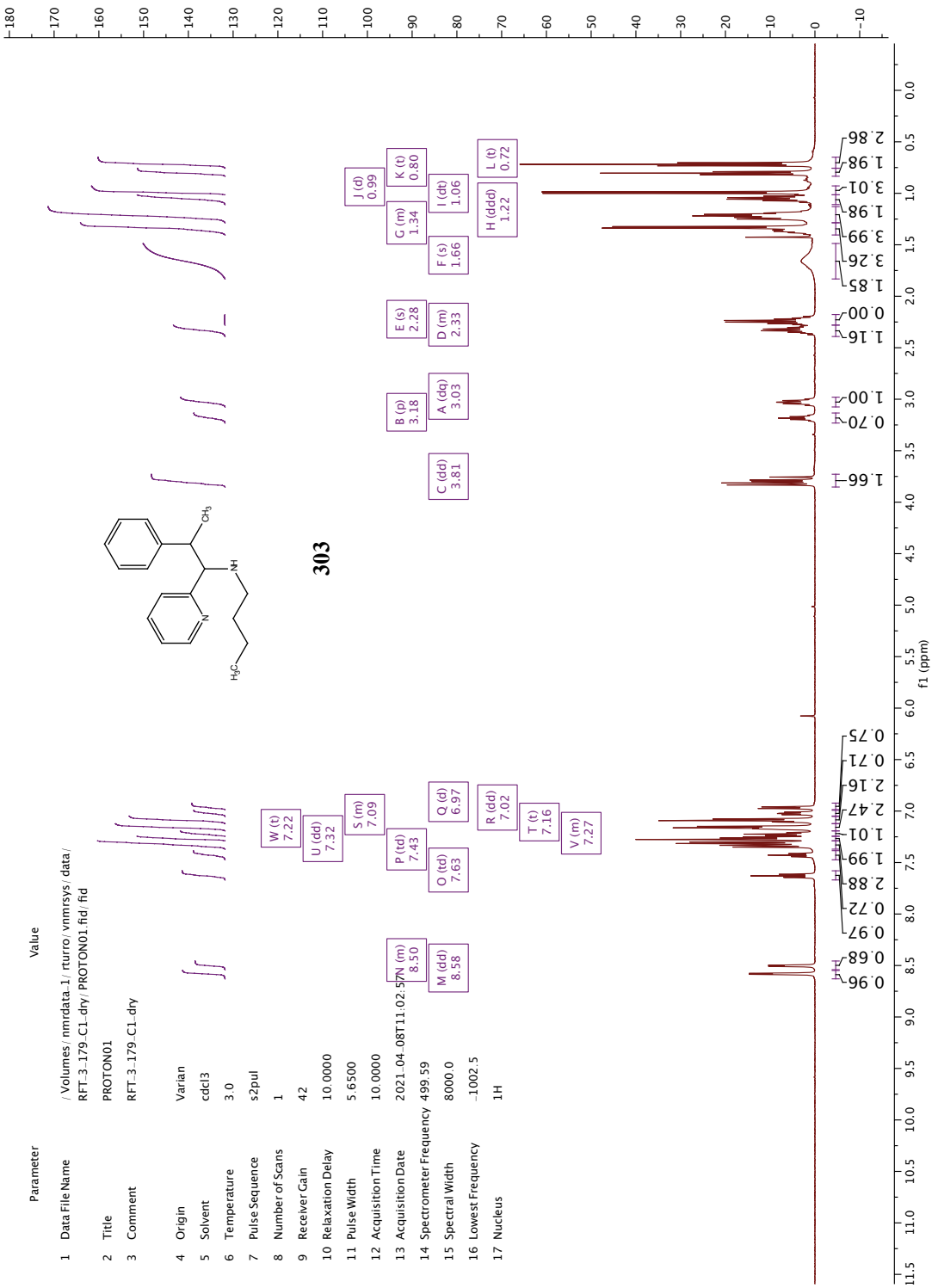
303
Parameter
Value
1 Data File Name /Volumes/nmrdata_1/rturro/vnmrsys/data/RFT_3-179_C1_dry/PROTON01.fid/fid
2 Title PROTON01
3 Comment RFT_3-179_C1_dry
4 Origin Varian
5 Solvent cdcl3
6 Temperature 3.0
7 Pulse Sequence s2pul
8 Number of Scans 1
9 Receiver Gain 42
10 Relaxation Delay 10.0000
11 Pulse Width 5.6500
12 Acquisition Time 10.0000
13 Acquisition Date 2021-04-08T11:02:57
14 Spectrometer Frequency 499.59
15 Spectral Width 8000.0
16 Lowest Frequency -1002.5
17 Nucleus 1H
N (m) 8.50
M (dd) 8.58
O (td) 7.63
P (td) 7.43
Q (d) 6.97
R (dd) 7.02
S (m) 7.09
T (t) 7.16
U (dd) 7.32
V (m) 7.27
W (t) 7.22
A (dq) 3.03
B (p) 3.18
C (dd) 3.81
D (m) 2.33
E (s) 2.28
F (s) 1.66
G (m) 1.34
H (ddd) 1.22
I (dt) 1.06
J (d) 0.99
K (t) 0.80
L (t) 0.72
f1 (ppm)

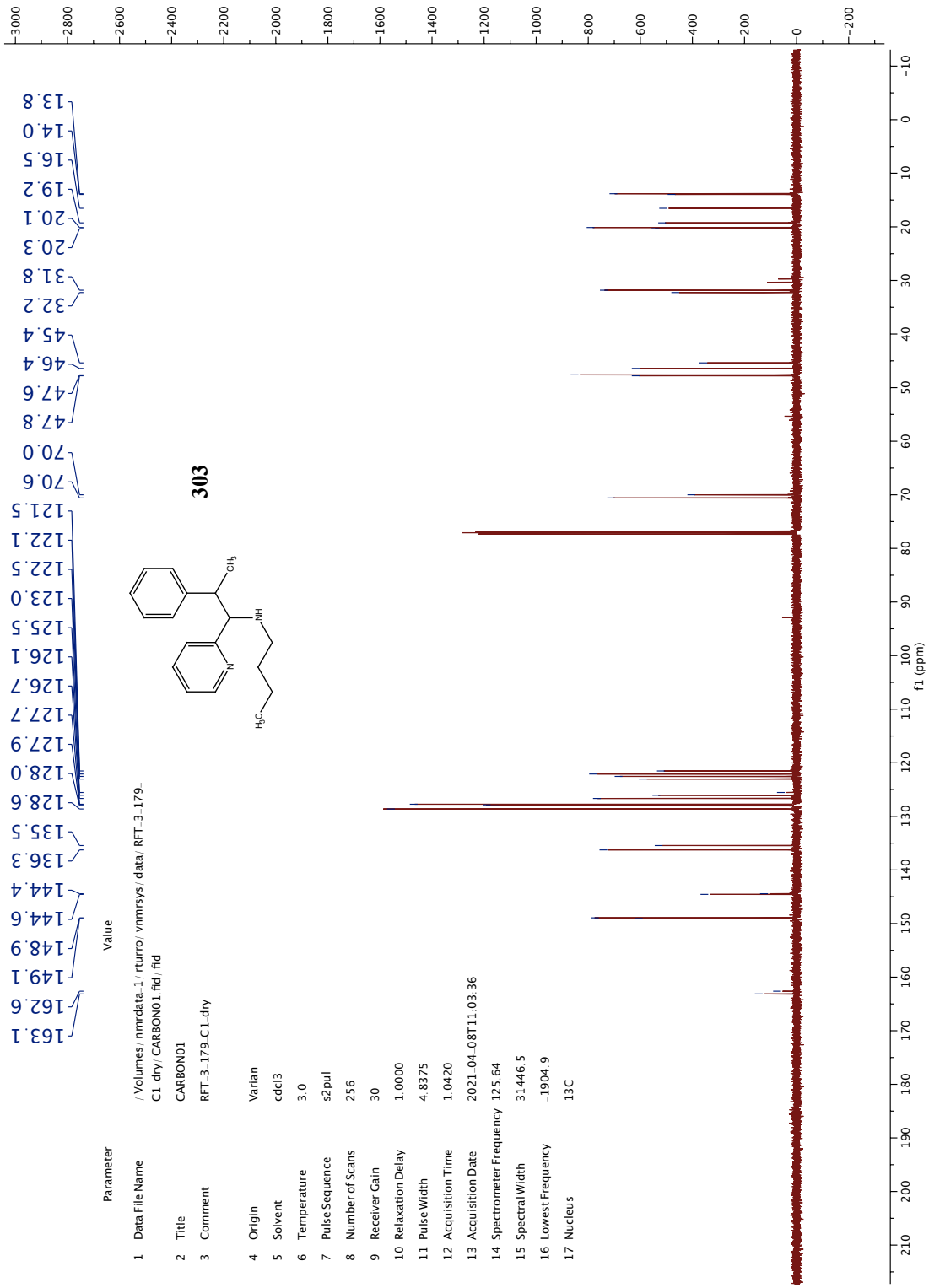
303
f1 (ppm)
Parameter
Value
1 Data File Name
/ Volumes/ nmrdata_1/ rturro/ vnmrsys/ data/ RFT_3_179_C1_dry/ CARBON01.fid/ fid
2 Title
CARBON01
3 Comment
RFT_3_179_C1_dry
4 Origin
Varian
5 Solvent
cdcl3
6 Temperature
3.0
7 Pulse Sequence
s2pul
8 Number of Scans
256
9 Receiver Gain
30
10 Relaxation Delay
1.0000
11 Pulse Width
4.8375
12 Acquisition Time
1.0420
13 Acquisition Date
2021_04_08T11:03:36
14 Spectrometer Frequency
125.64
15 Spectral Width
31446.5
16 Lowest Frequency
-1904.9
17 Nucleus
13C
13.8
14.0
16.5
19.2
20.1
20.3
31.8
32.2
45.4
46.4
47.6
47.8
70.0
70.6
121.5
122.1
122.5
123.0
125.5
126.1
126.7
127.7
127.9
128.0
128.6
135.5
136.3
144.4
144.6
148.9
149.1
162.6
163.1

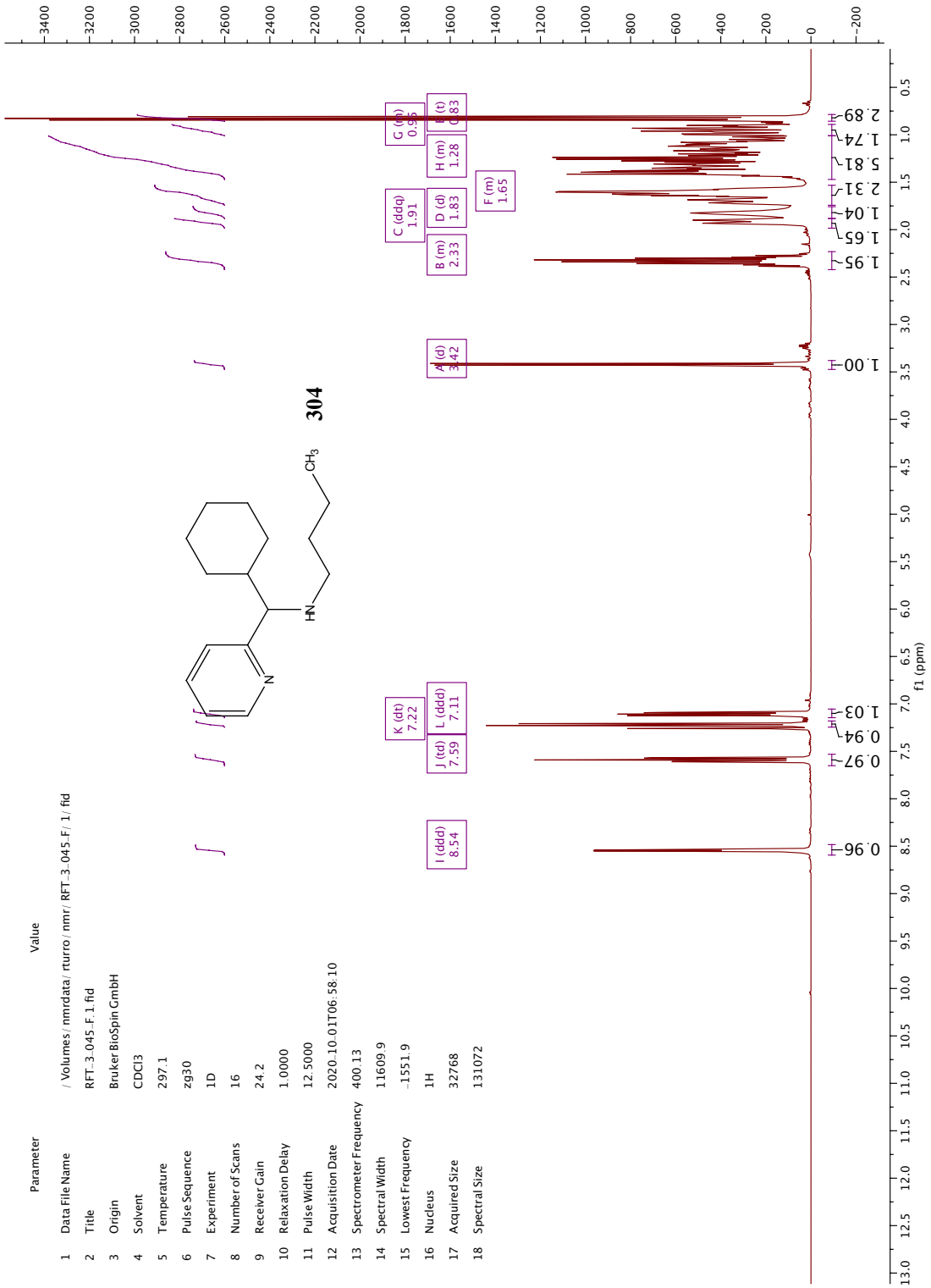

	Parameter	Value
1	Data File Name	/ Volumes / nmrdata / rturro / nmr / RFT_3_045_F / 1 / fid
2	Title	RFT_3_045_F_1.fid
3	Origin	Bruker BioSpin GmbH
4	Solvent	CDCl3
5	Temperature	297.1
6	Pulse Sequence	zg30
7	Experiment	1D
8	Number of Scans	16
9	Receiver Gain	24.2
10	Relaxation Delay	1.0000
11	Pulse Width	12.5000
12	Acquisition Date	2020-10-01T06:58:10
13	Spectrometer Frequency	400.13
14	Spectral Width	11609.9
15	Lowest Frequency	-1551.9
16	Nucleus	1H
17	Acquired Size	32768
18	Spectral Size	131072

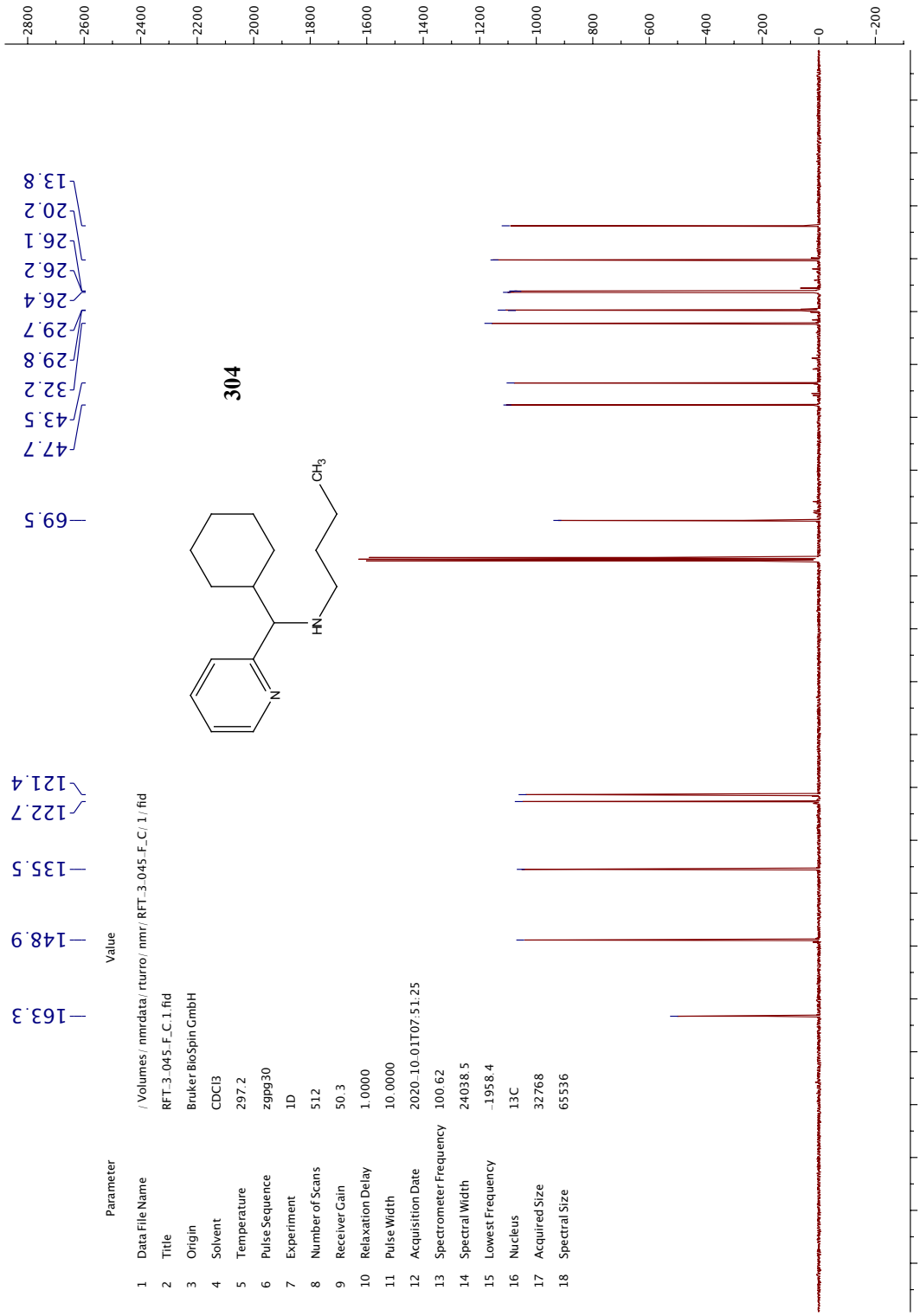

	Parameter	Value
1	Data File Name	/Volumes/nmrdata/rturro/nmr/RFT-3-045-F_C/1/fid
2	Title	RFT-3-045-F_C-1.fid
3	Origin	Bruker BioSpin GmbH
4	Solvent	CDCl3
5	Temperature	297.2
6	Pulse Sequence	zgpg30
7	Experiment	1D
8	Number of Scans	512
9	Receiver Gain	50.3
10	Relaxation Delay	1.0000
11	Pulse Width	10.0000
12	Acquisition Date	2020-10-01T07:51:25
13	Spectrometer Frequency	100.62
14	Spectral Width	24038.5
15	Lowest Frequency	-1958.4
16	Nucleus	13C
17	Acquired Size	32768
18	Spectral Size	65536

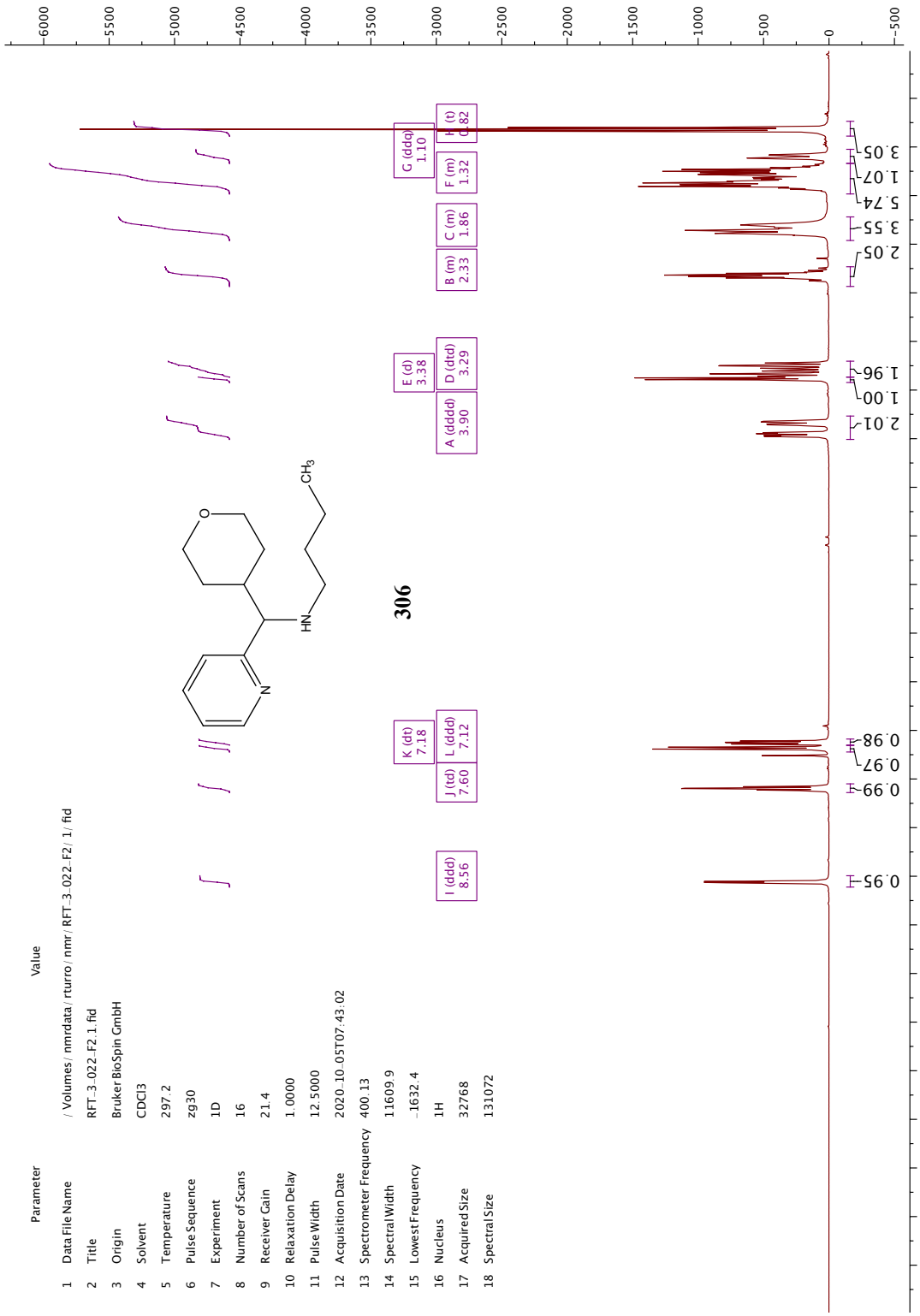
Parameter
Value
1 Data File Name / Volumes/ nmrdata/ rturro/ nmr/ RFT_3_022_F2/ 1/ fid
2 Title RFT_3_022_F2 1 fid
3 Origin Bruker BioSpin GmbH
4 Solvent CDCl3
5 Temperature 297.2
6 Pulse Sequence zg30
7 Experiment 1D
8 Number of Scans 16
9 Receiver Gain 21.4
10 Relaxation Delay 1.0000
11 Pulse Width 12.5000
12 Acquisition Date 2020_10_05T07:43:02
13 Spectrometer Frequency 400.13
14 Spectral Width 11609.9
15 Lowest Frequency -1632.4
16 Nucleus 1H
17 Acquired Size 32768
18 Spectral Size 131072
306
I (ddd) 8.56
J (td) 7.60
K (dt) 7.18
L (ddd) 7.12
A (dddd) 3.90
D (dtd) 3.29
E (d) 3.38
G (ddq) 1.10
B (m) 2.33
C (m) 1.86
F (m) 1.32
H (t) 0.82
0.95
0.99
0.97
0.98
2.01
1.00
1.96
2.05
3.55
5.74
1.07
3.05
f1 (ppm)

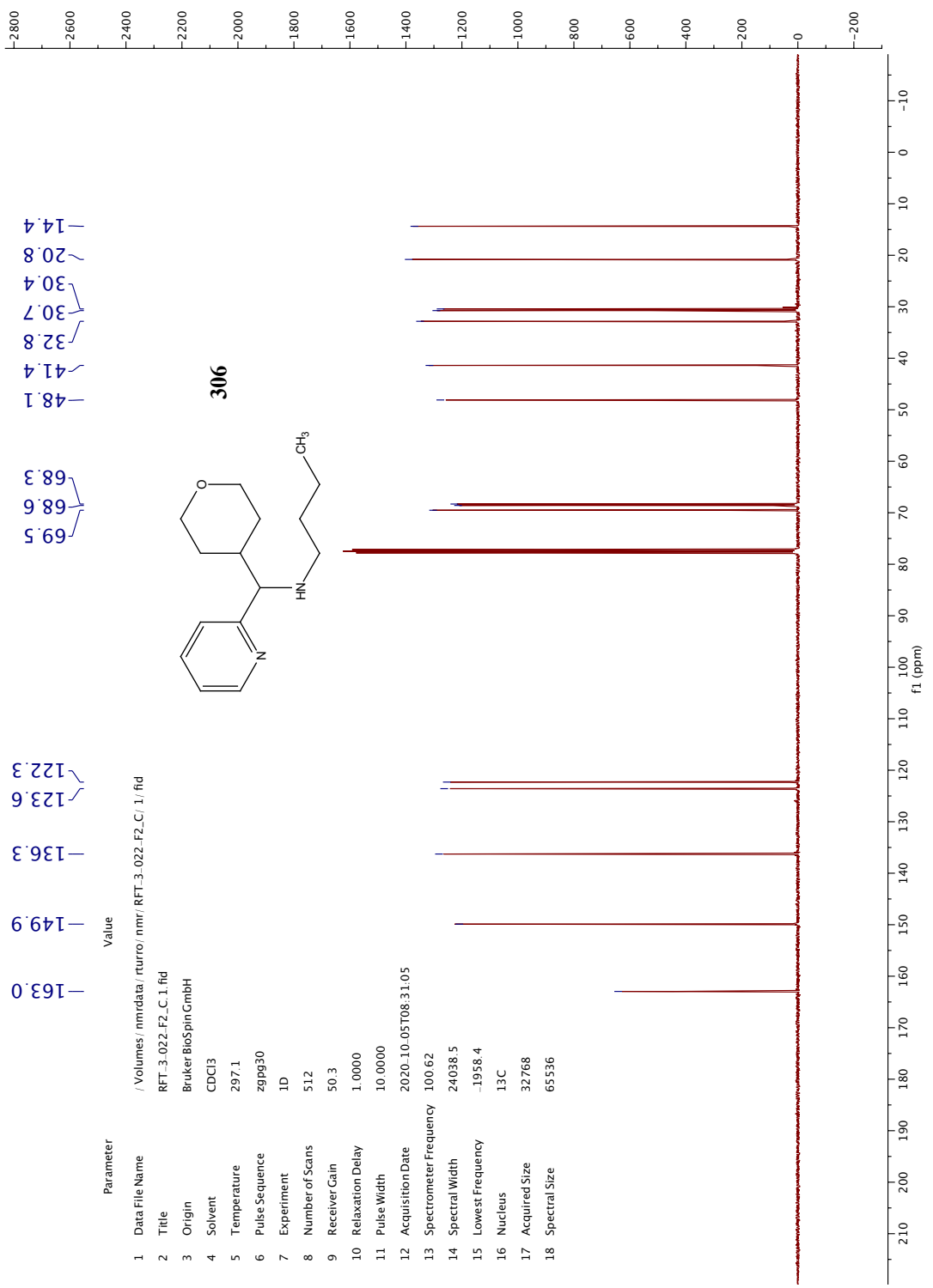

	Parameter	Value
1	Data File Name	/Volumes/nmrdata/rturro/nmr/RFT_3_022_F2_C/1/fid
2	Title	RFT_3_022_F2_C 1 fid
3	Origin	Bruker BioSpin GmbH
4	Solvent	CDCl3
5	Temperature	297.1
6	Pulse Sequence	zgpg30
7	Experiment	1D
8	Number of Scans	512
9	Receiver Gain	50.3
10	Relaxation Delay	1.0000
11	Pulse Width	10.0000
12	Acquisition Date	2020-10-05T08:31:05
13	Spectrometer Frequency	100.62
14	Spectral Width	24038.5
15	Lowest Frequency	-1958.4
16	Nucleus	13C
17	Acquired Size	32768
18	Spectral Size	65536

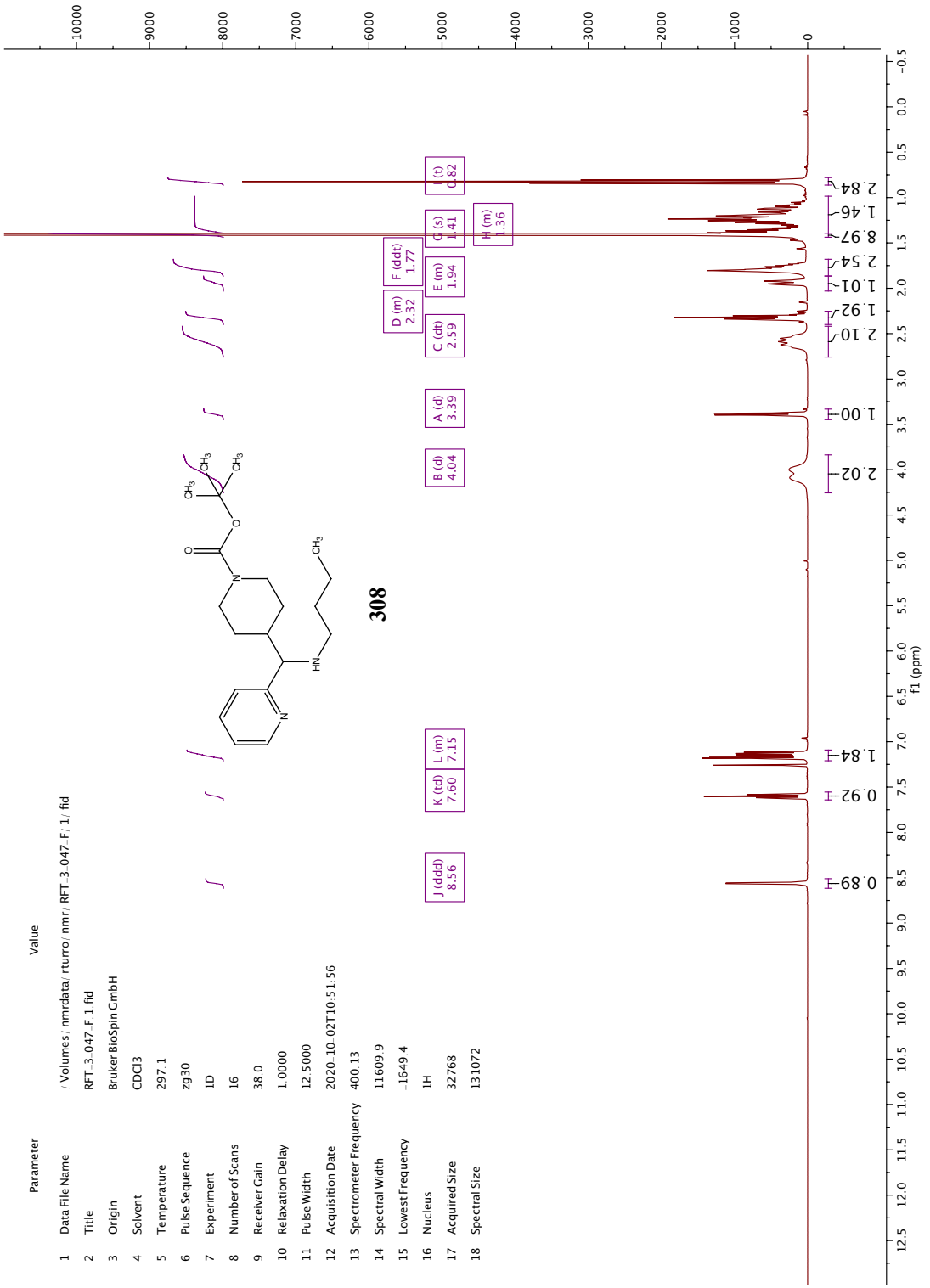
Parameter
Value
1 Data File Name / Volumes/ nmrdata/ rturro/ nmr/ RFT_3.047_F/ 1/ fid
2 Title RFT_3.047_F 1.fid
3 Origin Bruker BioSpin GmbH
4 Solvent CDCl3
5 Temperature 297.1
6 Pulse Sequence zg30
7 Experiment 1D
8 Number of Scans 16
9 Receiver Gain 38.0
10 Relaxation Delay 1.0000
11 Pulse Width 12.5000
12 Acquisition Date 2020_10_02T10_51_56
13 Spectrometer Frequency 400.13
14 Spectral Width 11609.9
15 Lowest Frequency -1649.4
16 Nucleus 1H
17 Acquired Size 32768
18 Spectral Size 131072
308
J (ddd) 8.56
K (td) 7.60
L (m) 7.15
B (d) 4.04
A (d) 3.39
C (dt) 2.59
D (m) 2.32
F (ddt) 1.77
E (m) 1.94
G (s) 1.41
H (m) 1.36
I (t) 0.82
0.89
0.92
1.84
2.02
1.00
2.10
1.92
1.01
2.54
8.97
1.46
2.84
f1 (ppm)

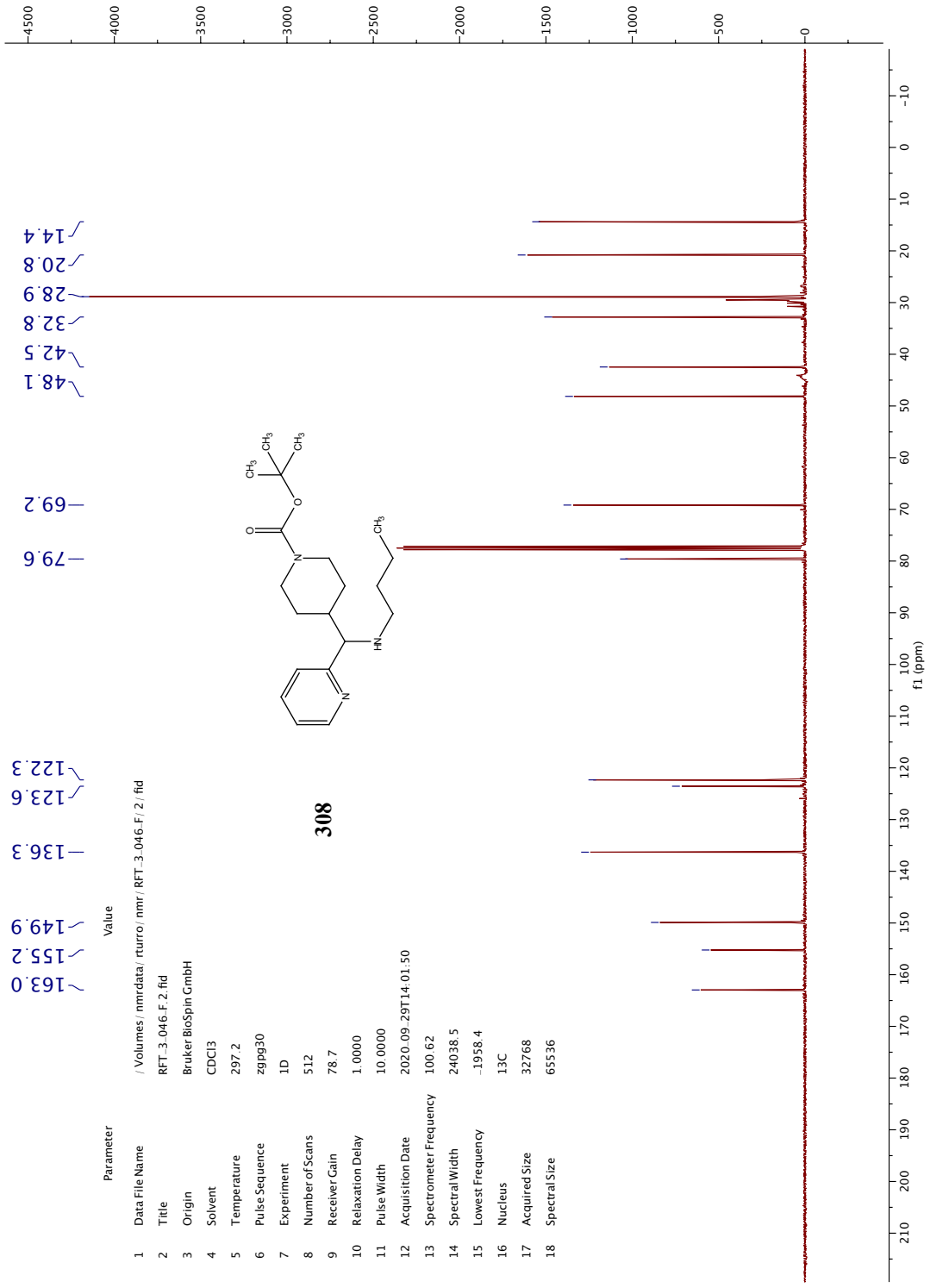

	Parameter	Value
1	Data File Name	/Volumes/nmrdata/rturro/nmr/RFT_3_046_F/2/fid
2	Title	RFT_3_046_F_2.fid
3	Origin	Bruker BioSpin GmbH
4	Solvent	CDCl3
5	Temperature	297.2
6	Pulse Sequence	zgpg30
7	Experiment	1D
8	Number of Scans	512
9	Receiver Gain	78.7
10	Relaxation Delay	1.0000
11	Pulse Width	10.0000
12	Acquisition Date	2020_09_29T14:01:50
13	Spectrometer Frequency	100.62
14	Spectral Width	24038.5
15	Lowest Frequency	-1958.4
16	Nucleus	13C
17	Acquired Size	32768
18	Spectral Size	65536

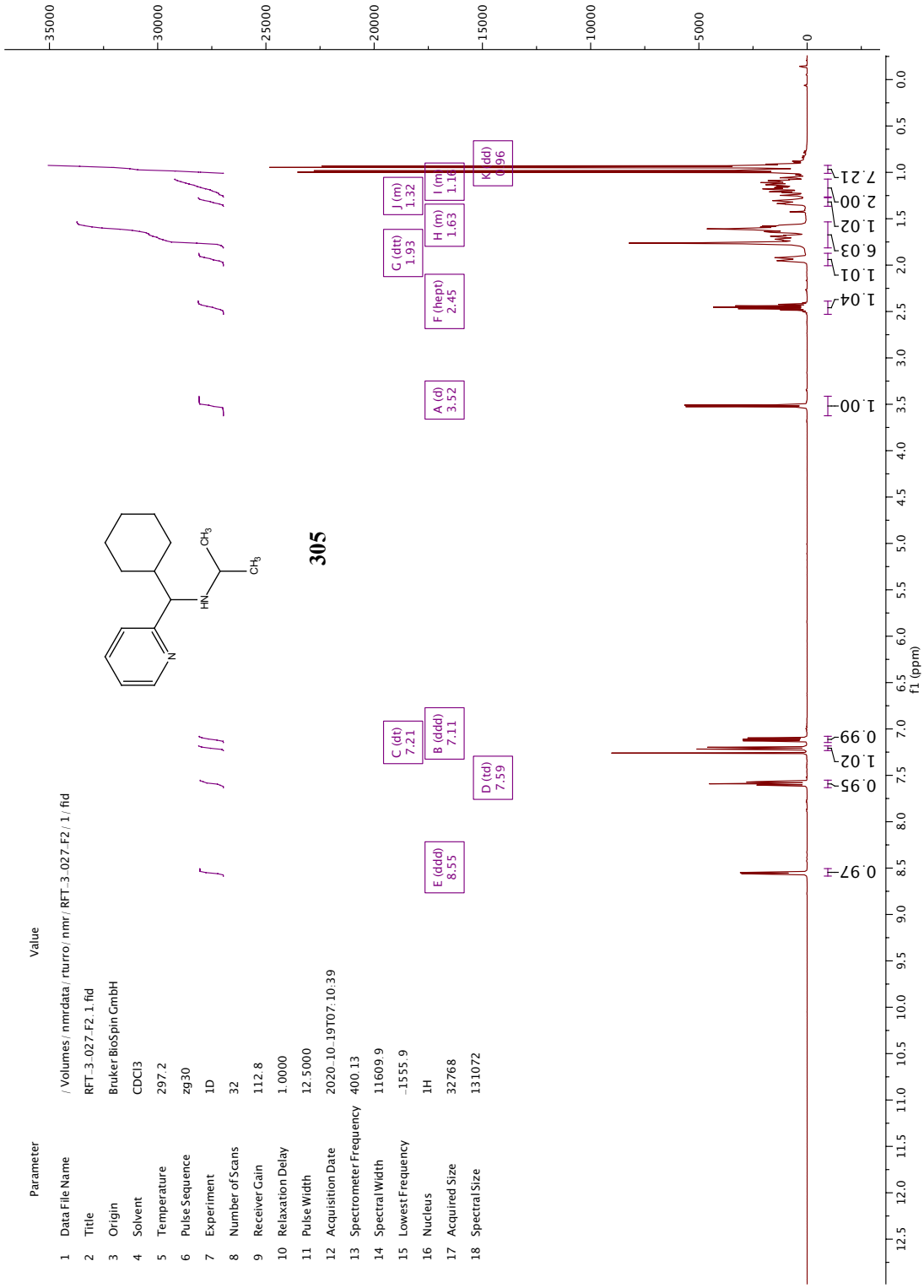
Parameter
Value
1 Data File Name / Volumes / nmrdata / rturro / nmr / RFT-3-027-F2 / 1 / fid
2 Title RFT-3-027-F2_1 fid
3 Origin Bruker BioSpin GmbH
4 Solvent CDCl3
5 Temperature 297.2
6 Pulse Sequence zg30
7 Experiment 1D
8 Number of Scans 32
9 Receiver Gain 112.8
10 Relaxation Delay 1.0000
11 Pulse Width 12.5000
12 Acquisition Date 2020_10_19T07.10.39
13 Spectrometer Frequency 400.13
14 Spectral Width 11609.9
15 Lowest Frequency -1555.9
16 Nucleus 1H
17 Acquired Size 32768
18 Spectral Size 131072
305
A (d) 3.52
B (ddd) 7.11
C (dt) 7.21
D (td) 7.59
E (ddd) 8.55
F (hept) 2.45
G (dtt) 1.93
H (m) 1.63
I (m) 1.16
J (m) 1.32
K (dd) 0.96
1.00
0.97
0.95
1.02
0.99
1.04
1.01
6.03
1.02
2.00
7.21
f1 (ppm)

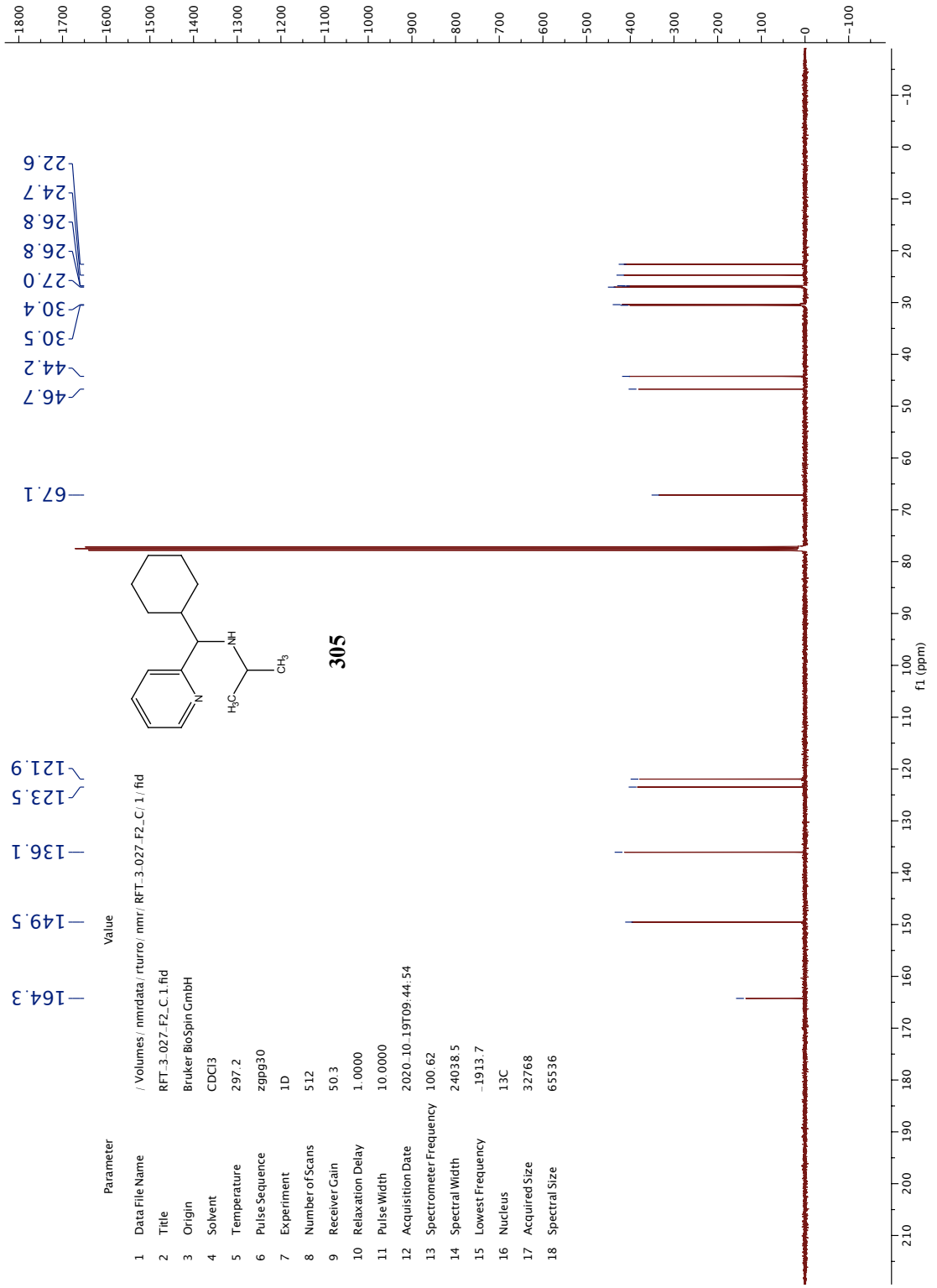

Parameter	Value
1 Data File Name	/ Volumes/ nmrdata/ rturro/ nmr/ RFT_3_027_F2_C/ 1/ fid
2 Title	RFT_3_027_F2_C_1.fid
3 Origin	Bruker BioSpin GmbH
4 Solvent	CDCl3
5 Temperature	297.2
6 Pulse Sequence	zgpg30
7 Experiment	1D
8 Number of Scans	512
9 Receiver Gain	50.3
10 Relaxation Delay	1.0000
11 Pulse Width	10.0000
12 Acquisition Date	2020_10_19T09:44:54
13 Spectrometer Frequency	100.62
14 Spectral Width	24038.5
15 Lowest Frequency	-1913.7
16 Nucleus	13C
17 Acquired Size	32768
18 Spectral Size	65536

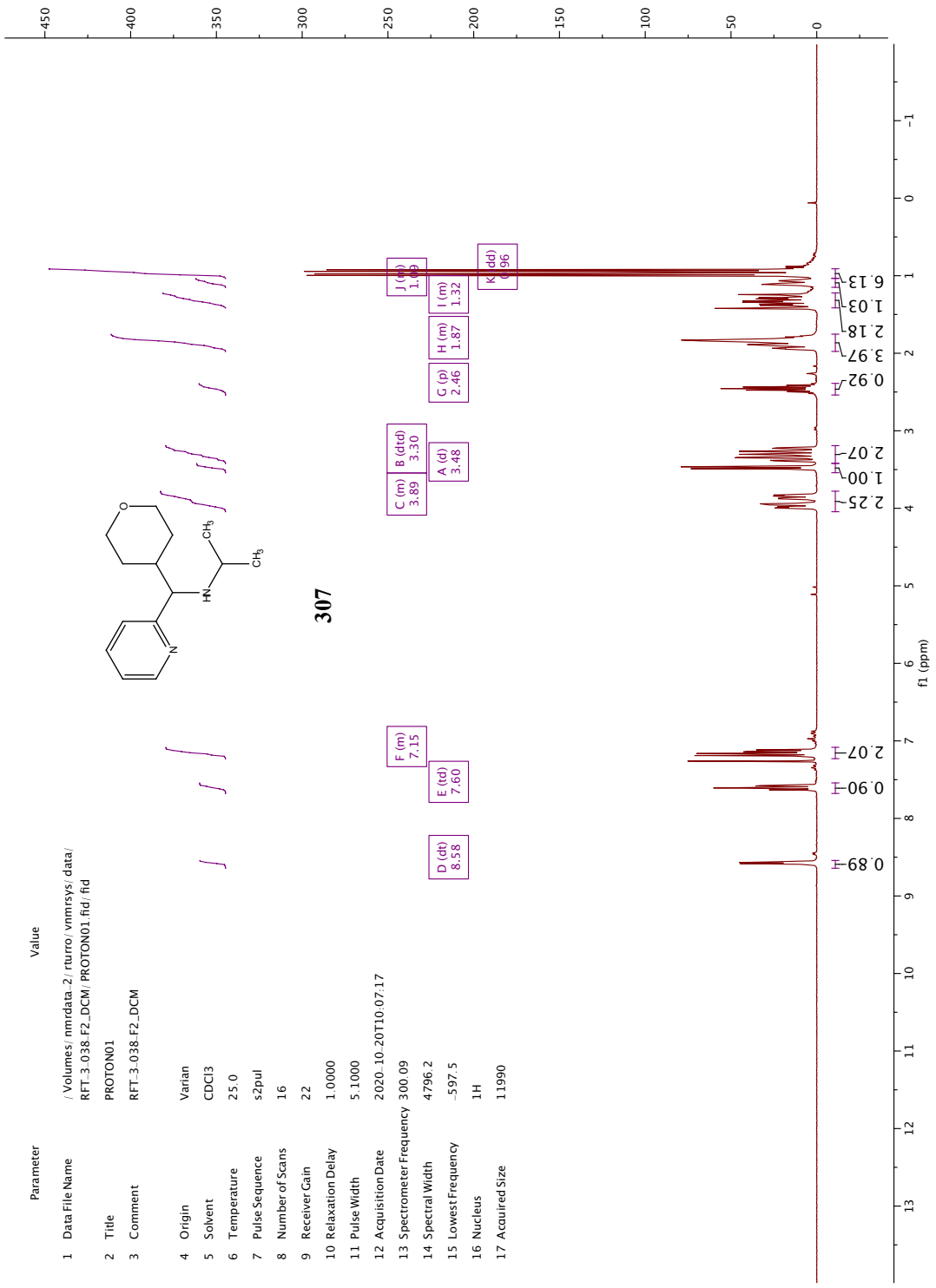
Parameter
Value
1 Data File Name
/ Volumes/ nmrdata_2/ rturro/ vnmrsys/ data/ RFT_3_038_F2_DCM/ PROTON01_fid/ fid
2 Title
PROTON01
3 Comment
RFT_3_038_F2_DCM
4 Origin
Varian
5 Solvent
CDCl3
6 Temperature
25.0
7 Pulse Sequence
s2pul
8 Number of Scans
16
9 Receiver Gain
22
10 Relaxation Delay
1.0000
11 Pulse Width
5.1000
12 Acquisition Date
2020_10_20T10:07:17
13 Spectrometer Frequency
300.09
14 Spectral Width
4796.2
15 Lowest Frequency
-597.5
16 Nucleus
1H
17 Acquired Size
11990
307
D (dt) 8.58
E (td) 7.60
F (m) 7.15
C (m) 3.89
B (dtd) 3.30
A (d) 3.48
G (p) 2.46
H (m) 1.87
I (m) 1.32
J (m) 1.09
K (dd) 0.96
0.89
0.90
2.07
2.25
1.00
2.07
0.92
3.97
2.18
1.03
6.13
f1 (ppm)

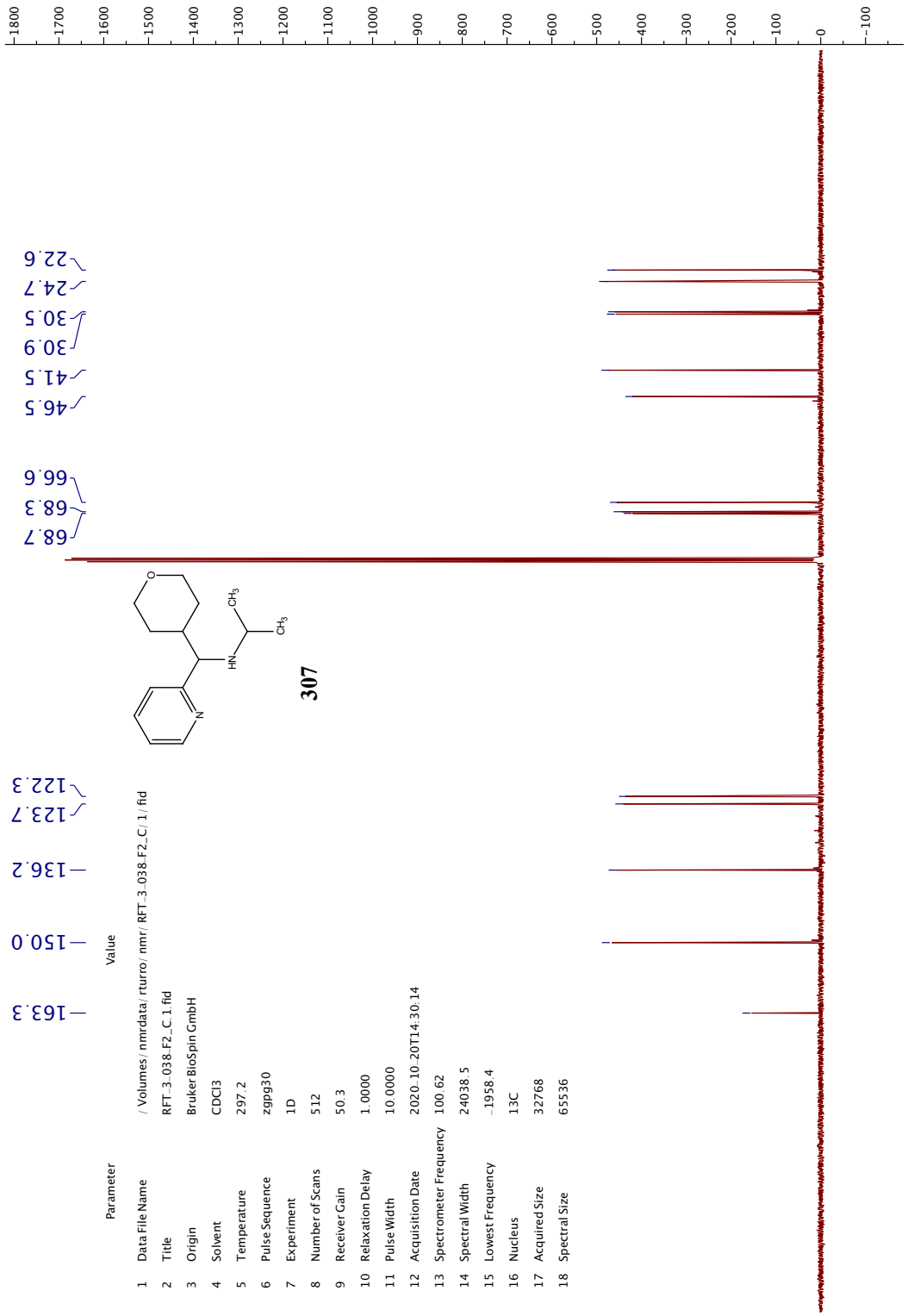

	Parameter	Value
1	Data File Name	/Volumes/nmrdata/rturro/nmr/RFT_3_038_F2_C/1/fid
2	Title	RFT_3_038_F2_C 1 fid
3	Origin	Bruker BioSpin GmbH
4	Solvent	CDCl3
5	Temperature	297.2
6	Pulse Sequence	zgpg30
7	Experiment	1D
8	Number of Scans	512
9	Receiver Gain	50.3
10	Relaxation Delay	1.0000
11	Pulse Width	10.0000
12	Acquisition Date	2020_10_20T14:30:14
13	Spectrometer Frequency	100.62
14	Spectral Width	24038.5
15	Lowest Frequency	-1958.4
16	Nucleus	13C
17	Acquired Size	32768
18	Spectral Size	65536

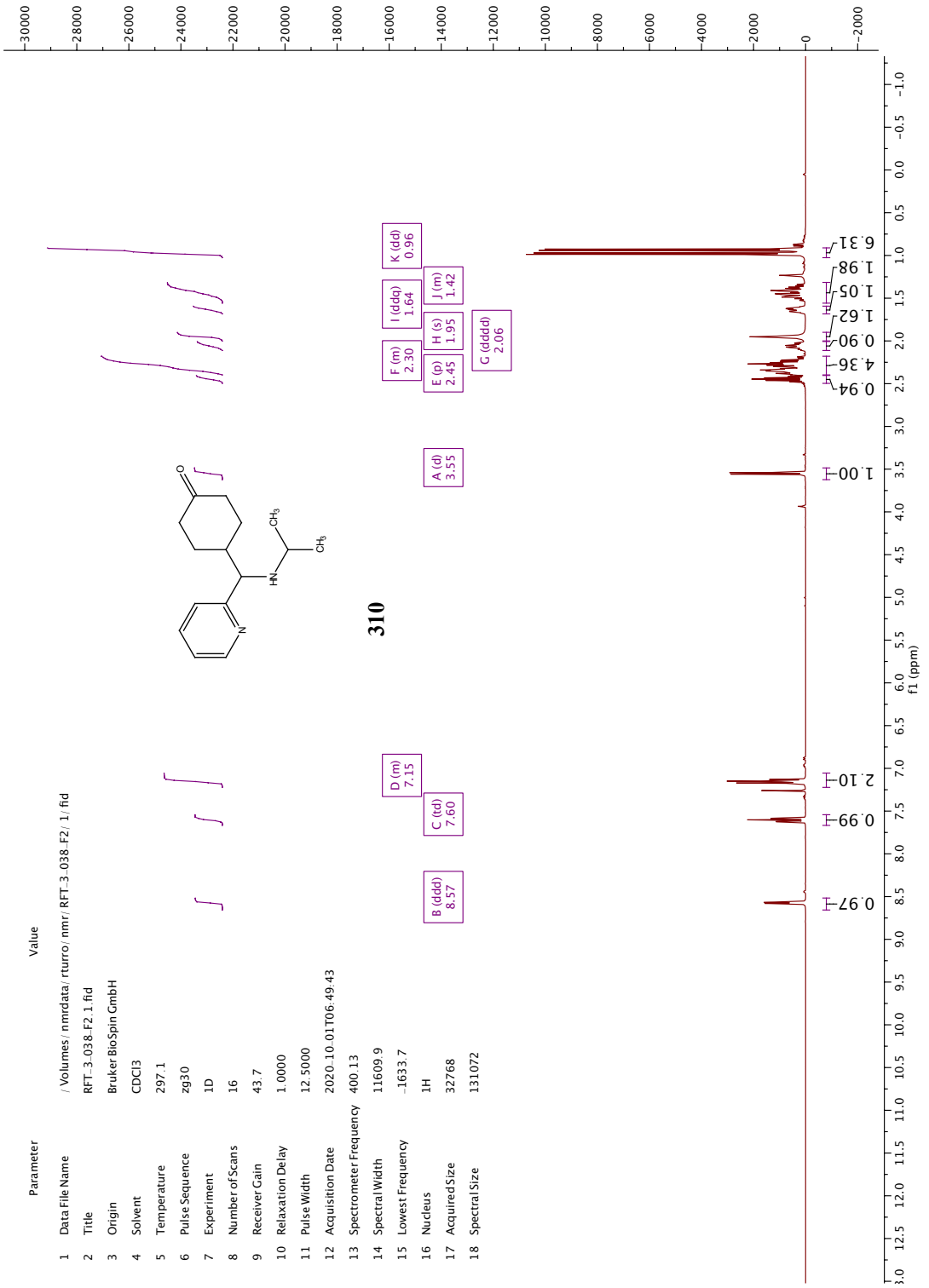
Parameter
Value
1 Data File Name / Volumes/ nmrdata/ rturro/ nmr/ RFT-3-038-F2/ 1/ fid
2 Title RFT-3_038-F2_1.fid
3 Origin Bruker BioSpin GmbH
4 Solvent CDCl3
5 Temperature 297.1
6 Pulse Sequence zg30
7 Experiment 1D
8 Number of Scans 16
9 Receiver Gain 43.7
10 Relaxation Delay 1.0000
11 Pulse Width 12.5000
12 Acquisition Date 2020_10_01T06:49:43
13 Spectrometer Frequency 400.13
14 Spectral Width 11609.9
15 Lowest Frequency -1633.7
16 Nucleus 1H
17 Acquired Size 32768
18 Spectral Size 131072
310
A (d) 3.55
B (ddd) 8.57
C (td) 7.60
D (m) 7.15
E (p) 2.45
F (m) 2.30
G (dddd) 2.06
H (s) 1.95
I (ddq) 1.64
J (m) 1.42
K (dd) 0.96
6.31
1.98
1.05
1.62
0.90
4.36
0.94
1.00
2.10
0.99
0.97
f1 (ppm)

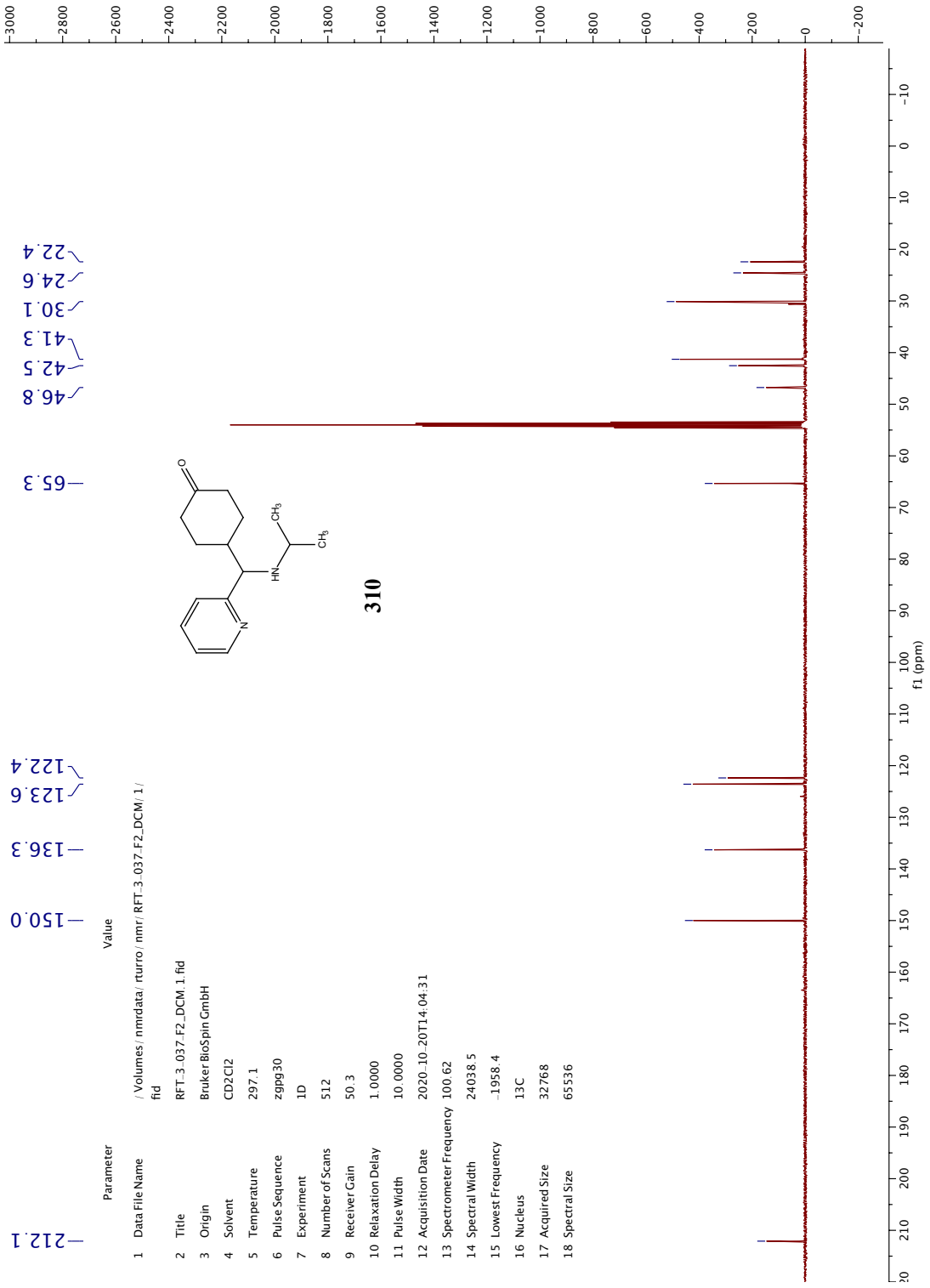

	Parameter	Value
1	Data File Name	/Volumes/nmrdata/rturro/nmr/RFT-3-037-F2_DCM/1/fid
2	Title	RFT_3_037_F2_DCM_1.fid
3	Origin	Bruker BioSpin GmbH
4	Solvent	CD2Cl2
5	Temperature	297.1
6	Pulse Sequence	zgpg30
7	Experiment	1D
8	Number of Scans	512
9	Receiver Gain	50.3
10	Relaxation Delay	1.0000
11	Pulse Width	10.0000
12	Acquisition Date	2020_10_20T14:04:31
13	Spectrometer Frequency	100.62
14	Spectral Width	24038.5
15	Lowest Frequency	-1958.4
16	Nucleus	13C
17	Acquired Size	32768
18	Spectral Size	65536

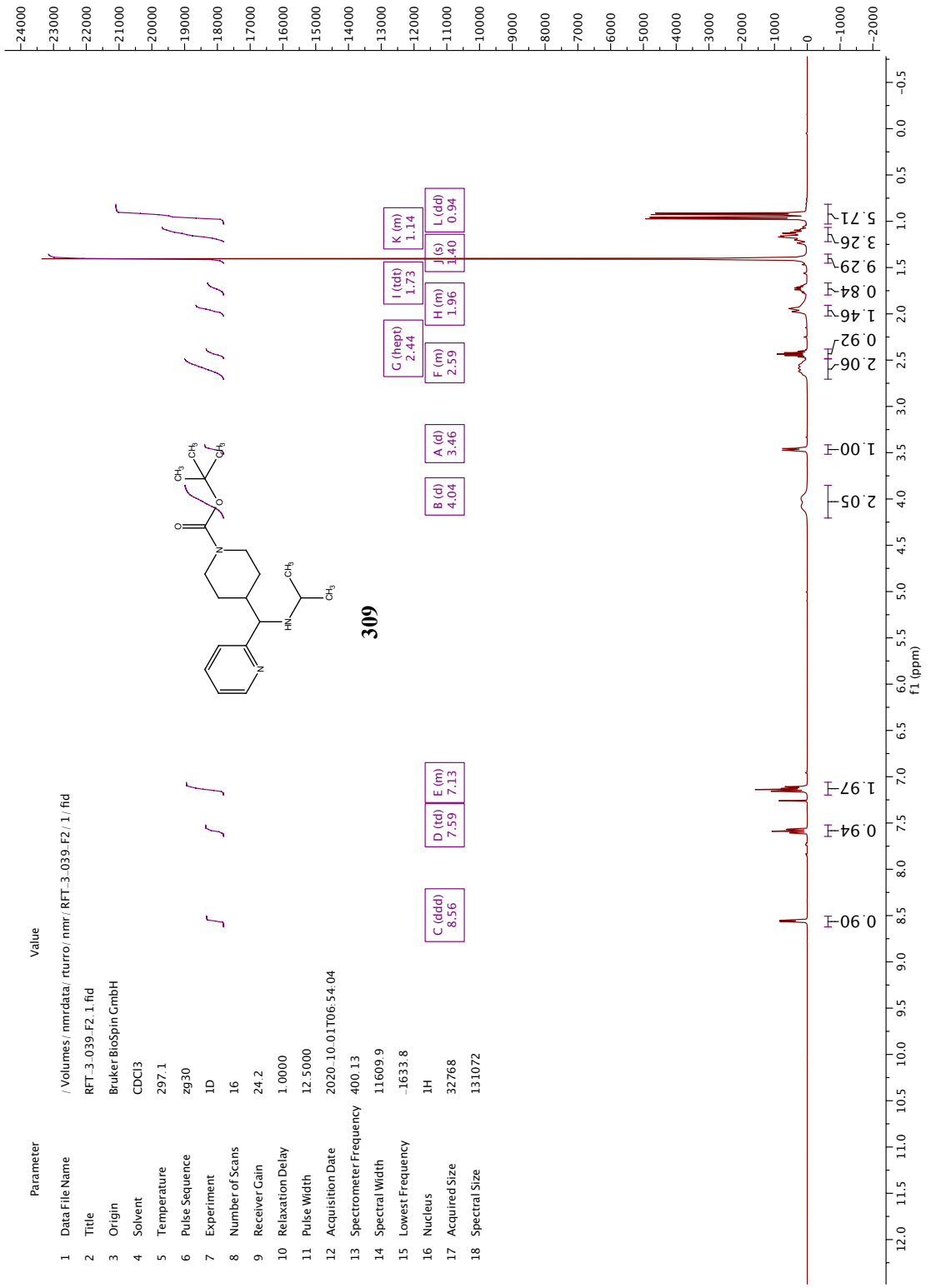
Parameter
Value
1 Data File Name / Volumes/ nmrdata/ rturro/ nmr/ RFT-3-039-F2/ 1/ fid
2 Title RFT-3-039-F2 1 fid
3 Origin Bruker BioSpin GmbH
4 Solvent CDCl3
5 Temperature 297.1
6 Pulse Sequence zg30
7 Experiment 1D
8 Number of Scans 16
9 Receiver Gain 24.2
10 Relaxation Delay 1.0000
11 Pulse Width 12.5000
12 Acquisition Date 2020-10-01T06:54:04
13 Spectrometer Frequency 400.13
14 Spectral Width 11609.9
15 Lowest Frequency -1633.8
16 Nucleus 1H
17 Acquired Size 32768
18 Spectral Size 131072
309
C (ddd) 8.56
D (td) 7.59
E (m) 7.13
B (d) 4.04
A (d) 3.46
G (hept) 2.44
F (m) 2.59
H (m) 1.96
I (tdt) 1.73
J (s) 1.40
K (m) 1.14
L (dd) 0.94
0.90
0.94
1.97
2.05
1.00
2.06
0.92
1.46
0.84
9.29
3.26
5.71
f1 (ppm)

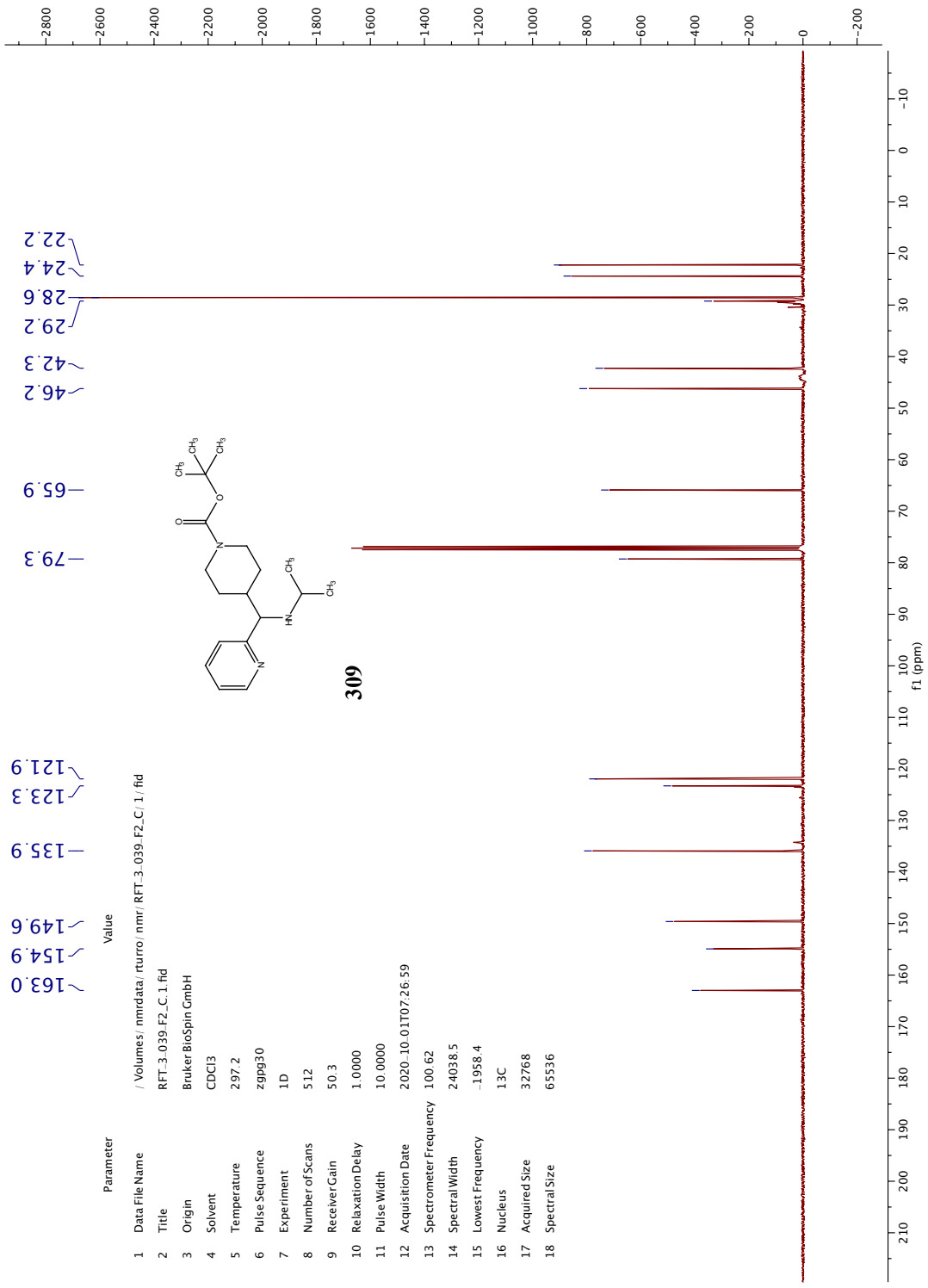

Parameter	Value
1 Data File Name	/Volumes/nmrdata/rturro/nmr/RFT_3_039_F2_C/1/fid
2 Title	RFT_3_039_F2_C_1 fid
3 Origin	Bruker BioSpin GmbH
4 Solvent	CDCl3
5 Temperature	297.2
6 Pulse Sequence	zgpg30
7 Experiment	1D
8 Number of Scans	512
9 Receiver Gain	50.3
10 Relaxation Delay	1.0000
11 Pulse Width	10.0000
12 Acquisition Date	2020_10_01T07:26:59
13 Spectrometer Frequency	100.62
14 Spectral Width	24038.5
15 Lowest Frequency	-1958.4
16 Nucleus	13C
17 Acquired Size	32768
18 Spectral Size	65536

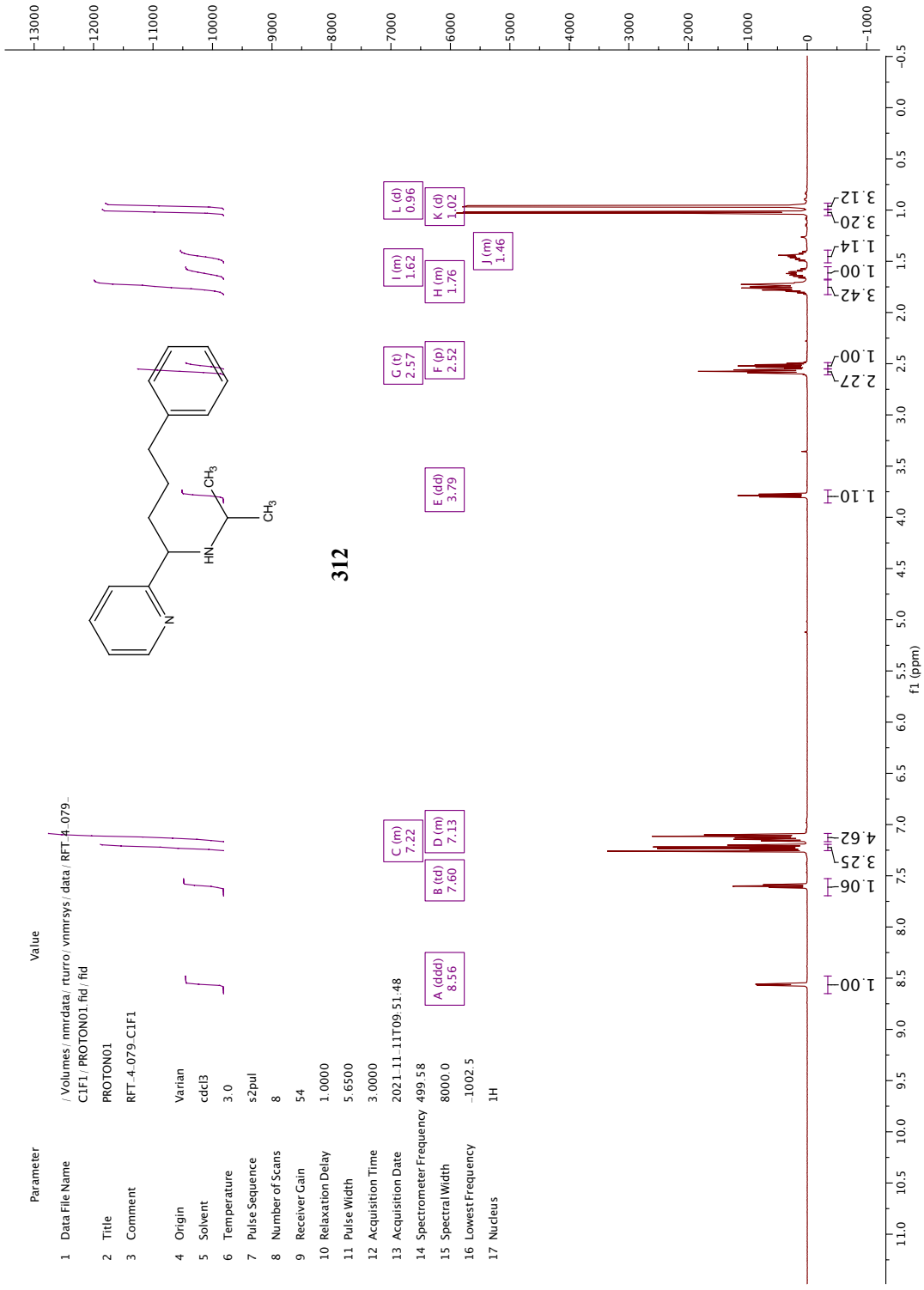

Parameter		Value
1	Data File Name	/ Volumes / nmrdata / rturro / vnmrsys / data / RFT_4.079_C1F1 / PROTON01.fid / fid
2	Title	PROTON01
3	Comment	RFT_4.079_C1F1
4	Origin	Varian
5	Solvent	cdcl3
6	Temperature	3.0
7	Pulse Sequence	s2pul
8	Number of Scans	8
9	Receiver Gain	54
10	Relaxation Delay	1.0000
11	Pulse Width	5.6500
12	Acquisition Time	3.0000
13	Acquisition Date	2021-11-11T09:51:48
14	Spectrometer Frequency	499.58
15	Spectral Width	8000.0
16	Lowest Frequency	-1002.5
17	Nucleus	1H

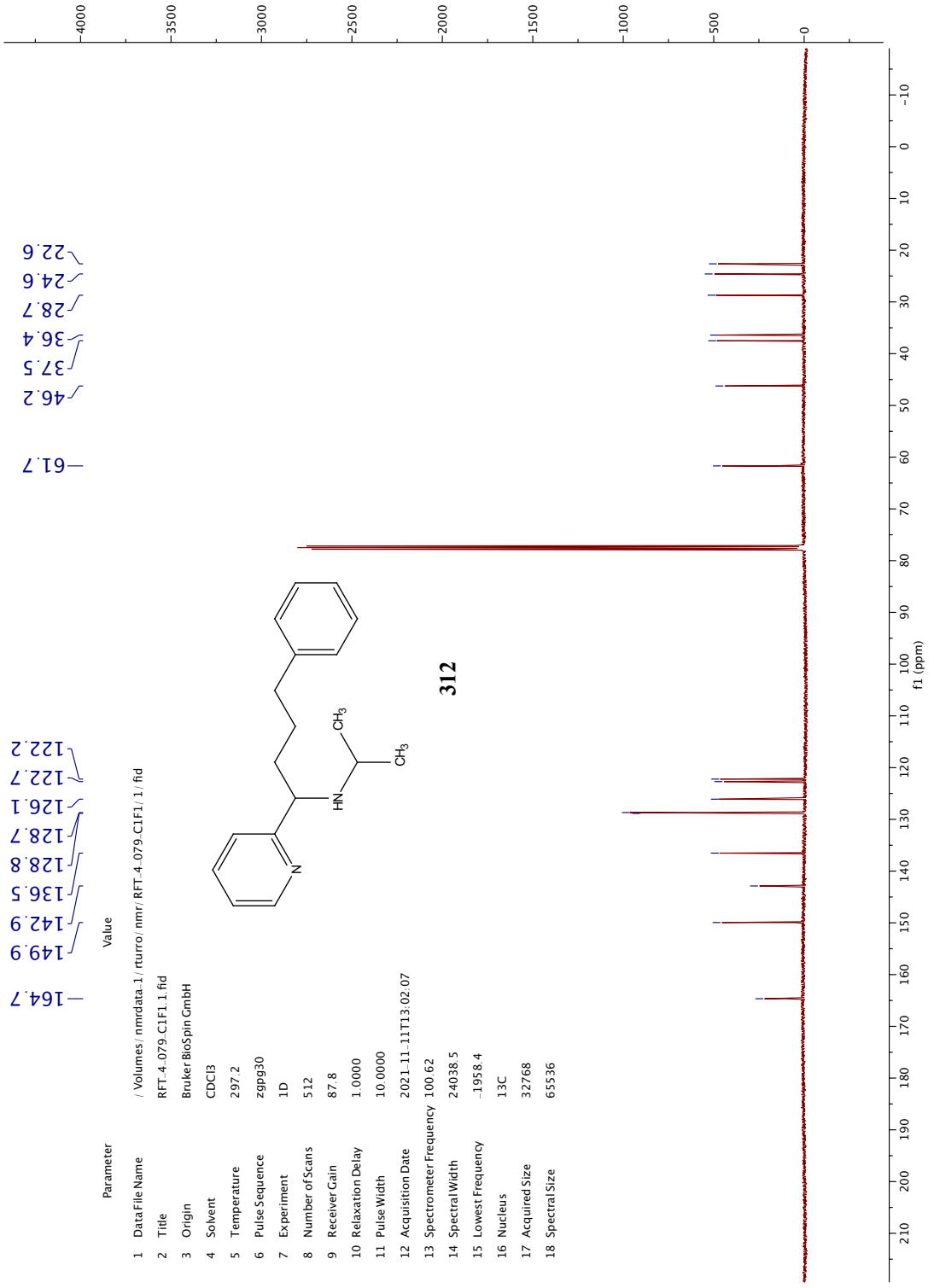

Parameter	Value
1 Data File Name	/ Volumes / nmrdata_1 / rturro / nmr / RFT-4-079_C1F1 / 1 / fid
2 Title	RFT-4-079_C1F1_1.fid
3 Origin	Bruker BioSpin GmbH
4 Solvent	CDCl3
5 Temperature	297.2
6 Pulse Sequence	zgpg30
7 Experiment	1D
8 Number of Scans	512
9 Receiver Gain	87.8
10 Relaxation Delay	1.0000
11 Pulse Width	10.0000
12 Acquisition Date	2021_11_11T13:02:07
13 Spectrometer Frequency	100.62
14 Spectral Width	24038.5
15 Lowest Frequency	-1958.4
16 Nucleus	13C
17 Acquired Size	32768
18 Spectral Size	65536

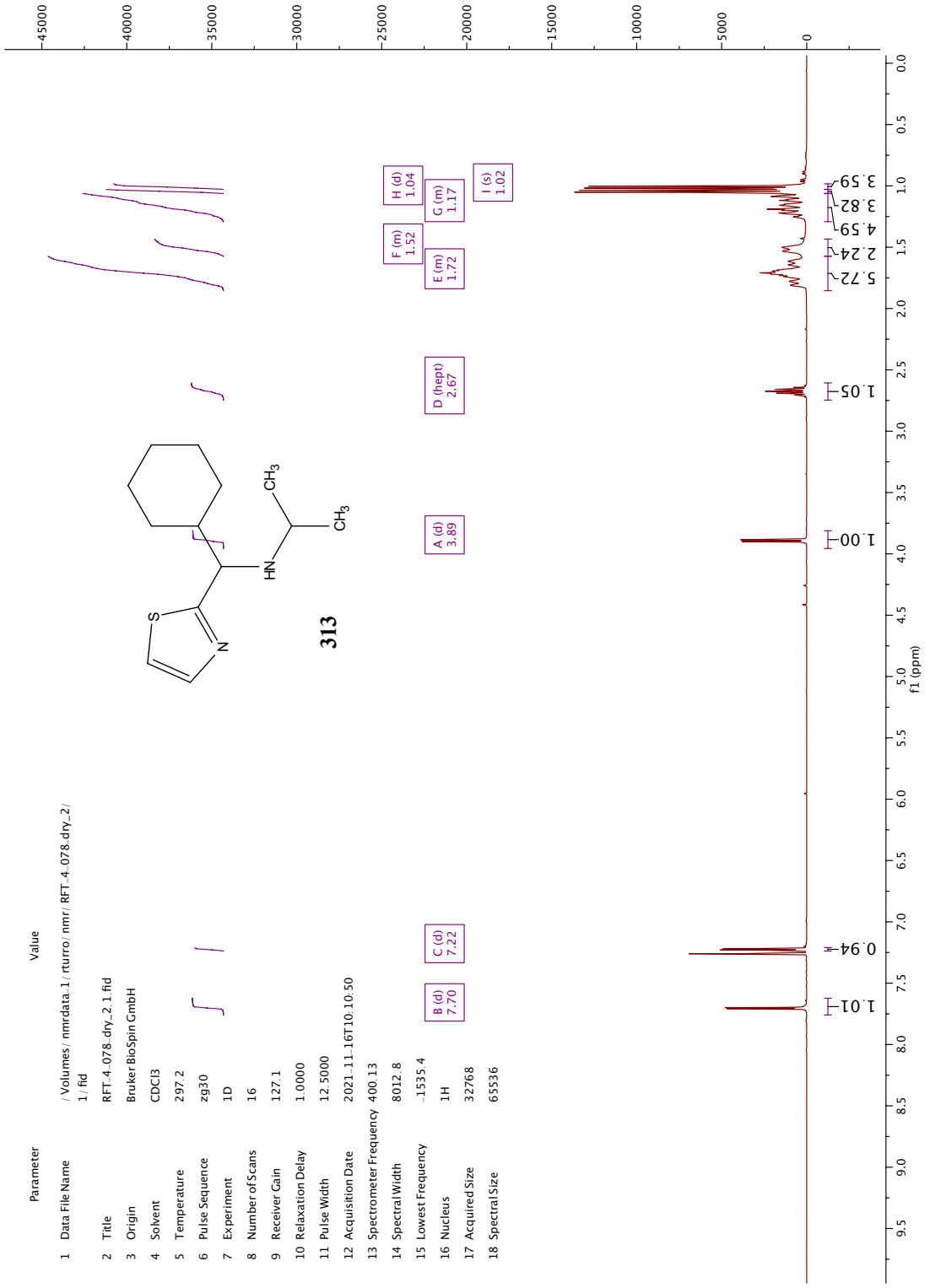

Parameter	Value
1 Data File Name	/Volumes/nmrdata_1/rturro/nmr/RFT_4_078_dry_2/1/fid
2 Title	RFT_4_078_dry_2 1 fid
3 Origin	Bruker BioSpin GmbH
4 Solvent	CDCl3
5 Temperature	297.2
6 Pulse Sequence	zg30
7 Experiment	1D
8 Number of Scans	16
9 Receiver Gain	127.1
10 Relaxation Delay	1.0000
11 Pulse Width	12.5000
12 Acquisition Date	2021-11-16T10:10:50
13 Spectrometer Frequency	400.13
14 Spectral Width	8012.8
15 Lowest Frequency	-1535.4
16 Nucleus	1H
17 Acquired Size	32768
18 Spectral Size	65536

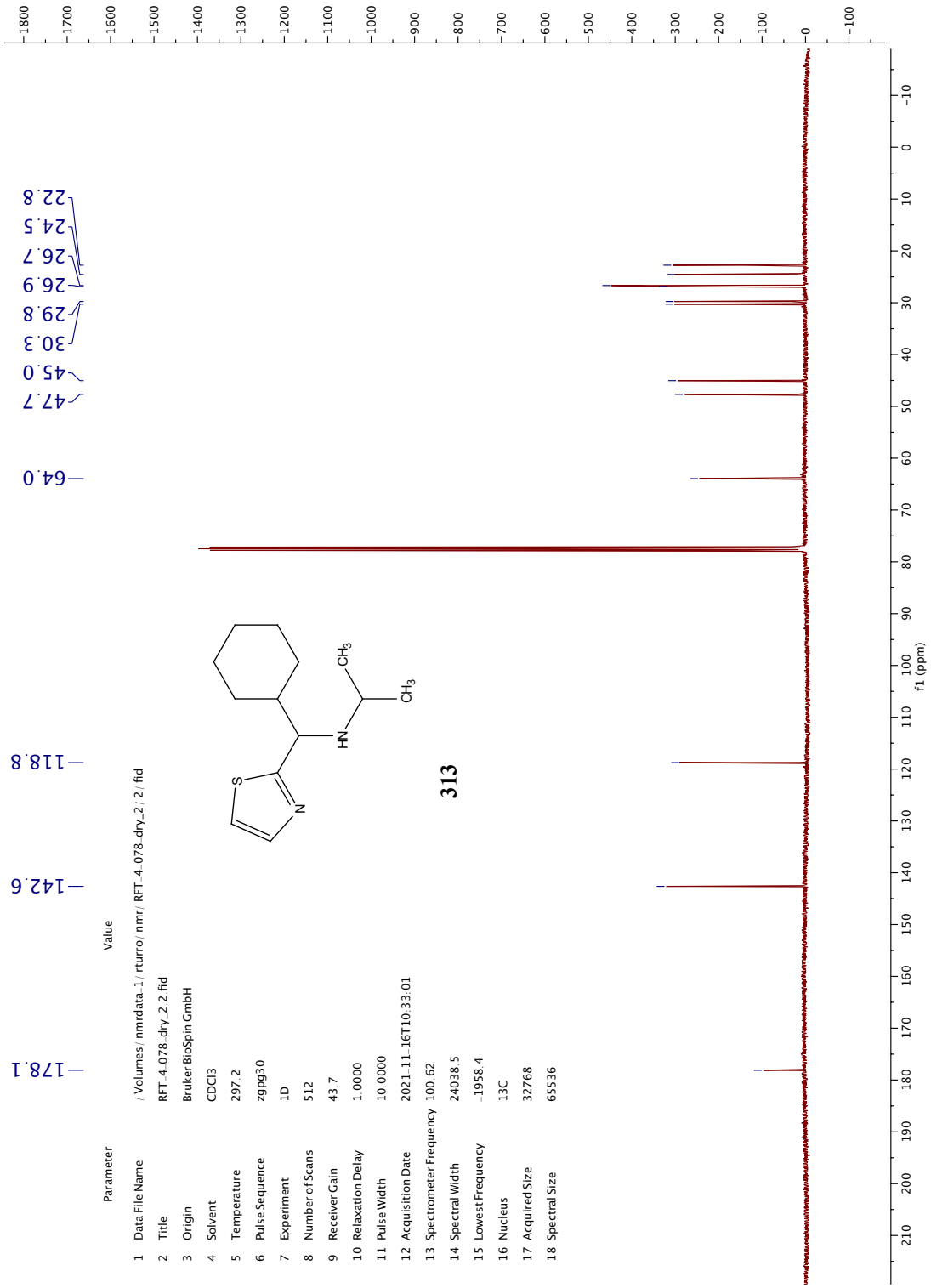

	Parameter	Value
1	Data File Name	/ Volumes / nmrdata_1 / rturro / nmr / RFT_4_078_dry_2 / 2 / fid
2	Title	RFT_4_078_dry_2_2.fid
3	Origin	Bruker BioSpin GmbH
4	Solvent	CDCl3
5	Temperature	297.2
6	Pulse Sequence	zgpg30
7	Experiment	1D
8	Number of Scans	512
9	Receiver Gain	43.7
10	Relaxation Delay	1.0000
11	Pulse Width	10.0000
12	Acquisition Date	2021-11-16T10:33:01
13	Spectrometer Frequency	100.62
14	Spectral Width	24038.5
15	Lowest Frequency	-1958.4
16	Nucleus	13C
17	Acquired Size	32768
18	Spectral Size	65536

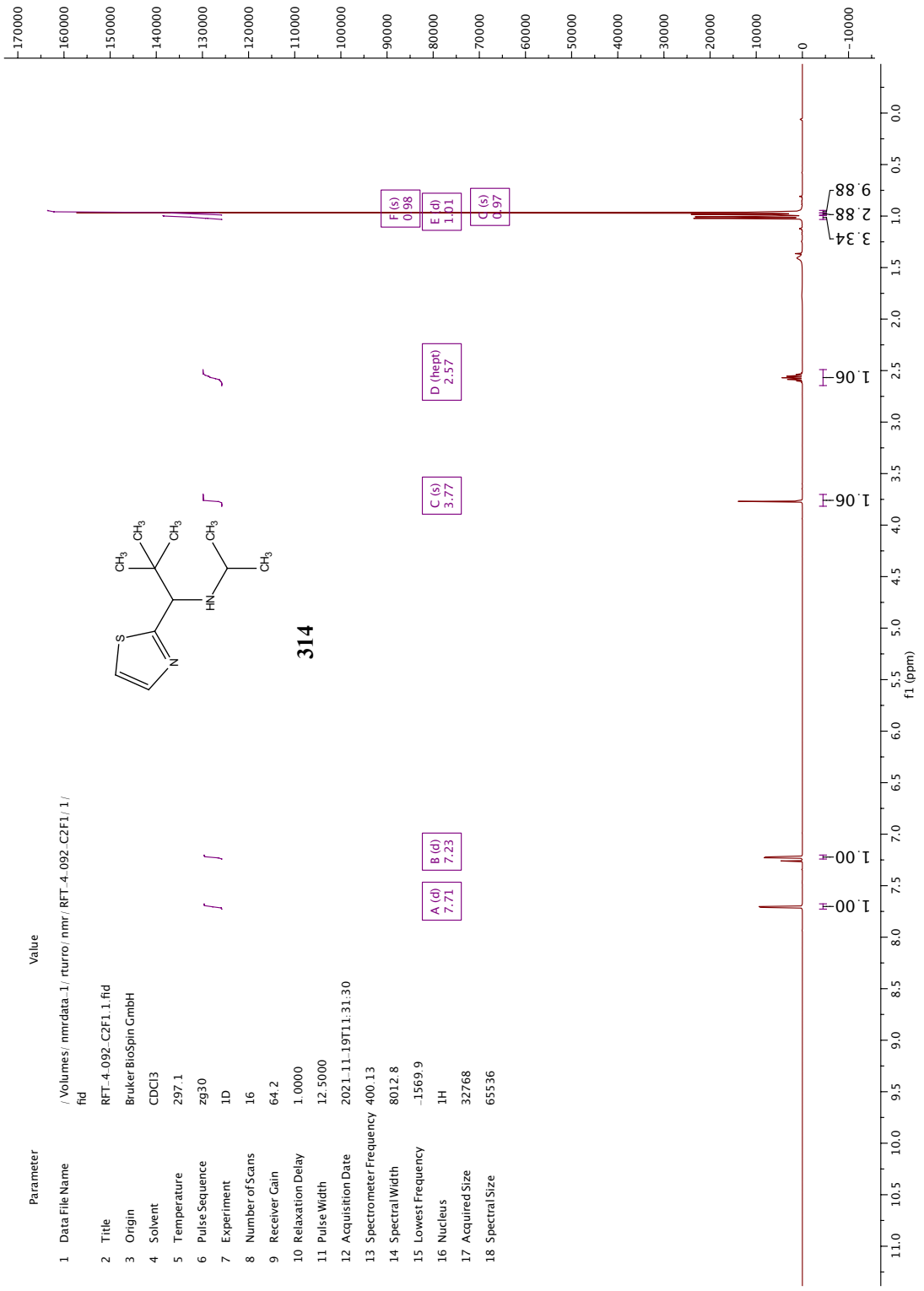

Parameter	Value
1 Data File Name	/ Volumes/ nmrdata_1/ rturro/ nmr/ RFT_4_092_C2F1/ 1 / fid
2 Title	RFT_4_092_C2F1_1.fid
3 Origin	Bruker BioSpin GmbH
4 Solvent	CDCl3
5 Temperature	297.1
6 Pulse Sequence	zg30
7 Experiment	1D
8 Number of Scans	16
9 Receiver Gain	64.2
10 Relaxation Delay	1.0000
11 Pulse Width	12.5000
12 Acquisition Date	2021-11-19T11:31:30
13 Spectrometer Frequency	400.13
14 Spectral Width	8012.8
15 Lowest Frequency	-1569.9
16 Nucleus	1H
17 Acquired Size	32768
18 Spectral Size	65536

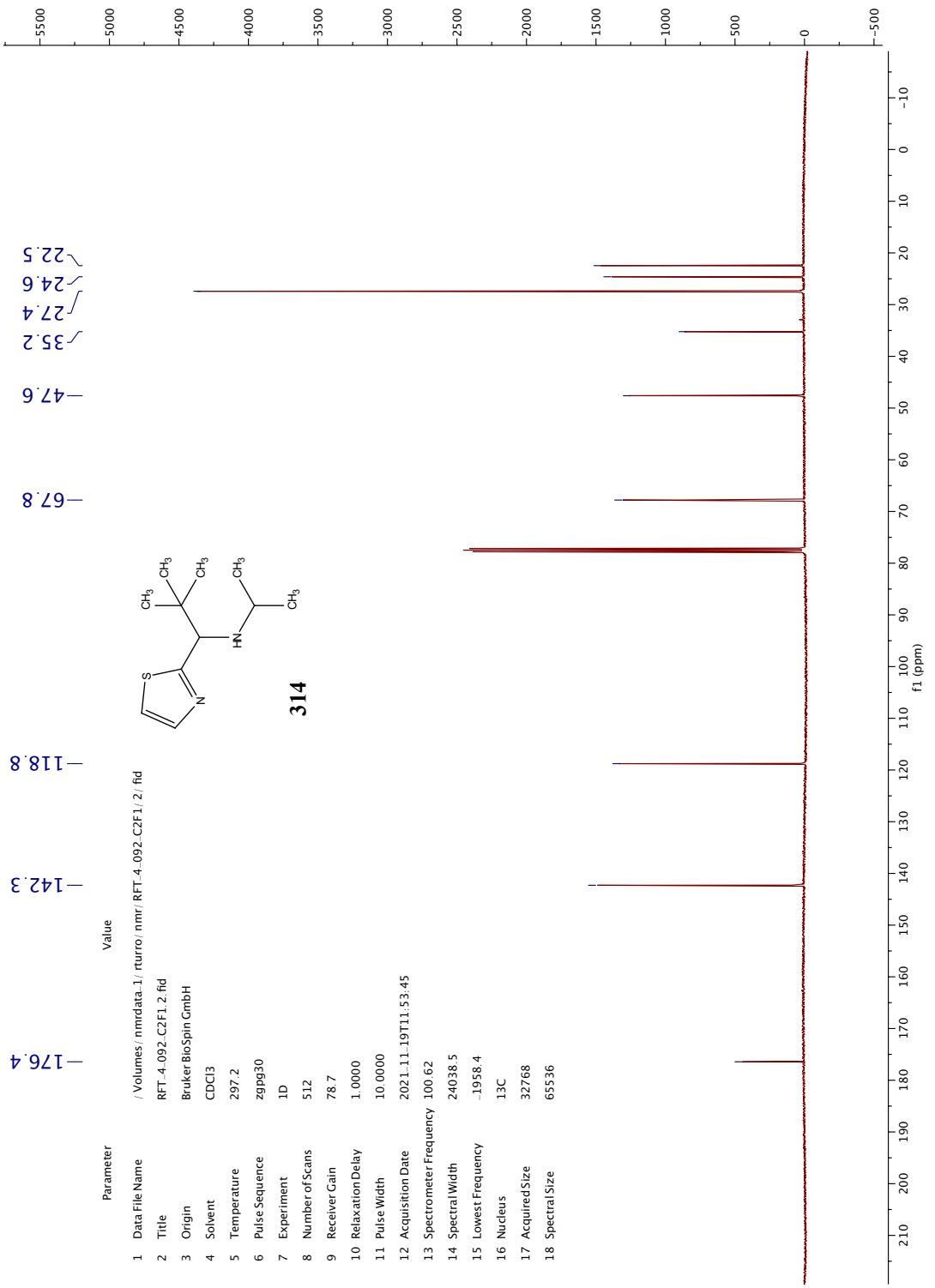

Parameter	Value
1 Data File Name	/Volumes/nmrdata_1/rturro/nmr/RFT-4-092-C2F1/2/fid
2 Title	RFT-4-092-C2F1 2 fid
3 Origin	Bruker BioSpin GmbH
4 Solvent	CDCl3
5 Temperature	297.2
6 Pulse Sequence	zgpg30
7 Experiment	1D
8 Number of Scans	512
9 Receiver Gain	78.7
10 Relaxation Delay	1.0000
11 Pulse Width	10.0000
12 Acquisition Date	2021-11-19T11:53:45
13 Spectrometer Frequency	100.62
14 Spectral Width	24038.5
15 Lowest Frequency	-1958.4
16 Nucleus	13C
17 Acquired Size	32768
18 Spectral Size	65536

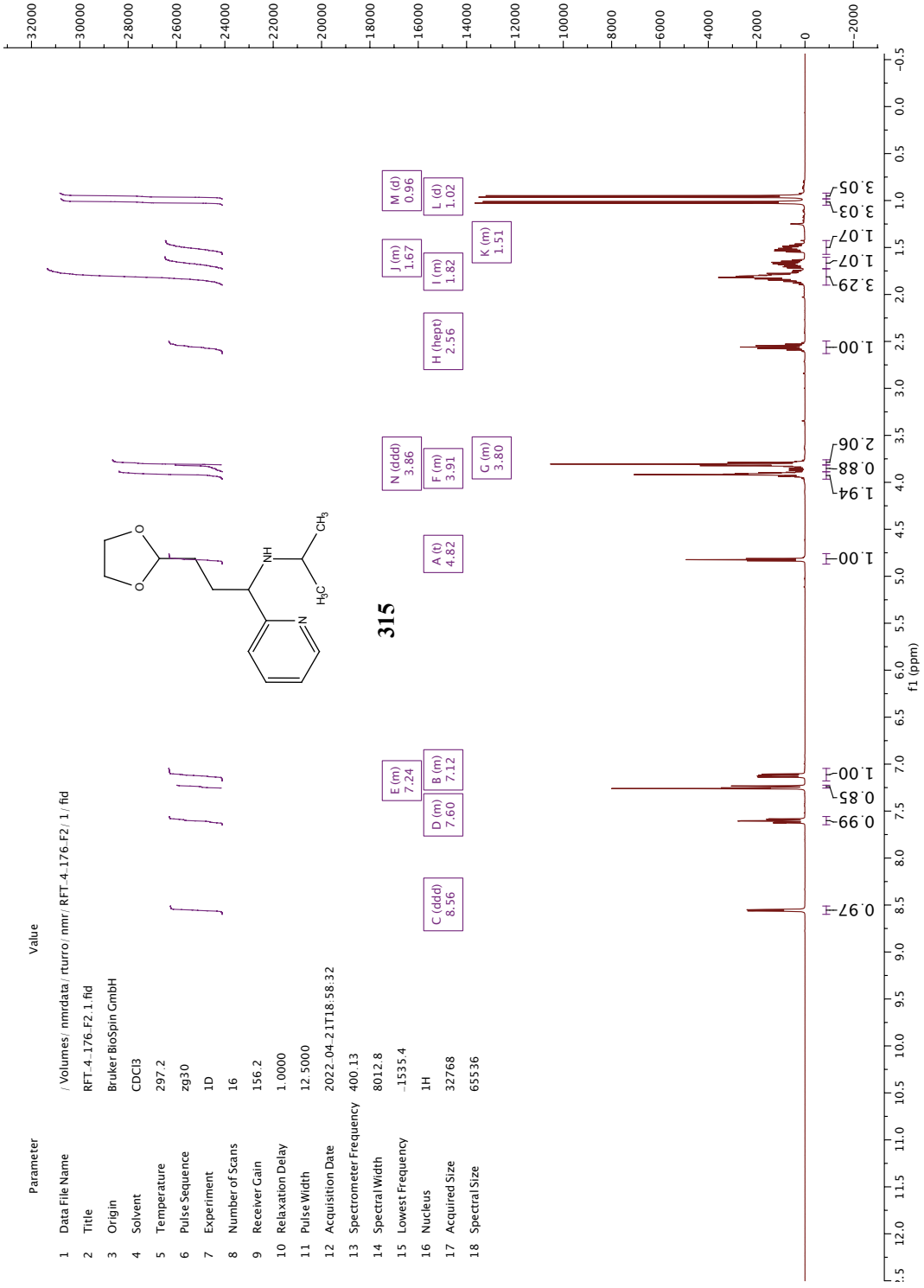

	Parameter	Value
1	Data File Name	/ Volumes/ nmrdata / rturro / nmr / RFT_4_176_F2 / 1 / fid
2	Title	RFT_4_176_F2_1.fid
3	Origin	Bruker BioSpin GmbH
4	Solvent	CDCl3
5	Temperature	297.2
6	Pulse Sequence	zg30
7	Experiment	1D
8	Number of Scans	16
9	Receiver Gain	156.2
10	Relaxation Delay	1.0000
11	Pulse Width	12.5000
12	Acquisition Date	2022_04_21T18:58:32
13	Spectrometer Frequency	400.13
14	Spectral Width	8012.8
15	Lowest Frequency	-1535.4
16	Nucleus	1H
17	Acquired Size	32768
18	Spectral Size	65536

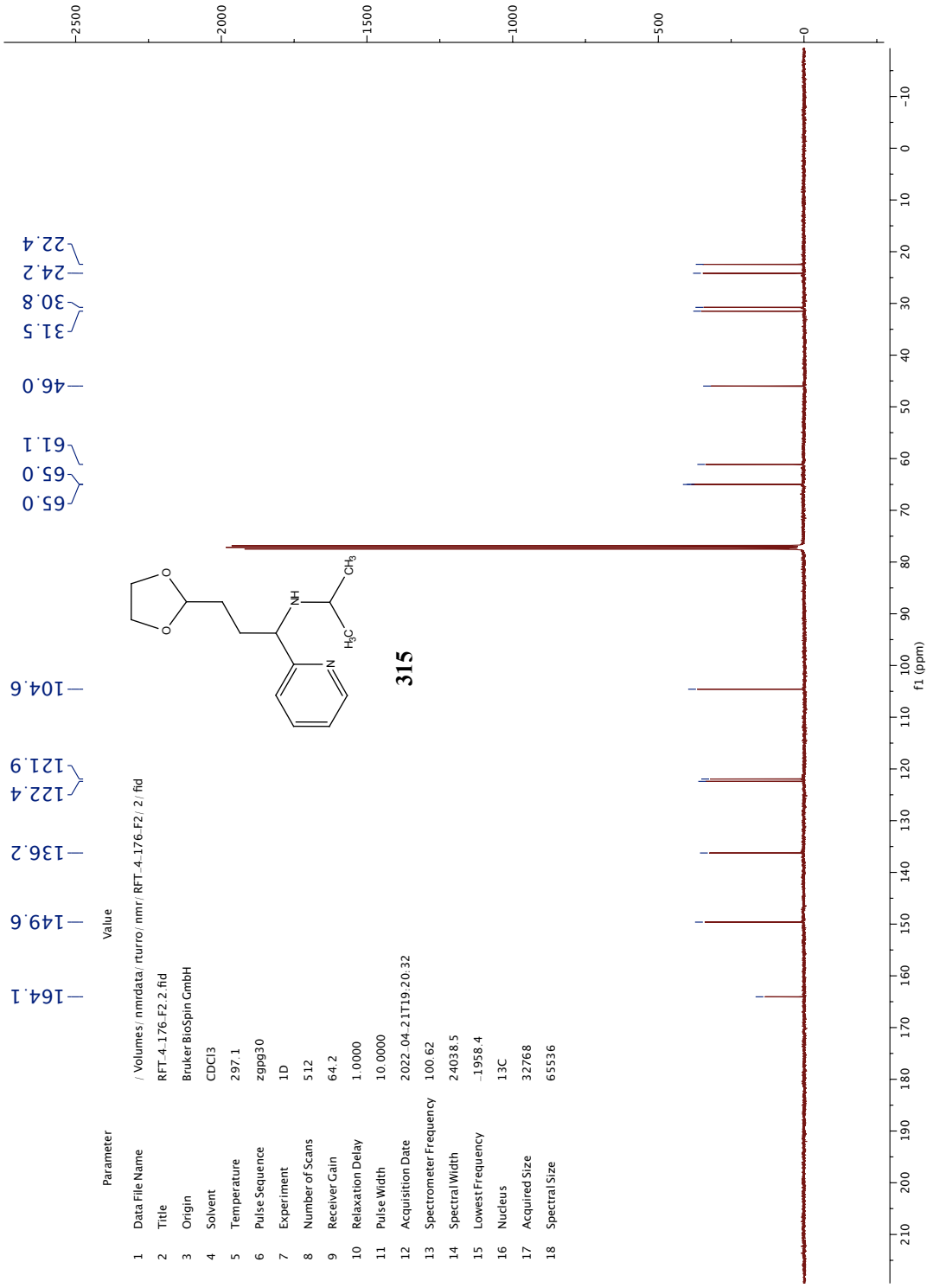

	Parameter	Value
1	Data File Name	/_Volumes/_nmrdata/_rturro/_nmr/_RFT_4_176-F2/_2_/_fid
2	Title	RFT_4_176_F2_2.fid
3	Origin	Bruker BioSpin GmbH
4	Solvent	CDCl3
5	Temperature	297.1
6	Pulse Sequence	zgpg30
7	Experiment	1D
8	Number of Scans	512
9	Receiver Gain	64.2
10	Relaxation Delay	1.0000
11	Pulse Width	10.0000
12	Acquisition Date	2022_04_21T19_20_32
13	Spectrometer Frequency	100.62
14	Spectral Width	24038.5
15	Lowest Frequency	-1958.4
16	Nucleus	13C
17	Acquired Size	32768
18	Spectral Size	65536

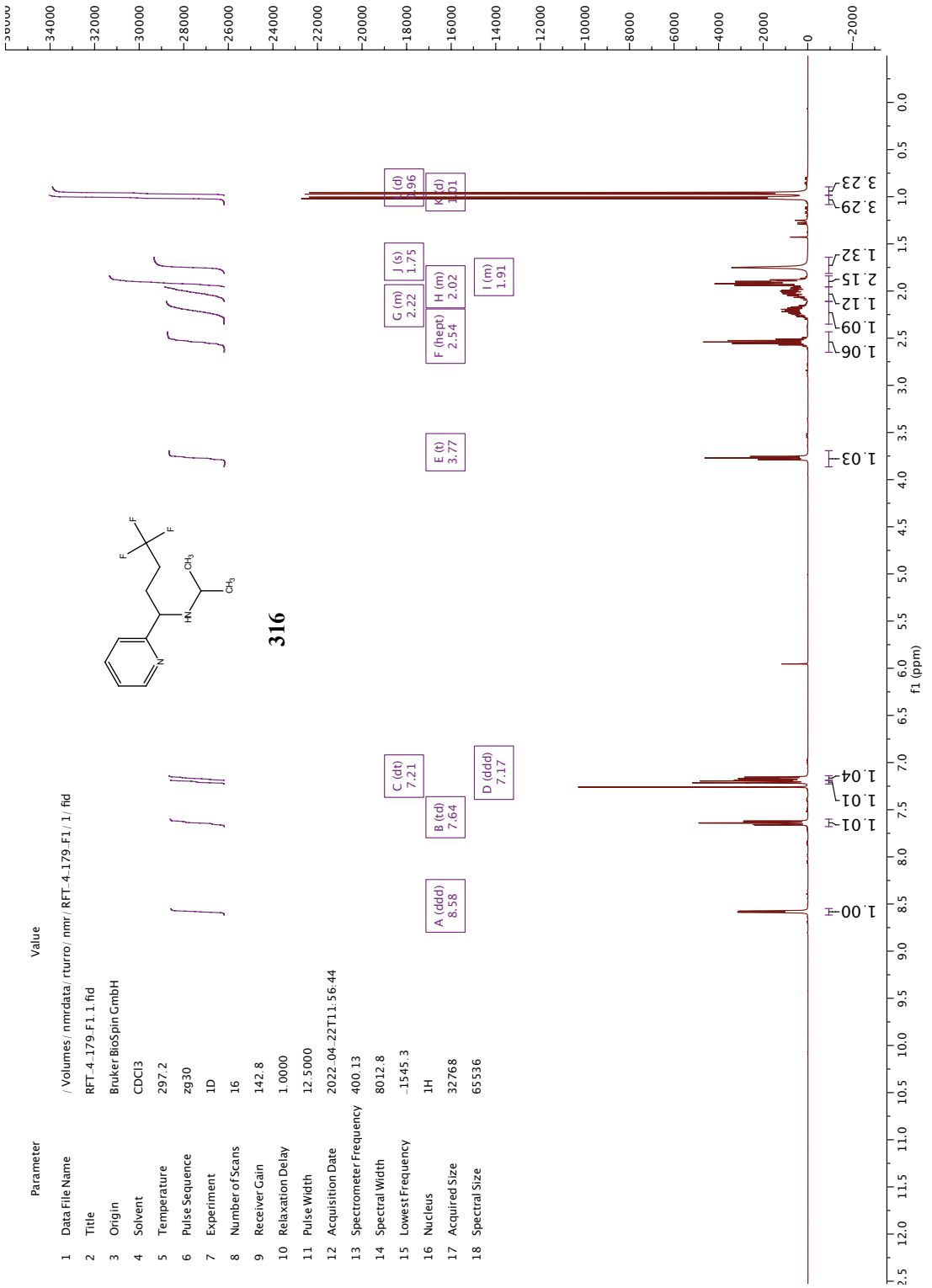
316
Parameter
Value
1 Data File Name / Volumes/ nmrdata/ rturro/ nmr/ RFT-4-179-F1 / 1/ fid
2 Title RFT_4_179_F1_1.fid
3 Origin Bruker BioSpin GmbH
4 Solvent CDCl3
5 Temperature 297.2
6 Pulse Sequence zg30
7 Experiment 1D
8 Number of Scans 16
9 Receiver Gain 142.8
10 Relaxation Delay 1.0000
11 Pulse Width 12.5000
12 Acquisition Date 2022_04_22T11.56.44
13 Spectrometer Frequency 400.13
14 Spectral Width 8012.8
15 Lowest Frequency -1545.3
16 Nucleus 1H
17 Acquired Size 32768
18 Spectral Size 65536
A (ddd) 8.58
B (td) 7.64
C (dt) 7.21
D (ddd) 7.17
E (t) 3.77
F (hept) 2.54
G (m) 2.22
H (m) 2.02
I (m) 1.91
J (s) 1.75
K (d) 1.01
L (d) 0.96
1.00
1.01
1.01
1.04
1.03
1.06
1.09
1.12
2.15
1.32
3.29
3.23
f1 (ppm)

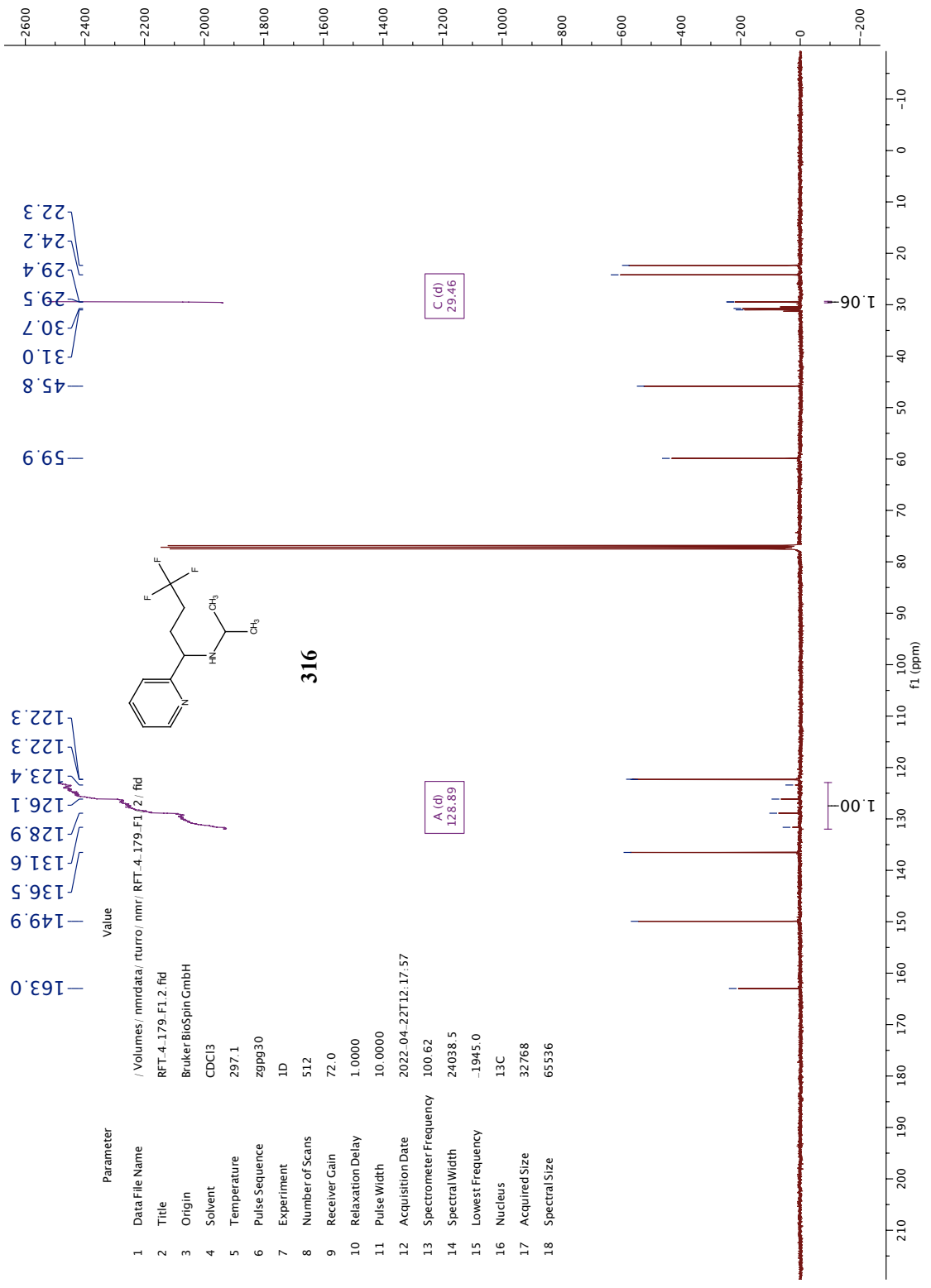
316
22.3
24.2
29.4
29.5
30.7
31.0
45.8
59.9
122.3
122.3
123.4
126.1
128.9
131.6
136.5
149.9
163.0
C (d) 29.46
A (d) 128.89
1.06
1.00
f1 (ppm)
Parameter
Value
1 Data File Name /Volumes/nmrdata/rturro/nmr/RFT-4-179-F1-2/2/fid
2 Title RFT-4-179-F1-2.fid
3 Origin Bruker BioSpin GmbH
4 Solvent CDCl3
5 Temperature 297.1
6 Pulse Sequence zgpg30
7 Experiment 1D
8 Number of Scans 512
9 Receiver Gain 72.0
10 Relaxation Delay 1.0000
11 Pulse Width 10.0000
12 Acquisition Date 2022-04-22T12:17:57
13 Spectrometer Frequency 100.62
14 Spectral Width 24038.5
15 Lowest Frequency -1945.0
16 Nucleus 13C
17 Acquired Size 32768
18 Spectral Size 65536

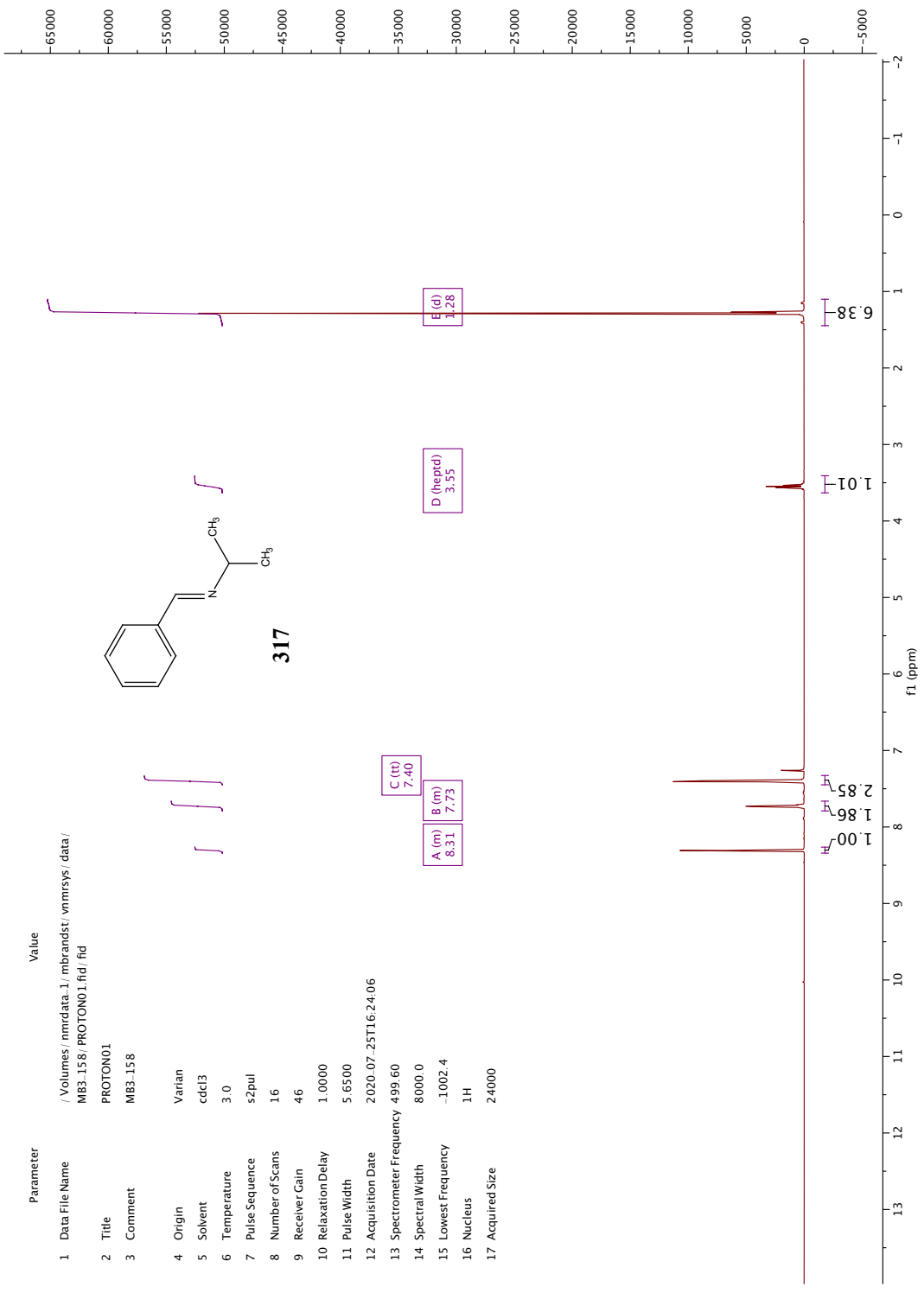

	Parameter	Value
1	Data File Name	/Volumes/nmrdata_1/mbrandst/vnmrsys/data/MB3-158/PROTON01.fid/fid
2	Title	PROTON01
3	Comment	MB3-158
4	Origin	Varian
5	Solvent	cdcl3
6	Temperature	3.0
7	Pulse Sequence	s2pul
8	Number of Scans	16
9	Receiver Gain	46
10	Relaxation Delay	1.0000
11	Pulse Width	5.6500
12	Acquisition Date	2020-07-25T16:24:06
13	Spectrometer Frequency	499.60
14	Spectral Width	8000.0
15	Lowest Frequency	-1002.4
16	Nucleus	1H
17	Acquired Size	24000

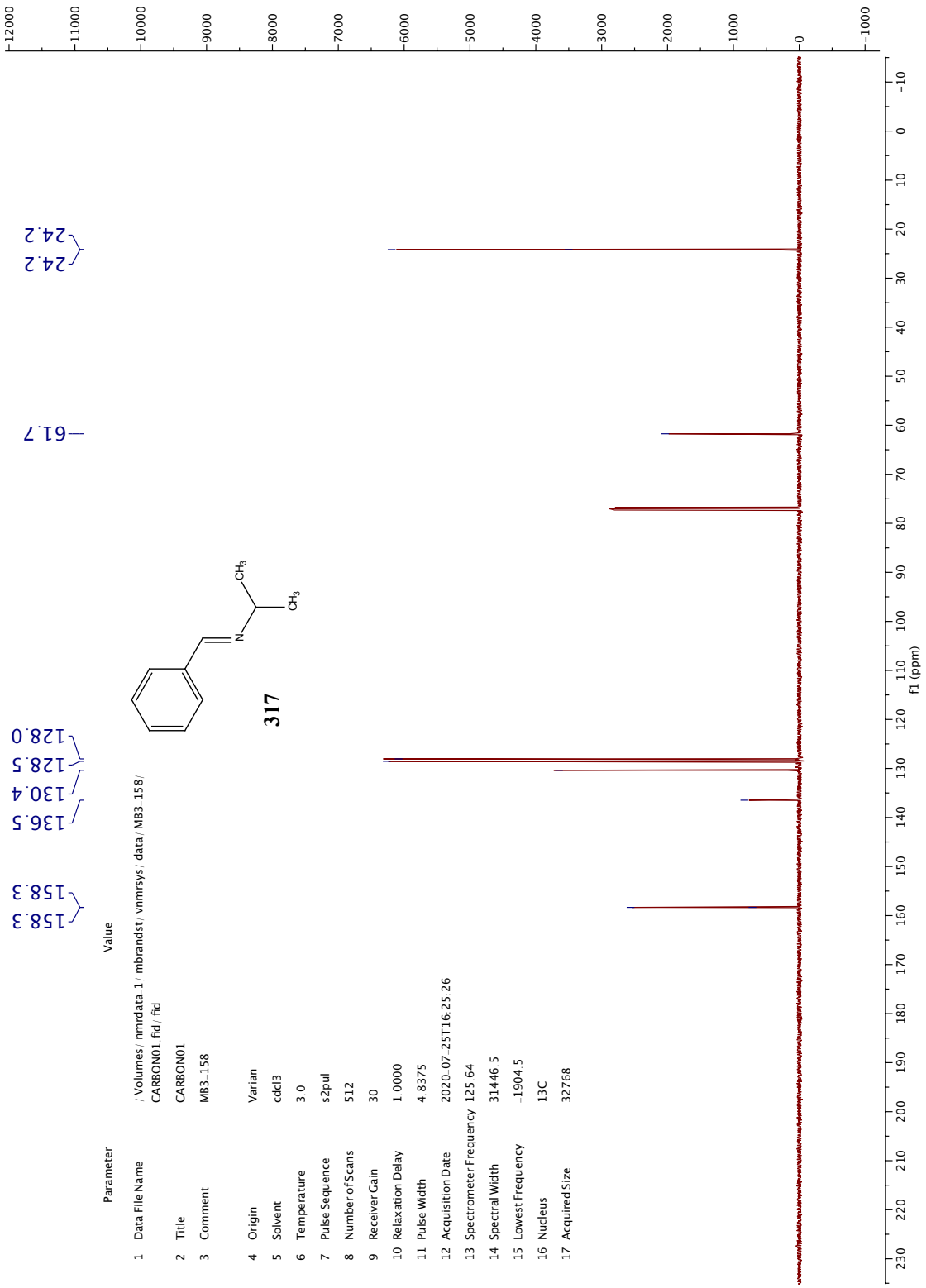

	Parameter	Value
1	Data File Name	/Volumes/nmrdata_1/mbrandst/vnmrsys/data/MB3-158/CARBON01.fid/fid
2	Title	CARBON01
3	Comment	MB3-158
4	Origin	Varian
5	Solvent	cdcl3
6	Temperature	3.0
7	Pulse Sequence	s2pul
8	Number of Scans	512
9	Receiver Gain	30
10	Relaxation Delay	1.0000
11	Pulse Width	4.8375
12	Acquisition Date	2020-07-25T16:25:26
13	Spectrometer Frequency	125.64
14	Spectral Width	31446.5
15	Lowest Frequency	-1904.5
16	Nucleus	13C
17	Acquired Size	32768

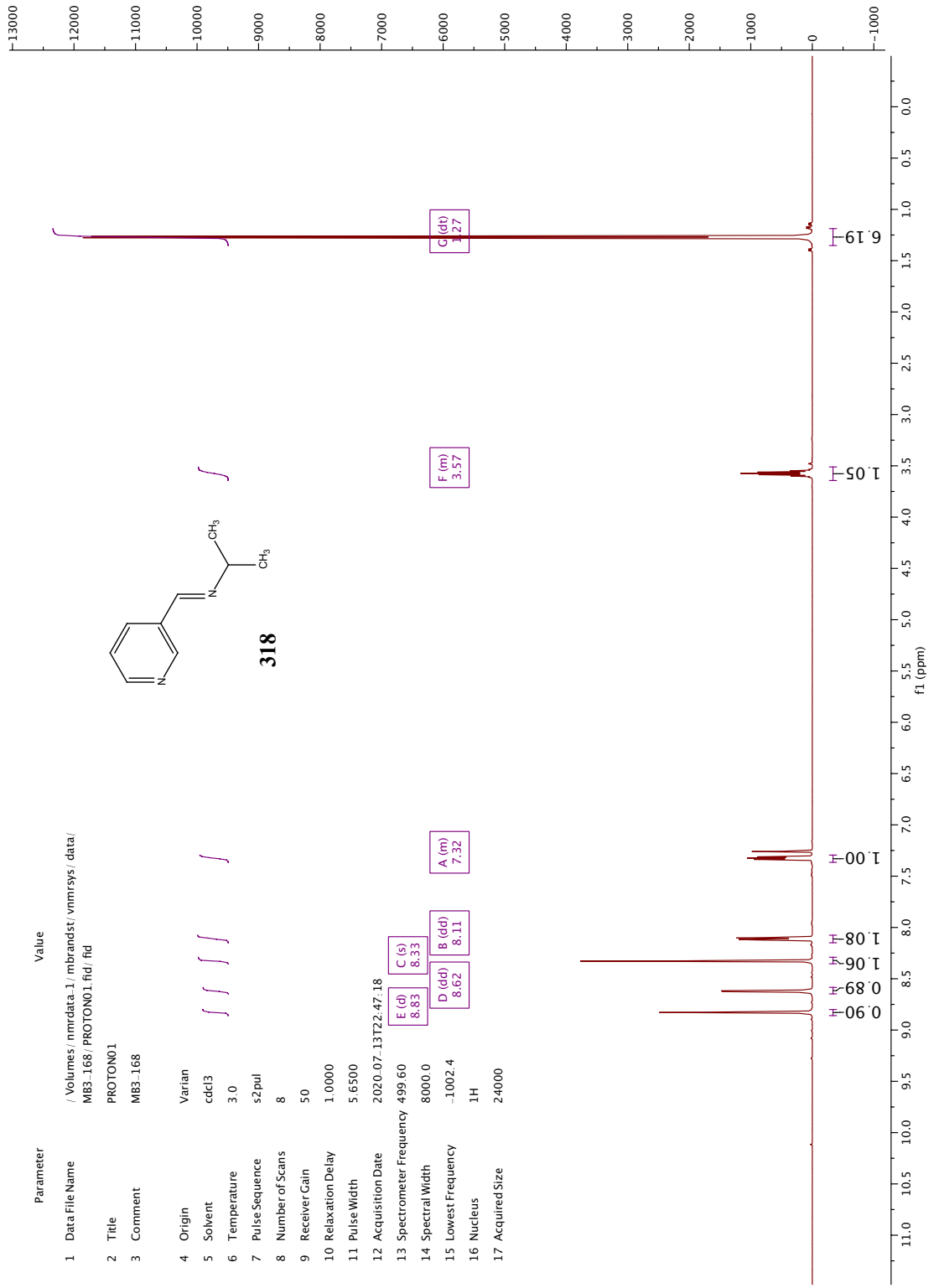
318
Parameter
Value
1 Data File Name
/ Volumes / nmrdata_1 / mbrandst / vnmrsys / data / MB3_168 / PROTON01.fid / fid
2 Title
PROTON01
3 Comment
MB3_168
4 Origin
Varian
5 Solvent
cdcl3
6 Temperature
3.0
7 Pulse Sequence
s2pul
8 Number of Scans
8
9 Receiver Gain
50
10 Relaxation Delay
1.0000
11 Pulse Width
5.6500
12 Acquisition Date
2020-07-13T22:47:18
13 Spectrometer Frequency
499.60
14 Spectral Width
8000.0
15 Lowest Frequency
-1002.4
16 Nucleus
1H
17 Acquired Size
24000
E (d) 8.83
C (s) 8.33
D (dd) 8.62
B (dd) 8.11
A (m) 7.32
F (m) 3.57
G (dt) 1.27
0.90
0.89
1.06
1.08
1.00
1.05
6.19
f1 (ppm)

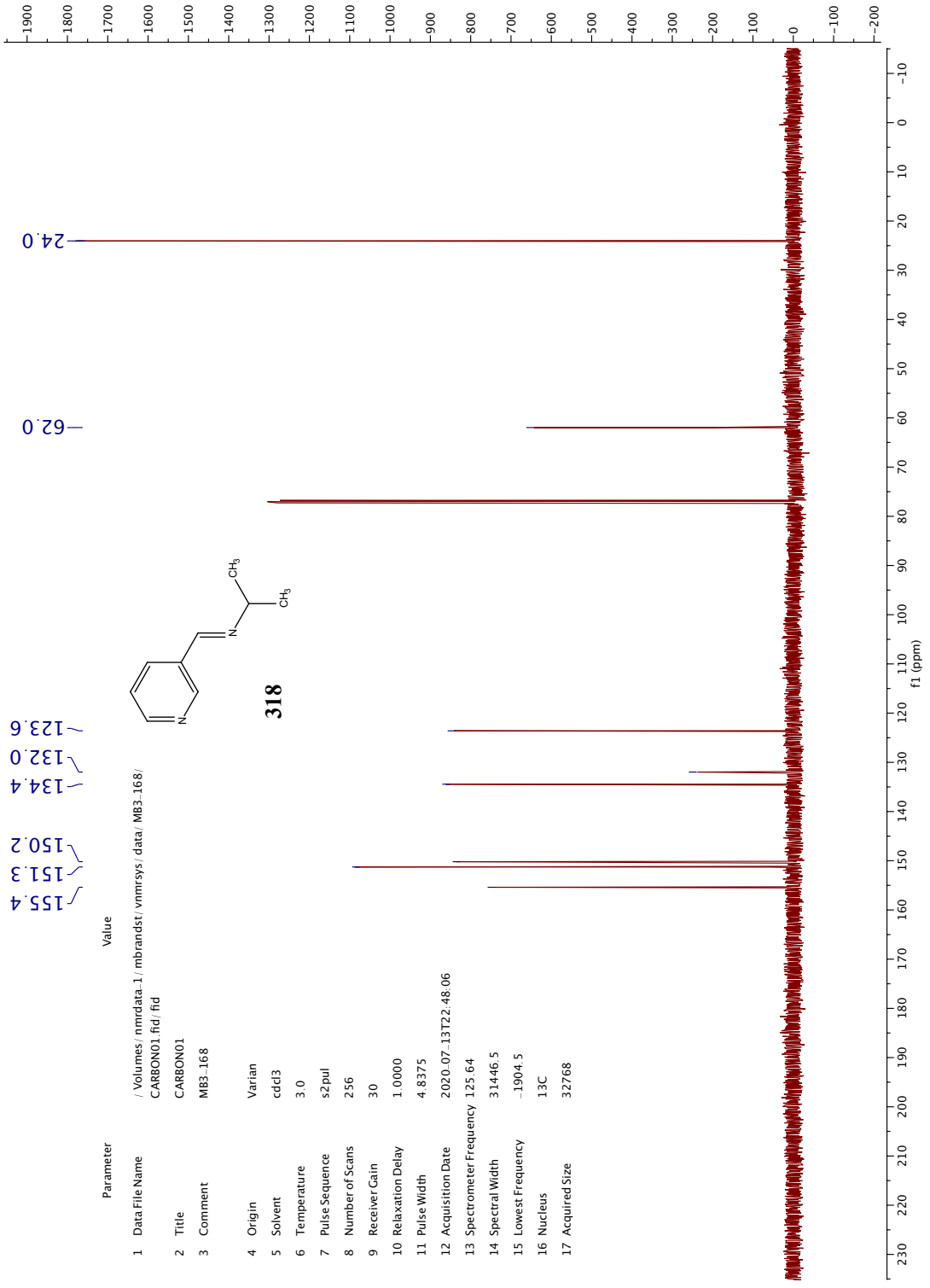

Parameter	Value
1 Data File Name	/ Volumes / nmrdata_1 / mbrandst / vnmrsys / data / MB3_168 / CARBON01 fid / fid
2 Title	CARBON01
3 Comment	MB3_168
4 Origin	Varian
5 Solvent	cdcl3
6 Temperature	3.0
7 Pulse Sequence	s2pul
8 Number of Scans	256
9 Receiver Gain	30
10 Relaxation Delay	1.0000
11 Pulse Width	4.8375
12 Acquisition Date	2020-07-13T22:48:06
13 Spectrometer Frequency	125.64
14 Spectral Width	31446.5
15 Lowest Frequency	-1904.5
16 Nucleus	13C
17 Acquired Size	32768

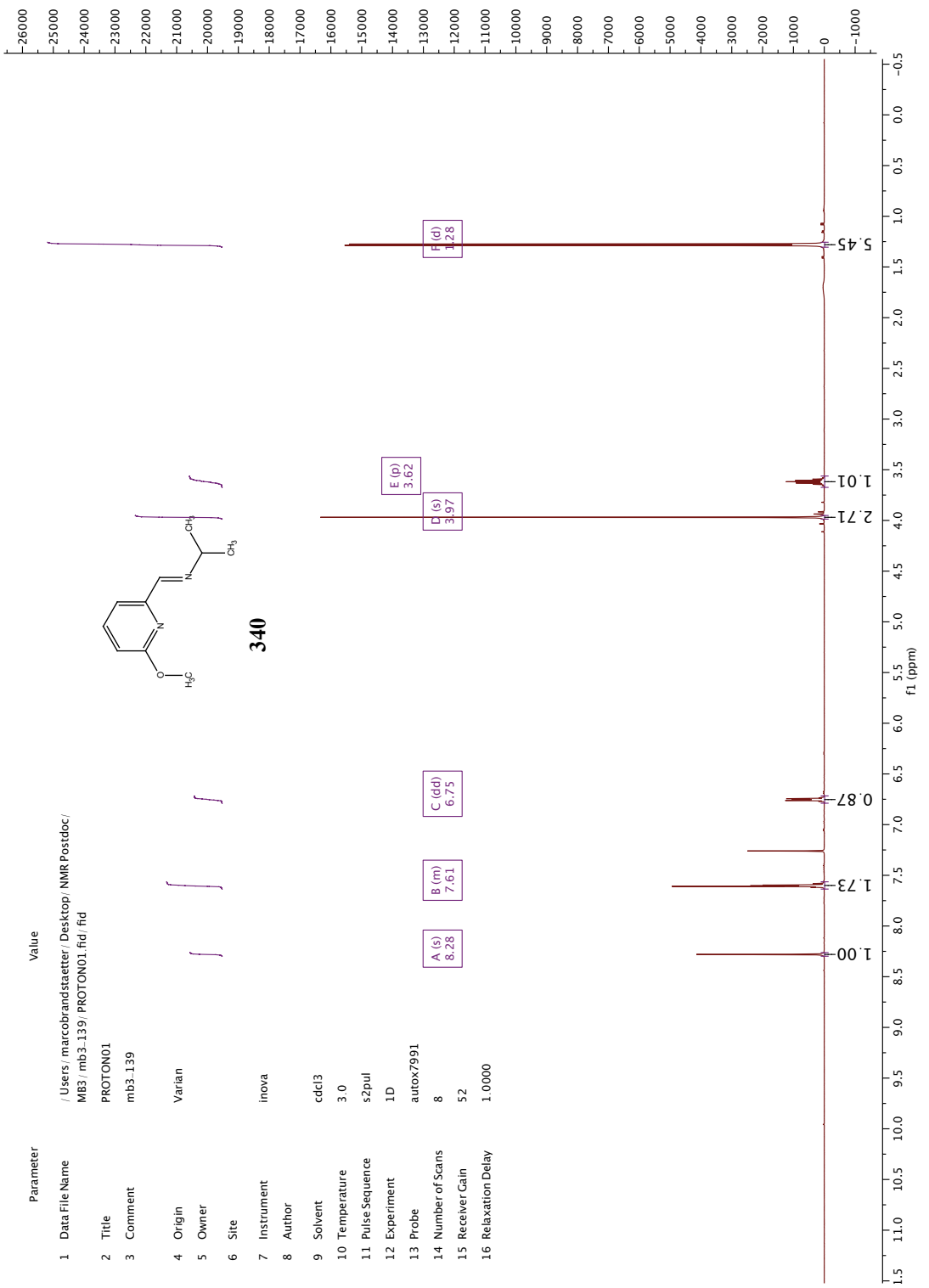
340
Parameter
Value
1 Data File Name / Users / marcobrandstaetter / Desktop / NMR Postdoc / MB3 / mb3-139 / PROTON01.fid / fid
2 Title PROTON01
3 Comment mb3-139
4 Origin Varian
5 Owner
6 Site
7 Instrument inova
8 Author
9 Solvent cdcl3
10 Temperature 3.0
11 Pulse Sequence s2pul
12 Experiment 1D
13 Probe autox7991
14 Number of Scans 8
15 Receiver Gain 52
16 Relaxation Delay 1.0000
A (s) 8.28
B (m) 7.61
C (dd) 6.75
D (s) 3.97
E (p) 3.62
F (d) 1.28
5.45
2.71
1.01
0.87
1.73
1.00
f1 (ppm)

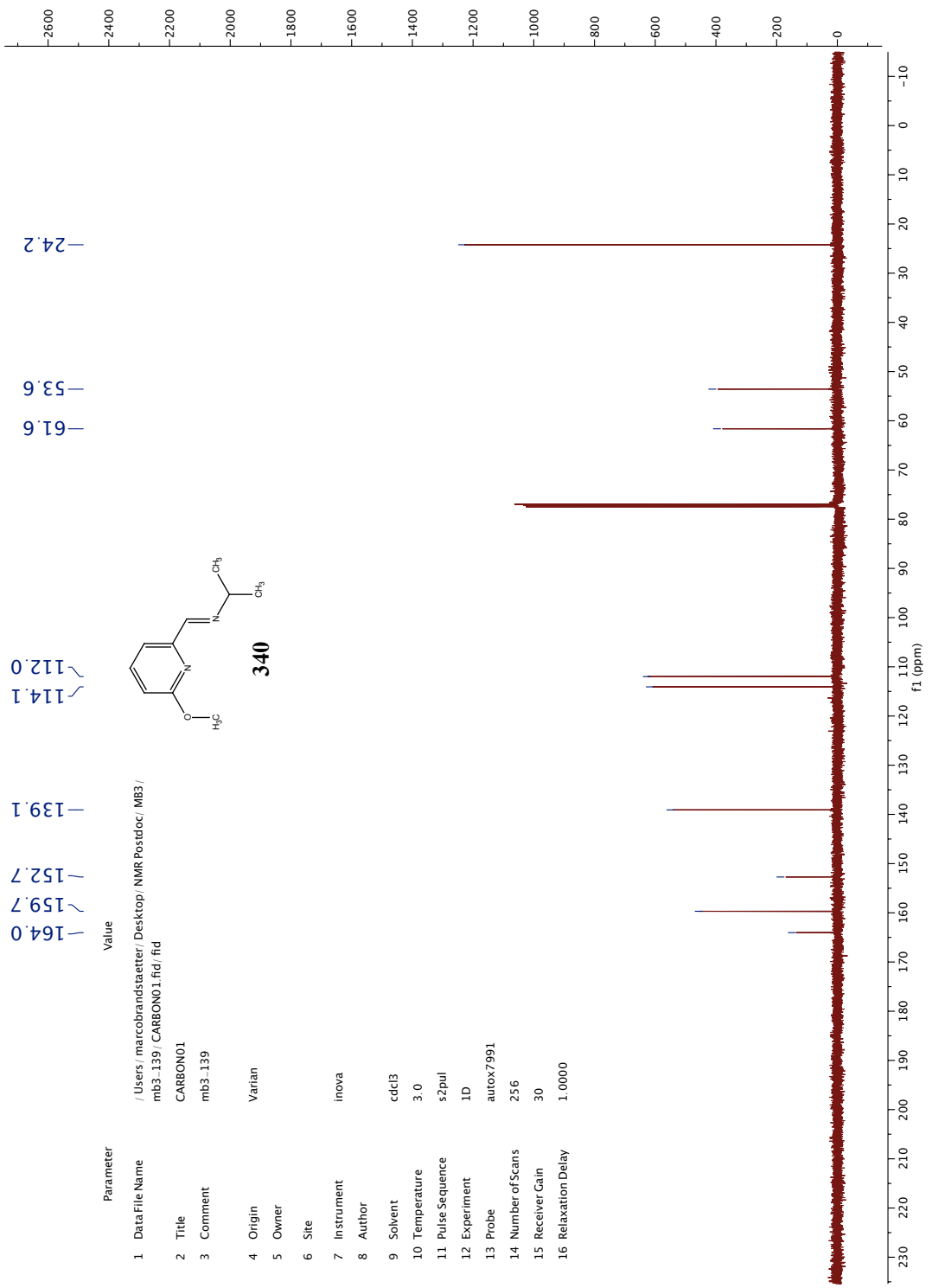

Parameter	Value
1 Data File Name	/Users/marcobrandstaetter/Desktop/NMR Postdoc/MB3/mb3_139/CARBON01.fid/fid
2 Title	CARBON01
3 Comment	mb3_139
4 Origin	Varian
5 Owner	
6 Site	
7 Instrument	inova
8 Author	
9 Solvent	cdcl3
10 Temperature	3.0
11 Pulse Sequence	s2pul
12 Experiment	1D
13 Probe	autox7991
14 Number of Scans	256
15 Receiver Gain	30
16 Relaxation Delay	1.0000

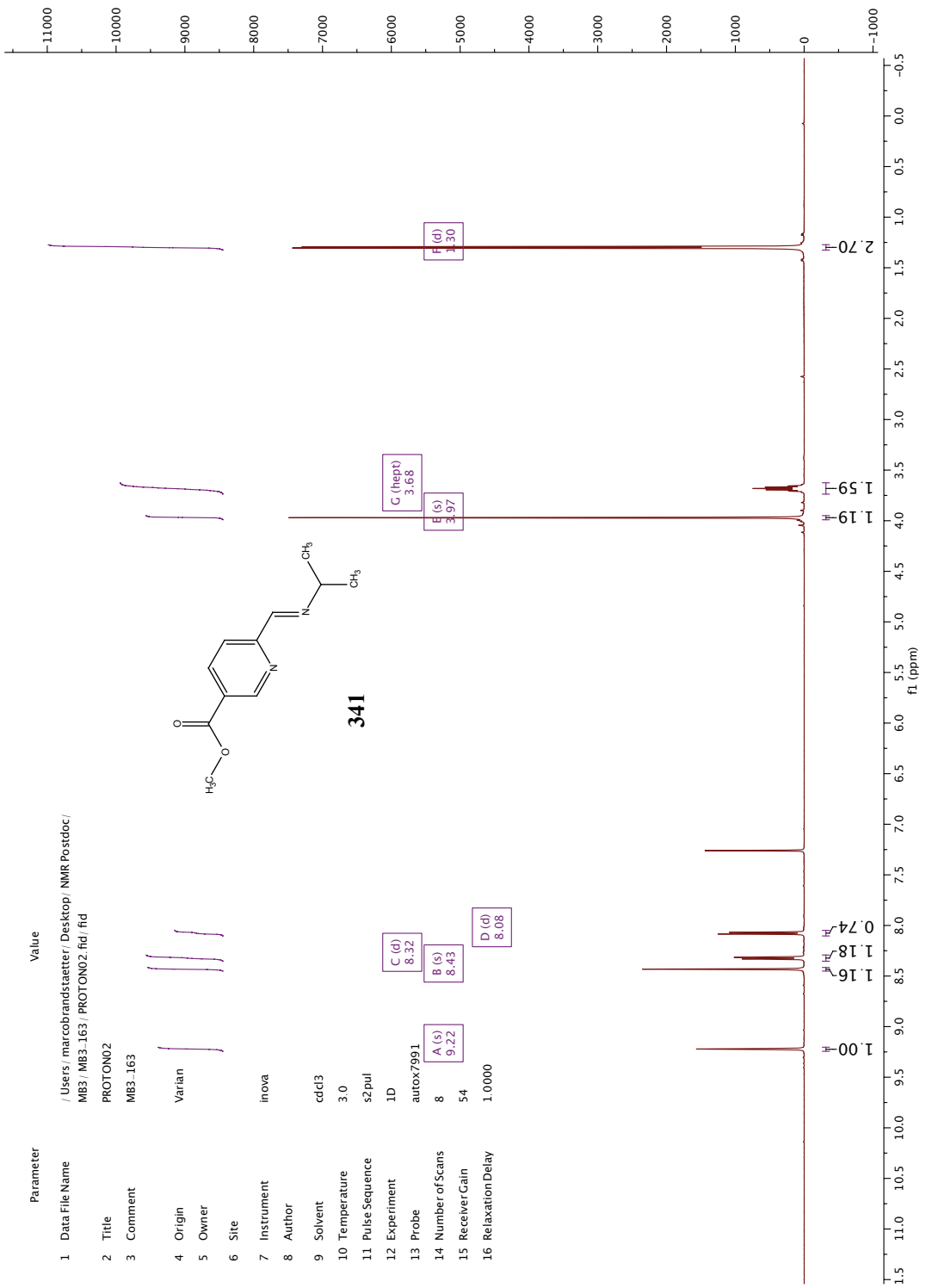
Parameter
Value
1 Data File Name / Users / marcobrandstaetter / Desktop / NMR Postdoc / MB3 / MB3_163 / PROTON02. fid / fid
2 Title PROTON02
3 Comment MB3_163
4 Origin Varian
5 Owner
6 Site
7 Instrument inova
8 Author
9 Solvent cdcl3
10 Temperature 3.0
11 Pulse Sequence s2pul
12 Experiment 1D
13 Probe autox7991
14 Number of Scans 8
15 Receiver Gain 54
16 Relaxation Delay 1.0000
A (s) 9.22
B (s) 8.43
C (d) 8.32
D (d) 8.08
E (s) 3.97
F (d) 1.30
G (hept) 3.68
341
2.70
1.59
1.19
1.16
1.18
0.74
1.00
f1 (ppm)

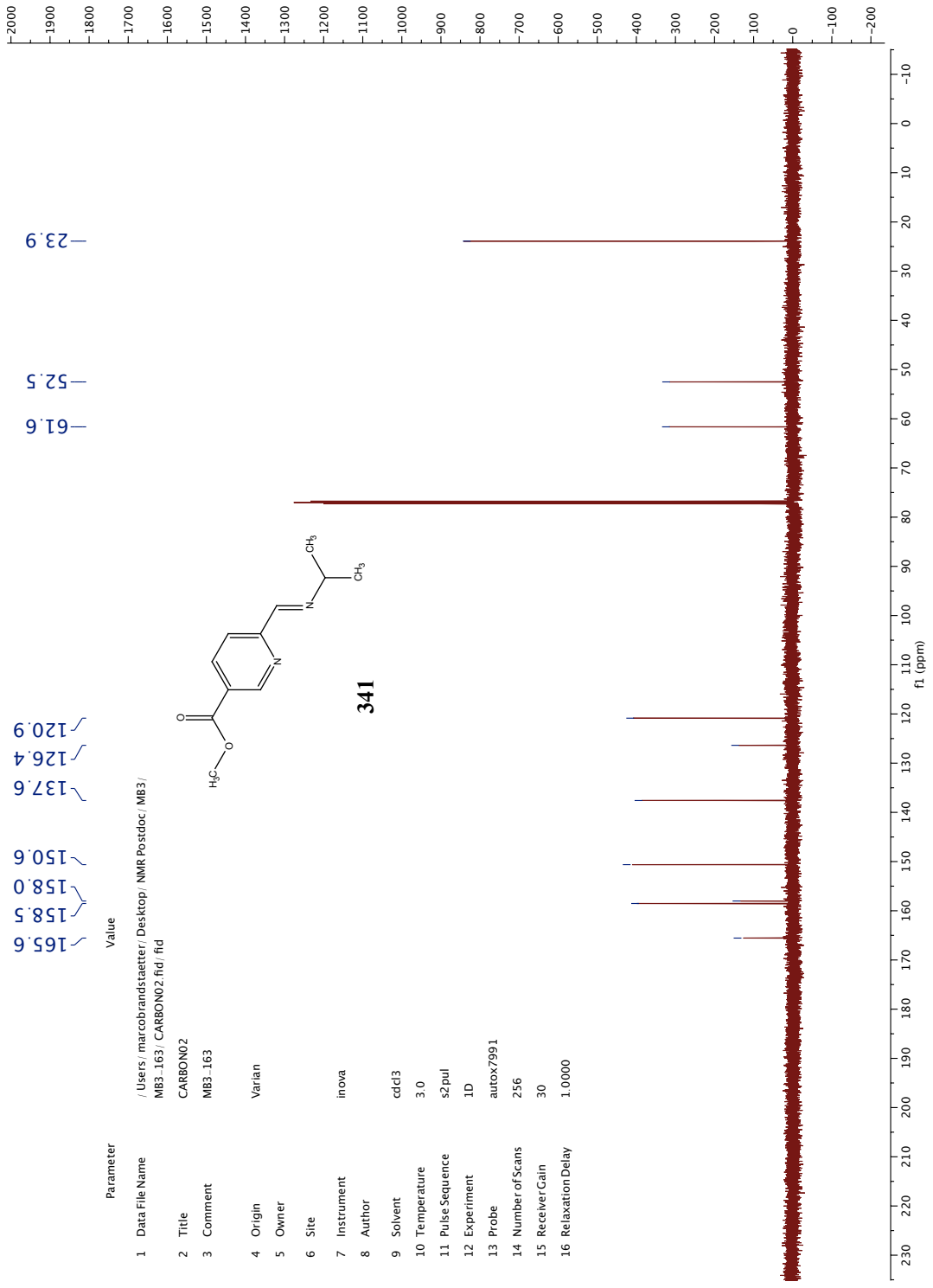

Parameter	Value
1 Data File Name	/Users/marcobrandstaetter/Desktop/NMR Postdoc/MB3/MB3-163/CARBON02 fid/fid
2 Title	CARBON02
3 Comment	MB3-163
4 Origin	Varian
5 Owner	
6 Site	
7 Instrument	inova
8 Author	
9 Solvent	cdcl3
10 Temperature	3.0
11 Pulse Sequence	s2pul
12 Experiment	1D
13 Probe	autox7991
14 Number of Scans	256
15 Receiver Gain	30
16 Relaxation Delay	1.0000

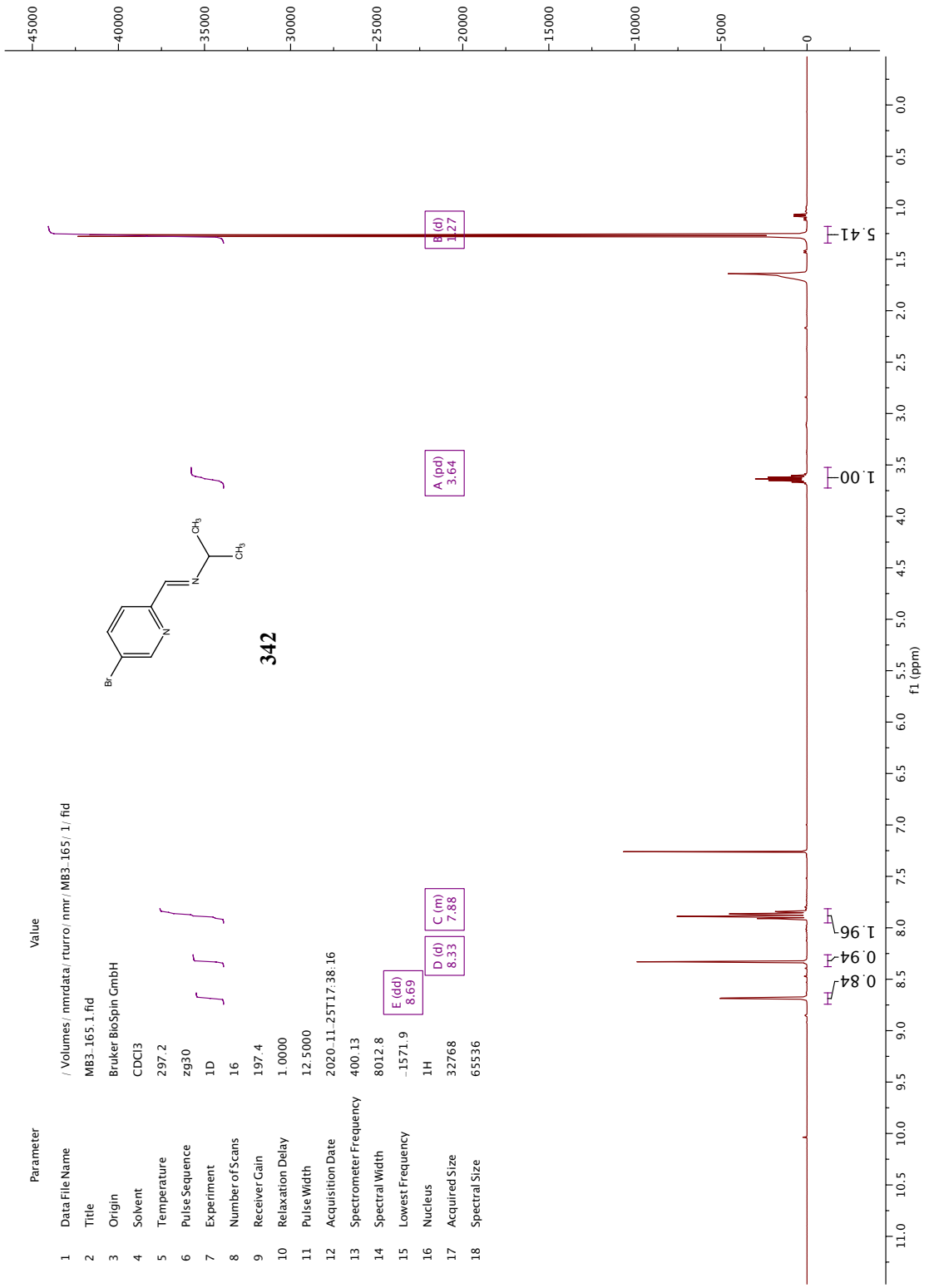

	Parameter	Value
1	Data File Name	/ Volumes/ nmrdata/ rturro/ nmr/ MB3_165/ 1/ fid
2	Title	MB3_165_1 fid
3	Origin	Bruker BioSpin GmbH
4	Solvent	CDCl3
5	Temperature	297.2
6	Pulse Sequence	zg30
7	Experiment	1D
8	Number of Scans	16
9	Receiver Gain	197.4
10	Relaxation Delay	1.0000
11	Pulse Width	12.5000
12	Acquisition Date	2020_11_25T17:38:16
13	Spectrometer Frequency	400.13
14	Spectral Width	8012.8
15	Lowest Frequency	-1571.9
16	Nucleus	1H
17	Acquired Size	32768
18	Spectral Size	65536

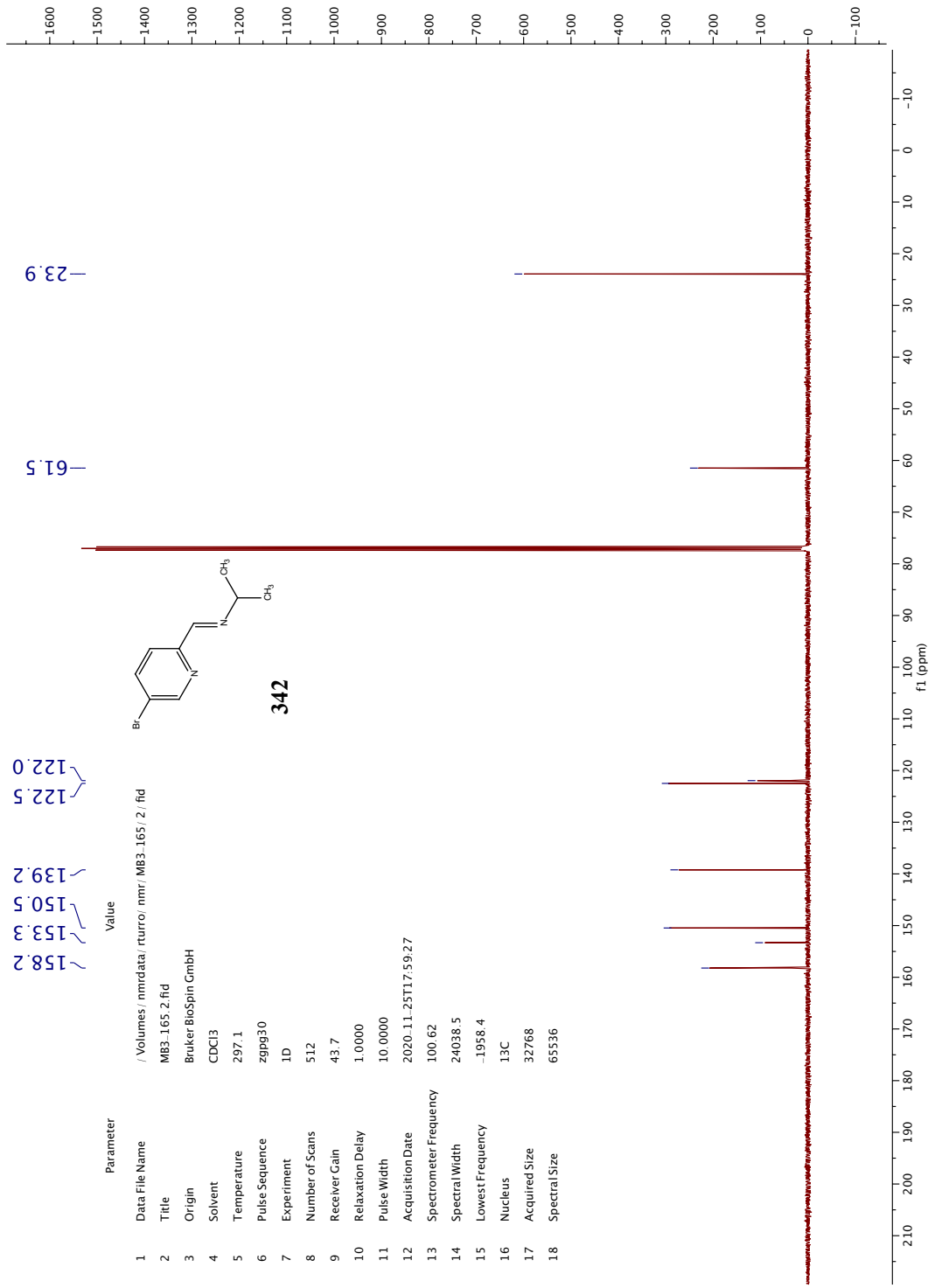

	Parameter	Value
1	Data File Name	/..Volumes/..nmrdata/..rturro/..nmr/..MB3_165/..2/..fid
2	Title	MB3_165_2.fid
3	Origin	Bruker BioSpin GmbH
4	Solvent	CDCl3
5	Temperature	297.1
6	Pulse Sequence	zgpg30
7	Experiment	1D
8	Number of Scans	512
9	Receiver Gain	43.7
10	Relaxation Delay	1.0000
11	Pulse Width	10.0000
12	Acquisition Date	2020_11_25T17:59:27
13	Spectrometer Frequency	100.62
14	Spectral Width	24038.5
15	Lowest Frequency	-1958.4
16	Nucleus	13C
17	Acquired Size	32768
18	Spectral Size	65536

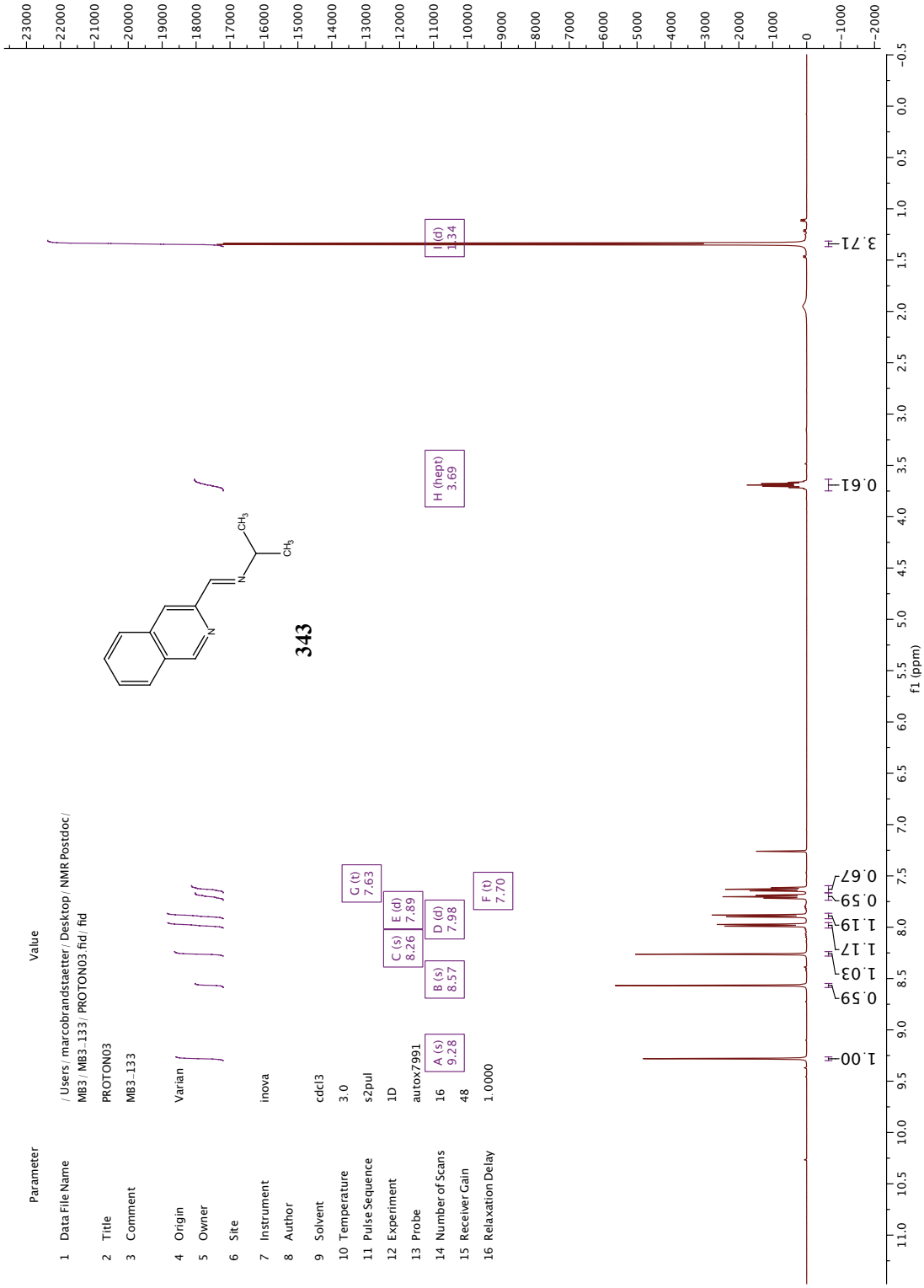
Parameter
Value
1 Data File Name / Users / marcobrandstaetter / Desktop / NMR Postdoc / MB3 / MB3_133 / PROTON03.fid / fid
2 Title PROTON03
3 Comment MB3_133
4 Origin Varian
5 Owner
6 Site
7 Instrument inova
8 Author
9 Solvent cdcl3
10 Temperature 3.0
11 Pulse Sequence s2pul
12 Experiment 1D
13 Probe autox7991
14 Number of Scans 16
15 Receiver Gain 48
16 Relaxation Delay 1.0000
A (s) 9.28
B (s) 8.57
C (s) 8.26
D (d) 7.98
E (d) 7.89
F (t) 7.70
G (t) 7.63
H (hept) 3.69
I (d) 1.34
343
1.00
0.59
1.03
1.17
1.19
0.59
0.67
0.61
3.71
f1 (ppm)

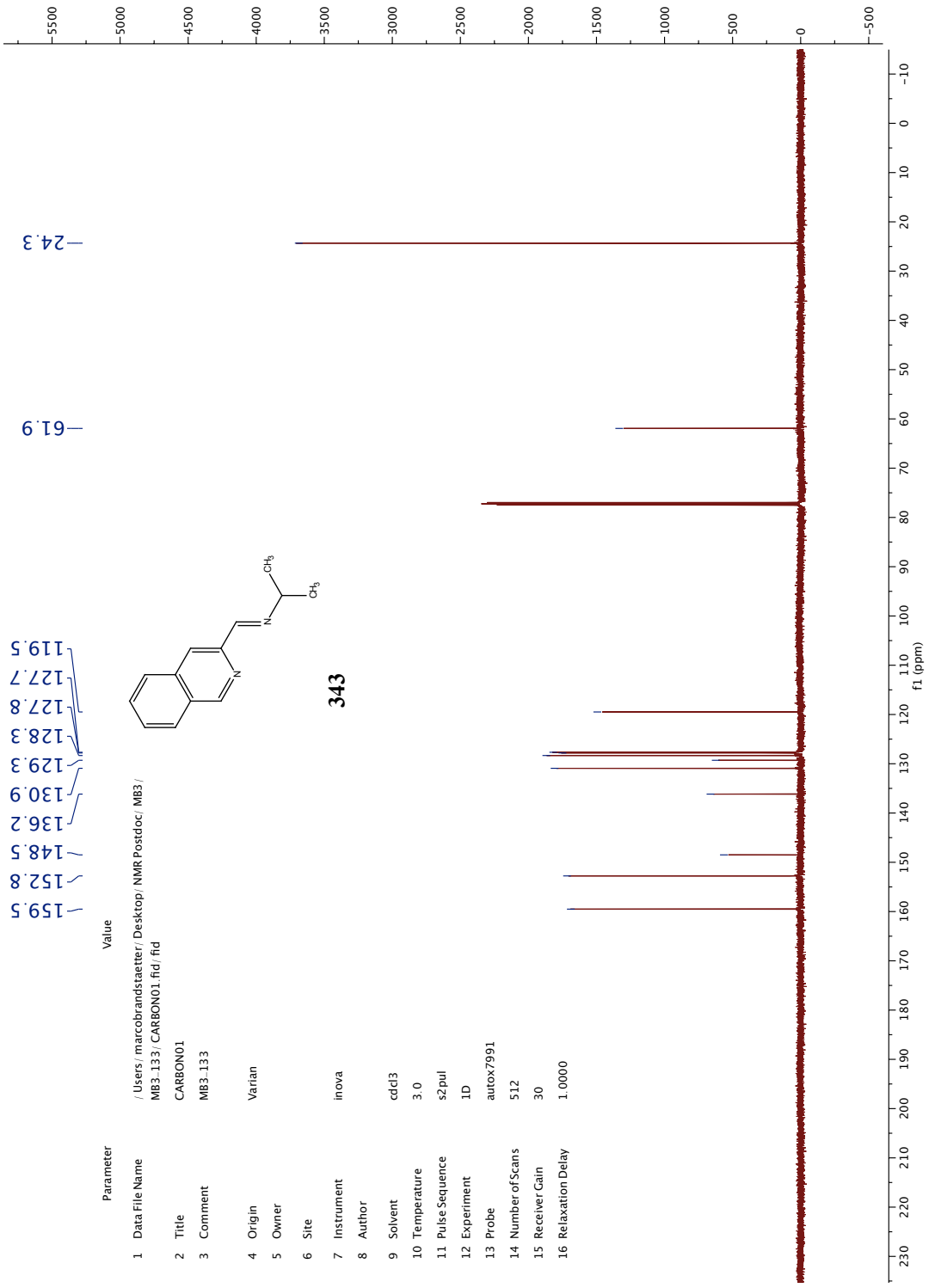

	Parameter	Value
1	Data File Name	/Users/marcobrandstaetter/Desktop/NMR Postdoc/MB3/MB3.133/CARBON01.fid/fid
2	Title	CARBON01
3	Comment	MB3.133
4	Origin	Varian
5	Owner	
6	Site	
7	Instrument	inova
8	Author	
9	Solvent	cdcl3
10	Temperature	3.0
11	Pulse Sequence	s2pul
12	Experiment	1D
13	Probe	autox7991
14	Number of Scans	512
15	Receiver Gain	30
16	Relaxation Delay	1.0000

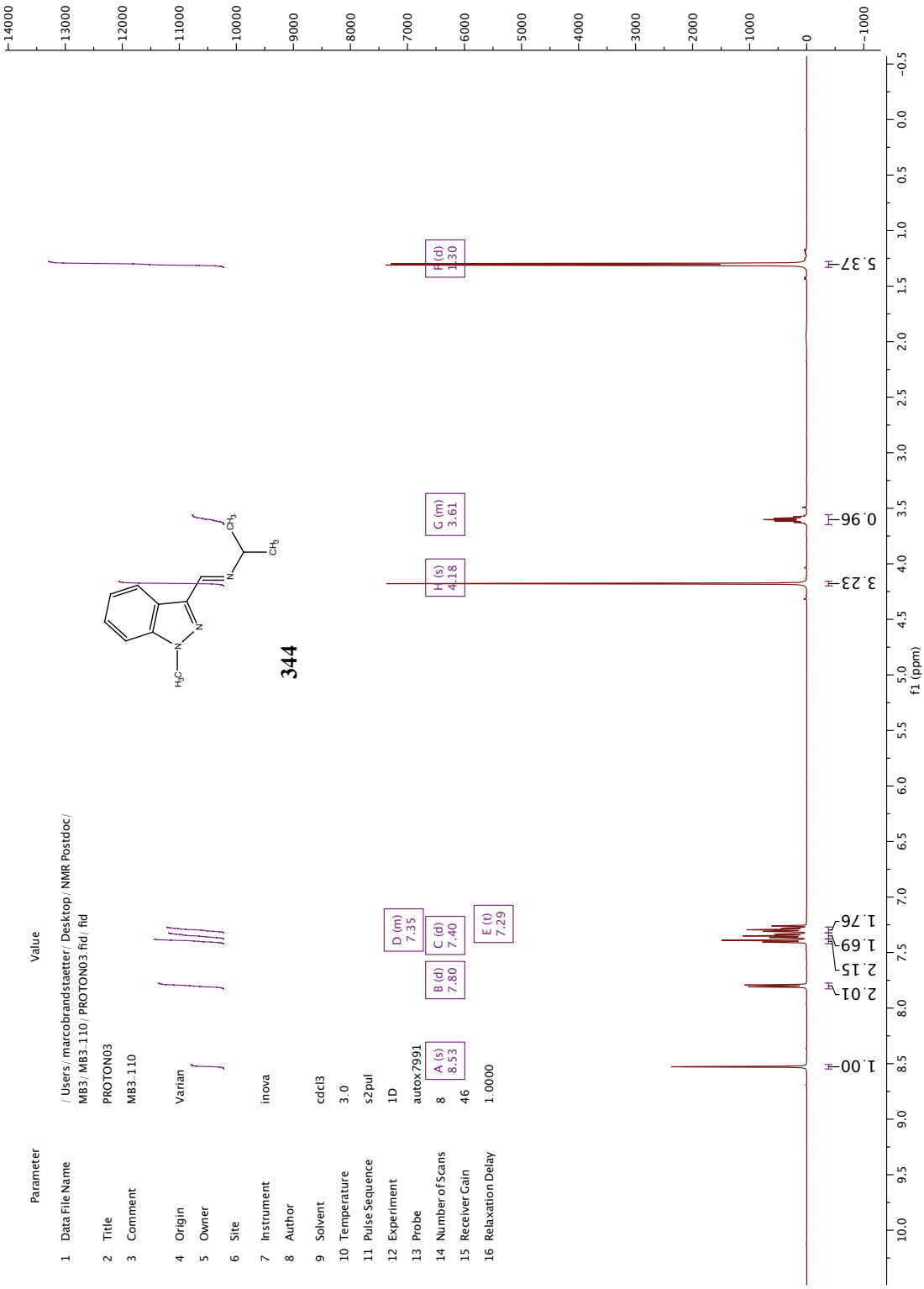
Parameter
Value
1 Data File Name / Users / marcobrandstaetter / Desktop / NMR Postdoc / MB3 / MB3_110 / PROTON03.fid / fid
2 Title PROTON03
3 Comment MB3_110
4 Origin Varian
5 Owner
6 Site
7 Instrument inova
8 Author
9 Solvent cdcl3
10 Temperature 3.0
11 Pulse Sequence s2pul
12 Experiment 1D
13 Probe autox7991
14 Number of Scans 8
15 Receiver Gain 46
16 Relaxation Delay 1.0000
A (s) 8.53
B (d) 7.80
C (d) 7.40
D (m) 7.35
E (t) 7.29
F (d) 1.30
G (m) 3.61
H (s) 4.18
344
1.00
2.01
2.15
1.69
1.76
5.37
0.96
3.23
f1 (ppm)

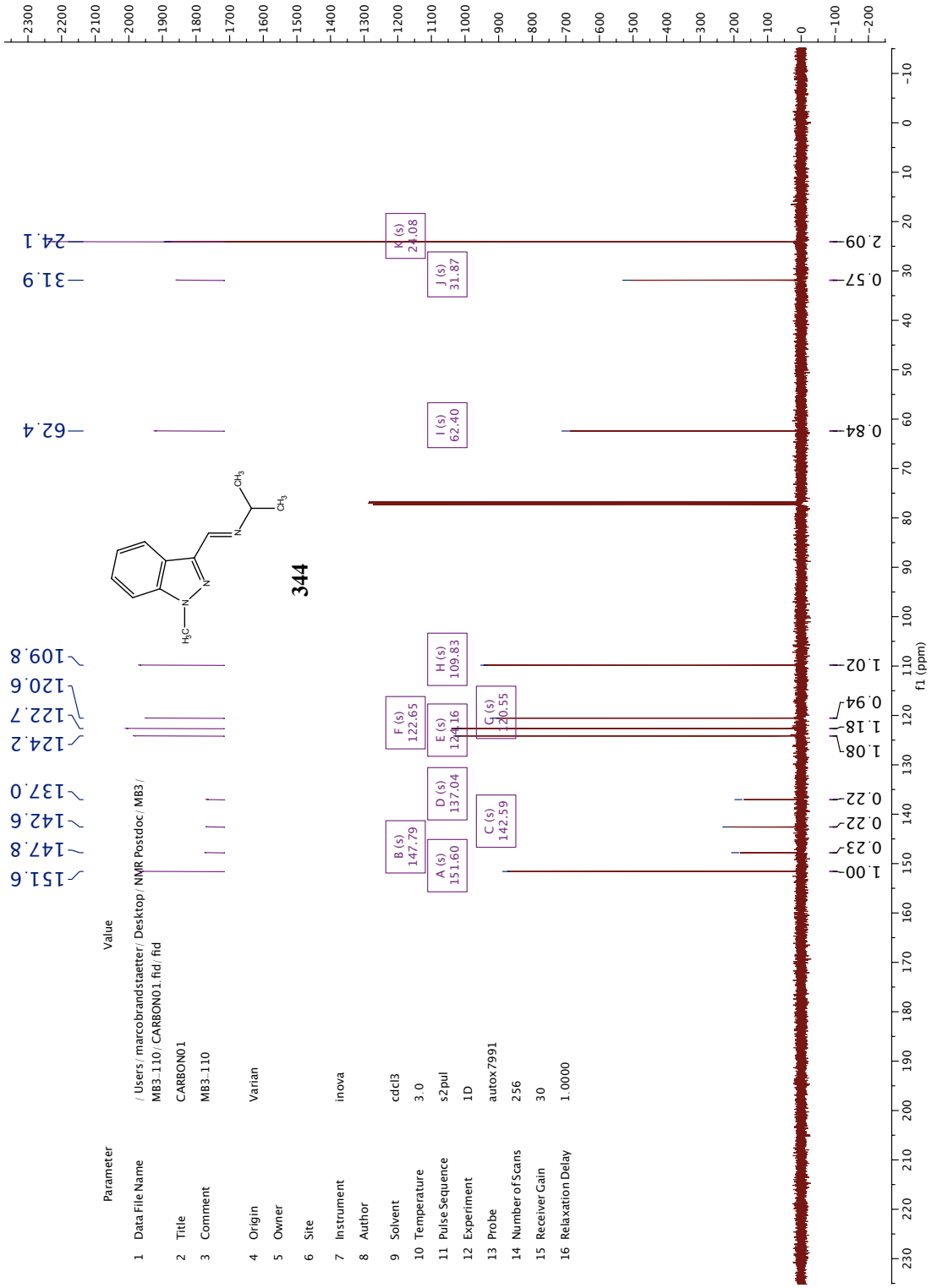
344
f1 (ppm)
Parameter
Value
1 Data File Name / Users / marcobrandstaetter / Desktop / NMR Postdoc / MB3 / MB3_110 / CARBON01.fid / fid
2 Title CARBON01
3 Comment MB3_110
4 Origin Varian
5 Owner
6 Site
7 Instrument inova
8 Author
9 Solvent cdcl3
10 Temperature 3.0
11 Pulse Sequence s2pul
12 Experiment 1D
13 Probe autox7991
14 Number of Scans 256
15 Receiver Gain 30
16 Relaxation Delay 1.0000
A (s) 151.60
B (s) 147.79
C (s) 142.59
D (s) 137.04
E (s) 124.16
F (s) 122.65
G (s) 120.55
H (s) 109.83
I (s) 62.40
J (s) 31.87
K (s) 24.08
151.6
147.8
142.6
137.0
124.2
122.7
120.6
109.8
62.4
31.9
24.1
1.00
0.23
0.22
0.22
1.08
1.18
0.94
1.02
0.84
0.57
2.09

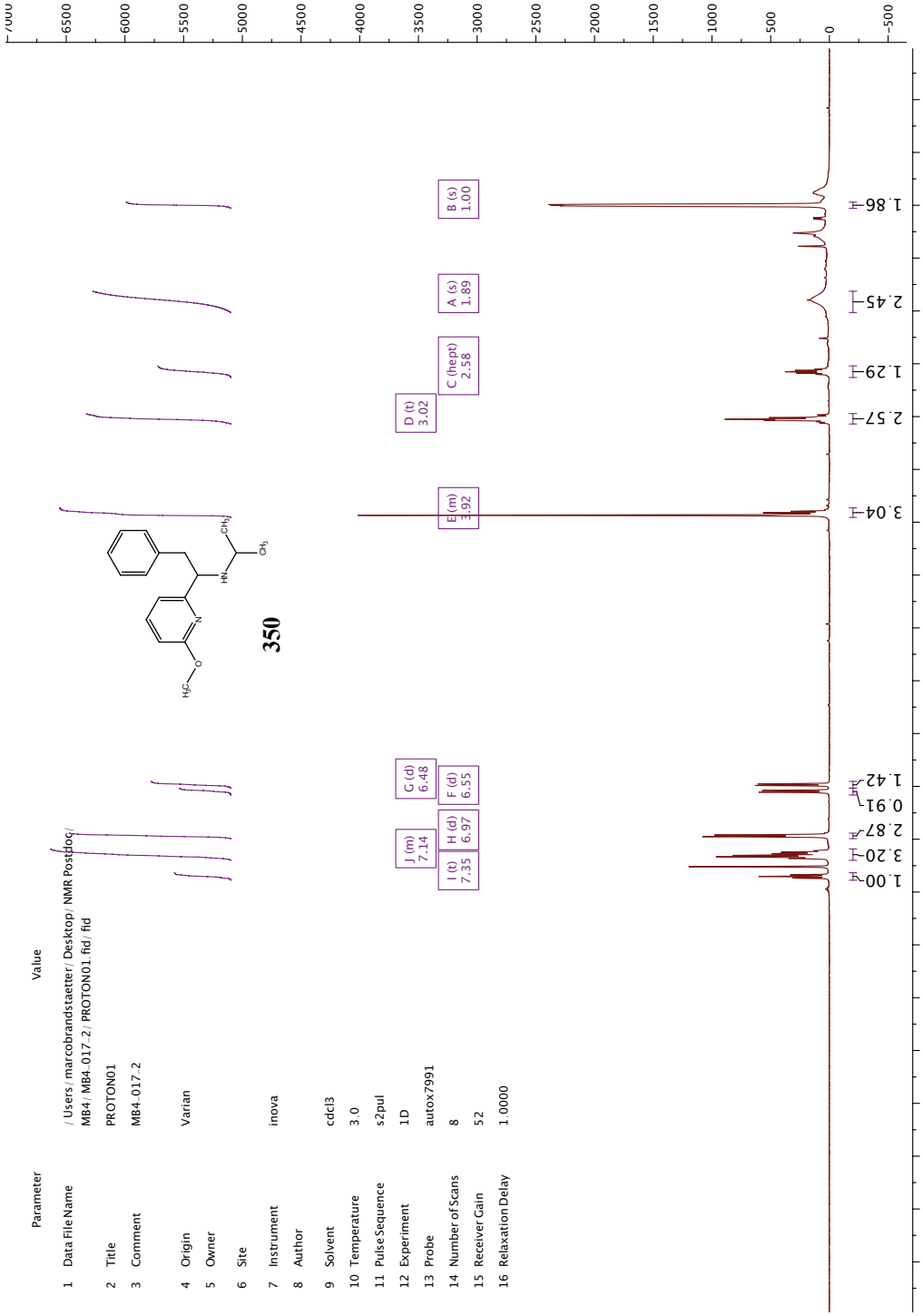
Parameter
Value
1 Data File Name
/ Users / marcobrandstaetter / Desktop / NMR Postdoc /
MB4 / MB4-017-2 / PROTON01.fid / fid
2 Title
PROTON01
3 Comment
MB4-017-2
4 Origin
Varian
5 Owner
6 Site
7 Instrument
inova
8 Author
9 Solvent
cdcl3
10 Temperature
3 0
11 Pulse Sequence
s2pul
12 Experiment
1D
13 Probe
autox7991
14 Number of Scans
8
15 Receiver Gain
52
16 Relaxation Delay
1.0000
350
I (t) 7.35
H (d) 6.97
J (m) 7.14
G (d) 6.48
F (d) 6.55
E (m) 3.92
D (t) 3.02
C (hept) 2.58
A (s) 1.89
B (s) 1.00
1.00
3.20
2.87
0.91
1.42
3.04
2.57
1.29
2.45
1.86
f1 (ppm)

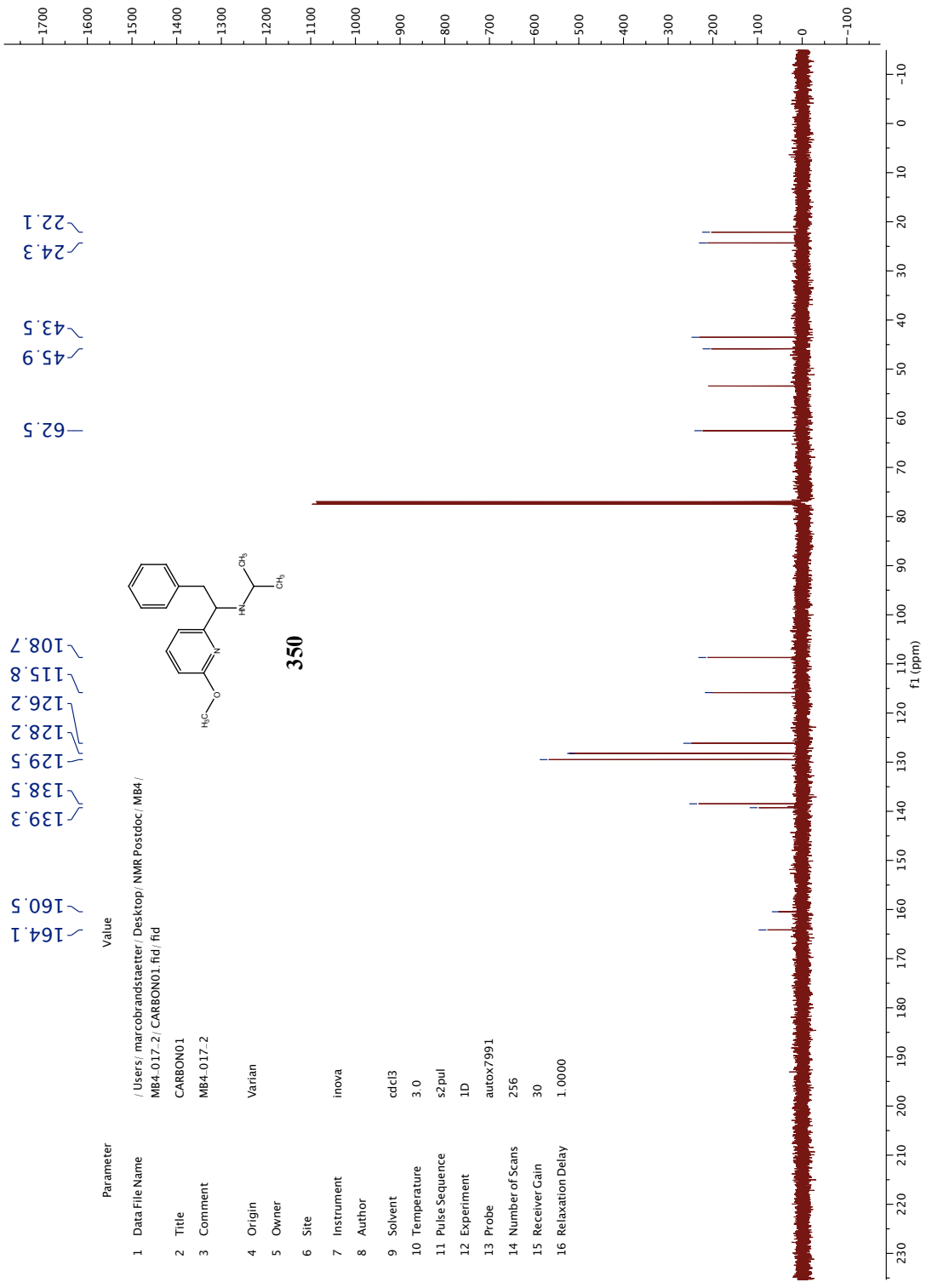

	Parameter	Value
1	Data File Name	/Users/marcobrandstaetter/Desktop/NMR Postdoc/MB4-MB4.017.2/CARBON01.fid/fid
2	Title	CARBON01
3	Comment	MB4.017.2
4	Origin	Varian
5	Owner	
6	Site	
7	Instrument	inova
8	Author	
9	Solvent	cdcl3
10	Temperature	3.0
11	Pulse Sequence	s2pul
12	Experiment	1D
13	Probe	autox7991
14	Number of Scans	256
15	Receiver Gain	30
16	Relaxation Delay	1.0000

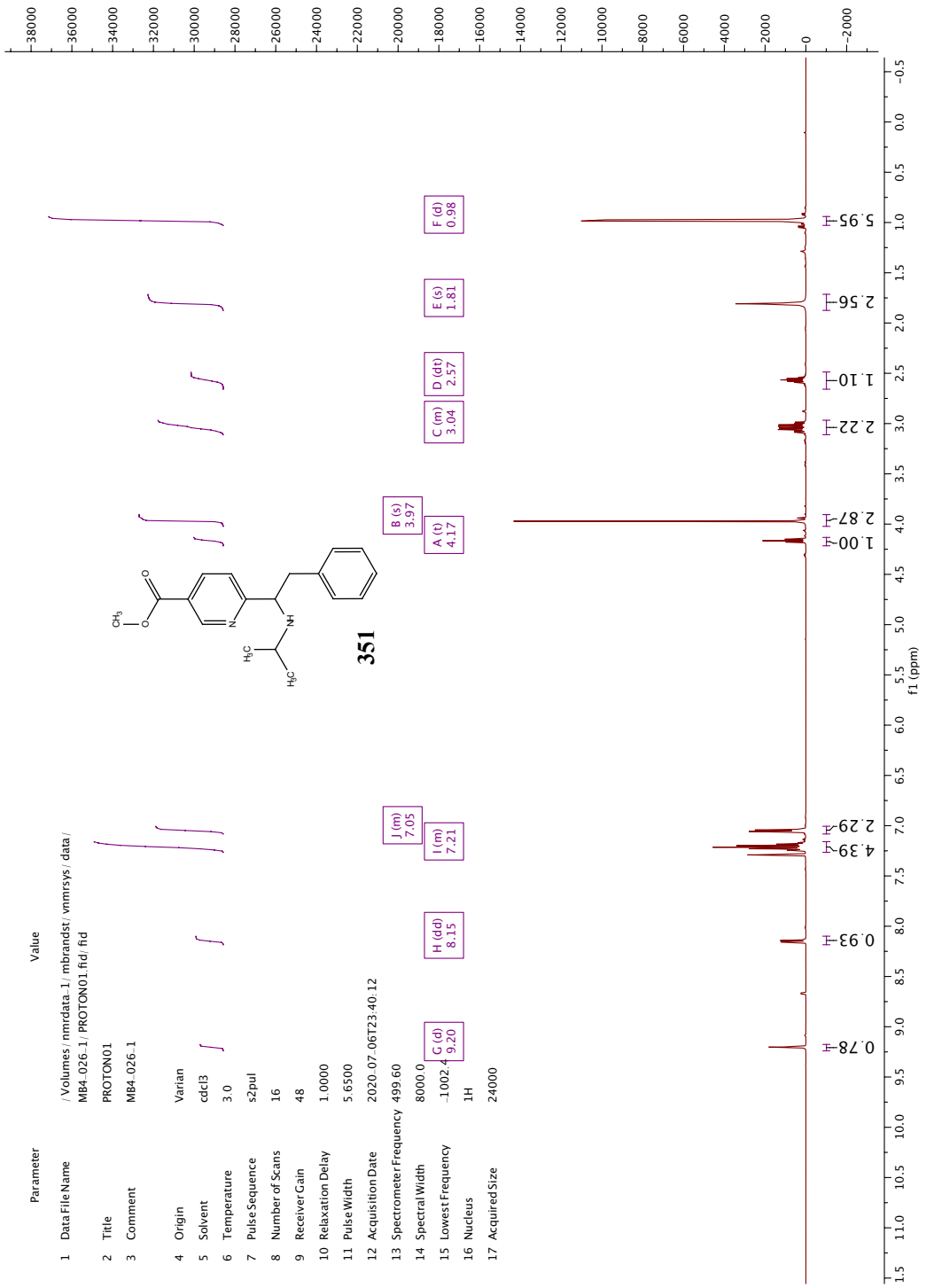
Parameter
Value
1 Data File Name
/ Volumes / nmrdata_1 / mbrandst / vnmrsys / data / MB4_026_1 / PROTON01.fid / fid
2 Title
PROTON01
3 Comment
MB4_026_1
4 Origin
Varian
5 Solvent
cdcl3
6 Temperature
3.0
7 Pulse Sequence
s2pul
8 Number of Scans
16
9 Receiver Gain
48
10 Relaxation Delay
1.0000
11 Pulse Width
5.6500
12 Acquisition Date
2020_07_06T23.40.12
13 Spectrometer Frequency
499.60
14 Spectral Width
8000.0
15 Lowest Frequency
-1002.4
16 Nucleus
1H
17 Acquired Size
24000
351
G (d) 9.20
H (dd) 8.15
I (m) 7.21
J (m) 7.05
A (t) 4.17
B (s) 3.97
C (m) 3.04
D (dt) 2.57
E (s) 1.81
F (d) 0.98
0.78
0.93
4.39
2.29
1.00
2.87
2.22
1.10
2.56
5.95
f1 (ppm)

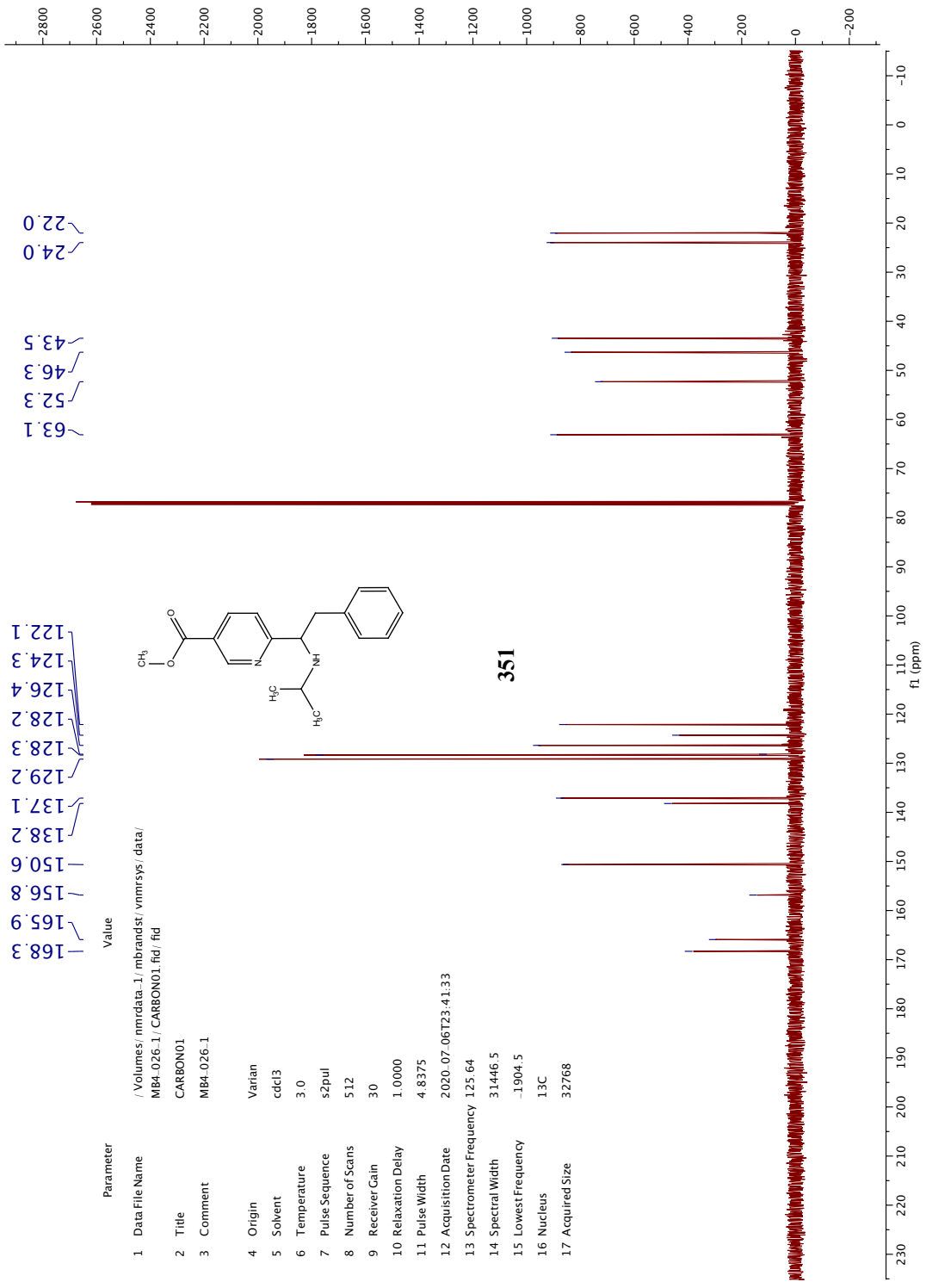

	Parameter	Value
1	Data File Name	/ Volumes/ nmrdata_1/ mbrandst/ vnmrsys/ data/ MB4.026.1/ CARBON01.fid/ fid
2	Title	CARBON01
3	Comment	MB4.026.1
4	Origin	Varian
5	Solvent	cdcl3
6	Temperature	3.0
7	Pulse Sequence	s2pul
8	Number of Scans	512
9	Receiver Gain	30
10	Relaxation Delay	1.0000
11	Pulse Width	4.8375
12	Acquisition Date	2020_07_06T23:41:33
13	Spectrometer Frequency	125.64
14	Spectral Width	31446.5
15	Lowest Frequency	-1904.5
16	Nucleus	13C
17	Acquired Size	32768

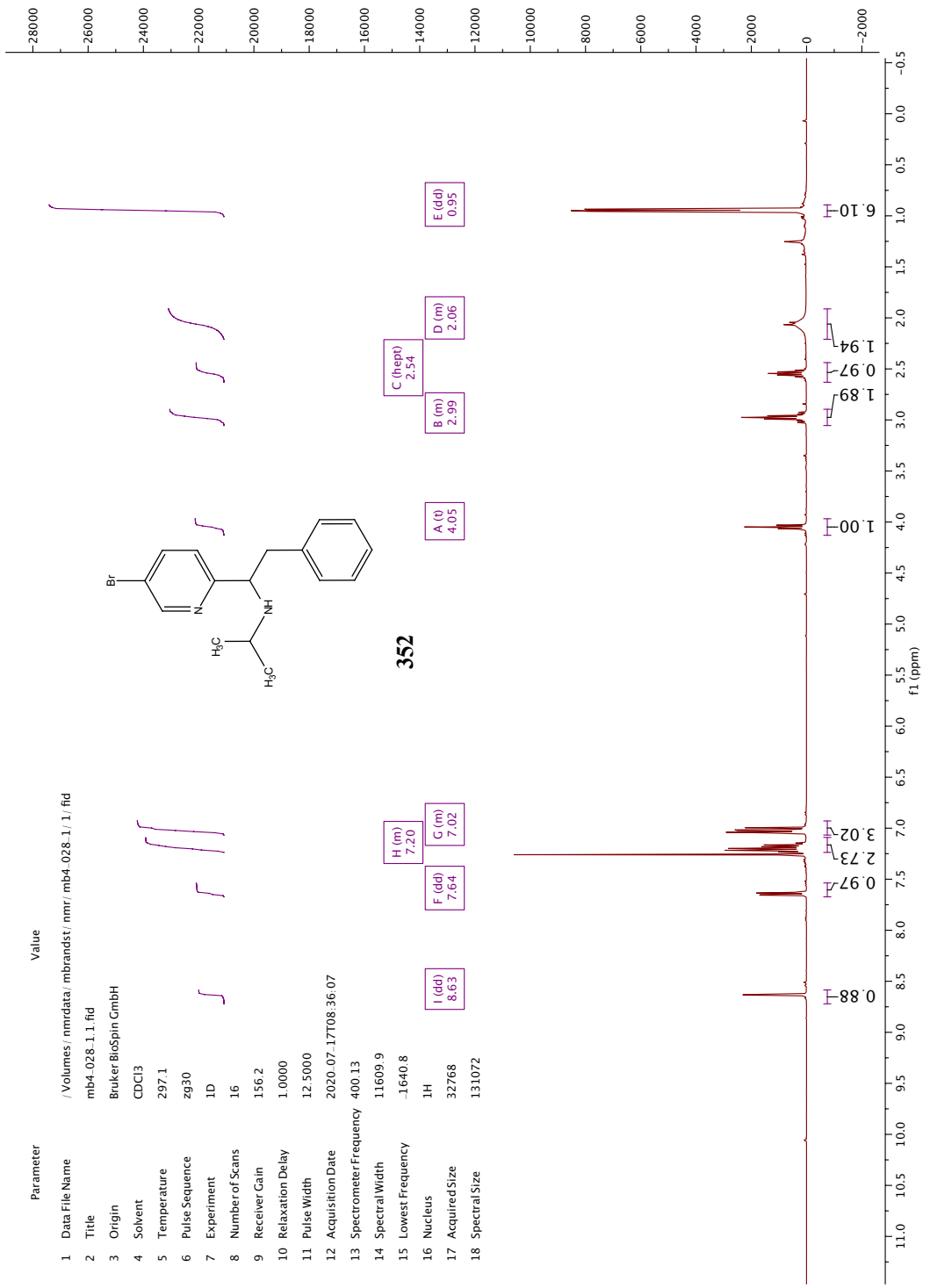
Parameter
Value
1 Data File Name / Volumes / nmrdata / mbrandst / nmr / mb4_028_1 / 1 / fid
2 Title mb4_028_1.1. fid
3 Origin Bruker BioSpin GmbH
4 Solvent CDCl3
5 Temperature 297.1
6 Pulse Sequence zg30
7 Experiment 1D
8 Number of Scans 16
9 Receiver Gain 156.2
10 Relaxation Delay 1.0000
11 Pulse Width 12.5000
12 Acquisition Date 2020_07_17T08:36:07
13 Spectrometer Frequency 400.13
14 Spectral Width 11609.9
15 Lowest Frequency -1640.8
16 Nucleus 1H
17 Acquired Size 32768
18 Spectral Size 131072
352
Br
N
NH
H3C
H3C
I (dd) 8.63
F (dd) 7.64
G (m) 7.02
H (m) 7.20
A (t) 4.05
B (m) 2.99
C (hept) 2.54
D (m) 2.06
E (dd) 0.95
0.88
0.97
2.73
3.02
1.00
1.89
0.97
1.94
6.10
f1 (ppm)

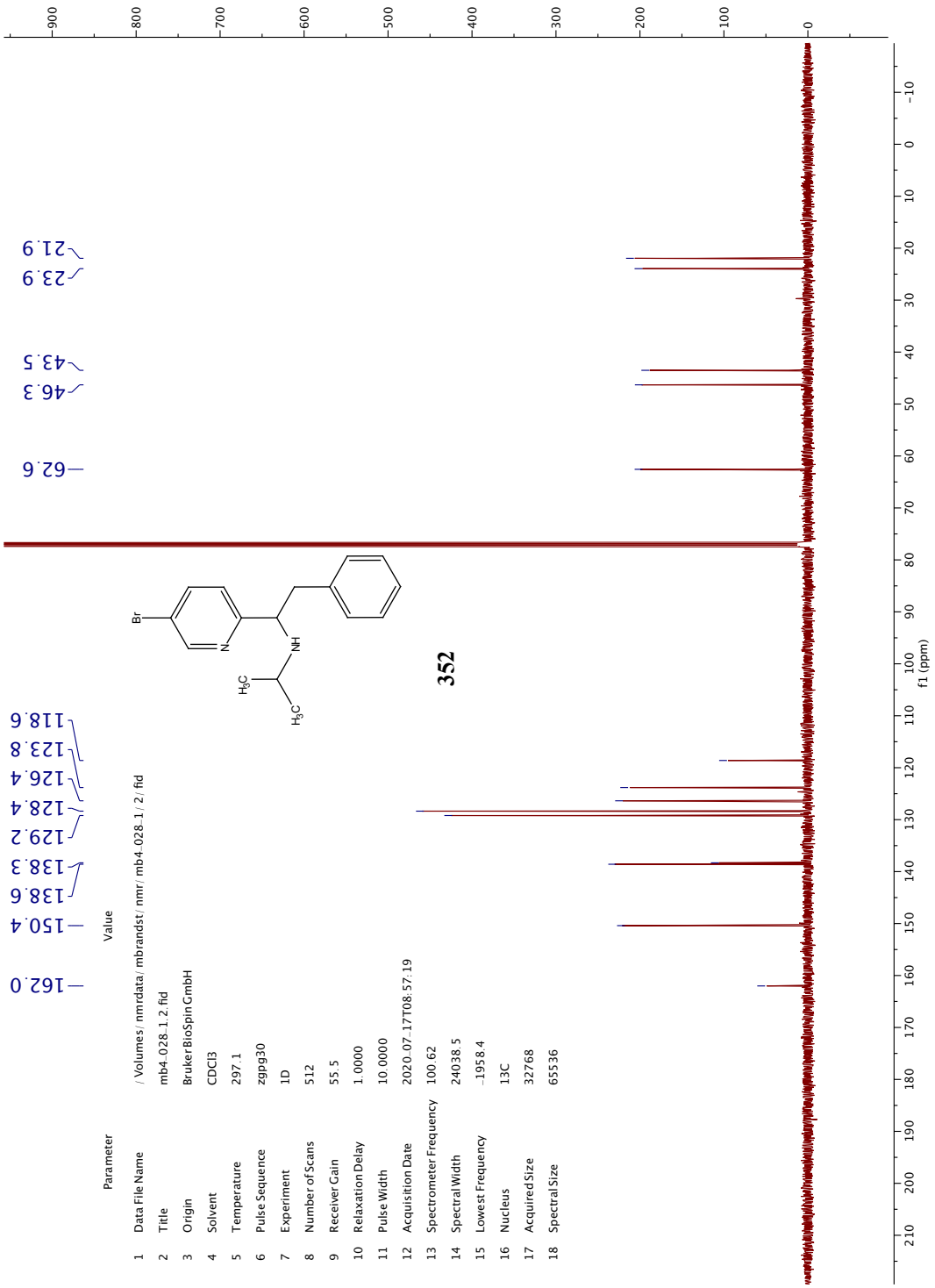

	Parameter	Value
1	Data File Name	/_Volumes/_nmrdata/_mbrandst/_nmr/_mb4_028_1_/_2/_fid
2	Title	mb4_028_1_2.fid
3	Origin	Bruker BioSpin GmbH
4	Solvent	CDCl3
5	Temperature	297.1
6	Pulse Sequence	zgpg30
7	Experiment	1D
8	Number of Scans	512
9	Receiver Gain	55.5
10	Relaxation Delay	1.0000
11	Pulse Width	10.0000
12	Acquisition Date	2020-07-17T08:57:19
13	Spectrometer Frequency	100.62
14	Spectral Width	24038.5
15	Lowest Frequency	-1958.4
16	Nucleus	13C
17	Acquired Size	32768
18	Spectral Size	65536

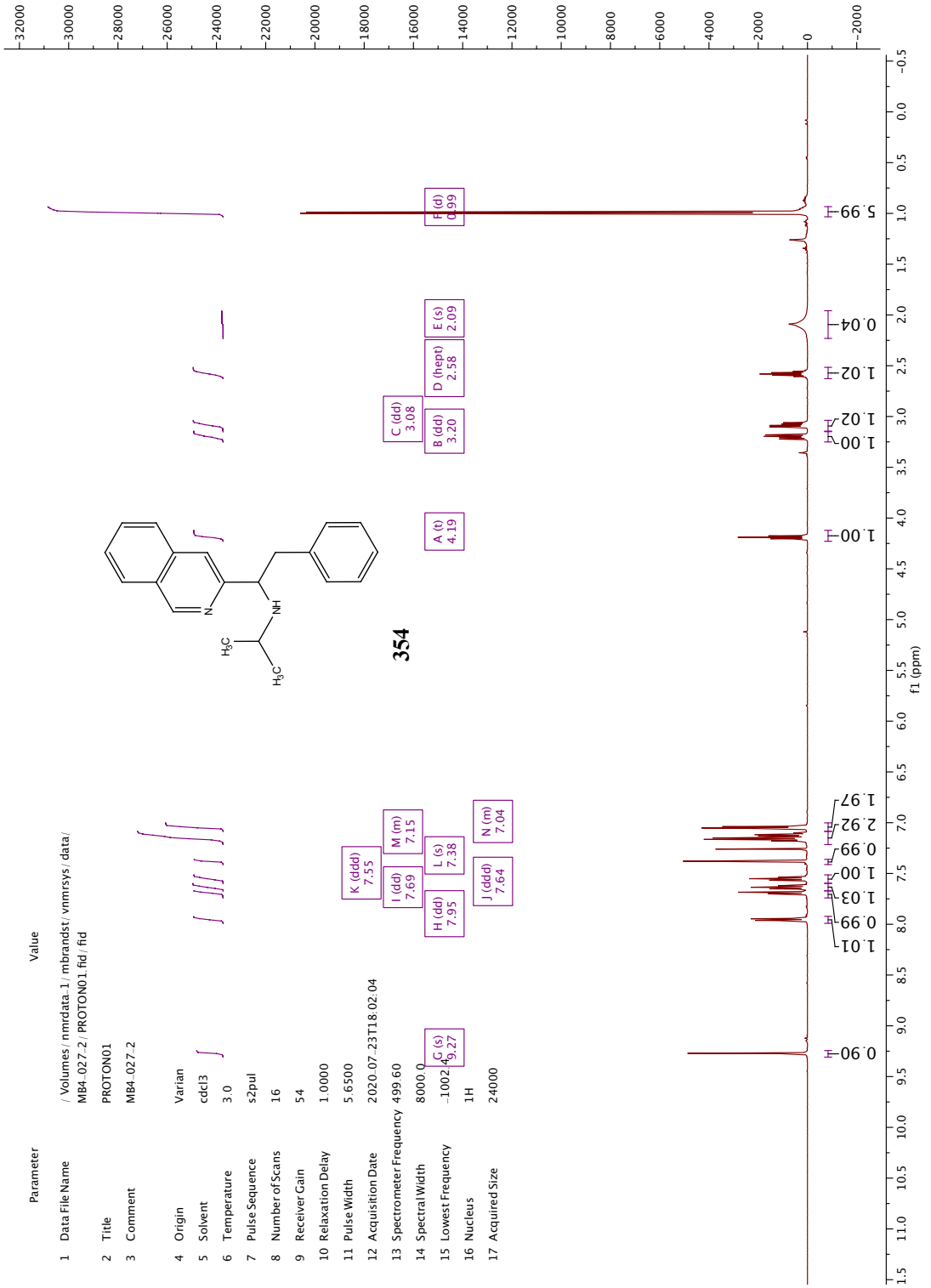
Parameter
Value
1 Data File Name / Volumes/ nmrdata_1/ mbrandst/ vnmrsys/ data/ MB4_027_2/ PROTON01.fid/ fid
2 Title PROTON01
3 Comment MB4_027_2
4 Origin Varian
5 Solvent cdcl3
6 Temperature 3.0
7 Pulse Sequence s2pul
8 Number of Scans 16
9 Receiver Gain 54
10 Relaxation Delay 1.0000
11 Pulse Width 5.6500
12 Acquisition Date 2020-07-23T18:02:04
13 Spectrometer Frequency 499.60
14 Spectral Width 8000.0
15 Lowest Frequency -1002.4
16 Nucleus 1H
17 Acquired Size 24000
354
A (t) 4.19
B (dd) 3.20
C (dd) 3.08
D (hept) 2.58
E (s) 2.09
F (d) 0.99
G (s) 9.27
H (dd) 7.95
I (dd) 7.69
J (ddd) 7.64
K (ddd) 7.55
L (s) 7.38
M (m) 7.15
N (m) 7.04
5.99
0.04
1.02
1.02
1.00
1.00
0.90
1.01
0.99
1.03
1.00
0.99
2.92
1.97
f1 (ppm)

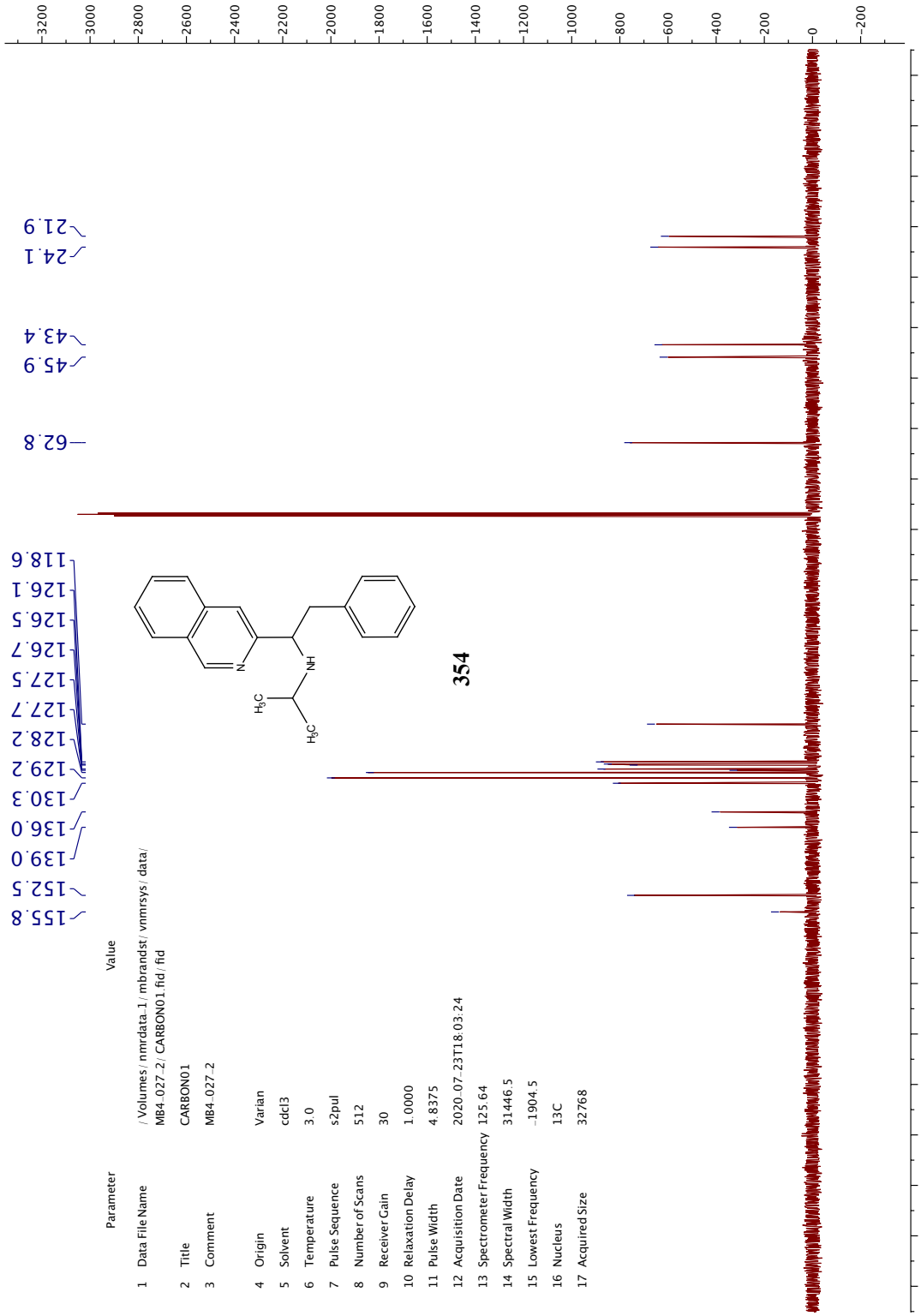

	Parameter	Value
1	Data File Name	/Volumes/nmrdata_1/mbrandst/vnmrsys/data/MB4_027_2/CARBON01.fid/fid
2	Title	CARBON01
3	Comment	MB4_027_2
4	Origin	Varian
5	Solvent	cdcl3
6	Temperature	3.0
7	Pulse Sequence	s2pul
8	Number of Scans	512
9	Receiver Gain	30
10	Relaxation Delay	1.0000
11	Pulse Width	4.8375
12	Acquisition Date	2020_07_23T18:03:24
13	Spectrometer Frequency	125.64
14	Spectral Width	31446.5
15	Lowest Frequency	-1904.5
16	Nucleus	13C
17	Acquired Size	32768

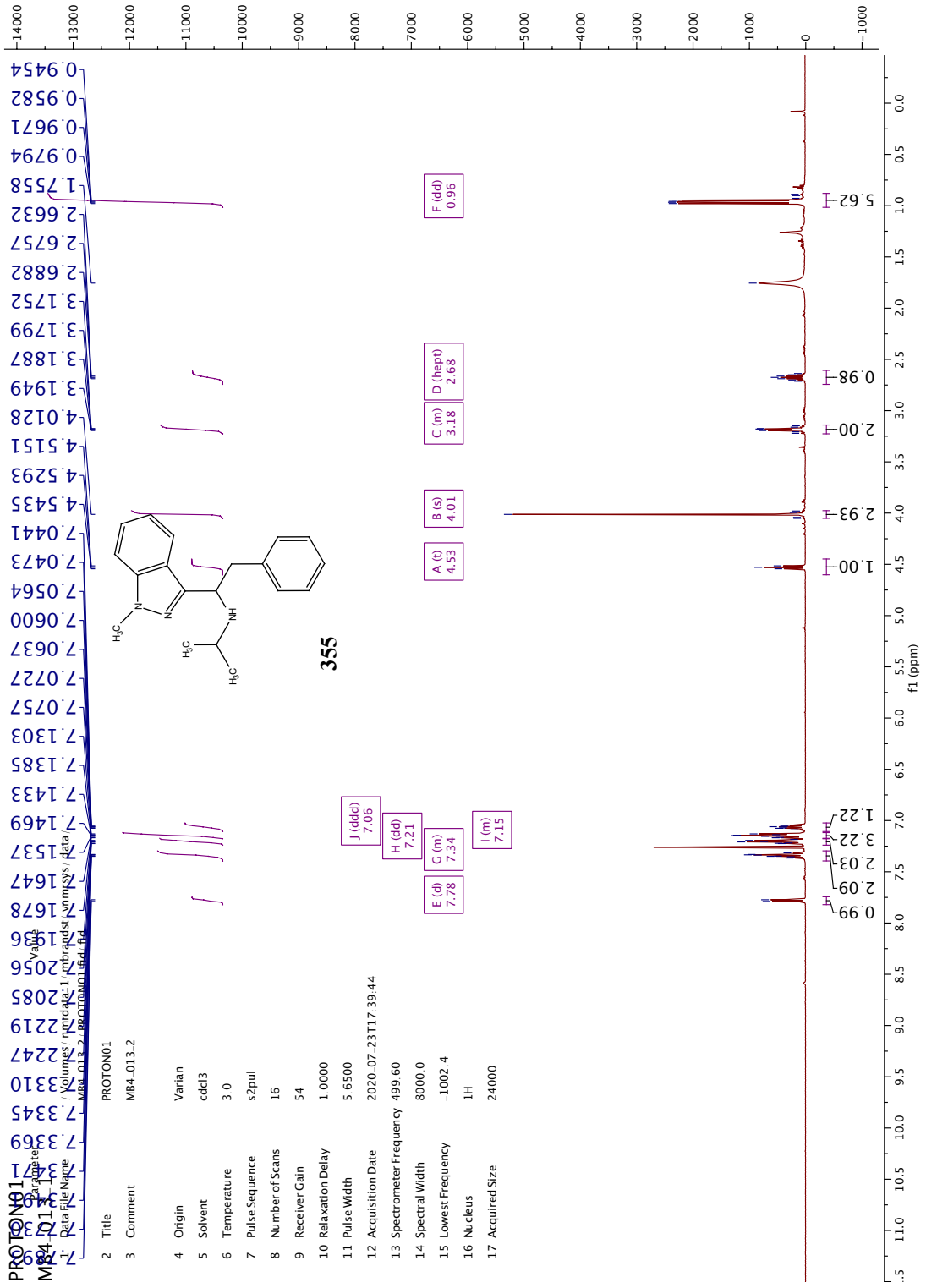
PROTON01
MB4_013_1
Parameter
Value
/ Volumes / nmrdata / 1 / nmrsys / data / MB4_013_2 / PROTON01.fid / fid
2 Title PROTON01
3 Comment MB4_013_2
4 Origin Varian
5 Solvent cdcl3
6 Temperature 3.0
7 Pulse Sequence s2pul
8 Number of Scans 16
9 Receiver Gain 54
10 Relaxation Delay 1.0000
11 Pulse Width 5.6500
12 Acquisition Date 2020_07_23T17:39:44
13 Spectrometer Frequency 499.60
14 Spectral Width 8000.0
15 Lowest Frequency -1002.4
16 Nucleus 1H
17 Acquired Size 24000
355
A (t) 4.53
B (s) 4.01
C (m) 3.18
D (hept) 2.68
E (d) 7.78
F (dd) 0.96
G (m) 7.34
H (dd) 7.21
I (m) 7.15
J (ddd) 7.06
5.62
0.98
2.00
2.93
1.00
1.22
3.22
2.03
2.09
0.99
f1 (ppm)

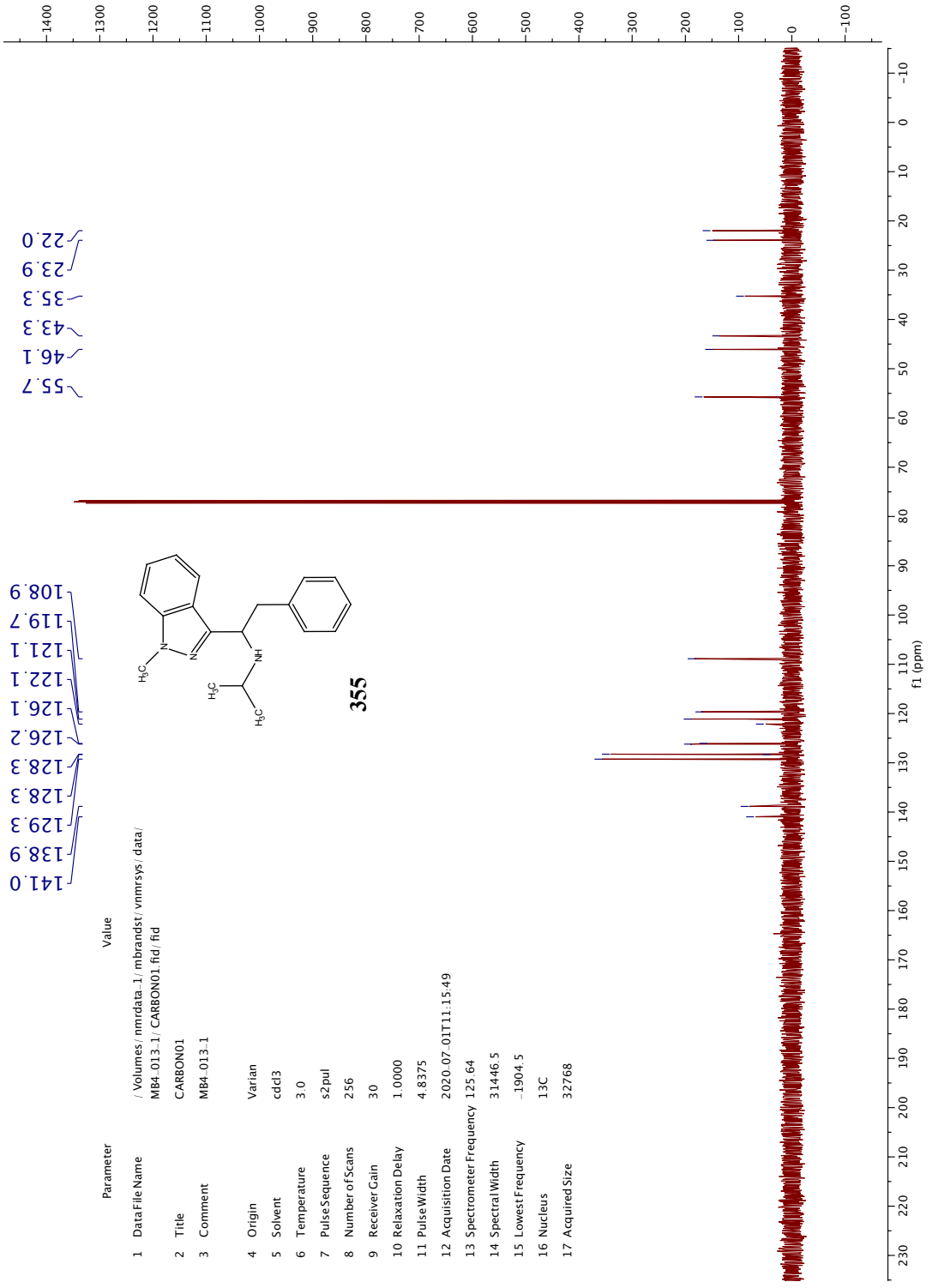

	Parameter	Value
1	Data File Name	/Volumes/nmrdata_1/mbrandst/vnmrsys/data/MB4_013.1/CARBON01.fid/fid
2	Title	CARBON01
3	Comment	MB4_013.1
4	Origin	Varian
5	Solvent	cdcl3
6	Temperature	3.0
7	Pulse Sequence	s2pul
8	Number of Scans	256
9	Receiver Gain	30
10	Relaxation Delay	1.0000
11	Pulse Width	4.8375
12	Acquisition Date	2020-07-01T11:15:49
13	Spectrometer Frequency	125.64
14	Spectral Width	31446.5
15	Lowest Frequency	-1904.5
16	Nucleus	13C
17	Acquired Size	32768

ABOUT THE AUTHOR

Raymond Farnon Turro was born in January 1996 in Ridgewood NJ, a suburb of New York City. He grew up there with his parents, Raymond and Joan Turro, as well as his younger sister Bridget. During this time he developed an interest in all things science with a particular interest in human health.

In 2014, Raymond began his undergraduate studies at Juniata College in Huntingdon, PA as a Biology major with the goal of going to medical school. His plans quickly changed after his first semester after taking part in Juniata's "Organic First" curriculum, where organic chemistry is taught to freshman students in lieu of general chemistry, causing him to first switch majors to biochemistry then chemistry shortly after. His newfound passion for organic chemistry in the classroom led him discovering a love for scientific research at the beginning of his sophomore year in the lab of Dr. John Unger where he developed asymmetric copper-catalyzed reactions. While at Juniata, Ray was active in the chemistry department serving as the department's chemistry seminar coordinator for 3 years as well as the department ombudsman.

Hungry for opportunities to do more research, Ray joined the lab of Dr. Uttam Tambar at UT Southwestern Medical Center in Dallas, TX for the summer of 2016 where he conducted research on small molecule drug development and chemical probe synthesis. This experience was so impactful that he returned the following summer in 2017 to develop methods for allylic fluorination.

After graduating Summa Cum Laude from Juniata College in 2018, Raymond moved across the country to Pasadena, CA to begin his graduate studies in the lab of Dr. Sarah Reisman at Caltech. His graduate research has focused on Ni-catalyzed reductive coupling

reactions as well as the total synthesis of C_{20}-diterpenoid alkaloids. After completing his organic chemistry training in the Reisman lab, Ray will move back to the east coast to join the Process Chemistry team at Takeda Pharmaceuticals in Cambridge, MA.